



**University Library**

Author/Filing Title ..... FONTECHA, J. ....

Class Mark ..... T .....

Please note that fines are charged on ALL  
overdue items.

**FOR REFERENCE ONLY**

0403271371





**POLYNUCLEAR COMPLEXES OF  
PSEUDOCALIXARENE  
MACROCYCLES**


**BY**

**JULIA BARREIRA FONTECHA**

**SUPERVISOR PROF. VICKIE MCKEE**

**A DOCTORAL THESIS SUBMITTED IN PARTIAL FULFILMENT OF THE  
REQUIREMENTS FOR THE AWARD OF DOCTOR OF PHILOSOPHY OF  
LOUGHBOROUGH UNIVERSITY**

**© JULIA BARREIRA FONTECHA 2006**

	<b>Loughborough University</b> Pitkin's library
Date	JAN 2007
Class	J
Acc No.	0403271371



## ABSTRACT

As part of a program to synthesise and investigate macrocyclic polynuclear arrays, a new range of phenol based pseudocalixarene macrocycles have been synthesized, combining some of the properties of the Schiff-base and calixarene macrocycle systems.

A series of dinuclear complexes of the pseudocalixarene macrocycle  $H_6L1$  containing two 2,2'-methylenediphenol groups have been synthesised and structurally characterised. Using divalent transition metal ions, complexes containing a common hyperbolic paraboloid (saddle)  $M_2(H_4L1)^{2+}$  core are formed. The structure is controlled by two strong O-H-O interactions resulting from metal-ion promoted monodeprotonation of the methylenediphenol units. The transition metal ions are located in a cleft within which neutral or anionic guests can bind. Use of trivalent transition metal ions leads to complete deprotonation of the phenol groups and loss of the saddle conformation.

A range of tri- and tetranuclear macrocyclic complexes of the pseudocalixarene macrocycle  $H_6L1$  have also been synthesised and structurally characterised. Depending on the counter anions present, the properties of the metal ion, the experimental conditions and the extent of deprotonation of the phenol groups, the nuclearity of the macrocycles can be manipulated. Similarly, bridging groups of various lengths can be accommodated between the bound metal ions. The synthesis and X-ray structures of several complexes along with some preliminary magnetic and spectroscopic studies are discussed.

Heteronuclear complexes of [2+2], [3+3] and [4+4] pseudocalixarene macrocyclic ligands have been synthesised by Schiff-base condensation of DHTMB with 1,3-diaminopropan-2-ol and first row transition, alkaline and alkaline-earth metal salts in the presence of a base. The effect of the metal template on the macrocyclic formation and relationships between the sizes and charges of the alkaline and alkaline-earth metal ions and the macrocycle's 'hole' are examined and the X-ray structures of some complexes are described.

## ACKNOWLEDGEMENTS

Firstly, I would like to start off by thanking my supervisor Prof. Vickie McKee for guiding me into the field of macrocyclic chemistry, for her supervision and encouragement during my PhD and for the many opportunities she has provided for development; in particular the opportunity to attend an international scientific meeting is very much appreciated. I am indebted to her for my achievements. Also the financial support from her and Loughborough University is gratefully acknowledged.

Many thanks to Drs. Martin Smith, Sandra Dann, Mark Elsegood and Paul Kelly from the Chemistry department at Loughborough University for their cooperation and many fruitful discussions I would also like to thank my work colleagues in the inorganic section: Paul, Gavin, Amy, Jo, Chris, Noelia, Allen, Andrew, Duncan, Sandrine, Richard B, Sophie, Julia, Katie, Sarah, Richard W., Liam and Emma, who made an invaluable contribution through their help and wide-ranging conversation. I also wish to thank Prof Jane Nelson for her general help and advice.

A special thanks goes to Pauline King and Alastair Daley at Loughborough University for all the elemental analysis, Dr. Mark Edgar for running the NMR studies, Dr Charlie Harding for carrying out the variable-temperature magnetic measurements, the EPSRC National Mass Spectrometry Service Centre in Swansea for the LSIMS and ESI spectra and the Synchrotron Radiation Source at Daresbury for use of stations 9 8 and 16 2.

My family, Esperanza, Vicente and Ana, deserve the biggest thanks for supporting me both mentally and financially during my long years of studies Thank you for your love and belief in me, I could not have done this without your help. Special thanks go to all my friends who made my years abroad such an amazing experience. And a very special thanks to Fabio whose love, support and unique friendship made each day special

## CONTENTS

Title	i
Abstract	ii
Acknowledgements	iii
Contents	iv
Ligands referred to in the thesis	xi
Colour pattern(s) of the atoms	xii
Abbreviations and symbols	xiii
Chapter 1: Introduction	1
Chapter 2: Dinuclear complexes of pseudocalixarene Schiff-base macrocycles	30
Chapter 3: Polynuclear complexes of pseudocalixarene Schiff-base macrocycles	104
Chapter 4: Heteronuclear complexes of pseudocalixarene Schiff-base macrocycles	145
Chapter 5: Experimental	203
References	244
Single X-ray crystallography	254
Appendix 1: Tables for crystal data and refinement for the compounds described	255
Appendix 2: Conferences and publications	274
Appendix 3: Single Crystal X-ray Crystallographic Data and NMR analyses	CD-ROM

## **Chapter 1: Introduction**

1.1. Introduction	2
1.2. Macrocyclic ligands	2
1.3. Synthesis of macrocyclic ligands	3
1.4. Schiff-base ligands	5
1.4.1. Phenol based Schiff-base ligands	7
1.4.1.1. Binucleating phenol based Schiff-base macrocycles	7
1.4.1.2. Tetranuclear phenol based Schiff-base macrocycles	12
1.4.1.3. Hexanuclear phenol based Schiff-base macrocycles	19
1.4.1.4. Pseudocalixarene Schiff-base macrocycles	21
1.5. Hydrogen bonding	26
1.6. Aims of this work	28

## **Chapter 2: Dinuclear complexes of pseudocalixarene Schiff-base macrocycles**

2.1. Introduction	31
2.2. Synthesis of 2,2'-dihydroxy-5,5'-di- <i>tert</i> -butyl-3,3'-methanediyl dibenzaldehyde (DHTMB)	33
2.2.1. Characterisation of 2,2'-dihydroxy-5,5'-di- <i>tert</i> -butyl-3,3'-methanediyl dibenzylalcohol (DHTMBA)	35
2.2.2. Characterisation of 2,2'-diallyloxy-5,5'-di- <i>tert</i> -butyl-3,3'-methanediyl dibenzylalcohol (AOTMBA)	36
2.2.3. Characterisation of 2,2'-diallyloxy-5,5'-di- <i>tert</i> -butyl-3,3'-methanediyl dibenzaldehyde (AOTMB)	37
2.2.4. Characterisation of 2,2'-dihydroxy-5,5'-di- <i>tert</i> -butyl-3,3'-methanediyl dibenzaldehyde (DHTMB)	37
2.3. Synthesis of 2,2'-dihydroxy-5,5'-di- <i>tert</i> -butyl-3,3'-methanediyl dibenzaldehyde (DHTMB) by direct oxidation	38
2.4. Dinuclear complexes of the pseudocalixarene macrocycle H <sub>6</sub> L1	39

2.4.1. Dinuclear complexes of H <sub>6</sub> L1 with intramolecular H-bonding	47
2.4.1.1 Synthesis and characterisation of [Cu <sub>2</sub> (H <sub>4</sub> L1)Cl]Cl·2MeOH, [Zn <sub>2</sub> (H <sub>4</sub> L1)Cl]Cl·H <sub>2</sub> O, [Ni <sub>2</sub> (H <sub>4</sub> L1)Cl]Cl·4H <sub>2</sub> O and [Mn <sub>2</sub> (H <sub>4</sub> L1)Cl]·Cl·H <sub>2</sub> O·EtOH	47
2.4.1.2. Structures of [Cu <sub>2</sub> (H <sub>4</sub> L1)Cl]Cl·1.6Et <sub>2</sub> O·EtOH and [Zn <sub>2</sub> (H <sub>4</sub> L1)Cl]Cl·Et <sub>2</sub> O·0.5EtOH·0.55H <sub>2</sub> O	51
2.4.1.3. Synthesis and characterisation of [Ni <sub>2</sub> (H <sub>4</sub> L1)(H <sub>2</sub> O) <sub>3</sub> ](ClO <sub>4</sub> ) <sub>2</sub> ·H <sub>2</sub> O, [Co <sub>2</sub> (H <sub>4</sub> L1)(H <sub>2</sub> O) <sub>3</sub> ](ClO <sub>4</sub> ) <sub>2</sub> ·3EtOH and [Co <sub>2</sub> (H <sub>4</sub> L1)(H <sub>2</sub> O) <sub>3</sub> ](BF <sub>4</sub> ) <sub>2</sub> ·2H <sub>2</sub> O	55
2.4.1.4. Structure of [Ni <sub>2</sub> (H <sub>4</sub> L1)(H <sub>2</sub> O)(EtOH) <sub>2</sub> ](ClO <sub>4</sub> ) <sub>2</sub> ·4EtOH	59
2.4.1.5. Synthesis and characterisation of [Ni <sub>2</sub> (H <sub>4</sub> L1)(NO <sub>3</sub> )(H <sub>2</sub> O) <sub>2</sub> ]NO <sub>3</sub> ·MeOH, [Zn <sub>2</sub> (H <sub>4</sub> L1)(NO <sub>3</sub> )(H <sub>2</sub> O) <sub>2</sub> ]NO <sub>3</sub> ·3H <sub>2</sub> O and [Co <sub>2</sub> (H <sub>3</sub> L1)(NO <sub>3</sub> ) <sub>2</sub> ]·5H <sub>2</sub> O	63
2.4.1.6. Structures of [Ni <sub>2</sub> (H <sub>4</sub> L1)(NO <sub>3</sub> )(EtOH) <sub>2</sub> ](NO <sub>3</sub> )·1.5EtOH·Et <sub>2</sub> O·H <sub>2</sub> O and [Zn <sub>2</sub> (H <sub>4</sub> L1)(NO <sub>3</sub> )(EtOH)](NO <sub>3</sub> )·H <sub>2</sub> O	65
2.4.1.7. Synthesis and characterisation of [Zn <sub>2</sub> (H <sub>4</sub> L1)(AcO)](AcO)·5H <sub>2</sub> O	70
2.4.1.8. Structure of [Zn <sub>2</sub> (H <sub>4</sub> L1)(AcO)](AcO)·5H <sub>2</sub> O·4Et <sub>2</sub> O	71
2.4.1.9. Synthesis and characterisation of [Ni <sub>2</sub> (H <sub>4</sub> L1)(MeOH) <sub>2</sub> ](ClO <sub>4</sub> ) <sub>2</sub> ·MeOH	74
2.4.1.10. Structure of [Ni <sub>2</sub> (H <sub>4</sub> L1)(MeOH) <sub>2</sub> ](ClO <sub>4</sub> ) <sub>2</sub> ·Et <sub>2</sub> O·1.5MeOH·0.5EtOH	75
2.4.1.11. Magnetic behaviour of [Ni <sub>2</sub> (H <sub>4</sub> L1)(MeOH) <sub>2</sub> ](ClO <sub>4</sub> ) <sub>2</sub> ·MeOH	79
2.4.2. Further structural studies of the dinuclear complexes with H-bonding	80
2.4.2.1. Nuclear Magnetic Resonance studies	80
2.4.2.2. Spectroscopic studies	85
2.4.3. Dinuclear complexes of H <sub>6</sub> L1 without intramolecular H-bonding	87
2.4.3.1. Synthesis and characterisation of [Mn <sub>2</sub> (H <sub>2</sub> L1)(Cl) <sub>2</sub> (EtOH) <sub>2</sub> ]·6H <sub>2</sub> O, [Co <sub>2</sub> (H <sub>2</sub> L1)(Cl) <sub>2</sub> (H <sub>2</sub> O) <sub>2</sub> ] and [Fe <sub>2</sub> (H <sub>2</sub> L1)(Cl) <sub>2</sub> (H <sub>2</sub> O) <sub>2</sub> ]	88
2.4.3.2. Structure of [Mn <sub>2</sub> (H <sub>2</sub> L1)(Cl) <sub>2</sub> (dmf)(dmsO)]·1.5dmf·0.3Et <sub>2</sub> O	91
2.4.3.3. Synthesis and characterisation of [Mn <sub>2</sub> (H <sub>2</sub> L1)(AcO) <sub>2</sub> (EtOH)], [Mn <sub>2</sub> (H <sub>2</sub> L1)(OH)(EtOH) <sub>2</sub> ](CF <sub>3</sub> SO <sub>3</sub> ) and [Co <sub>2</sub> (H <sub>2</sub> L1)](ClO <sub>4</sub> )	95
2.4.3.4. Synthesis and characterisation of [Cu <sub>2</sub> (H <sub>2</sub> L1)]·H <sub>2</sub> O and [Ni <sub>2</sub> (H <sub>2</sub> L1)(H <sub>2</sub> O) <sub>3</sub> ]	96
2.5. Conclusions	100

### Chapter 3: Polynuclear complexes of pseudocalixarene macrocycles

3.1. Introduction	105
3.2. Tri- and tetracopper complexes of the pseudocalixarene macrocycle H <sub>6</sub> L1	109
3.2.1. Structure of [Cu <sub>3</sub> (H <sub>2</sub> L1)(OH)(H <sub>2</sub> O)](NO <sub>3</sub> )·4EtOH	110
3.2.2. Structure of [Cu <sub>3</sub> (H <sub>2</sub> L1)(NO <sub>3</sub> )](NO <sub>3</sub> )(dmf) <sub>3</sub>	113
3.2.3. Structure of [Cu <sub>4</sub> (H <sub>2</sub> L1)(OH) <sub>2</sub> (H <sub>2</sub> O)(EtOH)](NO <sub>3</sub> ) <sub>2</sub> ·2EtOH·H <sub>2</sub> O	115
3.2.4. IR and LSIMS characterisation	119
3.2.5. Factors controlling the nuclearity	123
3.2.6. Further structural characterisations	126
3.2.6.1. UV-VIS spectroscopic studies	126
3.2.6.2. Magnetic studies	130
3.3. Other polynuclear complexes of the pseudocalixarene macrocycle H <sub>6</sub> L1	133
3.3.1. Synthesis and characterisation of trinuclear complexes of H <sub>6</sub> L1	135
3.3.2. Synthesis and characterisation of tetranuclear complexes of H <sub>6</sub> L1	136
3.4. Conclusions	141

### Chapter 4: Heteronuclear complexes of pseudocalixarene Schiff-base macrocycles

4.1. Introduction	146
4.2. Heteronuclear complexes of the pseudocalixarene macrocycle H <sub>6</sub> L1	149
4.2.1. Heteronuclear complexes of H <sub>6</sub> L1 with sodium	149
4.2.2. Heteronuclear complexes of H <sub>6</sub> L1 with calcium	159
4.2.3. Heteronuclear complexes of H <sub>6</sub> L1 with barium	162
4.2.4. Possible routes for the synthesis of the heteronuclear complexes of H <sub>6</sub> L1	173
4.3. Heteronuclear complexes of the pseudocalixarene macrocycle H <sub>9</sub> L8	175
4.3.1. Possible routes for the synthesis of the heteronuclear complexes of H <sub>9</sub> L8	183
4.4. Heteronuclear complexes of the pseudocalixarene macrocycle H <sub>12</sub> L9	185
4.4.1. Possible routes for the synthesis of the heteronuclear complexes of H <sub>12</sub> L9	192
4.5. Other heteronuclear barium complexes	197
4.6. Conclusions	199

## Chapter 5: Experimental

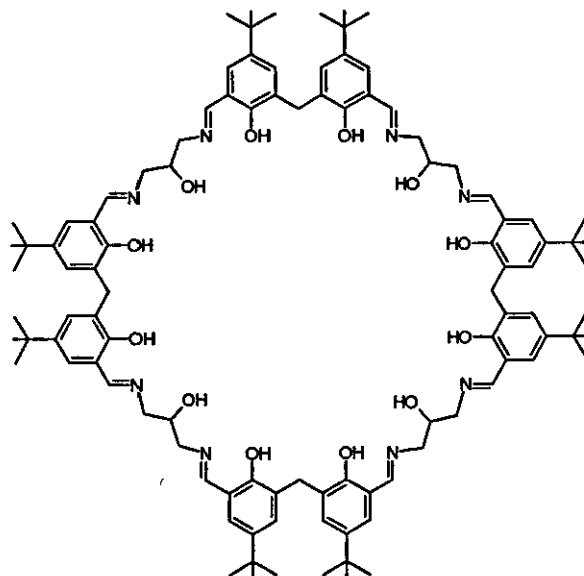
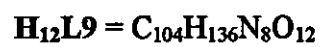
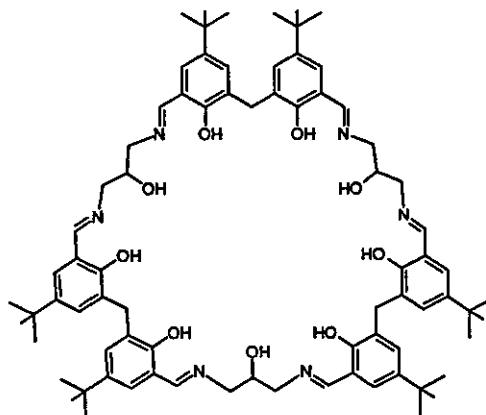
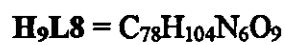
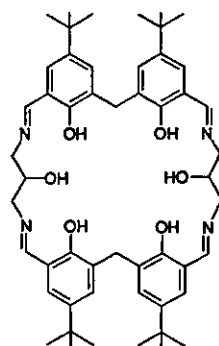
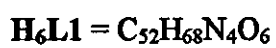
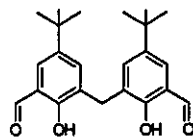
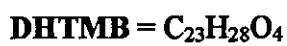
E.1 General experimental conditions	204
E.1.1. Solvents and reagents	204
E.1.2. Physical measurements	204
E.2. Dinuclear complexes of H <sub>6</sub> L1	205
E.2.1 Organic preparations	205
E.2.1.1. Synthesis of 2,2'-dihydroxy-5,5'-di- <i>tert</i> -butyl-3,3'-methanediyl-dibenzylalcohol (DHTMBA)	205
E.2.1.2. Synthesis of 2,2'-diallyloxy-5,5'-di- <i>tert</i> -butyl-3,3'-methanediyl-dibenzylalcohol (AOTMBA)	206
E.2.1.3. Synthesis of 2,2'-diallyloxy-5,5'-di- <i>tert</i> -butyl-3,3'-methanediyl-dibenzaldehyde (AOTMB)	207
E.2.1.4. Synthesis of 2,2'-dihydroxy-5,5'-di- <i>tert</i> -butyl-3,3'-methanediyl-dibenzaldehyde (DHTMB)	208
E.2.1.5. Synthesis of 2,2'-dihydroxy-5,5'-di- <i>tert</i> -butyl-3,3'-methanediyl-dibenzaldehyde (DHTMB) by direct oxidation	209
E.2.2. Complex syntheses	
E.2.2.1. [Cu <sub>2</sub> (H <sub>4</sub> L1)Cl]Cl·2MeOH (2.1)	210
E.2.2.2. [Zn <sub>2</sub> (H <sub>4</sub> L1)Cl]Cl·H <sub>2</sub> O (2.2)	211
E.2.2.3. [Ni <sub>2</sub> (H <sub>4</sub> L1)Cl]Cl·4H <sub>2</sub> O (2.3)	211
E.2.2.4. [Mn <sub>2</sub> (H <sub>4</sub> L1)Cl]Cl·H <sub>2</sub> O·EtOH (2.4)	212
E.2.2.5. [Ni <sub>2</sub> (H <sub>4</sub> L1)(H <sub>2</sub> O) <sub>3</sub> ](ClO <sub>4</sub> ) <sub>2</sub> ·H <sub>2</sub> O (2.5)	213
E.2.2.6. [Co <sub>2</sub> (H <sub>4</sub> L1)(H <sub>2</sub> O) <sub>3</sub> ](ClO <sub>4</sub> ) <sub>2</sub> ·3EtOH (2.6)	213
E.2.2.7. [Co <sub>2</sub> (H <sub>4</sub> L1)(H <sub>2</sub> O) <sub>3</sub> ](BF <sub>4</sub> ) <sub>2</sub> ·2H <sub>2</sub> O (2.7)	214
E.2.2.8. [Ni <sub>2</sub> (H <sub>4</sub> L1)(NO <sub>3</sub> )(H <sub>2</sub> O) <sub>2</sub> ](NO <sub>3</sub> )·H <sub>2</sub> O·MeOH (2.8)	215
E.2.2.9. [Zn <sub>2</sub> (H <sub>4</sub> L1)(NO <sub>3</sub> )(H <sub>2</sub> O) <sub>2</sub> ](NO <sub>3</sub> )·3H <sub>2</sub> O (2.9)	215
E.2.2.10. [Co <sub>2</sub> (H <sub>3</sub> L1)(NO <sub>3</sub> )]·5H <sub>2</sub> O (2.10)	216
E.2.2.11. [Zn <sub>2</sub> (H <sub>4</sub> L1)(AcO)](AcO)·5H <sub>2</sub> O (2.11)	217
E.2.2.12. [Ni <sub>2</sub> (H <sub>4</sub> L1)(MeOH) <sub>2</sub> ](ClO <sub>4</sub> ) <sub>2</sub> ·MeOH (2.12)	217

E.2.2.13. $[\text{Mn}_2(\text{H}_2\text{L1})(\text{Cl})_2(\text{EtOH})_2] \cdot 6\text{H}_2\text{O}$ (2.13)	218
E.2.2.14. $[\text{Co}_2(\text{H}_2\text{L1})(\text{Cl})_2(\text{H}_2\text{O})_2]$ (2.14)	219
E.2.2.15. $[\text{Fe}_2(\text{H}_2\text{L1})(\text{Cl})_2(\text{H}_2\text{O})_2]$ (2.15)	219
E.2.2.16. $[\text{Mn}_2(\text{H}_2\text{L1})(\text{AcO})_2(\text{EtOH})]$ (2.16)	220
E.2.2.17. $[\text{Mn}_2(\text{H}_2\text{L1})(\text{AcO})_2(\text{H}_2\text{O})_3]$	221
E.2.2.18. $[\text{Mn}_2(\text{H}_2\text{L1})(\text{EtOH})_2](\text{CF}_3\text{SO}_3) \cdot \text{H}_2\text{O}$ (2.17)	214
E.2.2.19. $[\text{Co}_2(\text{HL1})](\text{ClO}_4)$ (2.18)	222
E.2.2.20. $[\text{Cu}_2(\text{H}_2\text{L1})] \cdot \text{H}_2\text{O}$ (2.19)	222
E.2.2.21 $[\text{Ni}_2(\text{H}_2\text{L1})(\text{H}_2\text{O})_3]$ (2.20)	223
E 3. Polynuclear complexes of $\text{H}_6\text{L1}$	224
E 3.1 $[\text{Cu}_4(\text{H}_2\text{L1})(\text{OH})_2(\text{H}_2\text{O})_4](\text{NO}_3)_2$ (3.1)	224
E 3.2 $[\text{Cu}_3(\text{H}_2\text{L1})(\text{NO}_3)](\text{NO}_3)(\text{dmf})_3 \cdot \text{H}_2\text{O}$ (3.2c)	225
E.3.3. $[\text{Cu}_4(\text{H}_3\text{L1})(\text{OH})_2(\text{H}_2\text{O})_4](\text{NO}_3)_3$ (3.3)	226
E 3.4. $[\text{Ni}_3(\text{HL1})(\text{NO}_3)] \cdot 6\text{H}_2\text{O}$ (3.4)	227
E.3.5. $[\text{Ni}_3(\text{L1})((\text{NH}_2)_2\text{CO})] \cdot 2\text{EtOH} \cdot 2\text{H}_2\text{O}$ (3.5)	227
E.3.6. $[\text{Fe}_4(\text{L1})(\text{OH})_2(\text{EtO})_2](\text{NO}_3)_2 \cdot \text{H}_2\text{O}$ (3.6)	228
E 3.7. $[\text{Zn}_4(\text{H}_2\text{L1})(\text{EtO})_2(\text{EtOH})](\text{NO}_3)_2$ (3.7)	229
E.3.8 $[\text{Cu}_4(\text{H}_2\text{L1})(\text{OH})_2(\text{EtOH})](\text{ClO}_4)_2$ (3.8)	230
E.3.9. $[\text{Fe}_4(\text{L1})(\text{OH})_2(\text{EtO})_2](\text{ClO}_4)_2 \cdot 4\text{EtOH}$ (3.9)	230
E.3.10. $[\text{Ni}_4(\text{H}_2\text{L1})(\text{OH})_2(\text{H}_2\text{O})](\text{ClO}_4)_2$ (3.10)	231
E.3.11. $[\text{Cu}_4(\text{H}_2\text{L1})(\text{OH})_2(\text{EtOH})](\text{Cl})_2$ (3.11)	232
E 3.12. $[\text{Ni}_4(\text{H}_2\text{L1})(\text{OH})_2(\text{EtOH})_4](\text{Cl})_2$ (3.12)	232
E 3.13. $[\text{Cu}_4(\text{H}_2\text{L1})(\text{OH})_2(\text{H}_2\text{O})_2](\text{BF}_4)_2$ (3.13)	233
E 3.14 $[\text{Co}_4(\text{L1})(\text{OH})_4](\text{BF}_4)_2 \cdot 3\text{H}_2\text{O} \cdot 4\text{EtOH}$ (3.14)	234
E 3.15. $[\text{Ni}_4(\text{H}_2\text{L1})(\text{OH})_2(\text{EtO})](\text{AcO}) \cdot \text{H}_2\text{O}$ (3.15)	234
E 4. Heteronuclear complexes	235
E.4.1. $[\text{Ni}_2\text{Na}(\text{H}_2\text{L1})(\text{H}_2\text{O})_2](\text{AcO})$ (4.2)	235
E 4.2. $[\text{Zn}_2\text{Na}(\text{H}_2\text{L1})(\text{AcO})(\text{EtOH})](\text{AcOH})$ (4.3)	236
E 4.3 $[\text{Cu}_2\text{Ca}(\text{HL1})] \cdot \text{Cl}$ (4.4)	236
E.4.4. $[\text{Ni}_2\text{Ca}(\text{HL1})(\text{EtOH})](\text{NO}_3)$ (4.5)	237





E.4.5. $[\text{Cu}_4\text{Ba}(\text{H}_2\text{L1})_2](\text{ClO}_4)_2 \cdot \text{EtOH} \cdot 4\text{H}_2\text{O}$ (4.6a)	
$[\text{Cu}_4\text{Ba}(\text{H}_4\text{L9})](\text{ClO}_4)_2 \cdot 4\text{H}_2\text{O}$ (4.6b)	238
E.4.6. $[\text{Zn}_4\text{Ba}(\text{H}_2\text{L1})_2(\text{OH})](\text{ClO}_4) \cdot 3\text{H}_2\text{O}$ (4.7)	239
E.4.7. $[\text{Cu}_3\text{Ba}(\text{H}_2\text{L8})](\text{ClO}_4) \cdot 2\text{H}_2\text{O}$ (4.8)	240
E.4.8. $[\text{Ni}_3\text{Ba}(\text{HL8})](\text{EtOH}) \cdot \text{H}_2\text{O}$ (4.9a)	
$[\text{Ni}_4\text{Ba}(\text{H}_2\text{L1})_2(\text{EtOH})_2](\text{ClO}_4)_2 \cdot 3\text{H}_2\text{O}$ (4.9b)	241
E.4.9. $[\text{Cu}_3\text{Ca}(\text{H}_3\text{L8})](\text{NO}_3)_2 \cdot 3\text{EtOH} \cdot 2\text{H}_2\text{O}$ (4.10)	242
E.4.10. $[\text{Zn}_3\text{Ca}(\text{H}_3\text{L8})](\text{NO}_3)_2 \cdot 2\text{EtOH} \cdot 2\text{H}_2\text{O}$ (4.11)	243





## LIGANDS REFERRED TO IN THE THESIS




## COLOUR PATTERN(S) OF THE ATOMS

Carbon: 


Hydrogen: 


Oxygen:    or 

Nitrogen:   or 

Sulfur: 

Chlorine:  or 

Bromine: 

Sodium: 

Manganese:  or 


Iron:   or 

Cobalt:  or 

Nickel:  or 

Copper:   or 

Zinc: 

Lead: 

## ABBREVIATIONS AND SYMBOLS

DHTMBA	2,2'-Dihydroxy-5,5'-di- <i>tert</i> -butyl-3,3'-methanedioldibenzylalcohol
OATMBA	2,2'-Diallyloxy-5,5'-di- <i>tert</i> -butyl-3,3'-methanedioldibenzylalcohol
OATMB	2,2'-Diallyloxy-5,5'-di- <i>tert</i> -butyl-3,3'-methanedioldibenzaldehyde
DHTMB	2,2'-Dihydroxy-5,5'-di- <i>tert</i> -butyl-3,3'-methanedioldibenzaldehyde
Salen	<i>N,N'</i> -bis(salisylidene)ethylenediamine
Pd/C	Palladium on activated charcoal
PTSA	Para toluene sulfonic acid
DAHP	1,5-Diaminopentan-3-ol
DMF	<i>N,N</i> -dimethylformamide
DMA	<i>N,N</i> -dimethylacetamide
DMSO	Dimethylsulfoxide
Pet-ether	Petroleum ether
MeOH	Methanol
EtOH	Ethanol
Et <sub>2</sub> O	Diethylether
Et <sub>3</sub> N	Triethylamine
DCM	Methylene chloride
AcO	Acetate
AcOH	Acetic acid
Ar	Aryl ring
IR	Infrared
NMR	Nuclear magnetic resonance
DQF-COSY	Double quantum filtered correlated spectroscopy
NOE	Nuclear overhauser enhancement
DEPT	Distortionless enhancement by polarization transfer
HMBC	Heteronuclear multiple bond correlation
MS	Mass spectrometry
LSIMS	Liquid secondary ion mass spectrometry
FAB	Fast atom bombardment
ESI	Electrospray ionization

NOBA	3-Nitrobenxyl alcohol
CHN	Elemental analysis
UV	Ultraviolet
HOMO	Highest occupied molecular orbital
LUMO	Lowest unoccupied molecular orbital
HPLC	High performance liquid chromatography
Calc.	Calculated
Fig.	figure(s)
h.	hour(s)
min.	minute(s)
sec	second(s)
conc.	Concentrated or concentration
vs.	versus
ca.	circa
bp	boiling point
$\epsilon$	Extinction coefficient
<i>p</i>	para
<i>o</i>	orto
T	Temperature or Tesla
L	Litre(s) or Ligand
mL	milliliter(s)
M	Molar or Metal
mM	millimolar
mm	millimeter(s)
nm	nanometre(s)
Å	Angström unit $10^{-10}$ m
mMol	millimole
mol	mole
m/z	mass-to-charge ratio
Hz	Hertz, $\text{sec}^{-1}$
MHz	Megahertz, $10^6 \text{ sec}^{-1}$
ppm	parts per million

$\lambda$	Wavelength
$\nu$	Stretching frequency
$\delta$	Chemical shift in ppm
$\chi_M$	Molar magnetic susceptibility
$\mu_{\text{eff}}$	Effective magnetic moment
K	Kelvin
B.M.	Bohr magneton
N	Avogadro's number
$K_B$	Boltzmann's constant
C	Curie's constant
V	Volt
$e^-$	electron
°	degrees
°C	degrees centigrade
g	gram
$\text{cm}^{-1}$	wave number
b	broad
w	weak
m	medium
s	strong
equiv.	equivalent
<i>s</i>	singlet
<i>d</i>	duplet
<i>dd</i>	double duplet
<i>m</i>	multiplet

# **CHAPTER I**

## **INTRODUCTION**

## 1.1. Introduction

For much of the last forty years, the design and synthesis of macrocyclic ligands and their metal complexes has been the subject of increasing interest.<sup>1-5</sup> Macrocyclic molecules have attracted much attention because they can form a binding cavity for specific metals and possess host-guest complexation properties.

In particular, the design of macrocycles which complex metal ions with high stability and selectivity is a topic of growing interest not only due to its relevance in understanding many molecular processes occurring in biochemistry,<sup>7-11</sup> but also because of many possible applications in various areas such as materials science, catalysis, hydrometallurgy, transport and separation phenomena, selective extraction of metals, etc.<sup>12-20</sup>

A huge variety of macrocyclic ligands (e.g. calixarenes, polyporphyrins, crown ethers, cavitands, Schiff-bases, polyazamacrocycles, polyoxamacrocycles) and their respective complexes have been synthesised and characterised. This review, however, seeks to explore the development of the Schiff-base macrocyclic ligands and to focus particularly on polynucleating phenol-based Schiff-base macrocycles and related systems.

## 1.2. Macrocyclic ligands

A macrocyclic ligand is a large cyclic molecule with nine or more members containing three or more donor atoms which are able to form coordinate bonds with one or more metal centres within the central cavity.<sup>2</sup>

Although macrocyclic ligands have a similar coordination behaviour to that of non-cyclic polydentate ligands, the majority of the macrocycles are kinetically and thermodynamically more stable than their linear analogues. Thermodynamic stabilization comes from enthalpic contributions (macrocyclic ligands are less



strongly solvated than acyclic compounds because they present less solvent-accessible surface area) and entropic contributions (macrocycles are less conformationally flexible and thus lose fewer degrees of freedom upon complexation). Kinetic stabilization is achieved through large number of fixed donor atoms (both coordination and ligand dissociation reactions with macrocyclic ligands are slower than those with acyclic analogues). This trend is known as the *macrocyclic effect*.<sup>1,2</sup>

### 1.3. Synthesis of macrocyclic ligands

The growth of research in the area of macrocyclic chemistry has stimulated the development of diverse synthetic strategies. The synthesis of macrocyclic ligands can be divided into two main categories: direct synthesis (or non-template synthesis) and metal-directed synthesis (or template synthesis).<sup>1,2</sup>

In the *direct synthesis* the cyclisation process occurs by a conventional organic route. The macrocyclic ligand is obtained without the use of complexing metal ions. The main problem with this procedure is the possible polymerisation of the reactants. The two reactive functional groups have to be in close proximity in order for the cyclisation process to occur. Statistically it is more likely that the acyclic intermediate will react with another molecule, leading to polymerisation products rather than the desired cyclic compound. This problem can be reduced by using "high dilution" reaction conditions. The probability of an acyclic ligand reacting with another molecule decreases as the concentration in the reaction solution is reduced. This can be achieved by adding the reactants at a very slow rate so that the concentrations of unreacted materials are always very small. However, there are some cases where direct synthesis does not need high dilution and the macrocycles are obtained in good yields.<sup>21</sup> Although there are many examples of Schiff-base macrocycles obtained by direct synthesis,<sup>22-30</sup> template synthesis is generally preferred to get high yields and selective routes to new macrocycles

In *template synthesis* the yield of the cyclic product is noticeably increased by the presence of a metal ion in the cyclisation reaction. The metal ion directs the pathway of the reaction by coordinating the donor atoms and pre-organising the intermediate in the conformation necessary to obtain the cyclic product. This is known as the *metal template effect* and can be of two types. In the *kinetic template effect*, the metal ion directs the steric course of a condensation such that formation of the required cyclic product is facilitated. In the case of the *thermodynamic template effect*, the metal ion sequesters the cyclic product from the equilibrium mixture between products and reactants. Formation of the macrocycle as its metal complex is promoted.<sup>1,2</sup>

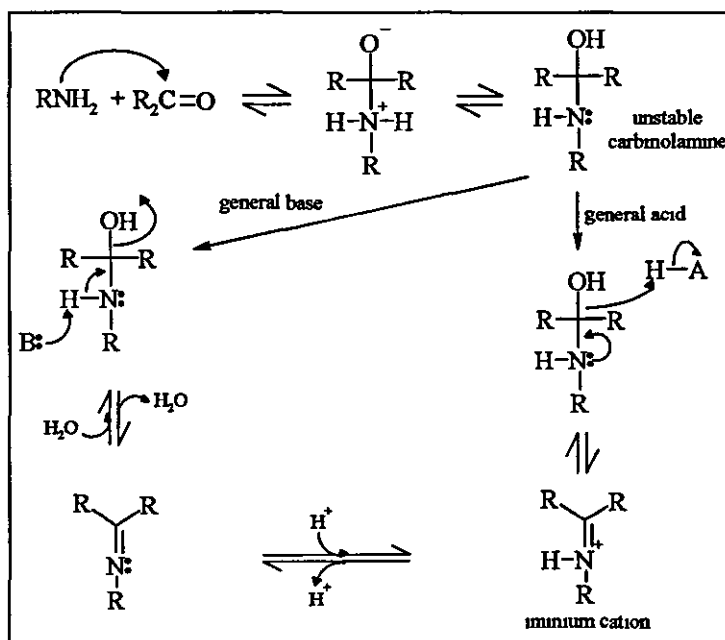
The most significant factors in the template synthesis appear to be the metal cation radius and geometric preferences, the nature of the donor atoms, and the size of the macrocyclic cavity. The success of the synthesis and the geometry of the resulting product are dependent on the compatibility of the macrocyclic cavity with the metal cation radius. Besides, the formation of the cyclic product depends on the strength of the interaction between the donor atoms and the metal ion<sup>1,2,31</sup> Template routes can be restrictive, as not all the metal ions will template a specific cyclisation reaction

Fenton *et al.* reported a way to use the sodium ion as an effective template in the synthesis of a series of macrocycles using 2,6-diformyl-4-methylphenolate as a precursor<sup>32</sup> They have shown that the sodium macrocyclic complex used as a “free macrocycle equivalent” readily undergoes transmetallation by transition metals to form dinuclear macrocyclic complexes with a high yield.<sup>33</sup> These complexes can also be viewed as sodium salts of the macrocycles. Sodium would not be expected to coordinate strongly to medium-soft donors such as nitrogen and might, in fact, not act as a strong template compared to, e.g. the synthesis of crown-ethers where all the coordinating donors are oxygen atoms.

#### 1.4. Schiff-base ligands

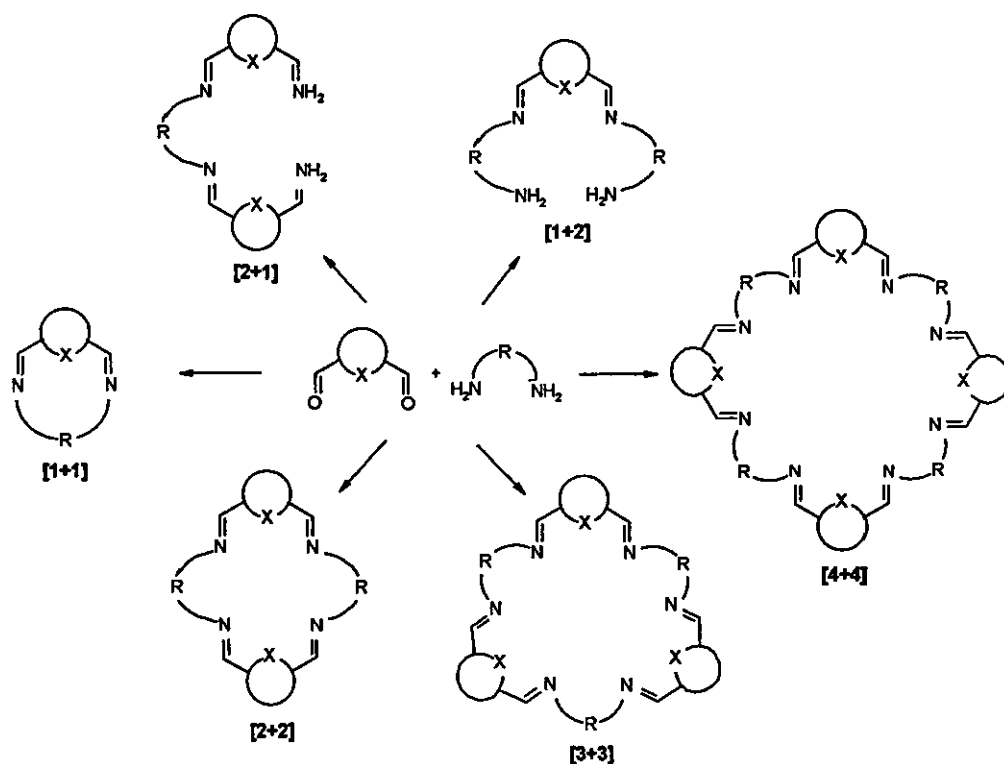
Professor H Schiff reported on the first synthesis of Schiff base metal complexes as early as the 1860s. Metal complexes with Schiff bases as ligands have played an important part in the development of coordination chemistry as a whole, however, it was not until the 1950s that concrete and rapid advances in this field became evident. A large variety of macrocyclic and macroacyclic Schiff-base ligands have been synthesised in order to determine correctly the role of the different donor atoms, their relative position, the number and size of the chelating rings formed, the flexibility and the shape of the coordinating moiety on the selective binding of charged or neutral species.

The Schiff-base condensation mechanism<sup>34</sup> consists of the addition of a nucleophilic molecule (amine) which forms a covalent intermediate with the reactant. The initial addition product (a carbinolamine) can become dehydrated, since the free pair of electrons on the N are more likely to be shared with the carbon to form a double bond than electrons from the original carbonyl O, which is more electronegative than the N. An imine or Schiff-base forms, with a pKa of about 7. The Schiff-base is often stabilized by resonance.



Scheme 1.1: Schiff-base condensation mechanism

Schiff-base macrocycles can be obtained by simple self-condensation of suitable diformyl (aldehyde or ketone) and primary diamine precursors. The condensation gives rise to cyclic and acyclic Schiff-bases which can have different size according to the experimental conditions used. Scheme 1.2 illustrates some examples of Schiff-base ligands synthesised from diformyl and primary diamine precursors. The numbers between brackets indicate the number of units of diformyl and diamine condensed to give rise to the ligands, e.g. [2+1] indicates two molecules of diformyl condensed with one molecule of diamine or [1+2] denotes that one unit of diformyl has condensed with 2 units of diamine, as shown in Scheme 1.2.



**Scheme 1.2:** Acyclic and macrocyclic Schiff-base ligands (X=O, N, S)

A wide variety of Schiff-base macrocycles has been synthesised depending on the precursors used (i.e. diformyl heterocycles, diformyl phenol rings, diamine alkane chains, diamine heterocycles).

### 1.4.1. Phenol based Schiff-base ligands

Schiff-base macrocycles containing potentially bridging phenol groups have been used to synthesise binucleating homo- and heteronuclear systems for approximately 30 years. The incorporation of a phenol fragment into the macrocyclic core leads to the formation of ligands that are particularly suitable for coordination of two metal ions. Detailed investigation of the chemistry of dinuclear<sup>35-38</sup> and, more recently, polynuclear<sup>39-43</sup> phenol-based macrocyclic complexes has permitted significant insights in a number of areas, including magnetochemistry, site selection, catalytic and bioinorganic model chemistry.

#### 1.4.1.1. Binucleating phenol based Schiff-base macrocycles

The term *binucleating* was used by Robson<sup>44</sup> when describing polydentate chelating ligands that are capable of simultaneously binding two metals. The two metal ions can be found in separated sites within the ligands or in close proximity, being able to interact with each other. This interaction is enhanced by the ability of ligand donor atoms to bridge two metal ions. Schiff-base complexes based on phenol head units have the ability to bridge the metal ions through the phenol oxygen atom.

In 1970 Robson and Pilkington<sup>45</sup> reported the first synthesis of a binucleating Schiff-base macrocyclic system derived from 2,6-diformyl-4-methylphenol (Fig.1.1). The macrocyclic system was synthesised by the metal template Schiff-base condensation of 2,6-diformyl-4-methylphenol with 1,3-diaminopropane in the presence of a range of first row transition metal ions.

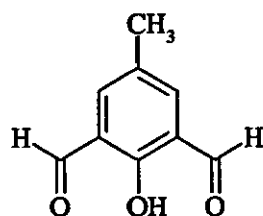


Fig.1.1: 2,6-diformyl-4-methylphenol

Since their first use by Robson *et al.*, extensive research has been carried out on "Robson-type" binucleating ligands and related systems derived from 2,6-diacetyl-4-substituted phenols (Fig. 1.2). Variations of R have included H,<sup>46,47</sup> CH<sub>3</sub>,<sup>38,48-51</sup> C(CH<sub>3</sub>)<sub>3</sub>,<sup>35,42,52-54</sup> OH,<sup>55</sup> NO<sub>2</sub>,<sup>56</sup> Cl,<sup>57-59</sup> Br,<sup>37,60,61</sup> F<sup>4</sup> and CF<sub>3</sub>.<sup>62,63</sup> While R' substitutes include for instance H, CH<sub>3</sub>, C<sub>6</sub>H<sub>6</sub> and OH.

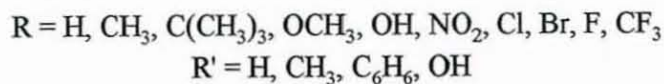
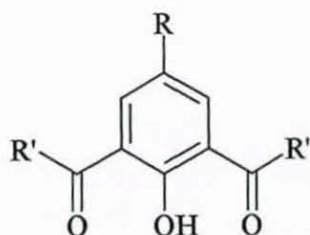


Fig. 1.2: 2,6-diacetyl-4-substituted phenol derivatives

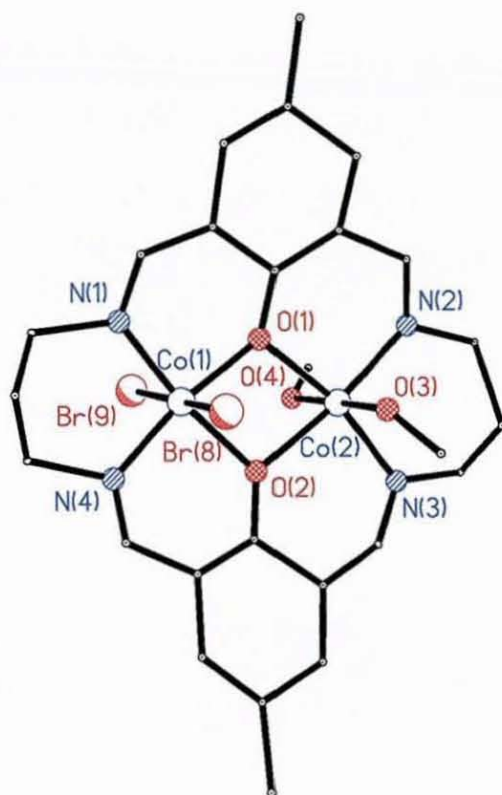


Fig. 1.3: Example of a typical Robson complex.  
 Structure<sup>48,64,65</sup> of the cation [Co<sub>2</sub>(L10)(Br)<sub>2</sub>(MeOH)<sub>2</sub>]<sup>+</sup>

The systems bridge two metal centres, holding them in close proximity, which has important implications for metal-metal interactions and magnetic exchange. It was found that complexes containing magnetic metal centres exhibit magnetic properties which are not simply the sum of those of the individual ions surrounded by their nearest-neighbour ligands. These properties result from both the nature and the magnitude of the interactions between the metal ions within the molecular unit. Using compartmental ligands, binuclear complexes can be synthesised where the two paramagnetic metal centres can interact with each other through the endogenous and/or exogenous ligand bridges in a ferromagnetic or antiferromagnetic way. By changing the type of ligand and the distance between the two chambers (and hence between the paramagnetic centres) it is possible to considerably vary the magnetic interaction.<sup>6</sup>

The large variety of complexes obtained with binucleating ligands has been recently divided in two groups.<sup>66</sup> The first group includes complexes with metals sharing at least one donor atom, these ligands have collectively been termed compartmental ligands. The other group consists of complexes in which the donor atoms are not shared. These complexes derive from ligands having isolated donor sets (Fig. 1.4).

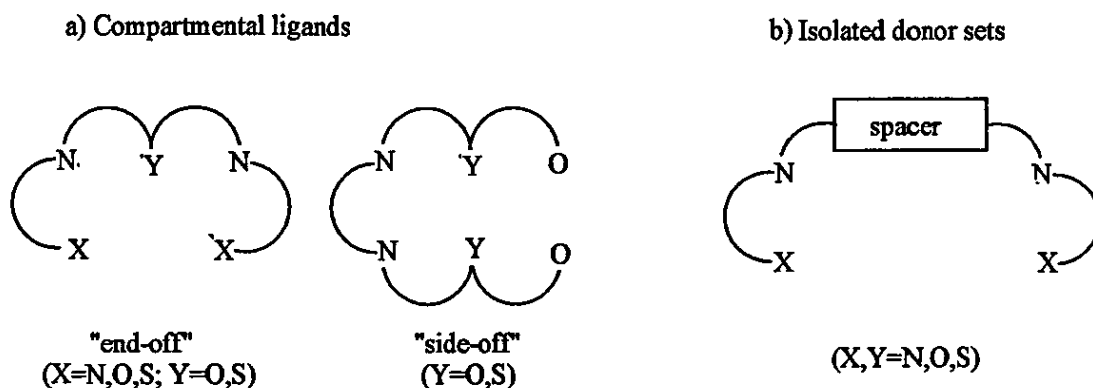


Fig. 1.4: Schematic representation of binucleating acyclic ligands

The Schiff-base macrocycles synthesised by [2+2] condensation of a 2,6-diacyl-4-substituted phenol and a diamine constitute a unique family of compartmental macrocyclic ligands (Fig 1.5), which is characterised by its ability to coordinate and bridge two metal ions by deprotonation of the phenol group. Many modifications can be made to the basic structure such as substitution of the *para* position of the phenol rings, provision of different lateral chains, introduction of additional donor atoms on the lateral chains, partial or full saturation of the imine bonds and introduction of auxiliary donor pendant arms in the diamine chains.

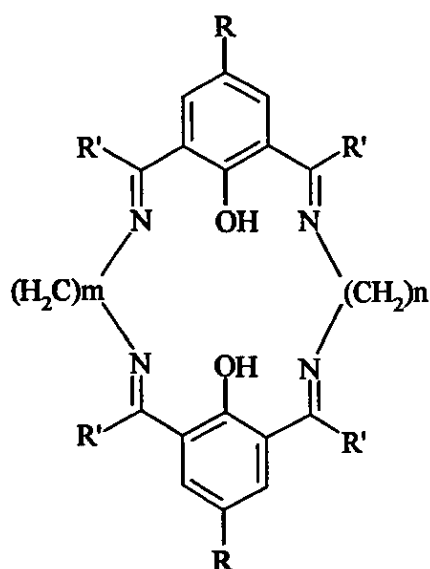
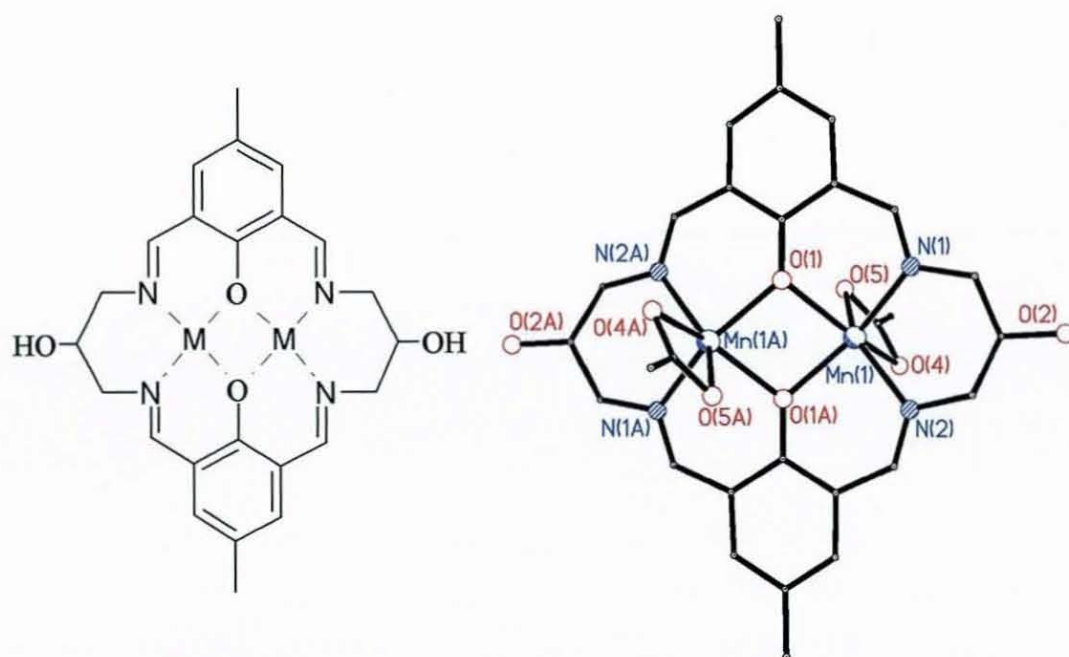


Fig. 1.5: "Robson-type" macrocycles

In particular, the incorporation of pendant alcohol groups on the diamine lateral chains allows the macrocycles to form endogenous alkoxide bridges between the adjacent metal centres.<sup>24</sup> The condensation of the phenol head-unit with a 1,3-diaminopropan-2-ol side chain yielded binuclear [2+2] complexes of H<sub>2</sub>L11 with Cu(II),<sup>67-69</sup> Ni(II),<sup>70</sup> Mn(II)<sup>70</sup> and Pb(II).<sup>24</sup> These complexes are structurally very similar to the complexes of the simple Robson-type ligands discussed previously. In the case of small transition metal ions (i.e. Cu<sup>2+</sup>, Ni<sup>2+</sup>, Mn<sup>2+</sup>) the pendant alcohol groups on the side chains remain protonated and pointing outside the cavity of the macrocycle, not participating on the coordination sphere of the metal



ions (Fig. 1.6). However, in the case of bigger cations such as  $\text{Pb}^{2+}$  the alcohol groups are weakly interacting with the metal in the apical position (Fig. 1.7).



**Fig. 1.6:** Structure<sup>64,65,70</sup> of  $[\text{Mn}_2(\text{H}_2\text{L11})(\text{AcO})_2]$  in which the pendant alcohol groups do not participate in the coordination of the metal ions

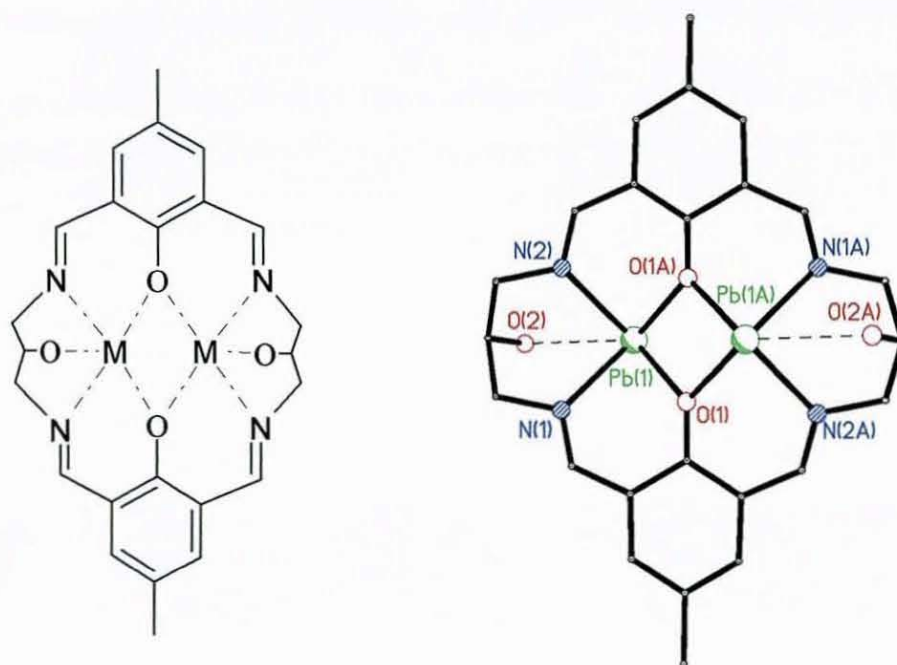


**Fig. 1.7:** Structure<sup>24,64,65</sup> of  $[\text{Pb}_2(\text{H}_2\text{L11})]^{2+}$  in which the pendant alcohol groups interact axially with the metal ions

### 1.4.1.2. Tetranuclear phenol based Schiff-base complexes

Recently, attention has been devoted to the synthesis and characterisation of polynuclear species, closely related to the dinuclear analogues, which can extend and in some cases considerably modify the unusual properties of dinuclear complexes.

A simple method of synthesising polynuclear complexes is the expansion of existing dinuclear ligands, thus facilitating the coordination of more metal ions. McKee *et al.* achieved this by increasing the diamine lateral chains containing the alcohol groups (Fig. 1.8). The presence of both phenol and alkoxide bridging groups within the macrocyclic cavity enhances the versatility of the ligand and the simple expansion from 1,3-diaminopropan-2-ol to 1,5-diaminopentan-3-ol allows it to bind from one to four metal ions,<sup>70,71</sup> increasing the nuclearity of the macrocycle. Tetranuclear complexes of Cu(II), Ni(II), Mn(II), Co(II) and Zn(II) have been reported.<sup>71-75</sup> The resulting macrocycles are made of two parts, the phenoldiimine heads which are the rigid part of the macrocycle and the five member carbon side chains containing the alcohol groups, which provide some flexibility to the system.

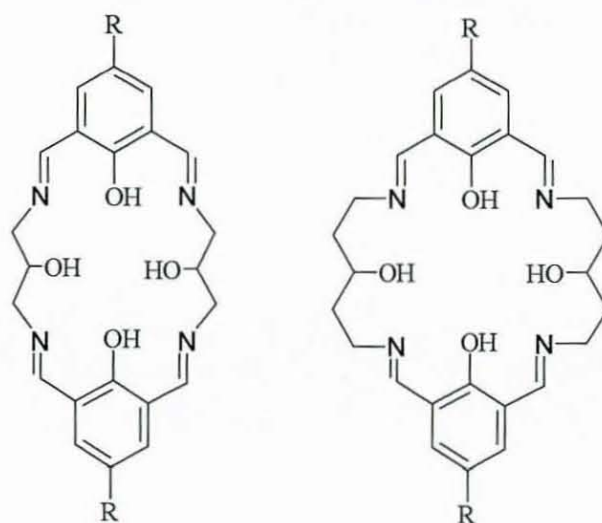


**Fig. 1.8:** Expansion of the ligand by increasing the diamine lateral chains

These macrocycles provide similar coordination geometries to the Robson tetraphenol macrocycles, although in this case the macrocycles provide three rather than four donors for each metal ion. The phenol and alcohol functions are usually deprotonated and shared between the side and length-ways metal neighbours, forming bridges between them. The coordination sphere is completed by exogenous ligands. In most cases, one of them is a central oxygen donor which is shared by the four metal ions, but it can be replaced by bridging azido and terminal azide donors<sup>42</sup> or by bridging pyrazolate molecules<sup>76</sup>.

The tetracopper complex  $[\text{Cu}_4(\text{L13})(\text{OH})(\text{H}_2\text{O})_2](\text{NO}_3)_3$ <sup>71</sup> illustrates the increase of the nuclearity achieved simply by expanding the lateral chains (Fig. 1.9). Use of the longer pentane derivative significantly expands the macrocyclic ring. The resulting macrocyclic ligand H<sub>4</sub>L13 is large enough to bind four transition metal ions, each bridged to neighbouring metal ions via deprotonated alkoxide and phenoxide donors.

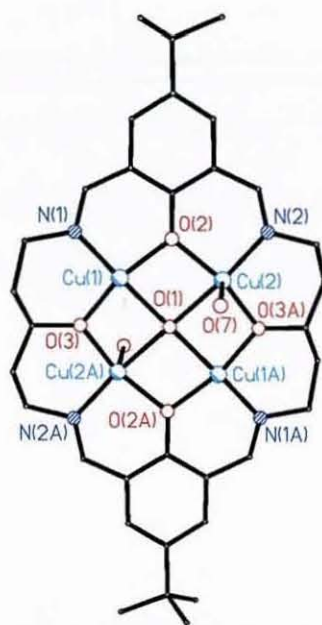


**Fig. 1.9:** Structure<sup>64,65,71</sup> of the cation  $[\text{Cu}_4(\text{L13})(\text{OH})(\text{H}_2\text{O})_2]^{3+}$

Tetranuclear complexes of transition metals are formed also by other extended macrocycles that contain four phenol and four diimine fragments. Such systems can be obtained by the [2+2] condensation of 2,6-diformylphenols with 1,2-



diphenylethylenediamine, or also by the [4+4] condensation of 2,6-diformylphenolate and 1,2-diaminoethane.

In 1987 Robson reported the synthesis of a new tetraphenol tetranucleating [2+2] macrocycle (Fig. 1.10) derived from the condensation of 2,6-diformyl-4-methylphenol with 2,6-bis(aminomethyl)-4-methylphenol.<sup>77</sup> The macrocycle H<sub>4</sub>L14 consists of four separate, essentially coplanar blocks having four phenoldiimine units. Reaction of 2,6-diformyl-4-methylphenol with 2,6-bis(aminoethyl)-4-methylphenol in the presence of nickel acetate produced a tetranuclear complex of H<sub>4</sub>L14 (Figs. 1.11 and 1.12).

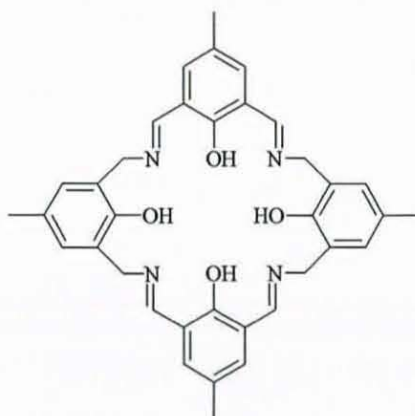


Fig. 1.10: Robson's tetraimine macrocycle H<sub>4</sub>L14

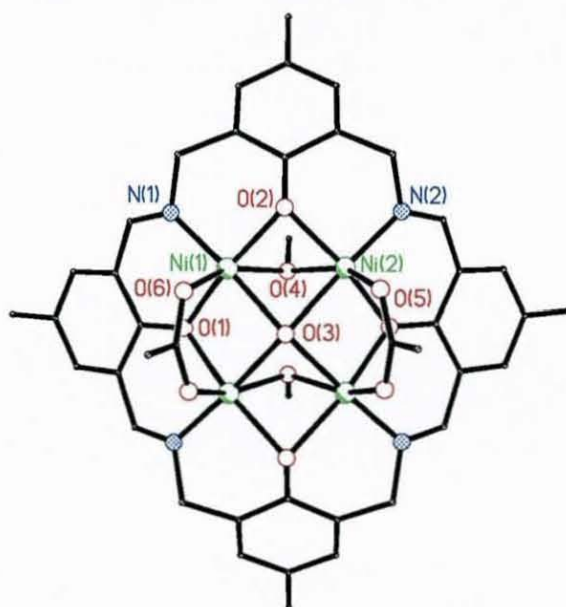
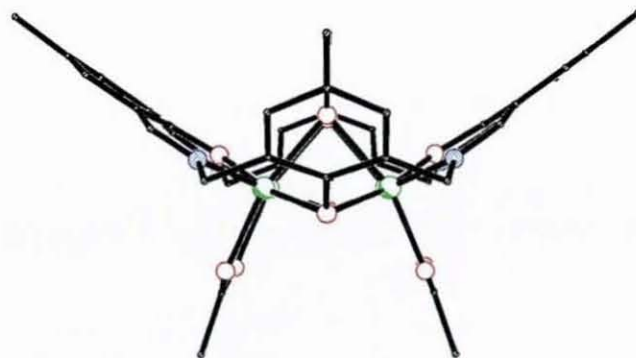


Fig. 1.11: Structure<sup>64,65,77</sup> of the complex [Ni<sub>4</sub>(L14)(OH)(AcO)<sub>2</sub>(MeO·H·OMe)]

The ligand H<sub>4</sub>L14 having four phenol units interconnected by carbons ortho to the hydroxyl groups is reminiscent of calixarenes. The four aromatic rings are inclined, all on the same side of the Ni<sub>4</sub> plane, at considerable angle to that plane, giving the overall molecular arrangement the shape of a bowl (Fig. 1.12).



**Fig. 1.12:** Side-on view of the complex  $[\text{Ni}_4(\text{L14})(\text{OH})(\text{AcO})_2(\text{MeO}\cdot\text{H}\cdot\text{OMe})]$  revealing the dished conformation of the macrocyclic ligand.

It is clearly apparent that this macrocycle has provided less flexibility than the tetranuclear macrocycles with saturated lateral chains containing alcohol groups, since the lateral chains in this case are aromatic rings and are relatively more rigid. The lack of flexibility within this macrocycle led Robson to synthesise the tetraamine derivative (Fig. 1.13) of this ligand.<sup>40,78</sup> The new ligand H<sub>4</sub>L15 gives more flexibility to allow metal-metal spatial relationships and individual metal coordination geometries to be accommodated.

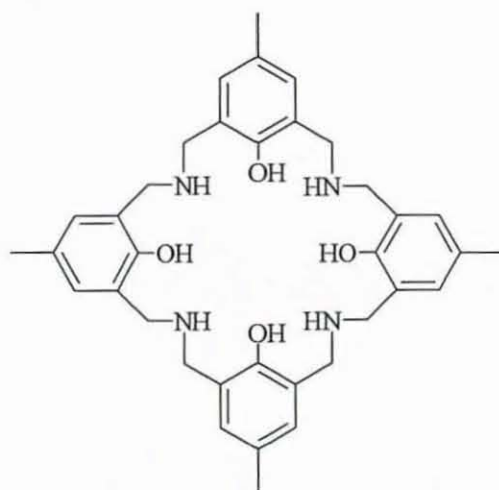


**Fig. 1.13:** Robson's tetraamine macrocycle H<sub>4</sub>L15

The tetranuclear zinc(II) complex  $[Zn_4(L15)(OH)(AcO)_3(MeOH)]$  was reported by Robson *et al.*<sup>40</sup> The bowl-shape conformation of the  $Ni_4$  complex of  $H_4L14$  is also present in the  $Zn_4$  complex of  $H_4L15$  but the symmetry is reduced. The phenol rings are all inclined on the same side of the  $Zn_4$  cluster but at four different angles to the mean plane that passes through the metals. The four zinc centres are not coplanar and the arrangement of the  $Zn_4$  cluster is markedly distorted from a square, the two “diagonals” differing significantly in length. With the loss of symmetry, probably due to a mismatch in size between the metal ions and the macrocyclic ligand, the strength of the four bonds linking the central group to the zinc centres differs, one of them being much weaker (represented with dotted line in Fig. 1.14).

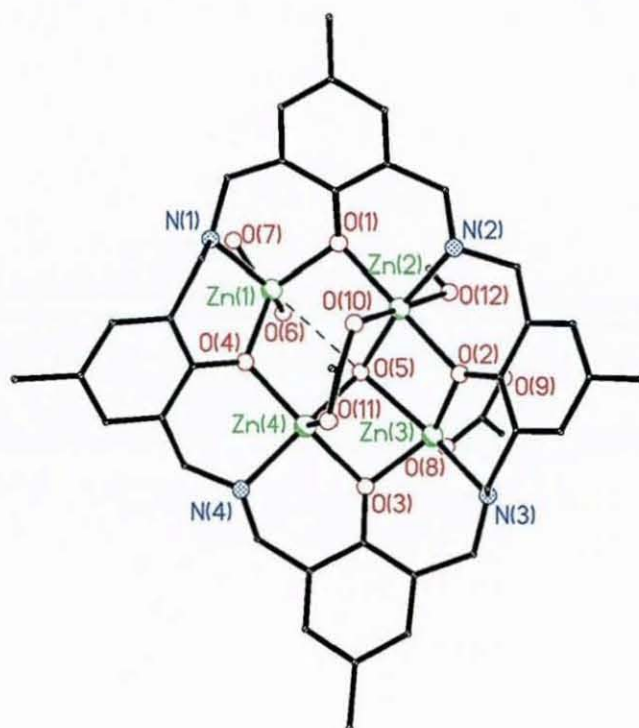


**Fig. 1.14:** Structure<sup>40,64,65</sup> of the complex  $[Zn_4(L15)(OH)(AcO)_3(MeOH)]$

Nag *et al.*<sup>79</sup> reported the synthesis of a more flexible [4+4] tetranuclear macrocycle  $H_4L16$  due to the introduction of aliphatic diamine chains which insert longer, flexible links between the phenol heads (Fig. 1.15). The new octaamine macrocycle was synthesised by template condensation of 2,6-diformyl-4-methylphenol and 1,2-diaminoethane in the presence of magnesium acetate,

obtaining the octaimine  $H_4L16$  macrocycle and subsequent reduction with  $NaBH_4$ . The synthesis of tetranickel(II) and tetracopper(II) complexes was achieved on reaction of the octaimine macrocycle  $H_4L17$  with the appropriate metal salt in the presence of  $Et_3N$ .<sup>80</sup>

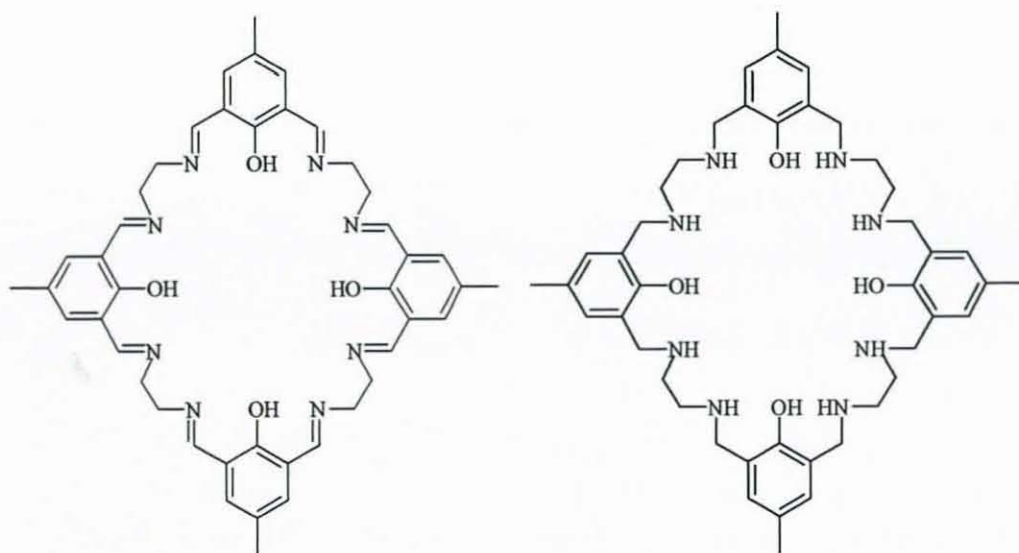


**Fig. 1.15:** Nag's tetraimine  $H_4L16$  and tetraamine  $H_4L17$  macrocycles

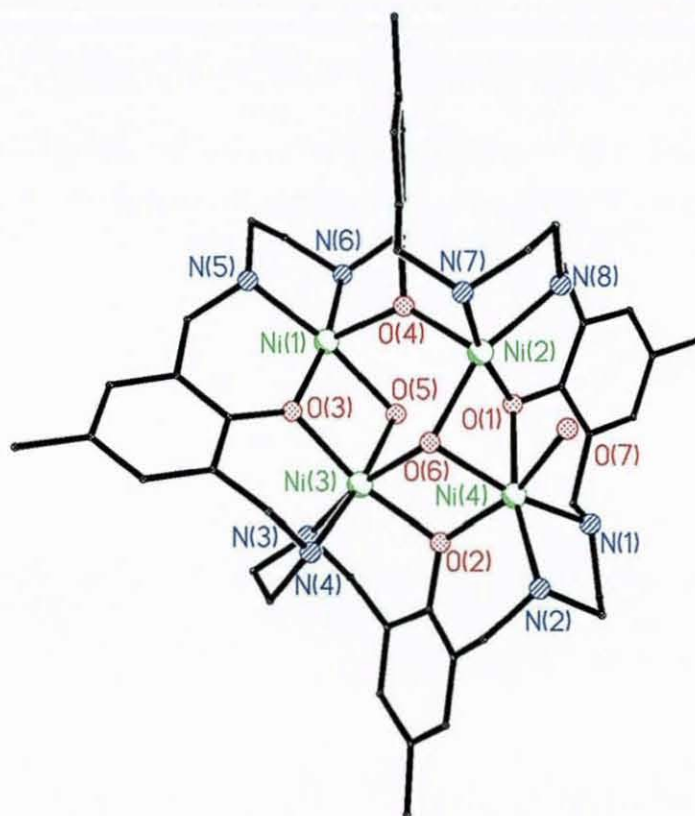


**Fig. 1.16:** Structure<sup>64,65,80</sup> of the cation  $[Ni_4(L17)(OH)(H_2O)_2]^{3+}$



The synthesis of a derivative of the previous macrocyclic ligand H<sub>4</sub>L16 was reported by Ōkawa *et al.*<sup>81</sup> The new tetranucleating macrocycle H<sub>4</sub>L18 (Fig. 1.17) presents two different types of coordination sites, two N<sub>(amine)2</sub>O<sub>2</sub> and two N<sub>(imine)2</sub>O<sub>2</sub> metal binding sites, which allows the formation of the heteronuclear Cu<sub>2</sub>M<sub>2</sub> complexes<sup>82</sup> (M= Co(II), Ni(II), Zn(II)). As with the previous macrocycles, the two amine side-chains give the macrocycle a certain degree of flexibility not possible with only imine donors.

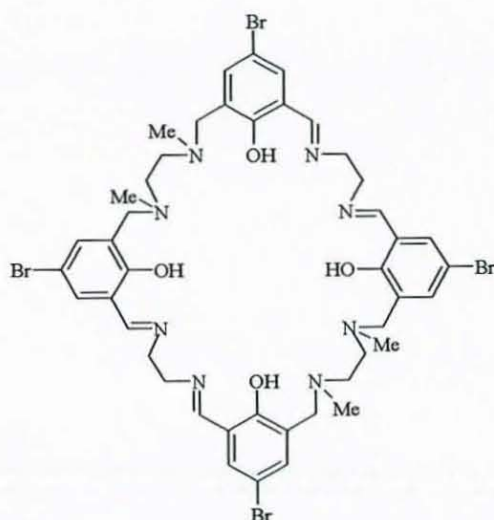


Fig. 1.17: Ōkawa's macrocyclic ligand H<sub>4</sub>L18

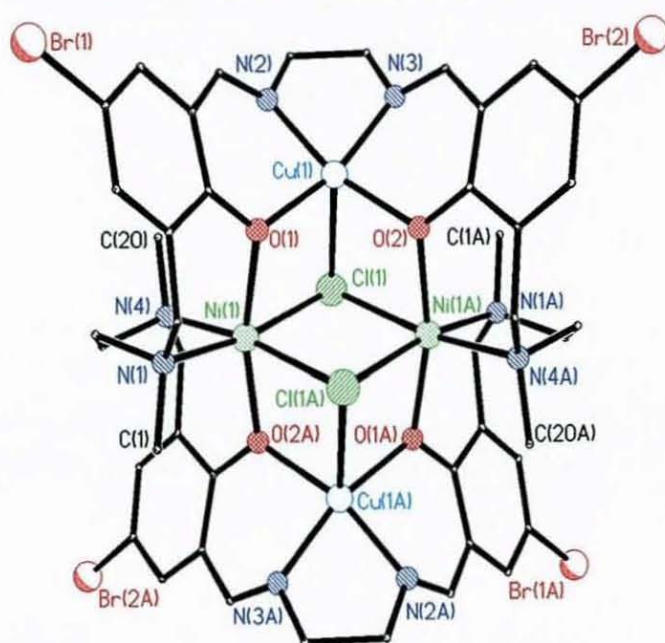
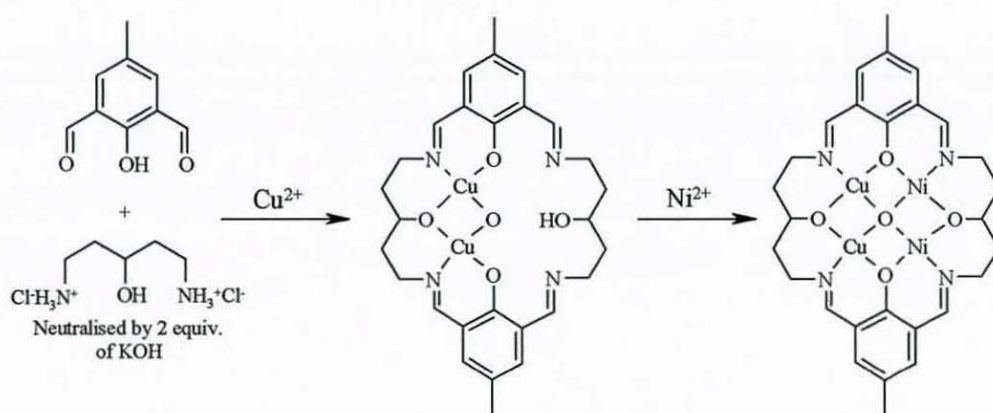


Fig. 1.18: Structure<sup>64,65,82</sup> of the cation [Cu<sub>2</sub>Ni<sub>2</sub>(L18)(Cl)<sub>2</sub>]<sup>2+</sup>



Most commonly, heteronuclear complexes of dinucleating Robson-type macrocycles are synthesised using ligands with dissimilar binding sites in either the final macrocyclic product or in a key non-cyclic intermediate in a stepwise synthesis, as for the previous heteronuclear complexes of H<sub>4</sub>L18. However, McKee *et al.*<sup>83</sup> were the first to isolate and structurally identify a heterotetranuclear macrocyclic complex with four identical binding sites. The controlled synthetic pathway involves in the initial formation of a dicopper precursor complex. The macrocycle has the ability to accommodate a bridging group (e.g. pyrazolate, hydroxo) to form dinuclear complexes. This yields two empty, if protonated, coordination sites having the potential to coordinate two further metal ions. The dinuclear complex is then reacted with an excess of Ni(II) to form the mixed metal complex of H<sub>4</sub>L19 (Fig. 1.19). The geometric arrangement of the metal ions in the tetranuclear product is controlled by the structure of the dinuclear intermediate.<sup>84</sup>



**Fig. 1.19:** Synthesis of the macrocyclic complex  $[\text{Cu}_2\text{Ni}_2(\text{L19})(\text{O})]^{2+}$

#### 1.4.1.3. Hexanuclear phenol based Schiff-base complexes

Hexanuclear complexes of transition metals are formed also by interesting extended macrocycles. Such systems can be obtained by the [3+3] condensation of 2,6-diformylphenols with 1,2-diethylenediaminephenols, or also by the [3+3] condensation of 2,6-diformylphenols and alcohol diamines.

In 1995 Tandon *et al.*<sup>67</sup> reported the synthesis of a triphenol hexanucleating [3+3] macrocycle derived from the condensation of 2,6-diformyl-4-methyl phenol with 1,3-diaminopropan-2-ol in the presence of copper nitrate and perchlorate or nickel nitrate and perchlorate as the template agents, yielding the ligand H<sub>6</sub>L20, which can accommodate six metal centres (Fig. 1.20) The hexacopper(II) complex is in fact a dodecanuclear dimer and can be described as hexagonal cyclic arrays of metal centres linked axially through hydroxo bridges.

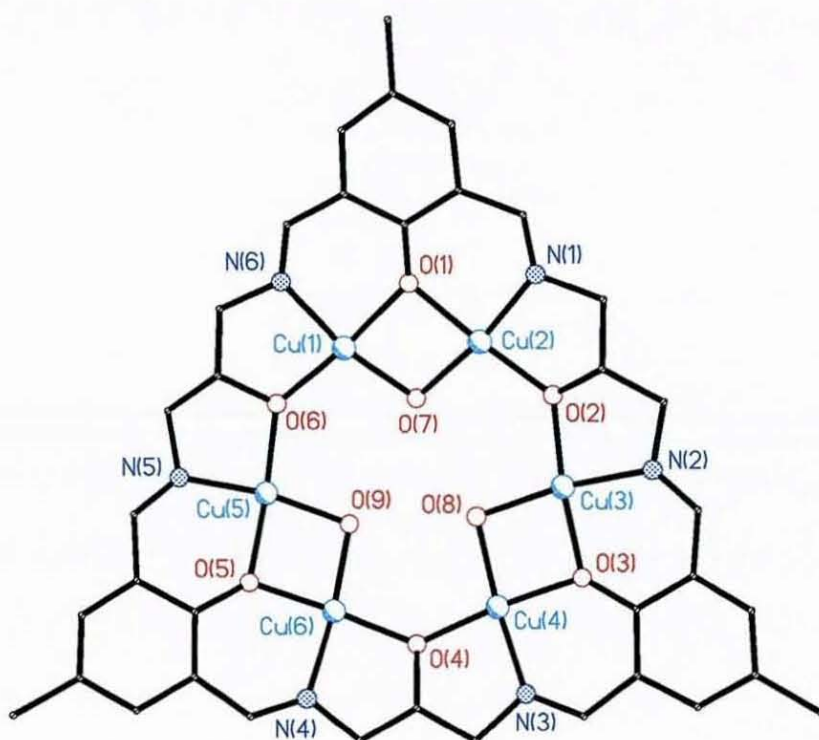


**Fig. 1.20:** Structure<sup>64,65,67</sup> of one hexanuclear ring for the dimer  $[\text{Cu}_6(\text{L}20)(\text{OH})_3]_2(\text{NO}_3)_6$

A related hexacopper complex of a more flexible macrocyclic ligand (H<sub>6</sub>L21) derived from the [3+3] template condensation of 2,6-diformyl-4-methylphenol and 2,6-bis(aminomethyl)-4-methylphenol in the presence of copper acetate reported by Robson *et al.*<sup>85</sup>, leads to a “cyclohexane boat” arrangement of six copper(II) centres (Fig. 1.21).

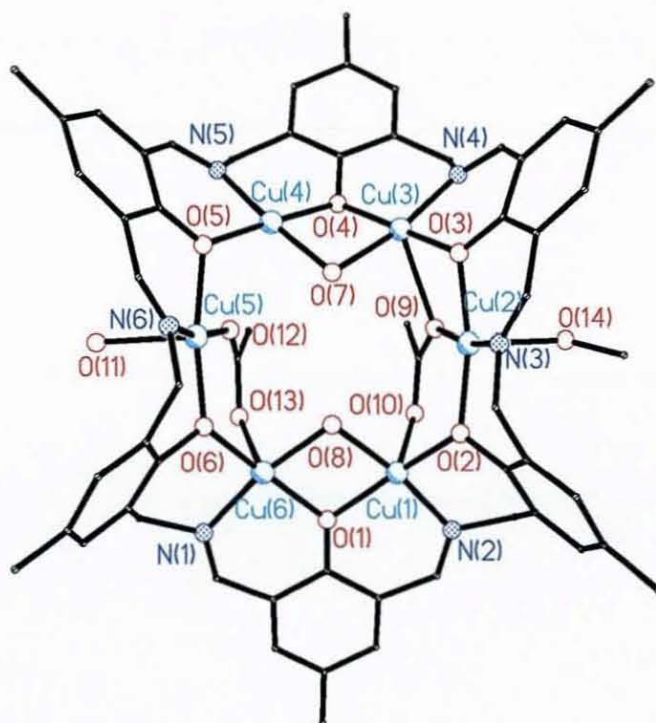


**Fig. 1.21:** Structure<sup>64,65,85</sup> of the cation  $[\text{Cu}_6(\text{L21})(\text{AcO})_2(\text{OH})_2(\text{MeOH})_2(\text{H}_2\text{O})]^{2+}$

#### 1.4.1.4. Pseudocalixarene Schiff-base macrocycles

There are two important differences in coordination chemistry between calixarenes and Robson macrocycles. First, the inclusion in the macrocycles of relatively soft imine or amine nitrogen donors in addition to the phenolic oxygen atoms widens the range of metal ions that might be expected to bind with high stability constants. Indeed, typically the macrocyclic ligands complex transition metals while the calixarenes are mainly viewed as hosts for hard metal ions. Second, the geometries of the metal complexes formed are significantly different. The calixarenes are relatively rigid, the only flexibility being at the methylene links, and the generally small size of the cavity means that in genuine calixarenes a planar conformation is sterically prohibited. For this reason coordinated metal ions cannot take advantage of the bridging potential of the phenol groups and the complexes are generally mononuclear. In contrast, macrocyclic ligands can complex using some or all of their phenolic oxygen donors in the bridging mode and are usually di- or polynuclear. They are also often close to planar, although



the more rigid tetraphenol examples are, to some extent, bowl-shaped (as shown for the complex  $[\text{Ni}_4(\text{L14})(\text{OH})(\text{AcO})_2(\text{MeO}\cdot\text{H}\cdot\text{OMe})]$ , Fig. 1.12).<sup>40,78, 88,89</sup>

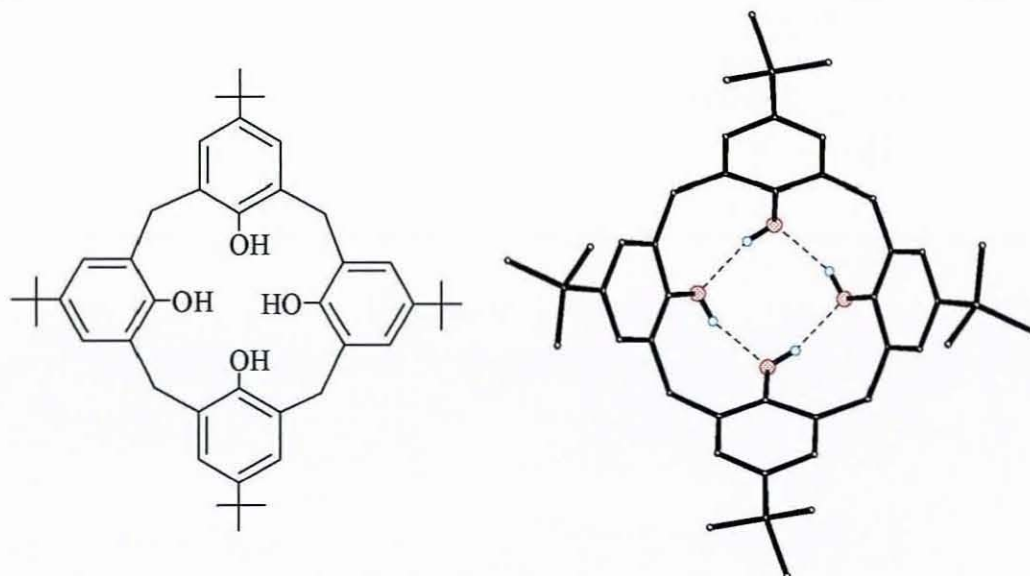


**Fig. 1.22:** Structure<sup>64,65</sup> of *p-tert*-butylcalix[4]arene showing the hydrogen bonding between the phenol groups



**Fig. 1.23:** Side-on view of *p-tert*-butylcalix[4]arene showing the bowl shape conformation

It is possible to introduce variation into the calixarene framework by extending the bridge between phenols to create a range of homocalixarenes.<sup>90-94</sup> In these species, two or more of the arene units are typically linked together with  $\text{CH}_2\text{-X-CH}_2$  spacers. This bridge may consist only of alkyl groups or may have heteroatoms, such as nitrogen, sulfur or oxygen, incorporated in the chain. Calixarenes with  $\text{X}=\text{CH}_2$  are considered the homocalixarenes, those with  $\text{X}=\text{O}$  are termed homooxalixarenes, and those with  $\text{X}=\text{NR}$  are termed

homoazacalixarenes. Introduction of heteroatoms has the additional interesting effect of combining crown ether (or azacrown ether) features with those of calixarenes. Homocalixarenes and their derivatives are the subject of recent interest due to their almost endless structural as well as functional possibilities that such backbones permit.

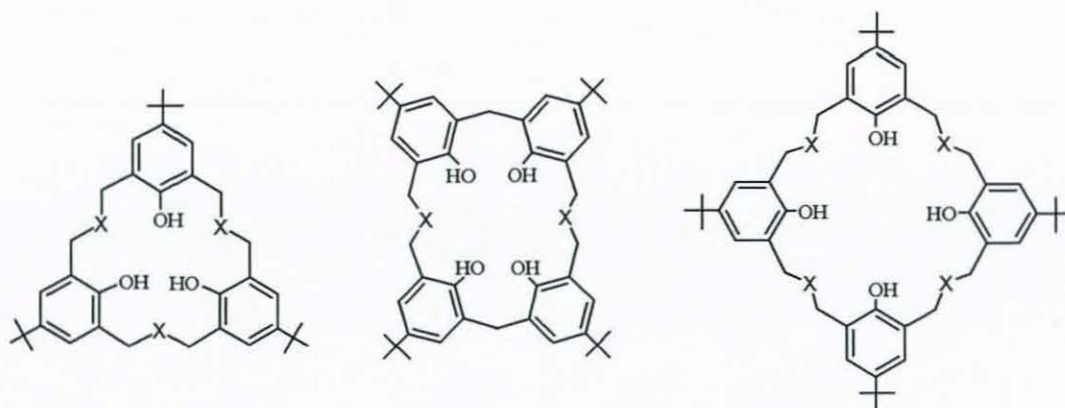


**Fig. 1.24:** Some examples of homocalixarenes (X = N, O, S)

Masci<sup>95</sup> reports the synthesis of uranyl complexes of the tetrahomodioxacalix[4]arenes (Fig. 1.25), where the conformation of the macrocycle is a distorted cone, held by intramolecular hydrogen bonds involving both phenolic and ether oxygen atoms in the free form, and by internal tetraphenoxide uranyl bonding in the complexes. Further work on uranyl complexes with larger homooxocalixarenes and mixed uranyl/alkali complexes has also been reported.<sup>96,97</sup>

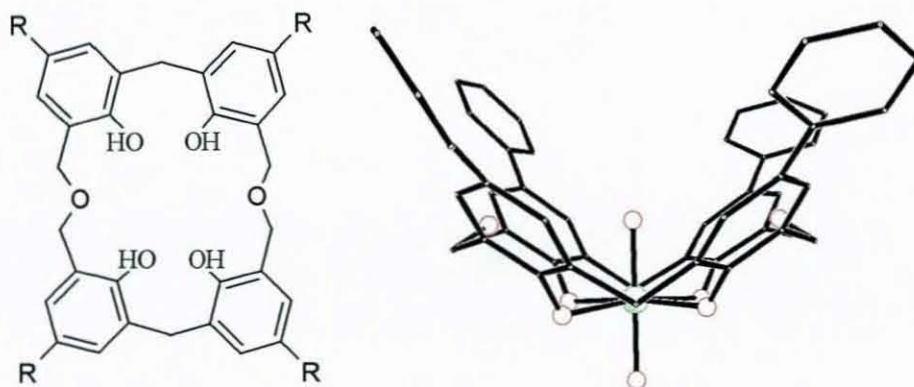


**Fig. 1.25:** *p*-R-tetrahomodioxacalix[4]arenes (R = methyl, phenyl) and the uranyl anionic complex<sup>64,64,96</sup>  $[\text{UO}_2(\text{L22})]^{2-}$

In an attempt to combine some of the properties of the Schiff-base and calixarene systems, McKee and Goetz further extended the macrocycles by developing a new range of Schiff-base pseudocalixarene macrocycles based on the new dialdehyde 2,2'-dihydroxy-5,5'-di-*tert*-butyl-3,3'-methanediyl dibenzaldehyde (DHTMB).<sup>98,99</sup>

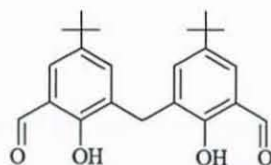


**Fig. 1.26:** DHTMB

The diphenolic head-unit DHTMB (Fig. 1.26) was prepared to study the influence of extended versions of the tetranuclear Schiff-base derived macrocycles previously reported.<sup>43,83</sup> Unlike most aza- or oxo-calixarenes, in which inserts are made at each methylene link, the new ligands (Fig. 1.27) preserve two methylenediphenol units intact while inserting softer imine donors along with other potentially bridging donors between them. The ligands can be viewed as formally derived from *p-tert*-butylcalix[4]arene (Fig. 1.22) by insertion of two diimine bridging sections ( $=N-R-N=$ ) into the ring i.e. they are members of the family of expanded calixarenes. Metal complexes of  $H_6L1$  and related macrocycles will be described in detail in the following chapters.

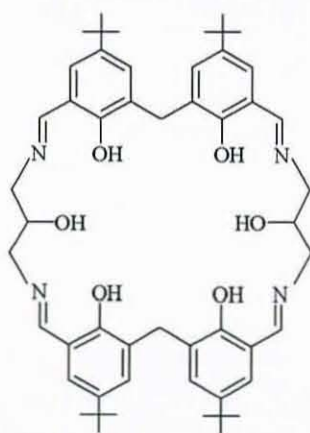


**Fig. 1.27:** Schiff-base macrocycle  $H_6L1$

A related macrocycle based on the dialdehyde precursor DHTMB has been reported by Hisaeda *et al.*<sup>100</sup> The macrocyclic dinucleating ligand has also two



$N_2O_2$  metal-binding sites doubly linked to each other with methylene spacers, but in this case the diamine used to form the macrocycle is *o*-phenylenediamine, which gives to the macrocycle a much rigid conformation than the related macrocycle  $H_6L1$ . The synthesis of dinickel(II), dicopper(II) and dicobalt(II) complexes was achieved on reaction of the macrocycle  $H_4L23$  (Fig. 1.28) with the appropriate metal salt. Dicobalt(III) complexes of  $H_4L23$  doubly bridged with bidentate diamine ligands axially coordinated. These have been shown to exhibit redox-switchable properties.<sup>101</sup>

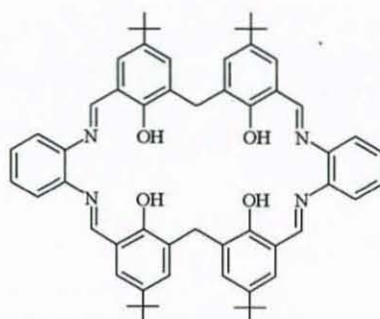


Fig. 1.28: Schiff-base macrocycle  $H_6L23$

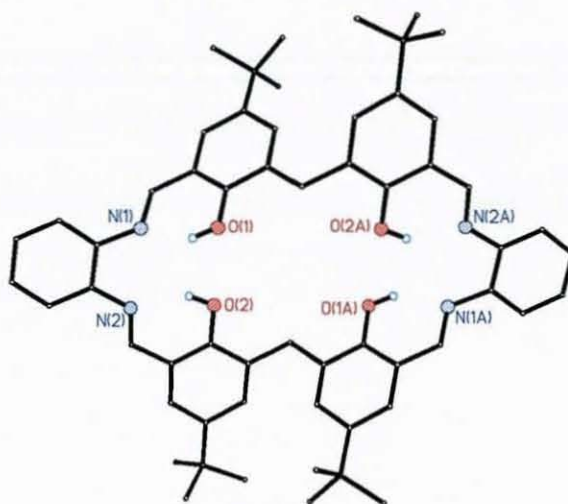


Fig. 1.29: Structure<sup>64,65,100</sup> of Hisaeda's macrocycle  $H_6L23$

Intramolecular hydrogen bonding interactions play an important role in the structural conformation of calixarene and pseudocalixarene macrocycles. Intramolecular H-bonding is a tool to control the cavity-forming process. When properly positioned within the same molecular structure, H-bonding sites are responsible for the formation, preorganization, and binding ability of the host.

### 1.5. Hydrogen bonding

The hydrogen bond is the most important of all directional intermolecular interactions. It is operative in determining molecular conformation, molecular aggregation, and the function of a large number of chemical systems ranging from inorganic to biological.

Hydrogen bonding occurs when an atom of hydrogen is attracted by rather strong forces to two atoms instead of only one, so that it may be considered to be acting as a bond between them. Typically this occurs where the partially positively charged hydrogen atom lies between partially negatively charged oxygen and nitrogen atoms, but is also found elsewhere, such as between fluorine ions in  $\text{HF}_2^-$  and between water and the smaller halide ions (i.e.  $\text{F}^-$ ,  $\text{Cl}^-$ ). They have been defined as follows<sup>102</sup>: "An  $\text{X-H}\cdots\text{A}$  interaction is called a "hydrogen bond", if it constitutes a local bond and X-H acts as proton donor to A" (X= O, N, halogen; A= O, N, S, halide, etc ).

Hydrogen bonds exist with a range of strengths. The classification of bonds as strong or weak appears to be rather a grey area. Jeffrey<sup>103</sup> called hydrogen bonds *moderate* if they resemble those between water molecules or in carbohydrates, and these are associated with energies in the range 16.7-62.8  $\text{kJ}\cdot\text{mol}^{-1}$ . Hydrogen bonds with energies above or below this range are called *strong* and *weak*, respectively. General properties of these categories are listed in Table 1.1.

**Table 1.1: Jeffrey's hydrogen bond classification**

Class	Strong	Moderate	Weak
Interaction type	strongly covalent	mostly electrostatic	electrostatic/dispers.
H $\cdots$ A length (Å)	1.2-1.5	1.5-2.2	>2.2
X-H bond length (Å)	0.08-0.25	0.02-0.08	<0.02
X-H versus H $\cdots$ A	X-H ~ H $\cdots$ A	X-H < H $\cdots$ A	X-H $\ll$ H $\cdots$ A
X $\cdots$ A distance (Å)	2.2-2.5	2.5-3.2	>3.2
Directionality	Strong	Moderate	Weak
Bond angles (°)	170-180	>130	>90
bond energy ( $\text{kJ}\cdot\text{mol}^{-1}$ )	62.8-167.5	16.7-62.8	<16.7



Gilli<sup>104,105</sup> gives an alternative classification for H-bonding. The O-H...O bonds observed in crystals can be grouped in five classes, three of strong, one of moderate and one of weak H-bonds, as summarised in Table 1.2

Table 1.2: Gilli's hydrogen bond classification

Class	Strength	Formula	Name	Acronym
A	Strong	$[-O\cdots H\cdots O]^-$	Negative Charge-Assisted H-Bonds	(-)CAHB
B	Strong	$[=O\cdots H\cdots O]^+$	Positive Charge-Assisted H-Bonds	(+)CAHB
C	Strong	$-O-H\cdots O=$	Resonance-Assisted H-Bonds	RAHB
D	Moderate	$\begin{array}{c} R_1 \\ \diagdown \\ \cdots O-H\cdots O-H \cdots \\ \diagup \\ R_2 \end{array}$	Polarization-Assisted H-Bonds	PAHB
E	Weak	$-O-H\cdots O<$	Isolated H-Bonds	IHB

The most frequent (-)CAHB are intermolecular bonds formed by acid salts of carboxylic and inorganic acids, although some intramolecular cases are also known, such as H-bonds in hydrogen maleate or in metal oximes. Almost all cases of (+)CAHB are intermolecular and derive from two oxygenated molecules trapping a proton coming from a strong acid. All RAHB H-bonds can be reduced to the general formula  $\cdots O=R_n-OH\cdots$  where  $R_n$  ( $n$  odd) is a resonant spacer of  $n$  atoms forming a chain of alternating single and double bonds.  $R_1$ -resonant bonds are associated with carboxylic acids and oxygenated inorganic or organometallic acids. Finally, examples of PAHB are found in ice, alcohol and phenol chemistry as well as in some hydroxylated inorganic compounds such as boric acid.

The ideas on the nature of the homonuclear X-H...X hydrogen bond are summarized in the *Electrostatic-Covalent H-bond Model* (ECHBM) developed by Gilli *et al.*,<sup>104,105</sup> that is: weak bonds are electrostatic in nature but become increasingly covalent with increasing strength; very strong H-bonds are essentially *three-centre-four-electron* covalent bonds; the strongest H-bonds must be homonuclear (X-H...X) and symmetrical as far as the distribution of chemical groups on the two sides of the H-bond is concerned, because only in this situation are the two VB resonance forms  $X-H\cdots X \leftrightarrow X\cdots H-X$  isoenergetic and able to mix

to the greatest extent; this last condition can be more generally expressed as a *condition of minimum  $\Delta PA$* , that is of minimum difference between the proton affinities (PA) of the H-bond donor and acceptor atoms.

The hydrogen bonding observed in the macrocyclic complexes described in this work is basically intermolecular H-bonding between the macrocyclic units and the lattice solvent molecules and counter ions present in the crystal lattice. Intramolecular H-bonding is also observed in some of the macrocyclic complexes and plays important role in the molecular conformation of the complexes, as will be described in the following chapters.

### **1.6. Aims of this work**

The polynuclear macrocyclic systems described above have achieved the aim of bringing the metal centres into close proximity with various degrees of constraint to the metal geometry and folding of the macrocycles. It has been shown that macrocycles containing imine donors provide less flexibility than those containing amine donors. However, within the group of imine-donor-macrocycles the flexibility can be enhanced by the introduction of side chains of different lengths. Here, the length and flexibility of the side-chain plays an important role allowing the macrocycle to adopt different conformations. In cases where the macrocycles are more flexible, the metals tend to impose their favoured geometry on the macrocycle whereas for more rigid macrocycles the situation is reversed. Generally, a compromise has to be found somewhere in between the two extreme positions.

The purpose of the work described in this thesis is to study the chemistry of the ligand systems derived from the [2+2], [3+3] or [4+4] Schiff-base template synthesis of the dialdehyde 2,2'-dihydroxy-5,5'-ditertiobutyl-3,3'-methanediyl-dibenzaldehyde (DHTMB) with 1,3-diaminopropan-2-ol and appropriate metal salts.

These extremely versatile macrocycles can be di-, tri- or tetranucleating, in the case of the [2+2] and [3+3] systems, or even pentanucleating in the case of the [4+4] macrocycle, and can incorporate a number of different bridging ligands. The flexibility of the saturated side chains allows the macrocycle to adjust the structural conformation and to accommodate the structural preferences of a range of different metal ions.

The introduction of different coordination sites within the polynuclear macrocycles opens the possibility of obtaining heteronuclear complexes, which is an interesting perspective due to already known dinuclear complexes exhibiting original physicochemical properties and functions arising from dissimilar metal ions in close proximity.

## **CHAPTER II**

# **DINUCLEAR COMPLEXES OF PSEUDOCALIXARENE SCHIFF-BASE MACROCYCLES**

## 2.1. Introduction

As previously outlined, a new diphenolic head-unit DHTMB (2,2'-dihydroxy-5,5'-di-*tert*-butyl-3,3'-methanediyl dibenzaldehyde, Fig. 2.1) has been developed by S. Goetz<sup>98,99</sup> with the intention of synthesising a new range of hybrid Schiff-base pseudocalixarene macrocycles, which combine some of the properties of the Schiff-base and calixarene systems. These new ligands can be viewed as formally derived from *p-tert*-butylcalix[4]arene<sup>106</sup> (Fig. 2.2) by insertion of two diimine bridging sections (=N-R-N=) into the ring

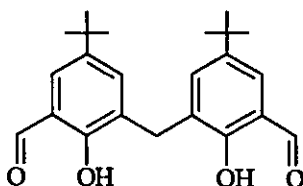


Fig. 2.1: DHTMB

The macrocycles can be regarded as being constructed of two distinct sections; the 2,2'-methylenediphenol unit, which normally is non-planar due to the saturated carbon linking the two aromatic rings, and the saturated side chains, inserting softer imine donors along with other potentially bridging donors (alcohol groups) between them. The introduction of longer, flexible links in the chain extends the range of conformational possibilities and thus permits some response to the coordination preferences of the metal ions. Therefore, these macrocycles would be expected to be considerably more flexible than the related calixarenes<sup>86,87,106</sup>

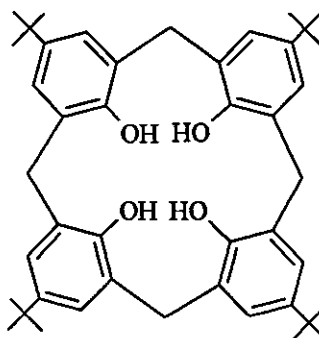


Fig. 2.2: *p-tert*-butylcalix[4]arene

Schiff-base condensation of DHTMB with 1,3-diaminopropan-2-ol in the presence of metal template ions yields complexes of the new macrocycle  $H_6L1$ . The most notable feature of this series of complexes is the variation in the nuclearity, which can be 2, 3 or 4 for the same ligand system<sup>107</sup>. This effect is related to the variation in the extent of deprotonation of the ligand, the orientation of the phenol groups, the counter anions present and the overall shape of the macrocyclic host.

Three types of metal binding site (Fig 2 3) are potentially available within this kind of macrocycle:

- "Salen-type" site A involves two phenol and two imine donors. There are two of these in the macrocycle.
- the unique central calixarene-type site B, which involves the four phenol (or phenolate) donors.
- four equivalent sites of type C, each involving one phenol, one imine and the alkoxo group of one of the saturated chains.

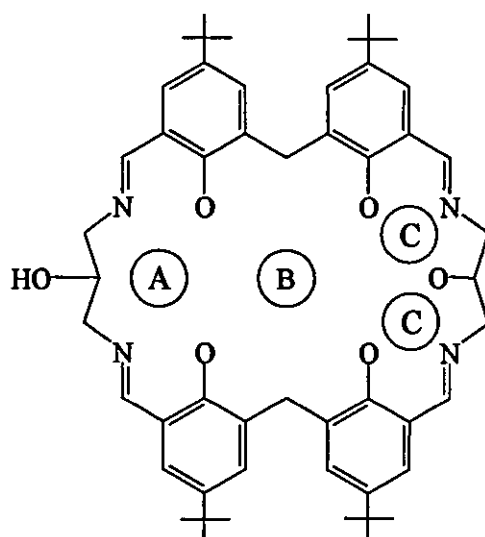


Fig. 2.3: Metal binding sites for the macrocycle  $H_6L1$

The transition metal template ions used (such as  $Cu(II)$ ,  $Ni(II)$ ,  $Co(II)$  and  $Zn(II)$ ) appear to coordinate first to the "A" binding site (or "C" binding site in the case of the tetranuclear complexes), consistent with their HSAB properties but the

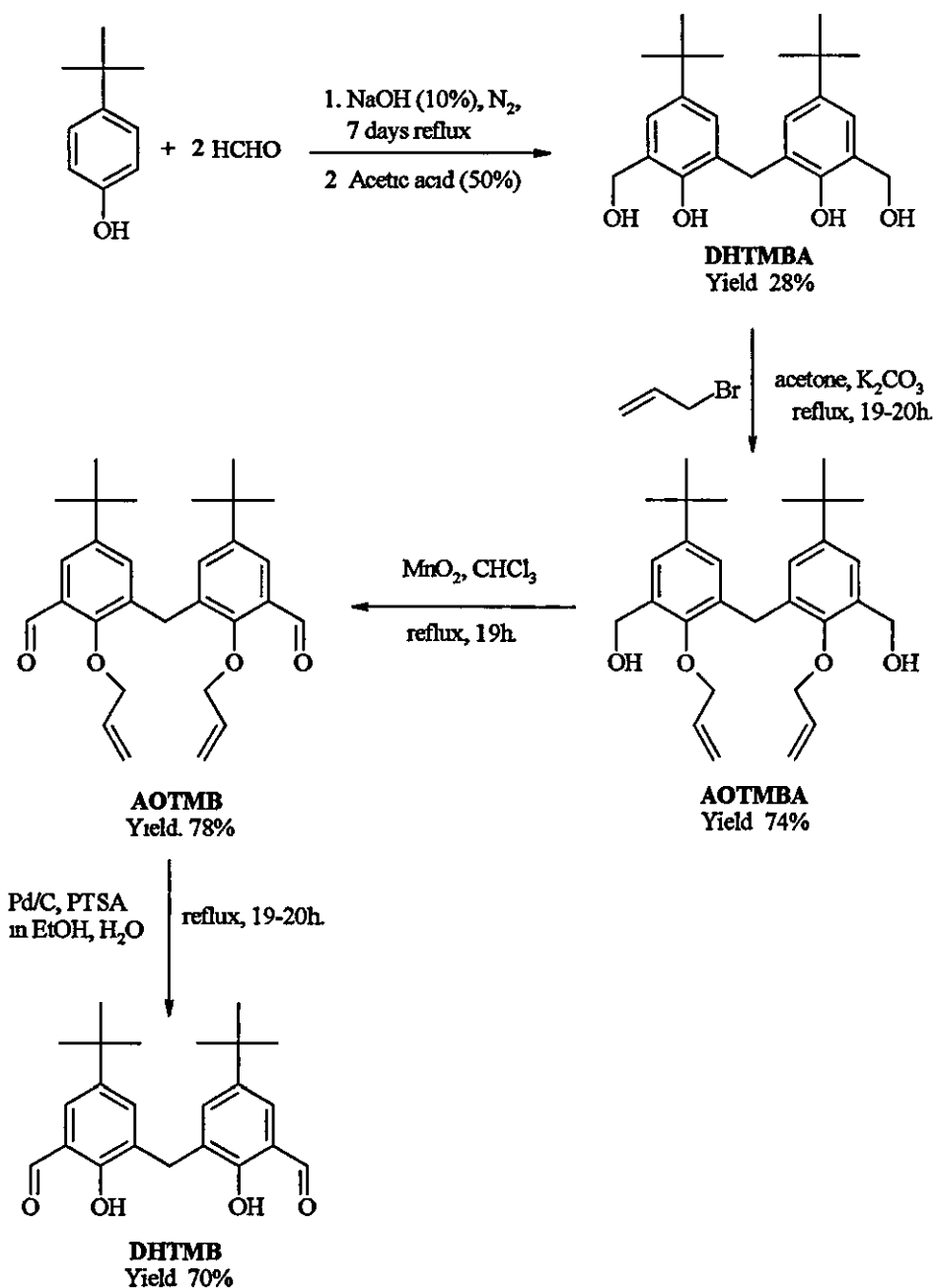
formation of the trinuclear(II) complexes shows that the central site is also available. Pearson's Hard and Soft Acid and Bases (HSAB) principle<sup>108,109</sup> simply states that hard acids prefer to coordinate to hard bases and soft acids to soft bases. Divalent first row metals are classified as intermediate Lewis acids in HSAB theory, thus preferentially will bind to intermediate Lewis base ligands. Comparison of "A" and "B" binding sites shows that the central binding site (B) contains harder Lewis bases, involving four phenol/phenolate donors, while the "A" binding site comprises less hard Lewis bases, consisting of two imine and two phenol/phenolate donors. Similarly, hard Lewis acids such as alkaline or alkaline earth metals will bind preferentially to the inner "B" site. It is possible then to take advantage of the different sites in this kind of macrocycle to synthesise heteronuclear complexes, as described in Chapter 4

This chapter summarises the investigation into the coordination chemistry of a set of dinuclear complexes of the macrocyclic ligand H<sub>6</sub>L1 (Fig. 2.3), derived from the [2+2] Schiff-base template reaction of DHTMB with 1,3-diaminopropan-2-ol and the metal salts of first row transition metals. In the dinuclear complexes of H<sub>6</sub>L1 the ligand provides four donor atoms for each metal ion and the coordination sphere is completed by exogenous ligands. In most cases a central external donor, bridging the metal ions, is incorporated. Special emphasis is given to the relationship between the metal oxidation state and the intramolecular hydrogen-bonding, which leads to an unusually rigid conformation in the complexes of divalent metal ions

## 2.2. Synthesis of 2,2'-dihydroxy-5,5'-di-*tert*-butyl-3,3'-methanediyl-dibenzaldehyde (DHTMB)

The DHTMB synthesis has been developed by Sandrine Goetz.<sup>98,99</sup> The procedure comprises four steps (Scheme 2.1), which include formation of the dialcohol precursor DHTMBA, protection of the phenol groups, oxidation of the alcohol groups to aldehydes and deprotection of the phenol groups. The overall yield is 5%, which is very low. The precursor (DHTMBA) to the synthesis of DHTMB was synthesised following the literature procedure reported by Gutsche *et al.*<sup>110</sup> in

1983 but the work up of the reaction was slightly changed. The oil that formed upon acidification was not separated but directly extracted from the aqueous layer with diethyl ether. The recrystallisation was performed as reported by Gutsche, with a comparable yield (*ca.* 28%). The low yield of this reaction, in addition to the following 3-step-reaction process, contributes to the very low overall yield.



Scheme 2.1: Four-step DHTMB synthesis



Initially, it was thought necessary to protect the phenol groups in order to oxidise the two alcohol groups cleanly to aldehyde groups. The protection reaction was carried out by reaction with allyl bromide in the presence of potassium carbonate in acetone, a method frequently applied to phenols<sup>111</sup> The protected compound was obtained with a reasonable yield of 74%. The value reported for the protection of one phenol group is 85%, which applied to the protection of two phenol groups would give a yield of 72%.

The method used to synthesise AOTMB is similar to that reported by Taniguchi *et al.*<sup>112</sup> The reaction is carried out using activated MnO<sub>2</sub> in chloroform with a yield of 78%.

The method used to deprotect the phenol groups is similar to that described by Boss *et al.*<sup>113</sup> The reaction was carried out using 10% Pd on activated charcoal and *p*-toluenesulfonic acid in ethanol with a yield of 70%, which seems quite low compared to the literature value. The value reported for the deprotection of one phenol group is 95%, which applied to the deprotection of two groups should give a yield of 90%.

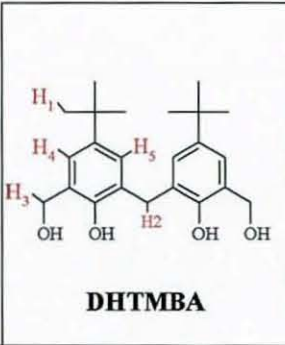
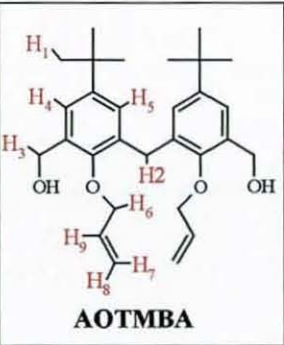
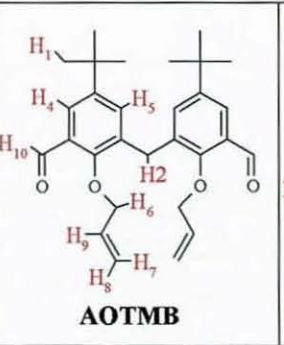
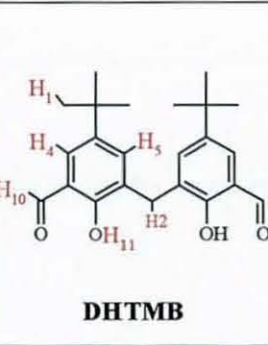
### **2.2.1. Characterisation of 2,2'-dihydroxy-5,5'-di-*tert*-butyl-3,3'-methanediyl-dibenzylalcohol (DHTMBA)**

The IR spectrum shows two broad bands corresponding to the O-H stretching vibration of the primary alcohol groups at 3210 and the phenol groups at 3420 cm<sup>-1</sup>. There is also a broad band at 1208 cm<sup>-1</sup> that can be assigned to the C-O stretching vibration of the phenol groups.<sup>114,115</sup>

There is additional confirmation of the formation of the precursor DHTMBA shown in the <sup>1</sup>H NMR analysis. The peak assigned to the saturated carbon linking the two phenol rings is seen at 3.88 ppm, confirming the condensation of the two *tert*-butylphenol molecules. Additionally, the peak at 4.77 ppm can be assigned to

the saturated carbon of the lateral alcohol groups (Table 2.1). These results together with the satisfactory elemental analysis data are consistent with the formation of DHTMBA.

**Table 2.1:** Proton assignments (ppm) of  $^1\text{H}$  NMR analysis for DHTMB and its precursor molecules DHTMBA, AOTMBA and AOTMB

				
	DHTMBA	AOTMBA	AOTMB	DHTMB
<b>H<sub>1</sub></b>	1.26 (s, 18)	1.26 (s, 18)	1.26 (s, 18)	1.26 (s, 18)
<b>H<sub>2</sub></b>	3.88 (s, 2)	4.07 (s, 2)	4.13 (s, 2)	4.03 (s, 2)
<b>H<sub>3</sub></b>	4.77 (s, 4)	4.70 (s, 4)		
<b>H<sub>4</sub></b>	6.94 (d, 2)	7.01 (d, 2)	7.30 (d, 2)	7.37 (d, 2)
<b>H<sub>5</sub></b>	7.26 (d, 2)	7.24 (d, 2)	7.75 (d, 2)	7.64 (d, 2)
<b>H<sub>6</sub></b>		4.34 (d, 4)		
<b>H<sub>7</sub></b>		5.30 (dd, 2)	4.40 (dd, 2)	
<b>H<sub>8</sub></b>		5.34 (dd, 2)	4.44 (dd, 2)	
<b>H<sub>9</sub></b>		6.07 (m, 2)	6.06 (m, 2)	
<b>H<sub>10</sub></b>			10.4 (s, 2)	9.86 (s, 2)
<b>H<sub>11</sub></b>				11.19 (s, 2)

### 2.2.2. Characterisation of 2,2'-diallyloxy-5,5'-di-tert-butyl-3,3'-methanediyl-dibenzylalcohol (AOTMBA)

Confirmation of the protection of the phenol groups is shown in the IR spectrum, where only one broad band appears corresponding to the O-H stretching vibration of the primary alcohol groups at  $3272\text{ cm}^{-1}$ . The peaks corresponding to the phenolic O-H bending vibration are not seen, which is another indication of the protection. There is also a weak band at  $3085\text{ cm}^{-1}$  that can be assigned to the allyl ( $=\text{CH}_2$ ) stretching vibration.

There are not many changes in the  $^1\text{H}$  NMR spectrum compared to the precursor DHTMBA except for the appearance of four new peaks at 6.07, 5.34, 5.30 and 4.34 ppm assigned to the allyl groups. The peaks assigned to the protons on the aromatic rings and the saturated carbon linking the two phenol rings are slightly shifted downfield (Table 2.1).

### **2.2.3. Characterisation of 2,2'-diallyloxy-5,5'-di-*tert*-butyl-3,3'-methanediyl-dibenzaldehyde (AOTMB)**

The IR spectrum shows a characteristic peak at  $1660\text{ cm}^{-1}$  corresponding to the C=O stretching vibration of the aldehydes.

The notable difference in the  $^1\text{H}$  NMR compared to AOTMBA is the peak at 10.4 ppm assigned to the aldehyde protons. The other peaks are slightly shifted as a consequence of the transformation of the alcohol groups into aldehyde groups (Table 2.1). The combined data from IR,  $^1\text{H}$  NMR and elemental analyses confirm the formation of AOTMB.

### **2.2.4. Characterisation of 2,2'-dihydroxy-5,5'-di-*tert*-butyl-3,3'-methanediyl-dibenzaldehyde (DHTMB)**

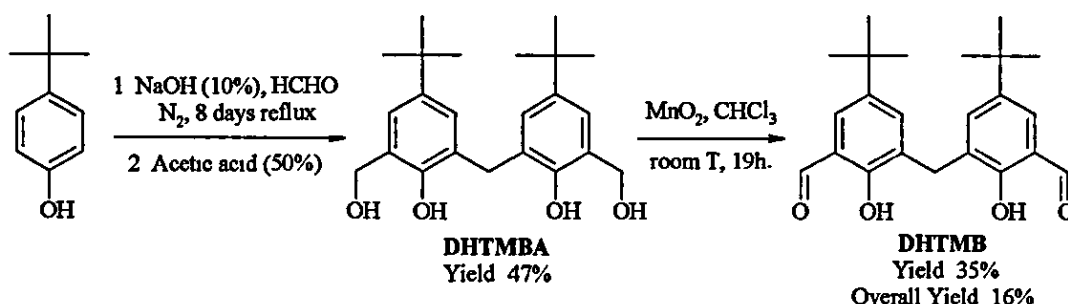
The IR spectrum shows the characteristic C=O stretching vibration at  $1658\text{ cm}^{-1}$  and the appearance of one peak at  $1270\text{ cm}^{-1}$  corresponding to the phenolic OH bending vibration of the two phenol groups

The  $^1\text{H}$  NMR shows the disappearance of the peaks assigned to the allyl groups (Table 2.1). These results combined with the elemental analysis data confirm the formation of DHTMB.

### 2.3. Synthesis of 2,2'-dihydroxy-5,5'-di-*tert*-butyl-3,3'-methanediyl-dibenzaldehyde (DHTMB) by direct oxidation

Formation of DHTMB was initially carried out according to the last procedure, involving four steps. This procedure gave low yields of only 5% and the reaction times were upwards of 14 days. In order to investigate the utility of DHTMB it needed to be made more accessible.

This method has recently been replaced by a new one here reported (Scheme 2.2) which involves only two steps: formation of the dialcohol precursor (DHTMBA) and direct oxidation of the dialcohol into the dialdehyde (DHMTB), which can be prepared more quickly and with less effort



**Scheme 2.2:** Two-step DHMTB synthesis

An extensive series of studies proved that the protection of the phenol groups is not necessary, and that simple manganese dioxide oxidation of the precursor DHTMBA produced the expected dialdehyde product, reducing the number of steps from four to two, and in a higher overall yield (16% vs. 5%). The precursor DHTMBA was synthesised following the previous procedure with slight variations. It was found that increasing the reacting time (8 days instead of 7) led to a considerable improvement in the yield to *ca.* 47% (*vs.* 28% in the four-step synthesis). The oxidation of the dialcohol DHTMBA was carried out using activated  $MnO_2$  with a yield of 35%. The solvent selected for the reaction was chloroform since it resulted in the best yields. Reactions were also carried out using toluene or ethanol but these only produced the product in lower yields (*ca.*

28%). The conditions providing the highest yield for the product were also performing the oxidation at room temperature, instead of refluxing as in the previous 4-step-reaction process.

In summary, the yields and reaction times of the synthesis of DHTMB have been significantly improved by varying the reaction conditions. The use of an appropriate oxidising agent (activated  $\text{MnO}_2$ ) that would not attack the phenol groups eases the synthesis of the dialdehyde, so the protection of the phenol groups would not be necessary, reducing the number of steps to two and thus reducing the product losses.

The IR spectrum shows the characteristic  $\text{C}=\text{O}$  stretching vibration at  $1659\text{ cm}^{-1}$  and the appearance of one peak at  $1271\text{ cm}^{-1}$  corresponding to the phenolic OH bending vibration of the two phenol groups. These results combined with the elemental analysis confirm the formation of DHTMB.

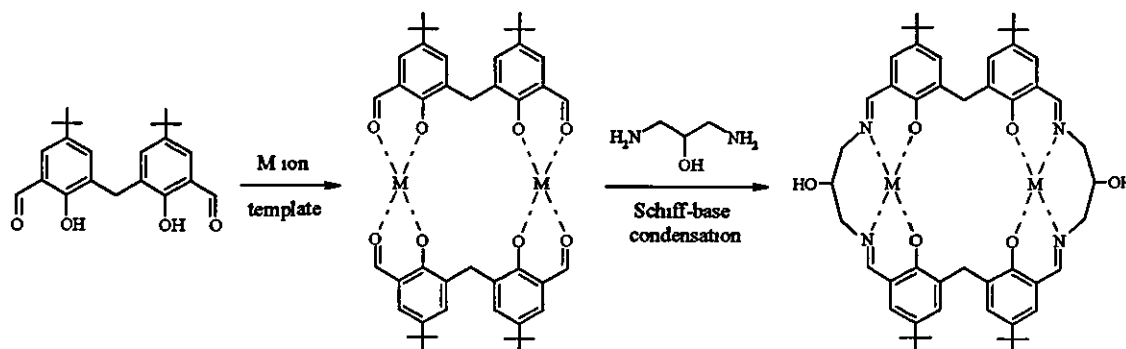
#### 2.4. Dinuclear complexes of the pseudocalixarene macrocycle $\text{H}_6\text{L1}$

The reaction of DHTMB with 1,3-diaminopropan-2-ol in the presence of a metal ion (Mn, Fe, Co, Ni, Cu and Zn salts) yields a variety of dinuclear complexes of  $\text{H}_6\text{L1}$  with very interesting conformations. Some of the work described in this chapter has been recently published.<sup>116</sup>

The mechanism for the synthesis of this series of dinuclear complexes could be described as a Schiff-base condensation (formation of an imine from an amine and a carbonyl compound) *via* the template route.<sup>2,4</sup> In the template synthesis the metal assists the Schiff-base reaction that leads to the formation of the macrocycle. Therefore, the structure of the final product is dependent on the order in which the different parts come together, and consequently on the way the metal ions are directing the course of the reaction. In the template synthesis the presence of a metal ion in the cyclisation reaction noticeably increases the yield of the

cyclic product. The metal ion plays a significant role in directing the pathway of the reaction.

It is likely that the formation of dinuclear complexes of  $H_6L1$  follow the route outlined in Scheme 2.3.



**Scheme 2.3:** [2+2] macrocycle synthesised via template condensation.

Thus, DHTMB molecules react with a metal ion to form a dinuclear complex. Evidence for this is the change of colour when reacting (from pale yellow colour of the DHTMB to green, brown or orange when reacted with the specific metal ions). Such species are then expected to readily form symmetrical [2+2] Schiff-base macrocycles upon condensation with the diamine, once the components have assembled around the template metal ions in the appropriate arrangement. It is widely accepted that in this type of synthesis the presence of the metal template restricts the rotation of the diamine through bidentate coordination, and this reduces the internal energy losses normally associated with cyclisation.<sup>4</sup> For the mechanism it is likely that the cyclisation step involves two molecules of the DHTMB which bind the two  $M(II)$  or  $M(III)$  ions, then the two diamine molecules condense with the aldehydes, forming the macrocycle (Scheme 2.3).

The dinuclear complexes listed in Table 2.2 were prepared by standard template techniques as described in the experimental chapter.

Table 2.2: Selected data for the dinuclear complexes investigated.

	Formula	Colour	IR bands (cm <sup>-1</sup> )
2.1	[Cu <sub>2</sub> (H <sub>4</sub> L1)Cl]Cl·2MeOH	Green	3326 (b,s,ν <sub>O-H</sub> ); 1627 (s,ν <sub>C-N</sub> ) 1560 (w,ν <sub>C-O</sub> )
2.2	[Zn <sub>2</sub> (H <sub>4</sub> L1)Cl]Cl·H <sub>2</sub> O	Pale yellow	3422 (b,s,ν <sub>O-H</sub> ); 1638 (s,ν <sub>C-N</sub> ) 1553 (w,ν <sub>C-O</sub> )
2.3	[Ni <sub>2</sub> (H <sub>4</sub> L1)Cl]Cl·4H <sub>2</sub> O	Green	3383 (b,m,ν <sub>O-H</sub> ); 1634 (s,ν <sub>C-N</sub> ) 1551 (w,ν <sub>C-O</sub> )
2.4	[Mn <sub>2</sub> (H <sub>4</sub> L1)Cl]Cl·H <sub>2</sub> O·EtOH	Orange	3384 (b, s,ν <sub>O-H</sub> ); 1648 (s,ν <sub>C-N</sub> ) 1545 (w,ν <sub>C-O</sub> )
2.5	[Ni <sub>2</sub> (H <sub>4</sub> L1)(H <sub>2</sub> O) <sub>3</sub> ](ClO <sub>4</sub> ) <sub>2</sub> ·H <sub>2</sub> O	Orange	3422 (b,m,ν <sub>O-H</sub> ); 1635 (s,ν <sub>C-N</sub> ) 1561 (w,ν <sub>C-O</sub> ); 1107 (b,s,ν <sub>3</sub> (ClO <sub>4</sub> <sup>-</sup> ) 624 (m,ν <sub>4</sub> (ClO <sub>4</sub> <sup>-</sup> ))
2.6	[Co <sub>2</sub> (H <sub>4</sub> L1)(H <sub>2</sub> O) <sub>3</sub> ](ClO <sub>4</sub> ) <sub>2</sub> ·3EtOH	Yellow	3440 (b,s,ν <sub>O-H</sub> ); 1636 (s,ν <sub>C-N</sub> ) 1560 (w,ν <sub>C-O</sub> ); 1106 (b,s,ν <sub>3</sub> (ClO <sub>4</sub> <sup>-</sup> ) 623 (m,ν <sub>4</sub> (ClO <sub>4</sub> <sup>-</sup> ))
2.7	[Co <sub>2</sub> (H <sub>4</sub> L1)(H <sub>2</sub> O) <sub>3</sub> ](BF <sub>4</sub> ) <sub>2</sub> ·2H <sub>2</sub> O	Yellow brownish	3448 (b,s,ν <sub>O-H</sub> ); 1647 (s,ν <sub>C-N</sub> ); 1560 (w,ν <sub>C-O</sub> ); 1084 and 1055 (b,ν <sub>3</sub> (BF <sub>4</sub> <sup>-</sup> ))
2.8	[Ni <sub>2</sub> (H <sub>4</sub> L1)(NO <sub>3</sub> )(H <sub>2</sub> O) <sub>2</sub> ](NO <sub>3</sub> )·H <sub>2</sub> O·MeOH	Green	3387 (b,s,ν <sub>O-H</sub> ); 1636 (s,ν <sub>C-N</sub> ); 1560 (w,ν <sub>C-O</sub> ), 1475 and 1366 (s,ν <sub>coord.NO3</sub> ), 1384 (s,ν <sub>freeNO3</sub> )
2.9	[Zn <sub>2</sub> (H <sub>4</sub> L1)(NO <sub>3</sub> )(H <sub>2</sub> O) <sub>2</sub> ](NO <sub>3</sub> )·3H <sub>2</sub> O	Pale yellow	3405 (b,s,ν <sub>O-H</sub> ); 1646 (s,ν <sub>C-N</sub> ); 1560 (w,ν <sub>C-O</sub> ); 1438 and 1364 (s,ν <sub>coord.NO3</sub> ), 1384 (s,ν <sub>freeNO3</sub> )
2.10	[Co <sub>2</sub> (H <sub>3</sub> L1)(NO <sub>3</sub> )]·5H <sub>2</sub> O	Orange	3396 (b,s,ν <sub>O-H</sub> ); 1636 (s,ν <sub>C-N</sub> ) 1460 and 1364 (s,ν <sub>coord.NO3</sub> ) 1384 (s,ν <sub>freeNO3</sub> )
2.11	[Zn <sub>2</sub> (H <sub>4</sub> L1)(AcO)](AcO)·5H <sub>2</sub> O	Pale yellow	3417 (b,s,ν <sub>O-H</sub> ); 1642 (s,ν <sub>C-N</sub> ) 1593 (s,ν <sub>C-O</sub> ), 1430 (s,ν <sub>COO</sub> <sup>-</sup> )
2.12	[Ni <sub>2</sub> (H <sub>4</sub> L1)(MeOH) <sub>2</sub> ](ClO <sub>4</sub> ) <sub>2</sub> ·MeOH	Red	3425 (b,m,ν <sub>O-H</sub> ); 1633 (s,ν <sub>C-N</sub> ) 1565 (w,ν <sub>C-O</sub> ); 1108 (b,s,ν <sub>3</sub> (ClO <sub>4</sub> <sup>-</sup> ) 624 (m,ν <sub>4</sub> (ClO <sub>4</sub> <sup>-</sup> ))
2.13	[Mn <sub>2</sub> (H <sub>2</sub> L1)(Cl) <sub>2</sub> (EtOH) <sub>2</sub> ] 6H <sub>2</sub> O	Brown	3422 (b,s,ν <sub>O-H</sub> ); 1617 (s,ν <sub>C-N</sub> ) 1550 (m,ν <sub>C-O</sub> )

2.14	$[\text{Co}_2(\text{H}_2\text{L1})(\text{Cl})_2(\text{H}_2\text{O})_2]$	Green Brownish	3366 (b,m, $\nu_{\text{O-H}}$ ); 1630 (s, $\nu_{\text{C-N}}$ ) 1560 (w, $\nu_{\text{C-O}}$ )
2.15	$[\text{Fe}_2(\text{H}_2\text{L1})(\text{Cl})_2(\text{H}_2\text{O})_2]$	Black Reddish	3423 (b,s, $\nu_{\text{O-H}}$ ); 1618 (s, $\nu_{\text{C-N}}$ ) 1549 (m, $\nu_{\text{C-O}}$ )
2.16	$[\text{Mn}_2(\text{H}_2\text{L1})(\text{AcO})_2(\text{EtOH})]$	Green brownish	3422 (b,m, $\nu_{\text{O-H}}$ ); 1618 (s, $\nu_{\text{C-N}}$ ) 1550 (s, $\nu_{\text{C-O}}$ ), 1439 (m, $\nu_{\text{COO}^-}$ )
2.17	$[\text{Mn}_2(\text{H}_2\text{L1})(\text{OH})(\text{EtOH})_2](\text{CF}_3\text{SO}_3^-)$	Dark green	3432 (b, s, $\nu_{\text{O-H}}$ ), 1616 (s, $\nu_{\text{C-N}}$ ) 1552 (m, $\nu_{\text{C-O}}$ ); 1269 (s, $\nu_{\text{SO}_3^-}$ ) 1031 (m, $\nu_{\text{C-F}}$ ); 640 (w, $\nu_{\text{C-F}}$ )
2.18	$[\text{Co}_2(\text{HL1})](\text{ClO}_4^-)$	Brown	3420 (b, s, $\nu_{\text{O-H}}$ ), 1637 (s, $\nu_{\text{C-N}}$ ) 1089 (b,s, $\nu_{\text{ClO}_4^-}$ ), 626 (m, $\nu_{\text{ClO}_4^-}$ )
2.19	$[\text{Cu}_2(\text{H}_2\text{L1})]\cdot\text{H}_2\text{O}$	Brown	3356 (b,w, $\nu_{\text{O-H}}$ ); 1618 (s, $\nu_{\text{C-N}}$ ) 1541 (s, $\nu_{\text{C-O}}$ )
2.20	$[\text{Ni}_2(\text{H}_2\text{L1})(\text{H}_2\text{O})_3]$	Brown	3406 (b,m, $\nu_{\text{O-H}}$ ), 1618 (s, $\nu_{\text{C-N}}$ ) 1543 (s, $\nu_{\text{C-O}}$ )

A range of analytical techniques, including infrared spectroscopy, elemental analysis, mass spectroscopy (liquid secondary ion mass spectrometry and electrospray ionisation), UV-visible spectroscopy, nuclear magnetic resonance and X-ray diffraction were used to characterise the dinuclear complexes.

Successful formation of the macrocycle was confirmed initially by IR spectroscopy (Table 2.2) where formation of the Schiff-base was indicated by disappearance of the carbonyl ( $1658\text{ cm}^{-1}$  in DHTMB) and amine stretches associated with the reactants, along with appearance of an imine stretching band at *ca.*  $1637\text{ cm}^{-1}$  for the M(II) complexes and at *ca.*  $1618\text{ cm}^{-1}$  for the M(III) complexes. This can be explained in terms of the higher charge of the metal ions M(III) ions are harder Lewis acids than M(II) ions, therefore attract more electron density from the N donor, consequently weakening the C=N bond more. Hence imine bonds vibrate at lower frequencies when coordinated to M(III) ions.



The weak band present in almost all of the complexes at *ca.* 1550  $\text{cm}^{-1}$  can be assigned to the C-O vibration of the phenol groups. Strong peaks in the range 1522-1529  $\text{cm}^{-1}$  are attributable to the phenolic C-O groups acquiring partial double bond character through conjugation with the imine system in the chelate ring<sup>114-115</sup>. A broad band in the region 3450-3350  $\text{cm}^{-1}$  indicative of O-H stretching vibrations of water was observed in the spectra of all the compounds (recorded in KBr discs).

Further indication of the dinuclear nature of the complexes was obtained from mass spectral data. Liquid Secondary Ion Mass Spectrometry (LSIMS), commonly referred to as FAB (Fast Atom Bombardment), has proved a very valuable characterisation technique for the complexes. In this technique<sup>117,118</sup> the samples dissolved in a liquid matrix (usually 3-nitrobenzyl alcohol, NOBA), are bombarded with a beam of caesium ions.

Chemical reactions occur between thermally equilibrated reagent ions (R) and sample molecules (M). Primary ions are formed in reagent gas ( $\text{R} + \text{e}^- \rightarrow \text{R}^+ + 2\text{e}^-$ ). These primary ions react with more reagent gas to form stable, reactive secondary cations by collisional hydrogen transfer ( $\text{R}^+ + \text{RH} \rightarrow \text{RH}^+ + \text{R}$ ). The ways of forming molecular ions are by protonation of the complexes ( $\text{RH}^+ + \text{M} \rightarrow \text{R} + \text{MH}^+$ ) or by charge exchange ( $\text{R}^+ + \text{M} \rightarrow \text{R} + \text{M}^+$ ), which normally will lead to reduction of some of the metal ions from M(II) to M(I) through the course of the LSIMS experiment. Therefore if one peak fits a formula which might be expected to have a charge of +2 or +3, the charge is actually +1 with the ion gaining one or two electrons through reduction, probably of the metal, during the mass spectrometry experiment<sup>117</sup>

Some of the mass spectrometry was performed by Electrospray Ionisation (ESI), which is a technique used to produce gaseous ionised species from a liquid solution (the compound dissolved in an appropriate solvent), generated by creating a fine spray of charged droplets in the presence of a strong electric field. The charged droplets are sprayed from the tip of a metal needle and then electrostatically directed towards the mass spectrometer inlet. Either gas, heat or a combination of both is applied to the droplets to induce vaporisation prior to entering the detector. As the solvent evaporates, the electric field density increases, hence the mutual repulsion between individual species becomes so great that it exceeds the surface tension and ions leave the droplet.

LSIMS spectra were usually preferred since they give singly charged ions at high mass uncomplicated by the presence of multi-charged species and this simplifies the interpretation of the spectra. It seemed also that LSIMS had less chance of generating ion pairs in the instrument than ESI, so the presence of cation and anion signals in LSIMS is reasonably suggestive of coordination rather than an ion pair formed within the instrument.

The spectrum shows different clusters of peaks at different  $m/z$  values ( $m$  = mass of the observed ion and  $z$  = charge of the observed ion) corresponding to different fragmented ions. Each cluster represents an isotopic distribution for one fragment (Fig. 2.4) due to the different isotopes of the atoms present in the molecule.

The value taken for  $m/z$  in the data tables is that of the most intense peak belonging to a set of peaks in the experimental spectrum. The value for the calculated mass is obtained by taking that of the most intense peak in the isotopic distribution pattern calculated by the Isotopic Distribution Calculator program.<sup>119</sup>

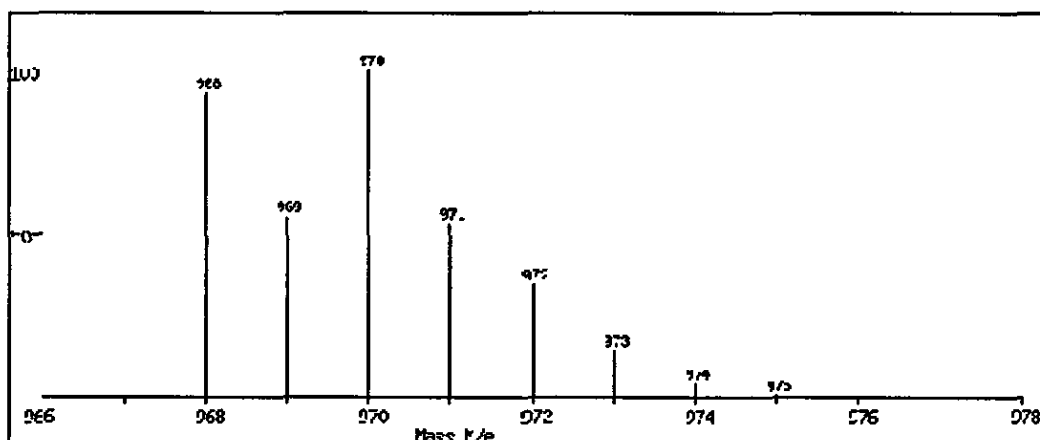


Fig. 2.4: Calculated isotopic distribution for the fragment  $[\text{Cu}_2(\text{H}_4\text{L1})+\text{e}]^+$

The dinuclear complexes studied generally afforded clean LSIMS spectra of singly charged fragments of the complexes with no peaks observed for  $m/2$ . Each of the dinuclear divalent metal complexes studied shows a peak corresponding to a singly charged ion containing the dimetallic fragment  $[\text{M}_2(\text{H}_4\text{L1})+\text{e}]^+$ ,  $[\text{M}_2(\text{H}_4\text{L1})-\text{H}]^+$  or  $[\text{M}_2(\text{H}_4\text{L1})-2\text{H}]^+$ . While the dinuclear trivalent metal complexes show peaks corresponding to the dimetallic fragment  $[\text{M}_2(\text{H}_2\text{L1})+\text{e}]^+$ . In a number of cases fragments including anions were also observed. In the case of the complexes characterised with ESI spectra, doubly charged fragments of the complexes were also observed (peaks assigned to the dimetallic fragment  $[\text{M}_2(\text{H}_4\text{L1})]^{2+}$  or  $[\text{M}_2(\text{H}_2\text{L1})]^{2+}$  at  $m/2$ ).

In general, the complexes were obtained from the reaction mixtures as powders and recrystallised to obtain crystals suitable for X-ray studies. Frequently the recrystallisation resulted in a different set of solvate molecules (coordinated and/or in the lattice) but the basic  $\text{M}_2(\text{H}_4\text{L1})$  or  $\text{M}_2(\text{H}_2\text{L1})$  unit remained unchanged. The detailed study of the LSIMS mass spectra allowed the recognition of fragmentation patterns for the series of complexes where no structure determination by X-ray crystallography was achieved. This data, together with elemental analysis, allowed structures to be proposed.

The dinuclear complexes here described can be separated into two different groups according to the topology adopted:

- dinuclear complexes with a folded structure (Fig. 2.5), which is maintained by two strong hydrogen bonds linking adjacent oxygen atoms of each monodeprotonated 2,2'-methylenediphenol unit of the macrocycle and generating a cleft within which guest molecules or ions can bind.

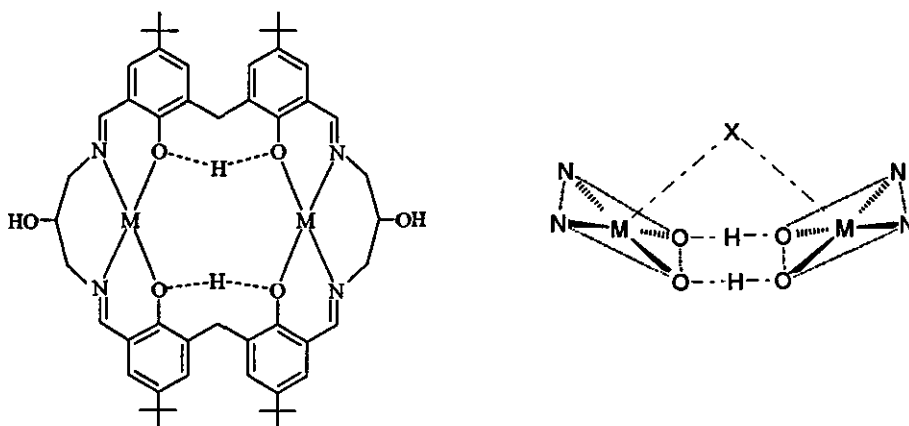


Fig. 2.5: complexes of the type  $[M_2(H_4L1)X]^{n+}$  ( $X = H_2O, Cl^-, NO_3^-,$  and  $AcO^-$ ).

- dinuclear complexes where all the phenol groups are fully deprotonated, the macrocycle opens out and the metal ions are far apart, lying at each end of the macrocyclic plane (Fig. 2.6)

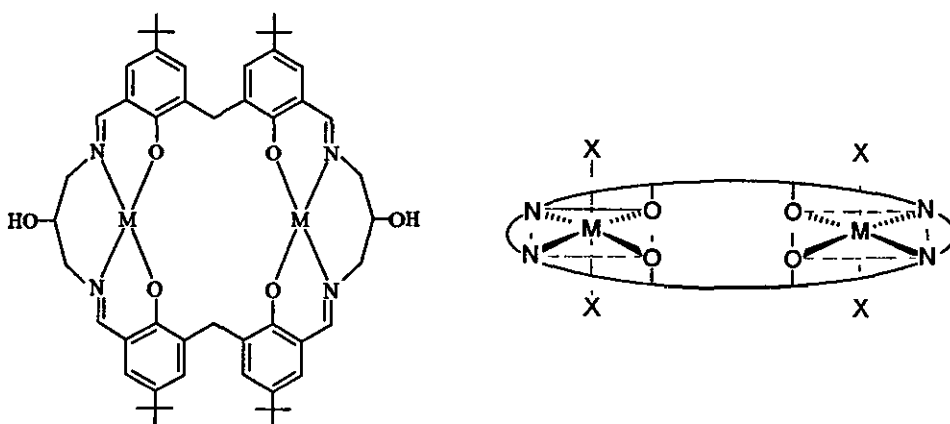


Fig. 2.6: complexes of the type  $[M_2(H_2L1)]^{n+}$ , ( $X = Cl^-, dmf$  and  $dmsO$ )

#### 2.4.1. Dinuclear complexes of $H_6L1$ with intramolecular H-bonding

**2.4.1.1. Synthesis and characterisation of  $[\text{Cu}_2(\text{H}_4\text{L1})\text{Cl}]\text{Cl}\cdot 2\text{MeOH}$ ,  $[\text{Zn}_2(\text{H}_4\text{L1})\text{Cl}]\text{Cl}\cdot \text{H}_2\text{O}$ ,  $[\text{Ni}_2(\text{H}_4\text{L1})\text{Cl}]\text{Cl}\cdot 4\text{H}_2\text{O}$  and  $[\text{Mn}_2(\text{H}_4\text{L1})\text{Cl}]\text{Cl}\cdot \text{H}_2\text{O}\cdot \text{EtOH}$**

Reaction of DHTMB with 1,3-diaminopropan-2-ol in the presence of the chloride salts of the transition metals Cu(II), Zn(II), Ni(II) and Mn(II) produces dinuclear complexes of the macrocycle  $\text{H}_6\text{L1}$ . They were all synthesised using the same procedure as described in the experimental chapter except the dimanganese(II) complex  $[\text{Mn}_2(\text{H}_4\text{L1})\text{Cl}]\text{Cl}\cdot \text{H}_2\text{O}\cdot \text{EtOH}$  (2.4), which was synthesised under nitrogen because it was found to quickly oxidise in solution. Once isolated as an orange powder the complex seems stable

In all four complexes the LSIMS or ESI mass spectrometry data confirm the formation of the dinuclear macrocyclic species. The divalent metal complexes show a peak corresponding to a singly charged ion containing the dimetallic fragment  $[\text{M}_2(\text{H}_4\text{L1})-2\text{H}]^+$  ( $[\text{M}_2(\text{H}_4\text{L1})+\text{e}]^+$  for the dicopper(II) (Fig. 2.7, Table 2.3) and dizinc(II) (Fig. 2.8, Table 2.4) complexes, suggesting that the complexes have been reduced by one electron in the LSIMS experiment). The peaks at  $m/z$  1006, 1009, 995, 987 and 1040 respectively support the presence of chloride ions in the complexes

**Table 2.3: Peak attributions for  $[\text{Cu}_2(\text{H}_4\text{L1})\text{Cl}]\text{Cl}\cdot 2\text{MeOH}$**

$m/z$	Rel. Intensity (%)	Fragments	Calc. Mass
889	40	$[\text{Na}_2(\text{H}_4\text{L1})+\text{e}]^+$	889
970	100	$[\text{Cu}_2(\text{H}_4\text{L1})+\text{e}]^+$	970
1006	15	$[\text{Cu}_2(\text{H}_4\text{L1})\text{Cl}+\text{H}]^+$	1006
1032	7	$[\text{Cu}_2(\text{H}_4\text{L1})(\text{MeOH})_2-2\text{H}]^+$	1032

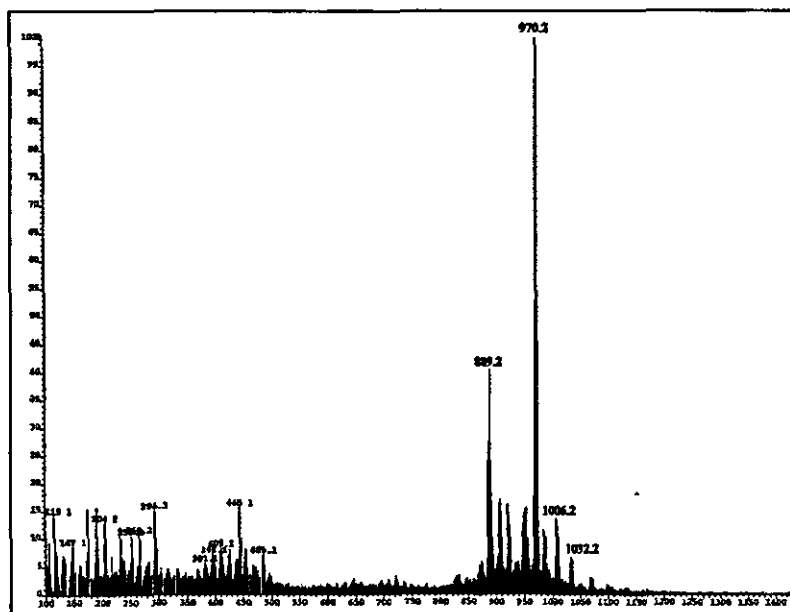


Fig. 2.7: LSI-MS spectrum of the complex  $[\text{Cu}_2(\text{H}_4\text{L1})\text{Cl}]\text{Cl}\cdot 2\text{MeOH}$

In the case of  $[\text{Zn}_2(\text{H}_4\text{L1})\text{Cl}]\text{Cl}\cdot\text{H}_2\text{O}$ , the relative intensity of the peaks is quite weak with respect to the peaks at  $m/z$  221 and  $m/z$  281 corresponding to fragmentation peaks of the complex (Fig. 2.8, Table 2.4)

Table 2.4: Peak attributions for  $[\text{Zn}_2(\text{H}_4\text{L1})\text{Cl}]\text{Cl}\cdot\text{H}_2\text{O}$

m/z	Rel. Intensity (%)	Fragments	Calc. Mass
973	25	$[\text{Zn}_2(\text{H}_4\text{L1}) + \text{e}]^+$	973
1009	50	$[\text{Zn}_2(\text{H}_4\text{L1})\text{Cl}]^+$	1009

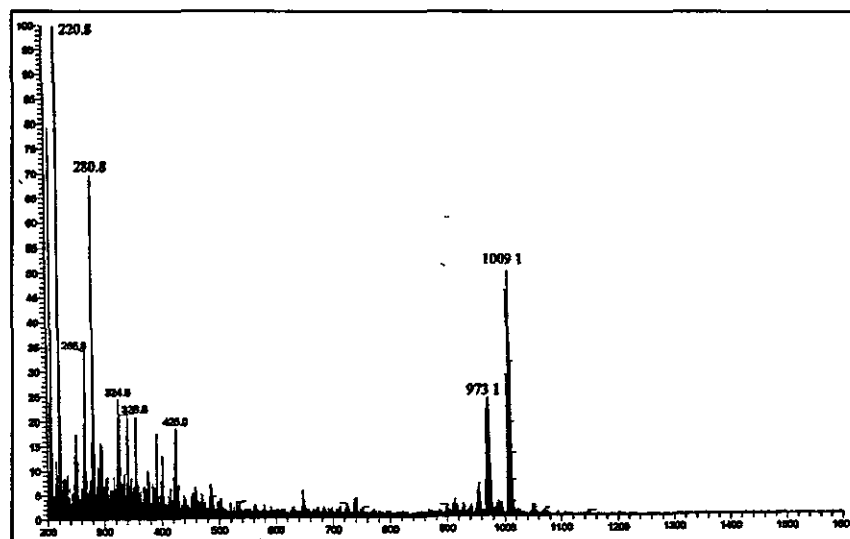


Fig. 2.8: LSI-MS spectrum of the complex  $[\text{Zn}_2(\text{H}_4\text{L1})\text{Cl}]\text{Cl}\cdot\text{H}_2\text{O}$

The ESI spectrum of the complex  $[\text{Ni}_2(\text{H}_4\text{L1})\text{Cl}]\text{Cl}\cdot 4\text{H}_2\text{O}$  shows the main peak at  $m/z$  957 which does not correspond with the calculated  $m/z$  959 of the molecular ion  $[\text{Ni}_2(\text{H}_4\text{L1}) - \text{H}]^+$ . The peak at  $m/z$  959 is observed at lower relative abundance (90%) in the main peak cluster (Fig 2.9). This can be explained in terms of isotopic distribution.

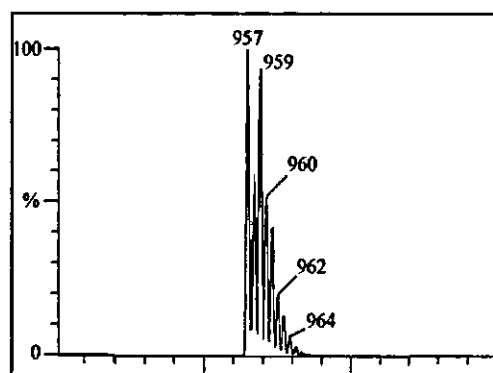


Fig. 2.9: ESI-MS spectrum fragment of the complex  $[\text{Ni}_2(\text{H}_4\text{L1})\text{Cl}]\text{Cl}\cdot 4\text{H}_2\text{O}$

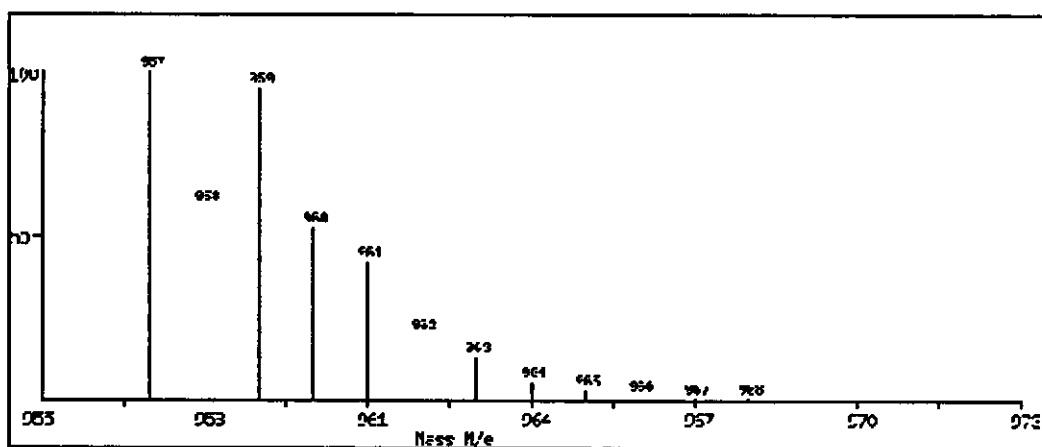


Fig. 2.10: Calculated isotopic distribution for the fragment  $[\text{Ni}_2(\text{H}_4\text{L1}) - \text{H}]^+$

As explained previously, the observed isotope distribution of an analyte will be characteristic and comparison with the theoretical isotope distribution (calculated by the Isotopic Distribution Calculator program<sup>119</sup>) is a very useful method of double checking the formula of the ion being measured. Figures 2.9 and 2.10 show experimental and calculated isotopic patterns for the molecular ion signal of  $[\text{Ni}_2(\text{H}_4\text{L1}) - \text{H}]^+$ . The agreement of calculated and experimental isotopic pattern confirms the formula given for the molecular ion.

**Table 2.5:** Peak attributions for  $[\text{Ni}_2(\text{H}_4\text{L1})\text{Cl}]\text{Cl}\cdot 4\text{H}_2\text{O}$   
(ESI-MS relative abundance is given for cone voltage = 90V)

m/z	Rel. Intensity (%)	Fragments	Calc. Mass
479	40	$[\text{Ni}_2(\text{H}_4\text{L1}) - 2\text{H}]^{2+}$	958
957	100	$[\text{Ni}_2(\text{H}_4\text{L1}) - \text{H}]^+$	959
995	10	$[\text{Ni}_2(\text{H}_4\text{L1})\text{Cl}]^+$	995

The LSIMS spectrum of  $[\text{Mn}_2(\text{H}_4\text{L1})\text{Cl}]\text{Cl}\cdot \text{H}_2\text{O}\cdot \text{EtOH}$  (Fig. 2.11, Table 2.6) confirms the formation of the dinuclear macrocyclic complex, showing a peak corresponding to a singly charged ion containing the dimetallic fragment  $[\text{Mn}_2(\text{H}_4\text{L1})\text{Cl} - \text{H}]^+$ . The peaks at m/z 987 and 1040 support the presence of chloride ions in the complex

**Table 2.6:** Peak attributions for  $[\text{Mn}_2(\text{H}_4\text{L1})\text{Cl}]\text{Cl}\cdot \text{H}_2\text{O}\cdot \text{EtOH}$

m/z	Rel. Intensity (%)	Fragments	Calc. Mass
898	7	$[\text{Mn}(\text{H}_4\text{L1}) - \text{e}]^+$	898
951	10	$[\text{Mn}_2(\text{H}_4\text{L1}) - 2\text{H}]^+$	951
987	100	$[\text{Mn}_2(\text{H}_4\text{L1})\text{Cl} - \text{H}]^+$	987
1040	35	$[\text{Mn}_2(\text{H}_4\text{L1})(\text{Cl})_2(\text{H}_2\text{O}) - \text{H}]^+$	1040

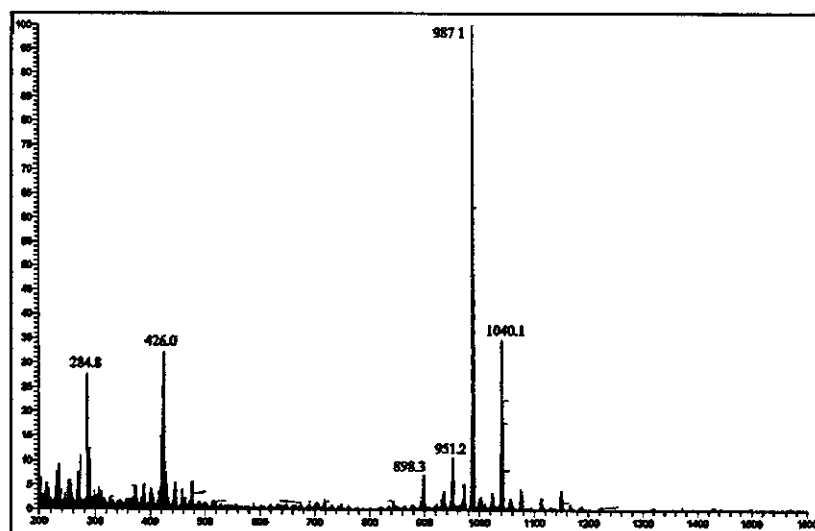


**Fig. 2.11:** LSI-MS spectrum of the complex  $[\text{Mn}_2(\text{H}_4\text{L1})\text{Cl}]\text{Cl}\cdot \text{H}_2\text{O}\cdot \text{EtOH}$

The stoichiometry of the complexes, derived from the elemental analyses, also suggests that the metal ions are in the +II oxidation state and therefore that the macrocycle is doubly deprotonated.



### 2.4.1.2. Structures of $[\text{Cu}_2(\text{H}_4\text{L1})\text{Cl}]\text{Cl}\cdot 1.6\text{Et}_2\text{O}\cdot \text{EtOH}$ and $[\text{Zn}_2(\text{H}_4\text{L1})\text{Cl}]\text{Cl}\cdot \text{Et}_2\text{O}\cdot 0.5\text{EtOH}\cdot 0.55\text{H}_2\text{O}$

Green crystals of  $[\text{Cu}_2(\text{H}_4\text{L1})\text{Cl}]\text{Cl}\cdot 1.6\text{Et}_2\text{O}\cdot \text{EtOH}$  (**2.1x**) and pale yellow crystals of  $[\text{Zn}_2(\text{H}_4\text{L1})\text{Cl}]\text{Cl}\cdot \text{Et}_2\text{O}\cdot 0.5\text{EtOH}\cdot 0.55\text{H}_2\text{O}$  (**2.2x**) suitable for X-ray studies were grown by slow diffusion of diethylether into an ethanol solution of the dicopper(II) complex **2.1** and the dizinc(II) complex **2.2** respectively. The recrystallisation resulted in a different set of solvate molecules for each structure but the basic  $\text{M}_2(\text{H}_4\text{L1})\text{Cl}$  unit remained intact. The two structures are isomorphous, thus only the dicopper(II) complex structure will be described in detail. Isomorphous, in this sense, means that the crystal of the dicopper structure is identical to the dizinc structure except for the presence of one or more different solvent molecules (i.e. the lattice, space group, cell dimensions and position and conformation of the macrocyclic complex within the unit cell is preserved). The solvent molecules simply occupy the empty spaces in the lattice in between the macrocyclic units, not affecting to the crystallographic factors mentioned.

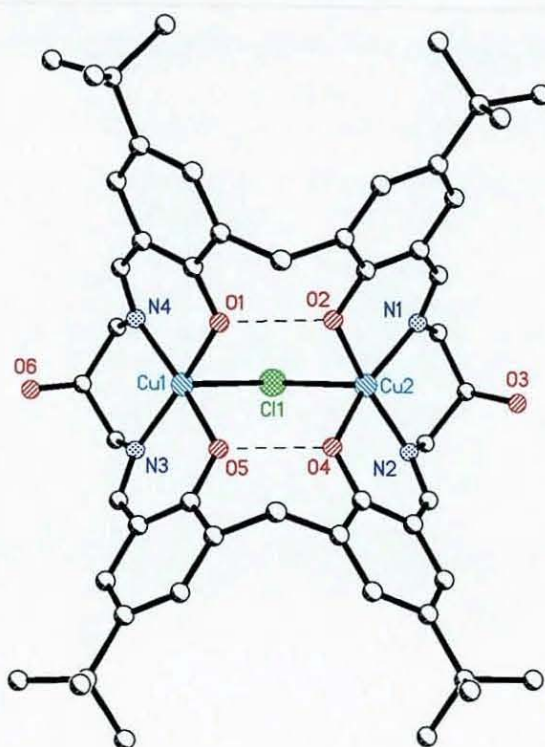


**Fig. 2.12:** Structure of the cation  $[\text{Cu}_2(\text{H}_4\text{L1})(\text{Cl})]^+$

All the X-ray data collection parameters for both structures are summarised in Tables 1 and 2 respectively of appendix 1 along with the details concerning the refinement and disorder. Perspective views of the cation  $[\text{Cu}_2(\text{H}_4\text{L1})(\text{Cl})]^+$  are shown in Figs. 2.12 and 2.13 and selected bond lengths and angles relevant to the metal ion coordination are given in Tables 2.7 and 2.8.

Each metal centre is five-coordinate and has identical macrocyclic donors. The geometry at each metal ion is square pyramidal with the two phenol oxygen atoms and the two imine nitrogen atoms forming the basal plane. The coordination sphere is completed by a central chloride donor in the axial site, which bridges the two metal ions (illustrated in Fig. 2.13). The formula unit is completed by a lattice chloride anion and solvent molecules (ether, ethanol and water).

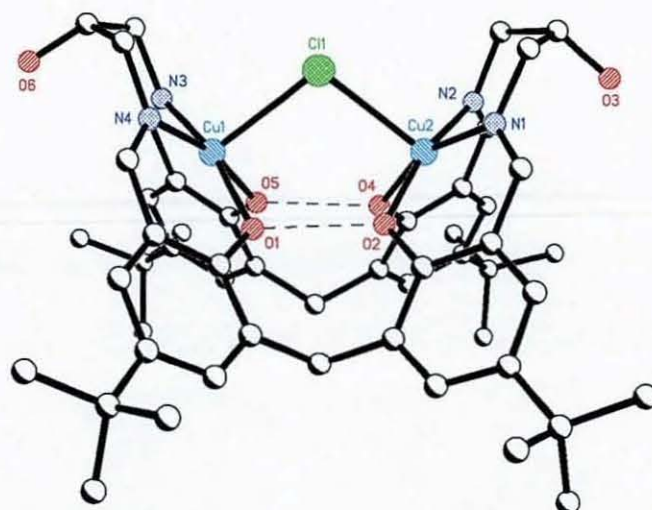


**Fig. 2.13:** Side-on view of the cation  $[\text{Cu}_2(\text{H}_4\text{L1})(\text{Cl})]^+$

The hydrogen atoms bonded to the oxygen atoms of the methylenediphenol units were located and not further refined. The structure is consistent with loss of one proton from each methylenediphenol unit, resulting in a phenol-phenolate interaction. It is also in agreement with the stoichiometric data which suggest the macrocycle is doubly deprotonated.

The macrocycle adopts a saddle conformation with the basal planes about each metal ion inclined to each other at *ca.*  $86^\circ$ . This shape is maintained by three



interactions: the M-Cl-M bridge ( $104.54(5)^\circ$  for Cu and  $104.99(9)^\circ$  for Zn) and two strong hydrogen bonds<sup>102-104</sup> linking adjacent phenol oxygen atoms (O1...O2 2.414(4) and O4...O5 2.402(4) Å for the dicopper complex and O1...O2 2.412(4) and O4...O5 2.406(4) Å for the dizinc complex). The Jahn-Teller effect explains the observation that the Cu-Cl bonds are significantly longer than the Zn-Cl equivalents (*ca.* 2.5 Å for Cu-Cl and *ca.* 2.3 Å for Zn-Cl). The metal-metal distances are 3.9998(12) Å and 3.656(3) Å for the dicopper and the dizinc complex respectively.

**Table 2.7:** Selected bond lengths [Å] and angles [°] for [Cu<sub>2</sub>(H<sub>4</sub>L)(Cl)]Cl·1.6Et<sub>2</sub>O·EtOH

Cu(1)-O(1)	1.958(3)	Cu(2)-O(2)	1.962(3)
Cu(1)-N(4)	1.978(4)	Cu(2)-N(1)	1.967(4)
Cu(1)-O(5)	1.989(3)	Cu(2)-O(4)	1.970(3)
Cu(1)-N(3)	1.952(4)	Cu(2)-Cl(1)	2.5423(14)
O(2)-O(1)	2.414(4)	Cu(1)-Cl(1)	2.5145(13)
O(5)-O(4)	2.402(4)	Cu(1)-Cu(2)	3.9998(12)
Cu(2)-N(2)	1.983(4)		
<hr/>			
N(4)-Cu(1)-O(5)	160.13(14)	N(1)-Cu(2)-O(4)	166.69(17)
O(1)-Cu(1)-N(3)	166.63(15)	N(2)-Cu(2)-N(1)	94.21(18)
O(1)-Cu(1)-N(4)	88.53(15)	N(2)-Cu(2)-O(4)	88.25(15)
O(1)-Cu(1)-O(5)	85.76(13)	O(2)-Cu(2)-O(4)	85.31(13)
N(4)-Cu(1)-N(3)	93.11(16)	O(2)-Cu(2)-N(1)	89.31(17)
O(5)-Cu(1)-N(3)	88.26(14)	Cu(2)-Cl(1)-Cu(1)	104.55(5)
N(2)-Cu(2)-O(2)	165.90(16)		

**Table 2.8:** Hydrogen bonds [Å] for [Cu<sub>2</sub>(H<sub>4</sub>L)(Cl)]Cl·1.6Et<sub>2</sub>O·EtOH

D-H...A	D(D-H)	D(H...A)	d(D...A)
O(2)-H(2)...O(1)	0.90	1.54	2.417(4)
O(4)-H(4)...O(5)	0.91	1.50	2.405(4)
O(3)-H(3A)...Cl(2)	0.84	2.26	3.098(3)
O(61)-H(61)...Cl(2)	0.84	2.28	3.102(6)
O(6)-H(6A)...Cl(2)*	0.84	2.33	3.149(6)

Symmetry transformations used to generate equivalent atoms: (\*) x, y-1, z

The pendant alcohol groups (O3 and O6) are pointing outside the cavity of the macrocycle and are not involved in bonding to the metal ions but they form

hydrogen bonds to the non-coordinated chloride ion Cl2, forming one-dimensional chains through the lattice (Fig. 2.14, Table 2.8). The solvate ethanol molecule is also hydrogen-bonded to Cl2 but the ether solvate molecules are non-bonded and lie in the channels between the cations.

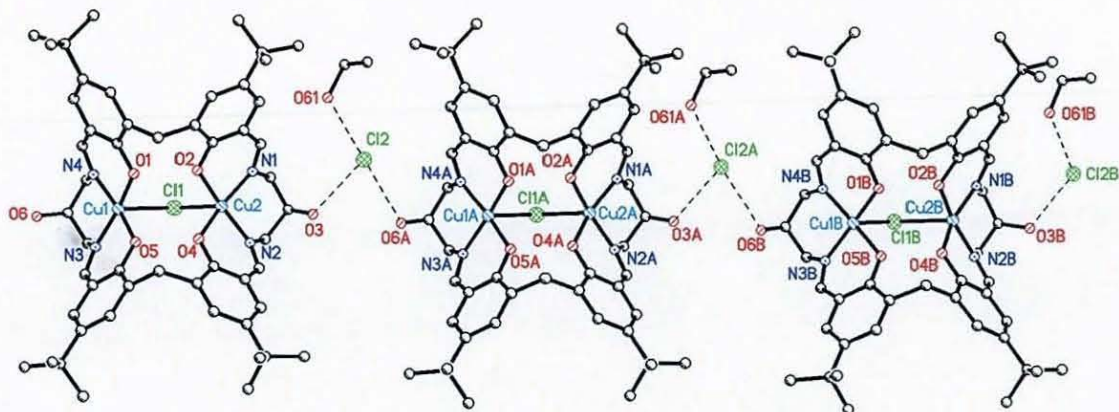


**Fig. 2.14:** H-bonding for  $[\text{Cu}_2(\text{H}_4\text{L})(\text{Cl})]\cdot\text{Cl}\cdot\text{EtOH}$  forming chains

In the dizinc complex there is some disorder at the metal sites involving minor six-coordinate components (20% at Zn1 and 40% at Zn2). In the minor component the zinc ions lie in the plane of their macrocyclic donors and each has a water molecule as a sixth ligand (Fig. 2.15, Table 2.9).

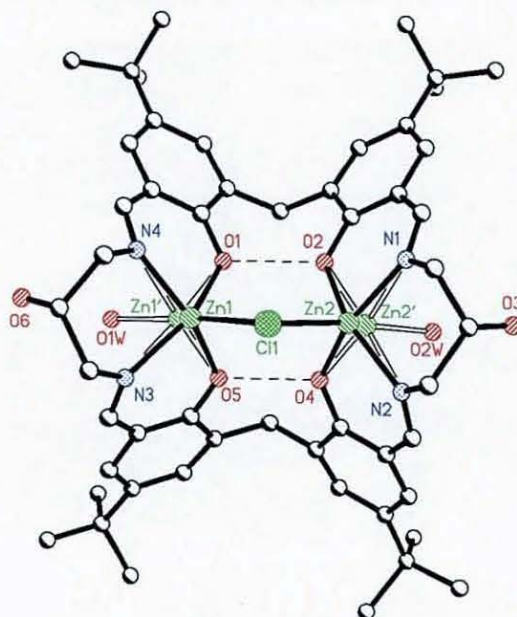


**Fig. 2.15:** Structure for the cation  $[\text{Zn}_2(\text{H}_4\text{L}_1)(\text{Cl})]^+$  showing the minor 6-coordinate component with white bonding

**Table 2.9:** Selected bond lengths [Å] and angles [°] for  $[\text{Zn}_2(\text{H}_4\text{L1})(\text{Cl})]\text{Cl}\cdot\text{Et}_2\text{O}\cdot 0.5\text{EtOH}\cdot 0.55\text{H}_2\text{O}$

Zn(1)-O(5)	2.042(5)	Zn(2)-O(4)	2.028(4)
Zn(1)-N(4)	2.052(5)	Zn(2)-N(1)	2.100(5)
Zn(1)-O(1)	2.083(5)	Zn(2)-N(2)	2.105(5)
Zn(1)-N(3)	2.087(5)	Zn(2)-Cl(1)	2.312(2)
Zn(1)-Cl(1)	2.300(2)	Zn(2')-N(2)	1.936(6)
Zn(1')-N(3)	1.949(17)	Zn(2')-N(1)	2.013(6)
Zn(1')-O(5)	1.999(18)	Zn(2')-O(4)	2.037(6)
Zn(1')-N(4)	2.009(18)	Zn(2')-O(2)	2.099(6)
Zn(1')-O(1)	2.094(18)	Zn(2')-O(2W)	2.178(10)
Zn(1')-O(1W)	2.401(3)	Zn(2')-Cl(1)	2.752(4)
Zn(1')-Cl(1)	2.630(11)	O(2)-O(1)	2.412(4)
Zn(2)-O(2)	2.022(4)	O(5)-O(4)	2.407(4)
O(5)-Zn(1)-N(4)	154.33(19)	O(2)-Zn(2)-O(4)	87.20(18)
O(5)-Zn(1)-O(1)	85.1(2)	O(2)-Zn(2)-N(1)	85.94(17)
N(4)-Zn(1)-O(1)	85.65(19)	O(4)-Zn(2)-N(1)	156.06(18)
O(5)-Zn(1)-N(3)	85.45(19)	O(2)-Zn(2)-N(2)	155.32(19)
N(4)-Zn(1)-N(3)	90.10(19)	O(4)-Zn(2)-N(2)	85.8(2)
O(1)-Zn(1)-N(3)	148.40(17)	N(1)-Zn(2)-N(2)	90.96(18)

The analogous nickel complex  $[\text{Ni}_2(\text{H}_4\text{L1})(\text{Cl})]\text{Cl}\cdot 4\text{H}_2\text{O}$  has been prepared but not crystallized. On the basis of analytical and mass spectral data it seems likely to contain the same chloro bridged structure, probably with water as sixth ligand to each nickel ion. It is therefore likely to be isostructural with the minor, 6-coordinate component of the zinc complex.

#### 2.4.1.3. Synthesis and characterisation of $[\text{Ni}_2(\text{H}_4\text{L1})(\text{H}_2\text{O})_3](\text{ClO}_4)_2\cdot\text{H}_2\text{O}$ , $[\text{Co}_2(\text{H}_4\text{L1})(\text{H}_2\text{O})_3](\text{ClO}_4)_2\cdot 3\text{EtOH}$ and $[\text{Co}_2(\text{H}_4\text{L1})(\text{H}_2\text{O})_3](\text{BF}_4)_2\cdot 2\text{H}_2\text{O}$

The dinickel(II) complex  $[\text{Ni}_2(\text{H}_4\text{L1})(\text{H}_2\text{O})_3](\text{ClO}_4)_2\cdot\text{H}_2\text{O}$  (2.5) was isolated as green crystals, grown by slow evaporation of an ethanol solution. However, the green crystalline powder (analysed as  $[\text{Ni}_2(\text{H}_4\text{L1})(\text{H}_2\text{O})(\text{EtOH})_2](\text{ClO}_4)_2\cdot 4\text{EtOH}$ ) turned orange under vacuum, presumably due to the loss of coordinated solvent molecules, probably ethanol. The dried orange complex analysed as  $[\text{Ni}_2(\text{H}_4\text{L1})](\text{ClO}_4)_2\cdot 4\text{H}_2\text{O}$ . Thus, the water molecules are thought to be non-coordinated in the orange powder and the Ni(II) ions are likely to be four-coordinated (the geometry around the metal is usually found to be square planar for

Ni(II) complexes isolated as orange or yellow powders) Alternatively, in the green crystals the ethanol and water molecules coordinate the nickel ions in a 6-coordinate environment (6-coordinate species of Ni(II) have green colour).

The complex  $[\text{Co}_2(\text{H}_4\text{L1})(\text{H}_2\text{O})_3](\text{ClO}_4)_2 \cdot 3\text{EtOH}$  (2.6) was synthesised under nitrogen because it was found to slowly oxidise in solution. Once isolated as a dark yellow powder the complex seems stable. All six coordinating sites about the cobalt are occupied as there is no change in colour when the dark yellow powder is dissolved in ethanol. An ethanol solution of the dicobalt(II) complex, which was yellow at the beginning, immediately turned dark brown when some drops of  $\text{H}_2\text{O}_2$  were added, suggesting the Co(III) complex has formed (complex  $[\text{Co}_2(\text{HL1})](\text{ClO}_4)$  (2.18), see section 2.4.3.3 of this chapter). The same oxidation process occurs when a solution of the dicobalt(II) complex is left in air, although this process is slower, taking 5-10 minutes to see the colour change.

For the dicobalt(II) complex the expected  $\nu_3$  and  $\nu_4$  vibrations for the perchlorate anions are detected *ca.*  $1106 \text{ cm}^{-1}$  (broad band) and  $623 \text{ cm}^{-1}$ . The  $\nu_3$  vibration is not split, which indicates a symmetrical environment for the  $\text{ClO}_4^-$  ions. For the dinickel(II) complex, the  $\nu_3$  and  $\nu_4$  vibrations for the perchlorate anions are detected  $1107$  and  $624 \text{ cm}^{-1}$ . The complex  $[\text{Co}_2(\text{H}_4\text{L1})(\text{H}_2\text{O})_3](\text{BF}_4)_2 \cdot 2\text{H}_2\text{O}$  (2.7) was also synthesised under nitrogen to avoid the slow oxidation of the cobalt(II) ions. The expected  $\nu_3$  vibrations for the tetrafluoroborate anions are detected at  $1084$  and  $1055 \text{ cm}^{-1}$  as a broad band. The  $\nu_3$  vibration is split into two bands, which indicates an unsymmetrical environment for the  $\text{BF}_4^-$  ions.

In all three complexes, the LSIMS or ESI mass spectrometry data support the formation of dinuclear macrocyclic species. The divalent metal complexes show a peak corresponding to a singly charged ion containing the dimetallic fragment  $[\text{M}_2(\text{H}_4\text{L1})-\text{H}]^+$ . The ESI spectrum of the dinickel(II) complex  $[\text{Ni}_2(\text{H}_4\text{L1})(\text{H}_2\text{O})_3](\text{ClO}_4)_2 \cdot \text{H}_2\text{O}$  shows the main peak at  $m/z$  479, which can be assigned as the doubly charged fragment  $[\text{Ni}_2(\text{H}_4\text{L1}) - 2\text{H}]^{2+}$  (Table 2.10).



**Table 2.10:** Peak attributions for  $[\text{Ni}_2(\text{H}_4\text{L1})(\text{H}_2\text{O})_3](\text{ClO}_4)_2 \cdot \text{H}_2\text{O}$   
(ESI-MS relative abundance is given for cone voltage = 90V)

m/z	Rel. Intensity (%)	Fragments	Calc. Mass
451	30	$[\text{Ni}(\text{H}_6\text{L1}) - \text{H}]^{2+}$	902
479	100	$[\text{Ni}_2(\text{H}_4\text{L1}) - 2\text{H}]^{2+}$	958
901	<5	$[\text{Ni}(\text{H}_4\text{L1}) - \text{H}]^+$	901
959	40	$[\text{Ni}_2(\text{H}_4\text{L1}) - \text{H}]^+$	959
1059	15	$[\text{Ni}_2(\text{H}_4\text{L1})(\text{ClO}_4)]^+$	1059

The LSIMS spectrum of complex  $[\text{Co}_2(\text{H}_4\text{L1})(\text{H}_2\text{O})_3](\text{ClO}_4)_2 \cdot 3\text{EtOH}$  shows a major peak at m/z 1059 that can be assigned to the cation  $[\text{Co}_2(\text{H}_4\text{L1})(\text{ClO}_4) - \text{H}]^+$  and a smaller peak at m/z 959 that can be assigned to the cation  $[\text{Co}_2(\text{H}_4\text{L1}) - \text{H}]^+$ . The peak at m/z 1131 suggests the presence of coordinating water molecules in the complex, completing the coordinating sphere of the cobalt ions (Table 2.11, Fig 2.16).

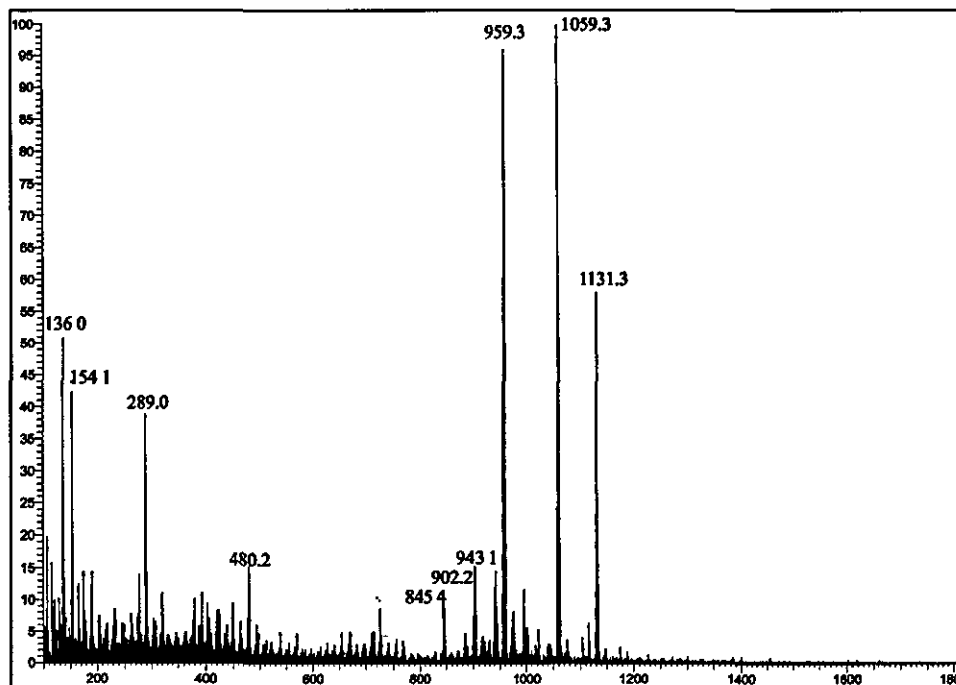


**Fig. 2.16:** LSIMS spectrum of  $[\text{Co}_2(\text{H}_4\text{L1})(\text{H}_2\text{O})_3](\text{ClO}_4)_2 \cdot 3\text{EtOH}$

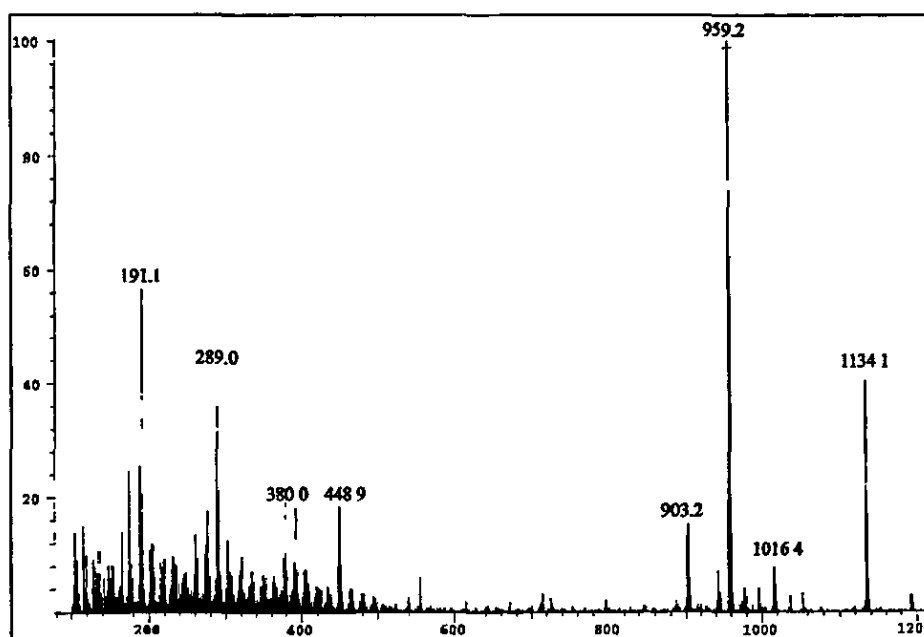
**Table 2.11:** Peak attributions for  $[\text{Co}_2(\text{H}_4\text{L1})(\text{H}_2\text{O})_3](\text{ClO}_4)_2 \cdot 3\text{EtOH}$ 

m/z	Rel. Intensity (%)	Fragments	Calc. Mass
902	15	$[\text{Co}(\text{H}_4\text{L1}) - \text{e}]^+$	902
943	14	$[\text{Co}(\text{H}_4\text{L1})(\text{H}_2\text{O}) + \text{Na}]^+$	943
959	95	$[\text{Co}_2(\text{H}_4\text{L1}) - \text{H}]^+$	959
1059	100	$[\text{Co}_2(\text{H}_4\text{L1})(\text{ClO}_4) - \text{H}]^+$	1059
1131	55	$[\text{Co}_2(\text{H}_4\text{L1})(\text{H}_2\text{O})_4(\text{ClO}_4) - \text{H}]^+$	1131

The LSIMS spectrum of complex  $[\text{Co}_2(\text{H}_4\text{L1})(\text{H}_2\text{O})_3](\text{BF}_4)_2 \cdot 2\text{H}_2\text{O}$  shows the main peak at m/z 959, assigned to the cation  $[\text{Co}_2(\text{H}_4\text{L1}) - \text{H}]^+$  (Table 2.12, Fig. 2.17). The peaks at m/z 1016 and 1134 suggest the presence of coordinating water and ethanol molecules in the complex, completing the coordinating sphere of the cobalt ions.

**Table 2.12:** Peak attributions for  $[\text{Co}_2(\text{H}_4\text{L1})(\text{H}_2\text{O})_3](\text{BF}_4)_2 \cdot 2\text{H}_2\text{O}$ 

m/z	Rel. Intensity (%)	Fragments	Calc. Mass
903	18	$[\text{Co}(\text{H}_4\text{L1}) + \text{H}]^+$	903
959	100	$[\text{Co}_2(\text{H}_4\text{L1}) - \text{H}]^+$	959
1016	10	$[\text{Co}_2(\text{H}_4\text{L1})(\text{H}_2\text{O})_3 + \text{H}]^+$	1016
1134	40	$[\text{Co}_2(\text{H}_4\text{L1})(\text{H}_2\text{O})_2(\text{EtOH})_3 - \text{H}]^+$	1134

**Fig. 2.17:** LSIMS spectrum of  $[\text{Co}_2(\text{H}_4\text{L1})(\text{H}_2\text{O})_3](\text{BF}_4)_2 \cdot 2\text{H}_2\text{O}$



#### 2.4.1.4. Structure of $[\text{Ni}_2(\text{H}_4\text{L1})(\text{H}_2\text{O})(\text{EtOH})_2](\text{ClO}_4)_2 \cdot 4\text{EtOH}$

Pale green crystals of  $[\text{Ni}_2(\text{H}_4\text{L1})(\text{H}_2\text{O})(\text{EtOH})_2](\text{ClO}_4)_2 \cdot 4\text{EtOH}$  (**2.5x**) suitable for X-ray studies were grown by slow evaporation of an ethanol solution of the dinickel(II) complex  $[\text{Ni}_2(\text{H}_4\text{L1})(\text{H}_2\text{O})_3](\text{ClO}_4)_2 \cdot \text{H}_2\text{O}$  (**2.5**). All the X-ray data collection parameters for the crystal structure are summarised in Table 3 of appendix 1 along with details concerning the refinement and disorder. Perspective views of the complex are shown in Figs. 2.18, 2.19 and 2.20 and selected bond lengths and angles relevant to the nickel coordination are given in Table 2.13.

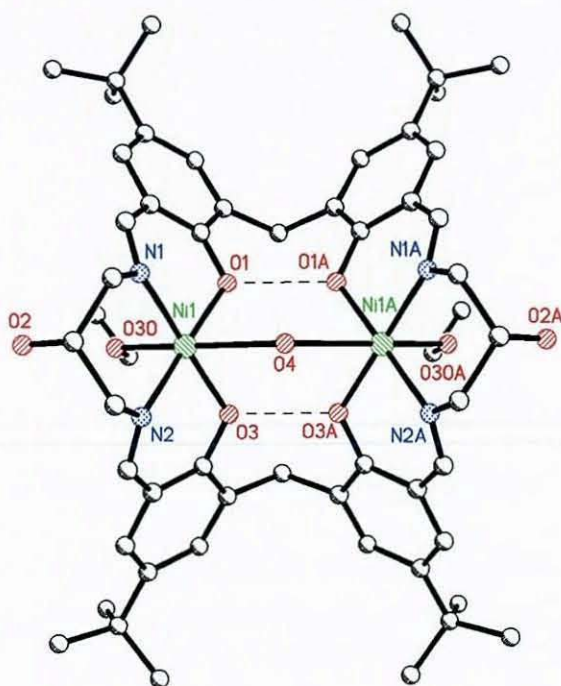


**Fig. 2.18:** Structure of the cation  $[\text{Ni}_2(\text{H}_4\text{L1})(\text{H}_2\text{O})(\text{EtOH})_2]^{2+}$

The crystal structure is very similar to the previous chloro bridged complexes, although in this cation the bridge has been replaced by water and the metal ions are six-coordinate. The additional ethanol ligands lie within the folds of the macrocycle and do not alter the overall shape of the macrocyclic cation. As demonstrated in Figs. 2.18 and 2.19, the structure is symmetric with a mirror plane passing through the saturated methylene carbons of each diphenol unit and the oxygen atom (O4) belonging to the bridging water molecule. The two nickel ions are each in a slightly distorted tetragonal environment, with the two phenol oxygen atoms and the two imine nitrogen atoms at the basal plane and the

bridging water and the ethanol molecules at the axial sites. The formula unit is completed by two lattice perchlorate anions and four ethanol lattice molecules, involved in hydrogen bonding to the macrocycle.

The pendant alcohol groups are not involved in bonding to the metal coordination sphere. Fig. 2.19 clearly shows that the hydroxy groups (both disordered positions O2 and O2') are pointing outside the cavity of the macrocycle.

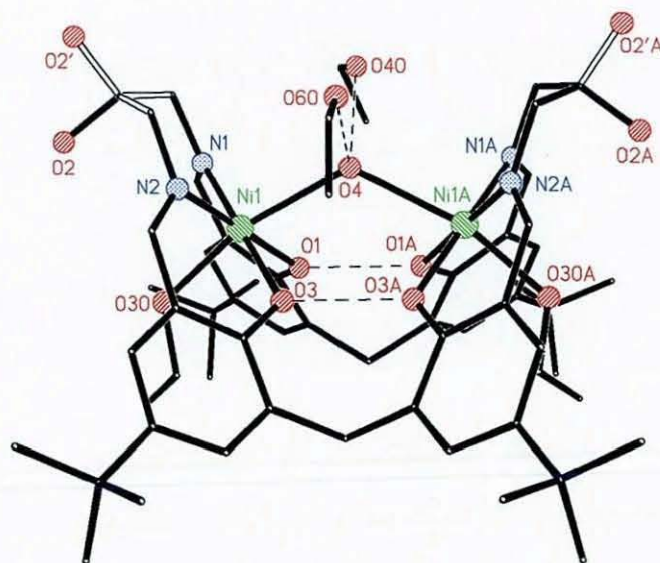


**Fig. 2.19:** Side-on view of the cation  $[\text{Ni}_2(\text{H}_4\text{L1})(\text{H}_2\text{O})(\text{EtOH})_2]^{2+} \cdot 2\text{EtOH}$  showing the pendant alcohol group disorder

**Table 2.13:** Selected bond lengths [ $\text{\AA}$ ] and angles [ $^\circ$ ] for  $[\text{Ni}_2(\text{H}_4\text{L1})(\text{H}_2\text{O})(\text{EtOH})_2](\text{ClO}_4)_2 \cdot 4\text{EtOH}$

Ni(1)-O(1)	1.994(3)	Ni(1)-N(1)	2.031(4)
Ni(1)-O(3)	2.012(3)	Ni(1)-O(30)	2.101(3)
Ni(1)-N(2)	2.025(4)	Ni(1)-O(4)	2.390(2)
O(1)-Ni(1)-O(3)	90.72(12)	N(2)-Ni(1)-O(30)	91.58(15)
O(1)-Ni(1)-N(2)	177.90(14)	N(1)-Ni(1)-O(30)	89.92(15)
O(3)-Ni(1)-N(2)	87.21(13)	O(1)-Ni(1)-O(4)	81.47(13)
O(1)-Ni(1)-N(1)	87.16(14)	O(3)-Ni(1)-O(4)	81.37(13)
O(3)-Ni(1)-N(1)	177.79(14)	N(2)-Ni(1)-O(4)	98.58(15)
N(2)-Ni(1)-N(1)	94.90(15)	N(1)-Ni(1)-O(4)	98.93(15)
O(1)-Ni(1)-O(30)	88.02(13)	O(30)-Ni(1)-O(4)	165.86(14)
O(3)-Ni(1)-O(30)	89.37(12)	Ni(1)-O(4)-Ni(1A)	123.9(2)

Symmetry transformations used to generate equivalent atoms: (A)  $x, -y+1/2, z$



As before, each 2,2'-methylenediphenol unit is monodeprotonated and the phenols are linked by short hydrogen bonds (O1...O1A 2.395(6) and O3...O3A 2.397(6) Å). The hydrogen atoms bonded to the methylenediphenol units were located and not further refined.

As shown in Figs. 2.19 and 2.20, the guest water molecule is hydrogen bonded to two ethanol solvate molecules (O4...O(ethanol) 2.707(8) and 2.718(7) Å) with one of the ethanol molecules hydrogen-bonded to one of the perchlorate ions. Considering this observation, there is at least one hydrogen on the bridging oxygen. Furthermore, the M-O distance (Ni(1)-O(4) 2.390(2) Å) would be too long for a bridging hydroxy group; therefore it can reasonably be assumed that the bridging unit is a water molecule.

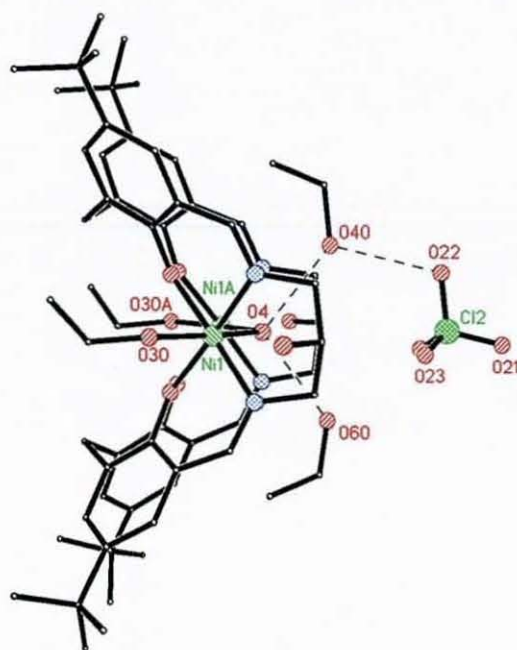


**Fig. 2.20:** Side-on view of the cation  $[\text{Ni}_2(\text{H}_4\text{L1})(\text{H}_2\text{O})(\text{EtOH})_2]^+ \cdot (\text{ClO}_4)^- \cdot 2\text{EtOH}$

Several studies<sup>79,80,120-124</sup> have reported a number of nickel complexes with aqua bridges where the metal-metal distance is controlled by other bridging groups. The mean M-OH<sub>2</sub> distance is 2.14 Å for nickel(II) and the range is 1.91-2.42 Å. It is also notable that the bridges with the longest Ni-OH<sub>2</sub> distances are unsymmetric with the second bond considerably shorter.<sup>79,80</sup>

In the nickel(II) structure described here, where the bridge has mirror symmetry, the Ni-OH<sub>2</sub> bonds are longer than those previously reported (Ni(1)-O(4) 2.389(2) Å) and also longer than the corresponding bonds to the coordinated ethanol molecules (Ni(1)-O(30) 2.099(3) Å). Examination of Fig. 2.19 shows that the Ni-OH<sub>2</sub> bonds are not perpendicular to the planes of the macrocyclic donors but inclined at an angle of *ca.* 77° and that the Ni-O(H<sub>2</sub>)-Ni angle has opened out to 123.9(2)°. Altogether, these observations suggest that the water is weakly bonded within the preformed cleft and therefore that the shape of the macrocycle is not enforced by the bridging group.

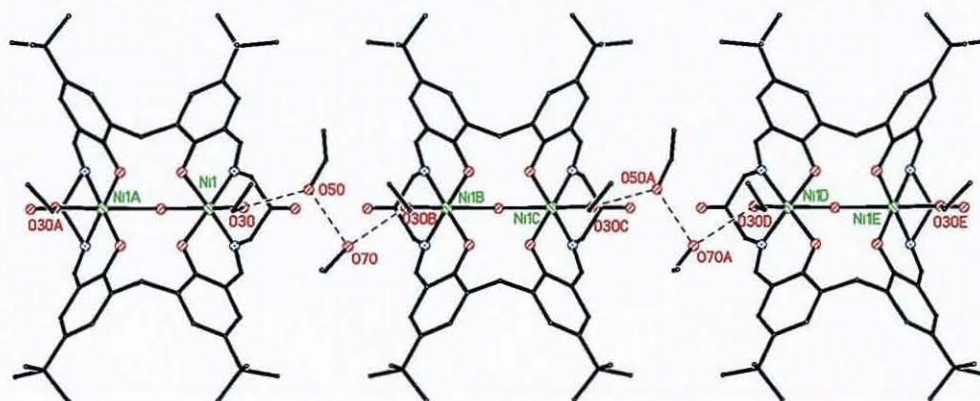


**Fig. 2.21:** H-bonding for  $[\text{Ni}_2(\text{H}_4\text{L1})(\text{H}_2\text{O})(\text{EtOH})_2]^{2+} \cdot 2\text{EtOH}$  forming chains.

Hydrogen bonding involving the two coordinated and two lattice ethanol molecules link the cations together, forming chains which run parallel to the *b* axis. The two other lattice ethanol molecules which are hydrogen bonded to the bridging water molecule (Figs. 2.19 and 2.20) have been omitted in the Figure 2.21 for clarity.

**Table 2.14:** Hydrogen bonds [Å] for  $[\text{Ni}_2(\text{H}_4\text{L1})(\text{H}_2\text{O})(\text{EtOH})_2](\text{ClO}_4)_2 \cdot 4\text{EtOH}$

D-H...A	d(D-H)	D(H...A)	d(D...A)
O(1)-H(1O)...O(1A)	1.22	1.22	2.394(6)
O(3)-H(3O)...O(3A)	1.22	1.22	2.397(6)
O(4)-H(4OA)...O(60)	0.85	1.87	2.718(7)
O(4)-H(4OB)...O(40)	0.86	1.85	2.702(8)
O(40)-H(40)...O(22)	0.81	2.05	2.850(9)
O(30)-H(30)...O(50)	0.85	1.78	2.632(10)
O(50)-H(50)...O(70)	0.86	1.85	2.705(14)
O(60)-H(60)...O(23)	0.99	2.32	3.155(9)
O(60)-H(60)...O(23A)	0.99	2.32	3.155(9)

Symmetry transformations used to generate equivalent atoms: (A)  $x, -y+1/2, z$



The analogous cobalt complex  $[\text{Co}_2(\text{H}_4\text{L1})(\text{H}_2\text{O})_3](\text{ClO}_4)_2 \cdot 3\text{EtOH}$  and the closely related complex  $[\text{Co}_2(\text{H}_4\text{L1})(\text{H}_2\text{O})_3](\text{BF}_4)_2 \cdot 2\text{H}_2\text{O}$  are likely to contain the same water bridged structure, with solvent molecules as sixth ligand to each cobalt ion. An analogous cobalt complex,  $[\text{Co}_2(\text{H}_4\text{L1})(\text{H}_2\text{O})(\text{EtOH})_2](\text{ClO}_4)_2 \cdot 4\text{EtOH}$ , was synthesised and characterised by S. Goetz.<sup>98</sup> The crystal structure of this cobalt complex is isomorphous with the nickel one here described.

#### 2.4.1.5. Synthesis and characterisation of $[\text{Ni}_2(\text{H}_4\text{L1})(\text{NO}_3)(\text{H}_2\text{O})_2](\text{NO}_3) \cdot \text{MeOH}$ , $[\text{Zn}_2(\text{H}_4\text{L1})(\text{NO}_3)(\text{H}_2\text{O})_2](\text{NO}_3) \cdot 3\text{H}_2\text{O}$ and $[\text{Co}_2(\text{H}_3\text{L1})(\text{NO}_3)] \cdot 5\text{H}_2\text{O}$

The complexes formed are similar to the previous dinuclear bridged complexes but this time with nitrate as counter anions. The nitrate ion vibration for the three complexes in the IR spectrum is indicative of both coordinated (*ca.* 1366 and *ca.* 1437  $\text{cm}^{-1}$ ) and free (1384  $\text{cm}^{-1}$ ) nitrate ions, which is consistent with the formula.

In the three complexes, the LSIMS data summarised in Tables 2.15, 2.16 and 2.17 reveal the formation of the dinuclear macrocyclic species. The divalent metal complexes show a peak corresponding to a singly charged ion containing the dimetallic fragment  $[\text{M}_2(\text{H}_4\text{L1})-\text{H}]^+$  or  $[\text{M}_2(\text{H}_4\text{L1})-2\text{H}]^+$ . For the nickel and zinc complexes the LSIMS does not provide supporting evidence of the presence of coordinating nitrate ions. However, the crystal structure reveals the presence of nitrate ions, as will be described further on in the discussion.

**Table 2.15:** Peak attributions for  $[\text{Ni}_2(\text{H}_4\text{L1})(\text{NO}_3)(\text{H}_2\text{O})_2](\text{NO}_3) \cdot \text{H}_2\text{O} \cdot \text{MeOH}$

m/z	Rel. Intensity (%)	Fragments	Calc. Mass
902	5	$[\text{Ni}(\text{H}_4\text{L1}) + \text{H}]^+$	902
942	9	$[\text{Ni}(\text{H}_4\text{L1})(\text{H}_2\text{O}) + \text{Na}]^+$	942
958	100	$[\text{Ni}_2(\text{H}_4\text{L1}) - 2\text{H}]^+$	958
980	7	$[\text{Ni}_2(\text{H}_4\text{L1})(\text{H}_2\text{O}) + 2\text{H}]^+$	980

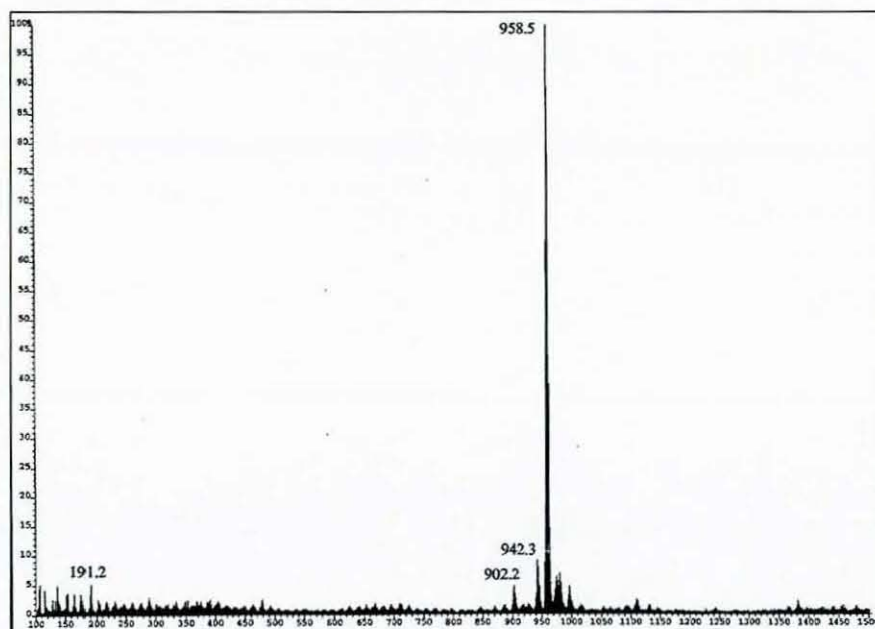


Fig. 2.22: LSIMS spectrum of  $[\text{Ni}_2(\text{H}_4\text{L1})(\text{NO}_3)(\text{H}_2\text{O})_2](\text{NO}_3)\cdot\text{H}_2\text{O}\cdot\text{MeOH}$

Table 2.16: Peak attributions for  $[\text{Zn}_2(\text{H}_4\text{L1})(\text{NO}_3)(\text{H}_2\text{O})_2](\text{NO}_3)\cdot 3\text{H}_2\text{O}$

m/z	Rel. Intensity (%)	Fragments	Calc. Mass
958	15	$[\text{Zn}(\text{H}_4\text{L1})(\text{EtOH}) + \text{H}]^+$	955
971	100	$[\text{Zn}_2(\text{H}_4\text{L1}) - 2\text{H}]^+$	971

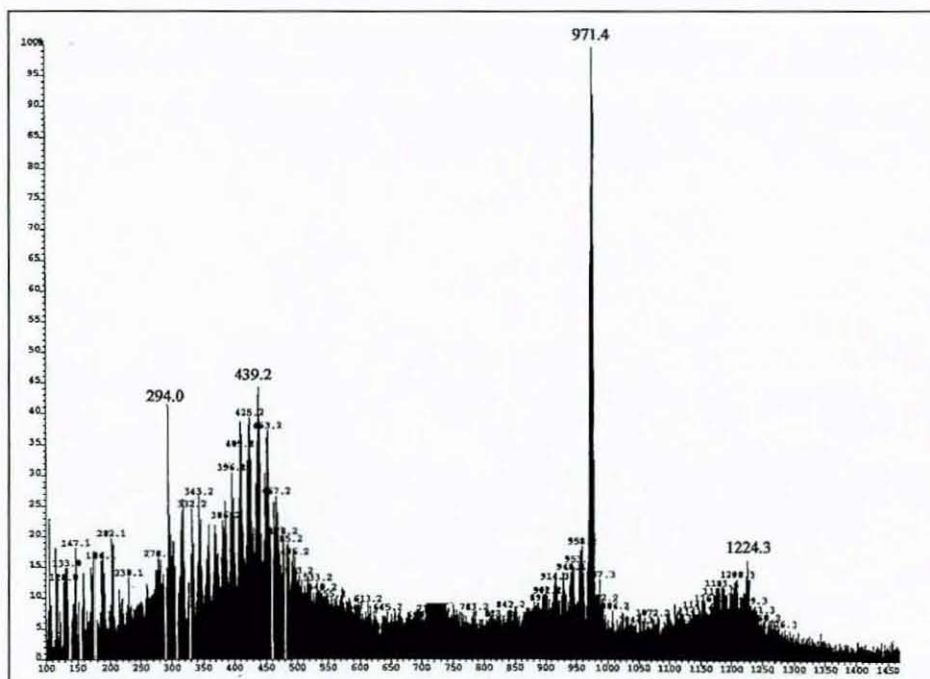


Fig. 2.23: LSIMS spectrum of  $[\text{Zn}_2(\text{H}_4\text{L1})(\text{NO}_3)(\text{H}_2\text{O})_2](\text{NO}_3)\cdot 3\text{H}_2\text{O}$



The LSIMS spectrum of the cobalt complex  $[\text{Co}_2(\text{H}_3\text{L1})(\text{NO}_3)] \cdot 5\text{H}_2\text{O}$  (**2.10**) shows the main peak corresponding to a singly charged ion containing the dimetallic fragment  $[\text{Co}_2(\text{H}_4\text{L1})-\text{H}]^+$  at  $m/z$  959. There is an indication of the presence of coordinating nitrate ions with the peaks at  $m/z$  1022 and 1079.

**Table 2.17:** Peak attributions for  $[\text{Co}_2(\text{H}_3\text{L1})(\text{NO}_3)] \cdot 5\text{H}_2\text{O}$

$m/z$	Rel. Intensity (%)	Fragments	Calc. Mass
902	11	$[\text{Co}(\text{H}_4\text{L1}) - \text{e}]^+$	902
959	33	$[\text{Co}_2(\text{H}_4\text{L1}) - \text{H}]^+$	959
1022	20	$[\text{Co}_2(\text{H}_4\text{L1})(\text{NO}_3)]^+$	1022
1079	7	$[\text{Co}_2(\text{H}_4\text{L1})(\text{NO}_3)(\text{H}_2\text{O})_3 + 2\text{H}]^+$	1079

The stoichiometry of the complexes, supported by the elemental analyses, shows that the metal ions are in the +II oxidation state and therefore that the macrocycle is again doubly deprotonated. The structure of the complexes is expected to be saddle-shaped again with intramolecular hydrogen-bonding between each monodeprotonated methylenediphenol group.

Interestingly, if an ethanol solution of the dizinc(II) complex  $[\text{Zn}_2(\text{H}_4\text{L1})(\text{NO}_3)(\text{H}_2\text{O})_2](\text{NO}_3) \cdot 3\text{H}_2\text{O}$  (**2.9**) is exposed to air for several days the nitrate ions appear to be slowly replaced by a carbonate anion, yielding a complex analysing as  $[\text{Zn}_2(\text{H}_4\text{L1})(\text{CO}_3)] \cdot 4\text{H}_2\text{O}$ . This reaction suggests the possibility of activating guest bound to the metal ions.

#### 2.4.1.6. Structures of $[\text{Ni}_2(\text{H}_4\text{L1})(\text{NO}_3)(\text{EtOH})_2](\text{NO}_3) \cdot 1.5\text{EtOH} \cdot \text{Et}_2\text{O} \cdot \text{H}_2\text{O}$ and $[\text{Zn}_2(\text{H}_4\text{L1})(\text{NO}_3)(\text{EtOH})](\text{NO}_3) \cdot \text{H}_2\text{O}$

The nitrato-bridged dinickel(II) and dizinc(II) structures of the complexes **2.8** and **2.9** are not isomorphous, unlike the two previous sets of bridged complexes, however they are similar. Again, they show short hydrogen bonds<sup>102-104</sup> across the monodeprotonated 2,2'-methylene-diphenol units and overall saddle conformation.

Green crystals of  $[\text{Ni}_2(\text{H}_4\text{L1})(\text{NO}_3)(\text{EtOH})_2]_2(\text{NO}_3) \cdot 1.5\text{EtOH} \cdot \text{Et}_2\text{O} \cdot \text{H}_2\text{O}$  (**2.8x**) suitable for X-ray studies were grown by slow diffusion of diethylether into an ethanol solution of  $[\text{Ni}_2(\text{H}_4\text{L1})(\text{NO}_3)(\text{H}_2\text{O})_2](\text{NO}_3) \cdot \text{H}_2\text{O} \cdot \text{MeOH}$  (**2.8**). All the X-ray data collection parameters are summarised in Table 4 of appendix 1 along with the details concerning the refinement and disorder. Perspective views of the complex are shown in Figs. 2.24 and 2.25 and selected bond lengths and angles relevant to the nickel coordination are given in Table 2.18. The asymmetric unit contains two equivalent molecules of  $[\text{Ni}_2(\text{H}_4\text{L1})(\text{NO}_3)(\text{EtOH})_2]^{2+}$ .

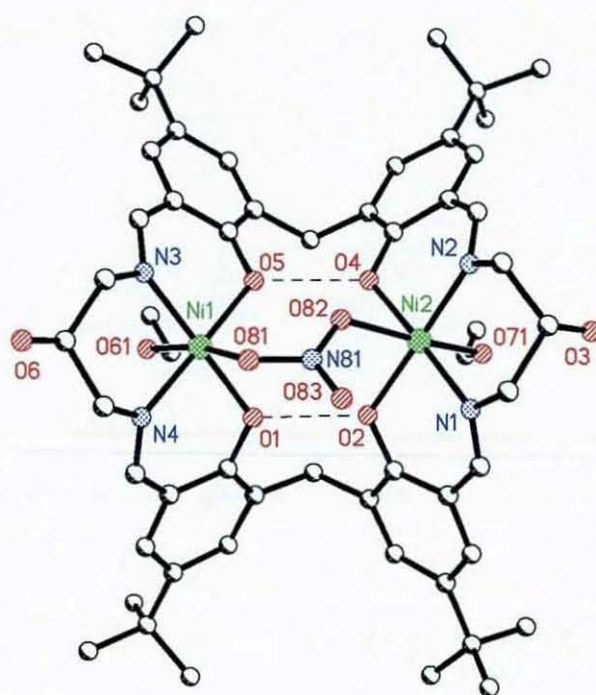


Fig. 2.24: Structure of the cation  $[\text{Ni}_2(\text{H}_4\text{L1})(\text{NO}_3)(\text{EtOH})_2]^{2+}$

The nitrate ion acts as a syn-anti-1,3-bridge with the mean plane of the nitrate ion inclined at ca.  $65^\circ$  with respect to the plane of Ni1A, Ni2A and O82A. The nickel ions are six-coordinate, the sixth ligand being an ethanol molecule in each case, and have quite regular geometry. The nickel ions are in a distorted octahedral environment, with an ethanol molecule and a bridging nitrate occupying the axial sites. The nitrate bridging unit is coordinated more strongly to the nickel ions (Ni(1A)-O(81A) 2.162(6) Å and Ni(2A)-O(82A) 2.090(7) Å) than was the bridging water molecule (Ni(1)-O(4) 2.389(2) Å) in the dinuclear complex  $[\text{Ni}_2(\text{H}_4\text{L1})(\text{H}_2\text{O})(\text{EtOH})_2](\text{ClO}_4)_2 \cdot 4\text{EtOH}$  (**2.5**).



**Table 2.18:** Selected bond lengths [ $\text{\AA}$ ] and angles [ $^\circ$ ] for  $[\text{Ni}_2(\text{H}_4\text{L1})(\text{NO}_3)(\text{EtOH})_2](\text{NO}_3) \cdot 1.5\text{EtOH} \cdot \text{Et}_2\text{O} \cdot \text{H}_2\text{O}$

Ni(1)-N(3)	2.025(7)	Ni(2)-O(4)	2.023(6)
Ni(1)-N(4)	2.030(7)	Ni(2)-N(1)	2.037(8)
Ni(1)-O(1)	2.032(6)	Ni(2)-O(2)	2.047(6)
Ni(1)-O(5)	2.059(6)	Ni(2)-O(82)	2.090(7)
Ni(1)-O(61)	2.117(6)	Ni(2)-O(71)	2.092(6)
Ni(1)-O(81)	2.162(6)	Ni(2)-Ni(1)	4.578(2)
Ni(2)-N(2)	2.001(7)		
<hr/>			
N(3)-Ni(1)-N(4)	93.5(3)	N(2)-Ni(2)-O(4)	87.8(2)
N(3)-Ni(1)-O(1)	177.8(3)	N(2)-Ni(2)-N(1)	95.1(3)
N(4)-Ni(1)-O(1)	88.1(3)	O(4)-Ni(2)-N(1)	177.1(3)
N(3)-Ni(1)-O(5)	87.9(3)	N(2)-Ni(2)-O(2)	177.4(3)
N(4)-Ni(1)-O(5)	176.5(3)	O(4)-Ni(2)-O(2)	89.7(2)
O(1)-Ni(1)-O(5)	90.4(2)	N(1)-Ni(2)-O(2)	87.4(3)
N(3)-Ni(1)-O(61)	91.0(3)	N(2)-Ni(2)-O(82)	90.6(3)
N(4)-Ni(1)-O(61)	91.6(3)	N(1)-Ni(2)-O(82)	100.8(3)
O(1)-Ni(1)-O(61)	87.4(2)	O(4)-Ni(2)-O(82)	79.2(2)
O(5)-Ni(1)-O(61)	85.2(2)	O(2)-Ni(2)-O(82)	88.4(3)
N(3)-Ni(1)-O(81)	91.7(3)	N(2)-Ni(2)-O(71)	92.0(3)
N(4)-Ni(1)-O(81)	79.3(3)	N(1)-Ni(2)-O(71)	89.5(3)
O(1)-Ni(1)-O(81)	90.1(2)	O(4)-Ni(2)-O(71)	90.3(2)
O(5)-Ni(1)-O(81)	103.9(3)	O(2)-Ni(2)-O(71)	88.5(2)
O(61)-Ni(1)-O(81)	170.6(2)	O(82)-Ni(2)-O(71)	169.1(3)

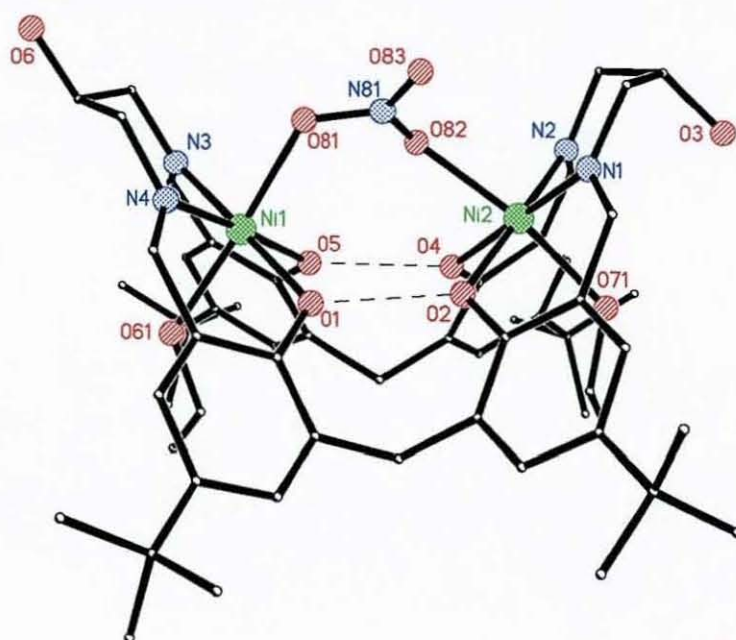


**Fig. 2.25:** Side-on view of the cation  $[\text{Ni}_2(\text{H}_4\text{L1})(\text{NO}_3)(\text{EtOH})_2]^{2+}$

The Ni-Ni distance is larger than for the aqua or chloro bridged analogues. It has expanded (4.5777(15) Å) to accommodate the longer syn-anti nitrate bridge, and the interplanar angle (ca. 83°) shows the cavity is a little more open. The two bonds linking the bridging unit to the nickel ions are of different lengths (Ni1A-O81A 2.1622(65) Å and Ni2A-O82A 2.0903(68) Å). Consequently, this insertion resulted in a loss of symmetry. The macrocycle is slightly twisted, and the two hydrogen bonds between adjacent phenol oxygen atoms are not parallel (Fig. 2.25). The values of the angle between the two phenyl rings of each DHTMB fragment are 72.08(26)° and 72.82(26)°.

Pale yellow crystals of  $[\text{Zn}_2(\text{H}_4\text{L1})(\text{NO}_3)(\text{EtOH})](\text{NO}_3)\cdot\text{H}_2\text{O}$  (**2.9x**) suitable for X-ray studies were grown by slow evaporation of an ethanol solution of the complex  $[\text{Zn}_2(\text{H}_4\text{L1})(\text{NO}_3)(\text{H}_2\text{O})_2](\text{NO}_3)\cdot 3\text{H}_2\text{O}$  (**2.9**). All the X-ray data collection parameters for the structure are summarised in Table 5 of appendix 1 along with the details concerning the refinement and disorder. A perspective view of the complex is shown in Fig. 2.26 and selected bond lengths and angles relevant to the zinc coordination are given in Table 2.19.

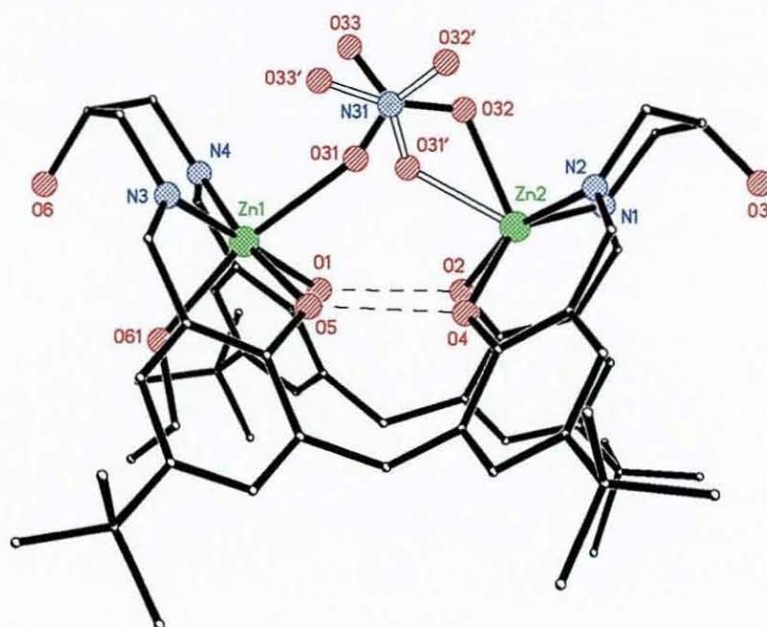


**Fig. 2.26:** Side-on view of the cation  $[\text{Zn}_2(\text{H}_4\text{L1})(\text{NO}_3)(\text{EtOH})]^+$

In the dizinc(II) cation one of the metal ions is six-coordinate, with ethanol as the sixth ligand, and the other is five-coordinate. The bound nitrate ion is disordered



and has been modelled with 60:40 occupancy of two positions, the major one is bound in the same way as the nitrate-bridged dinickel complex, but in the minor component is monodentate, coordinated only to the five-coordinate zinc ion (Zn2). Once again, the hydrogen atoms bonded to the methylenediphenol units were located and not further refined, and the hydrogen-bonded structure is consistent with loss of one proton from each methylenediphenol unit, resulting in a phenol-phenolate interaction.

**Table 2.19:** Selected bond lengths [ $\text{\AA}$ ] and angles [ $^\circ$ ] for  $[\text{Zn}_2(\text{H}_4\text{L1})(\text{NO}_3)(\text{EtOH})](\text{NO}_3)\cdot\text{H}_2\text{O}$

Zn(1)-O(1)	2.014(3)	Zn(2)-N(2)	2.065(3)
Zn(1)-N(4)	2.048(4)	Zn(2)-N(1)	2.071(3)
Zn(1)-N(3)	2.059(3)	Zn(2)-O(2)	2.108(3)
Zn(1)-O(5)	2.065(3)	Zn(2)-O(32)	2.104(7)
Zn(1)-O(61)	2.152(3)	Zn(2)-O(31')	2.025(10)
Zn(1)-O(31)	2.344(8)	Zn(1)-Zn(2)	4.4454(7)
Zn(2)-O(4)	1.999(3)		
O(1)-Zn(1)-N(4)	88.09(13)	O(4)-Zn(2)-N(2)	88.71(12)
O(1)-Zn(1)-N(3)	174.35(13)	O(4)-Zn(2)-N(1)	145.05(12)
N(4)-Zn(1)-N(3)	97.54(14)	N(2)-Zn(2)-N(1)	90.78(13)
O(1)-Zn(1)-O(5)	88.44(11)	O(4)-Zn(2)-O(2)	86.42(11)
N(4)-Zn(1)-O(5)	171.73(13)	N(2)-Zn(2)-O(2)	163.70(12)
N(3)-Zn(1)-O(5)	85.92(12)	N(1)-Zn(2)-O(2)	84.40(11)
O(1)-Zn(1)-O(61)	90.87(12)	O(4)-Zn(2)-O(32)	123.7(2)
O(5)-Zn(1)-O(61)	92.72(11)	O(2)-Zn(2)-O(32)	100.1(2)
N(4)-Zn(1)-O(61)	94.84(14)	N(1)-Zn(2)-O(32)	91.2(2)
N(3)-Zn(1)-O(61)	89.17(12)	N(2)-Zn(2)-O(32)	95.5(2)
O(1)-Zn(1)-O(31)	86.7(3)	O(4)-Zn(2)-O(31')	92.5(5)
O(5)-Zn(1)-O(31)	71.66(19)	O(2)-Zn(2)-O(31')	77.5(3)
N(4)-Zn(1)-O(31)	100.6(2)	N(1)-Zn(2)-O(31')	118.1(4)
N(3)-Zn(1)-O(31)	91.7(3)	N(2)-Zn(2)-O(31')	118.3(3)
O(61)-Zn(1)-O(31)	164.2(2)	O(32)-Zn(2)-O(31')	37.6(4)

**Table 2.20:** Hydrogen bonds [ $\text{\AA}$ ] for  $[\text{Zn}_2(\text{H}_4\text{L1})(\text{NO}_3)(\text{EtOH})](\text{NO}_3)\cdot\text{H}_2\text{O}$

D-H...A	d(D-H)	D(H...A)	d(D...A)
O(1)-H(1)...O(2)	1.09	1.34	2.426(4)
O(4)-H(4)...O(5)	0.98	1.51	2.480(3)
O(6)-H(6)...O(22)	1.11	1.54	2.650(5)
O(6)-H(6)...O(21)	1.11	2.53	3.282(6)
O(61)-H(61)...O(21)	0.94	1.85	2.794(5)

The cations are linked into chains by hydrogen bonding involving the pendant alcohols, the uncoordinated nitrate anion and the coordinated ethanol molecule. The water solvate molecules lie in the channels between the cations (Fig. 2.27).

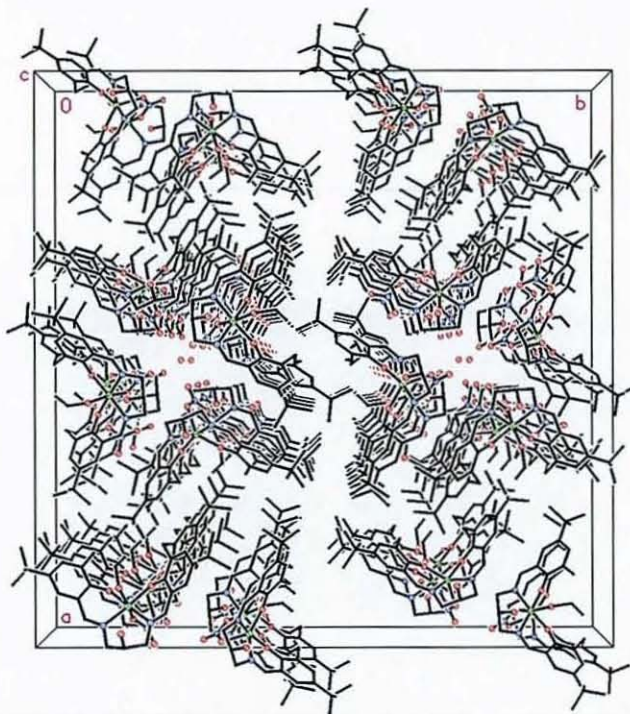


**Fig. 2.27:** Packing diagram for  $[\text{Zn}_2(\text{H}_4\text{L1})(\text{NO}_3)(\text{EtOH})](\text{NO}_3)\cdot\text{H}_2\text{O}$

The related cobalt complex  $[\text{Co}_2(\text{H}_4\text{L1})(\text{NO}_3)](\text{OH})\cdot 4\text{H}_2\text{O}$  has been prepared but not crystallized. On the basis of analytical and mass spectral data is likely to contain the same nitrate bridged structure, probably with one of the pendant alcohol groups deprotonated and coordinating the cobalt centre of another macrocyclic unit.

#### 2.4.1.7. Synthesis and characterisation of $[\text{Zn}_2(\text{H}_4\text{L1})(\text{AcO})](\text{AcO})\cdot 5\text{H}_2\text{O}$

Complex  $[\text{Zn}_2(\text{H}_4\text{L1})(\text{AcO})](\text{AcO})\cdot 5\text{H}_2\text{O}$  (**2.11**) is similar to the previous dinuclear bridged complexes but this time with acetate as counter anions. It was first isolated in our attempts to synthesise the heteronuclear zinc(II) complex of  $\text{H}_6\text{L1}$  with sodium (see Chapter 4). A strong band at  $1430\text{ cm}^{-1}$  in the IR spectrum can be assigned to the acetate symmetric vibration. The asymmetric vibration of



the acetate anions is a strong band at  $1563\text{ cm}^{-1}$ . The separation between the symmetric and asymmetric vibrations of the acetate anions is *ca.*  $130\text{ cm}^{-1}$ , which according to Deacon *et al.*<sup>125</sup> would suggest that the acetate anions are likely to adopt a chelating or bridging coordination mode; this is confirmed by crystallography. The LSIMS data (Fig. 2.28, Table 2.21) support the formation of the dinuclear macrocyclic species and also shows the presence of acetate ions.

**Table 2.21:** Peak attributions for  $[\text{Zn}_2(\text{H}_4\text{L1})(\text{AcO})](\text{AcO})\cdot 5\text{H}_2\text{O}$

m/z	Rel. Intensity (%)	Fragments	Calc. Mass
971	100	$[\text{Zn}_2(\text{H}_4\text{L1}) - 2\text{H}]^+$	971
1033	40	$[\text{Zn}_2(\text{H}_4\text{L1})(\text{AcO})]^+$	1033
1095	20	$[\text{Zn}_2(\text{H}_4\text{L1})(\text{AcO})_2 + \text{H}]^+$	1093

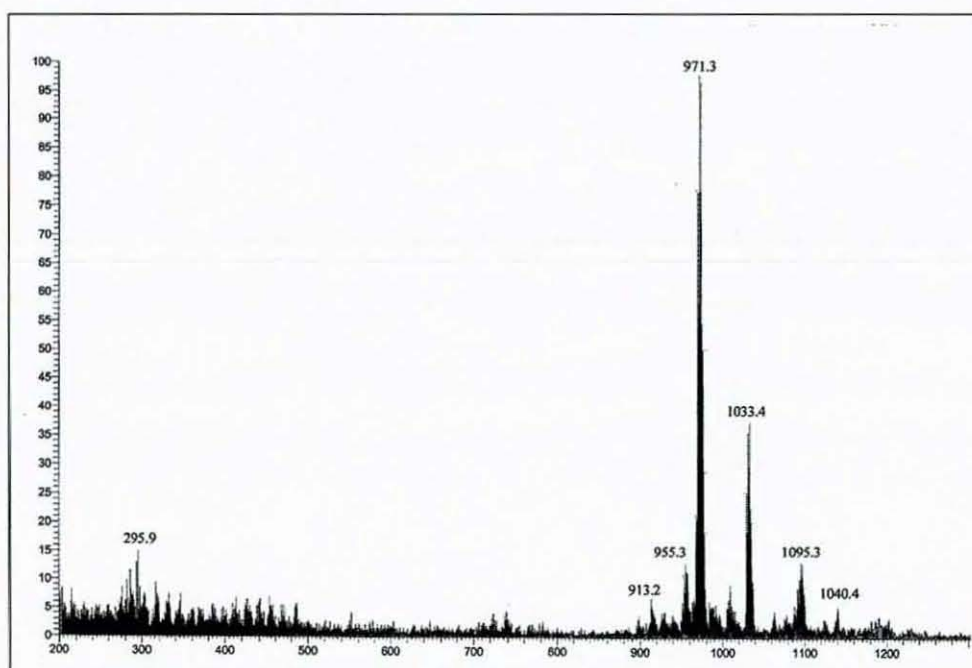


**Fig. 2.28:** LSIMS spectrum of  $[\text{Zn}_2(\text{H}_4\text{L1})(\text{AcO})](\text{AcO})\cdot 5\text{H}_2\text{O}$

#### 2.4.1.8. Structure of $[\text{Zn}_2(\text{H}_4\text{L1})(\text{AcO})](\text{AcO})\cdot 5\text{H}_2\text{O}\cdot 4\text{Et}_2\text{O}$

Pale yellow crystals of  $[\text{Zn}_2(\text{H}_4\text{L1})(\text{AcO})](\text{AcO})\cdot 5\text{H}_2\text{O}\cdot 4\text{Et}_2\text{O}$  (**2.11x**) were grown by slow diffusion of diethylether into an ethanol solution of the dizinc(II) complex  $[\text{Zn}_2(\text{H}_4\text{L1})(\text{AcO})](\text{AcO})\cdot 5\text{H}_2\text{O}$  (**2.11**). Perspective views of the cation

$[\text{Zn}_2(\text{H}_4\text{L1})(\text{AcO})]^+$  are shown in Figs. 2.29 and 2.30 and selected bond lengths and angles relevant to the metal ion coordination are given in Table 2.22. The structure of this dizinc complex resembles the previous bridged dinuclear complexes again showing hydrogen bonds across the monodeprotonated 2,2'-methylenediphenol units and the overall saddle conformation.

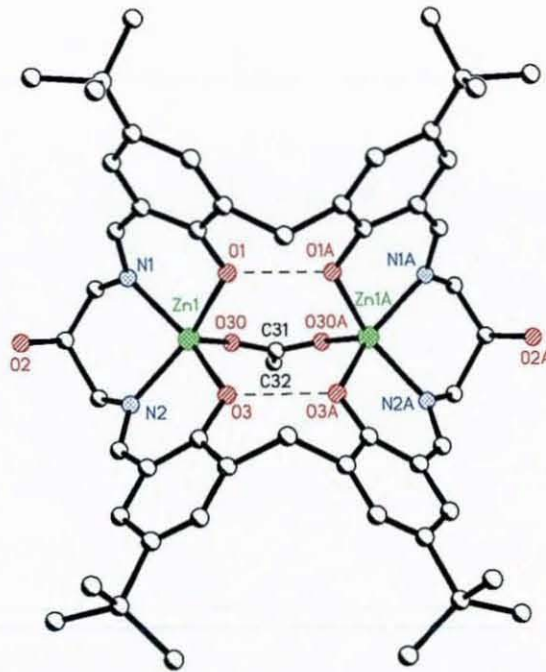


**Fig. 2.29:** Structure of the cation  $[\text{Zn}_2(\text{H}_4\text{L1})(\text{AcO})]^+$

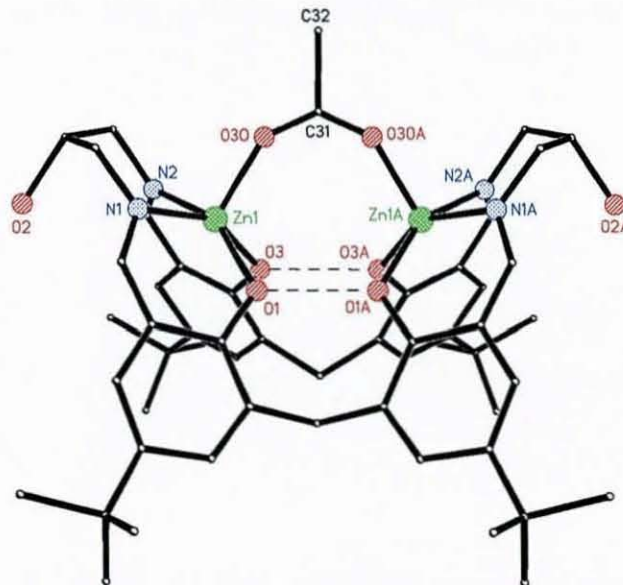


**Fig. 2.30:** Side-on view of cation  $[\text{Zn}_2(\text{H}_4\text{L1})(\text{AcO})]^+$

The crystals studied were not very good. Poor quality crystalline material will give rise to broader more diffuse diffraction peaks. This decreases the quality and resolution of the X-ray data and, consequently, the accuracy of the atomic positions. All the X-ray data collection parameters are summarised in Table 6 of appendix 1 along with the details concerning the refinement and disorder.

As demonstrated in Figs. 2.29 and 2.30, the cation is symmetric with a mirror plane passing through the two methylene carbons in between each pair of phenols and through the carbons of the bridging acetate ion (C31 and C32). The pendant alcohol groups are not involved in bonding to the zinc metals and are clearly pointing outside the cavity of the macrocycle. The zinc(II) ions are five-coordinate each bonded to two imine nitrogen atoms and two endogenous phenolate oxygen atoms. The coordination sphere is completed by a central acetate donor, which bridges the two metals. The geometry about the zinc ions is square pyramidal with the bridging acetate at the axial site. The formula unit is completed by lattice ethanol and water molecules and one acetate counter anion.

**Table 2.22:** Selected bond lengths [ $\text{\AA}$ ] and angles [ $^\circ$ ] for  $[\text{Zn}_2(\text{H}_4\text{L1})(\text{AcO})](\text{AcO}) \cdot 5\text{H}_2\text{O} \cdot 4\text{Et}_2\text{O}$

Zn(1)-O(30)	1.967(7)	Zn(1)-N(2)	2.047(10)
Zn(1)-O(3)	2.017(7)	Zn(1)-N(1)	2.098(10)
Zn(1)-O(1)	2.037(6)		
O(30)-Zn(1)-O(3)	108.1(3)	O(1)-Zn(1)-N(2)	154.0(3)
O(30)-Zn(1)-O(1)	106.8(3)	O(30)-Zn(1)-N(1)	100.7(4)
O(3)-Zn(1)-O(1)	85.0(3)	O(3)-Zn(1)-N(1)	151.1(3)
O(30)-Zn(1)-N(2)	99.2(4)	O(1)-Zn(1)-N(1)	84.9(3)
O(3)-Zn(1)-N(2)	85.7(3)	N(2)-Zn(1)-N(1)	91.7(4)



### 2.4.1.9. Synthesis and characterisation of $[\text{Ni}_2(\text{H}_4\text{L1})(\text{MeOH})_2](\text{ClO}_4)_2 \cdot \text{MeOH}$

The complex  $[\text{Ni}_2(\text{H}_4\text{L1})(\text{MeOH})_2](\text{ClO}_4)_2 \cdot \text{MeOH}$  (**2.12**) represents the exception to the series of dinuclear complexes just described. In this case, the complex does not contain an exogenous ligand bridging the two metal ions, although the topology of this complex is very similar to the previous dinickel bridged complexes, showing again the saddle-shaped conformation.

The LSIMS data (Fig. 2.31, Table 2.23) suggest the formation of the dinuclear macrocyclic species. The main peak corresponds to a singly charged ion containing the dimetallic fragment  $[\text{Ni}_2(\text{H}_4\text{L1})-\text{H}]^+$  at  $m/z$  959. The presence of the perchlorate anions in this complex is proved by the peak at  $m/z$  1059.

**Table 2.23:** Peak attributions for  $[\text{Ni}_2(\text{H}_4\text{L1})(\text{MeOH})_2](\text{ClO}_4)_2 \cdot \text{MeOH}$

$m/z$	Rel. Intensity (%)	Fragments	Calc. Mass
901	15	$[\text{Ni}(\text{H}_4\text{L1})-\text{e}]^+$	901
941	13	$[\text{Ni}(\text{H}_4\text{L1})(\text{H}_2\text{O})_2 + \text{Na}]^+$	942
957	100	$[\text{Ni}_2(\text{H}_4\text{L1})-\text{H}]^+$	959
1059	5	$[\text{Ni}_2(\text{H}_4\text{L1})(\text{ClO}_4)]^+$	1059

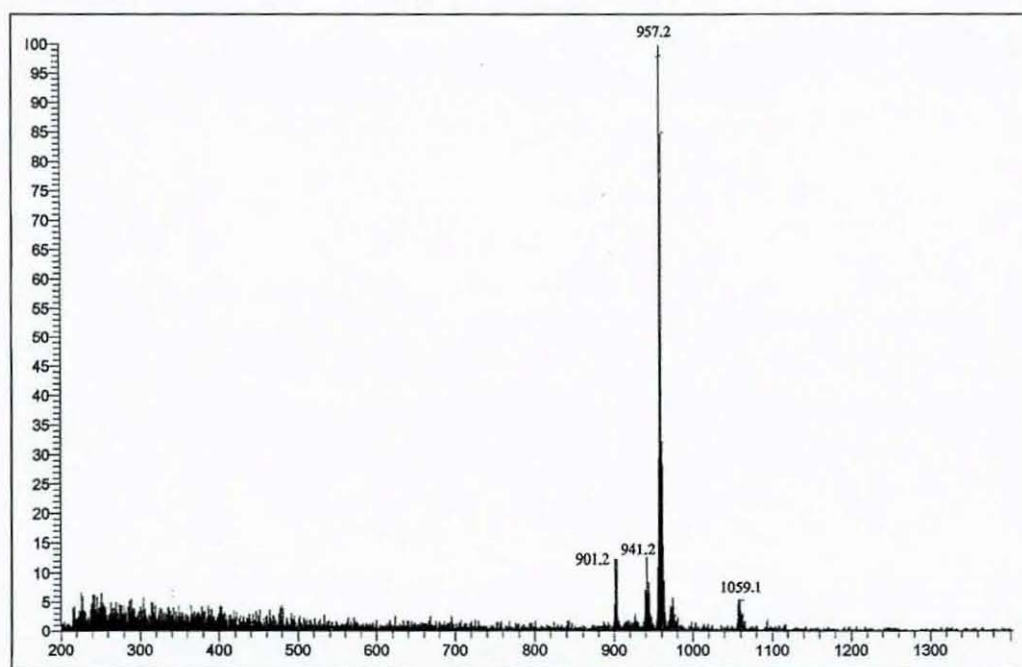


**Fig. 2.31:** LSIMS spectrum of  $[\text{Ni}_2(\text{H}_4\text{L1})(\text{MeOH})_2](\text{ClO}_4)_2 \cdot \text{MeOH}$



#### 2.4.1.10. Structure of $[\text{Ni}_2(\text{H}_4\text{L1})(\text{MeOH})_2](\text{ClO}_4)_2 \cdot \text{Et}_2\text{O} \cdot 1.5\text{MeOH} \cdot 0.5\text{EtOH}$

The complex  $[\text{Ni}_2(\text{H}_4\text{L1})(\text{MeOH})_2](\text{ClO}_4)_2 \cdot \text{MeOH}$  (**2.12**) was dissolved in methanol and left to evaporate slowly. After few days green crystals were formed. These green crystals could be the nickel(II) complex with water bridging (previously obtained for the dinickel(II) complex **2.5x**,  $[\text{Ni}_2(\text{H}_4\text{L1})(\text{H}_2\text{O})(\text{EtOH})_2](\text{ClO}_4)_2 \cdot 4\text{EtOH}$ ). When the green crystals were filtered and dried a red-orange powder was obtained (the solvate molecules were lost). This orange solid was dissolved again in methanol and diethylether was allowed to slowly diffuse into the green solution. Red crystals of  $[\text{Ni}_2(\text{H}_4\text{L1})(\text{MeOH})_2](\text{ClO}_4)_2 \cdot \text{Et}_2\text{O} \cdot 1.5\text{MeOH} \cdot 0.5\text{EtOH}$  (**2.12x**) suitable for X-ray studies were isolated within few days. The isolation of the red crystals was reproducible but only when green crystals were grown, filtered, dried and recrystallised by ether diffusion into a methanol solution. A possible explanation for this could be that by filtering the crystals from the mother liquor, water molecules and impurities present in the sample are being eliminated. The filtered sample is purer and the complex without water bridging molecule crystallises out.

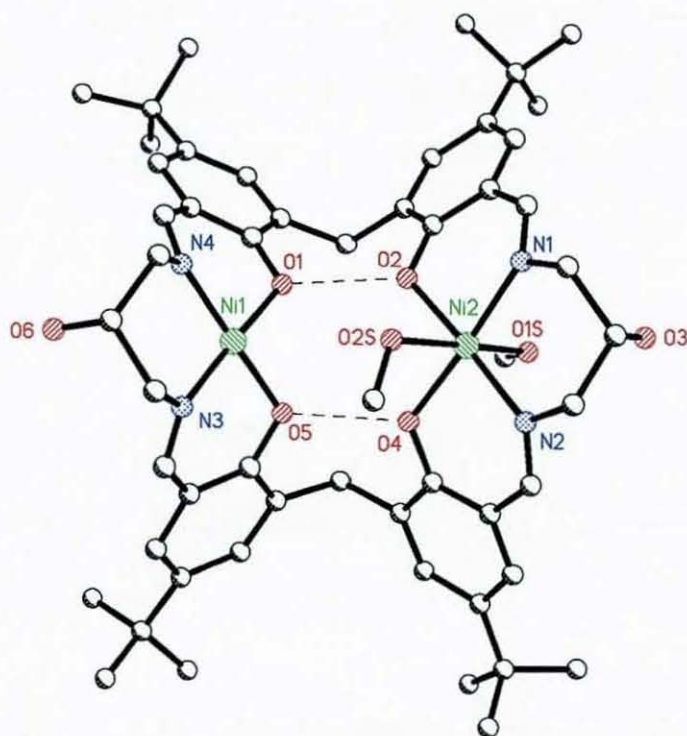
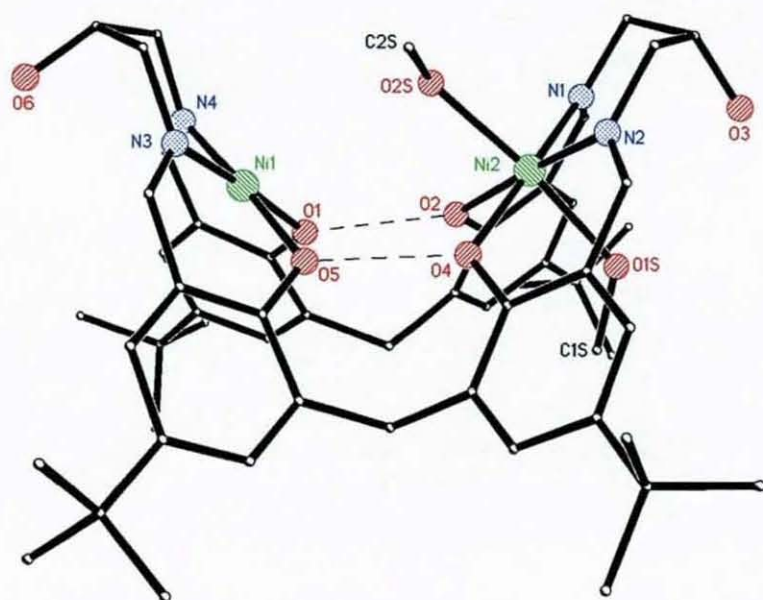


Fig. 2.32: Structure of the cation  $[\text{Ni}_2(\text{H}_4\text{L1})(\text{MeOH})_2]^{2+}$

All the X-ray data collection parameters for the crystal structure of  $[\text{Ni}_2(\text{H}_4\text{L1})(\text{MeOH})_2](\text{ClO}_4)_2 \cdot \text{Et}_2\text{O} \cdot 1.5\text{MeOH} \cdot 0.5\text{EtOH}$  are summarised in Table 7 of appendix 1 along with the details concerning the refinement and disorder. Perspective views of the complex are shown in Figs. 2.32 and 2.33 and selected bond lengths and angles relevant to the nickel coordination are given in Table 2.24.

Overall, the cation is very similar to the previous water bridged nickel(II) complex  $[\text{Ni}_2(\text{H}_4\text{L1})(\text{H}_2\text{O})(\text{EtOH})_2](\text{ClO}_4)_2 \cdot 4\text{EtOH}$ , showing the same saddle-shaped conformation, although there is now no exogenous ligand bridging the two metal ions. The distance from the nickel ion (Ni1) to the oxygen atom of the coordinated methanol molecule (O2S) is too long to represent a bond (Ni(1)-O(2S) 3.355(4) Å) therefore it can be concluded that the methanol molecule is not bridging both nickel ions but just coordinating the nickel ion Ni2 (illustrated in Figs. 2.32 and 2.33). This evidence confirms that the folded geometry adopted by the macrocycle is due to the hydrogen bonding links and not to the bridging groups. As before, each 2,2'-methylenediphenol unit is monodeprotonated and the phenols are linked by short<sup>102-104</sup> hydrogen bonds (O1...O2 2.432(5) and O4...O5 2.483(5) Å).



**Fig. 2.33:** Side-on view of the cation  $[\text{Ni}_2(\text{H}_4\text{L1})(\text{MeOH})_2]^{2+}$

Each nickel ion is bound by an identical set of macrocycle donors yet adopts differing stereochemistry. Ni1 is four-coordinate, with two imine nitrogen atoms and two endogenous phenolate oxygen atoms at the plane, presenting square planar geometry. While Ni2 is six-coordinate, it has identical macrocyclic donors in the plane of the chelating ligand and the coordination sphere is completed by two methanol molecules. The geometry at Ni2 is octahedral, with the two phenolic oxygen and the two imine nitrogen atoms at the basal plane, and two methanol molecules at the axial sites. The Ni-Ni distance (4.4830(8) Å) is larger than for the bridged analogues and the interplanar angle (86.53(9)°) shows the cavity a little more open. The angles between the two phenyl rings of each methylenediphenol fragment are 67.55(11)° and 72.82(11)°.

The simultaneous presence of four and six-coordinate nickel(II) ions in this complex deserves a comment. Combination of two centres in different spin states, especially with the macrocycle providing potentially identical metal-binding environments, is of great interest because of the rarity of such species.<sup>126-133</sup> Two different geometries were observed for the nickel(II) ions, specifically N<sub>2</sub>O<sub>4</sub> octahedral and N<sub>2</sub>O<sub>2</sub> square planar

Bonds between the macrocycle donors and the square-planar nickel ion (Ni1) are shorter, by 0.14-0.18 Å, than those to the octahedral nickel ion (Ni2). This is consistent with the observed difference in geometry. Since four-coordinate square planar nickel(II) complexes are low-spin, and six-coordinate octahedral nickel(II) derivatives are high-spin,<sup>134</sup> the 3d(x<sup>2</sup>-y<sup>2</sup>) orbital which is unpopulated in Ni1 will be singly populated in Ni2. Since this 3d(x<sup>2</sup>-y<sup>2</sup>) orbital is antibonding, the change in the spin state of the nickel(II) ions will affect the metal-ligand bond lengths, and thus it will be different for each nickel ion. Accordingly, an expansion of the chelating ligand core must take place, leading to Ni-N and Ni-O bond distances which become longer in Ni1 than in Ni2.<sup>126-133</sup>

**Table 2.24:** Selected bond lengths [Å] and angles [°] for  
 $[\text{Ni}_2(\text{H}_4\text{L1})(\text{MeOH})_2](\text{ClO}_4)_2 \cdot \text{Et}_2\text{O} \cdot 1.5\text{MeOH} \cdot 0.5\text{EtOH}$

Ni(1)-O(1)	1.865(3)	Ni(2)-O(4)	2.033(3)
Ni(1)-O(5)	1.869(3)	Ni(2)-N(2)	2.031(4)
Ni(1)-N(4)	1.883(4)	Ni(2)-O(2)	2.048(3)
Ni(1)-N(3)	1.881(4)	Ni(2)-O(2S)	2.078(4)
Ni(2)-N(1)	2.022(5)	Ni(2)-O(1S)	2.091(4)
Ni(1)-Ni(2)	4.483(1)	O(1)-O(2)	2.473(5)
Ni(1)-O(2S)	3.355(4)	O(4)-O(5)	2.483(5)
O(1)-Ni(1)-O(5)	86.50(14)	N(2)-Ni(2)-O(2)	174.75(15)
O(1)-Ni(1)-N(4)	90.27(16)	N(1)-Ni(2)-O(2S)	93.51(19)
O(5)-Ni(1)-N(4)	175.62(17)	O(4)-Ni(2)-O(2S)	86.89(14)
O(1)-Ni(1)-N(3)	175.65(16)	N(2)-Ni(2)-O(2S)	94.20(18)
O(5)-Ni(1)-N(3)	90.02(16)	O(2)-Ni(2)-O(2S)	87.40(15)
N(4)-Ni(1)-N(3)	93.06(17)	N(1)-Ni(2)-O(1S)	90.72(18)
N(1)-Ni(2)-O(4)	174.52(17)	O(4)-Ni(2)-O(1S)	88.46(14)
N(1)-Ni(2)-N(2)	98.38(18)	N(2)-Ni(2)-O(1S)	89.69(17)
O(4)-Ni(2)-N(2)	87.04(15)	O(2)-Ni(2)-O(1S)	88.30(14)
N(1)-Ni(2)-O(2)	86.49(16)	O(2S)-Ni(2)-O(1S)	173.77(15)
O(4)-Ni(2)-O(2)	88.06(13)		

A possible explanation for the formation of this complex could be described by studying the crystallographic results. The structure determination of the cation  $[\text{Ni}_2(\text{H}_4\text{L1})(\text{MeOH})_2]^{2+}$  reveals that the two nickel(II) ions have differing environments despite the fact that the macrocycle is capable of providing identical  $\text{N}_2\text{O}_2$  binding sites. When water molecules are present in the crystallisation solvents, the green complex formed is the one with a water molecule occupying the preformed macrocyclic cleft and bridging the two nickel ions (see section 2.4.1.4). Isolation of the green crystals, subsequent elimination of the water molecules by drying, and recrystallisation of the anhydrous complex by diffusion of diethylether into a methanol solution yields red crystals of the dinickel(II) complex  $[\text{Ni}_2(\text{H}_4\text{L1})(\text{MeOH})_2](\text{ClO}_4)_2 \cdot \text{Et}_2\text{O} \cdot 1.5\text{MeOH} \cdot 0.5\text{EtOH}$  with no water molecules present in the crystal structure. For both nickel ions to adopt 6-coordinate geometry there are two possibilities. First, the complex having one methanol molecule bridging both metal centres and further methanol molecules completing the coordination sphere for each nickel ion. The methanol molecule coordinated to one of the nickel ions in the cation  $[\text{Ni}_2(\text{H}_4\text{L1})(\text{MeOH})_2]^{2+}$  is not bridging the nickel centres (distance between the methanol oxygen and the nickel

not coordinated is too long). The other possibility would be each nickel ion having two methanol molecules as the axial ligands. It seems that the 4-coordinate nickel ion (Ni1) adopts this coordination number because there is not enough space in the macrocyclic cavity for both nickel ions to coordinate a methanol molecule on the concave side (Fig 2.33). It seems that the dinuclear macrocycle provides an intermediate ligand field strength which results in both geometries being present in the nickel complex.

#### 2.4.1.11. Magnetic behaviour of $[\text{Ni}_2(\text{H}_4\text{L1})(\text{MeOH})_2](\text{ClO}_4)_2 \cdot \text{MeOH}$

Variable temperature magnetic measurements were carried out by Dr. C. J. Harding for the complex  $[\text{Ni}_2(\text{H}_4\text{L1})(\text{MeOH})_2](\text{ClO}_4)_2 \cdot \text{MeOH}$  in the temperature range of 275 to 75 K.

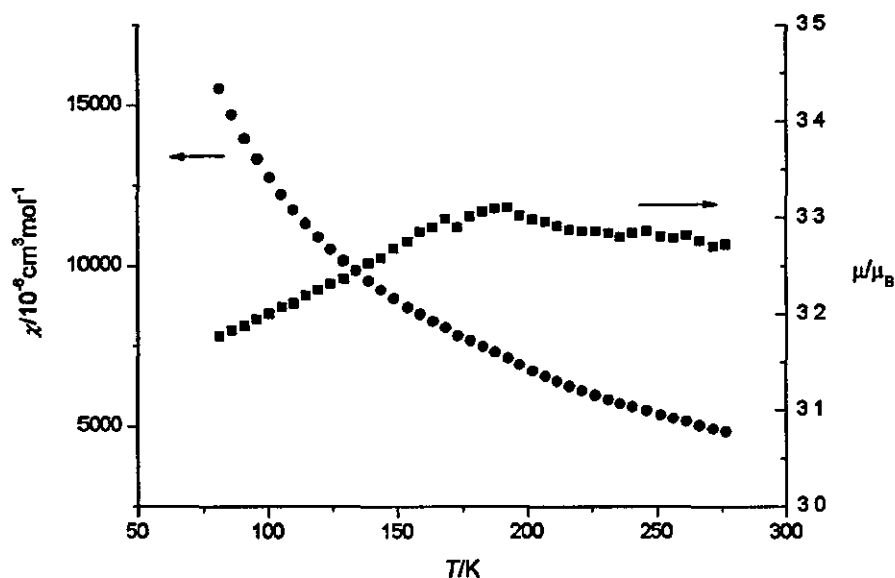


Fig. 2.34: Experimental temperature dependence of  $\chi_M$  (●) and  $\mu$  (■) per Ni, for  $[\text{Ni}_2(\text{H}_4\text{L1})(\text{MeOH})_2](\text{ClO}_4)_2 \cdot \text{MeOH}$

The values of molecular magnetic susceptibility ( $\chi_M$ ) increase steadily from 3.08 to 3.45 B.M. on decreasing the temperature from 300 to 75 K (Fig. 2.34). These values are expected for high-spin Ni(II) in an octahedral environment. The complex shows paramagnetism ( $\mu \sim 3.2$  B.M.) typical of one octahedral nickel(II) ion, consistent with the structure, which also has one square planar nickel(II) ion, presumably diamagnetic (the effect of paramagnetism is about 100 times greater



that that of diamagnetism)<sup>135,136</sup> These results indicate that the two nickel ions behave in an essentially independent manner. This is not surprising since there is no ligand bridging the nickel ions. The effective magnetic moment should be independent of the temperature yet there is a strange temperature dependence at the high temperature end of the scale, which is reproducible and not very large

The temperature dependence of the magnetic susceptibility ( $\chi_M$ ) for the complex is displayed in Figure 2 34 in the form of a  $\chi_M$  vs. T plot ( $\chi_M$  being the corrected magnetic susceptibility per two Ni(II) ions). Upon cooling of the sample from room temperature, the magnetic susceptibility value was observed to increase steadily. Paramagnetic susceptibilities are inversely proportional to temperature. The nickel complex follows the Curie's law ( $\chi = C/T$  and  $C = (N \cdot \mu^2)/K_B$  where C is Curie's constant, N is the Avogadro's number,  $\mu$  is an individual magnetic moment and  $K_B$  is Boltzmann's constant). Curie's constant relates the magnetic field and the temperature to the magnetisation of a paramagnetic substance.<sup>135,136</sup> The crystal structure of the nickel complex  $[\text{Ni}_2(\text{H}_4\text{L1})(\text{MeOH})_2](\text{ClO}_4)_2 \cdot \text{MeOH}$  clearly shows that one of the nickel ions has square planar geometry while the other nickel ion is in an octahedral environment. Square planar nickel(II) complexes are low-spin and diamagnetic, therefore it is not expected that the complex would show magnetic exchange interaction between the nickel ions.

## 2.4.2. Further structural studies of the dinuclear complexes with H-bonding

### 2.4.2.1. Nuclear Magnetic Resonance studies

In order to fully characterise the dinuclear complexes previously described, extensive NMR spectroscopy studies were performed for one of the zinc complexes obtained,  $[\text{Zn}_2(\text{H}_4\text{L1})\text{Cl}]\cdot\text{Cl}\cdot\text{H}_2\text{O}$  (2.2). The  $^1\text{H}$  spectrum was fully assigned (Figs. 2.35 and 2 36, Table 2.25) with a combination of NMR techniques involving NOE (nuclear Overhauser enhancement) and COSY (double quantum filtered correlated spectroscopy) experiments as well as variable temperature experiments. Electronic copies of the NMR plots are attached in the appendix 3.

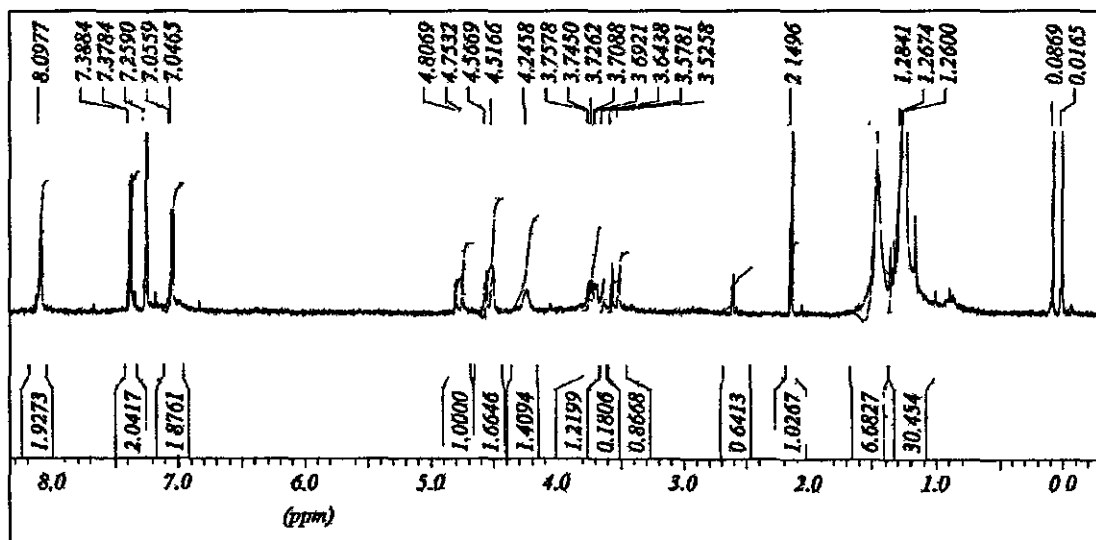


Fig. 2.35:  $^1\text{H}$  NMR spectrum of  $[\text{Zn}_2(\text{H}_4\text{L1})\text{Cl}]\cdot\text{Cl}\cdot\text{H}_2\text{O}$  in  $\text{CDCl}_3$

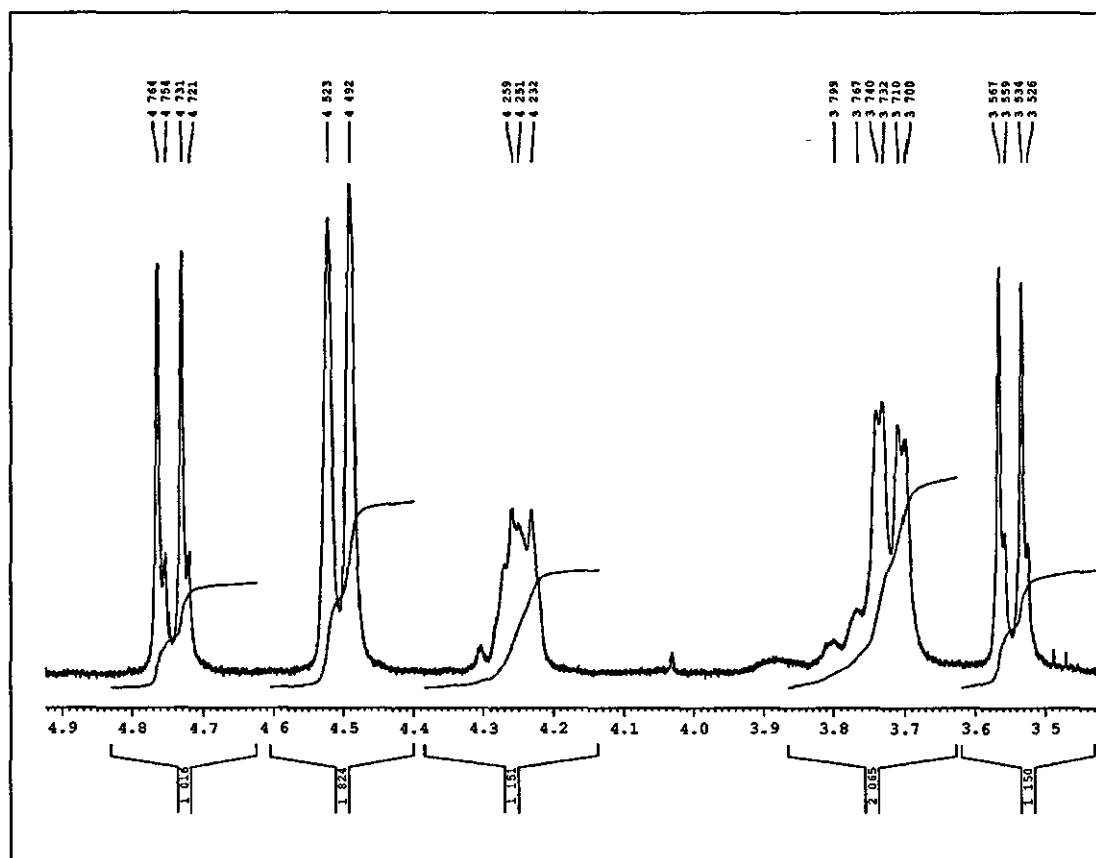
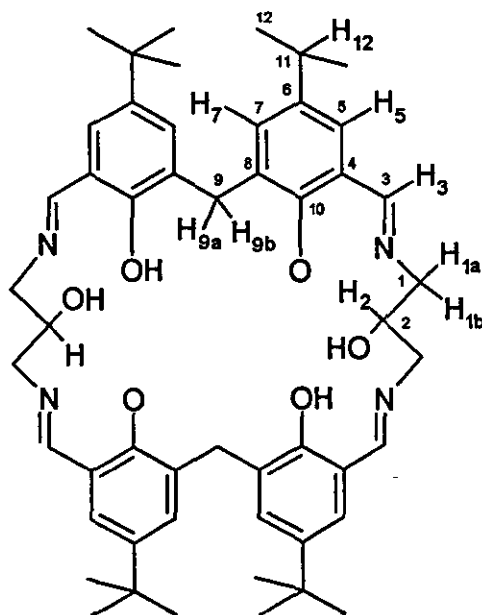


Fig. 2.36:  $^1\text{H}$  NMR spectrum expansion of  $[\text{Zn}_2(\text{H}_4\text{L1})\text{Cl}]\cdot\text{Cl}\cdot\text{H}_2\text{O}$  in  $\text{CDCl}_3$

Table 2.25: Proton assignments for  $^1\text{H}$  NMR of  $[\text{Zn}_2(\text{H}_6\text{L1})\text{Cl}]\cdot\text{Cl}\cdot\text{H}_2\text{O}$ 

H	$\delta$	Analyses
H <sub>1a</sub>	4.56	$^1\text{H}$ NMR, DQF-COSY
H <sub>1b</sub>	3.75	$^1\text{H}$ NMR, DQF-COSY
H <sub>2</sub>	4.24	$^1\text{H}$ NMR, DQF-COSY
H <sub>3</sub>	8.09	$^1\text{H}$ NMR, DQF-COSY
H <sub>5</sub>	7.05	$^1\text{H}$ NMR, DQF-COSY, NOE
H <sub>7</sub>	7.38	$^1\text{H}$ NMR, DQF-COSY, NOE
H <sub>9a</sub>	4.80	$^1\text{H}$ NMR, DQF-COSY
H <sub>9b</sub>	3.57	$^1\text{H}$ NMR, DQF-COSY
H <sub>12</sub>	1.28	$^1\text{H}$ NMR, DQF-COSY

Fig. 2.37: Proton and carbon labelling for macrocycle H<sub>6</sub>L1

The  $^1\text{H}$  spectrum reveals two singlets corresponding to the 36 *tert*-butyl protons ( $\delta$  1.28, H<sub>12</sub>) and to the four protons of the imine groups ( $\delta$  8.1, H<sub>3</sub>) respectively. It also shows a pair of doublets for the eight aromatic protons, the four H<sub>7</sub> ( $\delta$  7.38) and the four H<sub>5</sub> ( $\delta$  7.05). Aromatic protons H<sub>5</sub> and H<sub>7</sub> were definitely assigned by NOE analysis, where the  $^1\text{H}$  signals were monitored while irradiating at a series of frequencies, specifically the neighbouring H<sub>9B</sub> and H<sub>3</sub> proton signals. The  $^1\text{H}$  pattern for the saturated lateral chain protons comprises an AB system for the protons of the methylene groups, featuring a double doublet for the four protons H<sub>1B</sub> ( $\delta$  3.75–3.70) and a doublet for the four protons H<sub>1A</sub> ( $\delta$  4.56). It shows also a singlet corresponding to the protons H<sub>2</sub> ( $\delta$  4.24). The four methylene protons H<sub>9</sub>



also exhibit an AB system, appearing as a pair of doublets at 4.8 ppm for the two  $H_{9A}$  protons and at 3.57 ppm for the two  $H_{9B}$  protons. Thus, each methylene group shows two different proton environments.

It can be concluded then that the cation  $[Zn_2(H_4L1)Cl]^+$  (Fig. 2.38) in solution has two approximate mirror planes, dividing it in four approximate equivalent quarters (approximate  $mm$  symmetry), but also that the saddle conformation makes this molecule unsymmetrical respect of the planes of the phenols, which makes the proton environment for methylene protons different, the four protons  $H_9$  and the eight protons  $H_1$ , exhibiting two sets of resonances (AB system).

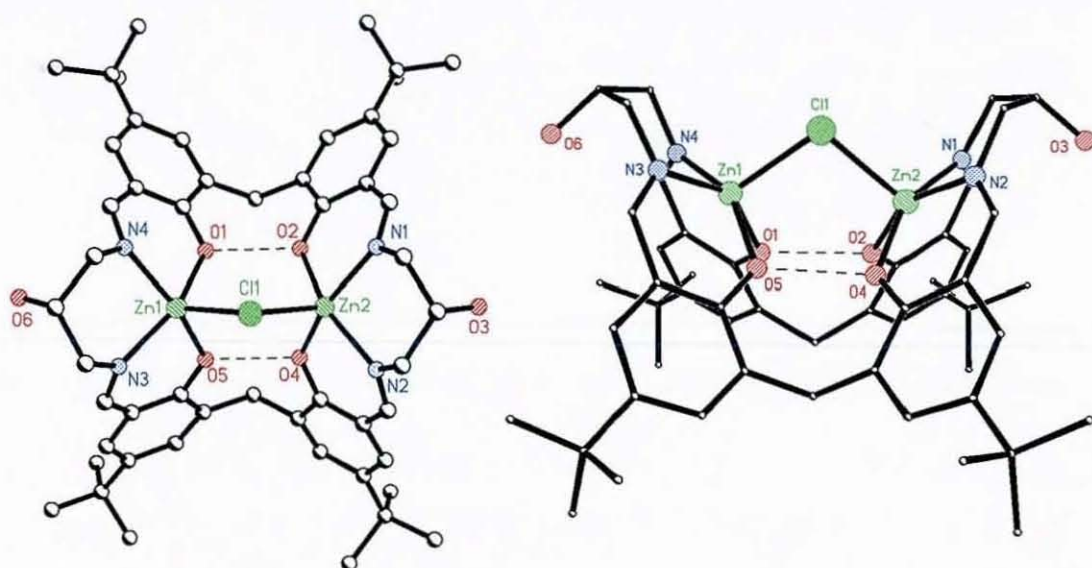


**Fig. 2.38:** Perspective views of cation  $[Zn_2(H_4L1)Cl]^+$

Protons  $H_{9A}$  and  $H_{9B}$  were assigned using proton-proton coupling experiments which showed strong coupling between them, suggesting that both protons bind the same carbon (this is reinforced by C-H coupling diagrams). The same occurs with  $H_{1A}$  and  $H_{1B}$ , and also with  $H_2$  and OH. These studies also reveal strong coupling between  $H_{1B}$  and  $H_2$  and weak coupling between  $H_{1A}$  and  $H_2$ , which could be explained in terms of the angle between both pairs of protons (angle of  $0^\circ$  or  $180^\circ$  between atoms shows strong coupling, angle of  $90^\circ$  or  $270^\circ$  between atoms shows no coupling). There is also proton-proton coupling between the

aromatic protons H<sub>5</sub> and H<sub>7</sub> and a weak coupling between imine protons, H<sub>3</sub>, and the methylene protons H<sub>1A</sub>.

Proton decoupled <sup>13</sup>C NMR spectra were also studied in order to assign the C atoms of the molecule. The methylene carbon resonances were assigned (Fig. 2.39, Table 2.26) from selective frequency on-resonance decoupling experiments. The rest of the carbon atoms were assigned by the proton-carbon coupling diagrams DQF-COSY (double quantum filtered correlated spectroscopy), by DEPT diagrams (distortionless enhancement by polarization transfer, which assigns C, CH, CH<sub>2</sub> and CH<sub>3</sub>) and by HMBC (heteronuclear multiple bond correlation, useful for verifying assignment of carbon signals, particularly quaternary carbons) connectivity experiments. Thus, the signal for the four *tert*-butyl carbons, C<sub>11</sub>, appears as a quaternary carbon at 30.97 ppm, the signal for the twelve methyl carbons, C<sub>12</sub>, at 31.27 ppm, methylene C<sub>9</sub> appears as a secondary carbon at 33.88 ppm, C<sub>1</sub> also secondary at 67.95 ppm and C<sub>2</sub> at 68.17 ppm. Aromatic C<sub>5</sub> and C<sub>7</sub> show at 129.73 and 132.30 ppm respectively and imine C<sub>3</sub> at 171.37 ppm. The remaining four carbon atoms, which are the quaternary aromatic carbons, are assigned as follows: δ 157.14 is thought to be C<sub>10</sub>, at higher ppm for being attached to such an electronegative atom as oxygen. C<sub>6</sub> appears at δ 141.62, as it is in para position to C<sub>10</sub> (π resonance in the ring favoured). The signal at δ 132.11 is assigned to C<sub>4</sub> as it is close to another electronegative atom (the imine nitrogen) and finally C<sub>8</sub> at 119.23 ppm.

**Table 2.26:** Carbon assignments for <sup>13</sup>C NMR of [Zn<sub>2</sub>(H<sub>4</sub>L1)Cl]·Cl·H<sub>2</sub>O

C	δ	Analyses
C <sub>1</sub>	67.95	<sup>13</sup> C NMR, DEPT, DQF-COSY
C <sub>2</sub>	68.17	<sup>13</sup> C NMR, DEPT, DQF-COSY
C <sub>3</sub>	171.37	<sup>13</sup> C NMR, DEPT, DQF-COSY
C <sub>4</sub>	132.11	<sup>13</sup> C NMR, DEPT, DQF-COSY
C <sub>5</sub>	129.73	<sup>13</sup> C NMR, DEPT, DQF-COSY
C <sub>6</sub>	141.62	<sup>13</sup> C NMR, DEPT, DQF-COSY, HMBC
C <sub>7</sub>	132.30	<sup>13</sup> C NMR, DEPT, DQF-COSY
C <sub>8</sub>	119.23	<sup>13</sup> C NMR, DEPT, DQF-COSY
C <sub>9</sub>	33.88	<sup>13</sup> C NMR, DEPT, DQF-COSY
C <sub>10</sub>	157.14	<sup>13</sup> C NMR, DEPT, DQF-COSY, HMBC
C <sub>11</sub>	30.97	<sup>13</sup> C NMR, DEPT, DQF-COSY
C <sub>12</sub>	31.27	<sup>13</sup> C NMR, DEPT, DQF-COSY



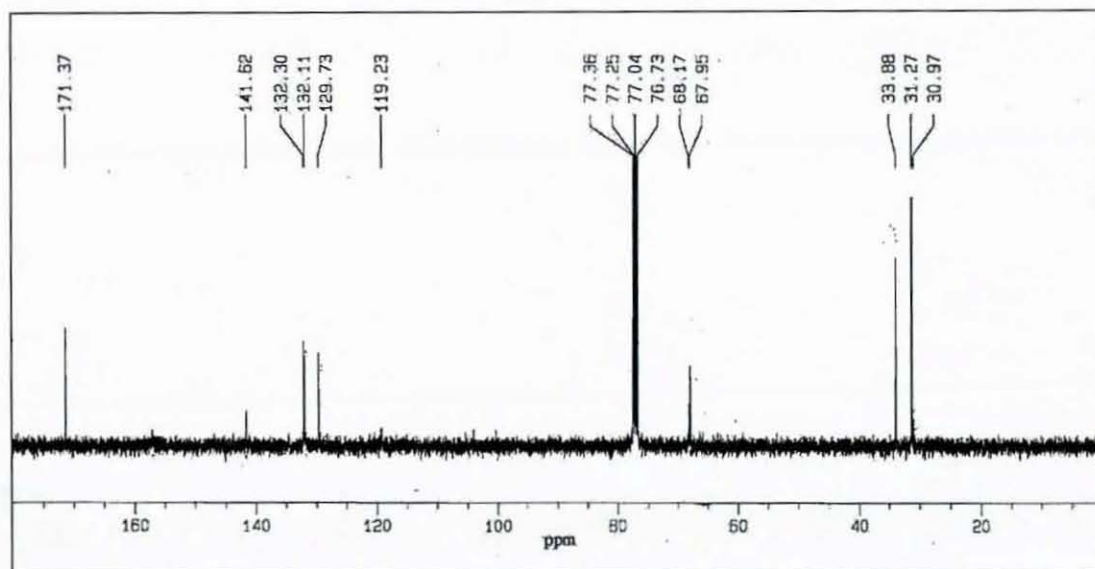


Fig. 2.39:  $^{13}\text{C}$  NMR spectrum of  $[\text{Zn}_2(\text{H}_4\text{L1})\text{Cl}]\cdot\text{Cl}\cdot\text{H}_2\text{O}$  in  $\text{CDCl}_3$

The NMR spectroscopy studies imply that the saddle conformation of this zinc complex persists in solution. There are no indications of fluxionality in the spectrum and the spectra are not significantly changed on heating to  $60^\circ\text{C}$ .

#### 2.4.2.2. Spectroscopic studies

In order to obtain more information and confirm the existence of the strong intramolecular hydrogen bonding in the structures described, UV electronic spectral studies were performed under acid or basic conditions.

Supposedly, if there are strong hydrogen bonds that link adjacent oxygen atoms of the 2,2'-methylenediphenol units of the macrocycle holding the saddle-shape conformation, they should break when a base is added to a solution of the complex, changing the overall structure and therefore varying its electronic spectrum. It should also be possible to see a change in its electronic spectrum when forming the intramolecular hydrogen bonding again by adding acid to that solution. The structure should also vary by adding acid to the solution, as this would protonate all the phenol groups and therefore the hydrogen bonds of the 2,2'-methylenediphenol units of the macrocycle would break.

The variation of the structure of the complex  $[\text{Zn}_2(\text{H}_4\text{L})\text{Cl}]\cdot\text{Cl}\cdot\text{H}_2\text{O}$  (**2.2**) was followed by monitoring the UV electronic spectra with acid/base variations. This spectral change was accomplished by dissolving the Zn complex in ethanol 96% ( $6.84\cdot 10^{-6}\text{M}$ ) and measuring the UV spectrum after adding drop-wise either diluted triethylamine solution or diluted hydrochloric acid solution in ethanol 96%. The pH of each solution was measured with a digital pH-meter. The apparatus was calibrated by immersion of the electrode in aqueous buffer (phosphate (pH 7) or borate (pH 10)) solution.

The UV spectra of the initial solution (pH=7) exhibit 4 bands (Fig. 2.40), due to  $\pi\text{-}\pi^*$  intraligand transitions: 348 nm ( $\epsilon=16959\text{ L}\cdot\text{mol}^{-1}\cdot\text{cm}^{-1}$ ), 263 nm ( $\epsilon=51506\text{ L}\cdot\text{mol}^{-1}\cdot\text{cm}^{-1}$ ), 221 nm ( $\epsilon=97924\text{ L}\cdot\text{mol}^{-1}\cdot\text{cm}^{-1}$ ) and 211 nm ( $\epsilon=102164\text{ L}\cdot\text{mol}^{-1}\cdot\text{cm}^{-1}$ ). These four bands are essentially unchanged from the DHTMB precursor.

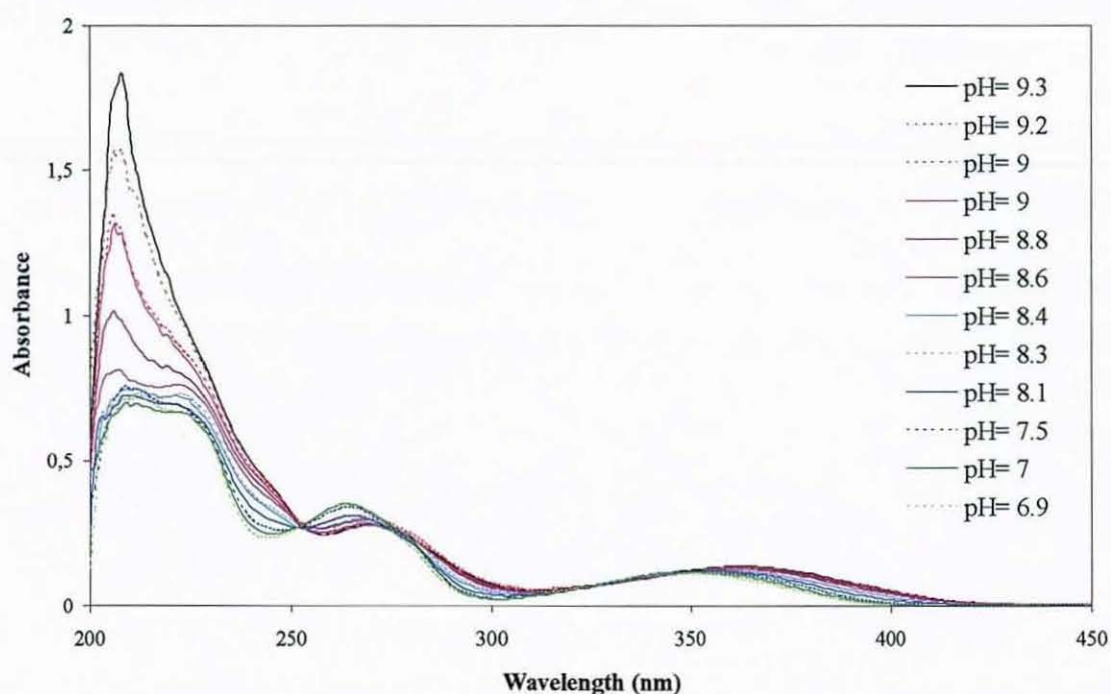


**Fig. 2.40:** UV spectrum for  $[\text{Zn}_2(\text{H}_4\text{L})\text{Cl}]\cdot\text{Cl}\cdot\text{H}_2\text{O}$  followed by acid-base variation

When acid or base was added, the bands at 348 and 263 nm were just slightly shifted, while the bands at 221 and 211 nm were significantly modified. By adding base to the complex (solid lines in the graph), the band at 221 nm either

disappears or is hidden and the band at 211 nm intensifies moving to 208 nm with an absorption coefficient of  $\epsilon=268085 \text{ L}\cdot\text{mol}^{-1}\cdot\text{cm}^{-1}$  at pH=9.3. The opposite process occurs on acidifying (dashed lines in the graph), the band at 221 nm appearing again as a shoulder (Fig. 2.40). This process can be explained in terms of breaking the H-bonds that link adjacent phenol oxygen atoms in the molecule by adding base, and reforming the strong H-bonding by adding acid again, showing therefore that the process is reversible. The band at 211 nm could be related to the phenolate groups of the ligand. The band is intensified by breaking the H-bonds that link adjacent phenol oxygen atoms, and *vice versa*, it decreases in intensity when forming the intramolecular H-bonds by acidifying again.

### 2.4.3. Dinuclear complexes of $\text{H}_6\text{L1}$ without intramolecular H-bonding

In this section, dinuclear complexes lacking the intramolecular hydrogen bonding will be discussed. These complexes have different characteristics from the previous series due to a different conformation adopted by the complexes

In the case of the dinuclear  $\text{M(III)}$  complexes, the use of trivalent metal ions leads to complete deprotonation of the phenol groups, due to the +III charge on the coordinated metal ion, which weakens the O-H bond. This deprotonation results in the loss of the saddle conformation and formation of a new topology, where all the phenols are fully deprotonated, the macrocycle opens out and the metal ions are far apart, lying above and below the macrocyclic plane respectively. The examples show clearly that the topology of the system is related to the oxidation state of the coordinated metal ions

In later studies, a new series of dinuclear  $\text{M(II)}$  complexes with different topology was obtained. The new dinuclear complexes were obtained by adding some base (triethylamine) to the reaction in order to fully deprotonate the phenol oxygen atoms. X-ray studies proved that the conformation of the complexes was not saddle-shaped. In contrast to the previous dinuclear  $\text{M(II)}$  structures, the metal ions are well separated and there is no exogenous bridge linking them. In these

cases, the difference in conformation can again be attributed to the complete deprotonation of the methylenediphenol groups. The absence of the intramolecular hydrogen bond allows the phenol oxygen atoms and metal ions to move apart. The resulting conformation is very similar to the preceding M(III) complexes, although the method of obtaining them is different.

#### 2.4.3.1. Synthesis and characterisation of $[\text{Mn}_2(\text{H}_2\text{L1})(\text{Cl})_2(\text{EtOH})_2] \cdot 6\text{H}_2\text{O}$ , $[\text{Co}_2(\text{H}_2\text{L1})(\text{Cl})_2(\text{H}_2\text{O})_2]$ and $[\text{Fe}_2(\text{H}_2\text{L1})(\text{Cl})_2(\text{H}_2\text{O})_2]$

Reaction of DHTMB with 1,3-diaminopropan-2-ol in the presence of Mn(II), Co(II) and Fe(II) chloride salts, followed by air oxidation produces dinuclear M(III) complexes of the macrocycle  $\text{H}_6\text{L1}$ , which were synthesised using the procedures described in the experimental chapter.

The complex  $[\text{Mn}_2(\text{H}_2\text{L1})(\text{Cl})_2(\text{EtOH})_2] \cdot 6\text{H}_2\text{O}$  (2.13) was initially synthesised from the Mn(II) salt. When the reaction was stopped and left to cool down in air, the yellow colour of the solution changed to dark brown, which is an indication of the oxidation of Mn(II) to Mn(III) ions. Some yellow powder, presumably Mn(II) complex, precipitated in the flask was isolated. The oxidation of the Mn(II) ions was also observed when a small amount of this yellow powder was dissolved and left to crystallise. The complex slowly oxidises in solution. The crystals obtained were brown, again an indication of Mn(III) ions.

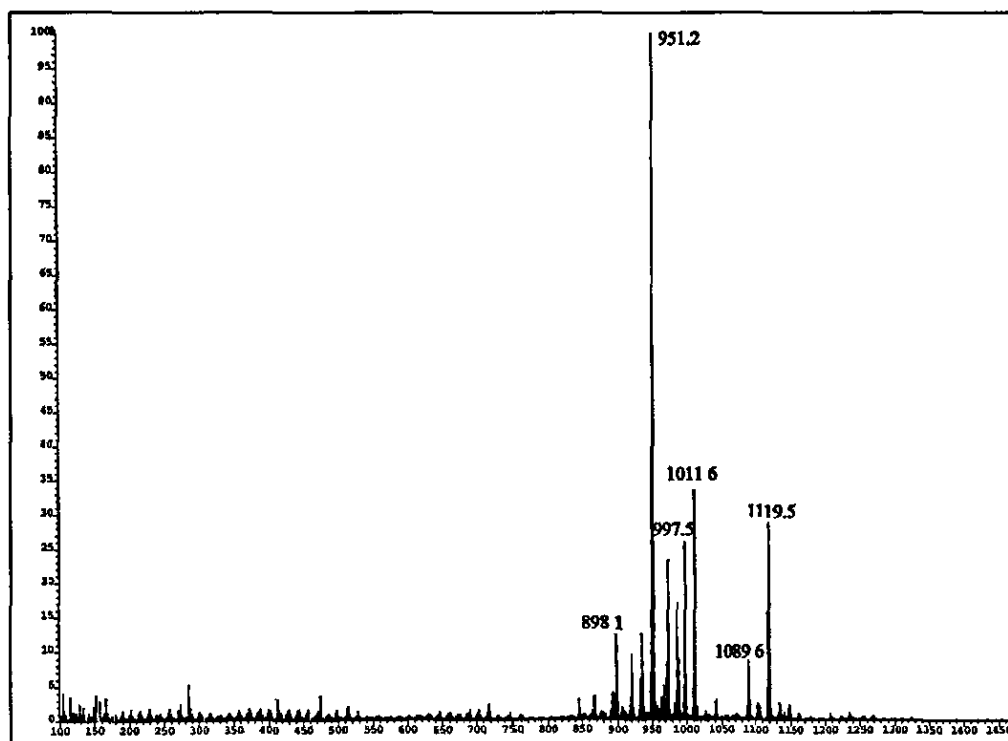
Complexes  $[\text{Co}_2(\text{H}_2\text{L1})(\text{Cl})_2(\text{H}_2\text{O})_2]$  (2.14) and  $[\text{Fe}_2(\text{H}_2\text{L1})(\text{Cl})_2(\text{H}_2\text{O})_2]$  (2.15) were also synthesised from their respective M(II) salts, but the products isolated were in the +III oxidation state. In all three cases the M(II) complexes are highly air sensitive and oxidise quite rapidly in solution to the corresponding M(III) complexes.

LSIMS spectra of the trivalent metal complexes  $[\text{Mn}_2(\text{H}_2\text{L1})(\text{Cl})_2(\text{EtOH})_2] \cdot 6\text{H}_2\text{O}$  (Table 2.27, Fig. 2.41) and  $[\text{Co}_2(\text{H}_2\text{L1})(\text{Cl})_2(\text{H}_2\text{O})_2]$  (Table 2.28, Fig. 2.42) show peaks corresponding to a singly charged ion containing the dimetallic fragment

$[\text{Mn}_2(\text{H}_2\text{L1})]^+$  The main peak for the manganese complex corresponds to the fragment  $[\text{Mn}_2(\text{H}_2\text{L1}) + e]^+$  at  $m/z$  951, while the main peak for the cobalt complex is assigned to the fragment  $[\text{Co}_2(\text{H}_2\text{L1})(\text{H}_2\text{O})_2 + e]^+$  at  $m/z$  995. The manganese complex also shows a peak at  $m/z$  1119, suggesting the presence of a dmsO molecule in the fragment (the complex was recrystallised in a mixture of dmsO and dmf solvents)

**Table 2.27:** Peak attributions for  $[\text{Mn}_2(\text{H}_2\text{L1})(\text{Cl})_2(\text{EtOH})_2] \cdot 6\text{H}_2\text{O}$

$m/z$	Rel. Intensity (%)	Fragments	Calc. Mass
951	100	$[\text{Mn}_2(\text{H}_2\text{L1}) + e]^+$	951
973	24	$[\text{Mn}_2(\text{H}_2\text{L1}) + \text{Na}]^+$	973
987	17	$[\text{Mn}_2(\text{H}_2\text{L1})\text{Cl} + \text{H}]^+$	987
997	27	$[\text{Mn}_2(\text{H}_2\text{L1})(\text{EtOH}) + e]^+$	997
1011	33	$[\text{Mn}_2(\text{H}_2\text{L1})(\text{Cl}) + \text{Na}]^+$	1009
1119	28	$[\text{Mn}_2(\text{H}_3\text{L1})(\text{Cl})_2(\text{dmsO})(\text{H}_2\text{O}) + \text{H}]^+$	1119

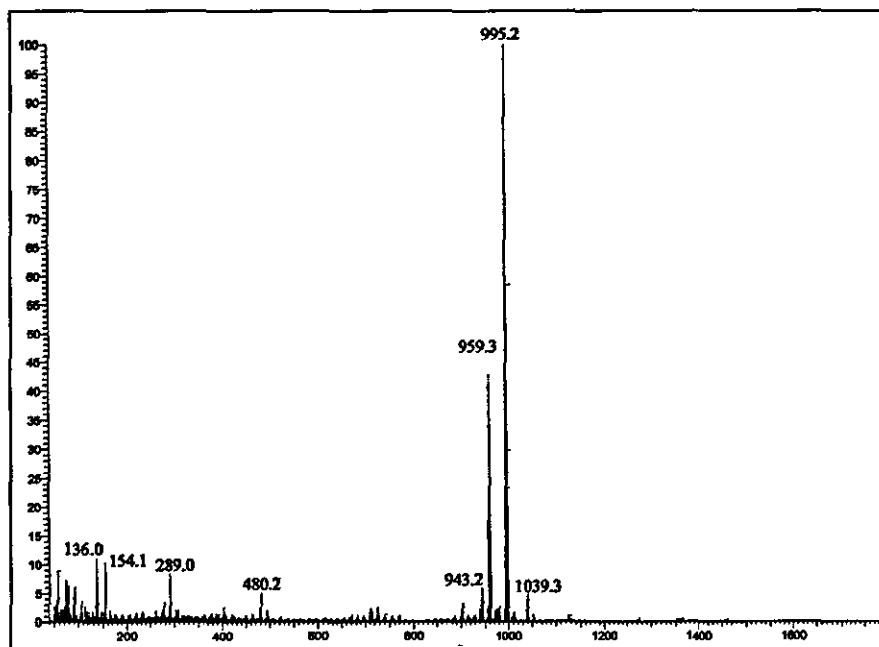


**Fig. 2.41:** LSIMS spectrum of  $[\text{Mn}_2(\text{H}_2\text{L1})(\text{Cl})_2(\text{EtOH})_2] \cdot 6\text{H}_2\text{O}$



**Table 2.28:** Peak attributions for  $[\text{Co}_2(\text{H}_2\text{L1})(\text{Cl})_2(\text{H}_2\text{O})_2]$ 

m/z	Rel. Intensity (%)	Fragments	Calc. Mass
959	45	$[\text{Co}_2(\text{H}_2\text{L1}) + \text{e}]^+$	959
995	100	$[\text{Co}_2(\text{H}_2\text{L1})(\text{Cl})]^+$	994
1039	5	$[\text{Co}_2(\text{H}_2\text{L1})(\text{Cl})(\text{H}_2\text{O})_2]^+$	1030

**Fig. 2.42:** LSIMS spectrum of  $[\text{Co}_2(\text{H}_2\text{L1})(\text{Cl})_2(\text{H}_2\text{O})_2]$ 

The ESI data of the iron complex  $[\text{Fe}_2(\text{H}_2\text{L1})(\text{Cl})_2(\text{H}_2\text{O})_2]$  (Table 2.29) suggest the formation of the dinuclear macrocyclic species. The main peak corresponds to a singly charged ion containing the dimetallic fragment  $[\text{Fe}_2(\text{H}_2\text{L1}) - \text{H}]^+$  at m/z 951. There are also two peaks of doubly charged ions which are assigned to  $[\text{Fe}_2(\text{H}_2\text{L1})]^{2+}$  and  $[\text{Fe}_2(\text{H}_2\text{L1})(\text{MeOH})]^{2+}$  at m/z 476 and 492 respectively.

**Table 2.29:** Peak attributions for  $[\text{Fe}_2(\text{H}_2\text{L1})(\text{Cl})_2(\text{H}_2\text{O})_2]$   
(ESI-MS relative abundance is given for cone voltage = 90V)

m/z	Rel. Intensity (%)	Fragments	Calc. Mass
476	20	$[\text{Fe}_2(\text{H}_2\text{L1})]^{2+}$	952
492	20	$[\text{Fe}_2(\text{H}_2\text{L1})(\text{MeOH})]^{2+}$	984
951	100	$[\text{Fe}_2(\text{H}_2\text{L1}) - \text{H}]^+$	951
987	60	$[\text{Fe}_2(\text{H}_2\text{L1})\text{Cl} - \text{H}]^+$	987

The stoichiometry of the complexes, derived from elemental analyses and supported from the LSIMS results, suggests that the metal ions are in the +III oxidation state and that the macrocycle has lost four protons, thus the phenol groups are likely to be fully deprotonated and the conformation of the complexes is likely to be similar to the structure of the Mn(III) complex following.

#### 2.4.3.2. Structure of $[\text{Mn}_2(\text{H}_2\text{L1})(\text{Cl})_2(\text{dmf})(\text{dmsO})]\cdot 1.5\text{dmf}\cdot 0.3\text{Et}_2\text{O}$

Brown crystals of  $[\text{Mn}_2(\text{H}_2\text{L1})(\text{Cl})_2(\text{dmf})(\text{dmsO})]\cdot 1.5\text{dmf}\cdot 0.3\text{Et}_2\text{O}$  (**2.13x**) suitable for X-ray studies were grown by slow diffusion of diethylether into a dmf-dmsO solution of  $[\text{Mn}_2(\text{H}_2\text{L1})(\text{Cl})_2(\text{EtOH})_2]\cdot 6\text{H}_2\text{O}$  (**2.13**).

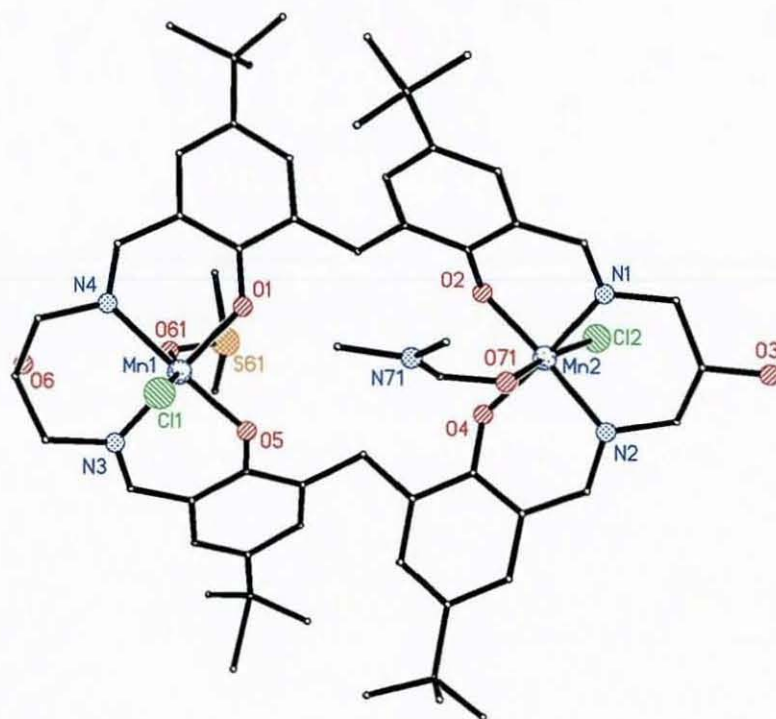


**Fig. 2.43:** Structure of the complex  $[\text{Mn}_2(\text{H}_2\text{L1})(\text{Cl})_2(\text{dmf})(\text{dmsO})]$

All the X-ray data collection parameters are summarised in Table 8 of appendix 1 along with the details concerning the refinement and disorder. Perspective views of the neutral complex  $[\text{Mn}_2(\text{H}_2\text{L1})(\text{Cl})_2(\text{dmf})(\text{dmsO})]$  are shown in Figs. 2.43, 2.44 and 2.45 and selected bond lengths and angles relevant to the manganese(III) ions coordination are given in Table 2.30.

The structure of the dimanganese(III) complex is very different from those discussed previously. The manganese ions are six-coordinate, each having chloride and a solvent molecule (dmf or dmsO) as the non-macrocyclic ligands and each showing the expected Jahn-Teller extension (Table 2.30). In contrast to the previous structures, the metal ions are well separated (7.625(1) Å) and there is no exogenous bridge linking them. The saddle-shape of the macrocycle has been lost and the phenolate groups in each methylenediphenolate are well separated (O1...O2 5.068(4) Å and O4...O5 5.067(4) Å) and rotated one with respect to the other, so that one is above the plane of the macrocycle and the other is below. The conformation resembles the 1,2-alternate form of the calixarenes<sup>86,87</sup> (Fig. 2.45). As a consequence of this, the metal ions are also on opposite sides of the macrocyclic plane (Fig. 2.44). The resulting conformation is very similar to that of the related mononuclear manganese(III) Schiff-base complex<sup>137</sup> [Mn(salpn)Cl(MeOH)] (Fig. 2.47) suggesting that the presence of the methylenediphenolate groups is not significant in determining the geometry in this case.

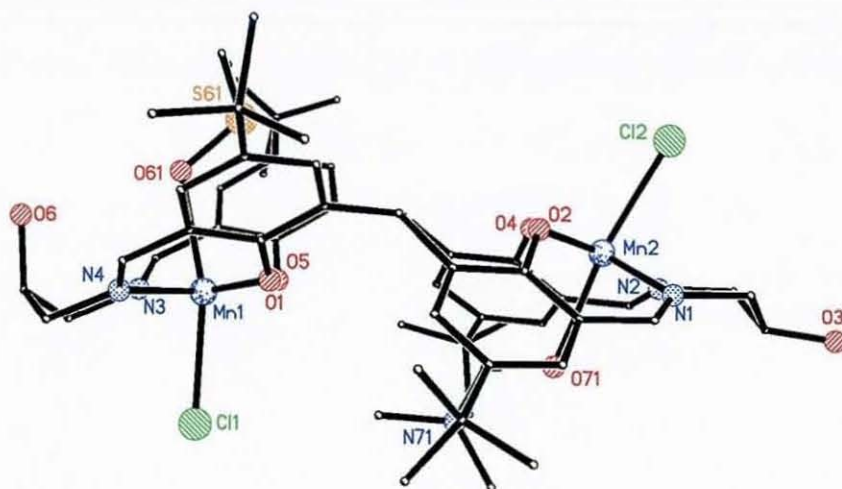


**Fig. 2.44:** Side-on view of the complex [Mn<sub>2</sub>(H<sub>2</sub>L1)(Cl)<sub>2</sub>(dmf)(dmsO)]

The difference in conformation between the previous hydrogen-bonded dinuclear M(II) complexes and this one can be related to the complete deprotonation of the 2,2'-methylenediphenol groups in the dimanganese(III) complex. This is due to the higher oxidation state of the Mn(III) ion, which is a better Lewis acid than the



M(II) ions and lowers the  $pK_a$  of the coordinated phenols, facilitating their deprotonation. In the absence of the intramolecular hydrogen bonding the phenol oxygen atoms and metal ions can move apart and the macrocyclic cleft opens out.

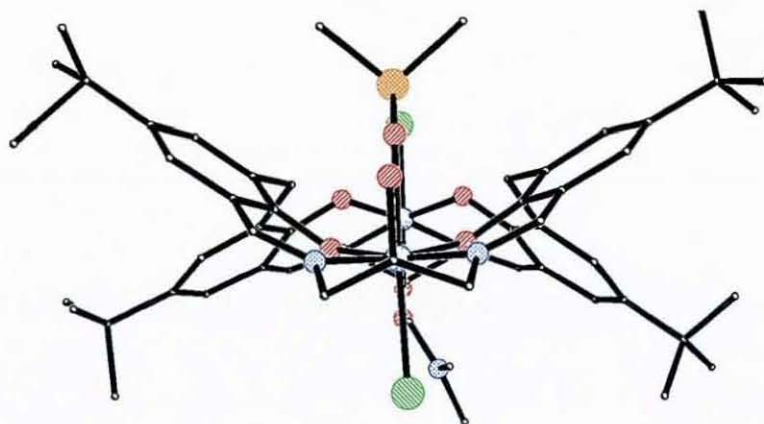


Fig. 2.45: Side-on view of the complex  $[\text{Mn}_2(\text{H}_2\text{L1})(\text{Cl})_2(\text{dmf})(\text{dmsO})]$

Hydrogen bonding between one of the coordinated chloride ions of one unit and a pendant alcohol group of another unit ( $\text{Cl1}\cdots\text{O3}$  3.035(7) Å) links the molecules into zigzag chains, forming channels in the lattice, which are occupied by the solvate diethylether molecules (Fig. 2.46).

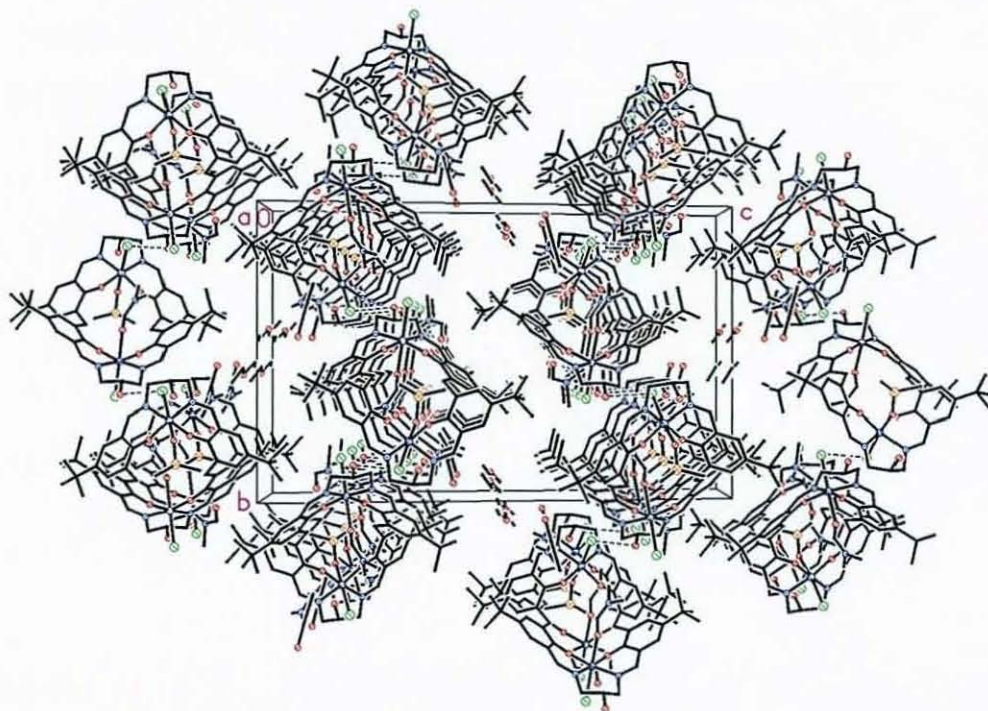
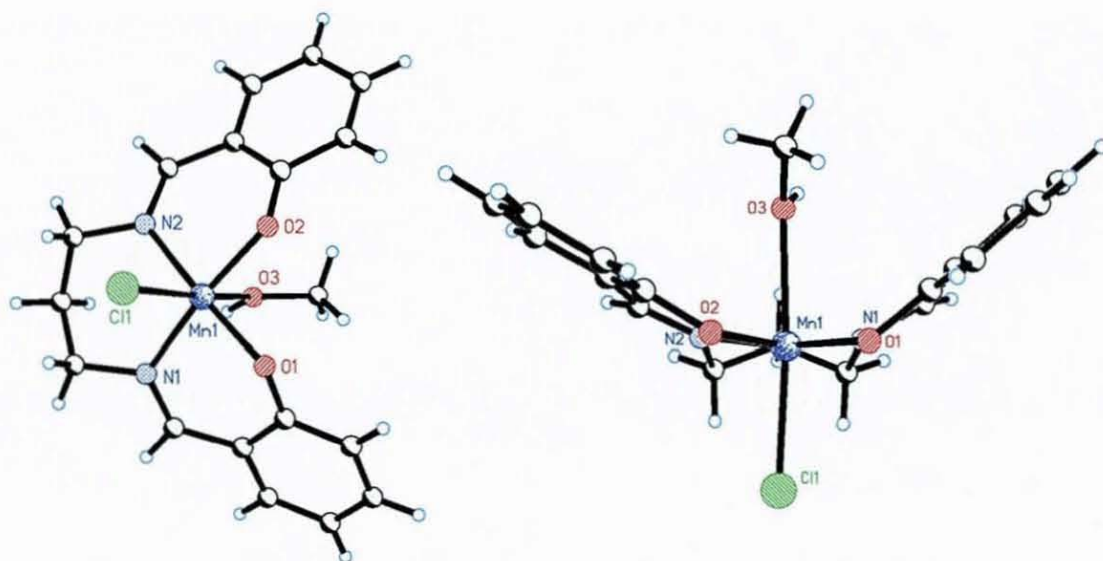


Fig. 2.46: Packing diagram for  $[\text{Mn}_2(\text{H}_2\text{L1})(\text{Cl})_2(\text{dmf})(\text{dmsO})] \cdot 1.5\text{dmf} \cdot 0.3\text{Et}_2\text{O}$

**Table 2.30:** Selected bond lengths [Å] and angles [°] for  
[Mn<sub>2</sub>(H<sub>2</sub>L1)(Cl)<sub>2</sub>(dmf)(dmsu)]

Mn(1)-O(1)	1.881(3)	Mn(2)-O(4)	1.876(3)
Mn(1)-O(5)	1.892(3)	Mn(2)-O(2)	1.892(3)
Mn(1)-N(3)	2.033(4)	Mn(2)-N(1)	2.026(4)
Mn(1)-N(4)	2.036(4)	Mn(2)-N(2)	2.027(4)
Mn(1)-O(61)	2.318(3)	Mn(2)-O(71)	2.349(3)
Mn(1)-Cl(1)	2.5073(14)	Mn(2)-Cl(2)	2.4792(12)
O(1)-Mn(1)-O(5)	87.85(13)	O(4)-Mn(2)-O(2)	88.12(12)
O(1)-Mn(1)-N(3)	171.38(15)	O(4)-Mn(2)-N(1)	170.59(13)
O(5)-Mn(1)-N(3)	88.63(14)	O(2)-Mn(2)-N(1)	88.41(13)
O(1)-Mn(1)-N(4)	89.97(14)	O(4)-Mn(2)-N(2)	90.23(13)
O(5)-Mn(1)-N(4)	172.00(15)	O(2)-Mn(2)-N(2)	172.28(13)
N(3)-Mn(1)-N(4)	92.45(16)	N(1)-Mn(2)-N(2)	92.05(14)
O(1)-Mn(1)-O(61)	89.56(13)	O(4)-Mn(2)-O(71)	86.97(12)
O(5)-Mn(1)-O(61)	91.43(12)	O(2)-Mn(2)-O(71)	88.12(11)
N(3)-Mn(1)-O(61)	82.66(14)	N(1)-Mn(2)-O(71)	84.18(13)
N(4)-Mn(1)-O(61)	80.86(14)	N(2)-Mn(2)-O(71)	84.26(12)
O(1)-Mn(1)-Cl(1)	98.63(11)	O(4)-Mn(2)-Cl(2)	97.90(9)
O(5)-Mn(1)-Cl(1)	100.10(10)	O(2)-Mn(2)-Cl(2)	98.36(9)
N(3)-Mn(1)-Cl(1)	89.73(11)	N(1)-Mn(2)-Cl(2)	91.25(10)
N(4)-Mn(1)-Cl(1)	87.84(12)	N(2)-Mn(2)-Cl(2)	89.34(10)
O(61)-Mn(1)-Cl(1)	166.05(9)	O(71)-Mn(2)-Cl(2)	171.98(9)



**Fig. 2.47:** Perspective views of the related complex [Mn(salpn)Cl(MeOH)]<sup>64,65,137</sup>

**2.4.3.3. Synthesis and characterisation of  $[\text{Mn}_2(\text{H}_2\text{L1})(\text{AcO})_2(\text{EtOH})]$ ,  
 $[\text{Mn}_2(\text{H}_2\text{L1})(\text{OH})(\text{EtOH})_2](\text{CF}_3\text{SO}_3)$  and  $[\text{Co}_2(\text{HL1})](\text{ClO}_4)$**

The complex  $[\text{Mn}_2(\text{H}_2\text{L1})(\text{AcO})_2(\text{EtOH})]$  (2.16) was synthesised both from the Mn(II) and the Mn(III) acetate salts. As for the previous manganese complexes, the Mn(II) complex is air sensitive and slowly oxidises in solution to the Mn(III) complex. The complex  $[\text{Mn}_2(\text{H}_2\text{L1})(\text{OH})(\text{EtOH})_2](\text{CF}_3\text{SO}_3)$  (2.17) was synthesised from the Mn(II) trifluorosulfonate salt. Again, the Mn(II) complex is air sensitive and slowly oxidises in solution to the Mn(III) complex. The ESI mass spectrometry data for both manganese(III) complexes  $[\text{Mn}_2(\text{H}_2\text{L1})(\text{AcO})_2(\text{EtOH})]$  and  $[\text{Mn}_2(\text{H}_2\text{L1})(\text{OH})(\text{EtOH})_2](\text{CF}_3\text{SO}_3)$  are listed in Tables 2.31 and 2.32. The trivalent metal complexes show the main peak corresponding to a doubly charged ion containing the dimetallic fragment  $[\text{M}_2(\text{H}_2\text{L1})]^{2+}$  at  $m/z$  475.

**Table 2.31: Peak attributions for  $[\text{Mn}_2(\text{H}_2\text{L1})(\text{AcO})_2(\text{EtOH})]$   
(relative abundance given for cone voltage = 20V)**

$m/z$	Rel. Intensity (%)	Fragments	Calc. Mass
475	100	$[\text{Mn}_2(\text{H}_2\text{L1})]^{2+}$	950
495	80	$[\text{Mn}(\text{H}_2\text{L1})(\text{EtOH})_2 + 2\text{H}]^{2+}$	990
516	10	$[\text{Mn}_2(\text{H}_2\text{L1})(\text{AcO}) + \text{Na}]^{2+}$	1033

**Table 2.32: Peak attributions for  $[\text{Mn}_2(\text{H}_2\text{L1})(\text{OH})(\text{EtOH})_2](\text{CF}_3\text{SO}_3)$   
(relative abundance given for cone voltage = 20V)**

$m/z$	Rel. Intensity (%)	Fragments	Calc. Mass
475	100	$[\text{Mn}_2(\text{H}_2\text{L1})]^{2+}$	950
495	25	$[\text{Mn}(\text{H}_2\text{L1})(\text{EtOH})_2 + 2\text{H}]^{2+}$	990
1099	5	$[\text{Mn}_2(\text{H}_2\text{L1})(\text{CF}_3\text{SO}_3) - \text{H}]^+$	1099

Complex  $[\text{Co}_2(\text{HL1})](\text{ClO}_4)$  (2.18) was synthesised from the cobalt(II) complex  $[\text{Co}_2(\text{H}_4\text{L1})(\text{H}_2\text{O})_3](\text{ClO}_4)_2 \cdot 3\text{EtOH}$  (2.6) by oxidising it with 4 drops of  $\text{H}_2\text{O}_2$  (50%). The solution colour changed from dark yellow (Co(II) ions) to dark brown (Co(III) ions). The elemental analysis and the LSIMS results are consistent with the formation of the complex. The LSIMS spectrum of the cobalt complex (Fig.



2.48, Table 2.33) shows the main peak at  $m/z$  959 corresponding to a singly charged ion containing the dimetallic fragment  $[\text{Co}_2(\text{H}_2\text{L1})+\text{e}]^+$ .

**Table 2.33:** Peak attributions for  $[\text{Co}_2(\text{HL1})](\text{ClO}_4)$

$m/z$	Rel. Intensity (%)	Fragments	Calc. Mass
849	40	$[(\text{H}_6\text{L1})+\text{H}]^+$	846
959	100	$[\text{Co}_2(\text{H}_2\text{L1})+\text{e}]^+$	959
981	55	$[\text{Co}_2(\text{HL1})+\text{Na}]^+$	981

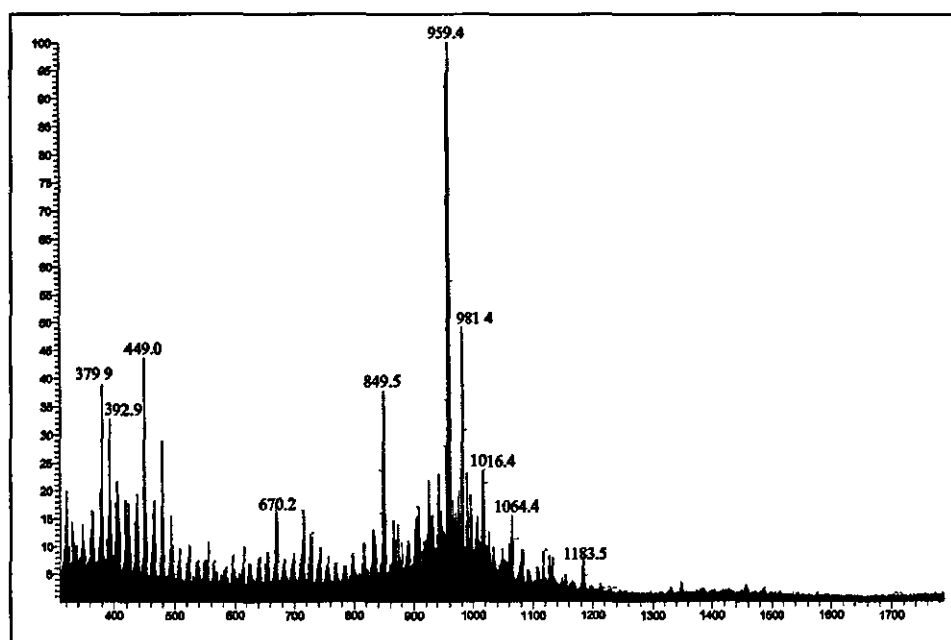


**Fig. 2.48:** LSIMS spectrum of  $[\text{Co}_2(\text{HL1})](\text{ClO}_4)$

#### 2.4.3.4. Synthesis and characterisation of $[\text{Cu}_2(\text{H}_2\text{L1})]\cdot\text{H}_2\text{O}$ and $[\text{Ni}_2(\text{H}_2\text{L1})(\text{H}_2\text{O})_3]$

Complexes  $[\text{Cu}_2(\text{H}_2\text{L1})]\cdot\text{H}_2\text{O}$  (2.19) and  $[\text{Ni}_2(\text{H}_2\text{L1})]\cdot 3\text{H}_2\text{O}$  (2.20) were obtained, in the presence of a base, as a by-product in the synthesis of the heteronuclear complex of the transition metals and alkali or alkali earth metals for the ligand  $\text{H}_6\text{L1}$  (Chapter 4). In this reaction some triethylamine was added in order to fully deprotonate the phenols and thus facilitate the coordination of the alkali or alkali earth metal. The by-product does not have the alkali or alkali earth ion coordinated but the phenol oxygen atoms are fully deprotonated and therefore the complex has lost the saddle conformation, typical of the dinuclear(II) complexes.

Brown orange needles of  $[\text{Cu}_2(\text{H}_2\text{L1})]\cdot\text{dmsO}\cdot\text{Et}_2\text{O}$  (**2.19x**) suitable for X-ray studies were grown by slow diffusion of diethylether into a dmf-dmsO-dcm solution of  $[\text{Cu}_2(\text{H}_2\text{L1})]\cdot\text{H}_2\text{O}$  (**2.19**). All the X-ray data collection parameters are summarised in Table 9 of appendix 1 along with the details concerning the refinement and disorder. Perspective views of the neutral complex  $[\text{Cu}_2(\text{H}_2\text{L1})]$  are shown in Figs. 2.49 and 2.50 and selected bond lengths and angles relevant to the copper(II) ions co-ordination are given in Table 2.34.

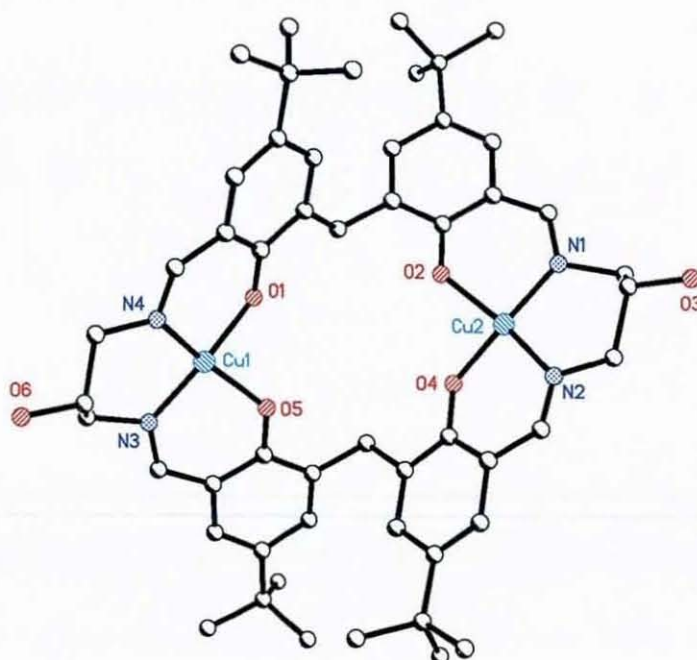


**Fig. 2.49:** Structure of the neutral complex  $[\text{Cu}_2(\text{H}_2\text{L1})]$

The structure of the dicopper(II) complex is very different from the dinuclear(II) discussed previously, but is similar to the related manganese(III) complex  $[\text{Mn}_2(\text{H}_2\text{L1})(\text{Cl})_2(\text{dmf})(\text{dmsO})]$ . The metal ions are well separated (7.043(4) Å) and there is no exogenous bridge linking them. The saddle-shape of the macrocycle has been stretched and the phenolate groups in each methylenediphenolate are well separated (O1...O2 4.480(9) Å and O4...O5 4.477(9) Å). The difference in conformation between the saddle-shaped dinuclear(II) series and this complex can be related to the complete deprotonation of the 2,2'-methylenediphenol groups by the use of a base (triethylamine). In the absence of the intramolecular hydrogen bonding the phenol oxygen atoms and the metal ions can spread out and the macrocyclic cleft relaxes.

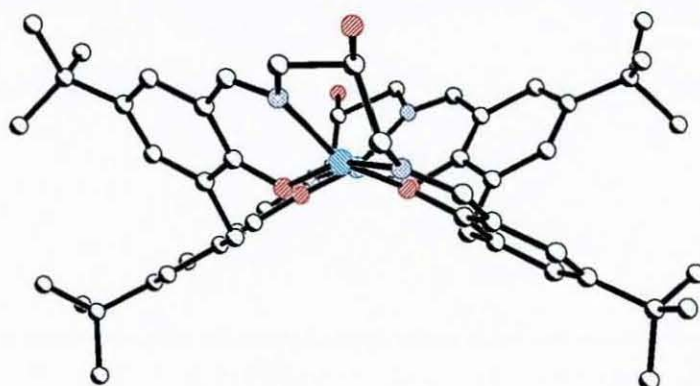


**Fig. 2.50:** Side-on view of the complex [Cu<sub>2</sub>(H<sub>2</sub>L1)]

The macrocyclic units are linked into chains by hydrogen bonding involving the pendant alcohol oxygen atoms and the imine nitrogen atoms, and also by weak electrostatic axial interactions between the copper ions of one macrocyclic unit and the imine nitrogen and pendant alcohol oxygen of other macrocyclic units. Figure 2.51 shows the electrostatic interactions between the macrocycles. The middle macrocycle has been represented with white bonding in order to differentiate clearly between the macrocyclic units. The lattice dmsu molecules are also hydrogen-bonded to the pendant alcohol groups of the macrocycle (Table 2.35).

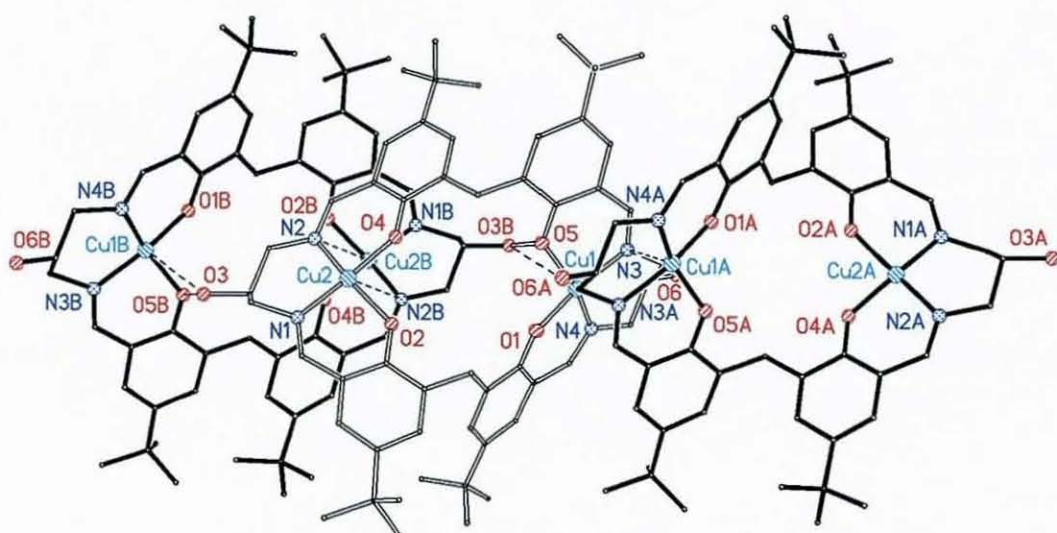


**Fig. 2.51:** Electrostatic interactions between the macrocyclic units of [Cu<sub>2</sub>(H<sub>2</sub>L1)]

**Table 2.34:** Selected bond lengths [Å] and angles [°] for [Cu<sub>2</sub>(H<sub>2</sub>L1)]·dmsO·Et<sub>2</sub>O

Cu(1)-O(1)	1.920(6)	Cu(2)-O(2)	1.911(6)
Cu(1)-O(5)	1.940(6)	Cu(2)-O(4)	1.910(6)
Cu(1)-N(4)	1.944(9)	Cu(2)-N(1)	1.972(10)
Cu(1)-N(3)	1.995(8)	Cu(2)-N(2)	1.965(9)
Cu(1)-Cu(2)	7.043(4)		
O(1)-Cu(1)-O(5)	86.7(3)	O(2)-Cu(2)-O(4)	85.6(3)
O(1)-Cu(1)-N(4)	93.1(3)	O(2)-Cu(2)-N(1)	92.7(4)
O(5)-Cu(1)-N(4)	155.5(4)	O(4)-Cu(2)-N(1)	155.2(4)
O(1)-Cu(1)-N(3)	158.6(3)	O(2)-Cu(2)-N(2)	157.0(3)
O(5)-Cu(1)-N(3)	91.6(3)	O(4)-Cu(2)-N(2)	94.3(3)
N(4)-Cu(1)-N(3)	97.2(4)	N(1)-Cu(2)-N(2)	96.6(4)

**Table 2.35:** Hydrogen bonds [Å] for [Cu<sub>2</sub>(H<sub>2</sub>L1)]·dmsO·Et<sub>2</sub>O

D-H...A	d(D-H)	D(H...A)	d(D...A)
O(3)-H(3A)...O(5A)	0.89	1.81	2.700(4)
O(3)-H(3B)...O(70B)	0.86	1.93	2.786(3)
O(6)-H(6)...O(70B)	0.84	1.92	2.726(5)
O(6)-H(6)...S(1B)	0.84	2.69	3.267(6)
O(6)-H(6)...N(3)	0.85	2.36	2.743(5)

Symmetry transformations used to generate equivalent atoms: (A) -x, -y, -z+1; (B) x, y+1, z

The LSIMS data listed in Tables 2.36 and 2.37 confirm the formation of the dinuclear macrocyclic complexes. The divalent metal complexes show a peak corresponding to a singly charged ion containing the dimetallic fragment [M<sub>2</sub>(H<sub>2</sub>L1)+/-H]<sup>+</sup>. The relative intensity of the peaks is weak and might be indicative of a poor solubility in the NOBA matrix. Indeed, once isolated, it is difficult to redissolve the compounds due to being neutral complexes

**Table 2.36:** Peak attributions for [Ni<sub>2</sub>(H<sub>2</sub>L1)]·3H<sub>2</sub>O

m/z	Rel. Intensity (%)	Fragments	Calc. Mass
942	5	[Ni <sub>1</sub> (H <sub>4</sub> L1)(H <sub>2</sub> O)+Na] <sup>+</sup>	942
959	30	[Ni <sub>2</sub> (H <sub>2</sub> L1)-H] <sup>+</sup>	959
1001	8	[Ni <sub>2</sub> (H <sub>2</sub> L1)(H <sub>2</sub> O)+Na] <sup>+</sup>	1001

**Table 2.37:** Peak attributions for  $[\text{Cu}_2(\text{H}_2\text{L1})]\cdot\text{H}_2\text{O}$ 

m/z	Rel. Intensity (%)	Fragments	Calc. Mass
845	25	$[(\text{H}_6\text{L1}) - \text{e}]^+$	845
906	15	$[\text{Cu}(\text{H}_4\text{L1}) - \text{e}]^+$	906
969	13	$[\text{Cu}_2(\text{H}_2\text{L1}) + \text{H}]^+$	969
989	22	$[\text{Cu}_2(\text{H}_2\text{L1})(\text{H}_2\text{O}) + \text{H}]^+$	987
1005	7	$[\text{Cu}_2(\text{H}_2\text{L1})\text{Cl} + 2\text{H}]^+$	1005

Elemental analysis suggests that the macrocycle has lost four protons. Phenol protons are more acidic ( $\text{pK}_a \sim 9.90$ ) than primary alcohol protons ( $\text{pK}_a = 13-16$ ). If a base is used to deprotonate the macrocycle, it will react first with the phenol protons of the macrocycle. On the basis of elemental analysis and mass spectrometry results, complex  $[\text{Ni}_2(\text{H}_2\text{L1})]\cdot 3\text{H}_2\text{O}$  is likely to have a similar structure to  $[\text{Cu}_2(\text{H}_2\text{L1})]\cdot\text{H}_2\text{O}$  previously described.

## 2.5. Conclusions

Yields and reaction times in the synthesis of the dialdehyde DHTMB have been significantly improved by varying the experimental conditions. DHTMB can be synthesised in a reasonable yield by direct oxidation of the dialcohol precursor DHTMBA, where the protection of the phenol groups is not necessary, reducing thus the number of steps to two.

The synthesis of a variety of dinuclear Schiff-base macrocyclic complexes has been achieved by condensing DHTMB with 1,3-diaminopropan-2-ol in the presence of various first row transition metal salts. The macrocycle  $\text{H}_6\text{L1}$  can be regarded as a Schiff-base pseudocalixarene macrocycle, preserving the two methylenediphenol units intact while inserting two diimine sections into the ring. It has been demonstrated that the DHTMB group introduces multiple geometrical variations, largely due to the presence of the saturated carbon linking the two phenol rings.



The structural studies indicated the diverse topology accessible in this series of dinuclear complexes, concluding that the conformation of the complexes is controlled primarily by the protonation level of the 2,2'-methylenediphenol units. The protonation level depends on the oxidation state of the metal ions and also on the pH.

In di-M(II) complexes two intramolecular phenol-phenolate strong hydrogen bonds, consistent with the loss of one proton from each methylenediphenol unit, hold the macrocycle in the saddle-shaped conformation incorporating a site for exogenous ligands to bridge the two metal ions. The structures of the  $M_2(H_4L1)$  frames of complexes **2.1-2.11** are almost superimposable (Fig. 2.52). Changing the non-macrocylic ligands or even the coordination number of the metal ions has very little effect on the overall structure of the cations.

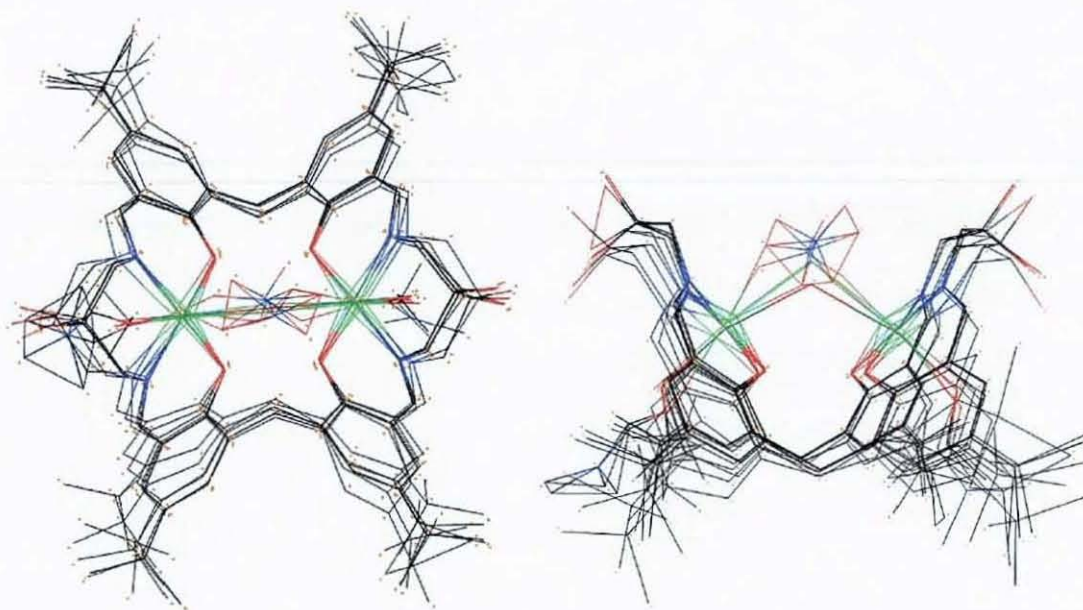


**Fig. 2.52:** Superposition of the  $M_2(H_4L1)$  core structures of the complexes **2.1-2.11**

The dinickel(II) complex  $[Ni_2(H_4L1)(MeOH)_2](ClO_4)_2 \cdot MeOH$  (**2.12**) does not contain an exogenous ligand bridging the two metal ions, unlike the other eleven examples of dinuclear complexes. However, it is very similar to the other bridged complexes, again showing the saddle-shaped conformation. This evidence confirms the hypothesis that the conformation of the complexes is controlled

primarily by the two intramolecular phenol-phenolate hydrogen bonds, which hold the macrocycle in this particular shape, and not by the bridging ligand, which is simply occupying the preformed cleft resulting from the hydrogen bonding.

The hydrogen bonds in the phenol-phenolate interaction of the complexes can be considered as strong, according to the classification of Jeffrey<sup>102,103</sup>, the distance being between 2.2 and 2.5 Å. The phenol-phenolate interaction can also be assigned to the (-)CAHB (negative charge-assisted hydrogen bonds) class<sup>104</sup>, although the presence of the coordinated metal ions might be expected to moderate the charge. This kind of hydrogen bond, where the interaction is strongly covalent, are associated with energies in the range of 62.8-167.5 kJ·mol<sup>-1</sup> and can probably be viewed as covalent bonds of three centres (O-H-O) with four electrons<sup>104</sup>. The hydrogen bonds in the complexes with a bridging water molecule are the shortest of this series and the distance increases with the size of the bridging group, suggesting some limited flexibility in the cleft and, possibly, that the nitrate ion is a tight fit.

In the case of dinuclear M(III) complexes 2.13-2.18, the different conformation is related to the complete deprotonation of the 2,2'-methylenediphenol groups, due to the higher oxidation state of the metal ion, which is a better Lewis acid and effectively lowers the pK<sub>a</sub> of the coordinated phenols. Without intramolecular hydrogen bonds binding adjacent phenol oxygen atoms, the conformation of the macrocycle relaxes and the phenol groups and metal ions move apart.

These dinuclear complexes show a real potential for host-guest chemistry as they can bind anions or neutral molecules acting as a bridge between the two metal centres and they could also bind further metal ions within the central cavity. The ability to accommodate different size of bridging molecules can be used in modelling studies of metalloenzymes,<sup>7,138-140</sup> such as urease in the case of dinickel complexes.<sup>122-124,139,140</sup> If two equivalents of anhydrous CuCl<sub>2</sub> are used and the reaction time is short, a dinuclear copper complex with a chloride ion bridging the two copper centres forms. If the reaction involves four equivalents of anhydrous

$\text{CuCl}_2$ , the tetracopper complex  $[\text{Cu}_4(\text{H}_2\text{L1})(\text{OH})_2(\text{EtOH})(\text{Cl})_2]$  (3.11) is isolated (see Chapter 3). Surprisingly, given the range of dinuclear complexes accessible with nickel or zinc, the only dinuclear bridged copper complex obtained so far is the chloride complex  $[\text{Cu}_2(\text{H}_4\text{L1})(\text{Cl})]\text{Cl}\cdot 2\text{MeOH}$  (2.1) and there is no evidence, as yet, of the isolation of a water or nitrate bridged dicopper complex in the other cases involving  $\text{Cu}(\text{NO}_3)_2$  or  $\text{Cu}(\text{ClO}_4)_2$ . Possibly the dicopper chloride complex is the most stable of those because the chloride ion is the perfect fit for the dicopper macrocyclic cavity.

The dependence of the structure on the oxidation state of the metal coordinated opens the possibility of developing redox switching systems in which clefts for guest binding can be opened or closed by external redox changes. It would be interesting to investigate the possibility of varying the oxidation states of the metal ions for the same complex and also inserting bridges across the cavity that could act as magnetic mediators. Indeed, a cobalt complex of a related macrocycle with redox-switching properties has been reported by Hisaeda *et al.*<sup>101</sup> It would also be interesting to investigate with more detail the influence of the pH in the structure of the complexes. These complexes show conformational changes with pH variations. The 2,2'-methylenediphenol unit could be used therefore as the basis of a two-way conformational switch. Formation or opening of the cleft being driven by redox changes at the metal ion or by pH changes.

Other reagents and conditions for the complex reactions could still be investigated and existing methods could be modified. It should be possible to vary the nature of the diamine without altering the hydrogen-bonded core structure of the complex; hence, it should also be possible to build specific properties into the sides of the guest-binding cleft in order to promote reactivity at the dinuclear site. Future work should also investigate electrochemical, magnetic, kinetic and thermodynamic aspects of the complexes synthesised in order to complete their characterisation.

## **CHAPTER III**

# **POLYNUCLEAR COMPLEXES OF PSEUDOCALIXARENE SCHIFF-BASE MACROCYCLES**

### 3.1. Introduction

Molecular magnetism and macrocyclic compounds are two active fields of research.<sup>2,141</sup> At the meeting point of these two fields, polynuclear complexes have received considerable attention.<sup>3,6,80,142-145</sup> Polynuclear complexes are of great interest for designing new magnetic materials and for investigating the structure and the role of the polymetallic active sites in biological systems

As mentioned in the previous chapter, the macrocyclic ligand H<sub>6</sub>L1 has been synthesised to explore the influence of the donor atoms and their relative position, the size of the chelate ring formed, the flexibility and the shape of the coordinating moiety, their planar or tridimensional architecture etc. on the metal ion binding and selectivity. The most remarkable characteristic of the series of complexes studied is the variation in the nuclearity, which can be 2, 3 or 4 for the same ligand system<sup>107</sup> This effect is linked to the variation in the extent of deprotonation of the ligand, the orientation of the phenol groups, the counter anions present and the overall shape of the macrocyclic host.

The previous chapter has focused on the formation of dinuclear complexes in order to study the mutual influence of the two metal centres on the physicochemical properties. In this chapter attention has been dedicated to the synthesis and characterisation of polynuclear species, closely related to the dinuclear analogues, which can extend or modify the properties of dinuclear complexes. The mechanism for the synthesis of this series of polynuclear complexes could be described again as a Schiff-base condensation *via* the template route.

The macrocyclic ligand H<sub>6</sub>L1 can potentially use all of the oxygen donors in the bridging mode. The presence of relatively soft imine donors in addition to the phenolic oxygen atoms also widens the range of metal ions that might be expected to bind with high stability constants.



The polynuclear complexes of the ligand  $H_6L1$  described in this chapter can be separated into two different groups:

- trinuclear complexes, where all the phenol groups are deprotonated in order to coordinate a third metal ion. In these type of complexes the metal ions occupy two different binding sites of  $H_6L1$ . Two of the metal ions occupy the  $N_2O_2$  sites (A in Fig 3 1), each coordinated to two imine groups and two phenol oxygen atoms. The third metal ion occupies the unique central calixarene-type site (B in Fig. 3 1), which involves the four phenolate donors.
- tetranuclear complexes, where four metal ions occupy the four lateral sites of the macrocycle (C in Fig. 3.1), each involving one phenol, one imine and a deprotonated alkoxy group of one of the saturated chains.

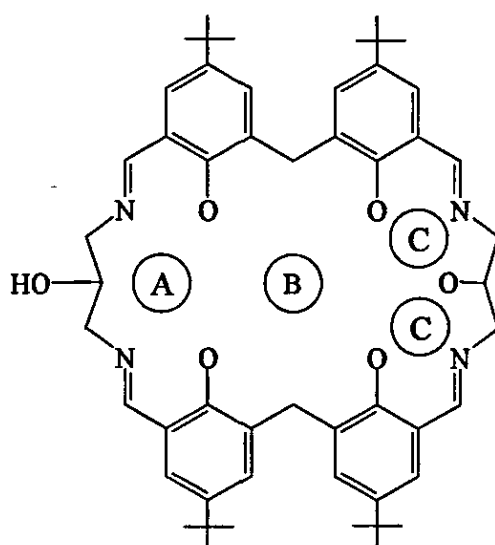
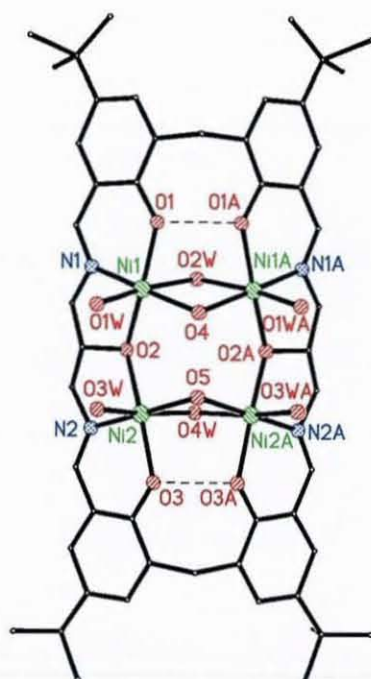


Fig. 3.1: Metal binding sites for the macrocycle  $H_6L1$

S. Goetz<sup>98</sup> first reported the synthesis of a tetranickel complex of the ligand  $H_6L1$ ,  $[Ni_4(H_2L1)(\mu_2-OH)_2(\mu_2-H_2O)_2(EtOH)_4](ClO_4)_2$ , which was synthesised by Schiff-base condensation of DHTMB with 1,3-diaminopropan-2-ol and nickel perchlorate in the presence of sodium hydroxide. This complex contains four nickel ions, each of them coordinated to three donors of the macrocycle (one phenoxy oxygen, one alkoxy oxygen and one imine nitrogen). The two sets of

opposite nickel ions (Ni1-Ni1A and Ni2-Ni2A) are doubly bridged by one hydroxo group and one water molecule. On each side of the macrocycle an alkoxo group bridges a pair of nickel atoms (Ni1-Ni2). Four ethanol molecules complete the coordination sphere of the nickel ions.



**Fig. 3.2:** Structure of the cation  $[\text{Ni}_4(\text{H}_2\text{L1})(\text{OH})_2(\text{H}_2\text{O})_2(\text{EtOH})_4]^{2+}$

As pictured in Fig. 3.3, the macrocycle is sharply folded at the saturated carbon of the methylenediphenol unit, allowing two coordinated nickel ions to share an edge. Similarly to the dinuclear complexes, the fold of the macrocycle is a consequence of a hydrogen bond between the adjacent phenolic oxygen atoms of each methylenediphenol fragment.

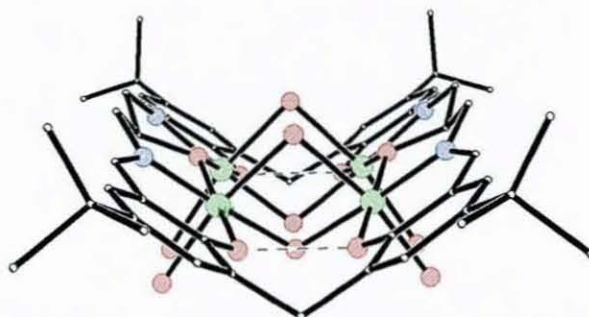


**Fig. 3.3:** Side-on view of the cation  $[\text{Ni}_4(\text{H}_2\text{L1})(\text{OH})_2(\text{H}_2\text{O})_2(\text{EtOH})_4]^{2+}$  showing the sharp fold of the macrocycle

A very closely related tetracopper complex,  $[\text{Cu}_4(\text{H}_2\text{L1})(\text{OH})_2(\text{H}_2\text{O})_2](\text{NO}_3)_2$ , was also synthesised by S. Goetz<sup>98</sup>. The structure is very similar to the tetranickel complex, with the same sharply folded conformation. The Cu(II) ions occupy the four equivalent lateral sites of the macrocycle, each linked to two other copper ions. Each metal has approximately square pyramidal geometry with macrocyclic phenoxo, alkoxo and imine donors as well as an exogenous hydroxo group at the basal sites. The hydroxo groups each bridge one pair of copper ions, which are also bridged by two water molecules at the axial sites. On each side of the macrocycle an alkoxo group bridges a different pair of copper ions.

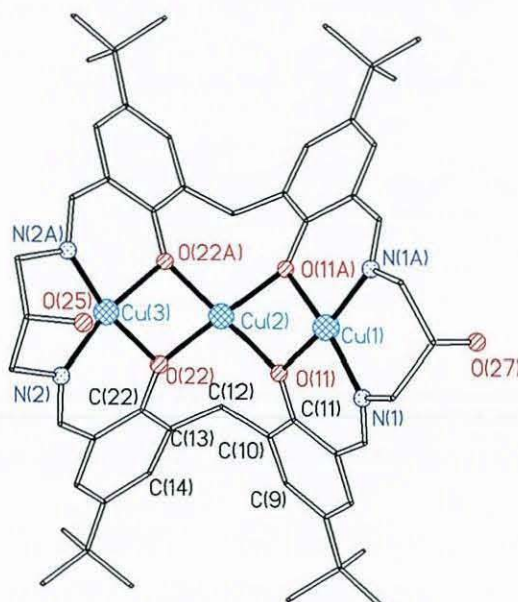


**Fig. 3.4:** Structure of  $[\text{Cu}_3(\text{L1})]$

The trinuclear complex  $[\text{Cu}_3(\text{L1})](\text{MeOH})_2$  was also isolated as a by-product of the reaction (Fig. 3.4). The tricopper complex is very similar to the previous dinuclear structures except that the central binding site is occupied by a third copper ion and that the macrocycle is completely deprotonated. The complex adopts the same saddle-shape conformation, which in this case is maintained by the copper ion in the central site rather than by two hydrogen bonds. The outer copper ions are separated from the central copper by 2.808(3) and 2.867(2) Å respectively. The distance separating the outer copper ions (5.162(3) Å) is longer than the metal-metal distances in the dinuclear complexes of ligand  $\text{H}_6\text{L1}$ . The insertion of the third metal in the central cavity causes the macrocycle to open



with the angle between the two phenyl rings of the each methylenediphenol unit being  $80.87(24)^\circ$ , which is almost  $10^\circ$  bigger than in the dinuclear species.

The formation of tri- and tetranuclear complexes indicated a range of coordination motifs that could be accessed with the ligand system  $H_6L1$ . However, Goetz's results<sup>98</sup> were preliminary and further work needed to be done in this area in order to completely understand the factors controlling the nuclearity and topology of the complexes of  $H_6L1$ .

This chapter summarises the investigation carried out into the coordination chemistry of tri- and tetranuclear complexes of the macrocyclic ligand  $H_6L1$ , derived from the [2+2] Schiff-base template synthesis of DHTMB with 1,3-diaminopropan-2-ol and the metal salts of first row transition metals. Some of the work described in this chapter has already been published.<sup>107</sup>

### 3.2. Tri- and tetracopper complexes of the pseudocalixarene macrocycle $H_6L1$

Reaction of 1,3-diaminopropan-2-ol and DHTMB with two equivalents of  $Cu(NO_3)_2 \cdot 6H_2O$  yielded a green solid on short reflux (1 h) analysing as the tetracopper complex  $[Cu_4(H_2L1)(OH)_2(H_2O)_4](NO_3)_2$  (**3.1**). A mixture of emerald green and brown crystals was obtained by slow diffusion of diethylether into a dimethylformamide solution of the tetracopper complex **3.1** in a few days. It was possible to separate these crystals by their different solubility in ethanol. The brown crystals were soluble in ethanol but not the green ones, which were filtered off. The brown product isolated was recrystallised by slow diffusion of diethylether into a dimethylformamide solution, yielding brown crystals analysing as the tricopper complex  $[Cu_3(H_2L1)(NO_3)](NO_3) \cdot dmf \cdot H_2O$  (**3.1a**). While the green product separated was recrystallised by slow evaporation of a mixture of ethanol, benzene and petroleum ether, yielding emerald green crystals of the tetracopper complex  $[Cu_4(H_2L1)(OH)_2(H_2O)(EtOH)](NO_3)_2 \cdot 2EtOH \cdot H_2O$  (**3.1b**) suitable for X-ray studies. The main product of the reaction is the tetracopper complex **3.1b**.

Reaction of 1,3-diaminopropan-2-ol and DHTMB with three equivalents of  $\text{Cu}(\text{NO}_3)_2 \cdot 6\text{H}_2\text{O}$  yielded a dark brown solid on long reflux (18 h). Brown and emerald green crystals were obtained by slow evaporation of the ethanol solution of the brown solid in a few days. These crystals were separated again by their different solubility in chloroform. The green crystals were soluble, but not the brown ones. The green product isolated analysed as  $[\text{Cu}_4(\text{HL1})(\text{NO}_3)_3(\text{H}_2\text{O})_3]$  (**3.2a**), while the brown product analysed as  $[\text{Cu}_3(\text{H}_3\text{L1})](\text{NO}_3)_3(\text{CHCl}_3)_2 \cdot 2\text{H}_2\text{O}$  (**3.2b**). Brown crystals of  $[\text{Cu}_3(\text{H}_2\text{L1})(\text{OH})(\text{H}_2\text{O})](\text{NO}_3) \cdot 4\text{EtOH}$  (**3.2d**) were obtained in a few days by slow diffusion of diethylether into an ethanol solution of the brown product isolated (**3.2b**). Brown crystals were also grown by slow diffusion of diethylether into an ethanol/dmf solution of the brown product (**3.2b**) and analysed as the tricopper complex  $[\text{Cu}_3(\text{H}_2\text{L1})(\text{NO}_3)](\text{NO}_3)(\text{dmf})_3 \cdot \text{H}_2\text{O}$  (**3.2c**). In this case the main product of the reaction is the tricopper complex **3.2b**, the ratio of brown and green crystals being approximately 5:3.

Reaction of 1,3-diaminopropan-2-ol and DHTMB with four equivalents of  $\text{Cu}(\text{NO}_3)_2 \cdot 6\text{H}_2\text{O}$  yields a green solid on short reflux (2 h) analysing as the tetracopper complex  $[\text{Cu}_4(\text{H}_3\text{L1})(\text{OH})_2(\text{H}_2\text{O})_4](\text{NO}_3)_3$  (**3.3**). When the green product was dissolved in DMF the colour changed to dark brown within a week, suggesting that the tetracopper complex has converted into the tricopper complex. Recrystallisation by slow diffusion of diethylether into the DMF/EtOH solution gave brown crystals of the trinuclear complex  $[\text{Cu}_3(\text{H}_2\text{L1})(\text{NO}_3)](\text{NO}_3)(\text{dmf})_3$  (**3.3a**) suitable for X-ray studies as the only product.

### 3.2.1. Structure of $[\text{Cu}_3(\text{H}_2\text{L1})(\text{OH})(\text{H}_2\text{O})](\text{NO}_3) \cdot 4\text{EtOH}$

Brown crystals of  $[\text{Cu}_3(\text{H}_2\text{L1})(\text{OH})(\text{H}_2\text{O})](\text{NO}_3) \cdot 4\text{EtOH}$  (**3.2d**) were grown by slow diffusion of diethylether into an ethanol solution of the tricopper(II) complex  $[\text{Cu}_3(\text{H}_3\text{L1})](\text{NO}_3)_3(\text{CHCl}_3)_2 \cdot 2\text{H}_2\text{O}$  (**3.2b**). The crystals studied were not very good, decreasing the quality and resolution of the X-ray data and, consequently, the accuracy of the atomic positions. All the X-ray data collection parameters are summarised in Table 10 of appendix 1 along with the details concerning the



refinement and disorder. Perspective views of the cation  $[\text{Cu}_3(\text{H}_2\text{L1})(\text{OH})(\text{H}_2\text{O})]_n^+$  are shown in Figs. 3.5 and 3.6 and selected bond lengths and angles relevant to the metals coordination are given in Table 3.1.

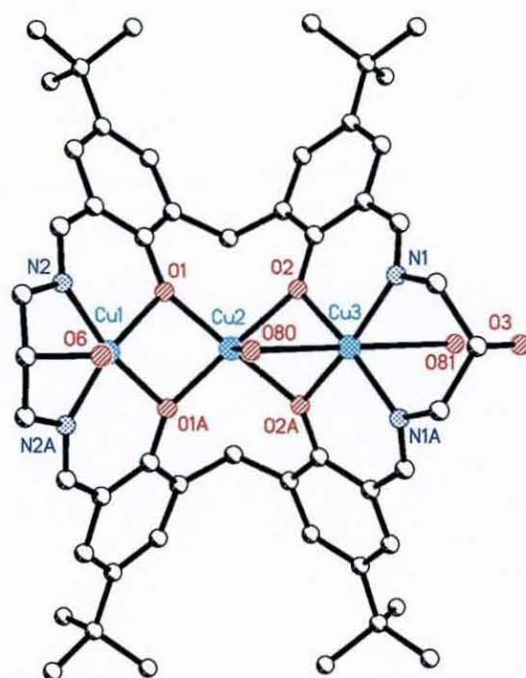


**Fig. 3.5:** Structure of the cation  $[\text{Cu}_3(\text{H}_2\text{L1})(\text{OH})(\text{H}_2\text{O})]_n^+$

The tricopper(II) complex is dark brown, presumably because of charge transfer between the fully deprotonated phenolate groups and the Cu(II) ions. One of the copper ions occupying a lateral site of the macrocycle (Cu1) and the copper atom that occupies the central site (Cu2) are in square pyramidal environments, while the remaining copper ion (Cu3) is in a tetragonal environment, with the atoms O80 and O81 as the axial ligands. The coordinated oxygen atoms O80 and O81 were not further refined because of the poor quality of the crystal and were modelled as an hydroxy group (O80), bridging the copper ions Cu2 and Cu3, and a water molecule (O81), axially coordinated to the copper ion Cu3.

As depicted in Fig. 3.6, one of the pendant alkoxy groups points inside the cavity of the macrocycle while the other one points outside. The latter one (O3) acts as an axial ligand (2.309(8) Å) to one of the copper ions (Cu1) belonging to the neighbouring macrocyclic unit resulting in a one-dimensional chain (Fig. 3.7).

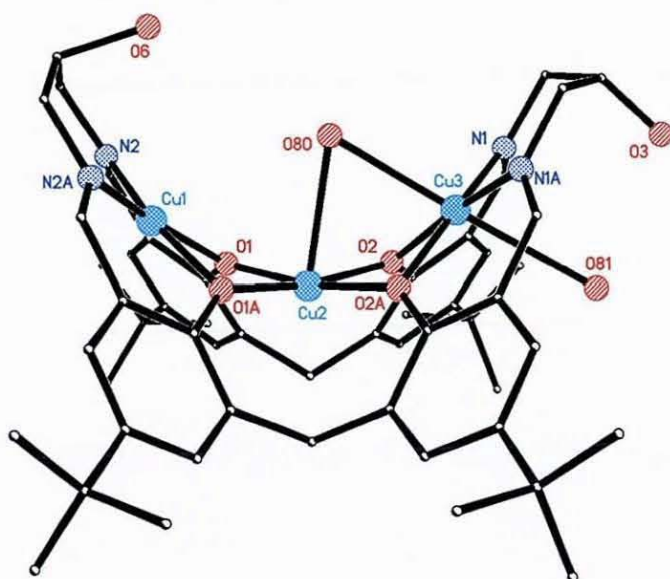


**Fig. 3.6:** Side-on view of the cation  $[\text{Cu}_3(\text{H}_2\text{L1})(\text{OH})(\text{H}_2\text{O})]_n^+$

The outer copper atoms are separated from the central copper atom (Cu2) by 2.839(2) and 2.778(2) Å respectively. The distance separating Cu1 and Cu3 is 5.162(3) Å, which is longer than the metal-metal distances in the dinuclear complexes of ligand  $\text{H}_6\text{L1}$ . The insertion of the third metal in the central cavity causes the macrocycle to open with the angle between the two phenyl rings of the each methylenediphenol unit being  $80.87(24)^\circ$ , which is almost  $10^\circ$  bigger than in the dinuclear species.

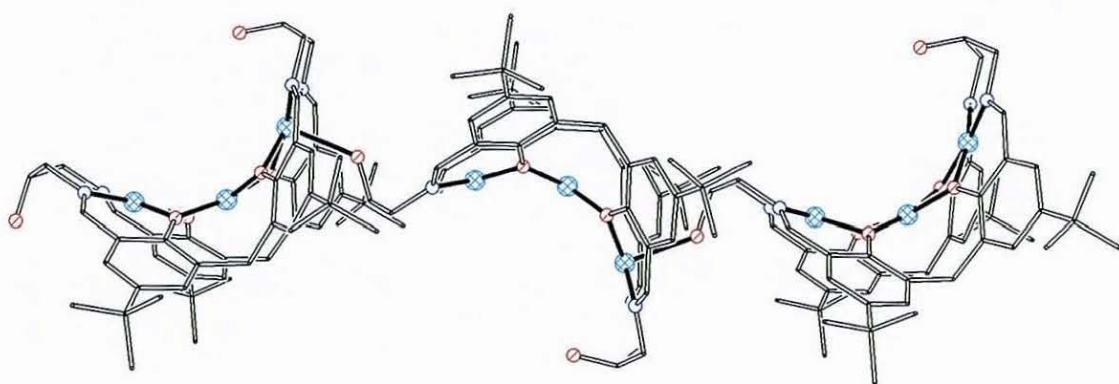


**Fig. 3.7:** One dimensional chain of cation  $[\text{Cu}_3(\text{H}_2\text{L1})]_n^{2+}$  (the coordinated water molecules and hydroxy ions have been omitted for more clarity)



**Table 3.1:** Selected bond lengths [ $\text{\AA}$ ] and angles [ $^\circ$ ] for  $[\text{Cu}_3(\text{H}_2\text{L1})(\text{OH})(\text{H}_2\text{O})](\text{NO}_3)\cdot 4\text{EtOH}$ 

Cu(3)-O(2)*	1.937(5)	Cu(2)-O(1)	1.890(5)	Cu(1)-O(1)*	1.968(5)
Cu(3)-O(2)	1.937(5)	Cu(2)-O(2)	1.923(5)	Cu(1)-O(1)	1.968(5)
Cu(3)-N(1)	1.955(6)	Cu(2)-O(2)*	1.923(5)	Cu(1)-O(3)**	2.330(9)
Cu(3)-N(1)*	1.955(6)	Cu(2)-Cu(1)	2.839(2)	Cu(1)-Cu(3)	5.162(3)
Cu(3)-Cu(2)	2.778(2)	Cu(1)-N(2)	1.928(7)		
Cu(2)-O(1)*	1.890(5)	Cu(1)-N(2)*	1.928(7)		
O(2)*-Cu(3)-O(2)	79.6(3)	O(1)*-Cu(2)-O(2)*	97.7(2)	O(1)*-Cu(1)-O(1)	78.4(3)
O(2)*-Cu(3)-N(1)	170.2(3)	O(1)-Cu(2)-O(2)*	169.5(2)	N(2)-Cu(1)-O(3)**	94.4(3)
O(2)-Cu(3)-N(1)	91.2(2)	O(2)-Cu(2)-O(2)*	80.3(3)	N(2)*-Cu(1)-O(3)**	94.4(3)
O(2)*-Cu(3)-N(1)*	91.2(2)	Cu(3)-Cu(2)-Cu(1)	129.87(7)	O(1)*-Cu(1)-O(3)**	91.3(2)
O(2)-Cu(3)-N(1)*	170.2(3)	N(2)-Cu(1)-N(2)*	98.3(4)	O(1)-Cu(1)-O(3)**	91.3(2)
N(1)-Cu(3)-N(1)*	97.9(4)	N(2)-Cu(1)-O(1)*	168.4(3)	Cu(2)-O(1)-Cu(1)	94.7(2)
O(1)*-Cu(2)-O(1)	82.4(3)	N(2)*-Cu(1)-O(1)*	91.3(3)	Cu(2)-O(2)-Cu(3)	92.1(2)
O(1)*-Cu(2)-O(2)	169.5(2)	N(2)-Cu(1)-O(1)	91.3(3)		
O(1)-Cu(2)-O(2)	97.7(2)	N(2)*-Cu(1)-O(1)	168.4(3)		

Symmetry transformations used to generate equivalent atoms: (\*)  $x, y, -z$  (\*\*)  $-x-7/2, y-1/2, -z$

### 3.2.2. Structure of $[\text{Cu}_3(\text{H}_2\text{L1})(\text{NO}_3)](\text{NO}_3)\cdot 3\text{dmf}$

During ongoing investigations of the tricopper/tetracopper reaction, a second form of the tricopper complex was obtained by crystallisation. Brown crystals of  $[\text{Cu}_3(\text{H}_2\text{L1})(\text{NO}_3)](\text{NO}_3)\cdot 3\text{dmf}$  (**3.3a**) suitable for X-ray studies were grown by slow diffusion of diethylether into a DMF solution of the tetracopper(II) complex  $[\text{Cu}_4(\text{H}_3\text{L1})(\text{OH})_2(\text{H}_2\text{O})_4](\text{NO}_3)_3$  (**3.3**).

This trinuclear copper(II) complex is very similar to the previous tricopper structure except that in this structure there is a coordinated nitrate ion which lies within the concave curve of the three copper sites. All the X-ray data collection parameters are summarised in Table 11 of appendix 1 along with the details concerning the refinement and disorder. A perspective view of the complex is shown in Fig. 3.8 and selected bond lengths and angles relevant to the metals coordination are given in Table 3.2.

As in the previous tricopper structure, the cations occupy the two lateral and the unique central sites of the macrocycle, with each ion bound to four macrocyclic donors in its basal plane. The coordinated nitrate ion is disordered (70:30) between two related positions; one site involves a single atom bridge between Cu1 and Cu2 and a three atom bridge between Cu2 and Cu3, while the minor site (white bonding in Fig. 3.8) provides a single atom bridge between Cu2 and Cu3 with a three atom bridge linking Cu1 and Cu2. The formula unit is completed by one nitrate counter-ion and three DMF lattice molecules, involved in hydrogen bonding to the complex.

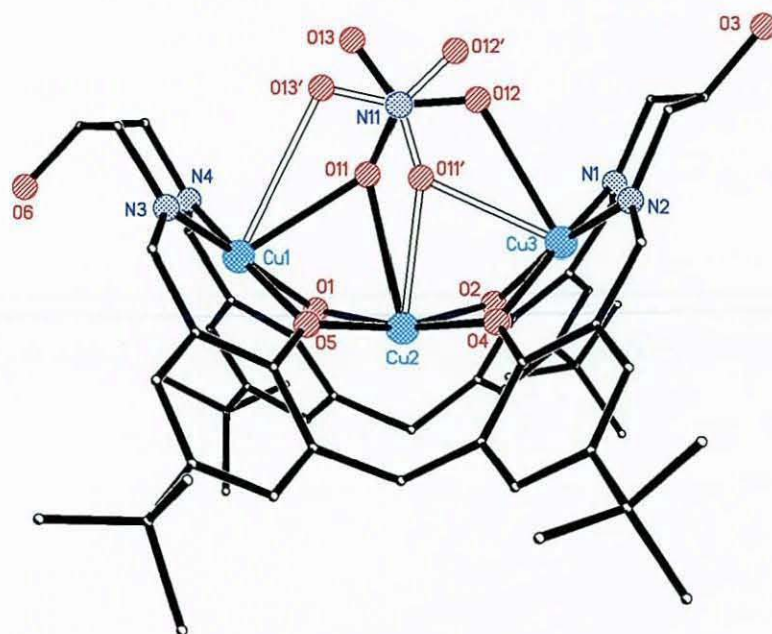


**Fig. 3.8:** Side-on view of  $[\text{Cu}_3(\text{H}_2\text{L1})(\text{NO}_3)]^+$  showing the nitrate disorder

The macrocycle adopts the same saddle-shape conformation as the previous tricopper complex. The macrocycle has lost the four protons of the phenol groups and the saddle-shape conformation is again maintained by the copper ion in the central site rather than by two hydrogen bonds linking adjacent phenol oxygen atoms as in the case of the dinuclear complexes of  $\text{H}_2\text{L1}$ .



**Table 3.2:** Selected bond lengths [ $\text{\AA}$ ] and angles [ $^\circ$ ] for  $[\text{Cu}_3(\text{H}_2\text{L1})(\text{NO}_3)]^+$ 

Cu(1)-N(3)	1.935(4)	Cu(2)-O(4)	1.929(3)
Cu(1)-N(4)	1.935(5)	Cu(2)-O(11)	2.490(5)
Cu(1)-O(5)	1.956(4)	Cu(2)-O(11')	2.400(14)
Cu(1)-O(1)	1.957(3)	Cu(2)-Cu(3)	2.8616(9)
Cu(1)-O(11)	2.432(5)	Cu(3)-N(2)	1.936(4)
Cu(1)-O(13')	2.98(3)	Cu(3)-N(1)	1.942(5)
Cu(1)-Cu(2)	2.8428(8)	Cu(3)-O(2)	1.945(3)
Cu(2)-O(1)	1.918(3)	Cu(3)-O(4)	1.952(3)
Cu(2)-O(5)	1.925(3)	Cu(3)-O(12)	2.613(9)
Cu(2)-O(2)	1.928(3)	Cu(3)-O(11')	2.444(17)
<hr/>			
N(3)-Cu(1)-N(4)	98.2(2)	O(4)-Cu(2)-O(11')	77.4(4)
N(3)-Cu(1)-O(5)	91.73(18)	O(1)-Cu(2)-O(11)	74.89(18)
N(4)-Cu(1)-O(5)	170.05(18)	O(5)-Cu(2)-O(11)	75.34(17)
N(3)-Cu(1)-O(1)	171.34(18)	O(2)-Cu(2)-O(11)	90.58(18)
N(4)-Cu(1)-O(1)	90.46(18)	O(4)-Cu(2)-O(11)	93.23(18)
O(5)-Cu(1)-O(1)	79.64(14)	N(2)-Cu(3)-N(1)	99.36(19)
N(3)-Cu(1)-O(11)	101.8(2)	N(2)-Cu(3)-O(2)	167.53(18)
N(4)-Cu(1)-O(11)	100.5(2)	N(1)-Cu(3)-O(2)	91.55(16)
O(5)-Cu(1)-O(1)	76.26(17)	N(2)-Cu(3)-O(4)	91.22(17)
O(1)-Cu(1)-O(11)	75.69(17)	N(1)-Cu(3)-O(4)	168.64(17)
N(3)-Cu(1)-O(13')	80.5(5)	O(2)-Cu(3)-O(4)	77.51(14)
N(4)-Cu(1)-O(13')	81.2(5)	N(2)-Cu(3)-O(11')	107.8(4)
O(5)-Cu(1)-O(13')	99.5(4)	N(1)-Cu(3)-O(11')	104.5(4)
O(1)-Cu(1)-O(13')	100.2(5)	O(2)-Cu(3)-O(11')	74.9(4)
O(1)-Cu(2)-O(5)	81.37(14)	O(4)-Cu(3)-O(11')	75.9(4)
O(1)-Cu(2)-O(2)	98.74(14)	N(2)-Cu(3)-O(12)	84.9(2)
O(5)-Cu(2)-O(2)	165.44(15)	N(1)-Cu(3)-O(12)	82.8(2)
O(1)-Cu(2)-O(4)	167.84(15)	O(2)-Cu(3)-O(12)	102.55(17)
O(5)-Cu(2)-O(4)	98.35(15)	O(4)-Cu(3)-O(12)	102.45(18)
O(2)-Cu(2)-O(4)	78.46(14)	Cu(1)-O(1)-Cu(2)	94.38(14)
O(1)-Cu(2)-O(11')	90.5(4)	Cu(2)-O(2)-Cu(3)	95.28(14)
O(5)-Cu(2)-O(11')	89.1(4)	Cu(2)-O(4)-Cu(3)	95.02(14)
O(2)-Cu(2)-O(11')	76.3(4)	Cu(2)-O(5)-Cu(1)	94.18(15)

**3.2.3. Structure of  $[\text{Cu}_4(\text{H}_2\text{L1})(\text{OH})_2(\text{H}_2\text{O})(\text{EtOH})](\text{NO}_3)_2 \cdot 2\text{EtOH} \cdot \text{H}_2\text{O}$** 

Green crystals of  $[\text{Cu}_4(\text{H}_2\text{L1})(\text{OH})_2(\text{H}_2\text{O})(\text{EtOH})](\text{NO}_3)_2 \cdot 2\text{EtOH} \cdot \text{H}_2\text{O}$  (**3.1b**) suitable for X-ray studies were obtained by slow evaporation of a solution of the tetracopper complex  $[\text{Cu}_4(\text{H}_2\text{L1})(\text{OH})_2(\text{H}_2\text{O})_4](\text{NO}_3)_2$  (**3.1**) in an ethanol, benzene and petroleum ether mixture. All the X-ray data collection parameters are summarised in Table 12 of appendix 1 along with the details concerning the refinement and disorder. Perspective views of the complex are shown in Figs. 3.9 and 3.10 and selected bond lengths and angles relevant to the metals coordination are given in Table 3.3.



The overall conformation of the tetracopper complex is very different to the previous dinuclear and trinuclear structures but very similar to the tetranickel(II) complex described above. Similarly to the dinuclear complexes, each adjacent pair of phenol oxygen atoms is monodeprotonated and linked by a hydrogen bond ( $O1\cdots O2$  2.395(7)Å and  $O4\cdots O5$  2.417(6)Å). Again, it is likely that the complex shape is maintained by the H-bonds and supported by bridging  $OH^-$  and solvent molecules. The macrocycle, however, does not adopt the saddle-shape conformation. The pendant alkoxy groups of the macrocycle are deprotonated and contribute to the coordinating sphere of the metal ions. The saturated portions of the ring are fully extended to allow each alkoxy group to bridge two copper ions and the macrocycle is sharply folded along its long axis, with each half approximately planar. The value of the angles between the planes formed by the adjacent phenol groups of each methylenediphenol fragment are  $65.6(2)$  and  $66.3(2)^\circ$ , which are smaller than in the related dinuclear species. As a result of accommodating four metal centres the macrocycle has stretched, which shows the extent of flexibility of the macrocyclic ligand  $H_6L1$  due to the presence flexible lateral chains.

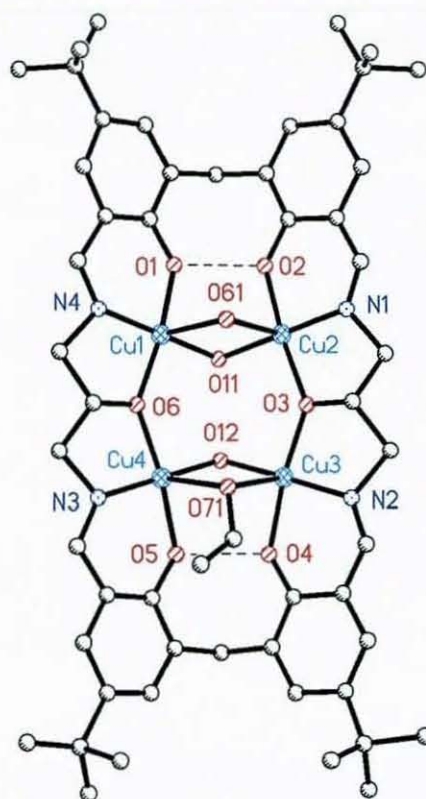


**Fig. 3.9:** Structure of the cation  $[Cu_4(H_2L1)(OH)_2(H_2O)(EtOH)]^+$

The Cu(II) ions occupy the four equivalent lateral sites of the macrocycle, each linked to two other copper ions. Each metal has approximately square pyramidal geometry with macrocyclic phenoxo, alkoxo and imine donors as well as an exogenous  $\mu_2$ -hydroxo group at the basal sites situated in the fold of the macrocycle. The axial ligands are disordered and have been modelled as having 50% occupancy of water and ethanol at each site. The Jahn-Teller effect explains the observation that one of the bridging units (the oxygen atom on one of the basal coordination sites) is coordinated more strongly to the copper ions at a distance of *ca.* 1.91 Å, while the other unit (the oxygen atom on the axial coordination site) is at a distance of *ca.* 2.47 Å.

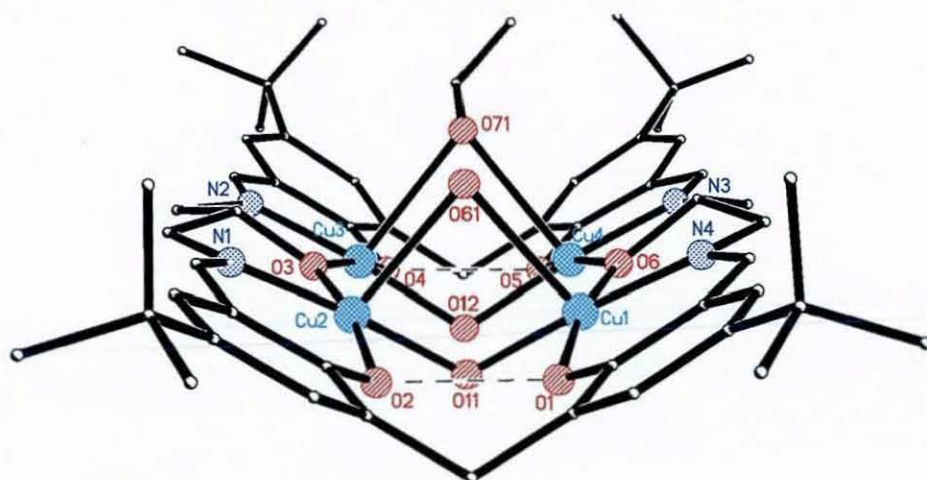


**Fig. 3.10:** Side-on view of the cation  $[\text{Cu}_4(\text{H}_2\text{L1})(\text{OH})_2(\text{H}_2\text{O})(\text{EtOH})]^+$  showing the sharp fold of the macrocycle

The bridging equatorial hydroxo groups might influence the metal-metal distance by pulling the copper ions together, in contrast to the dinuclear complexes where no hydroxo groups are present. The distance separating opposite metal ions ( $\text{Cu1}\cdots\text{Cu2}$  3.143(2) Å and  $\text{Cu3}\cdots\text{Cu4}$  3.160(1) Å) is smaller than the M-M distance in the dinuclear complexes studied.

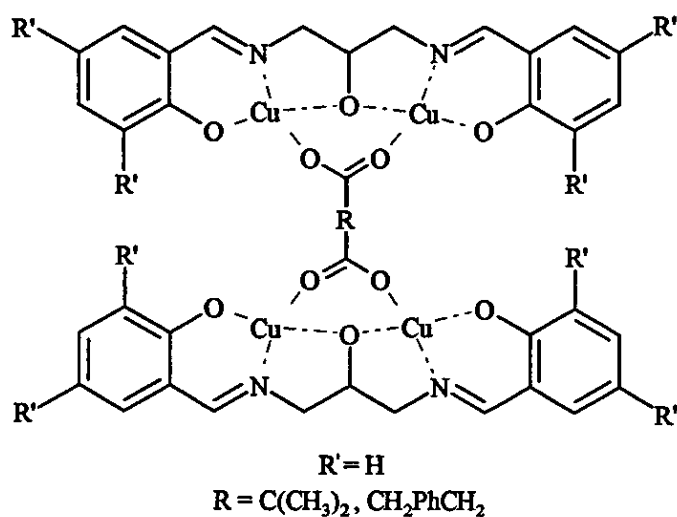
As previously mentioned, two very closely related tetranuclear complexes,  $[\text{Cu}_4(\text{H}_2\text{L1})(\text{OH})_2(\text{H}_2\text{O})_2](\text{NO}_3)_2$  and  $[\text{Ni}_4(\text{H}_2\text{L1})(\text{OH})_2(\text{H}_2\text{O})_2(\text{EtOH})_4](\text{ClO}_4)_2$ , were synthesised and characterised by S. Goetz during the course of her PhD

project.<sup>98</sup> The crystal structures of both complexes are virtually identical to the tetracopper complex structure here described in that the sharply folded conformation of the macrocycle is the same in each case (superimposable). This is likely to be a consequence of the hydrogen links between the phenolate oxygen atoms of each monodeprotonated 2,2'-methylenediphenol unit, as previously observed in the dinuclear complexes described in Chapter 2.

**Table 3.3:** Selected bond lengths [Å] and angles [°] for  $[\text{Cu}_4(\text{H}_2\text{L})(\text{OH})_2(\text{H}_2\text{O})(\text{EtOH})(\text{NO}_3)_2 \cdot 2\text{EtOH} \cdot \text{H}_2\text{O}]$

Cu(1)-O(11)	1 927(5)	Cu(3)-O(3)	1.963(5)
Cu(1)-N(4)	1 932(8)	Cu(3)-O(4)	2.007(5)
Cu(1)-O(6)	1 961(5)	Cu(3)-O(71)	2.520(7)
Cu(1)-O(1)	1 995(5)	Cu(4)-N(3)	1.898(7)
Cu(1)-O(61)	2 420(6)	Cu(4)-O(12)	1.909(5)
Cu(2)-N(1)	1 904(6)	Cu(4)-O(6)	1.979(5)
Cu(2)-O(11)	1 928(5)	Cu(4)-O(5)	1.997(5)
Cu(2)-O(3)	1 963(5)	Cu(4)-O(71)	2.527(7)
Cu(2)-O(2)	1 977(5)	Cu(1)-Cu(2)	3.143(2)
Cu(2)-O(61)	2 402(6)	Cu(3)-Cu(4)	3.160(1)
Cu(3)-O(12)	1 889(5)	Cu(2)-Cu(3)	3 681(1)
Cu(3)-N(2)	1.935(7)	Cu(1)-Cu(4)	3 677(1)
O(11)-Cu(1)-N(4)	176.3(3)	O(12)-Cu(3)-O(4)	88 9(2)
O(11)-Cu(1)-O(6)	95.9(2)	N(2)-Cu(3)-O(4)	89 0(2)
N(4)-Cu(1)-O(6)	85 0(2)	O(3)-Cu(3)-O(4)	170 4(2)
O(11)-Cu(1)-O(1)	88.04(19)	O(12)-Cu(3)-O(71)	83 9(2)
N(4)-Cu(1)-O(1)	90.5(2)	N(2)-Cu(3)-O(71)	100 6(3)
O(6)-Cu(1)-O(1)	170.3(2)	O(3)-Cu(3)-O(71)	102 1(2)
O(11)-Cu(1)-O(61)	82.5(2)	O(4)-Cu(3)-O(71)	87.2(2)
N(4)-Cu(1)-O(61)	101.0(3)	N(3)-Cu(4)-O(12)	175 6(3)
O(6)-Cu(1)-O(61)	98.7(2)	N(3)-Cu(4)-O(6)	85 4(2)
O(1)-Cu(1)-O(61)	90.6(2)	O(12)-Cu(4)-O(6)	95.2(2)
N(1)-Cu(2)-O(11)	175.3(3)	N(3)-Cu(4)-O(5)	90 7(2)
N(1)-Cu(2)-O(3)	86.0(2)	O(12)-Cu(4)-O(5)	88 08(19)
O(11)-Cu(2)-O(3)	95.0(2)	O(6)-Cu(4)-O(5)	170 3(2)
N(1)-Cu(2)-O(2)	90.4(2)	N(3)-Cu(4)-O(71)	100 9(3)
O(11)-Cu(2)-O(2)	87.9(2)	O(12)-Cu(4)-O(71)	83 3(2)
O(3)-Cu(2)-O(2)	170 6(2)	O(6)-Cu(4)-O(71)	102 3(2)
N(1)-Cu(2)-O(61)	101.4(3)	O(5)-Cu(4)-O(71)	87 1(2)
O(11)-Cu(2)-O(61)	83.0(2)	Cu(3)-O(3)-Cu(2)	139 4(3)
O(3)-Cu(2)-O(61)	97.8(2)	Cu(1)-O(6)-Cu(4)	137.9(3)
O(2)-Cu(2)-O(61)	91.4(2)	Cu(1)-O(11)-Cu(2)	109 2(2)
O(12)-Cu(3)-N(2)	174.9(3)	Cu(3)-O(12)-Cu(4)	112 6(2)
O(12)-Cu(3)-O(3)	94.5(2)	Cu(2)-O(61)-Cu(1)	81.36(16)
N(2)-Cu(3)-O(3)	86.9(2)	Cu(3)-O(71)-Cu(4)	77.54(18)

The related tetracopper complex  $[\{\text{Cu}_2(\text{L24})\}_2(\text{O}_2\text{C-R-CO}_2)]$  (Scheme 3.1) has been reported by Lee *et al.*<sup>146</sup> The acyclic complex presents similar metal sites to the tetracopper complex  $[\text{Cu}_4(\text{H}_2\text{L1})(\text{OH})_2(\text{H}_2\text{O})(\text{EtOH})](\text{NO}_3)_2 \cdot 2\text{EtOH} \cdot \text{H}_2\text{O}$  (3.1b) just described, each of the metals being coordinated by the imine nitrogen, phenoxo oxygen, and the bridging alkoxo oxygen afforded by the ligand. Two copper ions are bridged by the alkoxo oxygen, similarly to the complex 3.1b, but in this case the pair of copper ions is doubly bridged and linked to another dicopper unit by a ligand containing two dicarboxylato groups, forming the tetracopper dimer (Scheme 3.1). An analogous tetranuclear copper(II) complex in which the two dimeric  $\{\text{Cu}_2\text{L24}\}$  units are linked instead by 3-phenylpyrazole ligands was also reported by Chakravarty *et al.*<sup>147</sup>



**Scheme 3.1:**  $\mu$ -alkoxo- $\mu$ -dicarboxylato doubly bridged tetranuclear copper(II) complex  $[\{\text{Cu}_2(\text{L24})\}_2(\text{O}_2\text{C-R-CO}_2)]$

### 3.2.4. IR and LSIMS characterisation

The tri- and tetracopper complexes studied were initially characterised by IR spectroscopy, where formation of the Schiff-base macrocycle was indicated by disappearance of the carbonyl ( $1658\text{ cm}^{-1}$  in DHTMB) and amine stretches associated with the reactants, along with appearance of an imine stretching band

at  $1625\text{ cm}^{-1}$  for the tricopper complex  $[\text{Cu}_3(\text{H}_2\text{L1})(\text{OH})(\text{H}_2\text{O})](\text{NO}_3)\cdot 4\text{EtOH}$  (3.2d) and at  $1647\text{ cm}^{-1}$  or for the tetracopper complex  $[\text{Cu}_4(\text{H}_2\text{L1})(\text{OH})_2(\text{H}_2\text{O})_4](\text{NO}_3)_2$  (3.1) or at  $1630\text{ cm}^{-1}$  for the tetracopper complex  $[\text{Cu}_4(\text{H}_3\text{L1})(\text{OH})_2(\text{H}_2\text{O})_4](\text{NO}_3)_3$  (3.3). The band at  $1383\text{ cm}^{-1}$  is indicative of the presence of nitrate ions in both tri- and tetracopper complexes. Free nitrate ions normally exhibit three NO stretching bands, related to the three normal modes of vibration of the planar ions ( $\nu_{\text{asym}}(\text{NO}_2)$  at  $\sim 1455\text{ cm}^{-1}$ ;  $\nu_{\text{sym}}(\text{NO}_2)$  at  $\sim 1383\text{ cm}^{-1}$  and  $\nu(\text{NO})$  at  $\sim 830\text{ cm}^{-1}$ ). The IR analyses performed showed the band at  $1383\text{ cm}^{-1}$  as the most intense, although the other two bands could also be observed at less intensity.

Further indication of the tri- or tetranuclear nature of the complexes was obtained from mass spectral data. The LSIMS spectrum of the complex  $[\text{Cu}_3(\text{H}_2\text{L1})(\text{NO}_3)](\text{NO}_3)(\text{dmf})_3\cdot\text{H}_2\text{O}$  (3.2c) (Table 3.4, Fig. 3.11) shows a peak at  $m/z$  1029 corresponding to a singly charged ion containing the trimetallic fragment  $[\text{Cu}_3(\text{HL1})-\text{H}]^+$ . The peaks at  $m/z$  1089, 1094 and 1136 also suggest the formation of the trinuclear complex. The presence of clusters of peaks at higher mass attributable to dimerisation of the tricopper complex is in agreement with the results obtained by X-ray crystallographic studies, which suggested that individual units of complex  $[\text{Cu}_3(\text{L1})]$  form one dimensional chains

**Table 3.4:** Peak attributions for  $[\text{Cu}_3(\text{H}_2\text{L1})(\text{NO}_3)](\text{NO}_3)(\text{dmf})_3\cdot\text{H}_2\text{O}$

M/z	Rel. Intensity (%)	Fragments	Calc. Mass
969	95	$[\text{Cu}_2(\text{H}_2\text{L1})+\text{H}]^+$	969
1029	97	$[\text{Cu}_3(\text{HL1})-\text{H}]^+$	1029
1089	100	$[\text{Cu}_3(\text{H}_2\text{L1})(\text{OH})_2+\text{Na}]^+$	1088
1094	75	$[\text{Cu}_3(\text{H}_2\text{L1})(\text{NO}_3)+\text{H}]^+$	1094
1136	25	$[\text{Cu}_3(\text{H}_2\text{L1})(\text{NO}_3)(\text{EtOH})-\text{H}]^+$	1138
1934	8	$[(\text{Cu}_2(\text{H}_2\text{L1}))_2-\text{H}]^+$	1936
1995	4	$[(\text{Cu}_3(\text{L1}))_2-\text{Cu}]^+$	1995
2058	5	$[(\text{Cu}_3(\text{L1}))_2+\text{H}]^+$	2058
2119	5	$[(\text{Cu}_3(\text{L1}))_2(\text{NO}_3)_2-\text{Cu}]^+$	2119
2201	5	$[(\text{Cu}_3(\text{HL1}))_2(\text{NO}_3)]^+$	2123



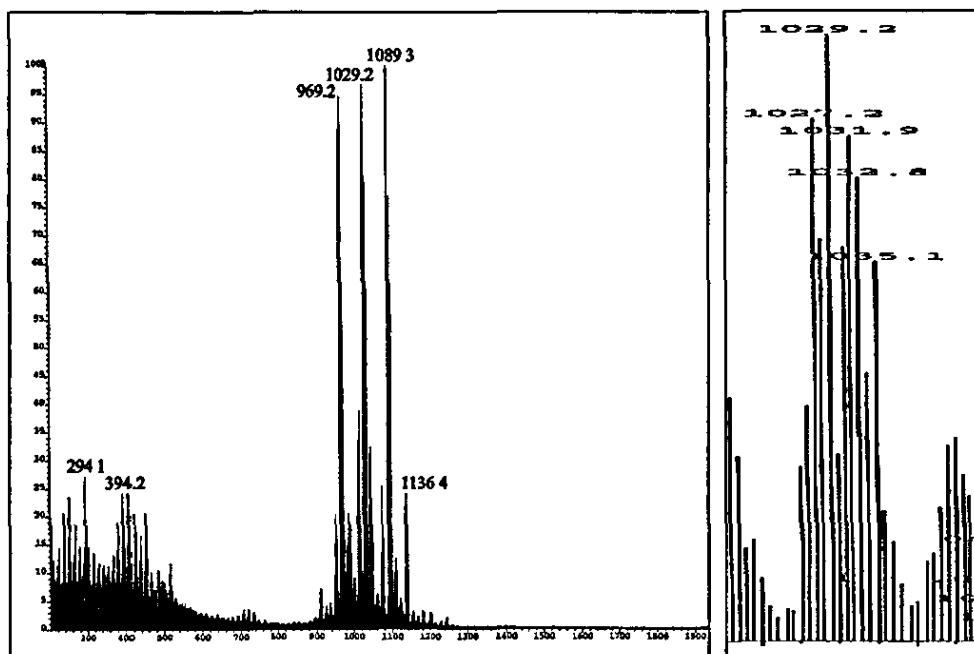


Fig. 3.11: LSIMS spectrum of  $[\text{Cu}_3(\text{H}_2\text{L1})(\text{NO}_3)](\text{NO}_3)(\text{dmf})_3 \cdot \text{H}_2\text{O}$  and fragment expansion of the peak at  $m/z$  1029

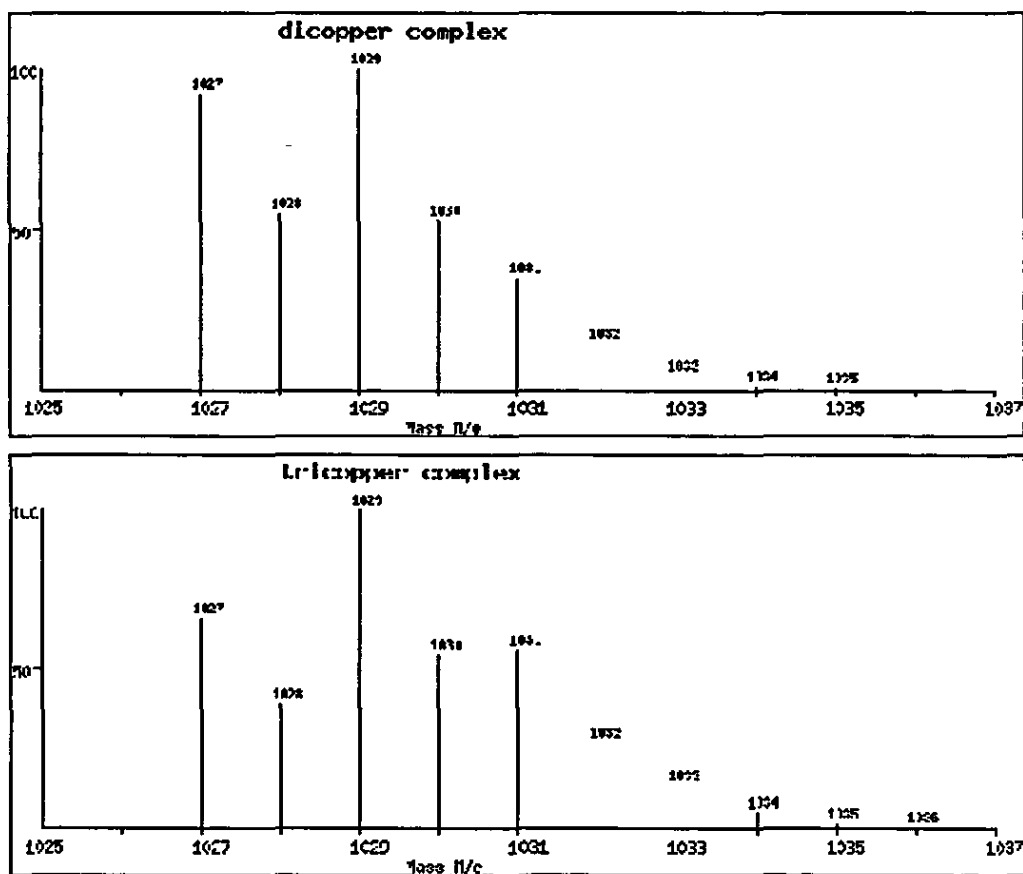


Fig. 3.12: Calculated isotopic distribution for the fragments  $[\text{Cu}_2(\text{H}_4\text{L1})(\text{NO}_3)-3\text{H}]^+$  and  $[\text{Cu}_3(\text{HL1})-\text{H}]^+$

The case of LSIMS spectra of complexes containing both copper(II) and nitrate counter ions deserves special attention. The fact that the mass of the copper and the nitrate ions are 63 and 62 g/mol respectively could lead to errors in the calculation of the fragments present in the spectra (e.g. the peak at  $m/z$  1029 could be attributed to the dicopper fragment  $[\text{Cu}_2(\text{H}_4\text{L1})(\text{NO}_3)_3\text{H}]^+$  or to the tricopper fragment  $[\text{Cu}_3(\text{HL1})\text{-H}]^+$ ). The observed isotope distribution of each peak in the spectrum for a given complex is characteristic and comparison with the theoretical isotope distribution pattern (calculated by the Isotopic Distribution Calculator program<sup>119</sup>) is a very useful method of double checking the formula of the ion being measured. Figures 3.11 and 3.12 show experimental and calculated isotopic patterns for the molecular ion signal at  $m/z$  1029. The agreement of calculated and experimental isotopic pattern confirms the formula given for the molecular ion fragment  $[\text{Cu}_3(\text{HL1})\text{-H}]^+$ . However, even with the isotopic distributions, the difference between the peaks is not always clear (Figs 3.12). The presence of little impurities in the sample could change the relative intensities of the peaks and this would lead to confusion between complexes.

The LSIMS spectrum of  $[\text{Cu}_4(\text{H}_2\text{L1})(\text{OH})_2(\text{H}_2\text{O})_2](\text{NO}_3)_2 \cdot 2\text{H}_2\text{O}$  (3.1) shows peaks corresponding to singly charged ions for both the trimetallic and the tetrametallic species (Table 3.5, Fig. 3.13). It shows the main peak at  $m/z$  1091 which can be assigned to the fragment  $[\text{Cu}_4(\text{L1}) + e]^+$ . The peaks at  $m/z$  1111, 1127 and 1156 also suggest the formation of the tetranuclear complex, while the peak at  $m/z$  1032 could be attributed to the trimetallic fragment  $[\text{Cu}_3(\text{H}_2\text{L1}) + e]^+$  or also to the tetrametallic fragment  $[\text{Cu}_4(\text{H}_2\text{L1}) - \text{Cu}]^+$ .

**Table 3.5:** Peak attributions for  $[\text{Cu}_4(\text{H}_2\text{L1})(\text{OH})_2(\text{H}_2\text{O})_2](\text{NO}_3)_2 \cdot 2\text{H}_2\text{O}$

$m/z$	Rel. Intensity (%)	Fragments	Calc. Mass
1032	37	$[\text{Cu}_3(\text{H}_2\text{L1}) + e]^+$	1032
1091	100	$[\text{Cu}_4(\text{L1}) + e]^+$	1093
1111	82	$[\text{Cu}_4(\text{L1})(\text{OH}) + \text{H}]^+$	1111
1127	83	$[\text{Cu}_4(\text{H}_2\text{L1})(\text{OH})_2 - \text{H}]^+$	1127
1156	60	$[\text{Cu}_4(\text{H}_2\text{L1})(\text{OH})(\text{EtO}) - \text{H}]^+$	1156

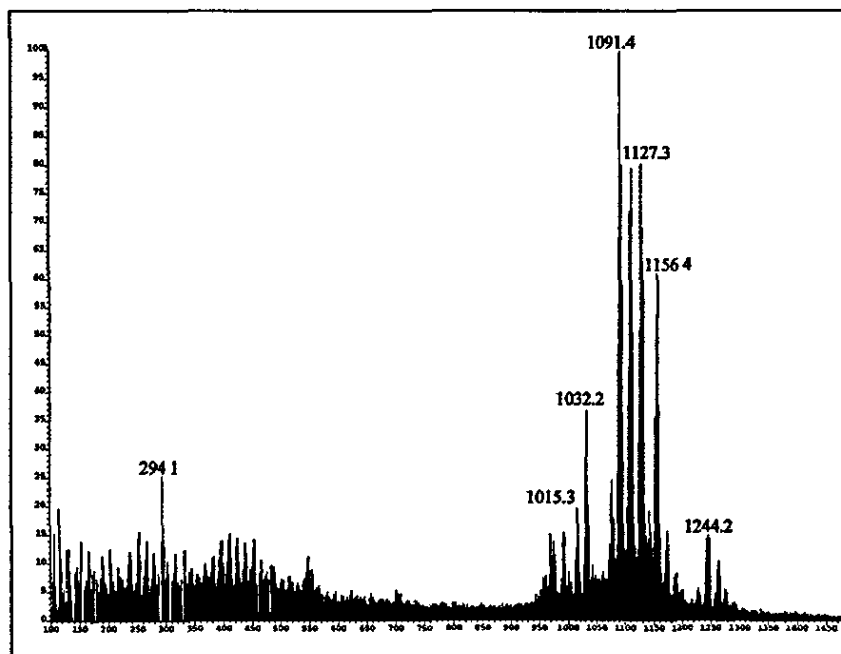


Fig. 3.13: LSIMS spectrum of  $[\text{Cu}_4(\text{H}_2\text{L1})(\text{OH})_2(\text{H}_2\text{O})_2](\text{NO}_3)_2 \cdot 2\text{H}_2\text{O}$

### 3.2.5. Factors controlling the nuclearity

As explained previously, in the course of attempts to synthesise polynuclear species of the macrocyclic ligand  $\text{H}_6\text{L1}$ , mixtures of both trinuclear and tetranuclear copper(II) complexes were isolated by crystallisation when the reaction between 1,3-diaminopropan-2-ol and DHTMB with  $\text{Cu}(\text{NO}_3)_2 \cdot 6\text{H}_2\text{O}$  was performed. The reaction mixture yielded brown tricopper and green tetracopper crystals in different crystallisation solvent combinations, which could be separated by different solubility in ethanol or chloroform (see section 3.2). Even varying the experimental conditions (reacting time and stoichiometry) this mixture of tri- and tetranuclear copper(II) complexes was obtained by crystallisation. Instead, when the reaction was performed with  $\text{Cl}^-$ ,  $\text{ClO}_4^-$  or  $\text{BF}_4^-$  as the counter-ion, only one product was obtained (either dinuclear or tetranuclear complex). However, these reactions were performed on short reflux (2-3 h) and it might be possible to obtain the trinuclear complex on long reflux (e.g. 24 h). Extensive studies were performed in order to study the influence of the factors controlling the nuclearity of the complexes of  $\text{H}_6\text{L1}$ . The Table 3.6 contains all the relevant data of the experimental conditions for the syntheses of the copper(II) complexes studied.

STOICHIOMETRY	COUNTER ION	REACTION TIME	SOLUTION COLOUR	COMPLEXES ISOLATED		CRYSTALS		
2 equivalents	Cl <sup>-</sup>	2 h	Green	2.1	[Cu <sub>2</sub> (H <sub>4</sub> L1)Cl]Cl·2MeOH	[Cu <sub>2</sub> (H <sub>4</sub> L1)Cl]Cl·1.6Et <sub>2</sub> O·EtOH	2.1a	Green
4 equivalents	Cl <sup>-</sup>	18 h	Green	3.11	[Cu <sub>4</sub> (H <sub>2</sub> L1)(OH) <sub>2</sub> (EtOH)](Cl) <sub>2</sub>			
2 equivalents	NO <sub>3</sub> <sup>-</sup>	1 h	Green	3.1	[Cu <sub>4</sub> (H <sub>2</sub> L1)(OH) <sub>2</sub> (H <sub>2</sub> O) <sub>4</sub> ](NO <sub>3</sub> ) <sub>2</sub>	[Cu <sub>3</sub> (H <sub>2</sub> L1)](NO <sub>3</sub> ) <sub>2</sub> (dmf)(H <sub>2</sub> O)	3.1a	Brown
						[Cu <sub>4</sub> (H <sub>2</sub> L1)(OH) <sub>2</sub> (H <sub>2</sub> O)(EtOH)](NO <sub>3</sub> ) <sub>2</sub> ·2EtOH·H <sub>2</sub> O	3.1b	Green
3 equivalents	NO <sub>3</sub> <sup>-</sup>	18 h	Brown	3.2a	[Cu <sub>4</sub> (HL1)(NO <sub>3</sub> ) <sub>3</sub> (H <sub>2</sub> O) <sub>3</sub> ]			
				3.2b	[Cu <sub>3</sub> (H <sub>3</sub> L1)](NO <sub>3</sub> ) <sub>3</sub> (CHCl <sub>3</sub> ) <sub>2</sub> ·2H <sub>2</sub> O	[Cu <sub>3</sub> (H <sub>2</sub> L1)(NO <sub>3</sub> )](NO <sub>3</sub> )(dmf) <sub>3</sub> ·H <sub>2</sub> O	3.2c	Brown
						[Cu <sub>3</sub> (H <sub>2</sub> L1)(O) <sub>2</sub> ](NO <sub>3</sub> ) <sub>2</sub> ·3EtOH	3.2d	Brown
4 equivalents	NO <sub>3</sub> <sup>-</sup>	2 h	Green	3.3	[Cu <sub>4</sub> (H <sub>3</sub> L1)(OH) <sub>2</sub> (H <sub>2</sub> O) <sub>4</sub> ](NO <sub>3</sub> ) <sub>3</sub>	[Cu <sub>3</sub> (H <sub>2</sub> L1)(NO <sub>3</sub> )](NO <sub>3</sub> )(dmf) <sub>3</sub>	3.3a	Brown
4 equivalents	ClO <sub>4</sub> <sup>-</sup>	3 h	Green	3.8	[Cu <sub>4</sub> (H <sub>2</sub> L1)(OH) <sub>2</sub> (EtOH)](ClO <sub>4</sub> ) <sub>2</sub>			
4 equivalents	BF <sub>4</sub> <sup>-</sup>	3 h	Green	3.13	[Cu <sub>4</sub> (H <sub>2</sub> L1)(OH) <sub>2</sub> (H <sub>2</sub> O) <sub>2</sub> ](BF <sub>4</sub> ) <sub>2</sub>			

**Table 3.6:** Data for the polynuclear copper complexes of H<sub>6</sub>L1 investigated

To date, the dicopper complex has only been isolated in the presence of chloride, a good coordinating anion which is also large enough to fit the cavity defined by the hydrogen-bonding interactions to the ligand. When  $\text{NO}_3^-$ ,  $\text{ClO}_4^-$  or  $\text{BF}_4^-$  were used, the initial product of the reaction was the tetracopper complex.

Initially, the ligand:metal ratio used in the reaction with  $\text{Cu}(\text{NO}_3)_2 \cdot 6\text{H}_2\text{O}$  was 1:2 intending to obtain the dicopper complex, but the product of the reaction was the tetracopper complex  $[\text{Cu}_4(\text{H}_2\text{L1})(\text{OH})_2(\text{H}_2\text{O})_4](\text{NO}_3)_2$  (3.1), which gave mixtures of the polynuclear complexes  $[\text{Cu}_3(\text{H}_2\text{L1})](\text{NO}_3)_2 \cdot \text{dmf} \cdot \text{H}_2\text{O}$  (3.1a) and  $[\text{Cu}_4(\text{H}_2\text{L1})(\text{OH})_2(\text{H}_2\text{O})(\text{EtOH})](\text{NO}_3)_2 \cdot 2\text{EtOH} \cdot \text{H}_2\text{O}$  (3.1b) by crystallisation. When the reaction was performed with a ligand:metal ratio of 1:3 or 1:4 the products were again mixtures of tri- and tetracopper complexes, showing that the product of the template reaction is independent of the stoichiometry of the reaction when using  $\text{Cu}(\text{NO}_3)_2 \cdot 6\text{H}_2\text{O}$ .

Another important factor controlling the nuclearity of the complexes is the reaction times. If the reacting times were short (1-2 h) the green tetracopper complex was obtained. Extended reflux (18 h) of the template mixture caused the green colour to darken to brown and mixtures of tri- and tetracopper were formed, as indicated by LSIMS spectrometry and X-ray crystallography.

The same colour change occurred when the tetracopper complex  $[\text{Cu}_4(\text{H}_3\text{L1})(\text{OH})_2(\text{H}_2\text{O})_4](\text{NO}_3)_3$  (3.3) was dissolved in DMF and clean tricopper  $[\text{Cu}_3(\text{H}_2\text{L1})(\text{NO}_3)](\text{NO}_3) \cdot 3\text{dmf}$  (3.3a) was obtained. The tetracopper complex converts into the brown tricopper complex on recrystallisation from slow diffusion of diethylether into the DMF solution in a few days. So it seems that there is a structural rearrangement from tetra- to tricopper complex either in alcohol (the green colour of the reaction mixture in ethanol turned dark brown after 18 hours refluxing, see synthesis E.3.2 of the experimental chapter) or in a solvent with better donor properties (green solution in DMF turned dark brown within a week, synthesis E.3.3 of the experimental chapter).



Similar change of nuclearity by rearrangement of a dinuclear complex into the trinuclear analogue under crystallisation was reported by McKee, Nelson and co-workers.<sup>148</sup> Despite the apparently good coordination stabilisation of the dinuclear silver(I) complex, it was not stable long-term in solution. When the dinuclear complex was allowed to stand for several days in solution, crystals of a trinuclear silver cryptate could be isolated. The nuclearity of the product depended on the time allowed for rearrangement and also on the ligand to silver ratio.

### 3.2.6. Further structural characterisations

#### 3.2.6.1. UV-VIS spectroscopic studies

An important characteristic of these complexes, as mentioned before, is the variation of the nuclearity within the same ligand system and more importantly, rearrangements from one nuclearity to another. Preliminary studies of the process and conditions required for interconversion of the polynuclear structures were undertaken. The experiments were carried out for the di-, tri- and tetranuclear copper complexes of the same ligand system<sup>107</sup> (Fig. 3.14).

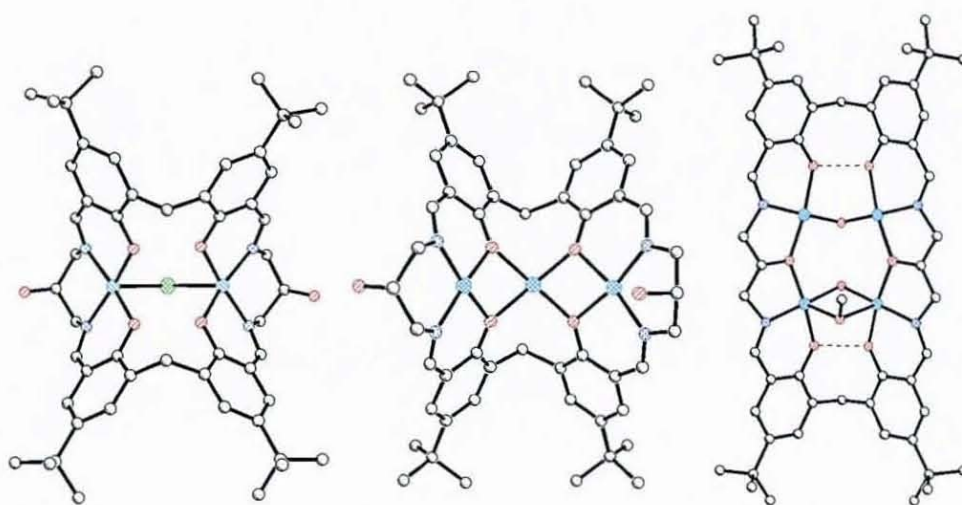
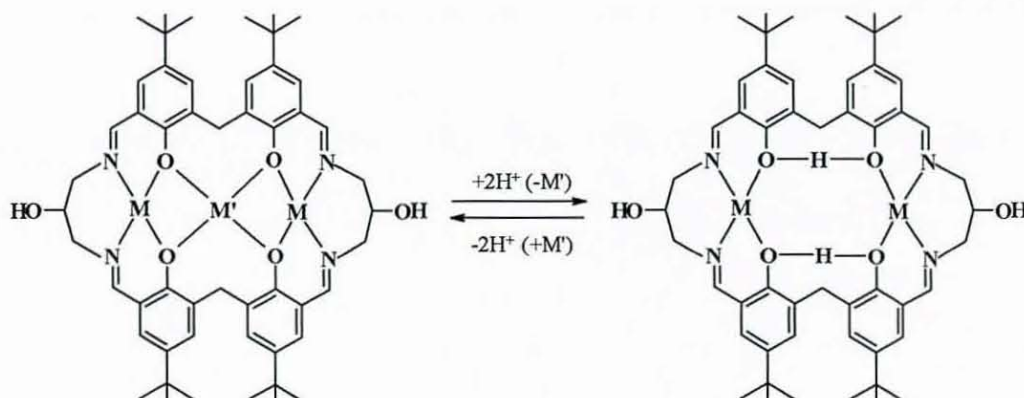


**Fig. 3.14:**  $[\text{Cu}_2(\text{H}_4\text{L1})(\text{Cl})]^+$ ,  $[\text{Cu}_3(\text{H}_2\text{L1})]_n^{2+}$  and  $[\text{Cu}_4(\text{H}_2\text{L1})(\text{OH})_2(\text{H}_2\text{O})]^{2+}$  ions.

### Exchange between dinuclear and trinuclear structures

During preliminary investigations designed to examine the chemical stability of the complexes, it was found that under acid or basic conditions exchange between dinuclear and trinuclear structures could occur, as shown by UV-VIS spectroscopic analysis.



**Scheme 3.2:** Interconversion of trinuclear and dinuclear structures by pH changes.

The similarity of the structures between the di- and the tricopper suggested that it would be possible to obtain the dicopper complex by adding a certain amount of acid to the tricopper solution. Formally, the dicopper complex would be generated from the trinuclear analogue by displacement of the central metal ion ( $M'$ ) by two hydrogen-bonding protons when acidifying. This change should be reversible by adding base to the solution. The base breaks the hydrogen-bonding by deprotonation of the phenol groups and the metal coordinates the four phenolate oxygen groups (Scheme 3.2).

The transformation of the dark brown tricopper complex to the green dicopper one was followed by monitoring their electronic spectra in ethanol (Fig. 3.15). This spectral change can be accomplished in a few seconds by addition of a small amount of acid (1 drop of diluted  $\text{HNO}_3$  in ethanol) to the tricopper solution (conc. =  $6.4 \cdot 10^{-4} \text{M}$ ).

The spectrum obtained (green curve) is very similar to the dicopper one, showing the expected d-d transition band at 624 nm ( $\epsilon=140 \text{ L}\cdot\text{mol}^{-1}\cdot\text{cm}^{-1}$ ). It is likely that the green solution obtained after adding acid is the dicopper complex and not the tetracopper analogue since the d-d transition band for the dicopper complex  $[\text{Cu}_2(\text{H}_4\text{L1})(\text{Cl})]^+$  is found at 620 nm ( $\epsilon=114 \text{ L}\cdot\text{mol}^{-1}\cdot\text{cm}^{-1}$ ) while for the tetracopper complex  $[\text{Cu}_4(\text{H}_2\text{L1})(\text{OH})_2(\text{H}_2\text{O})(\text{EtOH})]^{2+}$  it appears at 644 nm ( $\epsilon=498 \text{ L}\cdot\text{mol}^{-1}\cdot\text{cm}^{-1}$ ). Addition of a non-coordinating base, such as triethylamine (1 drop of diluted  $\text{Et}_3\text{N}$  in ethanol), will readily reverse the process (blue curve), but excess of base leads to other, unidentified products.

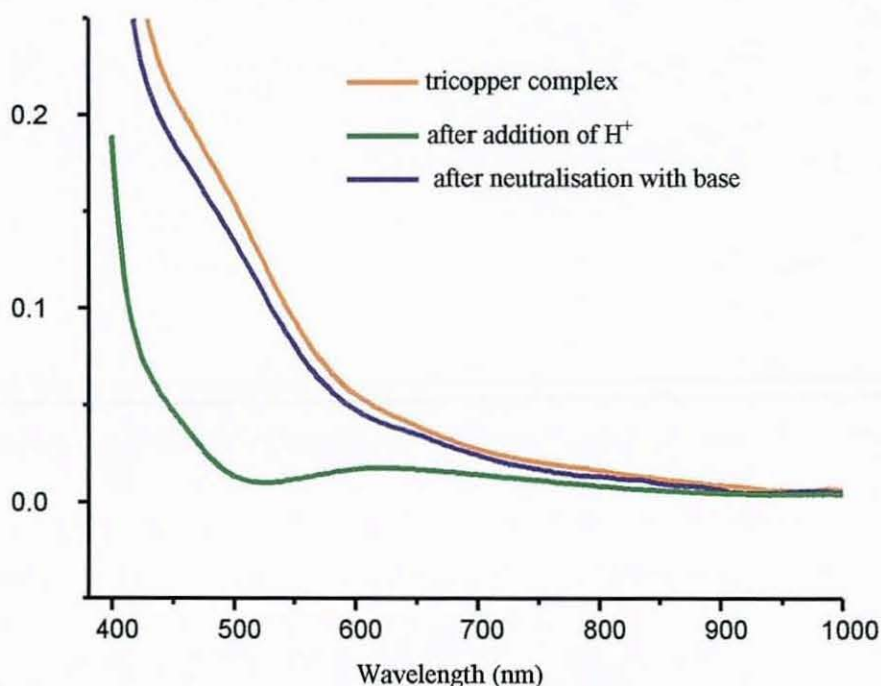


**Fig. 3.15:** Structural interconversion of the dicopper and tricopper complexes with acid-base variation followed by visible spectrometry.

The expected d-d transition band for the tricopper only appears as a shoulder (*ca.* 500 nm;  $\epsilon=1204 \text{ L}\cdot\text{mol}^{-1}\cdot\text{cm}^{-1}$ ) as a result of the presence of near-UV region of intense bands of either  $\pi\text{-}\pi^*$  ligand transitions or ligand-to-metal charge transfer. The brown colour is presumably due to charge transfer between the fully deprotonated phenolate groups and the copper ions. This behaviour can be explained in terms of competition for the phenol oxygen donor between protons and copper ions.



No changes were observed when base was added to the tetracopper solution. It seems that the exchange between tri- and tetracopper complexes is not promoted under basic conditions.

### Exchange between trinuclear and tetranuclear structures

Preliminary studies designed to examine the structural interconversion of the trinuclear and tetranuclear complexes were performed. The experimental results suggest that transformation of trinuclear into tetranuclear complexes is possible in the presence of a good donor solvent, as shown by visible spectrometry.

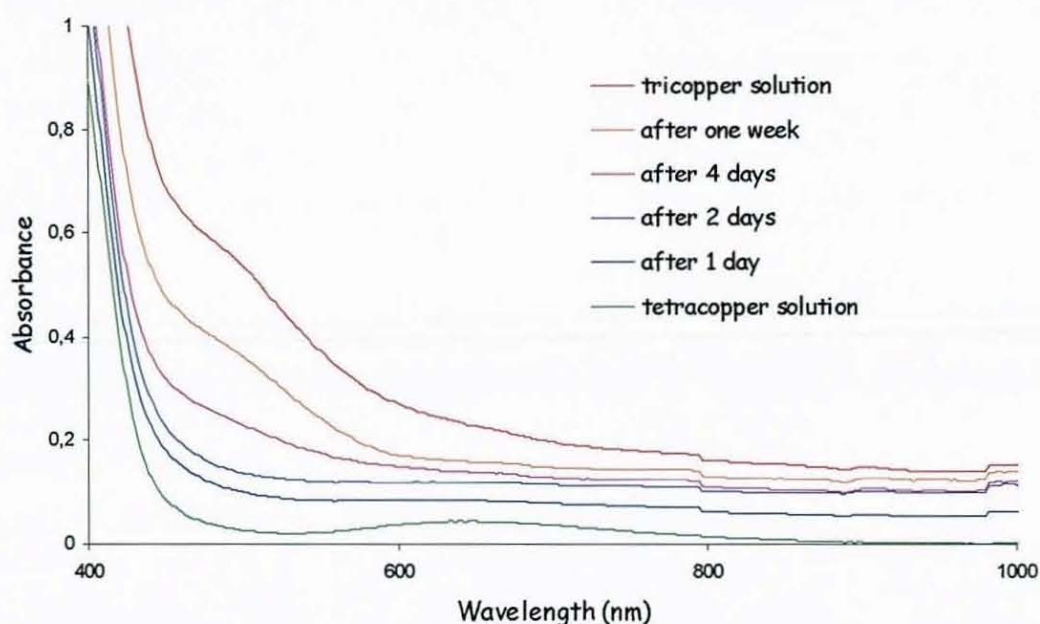


**Fig. 3.16:** Structural exchange of tetracopper to tricopper complex in DMA followed by visible spectrometry.

The transformation of the green tetracopper complex to the brown tricopper one was followed again by monitoring the electronic spectra (Fig. 3.16). This spectral change was accomplished by dissolving the tetracopper complex  $[\text{Cu}_4(\text{H}_2\text{L1})(\text{OH})_2(\text{H}_2\text{O})_4](\text{NO}_3)_2$  in dimethylacetamide (DMA) and measuring the visible spectrum at different times (conc. =  $2 \cdot 10^{-3} \text{M}$ ). The copper d-d transition for the tetranuclear complex is seen as a broad band at 644 nm ( $\epsilon = 110 \text{ L} \cdot \text{mol}^{-1} \cdot \text{cm}^{-1}$ ).

Exchange between polynuclear species was evidenced by these visible spectroscopic studies. Interconversion between tricopper and dicopper complexes was driven by acid/base equilibria. This phenomenon explicitly illustrates the critical role protons play in the rearrangement of the macrocycle in coordination with metal ions. Rearrangement of the tetracopper complex into the tricopper analogue was achieved by dissolving the tetracopper complex in a good donor solvent, suggesting that the tetranuclear complex is the kinetic product of the template reaction and the trinuclear complex is the thermodynamic product.

Similar spectrometric experiments studying the binding behaviour of a "calix-salen" macrocycle were reported by Martell *et al.*<sup>149</sup> along with many others. Reaction of the Schiff base macrocycle with Ni(II) can produce mono-, di-, and trinuclear complexes, depending on the ligand/metal ion ratio. The stepwise binding behaviour of the macrocycle with Ni(II) was monitored by means of spectrophotometric titration.

### 3.2.6.2. Magnetic studies

Variable temperature magnetic measurements were carried out by Dr. C. J. Harding. The magnetic susceptibility data were collected for powdered samples of tricopper and tetracopper complexes working in the temperature range 80-280 K.

The variation of molar magnetic susceptibility ( $\chi_M$ ) with temperature for the tetracopper complex  $[\text{Cu}_4(\text{H}_2\text{L1})(\text{OH})_2(\text{H}_2\text{O})_4](\text{NO}_3)_2$  is illustrated in the plot of  $(\chi_M T)$  vs.  $T$  (Fig. 3.17) showing that the Curie/Weiss law is roughly obeyed ( $\chi_M$  being the corrected magnetic susceptibility per two Cu(II) ions). The overall magnetic exchange interaction is strongly antiferromagnetic with a Weiss temperature of about  $-100\text{K}$ .



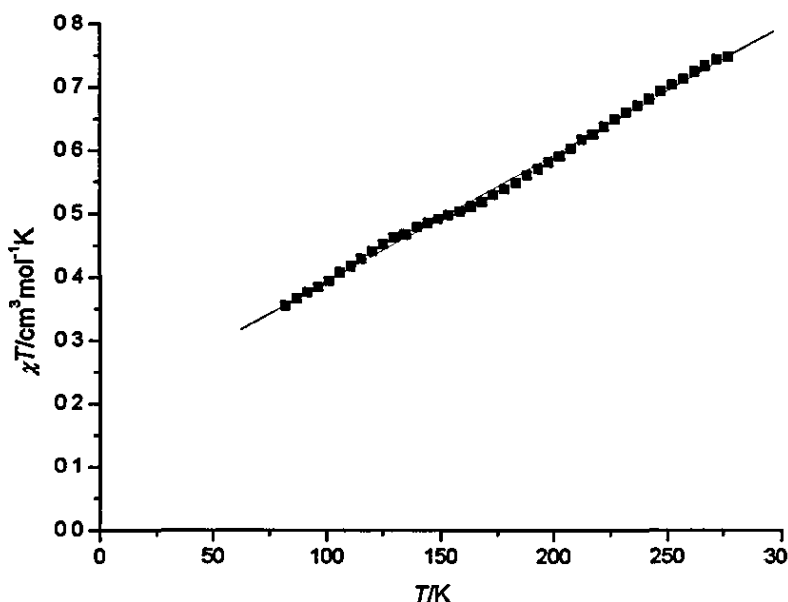


Fig. 3.17: Experimental temperature dependence of  $\chi_M T$  for  $[\text{Cu}_4(\text{H}_2\text{L1})(\text{OH})_2(\text{H}_2\text{O})_4](\text{NO}_3)_2$

For the tricopper complex  $[\text{Cu}_3(\text{H}_2\text{L1})(\text{NO}_3)](\text{NO}_3) \cdot 3\text{dmf}$ , antiferromagnetic interaction is expected within each pair of neighbouring bridged copper ions, Cu(1)-Cu(2) and Cu(2)-Cu(3), respectively. The interaction between Cu(1) and Cu(3), separated by 5.162(3) Å, is expected to be much weaker. The temperature dependence of the molar magnetic susceptibility for the tricopper complex is displayed in the form of a plot of  $\chi_M^{-1}$  vs. T (Curie/Weiss law plot), which gives an intercept of -22K, so the magnetic exchange interaction is again antiferromagnetic (Fig. 3.18). Magnetic susceptibility measurements are in agreement with the trinuclear nature of this compound and could be fitted for an antiferromagnetic interaction between nearest neighbour copper(II) ions

The experimental data are not linear. There are evident wobbles in the experimental lines, which may be significant. The  $\chi_M^{-1}$  vs. T curve exhibits a change in the slope, characteristic for trinuclear compounds with antiferromagnetic exchange interaction between nearest neighbours.<sup>150</sup> This behaviour could be also related to possible intermolecular interactions between trinuclear units of the complex.<sup>151</sup> Nevertheless, these data are preliminary and low temperature experiments should be done.

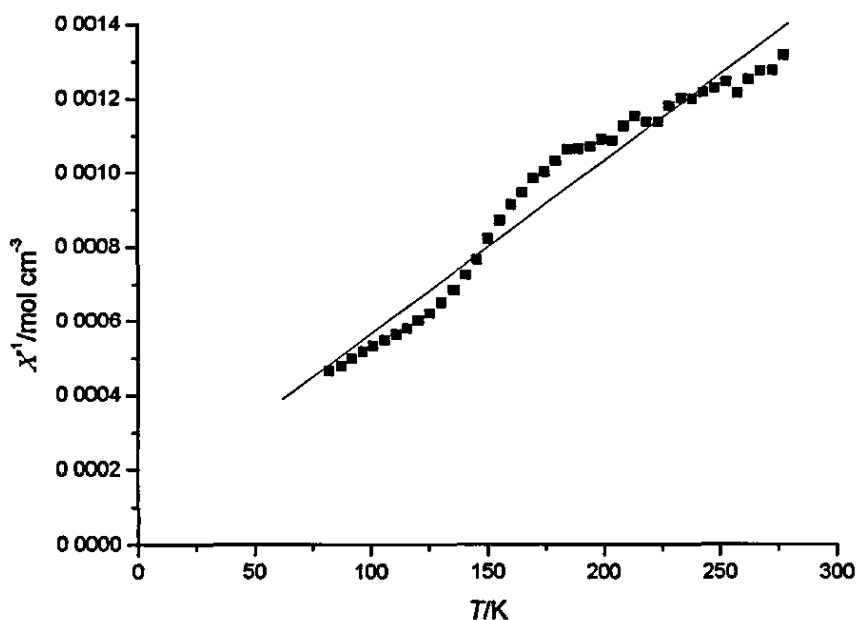


Fig. 3.18: Experimental temperature dependence of  $\chi_M^{-1}$  for  $[\text{Cu}_3(\text{H}_2\text{L1})(\text{NO}_3)](\text{NO}_3)\cdot 3\text{dmf}$

Magneto-structural correlations for several hydroxo-, alkoxo- and phenoxo-bridged<sup>52,60,152-157</sup> dicopper complexes have been extensively studied and show that a major factor controlling the exchange interactions is the Cu-O-Cu bridge angle and thence the Cu...Cu separation. Therefore, it is supposed that the antiferromagnetic coupling between the copper centres of the tri- and tetracopper complexes occurs via a superexchange mechanism through the oxygen bridges of the complexes. In the case of the complex  $[\text{Cu}_3(\text{H}_2\text{L1})(\text{NO}_3)](\text{NO}_3)\cdot 3\text{dmf}$  it is probable that the antiferromagnetic interaction is due to the combination of each pair of neighbouring phenoxo-bridged copper ions contributions. While for the tetracopper  $[\text{Cu}_4(\text{H}_2\text{L1})(\text{OH})_2(\text{H}_2\text{O})_4](\text{NO}_3)_2$  complex the interaction would be the combination of the neighbouring alkoxo-bridged copper ions contributions. The alkoxo bridging groups (O3 and O6, Fig. 3.10) are in the same plane as the orbitals containing the unpaired electrons of the bridged copper ions (coplanar Cu2-O3-Cu3 and Cu1-O6-Cu4) and therefore the antiferromagnetic interaction will be stronger than for the hydroxo bridging groups, which are at angle of *ca.* 90° with respect to the plane of the orbitals containing the unpaired electrons of the copper ions (Cu1-O11-Cu2 109.2(2)° and Cu3-O12-Cu4 112.6(2)°), and thus the antiferromagnetic interaction is likely to be very small.

### 3.3. Other polynuclear complexes of the pseudocalixarene macrocycle H<sub>6</sub>L1

The polynuclear complexes described above are a good example of how the macrocycle can accommodate different nuclearities due to its flexibility. As mentioned previously, S. Goetz prepared tricopper, tetracopper and tetranickel complexes of H<sub>6</sub>L1 in the course of her PhD project<sup>98</sup>, by reacting DHTMB with 1,3-diaminopropan-2-ol and metal salts in the presence of sodium hydroxide. However, tri- and tetranuclear complexes of the ligand H<sub>6</sub>L1 can be also synthesised without addition of a base. The polynuclear complexes listed in Table 3.7 were prepared by standard template techniques as described in the experimental chapter. The synthesis of the polynuclear complexes involved reaction of DHTMB and 1,3-diaminopropan-2-ol with three equivalents of the metal salt to yield the trinuclear complexes while reaction with four equivalents of the metal salt yielded the tetranuclear complexes

Successful formation of the macrocycle was confirmed initially by IR spectroscopy (Table 3.7) showing evidence that the Schiff-base condensation has taken place with the band in the range of 1619-1648 cm<sup>-1</sup> that can be assigned to the vibration of the imine groups, along with the disappearance of the carbonyl (1658 cm<sup>-1</sup> in DHTMB) and amine stretches associated with the reactants. The weak band at *ca.* 1550 cm<sup>-1</sup> can be assigned to the C-O vibration of the phenol groups.<sup>114,115</sup> A broad band in the region 3450-3350 cm<sup>-1</sup> indicative of O-H stretching vibrations of water was observed in the spectra of all the compounds.

Further indication of the polynuclear nature of the complexes was obtained from mass spectral data. The polynuclear complexes studied afforded LSIMS spectra of singly charged fragments of the complexes with no peaks observed for  $m/2$ . Each of the trinuclear metal complexes studied shows peaks corresponding to a singly charged ion containing the trimetallic fragment  $[M_3(H_2L1)]^+$  along with anion or solvate molecules. Whereas the LSIMS spectra of each of the tetranuclear metal complexes studied show peaks corresponding to the fragments  $[M_4(L1)+e]^+$  or

$[M_4(H_2L1)(X)]^+$ , where X are anion or solvate molecules. The detailed study of the LSIMS spectra and also the elemental analyses allowed the recognition of a fragmentation pattern for the complexes where no structure determination by X-ray crystallography was achieved, supporting the structure proposed.

**Table 3.7:** Selected data for the polynuclear complexes of  $H_6L1$  investigated.

	Formula	Colour	IR bands (cm <sup>-1</sup> )
3.4	$[Ni_3(HL1)(NO_3)] \cdot 6H_2O$	Green brownish	3426 (b,s, $\nu_{O-H}$ ); 1638 (m, $\nu_{C-N}$ ) 1549 (w, $\nu_{C-O}$ ); 1384 (m, $\nu_{NO_3}$ )
3.5	$[Ni_3(L1)((NH_2)_2CO)] \cdot 2EtOH \cdot 2H_2O$	Brown	3405 (b,m, $\nu_{O-H}$ ); 1638 (m, $\nu_{C-N}$ ), 1660 (s, urea $\nu_{C-O}$ )
3.6	$[Fe_4(L1)(OH)_2(EtO)_2](NO_3)_2 \cdot H_2O$	Black	3424 (b,m, $\nu_{O-H}$ ), 1623 (s, $\nu_{C-N}$ ) 1543 (s, $\nu_{C-O}$ ), 1385 (m, $\nu_{freeNO_3}$ )
3.7	$[Zn_4(H_2L1)(EtO)_2(EtOH)](NO_3)_2$	Yellow	3421 (b,m, $\nu_{O-H}$ ); 1637 (s, $\nu_{C-N}$ ); 1545 (w, $\nu_{C-O}$ ), 1458 and 1363 (m, $\nu_{coord,NO_3}$ )
3.8	$[Cu_4(H_2L1)(OH)_2(EtOH)](ClO_4)_2$	Green	3448 (b,m, $\nu_{O-H}$ ); 1646 (s, $\nu_{C-N}$ ), 1560 (w, $\nu_{C-O}$ ); 1104 (b, s, $\nu_{3(ClO_4^-)}$ ); 623 (m, $\nu_{4(ClO_4^-)}$ )
3.9	$[Fe_4(L1)(OH)_2(EtO)_2](ClO_4)_2 \cdot 4EtOH$	Black	3427 (b,m, $\nu_{O-H}$ ); 1619 (s, $\nu_{C-N}$ ); 1549 (m, $\nu_{C-O}$ ), 1107 (b, s, $\nu_{3(ClO_4^-)}$ ); 624 (m, $\nu_{4(ClO_4^-)}$ )
3.10	$[Ni_4(H_2L1)(OH)_2(H_2O)](ClO_4)_2$	Brown yellowish	3447 (b,m, $\nu_{O-H}$ ); 1628 (m, $\nu_{C-N}$ ); 1114, 1107 and 1090 (s, $\nu_{3(ClO_4^-)}$ ), 627 (m, $\nu_{4(ClO_4^-)}$ )
3.11	$[Cu_4(H_2L1)(OH)_2(EtOH)](Cl)_2$	Green brownish	3422 (b,m, $\nu_{O-H}$ ); 1637 (s, $\nu_{C-N}$ ); 1542 (w, $\nu_{C-O}$ )
3.12	$[Ni_4(H_2L1)(OH)_2(EtOH)_4](Cl)_2$	Green	3417 (b,m, $\nu_{O-H}$ ), 1648 (s, $\nu_{C-N}$ ); 1547 (w, $\nu_{C-O}$ )
3.13	$[Cu_4(H_2L1)(OH)_2(H_2O)_2](BF_4)_2$	Green	3422 (b,m, $\nu_{O-H}$ ); 1639 (s, $\nu_{C-N}$ ); 1543 (w, $\nu_{C-O}$ ); 1061 (b, s, $\nu_{BF_4}$ )
3.14	$[Co_4(L1)(OH)_4](BF_4)_2 \cdot 3H_2O \cdot 4EtOH$	Brown	3482 (b,m, $\nu_{O-H}$ ); 1646 (s, $\nu_{C-N}$ ); 1545 (w, $\nu_{C-O}$ ), 1084 (b, s, $\nu_{BF_4}$ )
3.15	$[Ni_4(H_2L1)(OH)_2(EtO)](AcO) \cdot H_2O$	Brown yellowish	3410 (b,m, $\nu_{O-H}$ ), 1619 (s, $\nu_{C-N}$ ); 1547 (m, $\nu_{C-O}$ ), 1449 (s, $\nu_{COO}$ )

### 3.3.1. Synthesis and characterisation of trinuclear complexes of H<sub>6</sub>L1

Reaction of DHTMB with 1,3-diaminopropan-2-ol in the presence of three equivalents of Ni(II) yields trinuclear complexes of the macrocycle H<sub>6</sub>L1. The LSIMS or ESI mass spectral data confirm the formation of the trinuclear macrocyclic species. The elemental analyses are also consistent with the formation of the trinickel complexes. In the case of the trinickel(II) complex [Ni<sub>3</sub>(HL1)(NO<sub>3</sub>)]·6H<sub>2</sub>O (3.4), the relative intensity of the peaks is quite weak with respect to the base peak at m/z 425 corresponding to the NOBA matrix. This could suggest a lack of solubility of the nickel complex in the LSIMS medium (NOBA matrix). The fragmentation pattern (Table 3.8) shows a peak at m/z 1164 which can be assigned to [Ni<sub>3</sub>(H<sub>2</sub>L1)(NO<sub>3</sub>)<sub>2</sub>+Na]<sup>+</sup>, suggesting the formation of the trinickel product

**Table 3.8:** Peak attributions for [Ni<sub>3</sub>(HL1)(NO<sub>3</sub>)]·6H<sub>2</sub>O

M/z	Rel. Intensity (%)	Fragments	Calc. Mass
901	5	[Ni(H <sub>3</sub> L1) -H] <sup>+</sup>	901
957	35	[Ni <sub>2</sub> (H <sub>3</sub> L1) -2H] <sup>+</sup>	957
1164	2	[Ni <sub>3</sub> (H <sub>2</sub> L1)(NO <sub>3</sub> ) <sub>2</sub> +Na] <sup>+</sup>	1164

The spectrum of the complex [Ni<sub>3</sub>(L1)((NH<sub>2</sub>)<sub>2</sub>CO)]·2EtOH·2H<sub>2</sub>O (3.5) shows two peaks which suggest again the formation of the trinuclear complex. Initially, the reaction was developed with the intention to model the properties of the dinuclear active sites of the urease enzyme. The aim was to synthesise the dinickel complex with the urea molecule coordinated to the nickel ions. However, the ESI spectrum suggests that the reaction yielded the trinickel complex with the urea molecule, showing one peak at m/z 1131 assigned to [Ni<sub>3</sub>(H<sub>2</sub>L1)((NH<sub>2</sub>)<sub>2</sub>CO)(OH)(H<sub>2</sub>O)<sub>2</sub>+H]<sup>+</sup> and another peak at m/z 1165 assigned to the fragment [Ni<sub>3</sub>(H<sub>2</sub>L1)((NH<sub>2</sub>)<sub>2</sub>CO)(BF<sub>4</sub>)+H]<sup>+</sup>.



**Table 3.9:** Peak attributions for  $[\text{Ni}_3(\text{L1})(\text{NH}_2)_2\text{CO}]\cdot 2\text{EtOH}\cdot 2\text{H}_2\text{O}$   
(ESI-MS relative abundance is given for cone voltage = 90V)

m/z	Rel. Intensity (%)	Fragments	Calc. Mass
479	35	$[\text{Ni}_2(\text{H}_4\text{L1}) - 2\text{H}]^{2+}$	958
847	5	$[(\text{H}_7\text{L1}) + \text{H}]^+$	847
957	40	$[\text{Ni}_2(\text{H}_3\text{L1}) - 2\text{H}]^+$	957
1131	5	$[\text{Ni}_3(\text{H}_2\text{L1})(\text{NH}_2)_2\text{CO}(\text{OH})(\text{H}_2\text{O})_2 + \text{H}]^+$	1131
1165	3	$[\text{Ni}_3(\text{H}_2\text{L1})(\text{NH}_2)_2\text{CO}(\text{BF}_4) + \text{H}]^+$	1165

The stoichiometry of the complexes, derived from elemental analyses, shows that the metal ions are in the +II oxidation state and therefore that the macrocycle has lost four protons, which are most probably the four phenolic hydrogen atoms. In the trinuclear complexes of the macrocycle  $\text{H}_6\text{L1}$  all the phenol groups are deprotonated in order to coordinate a third metal ion in the central site.

### 3.3.2. Synthesis and characterisation of tetranuclear complexes of $\text{H}_6\text{L1}$

In general, reaction of DHTMB with 1,3-diaminopropan-2-ol in the presence of four equivalents of the transition metals Cu(II), Ni(II) and Zn(II) produces tetranuclear complexes of the macrocycle  $\text{H}_6\text{L1}$ . However, the Fe(III) complexes  $[\text{Fe}_4(\text{L1})(\text{OH})_2(\text{EtO})_2](\text{NO}_3)_2\cdot\text{H}_2\text{O}$  and  $[\text{Fe}_4(\text{L1})(\text{OH})_2(\text{EtO})_2](\text{ClO}_4)_2\cdot 4\text{EtOH}$  were obtained by reacting DHTMB and 1,3-diaminopropan-2-ol with equimolar amounts of iron salts. While complexes  $[\text{Ni}_4(\text{H}_2\text{L1})(\text{OH})_2(\text{EtO})_2]\cdot\text{EtOH}$  and  $[\text{Ni}_4(\text{H}_2\text{L1})(\text{OH})_2(\text{EtO})](\text{AcO})\cdot\text{H}_2\text{O}$  were synthesised by reacting DHTMB and 1,3-diaminopropan-2-ol with three equivalents of nickel(II) salts. In these later cases the products obtained were the tetranuclear complexes, suggesting that the product is independent of the amount of nickel salts used in the template reaction.

In the case of  $[\text{Fe}_4(\text{L1})(\text{OH})_2(\text{EtO})_2](\text{NO}_3)_2\cdot\text{H}_2\text{O}$  (3.6), the relative intensity of the peaks is quite weak with respect to the peak at m/z 136 (100%) corresponding to the NOBA matrix. This could suggest a lack of solubility of the iron complex in the LSIMS medium. The fragmentation pattern (Table 3 10) shows a peak at m/z 1299 which can be assigned to  $[\text{Fe}_4(\text{L1})(\text{NO}_3)_2(\text{EtO})_2\text{Na} + 2\text{e}^-]^+$ .

**Table 3.10: Peak attributions for  $[\text{Fe}_4(\text{L1})(\text{OH})_2(\text{EtO})_2](\text{NO}_3)_2 \cdot \text{H}_2\text{O}$** 

m/z	Rel. Intensity (%)	Fragments	Calc. Mass
932	6	$[\text{Fe}(\text{H}_3\text{L1})(\text{MeOH})]^+$	932
992	4	$[\text{Fe}_2(\text{HL1})(\text{OH}) + \text{Na}]^+$	992
1064	3	$[\text{Fe}_2(\text{H}_4\text{L1})(\text{NO}_3)(\text{EtO}) + \text{e}]^+$	1062
1092	2	$[\text{Fe}_2(\text{H}_2\text{L1})(\text{NO}_3)(\text{EtOH})(\text{MeOH}) - \text{H}]^+$	1092
1299	4	$[\text{Fe}_4(\text{L1})(\text{NO}_3)_2(\text{EtO})_2\text{Na} + 2\text{e}]^+$	1299

The fragmentation pattern for  $[\text{Zn}_4(\text{H}_2\text{L1})(\text{EtO})_2(\text{EtOH})](\text{NO}_3)_2$  (3.7) shows a peak at m/z 1099 corresponding to the tetrametallic fragment  $[\text{Zn}_4(\text{L1}) + \text{e}]^+$ . The peaks at m/z 1195 and 1273 also suggest both the formation of the tetranuclear complex and presence of nitrate ions in the complex.

**Table 3.11: Peak attributions for  $[\text{Zn}_4(\text{H}_2\text{L1})(\text{EtO})_2(\text{EtOH})](\text{NO}_3)_2$** 

m/z	Rel. Intensity (%)	Fragments	Calc. Mass
969	25	$[\text{Zn}_2(\text{H}_3\text{L1}) - 3\text{H}]^+$	969
1033	17	$[\text{Zn}_2(\text{H}_4\text{L1})(\text{NO}_3) - 2\text{H}]^+$	1033
1099	10	$[\text{Zn}_4(\text{L1}) + \text{e}]^+$	1100
1195	11	$[\text{Zn}_4(\text{H}_2\text{L1})(\text{NO}_3)(\text{MeO}) + \text{e}]^+$	1195
1273	10	$[\text{Zn}_4(\text{H}_2\text{L1})(\text{NO}_3)_2(\text{EtO}) + 2\text{H}]^+$	1273

The fragmentation pattern for the complex  $[\text{Cu}_4(\text{H}_2\text{L1})(\text{OH})_2(\text{EtOH})](\text{ClO}_4)_2$  (3.8) (Table 3.12) shows again peaks corresponding to a singly charged ion for both the trimetallic and the tetrametallic complexes

**Table 3.12: Peak attributions for  $[\text{Cu}_4(\text{H}_2\text{L1})(\text{OH})_2(\text{EtOH})](\text{ClO}_4)_2$** 

m/z	Rel. Intensity (%)	Fragments	Calc. Mass
977	14	$[\text{Cu}(\text{H}_3\text{L1})(\text{H}_2\text{O})_4 - 2\text{H}]^+$	977
1031	10	$[\text{Cu}_3(\text{H}_2\text{L1}) + \text{e}]^+$	1031
1130	5	$[\text{Cu}_4(\text{H}_2\text{L1})(\text{OH})_2 + \text{e}]^+$	1129
1193	5	$[\text{Cu}_4(\text{HL1})(\text{ClO}_4) + \text{e}]^+$	1193
1337	10	$[\text{Cu}_4(\text{H}_2\text{L1})(\text{ClO}_4)_2(\text{EtO}) - 2\text{H}]^+$	1337

In the case of  $[\text{Fe}_4(\text{L1})(\text{OH})_2(\text{EtO})_2](\text{ClO}_4)_2 \cdot 4\text{EtOH}$  (3.9), the relative intensity of the peaks is quite weak with respect to the peak at  $m/z$  191 corresponding to the fragment  $[(\text{C}_{12}\text{H}_{14}\text{O}_2) + \text{H}]^+$ , which suggests that the complex is not very soluble within the NOBA matrix. The fragmentation pattern shows two peaks at  $m/z$  1266 and 1373, attributed to the fragments  $[\text{Fe}_4(\text{L1})(\text{ClO}_4)(\text{OH})_4(\text{H}_2\text{O})_2 - 2\text{H}]^+$  and  $[\text{Fe}_4(\text{L1})(\text{ClO}_4)_2(\text{OH})_2(\text{EtO})(\text{H}_2\text{O})_2]^+$ .

**Table 3.13** Peak attributions for  $[\text{Fe}_4(\text{L1})(\text{OH})_2(\text{EtO})_2](\text{ClO}_4)_2 \cdot 4\text{EtOH}$

$m/z$	Rel. Intensity (%)	Fragments	Calc. Mass
897	17	$[\text{Fe}(\text{H}_4\text{L1}) - \text{H}]^+$	897
940	15	$[\text{Fe}(\text{H}_3\text{L1})(\text{H}_2\text{O}) + \text{Na}]^+$	940
951	15	$[\text{Fe}_2(\text{H}_2\text{L1}) - \text{H}]^+$	951
994	14	$[\text{Fe}_2(\text{L1})(\text{H}_2\text{O})\text{Na} + \text{H}]^+$	994
1266	6	$[\text{Fe}_4(\text{L1})(\text{ClO}_4)(\text{OH})_4(\text{H}_2\text{O})_2 - 2\text{H}]^+$	1266
1373	5	$[\text{Fe}_4(\text{L1})(\text{ClO}_4)_2(\text{OH})_2(\text{EtO})(\text{H}_2\text{O})_2]^+$	1375

The complex  $[\text{Ni}_4(\text{H}_2\text{L1})(\text{OH})_2(\text{H}_2\text{O})](\text{ClO}_4)_2$  (3.10) afforded a clean LSIMS spectrum of singly charged fragments of the tetranuclear complex (Fig. 3.19, Table 3.14). This complex, unlike the previous ones, was synthesised using a base (triethylamine) to promote the coordination of four metals more easily. The use of base does not determine the formation of the tetranuclear complexes, since previous tetranuclear complexes have been synthesised without the use of base. But the study of the LSIMS spectrum of the tetranickel complex 3.10 (and comparison with the spectra of the previous tetranuclear complexes) leads to the assumption that the use of base promotes the formation of tetranuclear species in a better yield, since the spectrum of the tetranickel(II) just shows peaks for tetranuclear species (and not mixtures of di-, tri- and tetranuclear species).

**Table 3.14:** Peak attributions for  $[\text{Ni}_4(\text{H}_2\text{L1})(\text{OH})_2(\text{H}_2\text{O})](\text{ClO}_4)_2$

$m/z$	Rel. Intensity (%)	Fragments	Calc. Mass
1239	23	$[\text{Ni}_4(\text{H}_2\text{L1})(\text{ClO}_4)(\text{EtO})(\text{OH}) + 2\text{H}]^+$	1239
1256	90	$[\text{Ni}_4(\text{H}_2\text{L1})(\text{EtO})_3(\text{EtOH}) - \text{H}]^+$	1256
1298	12	$[\text{Ni}_4(\text{H}_2\text{L1})(\text{ClO}_4)(\text{EtOH})_2(\text{OH})_2 - \text{H}]^+$	1300

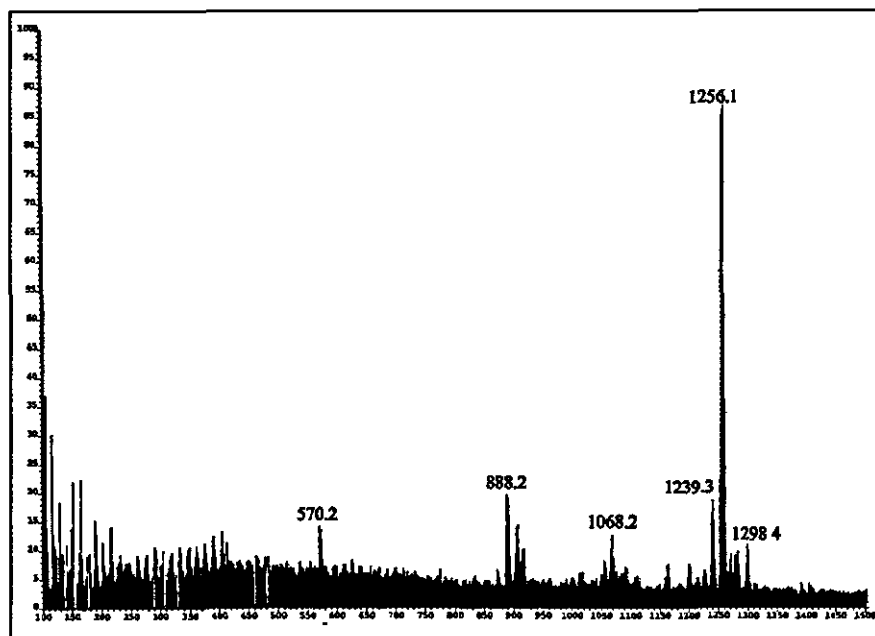


Fig. 3.19: LSIMS spectrum of  $[\text{Ni}_4(\text{H}_2\text{L1})(\text{OH})_2(\text{H}_2\text{O})](\text{ClO}_4)_2$

The LSIMS spectrum of the complex  $[\text{Cu}_4(\text{H}_2\text{L1})(\text{OH})_2(\text{EtOH})](\text{Cl})_2$  (3.11) shows peaks corresponding to singly charged ion fragments for di-, tri- and tetrametallic complexes (Table 3.15). The main peak corresponds to the tricopper fragment  $[\text{Cu}_3(\text{H}_2\text{L1}) + \text{e}]^+$ , while the peak at  $m/z$  1202 could be attributed to the tetranuclear fragment  $[\text{Cu}_4(\text{H}_2\text{L1})(\text{Cl})_2(\text{H}_2\text{O})_2 + \text{e}]^+$

Table 3.15: Peak attributions for  $[\text{Cu}_4(\text{H}_2\text{L1})(\text{OH})_2(\text{EtOH})](\text{Cl})_2$

$m/z$	Rel. Intensity (%)	Fragments	Calc. Mass
967	42	$[\text{Cu}_2(\text{H}_4\text{L1}) - \text{H}]^+$	967
1031	100	$[\text{Cu}_3(\text{H}_2\text{L1}) + \text{e}]^+$	1031
1202	5	$[\text{Cu}_4(\text{H}_2\text{L1})(\text{Cl})_2(\text{H}_2\text{O})_2 + \text{e}]^+$	1202

The spectrum of  $[\text{Ni}_4(\text{H}_2\text{L1})(\text{OH})_2(\text{EtOH})_4](\text{Cl})_2$  (3.12) shows peaks which suggest again the formation of the tetranuclear complex (Table 3.16). The fragmentation pattern for the tetranickel(II) complex shows peaks at  $m/z$  1163, 1327 and 1349 corresponding to a singly charged ion containing tetrametallic fragments  $[\text{Ni}_4(\text{H}_2\text{L1})(\text{Cl})_2(\text{OH})]^+$ ,  $[\text{Ni}_4(\text{H}_2\text{L1})(\text{Cl})_2(\text{EtO})(\text{EtOH})_3 - \text{H}]^+$  and  $[\text{Ni}_4(\text{H}_2\text{L1})(\text{Cl})_2(\text{OH})(\text{EtOH})_4 + \text{H}]^+$  respectively.

**Table 3.16:** Peak attributions for  $[\text{Ni}_4(\text{H}_2\text{L1})(\text{OH})_2(\text{EtOH})_4](\text{Cl})_2$ 

m/z	Rel. Intensity (%)	Fragments	Calc. Mass
957	100	$[\text{Ni}_2(\text{H}_4\text{L1}) - \text{H}]^+$	957
979	15	$[\text{Ni}_2(\text{H}_3\text{L1})(\text{H}_2\text{O}) + 2\text{H}]^+$	979
1163	10	$[\text{Ni}_4(\text{H}_2\text{L1})(\text{Cl})_2(\text{OH})]^+$	1163
1327	10	$[\text{Ni}_4(\text{H}_2\text{L1})(\text{Cl})_2(\text{EtO})(\text{EtOH})_3 - \text{H}]^+$	1329
1349	10	$[\text{Ni}_4(\text{H}_2\text{L1})(\text{Cl})_2(\text{OH})(\text{EtOH})_4 + \text{H}]^+$	1349

The low intensity of the peaks for  $[\text{Cu}_4(\text{H}_2\text{L1})(\text{OH})_2(\text{H}_2\text{O})_2](\text{BF}_4)_2$  (3.13) suggest the low solubility of the copper complex in the LSIMS medium (NOBA matrix). The fragmentation pattern shows two peaks at m/z 1264 and 1460 which suggest the formation of the tetranuclear product.

**Table 3.17:** Peak attributions for  $[\text{Cu}_4(\text{H}_2\text{L1})(\text{OH})_2(\text{H}_2\text{O})_2](\text{BF}_4)_2$ 

m/z	Rel. Intensity (%)	Fragments	Calc. Mass
977	20	$[\text{Cu}(\text{H}_4\text{L1})(\text{H}_2\text{O})_4 - \text{H}]^+$	977
1067	19	$[\text{Cu}_3(\text{H}_2\text{L1})(\text{H}_2\text{O})_2 + \text{e}]^+$	1067
1264	8	$[\text{Cu}_4(\text{H}_2\text{L1})(\text{BF}_4)(\text{EtOH})(\text{OH})_2 + 2\text{H}]^+$	1264
1460	21	$[\text{Cu}_4(\text{H}_2\text{L1})(\text{BF}_4)_2(\text{OH})(\text{EtOH})_3(\text{H}_2\text{O})_2]^+$	1460

The brown product characterised as the tetracobalt(III) complex  $[\text{Co}_4(\text{L1})(\text{OH})_4](\text{BF}_4)_2 \cdot 3\text{H}_2\text{O} \cdot 4\text{EtOH}$  (3.14) has a fragmentation pattern with peaks corresponding to singly charged ions for both dimetallic, trimetallic and tetrametallic complexes. The peak at m/z 1327 can be attributed to the tetracobalt fragment  $[\text{Co}_4(\text{L1})(\text{OH})_4(\text{EtOH})_4 + \text{e}]^+$  and the peak at m/z 1384 assigned to the fragment  $[\text{Co}_4(\text{L1})(\text{EtOH})_4(\text{OH})_4(\text{H}_2\text{O})_2 + \text{Na}]^+$ .

**Table 3.18:** Peak attributions for  $[\text{Co}_4(\text{L1})(\text{OH})_4](\text{BF}_4)_2 \cdot 3\text{H}_2\text{O} \cdot 4\text{EtOH}$ 

m/z	Rel. Intensity (%)	Fragments	Calc. Mass
847	80	$[(\text{H}_6\text{L1}) + \text{H}]^+$	846
937	100	$[\text{Co}(\text{H}_2\text{L1})(\text{H}_2\text{O})_2 + \text{H}]^+$	937
977	53	$[\text{Co}_2(\text{H}_2\text{L1})(\text{H}_2\text{O}) + \text{e}]^+$	977
1052	30	$[\text{Co}_3(\text{L1})(\text{OH})_2 + \text{H}]^+$	1050
1327	25	$[\text{Co}_4(\text{L1})(\text{OH})_4(\text{EtOH})_4 + \text{e}]^+$	1327
1384	40	$[\text{Co}_4(\text{L1})(\text{EtOH})_4(\text{OH})_4(\text{H}_2\text{O})_2 + \text{Na}]^+$	1384



The spectrum of  $[\text{Ni}_4(\text{H}_2\text{L1})(\text{OH})_2(\text{EtO})]\cdot\text{AcO}\cdot\text{H}_2\text{O}$  (3.15) shows peaks that confirm the formation of the tetranuclear complex (Table 3.19). The fragmentation pattern for the tetranickel(II) complex shows peaks at  $m/z$  1089 and 1161, corresponding to singly charged ions containing tetrametallic fragments  $[\text{Ni}_4(\text{L1})(\text{OH})-\text{H}]^+$  and  $[\text{Ni}_4(\text{L1})(\text{EtO})(\text{EtOH})-\text{H}]^+$  respectively.

**Table 3.19:** Peak attributions for  $[\text{Ni}_4(\text{H}_2\text{L1})(\text{OH})_2(\text{EtO})]\cdot\text{AcO}\cdot\text{H}_2\text{O}$

$m/z$	Rel. Intensity (%)	Fragments	Calc. Mass
957	82	$[\text{Ni}_2(\text{H}_4\text{L1})-\text{H}]^+$	959
979	84	$[\text{Ni}_2(\text{H}_4\text{L1})(\text{OH})+\text{H}]^+$	981
1016	52	$[\text{Ni}_2(\text{H}_4\text{L1})(\text{AcO})-\text{H}]^+$	1018
1073	42	$[\text{Ni}_2(\text{H}_4\text{L1})(\text{AcO})(\text{H}_2\text{O})_3]^+$	1073
1089	44	$[\text{Ni}_4(\text{L1})(\text{OH})-\text{H}]^+$	1089
1161	57	$[\text{Ni}_4(\text{L1})(\text{EtO})(\text{EtOH})-\text{H}]^+$	1163

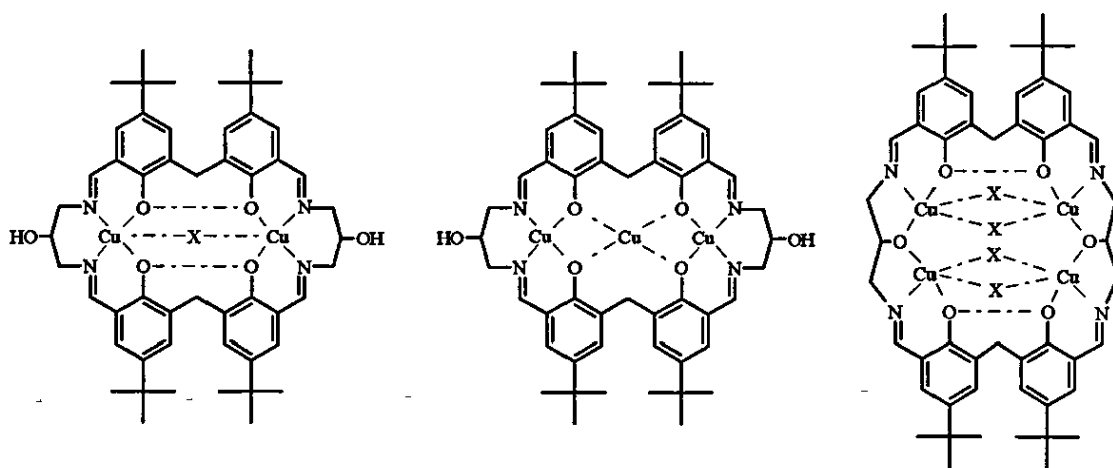
The stoichiometry of the tetranuclear  $\text{M}(\text{II})$  complexes, derived from elemental analyses, shows that the macrocycle has lost four protons in order to coordinate all four metal ions, while the stoichiometry of the trivalent complexes shows that the macrocycle is fully deprotonated due to the +III charge of the coordinated metal ions

### 3.4. Conclusions

These studies indicate the diverse topology accessible in this series of complexes of  $\text{H}_6\text{L1}$  and show that exchange between complexes of differing nuclearity can be achieved, both as part of the template reaction and driven by acid/base equilibria. The conformation of the complexes is controlled primarily by the two intramolecular phenol-phenolate strong hydrogen bonds.

The experimental results discussed in the previous chapter suggest that the dicopper complex is only isolated in the presence of a good coordinating anion

which is also large enough to fit the cavity defined by the hydrogen-bonding interactions of the ligand. When the counter ion used is chloride and the reaction time is short, the dinuclear copper complex  $[\text{Cu}_2(\text{H}_4\text{L1})\text{Cl}]\cdot\text{Cl}\cdot 2\text{MeOH}$  (**2.1**) with a chloride ion bridging the two copper centres forms. When  $\text{NO}_3^-$  was used, the initial product of the template reaction was the tetracopper complex, irrespective of the stoichiometry of the template reaction. There is no evidence, as yet, of the isolation of a water or nitrate bridged dicopper complex in the other cases involving  $\text{Cu}(\text{NO}_3)_2$ . In this case, copper seems to opt for the tetranuclear or trinuclear option, as discussed previously.



**Scheme 3.3:** Representation of the di-, tri- and tetranuclear copper species of  $\text{H}_6\text{L1}$

A great amount of rearrangement would not be necessary to pass from the dinuclear species to the trinuclear species (Scheme 3.3). However, if we assume the tetranuclear species forms before the trinuclear species, the process would involve a lot of rearrangement (more bonds to be broken and major geometrical change).

Formally, the tricopper could be generated from the dinuclear analogue by displacement of the two central hydrogen-bonding protons by a  $\text{Cu}(\text{II})$  ion. In dinuclear complexes of  $\text{M}(\text{II})$  ions, the sites occupied by the metal are equivalent, and each methylenediphenol unit is monodeprotonated. The saddle shape of the macrocycle is maintained by two hydrogen bonds linking adjacent phenol oxygen

atoms. The dinuclear complex is essentially pre-organised for binding a third metal ion in the central site; the protons of the two hydrogen bonds are lost and, if the incoming metal ion is of suitable size, the overall conformation of the complex need not undergo major change. On going from dinuclear to trinuclear the distance between adjacent phenol oxygen atoms increases significantly, the diagonal distance across the cavity increases, and the angular geometry at the  $N_2O_2$  sites becomes strained. Interconversion between di- and tricopper species was evidenced by visible spectroscopic studies (section 3.2.6.1).

Surprisingly, however, it seems that the tricopper complex is actually formed by rearrangement of the tetracopper complex. Reaction of 1,3-diaminopropan-2-ol and DHTMB with two equivalents of  $Cu(NO_3)_2 \cdot 6H_2O$  yields a green tetracopper  $[Cu_4(H_2L1)(OH)_2(H_2O)_4](NO_3)_2$  product on short reflux. Extended reflux of the template mixture causes the green colour to darken to brown and mixtures of tricopper and tetracopper complexes are formed. The same colour change occurs if the tetracopper complex is dissolved in a good donor solvent (such as dimethylacetamide or dimethylformamide) and clean tricopper complex is obtained, although the rate of interconversion is slow. Conversion of tetra- to tricopper species was evidenced both by crystallisation and by visible spectroscopic studies (section 3.2.6.1).

Consequently, it seems that the tetranuclear complex is the kinetic product of the template reaction and the trinuclear complex is the thermodynamic product. In view of the extensive structural rearrangement required (Scheme 3.3), it is not unexpected that the rearrangement is slow in alcohol but faster in a solvent with better donor properties. Good electron-donor solvents clearly will favour the conversion of tetracopper into tricopper complex by coordinating the copper ions of the complex while rearranging the conformation. However, the reasons or driving forces of the processes occurring in this reaction are still obscure and need further investigation.

Finally, the experimental results suggest that the synthesis of polynuclear complexes of Ni(II), Zn(II), Co(III) and Fe(III) ions can be achieved. The use of base promotes the formation of tetranuclear complexes over trinuclear by favouring the deprotonation of the alkoxo groups of the side chains of the macrocycle and thus promoting their participation in the coordination spheres of the metal ions. Alternatively, it could be that the addition of base provides the bridging OH ions that favour the formation of the tetranuclear complex. This is evidenced in the LSIMS spectrum of the complex  $[\text{Ni}_4(\text{H}_2\text{L1})(\text{OH})_2(\text{H}_2\text{O})](\text{ClO}_4)_2$  (3.10), where the main peak is the tetranuclear fragment and there are no peaks of trinuclear or dinuclear fragments present. However, trinuclear nickel(II) complexes can also be synthesised, such as  $[\text{Ni}_3(\text{HL1})(\text{NO}_3)] \cdot 6\text{H}_2\text{O}$  (3.4) and  $[\text{Ni}_3(\text{L1})((\text{NH}_2)_2\text{CO})] \cdot 2\text{EtOH} \cdot 2\text{H}_2\text{O}$  (3.5).

## **CHAPTER IV**

# **HETERONUCLEAR COMPLEXES OF PSEUDOCALIXARENE SCHIFF-BASE MACROCYCLES**



#### 4.1. Introduction

Heteronuclear complexes are of interest for their unique physicochemical properties (such as molecular recognition, mimicry of the active sites of some metalloenzymes and special magnetic and photophysical properties) associated with metal-metal interaction and exceptional functions due to the cooperative effect of dissimilar metal ions in close proximity.<sup>3,158,159</sup> The majority of heteronuclear complexes reported are dinuclear systems. Most commonly, these heteronuclear complexes are synthesised using ligands with dissimilar binding sites in either the final macrocyclic product or in a key non-cyclic intermediate in a step-wise synthesis

Phenol-based macrocyclic ligands having two dissimilar metal-binding sites sharing two phenolic oxygen atoms have been used for the study of phenolate-bridged heterodinuclear metal complexes.<sup>5,37,61,160-162</sup> In contrast, less attention has been paid to polynucleating ligands with dissimilar binding sites that can provide mixed-metal complexes with higher nuclearities.<sup>81,83,84</sup>

Schiff-base metal complexes with  $N_2O_2$  donor atom sets can act as chelating ligands for different cations to produce heteronuclear complexes, such as  $[Co(salen)M]$  complexes<sup>163</sup> (where  $M$ =alkaline metal ions),  $[Cu(salen)M']$  complexes<sup>164</sup> (where  $M'$ =divalent first row transition metal ions) or  $[Ni(L)Zn]$  complexes<sup>165</sup> (where  $L$  is a ligand with a  $N_2O_2$  donor atom set). Interest in these complexes is due to the fact that, since they have two metal centers with different Lewis acid-base properties, they may promote coordination and activation of small molecules. Metal complexes with acyclic salen-type ligands are important catalysts for organic synthesis (e.g. epoxidation,<sup>166</sup> hydrolysis of epoxides,<sup>167</sup> aziridation,<sup>168</sup> asymmetric cyclopropanation,<sup>169</sup> ring opening<sup>170</sup>)

These facts lead to the suggestion that many interesting metal complexes could be prepared from ligands that have the ability to coordinate two or more metal ions per molecule in which the coordinating sites contain different types of donor

atoms. A versatile class of ligands that fulfils these requirements is the Schiff-base pseudocalixarene macrocycles, e.g.  $H_6L1$ ,  $H_9L8$  and  $H_{12}L9$ .

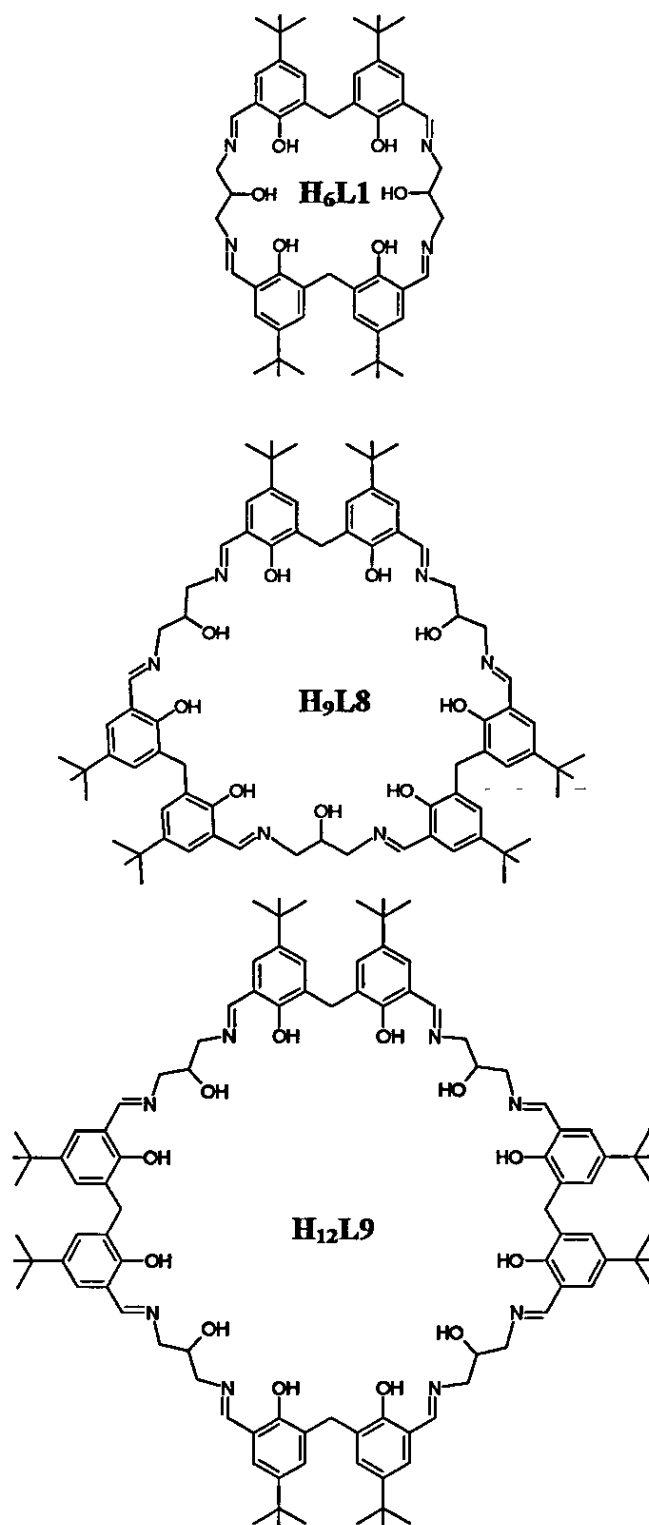


**Fig. 4.1:** Pseudocalixarene Schiff-base macrocycles

As discussed in the previous chapters, the transition metal template ions used to synthesise  $H_6L1$  are likely to coordinate first to the  $N_2O_2$ , salen-type binding sites, consistent with their HSAB properties. Despite the surprising isolation of  $[Cu_3(H_2L1)(OH)(H_2O)](NO_3) \cdot 4EtOH$  (**3.2d**) and  $[Cu_3(H_2L1)(NO_3)](NO_3)(dmf)_3$  (**3.3a**, see section 3.2 of previous chapter), the “hard” HSAB character of the tetraphenolic site is not ideally suited to bind first row transition metal ions. Consequently, attention has been focused on binding harder group 1 and group 2 metal ions at the central site. Heteronuclear complexes incorporating two or more transition metal ions and one alkali or alkaline earth metal ion should be accessible for this type of macrocycles. Analogous heteronuclear complexes that have one compartment for complexation of alkaline or alkaline-earth cations and two or more compartments for transition metal ions have been reported previously (e.g. heteronuclear cation  $[Ni_2Ba(L25)]^{2+}$ , Fig. 4.2).<sup>171,172</sup>

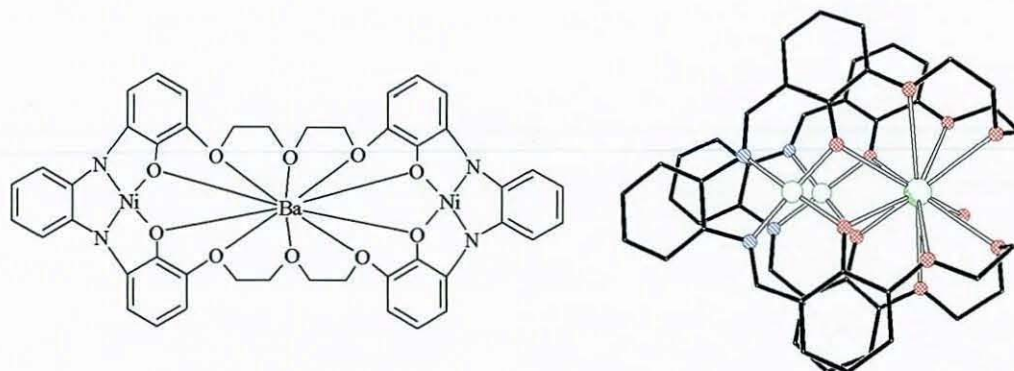


**Fig. 4.2:** Structure<sup>64,65</sup> of the heteronuclear cation  $[Ni_2Ba(L25)]^{2+}$

This chapter concerns the investigation into the coordination chemistry of a set of heteronuclear complexes of the macrocyclic ligands  $H_6L1$ ,  $H_9L8$  and  $H_{12}L9$  derived from the [2+2], [3+3] and [4+4] Schiff-base template condensation of DHTMB (2,2'-dihydroxy-5,5'-di-*tert*-butyl-3,3'-methanediyl dibenzaldehyde) with 1,3-diaminopropan-2-ol respectively (or possibly by rearrangement of the macrocyclic ligands). The relationships between the sizes and charges of the alkaline and alkaline-earth metal ions and the macrocyclic ‘hole’ are examined and the X-ray structures of some complexes are described.

## 4.2. Heteronuclear complexes of the pseudocalixarene macrocycle H<sub>6</sub>L1

The heteronuclear complexes were prepared by standard template techniques as described in the experimental chapter. The reaction of the dialdehyde DHTMB with the diamine 1,3-diaminopropan-2-ol in the presence of a first row transition metal ion (Ni<sup>2+</sup>, Cu<sup>2+</sup> and Zn<sup>2+</sup> salts), an alkaline or alkaline earth metal ion (Na<sup>+</sup>, Ca<sup>2+</sup> and Ba<sup>2+</sup> salts) and base (Et<sub>3</sub>N) yields a variety of heteronuclear complexes derived from H<sub>6</sub>L1. In the absence of added base the group 1 or 2 ions were not incorporated and only the dinuclear transition metal complexes were obtained, because the phenol groups remain protonated and therefore not coordinating the group 1 or 2 metal ions.

### 4.2.1. Heteronuclear complexes of H<sub>6</sub>L1 with sodium

Initially, complex [Cu<sub>2</sub>Na(H<sub>2</sub>L1)(H<sub>2</sub>O)](AcO) (**4.1**) was obtained accidentally, apparently through use of solvent contaminated with sodium hydroxide. Cu(AcO)<sub>2</sub>·4H<sub>2</sub>O salts were added to a solution of DHTMB in ethanol, followed by addition of the diamine 1,3-diaminopropan-2-ol and left refluxing for 2 hours. The complex was initially identified by X-ray crystallography. Green-brown dichroic crystals of [Cu<sub>2</sub>Na(H<sub>2</sub>L1)(H<sub>2</sub>O)](AcO)·10EtOH·4H<sub>2</sub>O (**4.1x**) were grown by slow evaporation of an ethanol solution of complex **4.1** and used for X-ray studies. The data quality was poor but the main features of the structure are clear. It was not possible to reproduce the reaction and obtain the heteronuclear complex again without the use of added base. All the X-ray data collection parameters are summarised in Table 13 of appendix 1 along with the details concerning the refinement and disorder. Perspective views of the cation [Cu<sub>2</sub>Na(H<sub>2</sub>L1)(H<sub>2</sub>O)]<sup>+</sup> are shown in Figs. 4.3 and 4.4 and selected bond lengths and angles relevant to the metal ion coordination are given in Table 4.1.

As demonstrated in Fig. 4.3, the structure has a two-fold axis of symmetry, lying along the sodium ion and the middle point of the bond between the imine carbon and the phenol carbon bonded to it, and passing perpendicularly through the



sodium ion (Na1) and the oxygen atom (O3W). Each copper ion is four-coordinate and has identical macrocyclic donors, two phenol oxygen and two imine nitrogen atoms. The geometry at each copper ion is distorted square planar. The sodium ion seems to be five-coordinate and has square pyramidal geometry with the four phenolate oxygen atoms at the basal plane and a water molecule in the axial site. However since the X-ray data for this crystal are poor, the coordination at the sodium ion is not certain.

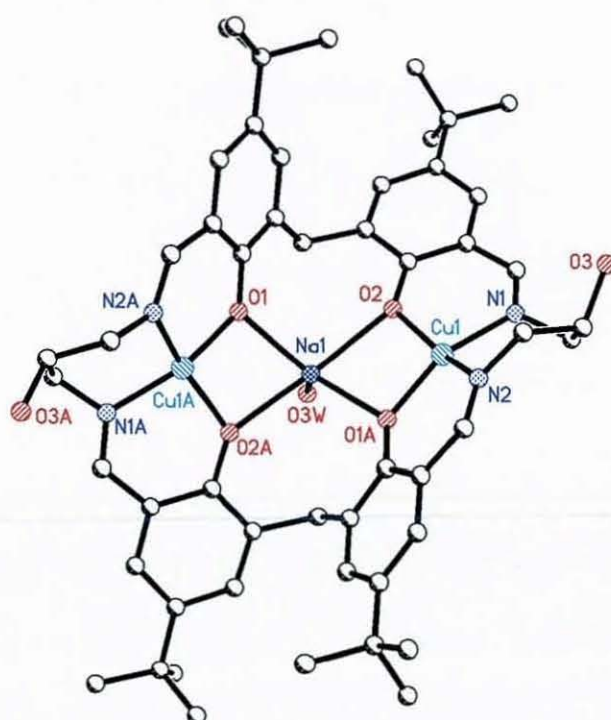


**Fig. 4.3:** Structure of the cation  $[\text{Cu}_2\text{Na}(\text{H}_2\text{L1})(\text{H}_2\text{O})]^+$

The general conformation of this complex is slightly different from the saddle-shape seen in the dinuclear and trinuclear complexes discussed previously. The difference in conformation can be related to the complete deprotonation of the 2,2'-methylenediphenol groups by the use of a base. As for the tricopper complex described in chapter 2, the shape of the complex is now determined by the central metal ion which is coordinated to the four phenolate donors. Since the radius of the  $\text{Na}^+$  ion is larger than that of the  $\text{Cu}^{2+}$ , the phenol oxygen atoms are further apart (e.g.  $\text{O1}\cdots\text{O2}$  3.56 Å) and the saddle-shape of the macrocycle has been stretched. The distance between adjacent phenol oxygen atoms has increased



approximately 1.15 Å compared to the dicopper precursor  $[\text{Cu}_2(\text{H}_4\text{L1})\text{Cl}]\text{Cl}\cdot 1.6\text{Et}_2\text{O}\cdot \text{EtOH}$  (see section 2.4.1.2 of Chapter 2).

The copper ions are separated from the central sodium ion by 3.243(2) Å and the distance separating the copper ions is 5.783(3) Å, which are longer than the metal-metal distances in the dinuclear and trinuclear analogues of ligand  $\text{H}_6\text{L1}$ . The central cavity of the macrocycle has stretched in order to accommodate the large  $\text{Na}^+$  ion, which lies out of the mean plane of the phenolate oxygen donors (illustrated in Fig. 4.4). The pendant alcohol groups are pointing outside the cavity of the macrocycle and are not involved in bonding to the metal ions but they form hydrogen bonds to solvate ethanol molecules.

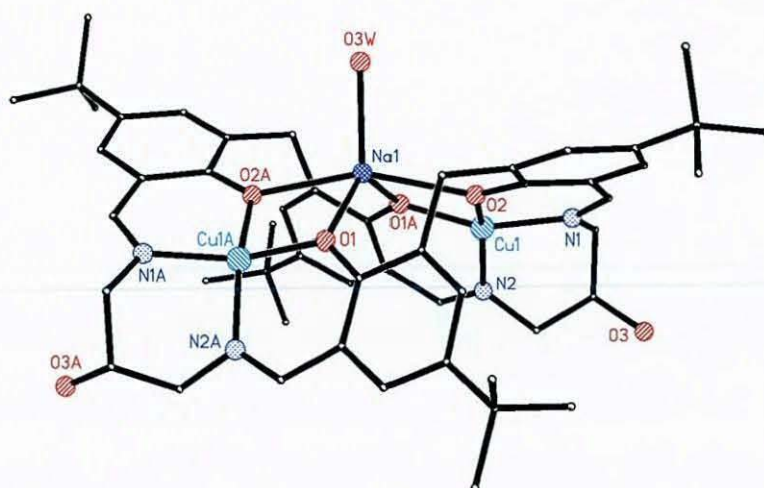


**Fig. 4.4:** Side-on view of the cation  $[\text{Cu}_2\text{Na}(\text{H}_2\text{L1})(\text{H}_2\text{O})]^+$

**Table 4.1:** Selected bond lengths [Å] and angles [°] for  $[\text{Cu}_2\text{Na}(\text{H}_2\text{L1})(\text{H}_2\text{O})](\text{AcO})\cdot 10\text{EtOH}\cdot 4\text{H}_2\text{O}$

Na(1)-O(1)	2.293(6)	Cu(1)-O(2)	1.906(6)
Na(1)-O(3W)	2.315(15)	Cu(1)-N(1)	1.947(7)
Na(1)-O(2)	2.393(6)	Cu(1)-N(2)	1.943(7)
Na(1)-Cu(1)	3.243(2)		
O(1)-Na(1)-O(3W)	116.37(18)	O(2)-Cu(1)-N(1)	94.8(3)
O(1)-Na(1)-O(2)	99.0(2)	O(2)-Cu(1)-N(2)	154.7(3)
O(3W)-Na(1)-O(2)	101.34(18)	N(1)-Cu(1)-N(2)	92.0(3)
O(1)-Na(1)-Cu(1)	114.4(2)	O(2)-Cu(1)-Na(1)	47.04(17)
O(3W)-Na(1)-Cu(1)	116.92(8)	N(1)-Cu(1)-Na(1)	138.8(2)
O(2)-Na(1)-Cu(1)	35.67(14)	N(2)-Cu(1)-Na(1)	129.1(2)

The LSIMS spectrum of the heteronuclear complex  $[\text{Cu}_2\text{Na}(\text{H}_2\text{L1})(\text{H}_2\text{O})](\text{AcO})$  (**4.1**) shows the main peak at  $m/z$  989 corresponding to a singly charged ion containing the trimetallic fragment  $[\text{Cu}_2\text{Na}(\text{H}_2\text{L1})-2\text{H}]^+$ . There is no evidence of acetate ions in the LSIMS spectrum, which suggests that the acetate ions may not be coordinated to the heteronuclear complex.

**Table 4.2:** Peak attributions for  $[\text{Cu}_2\text{Na}(\text{H}_2\text{L1})(\text{H}_2\text{O})](\text{AcO})$

M/z	Rel. Intensity (%)	Fragments	Calc. Mass
975	15	$[\text{CuNa}(\text{H}_2\text{L1})(\text{EtOH})+2\text{H}]^+$	975
989	100	$[\text{Cu}_2\text{Na}(\text{H}_2\text{L1})-2\text{H}]^+$	989
1035	10	$[\text{Cu}_2\text{Na}(\text{H}_2\text{L1})(\text{EtOH})-2\text{H}]^+$	1035

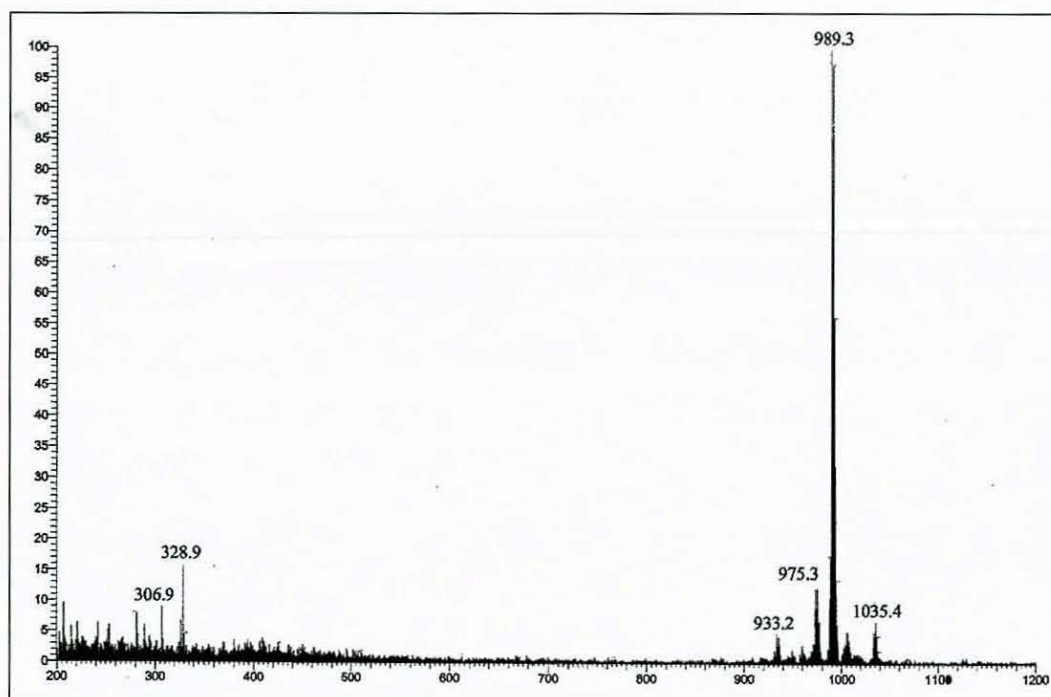


**Fig. 4.5:** LSIMS spectrum of  $[\text{Cu}_2\text{Na}(\text{H}_2\text{L1})(\text{H}_2\text{O})](\text{AcO})$

Following the isolation of complex **4.1**, similar reactions of the dialdehyde DHTMB with the diamine 1,3-diaminopropan-2-ol in the presence of a first row transition metal ion ( $\text{Ni}^{2+}$ ,  $\text{Cu}^{2+}$  and  $\text{Zn}^{2+}$  salts) and sodium were attempted and yielded heteronuclear complexes of  $\text{H}_6\text{L1}$  (Table 4.3).



**Table 4.3:** Selected data for the heteronuclear sodium complexes of H<sub>6</sub>L1

	Formula	Colour	IR bands (cm <sup>-1</sup> )
4.1	[Cu <sub>2</sub> Na(H <sub>2</sub> L1)(H <sub>2</sub> O)](AcO)	Green	3396 (b, m, ν <sub>O-H</sub> ); 1624 (s, ν <sub>C=N</sub> ); 1543 (m, ν <sub>C-O</sub> ); 1442 (s, ν <sub>COO<sup>-</sup></sub> )
4.2	[Ni <sub>2</sub> Na(H <sub>2</sub> L1)(H <sub>2</sub> O) <sub>2</sub> ](AcO)	Brown	3422 (b, m, ν <sub>O-H</sub> ); 1618 (s, ν <sub>C=N</sub> ); 1545 (m, ν <sub>C-O</sub> ); 1450 (m, ν <sub>COO<sup>-</sup></sub> )
4.3	[Zn <sub>2</sub> Na(H <sub>2</sub> L1)(AcO)(EtOH)](AcOH)	Yellow	3388 (b, w, ν <sub>O-H</sub> ); 1634 (s, ν <sub>C=N</sub> ); 1581 (m, ν <sub>C-O</sub> ); 1442 (m, ν <sub>COO<sup>-</sup></sub> )

It is essential in the synthesis of the heteronuclear complexes that the reaction is carried out in the presence of a base. Attempts to synthesise heteronuclear complexes have demonstrated that the use of a base favoured the formation of the heteronuclear species as it assists the deprotonation of the phenol groups and therefore favours coordination of the alkaline or alkaline earth metal in the central site of the macrocyclic cavity. Such is the case of the related genuine calixarene ligands, which form complexes with group 1 and 2 metal ions by deprotonation of the phenol groups in basic solution.<sup>173-175</sup> The heteronuclear complexes here described were synthesised by adding triethylamine to the reaction mixture, as described in the experimental chapter.

Successful formation of the macrocycle H<sub>6</sub>L1 was confirmed by IR spectroscopy (Table 4.3) where formation of the Schiff-base was indicated by disappearance of the carbonyl (1658 cm<sup>-1</sup> in DHTMB) and amine stretches associated with the reactants, along with appearance of an imine stretching band at 1618-1634 cm<sup>-1</sup>. The weak band present in almost all of the complexes at *ca.* 1550 cm<sup>-1</sup> can be assigned to the C-O vibration of the phenol groups.<sup>114,115</sup> A broad band in the region 3350-3500 cm<sup>-1</sup> indicative of O-H stretching vibrations of water was observed in the spectra of all the compounds (recorded as KBr discs).

The heteronuclear complex [Zn<sub>2</sub>Na(H<sub>2</sub>L1)(AcO)(EtOH)](AcOH) (**4.3**) was also characterised by X-ray crystallography. Pale yellow crystals of [Zn<sub>2</sub>Na(H<sub>2</sub>L1)(AcO)(EtOH)]<sub>2</sub>·2EtOH (**4.3x**) suitable for X-ray studies were

grown by slow evaporation of an ethanol solution of the complex **4.3**. Perspective views of the complex are shown in Figs. 4.6, 4.7 and 4.8 and selected bond lengths and angles relevant to the metal ion coordination are given in Table 4.4. All the X-ray data collection parameters are summarised in Table 14 of appendix 1 along with the details concerning the refinement and disorder.

The general conformation of this complex is similar to the previous  $[\text{Cu}_2\text{Na}(\text{H}_2\text{L1})(\text{H}_2\text{O})](\text{AcO})\cdot 4\text{EtOH}\cdot 4\text{H}_2\text{O}$  structure (**4.1x**). The two transition metal ions occupy the salen-type sites of the macrocycle while the alkali metal binds the tetraphenolate central site. The sodium cation is six-coordinate with the four phenolic oxygen donors of the macrocycle and an ethanol and acetate exogenous oxygen donors (Figs. 4.6 and 4.7).

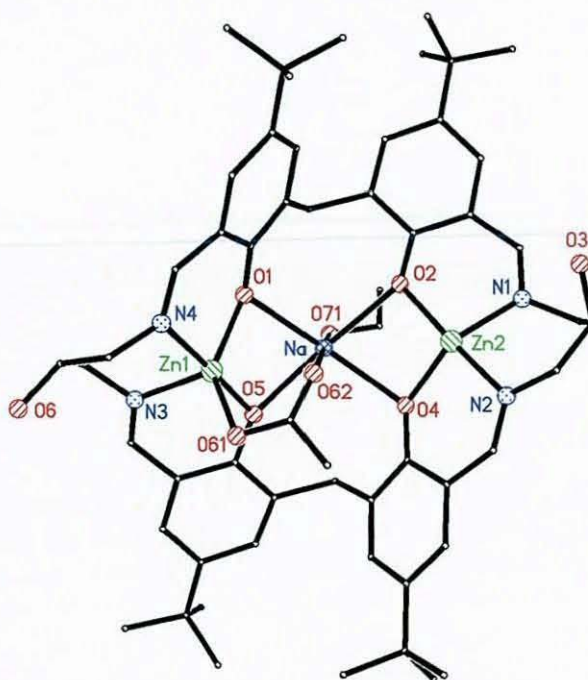


**Fig. 4.6:** Structure of one half of the dimeric complex  $[\text{Zn}_2\text{Na}(\text{H}_2\text{L1})(\text{AcO})(\text{EtOH})]_2$

The zinc atoms are separated from the central sodium ion by 3.111(2) and 3.173(2) Å respectively and the distance separating the zinc ions is 5.556(3) Å, which are again longer than the metal-metal distances in the dinuclear and trinuclear analogues. The macrocyclic cavity can not stretch further to accommodate the large cation and therefore the sodium lies somewhat above the mean plane of the



four phenolate oxygen donors (Fig. 4.7). One of the pendant alcohol groups (O3) is involved in the coordination sphere of the one of the zinc ions (Zn2) of other macrocyclic unit while the other pendant alcohol group (O6) is pointing outside the cavity of the macrocycle and not involved in bonding to the metal ions but forming hydrogen bonds to the coordinated and lattice ethanol molecules (Table 4.5).

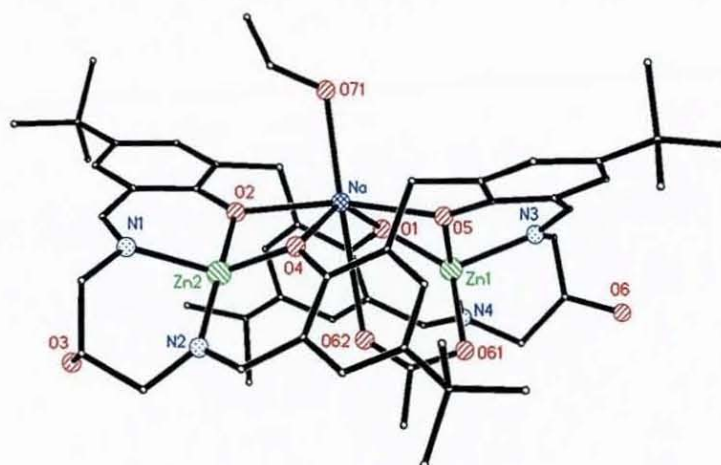


**Fig. 4.7:** Side-on view of one half of the dimeric complex  $[\text{Zn}_2\text{Na}(\text{H}_2\text{L1})(\text{AcO})(\text{EtOH})_2]$

The zinc ions are not equivalent. Both zinc centres are 5-coordinate, but for one of the zinc(II) ions the apical ligand is the oxygen of the acetate counterion, while for the other zinc(II) ion the apical donor is the alkoxo group of the other macrocyclic unit, leading to the dimeric structure shown in Fig. 4.8.

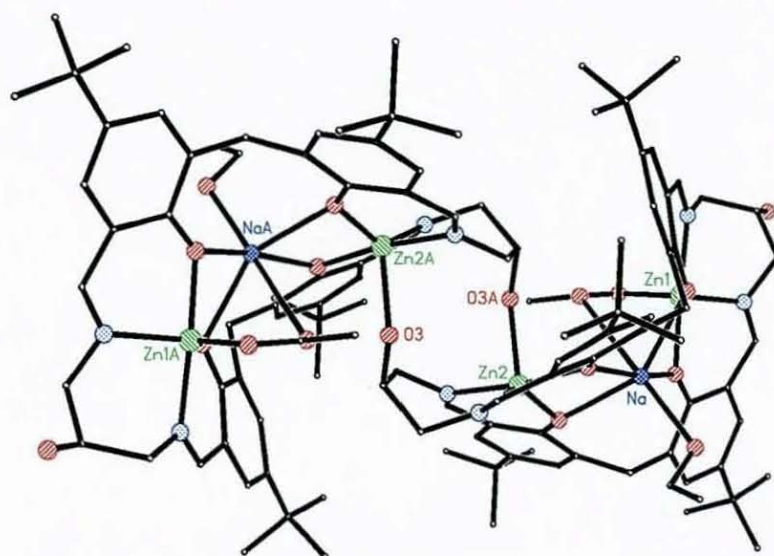


**Fig. 4.8:** Structure of the dimer  $[\text{Zn}_2\text{Na}(\text{H}_2\text{L1})(\text{AcO})(\text{EtOH})_2]$



**Table 4.4:** Selected bond lengths [ $\text{\AA}$ ] and angles [ $^\circ$ ] for  $[\text{Zn}_2\text{Na}(\text{H}_2\text{L1})(\text{AcO})(\text{EtOH})]_2 \cdot 2\text{EtOH}$

Zn(1)-O(1)	2 006(4)	Zn(2)-N(2)	2.057(4)
Zn(1)-O(5)	2 016(4)	Zn(2)-O(3A)	2.220(3)
Zn(1)-N(3)	2 055(4)	Zn(2)-Na	3.173(2)
Zn(1)-N(4)	2 091(5)	Na-O(5)	2.274(4)
Zn(1)-O(61)	2.114(4)	Na-O(2)	2.342(4)
Zn(1)-Na	3.111(2)	Na-O(4)	2.384(4)
Zn(2)-O(4)	1.949(3)	Na-O(1)	2 420(4)
Zn(2)-O(2)	1.999(3)	Na-O(71)	2.429(5)
Zn(2)-N(1)	2.046(4)	Na-O(62)	3 017(5)
O(1)-Zn(1)-O(5)	91.97(15)	N(1)-Zn(2)-O(3A)	118 42(15)
O(1)-Zn(1)-N(3)	119.75(16)	N(2)-Zn(2)-O(3A)	83.62(14)
O(5)-Zn(1)-N(3)	89.32(16)	O(5)-Na-O(2)	167.30(16)
O(1)-Zn(1)-N(4)	88 97(17)	O(5)-Na-O(4)	99 94(15)
O(5)-Zn(1)-N(4)	177 01(16)	O(2)-Na-O(4)	74.10(13)
N(3)-Zn(1)-N(4)	87.75(18)	O(5)-Na-O(1)	76 02(13)
O(1)-Zn(1)-O(61)	134 88(14)	O(2)-Na-O(1)	101.92(14)
O(5)-Zn(1)-O(61)	90 88(16)	O(4)-Na-O(1)	143.58(15)
N(3)-Zn(1)-O(61)	105 30(17)	O(5)-Na-O(71)	103.82(16)
N(4)-Zn(1)-O(61)	90.46(17)	O(2)-Na-O(71)	88 60(15)
O(4)-Zn(2)-O(2)	92 32(14)	O(4)-Na-O(71)	103.53(15)
O(4)-Zn(2)-N(1)	134.54(16)	O(1)-Na-O(71)	112.64(15)
O(2)-Zn(2)-N(1)	91 05(15)	O(5)-Na-O(62)	73.57(13)
O(4)-Zn(2)-N(2)	92.56(15)	O(2)-Na-O(62)	93.97(13)
O(2)-Zn(2)-N(2)	173.15(15)	O(4)-Na-O(62)	76.10(12)
N(1)-Zn(2)-N(2)	88 95(16)	O(1)-Na-O(62)	67.99(12)
O(4)-Zn(2)-O(3A)	106 89(14)	O(71)-Na-O(62)	177.17(16)
O(2)-Zn(2)-O(3A)	90 36(13)	Zn(1)-Na-Zn(2)	124.25(7)

Symmetry transformations used to generate equivalent atoms: (A)  $-x+1, -y+2, -z$

**Table 4.5:** Hydrogen bonds for  $[\text{Zn}_2\text{Na}(\text{H}_2\text{L1})(\text{AcO})(\text{EtOH})]_2 \cdot 2\text{EtOH}$  (atoms O81 and O91 belong to the ethanol solvate molecules)

D-H...A	D(D-H)	D(H...A)	D(D...A)
O(3)-H(3) ..O(62A)	0 84	1.77	2.584(5)
O(6)-H(6).. O(91)	0 84	1.92	2.739(11)
O(71)-H(71)...O(6B)	0.84	2.15	2 979(7)
O(81)-H(81)...O(61)	0.84	1.86	2 694(7)
O(91)-H(91).. O(81)	0.84	1.87	2 706(11)

Symmetry transformations used to generate equivalent atoms: (A)  $-x+1, -y+2, -z$  (B)  $-x+1, -y+2, -z+1$

The analogous nickel and sodium heteronuclear complex  $[\text{Ni}_2\text{Na}(\text{H}_2\text{L1})(\text{H}_2\text{O})_2] \cdot \text{AcO}$  (4.2) has been prepared and characterised by IR and LSIMS analyses, although no crystal structure was obtained.

Further indication of the heteronuclear nature of the complexes was obtained from mass spectral data. The heteronuclear sodium complexes of  $H_6L1$  studied afforded clean LSIMS spectra of singly charged fragments of the complexes with no peaks observed for  $m/2$ . Each of the heteronuclear metal complexes studied shows a peak corresponding to a singly charged ion containing the trimetallic fragment  $[M_2Na(H_2L1)]^+$  or  $[M_2Na(H_2L1)-2H]^+$  ( $M = Cu^{2+}, Ni^{2+}$  or  $Zn^{2+}$ ). Fragments including anions or solvent molecules are also observed. In LSIMS spectrometry is common to find peaks of sodium-adducted molecular ions  $[M+Na]^+$ . However, no peaks with such high intensity were observed in the dinuclear complexes reported in chapter 2. Furthermore, the similarity of the two structurally characterised complexes,  $[Cu_2Na(H_2L1)(H_2O)](AcO) \cdot 4EtOH \cdot 4H_2O$  (**4.1x**) and  $[Zn_2Na(H_2L1)(AcO)(EtOH)_2] \cdot 2EtOH$  (**4.3x**), is a good evidence of the formation of the heteronuclear complexes.

The spectrum of the complex  $[Ni_2Na(H_2L1)(H_2O)_2](AcO)$  (**4.2**) shows the main peak at  $m/z$  979 which is assigned to the fragment  $[Ni_2Na(H_2L1)-2H]^+$ , suggesting the formation of the heteronuclear complex (Fig. 4.9, Table 4 6)

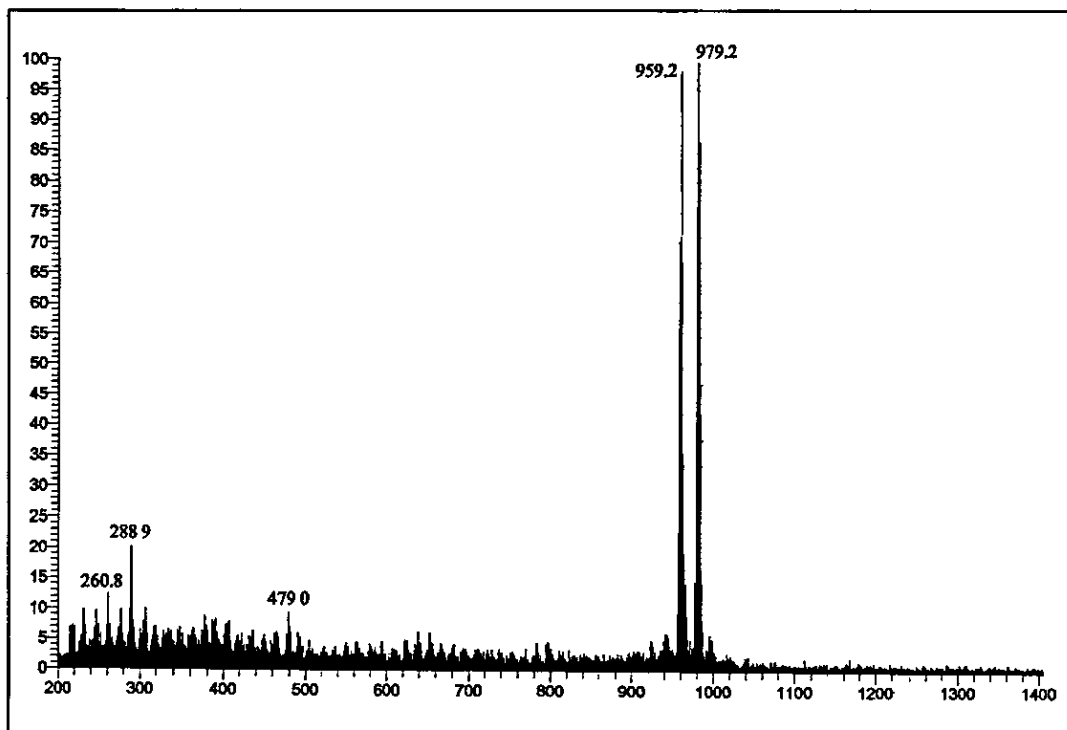


Fig. 4.9: LSIMS spectrum of  $[Ni_2Na(H_2L1)(H_2O)_2](AcO)$

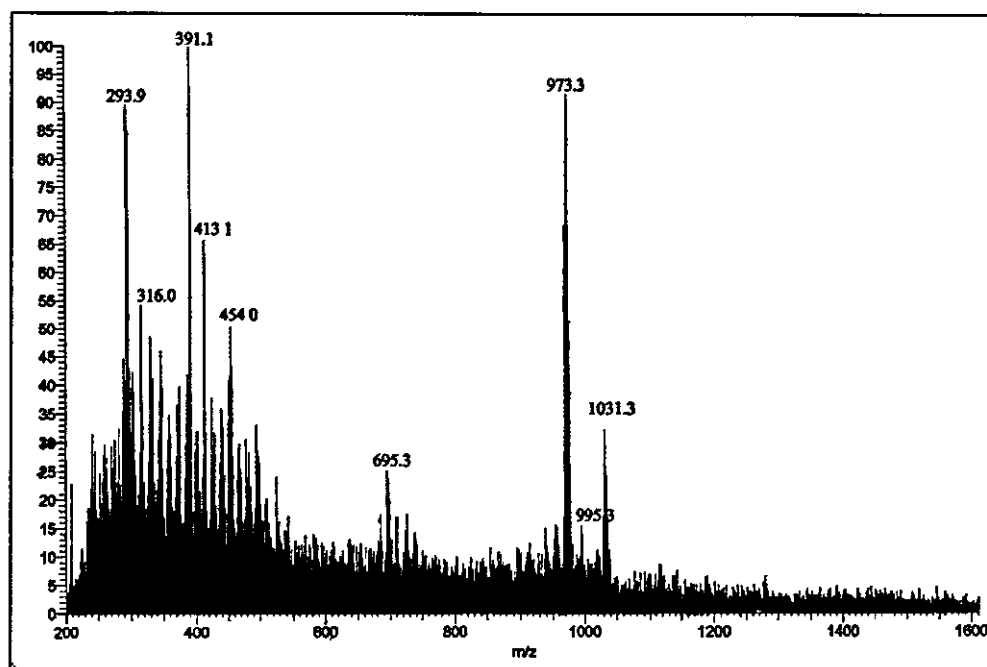
**Table 4.6:** Peak attributions for  $[\text{Ni}_2\text{Na}(\text{H}_2\text{L1})(\text{H}_2\text{O})_2](\text{AcO})$ 

M/z	Rel. Intensity (%)	Fragments	Calc. Mass
959	97	$[\text{Ni}_2(\text{H}_2\text{L1})-\text{H}]^+$	959
979	100	$[\text{Ni}_2\text{Na}(\text{H}_2\text{L1})-2\text{H}]^+$	979

In the case of the complex  $[\text{Zn}_2\text{Na}(\text{H}_2\text{L1})(\text{AcO})(\text{EtOH})](\text{AcOH})$  (4.3), the relative intensity of the peaks with respect to the peaks at  $m/z$  293 and  $m/z$  391, corresponding to fragmentation peaks of the complex, suggests low solubility of the complex within the NOBA matrix (Fig 4 10, Table 4.7). The fragmentation pattern of the complex shows two peaks at  $m/z$  995 and 1031 which are attributable to the heteronuclear fragments  $[\text{Zn}_2\text{Na}(\text{H}_2\text{L1})]^+$  and  $[\text{Zn}_2\text{Na}(\text{H}_2\text{L1})(\text{H}_2\text{O})_2]^+$  respectively.

**Table 4.7:** Peak attributions for  $[\text{Zn}_2\text{Na}(\text{H}_2\text{L1})(\text{AcO})(\text{EtOH})](\text{AcOH})$ 

m/z	Rel. Intensity (%)	Fragments	Calc. Mass
293	90	$[\text{C}_{21}\text{H}_{25}\text{O}]^+$	293
391	100	$[\text{C}_{25}\text{H}_{31}\text{N}_2\text{O}_2]^+$	391
973	93	$[\text{Zn}_2(\text{H}_2\text{L1})+2\text{H}]^+$	973
995	15	$[\text{Zn}_2\text{Na}(\text{H}_2\text{L1})]^+$	995
1031	30	$[\text{Zn}_2\text{Na}(\text{H}_2\text{L1})(\text{H}_2\text{O})_2]^+$	1031

**Fig. 4.10:** LSIMS spectrum of  $[\text{Zn}_2\text{Na}(\text{H}_2\text{L1})(\text{AcO})(\text{EtOH})](\text{AcOH})$

Is worth mentioning that the synthesis of the heteronuclear sodium complexes of the macrocycle  $H_6L1$  seems to be independent of the order in which the reagents were added to reaction mixture. In the case of the heteronuclear complexes  $[Cu_2Na(H_2L1)(H_2O)](AcO)$  (4.1) and  $[Ni_2Na(H_2L1)(H_2O)_2](AcO)$  (4.2), the transition metal and the sodium salts were added at the same time to the reaction mixture. While in the case of the complex  $[Zn_2Na(H_2L1)(AcO)(EtOH)](AcOH)$  (4.3), the sodium salts were added first and left to react with the DHTMB and the diamine for long reflux (22 h) before adding the zinc(II) salts to the reaction mixture. Both procedures produced the heteronuclear complexes as the only product with good yields (75-85%)

#### 4.2.2. Heteronuclear complexes of $H_6L1$ with calcium

In subsequent studies attention was focused on binding group 2 metal ions at the central site of the macrocycle  $H_6L1$ . The  $Ca^{2+}$  ion has a similar radius to  $Na^+$  ion ( $r(Ca^{2+})= 1.14 \text{ \AA}$ ;  $r(Na^+)= 1.16 \text{ \AA}$ )<sup>176</sup> and might be expected to bind more strongly to the central site of the macrocycle due to the higher charge of the ion. Template synthesis of the dialdehyde DHTMB and the diamine 1,3-diaminopropan-2-ol with a first row transition metal ion ( $Cu^{2+}$  or  $Ni^{2+}$  salts) and the alkaline earth metal ion  $Ca^{2+}$  in the presence of base produced heteronuclear complexes of  $H_6L1$  (Table 4.8).

**Table 4.8:** Selected data for the heteronuclear calcium complexes of  $H_6L1$

	Formula	Colour	IR bands ( $cm^{-1}$ )
4.4	$[Cu_2Ca(HL1)]\cdot Cl$	Green	3407 (b, m, $\nu_{O-H}$ ); 1628 (s, $\nu_{C-N}$ ); 1560 (w, $\nu_{C-O}$ )
4.5	$[Ni_2Ca(HL1)(EtOH)](NO_3)$	Brown	3384 (b, m, $\nu_{O-H}$ ); 1619 (s, $\nu_{C-N}$ ); 1449 and 1363 (m, $\nu_{coord.NO_3^-}$ ); 1392 (m, $\nu_{freeNO_3^-}$ )

In these complexes the macrocycle is monoprotonated, suggesting that one of the pendant alcohol groups is deprotonated and possibly coordinating a metal ion of other macrocyclic unit, forming dimers or macrocyclic chains

The detailed study of the LSIMS mass spectra allowed the recognition of fragmentation patterns for the heteronuclear calcium complexes although no structure determination by X-ray crystallography was achieved. The fragmentation pattern for the complex  $[\text{Cu}_2\text{Ca}(\text{HL1})]\cdot\text{Cl}$  (4.4) shows the main peak at  $m/z$  1043 corresponding to a singly charged ion containing the trimetallic fragment  $[\text{Cu}_2\text{Ca}(\text{H}_2\text{L1})\text{Cl}]^+$  and another peak at  $m/z$  1006 assigned to the fragment  $[\text{Cu}_2\text{Ca}(\text{HL1})-\text{H}]^+$  (Fig. 4.11, Table 4.9).

Table 4.9: Peak attributions for  $[\text{Cu}_2\text{Ca}(\text{HL1})]\cdot\text{Cl}$

M/z	Rel. Intensity (%)	Fragments	Calc. Mass
906	30	$[\text{Cu}(\text{H}_3\text{L1})-\text{H}]^+$	906
969	55	$[\text{Cu}_2(\text{H}_3\text{L1})]^+$	969
1006	50	$[\text{Cu}_2\text{Ca}(\text{HL1})-\text{H}]^+$	1006
1043	100	$[\text{Cu}_2\text{Ca}(\text{H}_2\text{L1})\text{Cl}]^+$	1043
1147	15	$[\text{Cu}_2\text{Ca}(\text{HL1})(\text{Cl})_2(\text{EtOH})_2+2\text{H}]^+$	1147

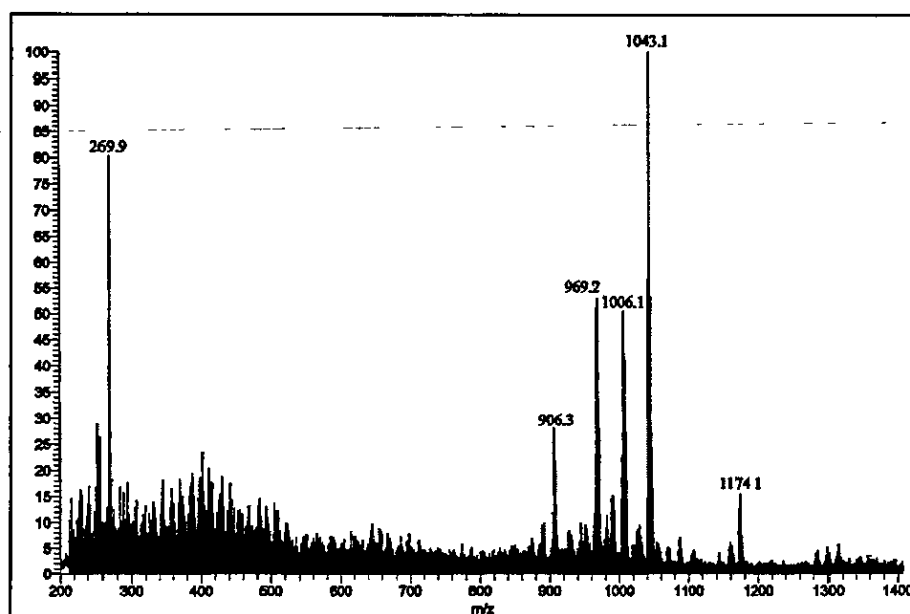


Fig. 4.11: LSIMS spectrum of  $[\text{Cu}_2\text{Ca}(\text{HL1})]\cdot\text{Cl}$

The fragmentation pattern for the complex  $[\text{Ni}_2\text{Ca}(\text{HL1})(\text{EtOH})](\text{NO}_3)$  (4.5) shows the main peak at  $m/z$  959 corresponding to a singly charged ion containing the dimetallic fragment  $[\text{Ni}_2(\text{H}_2\text{L1})-\text{H}]^+$ . The peak at  $m/z$  479 is assigned to the doubly charged fragment  $[\text{Ni}_2(\text{H}_2\text{L1})]^{2+}$ . Another peak at  $m/z$  1058 attributable to



the trimetallic fragment  $[\text{Ni}_2\text{Ca}(\text{H}_2\text{L1})(\text{NO}_3) - 2\text{H}]^+$  suggests the formation of the heteronuclear complex (Fig. 4.12, Table 4.10).

**Table 4.10:** Peak attributions for  $[\text{Ni}_2\text{Ca}(\text{HL1})(\text{EtOH})](\text{NO}_3)$

M/z	Rel. Intensity (%)	Fragments	Calc. Mass
479	83	$[\text{Ni}_2(\text{H}_2\text{L1})]^{2+}$	958
957	100	$[\text{Ni}_2(\text{H}_2\text{L1}) - \text{H}]^+$	959
1058	55	$[\text{Ni}_2\text{Ca}(\text{H}_2\text{L1})(\text{NO}_3) - 2\text{H}]^+$	1058

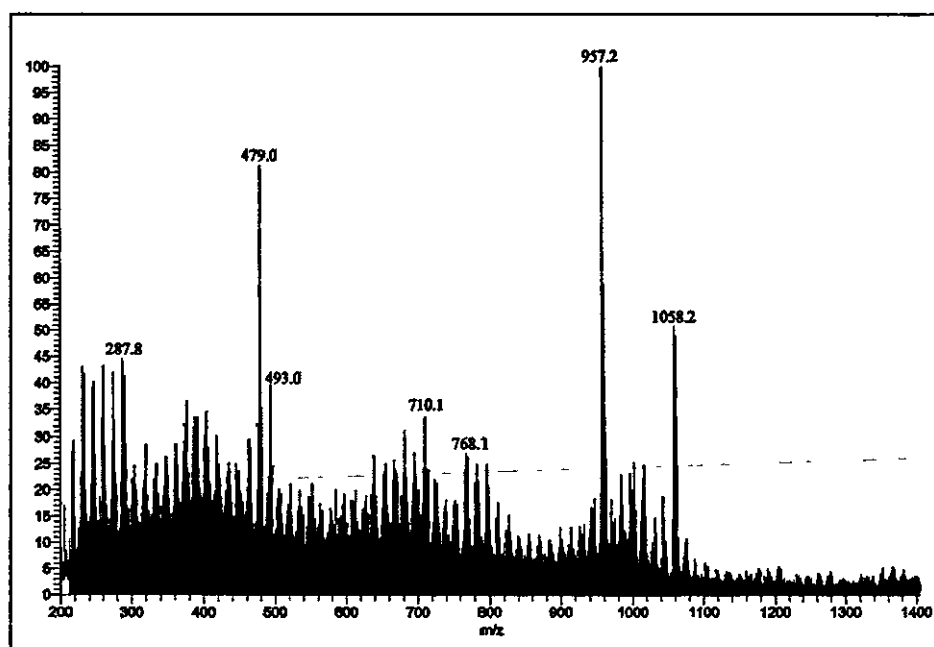


**Fig. 4.12:** LSIMS spectrum of  $[\text{Ni}_2\text{Ca}(\text{HL1})(\text{EtOH})](\text{NO}_3)$

Contrary to the results obtained for the heteronuclear sodium complexes of the macrocycle  $\text{H}_6\text{L1}$ , the synthesis of the heteronuclear calcium complexes depends on the order in which the reagents are added to the reaction mixture. The heteronuclear complexes  $[\text{Cu}_2\text{Ca}(\text{HL1})]\cdot\text{Cl}$  (4.4) and  $[\text{Ni}_2\text{Ca}(\text{HL1})(\text{EtOH})](\text{NO}_3)$  (4.5) were synthesised by adding simultaneously the transition metal and the calcium salts to the reaction mixture. Alternatively, heteronuclear calcium complexes of the new [3+3] macrocyclic ligand  $\text{H}_9\text{L8}$  were isolated if the calcium salts were added and left to react with the ligands on long reflux before adding the transition metal salts to the reaction mixture. The heteronuclear complexes of the macrocycle  $\text{H}_9\text{L8}$  will be described in section 4.3.

### 4.2.3. Heteronuclear complexes of H<sub>6</sub>L1 with barium

The next step in the synthesis of the heteronuclear complexes was to obtain complexes with larger group 2 metal ions. When the metal ion is a little too large for the macrocyclic cavity we expect to see it sitting above the donor set, as indeed we do in the heteronuclear complexes described previously where the fit was not perfect. An extension of this pattern leads to a second structural motif, in which two of the macrocyclic ligands sandwich the metal ion (e.g. the heteronuclear sandwich complex [Na<sub>2</sub>Ba(L26)<sub>2</sub>(Py)](Py)<sub>3</sub> where two calixarene macrocycles sandwich a barium ion<sup>177</sup>, Fig. 4.13). Sodium and calcium ions were already a little too large for the macrocyclic cavity of H<sub>6</sub>L1 and were lying somewhat above the mean plane of the four phenol oxygen atoms. Ba<sup>2+</sup> ion is considerably larger than Ca<sup>2+</sup> or Na<sup>+</sup> ions and is not likely to fit in the macrocyclic cavity of H<sub>6</sub>L1.

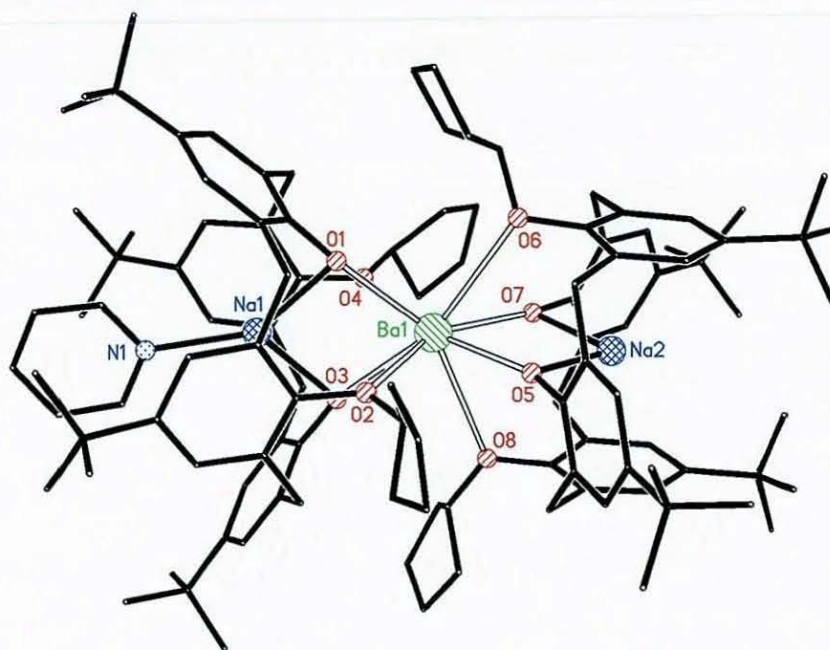


**Fig. 4.13:** Structure<sup>64,65,177</sup> of the heteronuclear sandwich complex [Na<sub>2</sub>Ba(L26)<sub>2</sub>(Py)]

The distance between opposite pairs of phenol oxygen atoms is *ca.* 2.75 Å in the heteronuclear sodium complexes of the [2+2] macrocycle H<sub>6</sub>L1, so the macrocyclic hole radius may be defined as *ca.* 1.37 Å. Taking the eight-coordinate radii of the metal ions as a basis of comparison of their effective sizes in these complexes it seems that Ba<sup>2+</sup> is a little too large ( $r(\text{Ba}^{2+}) = 1.56 \text{ \AA}$ )<sup>176</sup> for the macrocyclic hole of H<sub>6</sub>L1. Instead, barium complexes are likely to form sandwich complexes of the macrocycle H<sub>6</sub>L1 or to form bigger macrocycles with a larger macrocyclic cavity. This is rationalized taking into account the ionic radii and coordination numbers of the cations, and the conformational restraints of H<sub>6</sub>L1 macrocyclic molecules, which only offer six oxygen donors per macrocycle. It is likely that cations with coordination numbers of about six and ionic radii that match the hole size of the macrocycle (Ca<sup>2+</sup> or Na<sup>+</sup> ions) form the 1:1 metal:macrocyclic complexes whereas those with higher coordination numbers and ionic radii that mismatches the size of the macrocyclic cavity (Ba<sup>2+</sup> ions) form 1:2 metal:macrocyclic complexes or complexes with larger macrocycles. Other examples of barium macrocyclic sandwich complexes have been reported previously.<sup>178-181</sup>

The reaction of DHTMB and 1,3-diaminopropan-2-ol in the presence of the alkaline earth metal ion Ba<sup>2+</sup> and first row transition metal ions (Ni<sup>2+</sup>, Cu<sup>2+</sup> and Zn<sup>2+</sup> salts) yields a variety of new heteronuclear complexes. Two different types of product are formed when barium salts are used: heteronuclear sandwich complexes of the [2+2] macrocycle H<sub>6</sub>L1 and heteronuclear complexes of larger [3+3] and [4+4] macrocycles. This section will focus on the heteronuclear sandwich complexes of H<sub>6</sub>L1.

Simultaneous addition of barium and copper(II) perchlorate salts to an ethanol solution of DHTMB and further reaction with 1,3-diaminopropan-2-ol in the presence of base yielded a green brownish solid. A mixture of brown and green crystals was obtained by slow evaporation of an ethanol solution of the solid isolated. These crystals could be separated by different solubility. The green crystals were soluble in chloroform but not the brown ones, so the mixture was



dissolved in chloroform and the brown solid was filtered off. The brown solid analysing as  $[\text{Cu}_4\text{Ba}(\text{H}_2\text{L1})_2](\text{ClO}_4)_2 \cdot \text{EtOH} \cdot 4\text{H}_2\text{O}$  (**4.6a**) was recrystallised and further characterised by X-ray crystallography. The green solid obtained as the major product analysed as  $[\text{Cu}_4\text{Ba}(\text{H}_4\text{L9})](\text{ClO}_4)_2 \cdot 4\text{H}_2\text{O}$  (**4.6b**) and will be described in section 4.4.

Brown crystals of  $[\text{Cu}_4\text{Ba}(\text{H}_2\text{L1})_2](\text{ClO}_4)_2 \cdot \text{EtOH}$  (**4.6ax**) suitable for X-ray studies were grown by slow diffusion of diethylether into an ethanol solution of the heteronuclear complex  $[\text{Cu}_4\text{Ba}(\text{H}_2\text{L1})_2](\text{ClO}_4)_2 \cdot \text{EtOH} \cdot 4\text{H}_2\text{O}$  (**4.6a**). All the X-ray data collection parameters are summarised in Table 15 of appendix 1 along with the details concerning the refinement and disorder. Perspective views of the cation  $[\text{Cu}_4\text{Ba}(\text{H}_2\text{L1})_2]^{2+}$  are shown in Figs. 4.12 and 4.13 and selected bond lengths and angles relevant to the metal ion coordination are given in Table 4.11.

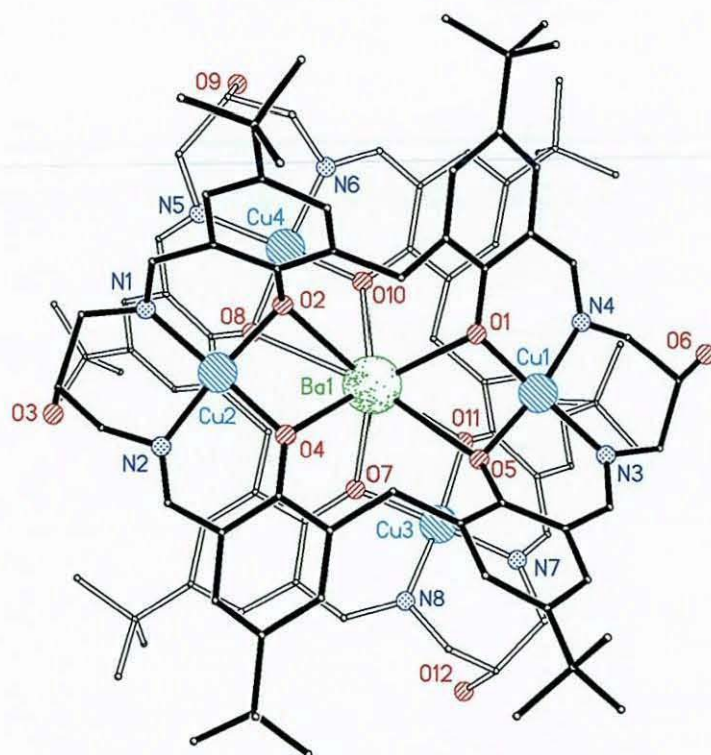


**Fig. 4.12:** Structure of the cation  $[\text{Cu}_4\text{Ba}(\text{H}_2\text{L1})_2]^{2+}$

Two of the macrocyclic ligands ( $\text{H}_2\text{L1}$ ) sandwich the barium ion (in order to appreciate clearly both macrocyclic ligands in the complex structure, one of them

has been represented with white bonds and the other with black bonds, Figs. 4.12 and 4.13). The two transition metal ions of each macrocyclic unit occupy the salen-type sites of the macrocycle while the barium ion coordinates the tetraphenolate central site of both macrocyclic units. The geometry of the copper(II) ions is square pyramidal, with two imine nitrogen and two phenolate oxygen donors of one of the macrocyclic units at the basal plane and a phenolate oxygen donor of the other macrocyclic unit weakly bonded as the apical ligand (e.g. Cu1-O11 2.765(8) Å, Table 4.11).

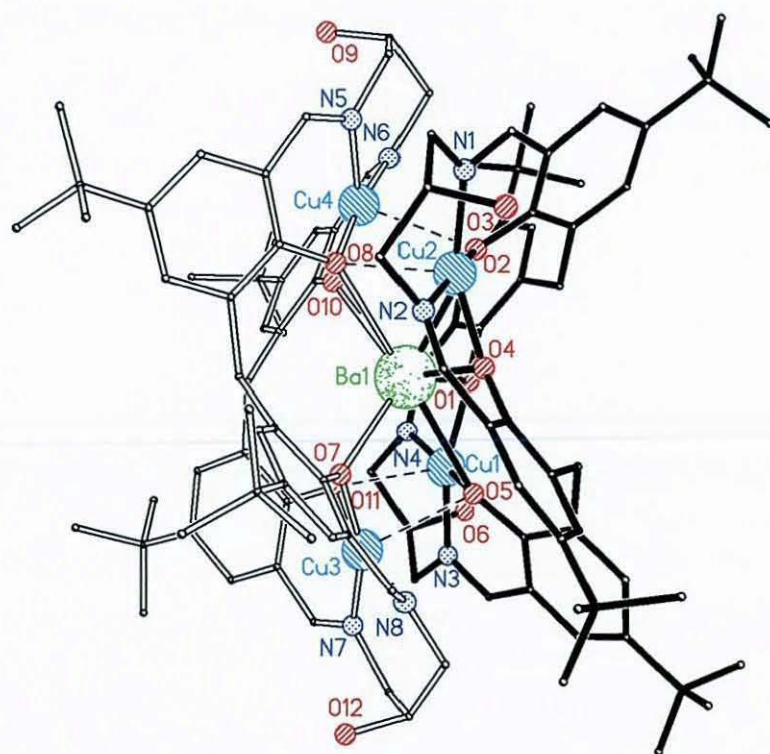


**Fig. 4.13:** Side-on view of the cation  $[\text{Cu}_4\text{Ba}(\text{H}_2\text{L}1)_2]^{2+}$

The general conformation of each macrocyclic unit of this complex is similar to the heteronuclear structures previously described. The 2,2'-methylenediphenol groups are completely deprotonated (there is no intramolecular hydrogen bonding), the phenol oxygen atoms are well separated (e.g. O1...O2 4.046(11) Å, Table 4.11) and the saddle-shape of the macrocycle has been stretched. The distance between adjacent phenol oxygen atoms has increased approximately 1.63



Å compared to the dicopper precursor  $[\text{Cu}_2(\text{H}_4\text{L1})\text{Cl}]\text{Cl}\cdot 1.6\text{Et}_2\text{O}\cdot\text{EtOH}$  (see section 2.4.1.2 of Chapter 2).

The barium cation is eight-coordinate and has rectangular antiprism geometry, coordinating the four phenolic oxygen donors of the each macrocycle (oxygen atoms O1, O2, O4 and O5 belong to one macrocycle while O7, O8, O10 and O11 donors belong to the other macrocycle).

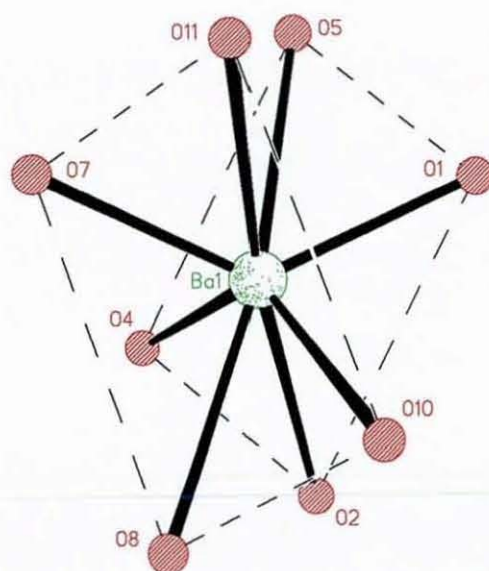


**Fig. 4.14:** Coordination sphere of the barium cation in  $[\text{Cu}_4\text{Ba}(\text{H}_2\text{L1})_2]^{2+}$

The average O-Ba bond length is 2.77 Å and the barium lies on the intersection between the two  $\text{O}_4$  planes. The bond lengths of barium coordination are not equivalent, having four bond distances approximately 0.3 Å longer than the other four (Table 4.11). Interestingly, each of the methylenediphenol units coordinates the barium ion with a long bond ( $\sim 2.92$  Å) from one of the phenolate groups and with a short bond ( $\sim 2.62$  Å) from the other phenolate group. The reason for one Ba-O bond being longer is because the phenolate oxygen participating on that bond also interacts with the opposite copper ion of the other macrocyclic unit, weakly coordinating as the axial ligand for that copper ion, and therefore weakening the bond to the barium ion.

**Table 4.11:** Selected interatomic distances [Å] and angles [°]  
for [Cu<sub>4</sub>Ba(H<sub>2</sub>L1)<sub>2</sub>](ClO<sub>4</sub>)<sub>2</sub>·EtOH

Ba(1)-O(7)	2.603(7)	Cu(2)-O(2)	1.955(7)
Ba(1)-O(1)	2.614(8)	Cu(2)-N(1)	1.974(10)
Ba(1)-O(10)	2.624(7)	Cu(2)-N(2)	1.999(9)
Ba(1)-O(4)	2.638(7)	Cu(2)-O(8)	2.551(8)
Ba(1)-O(11)	2.867(8)	Cu(3)-O(7)	1.913(8)
Ba(1)-O(5)	2.877(8)	Cu(3)-O(11)	1.924(8)
Ba(1)-O(2)	2.945(8)	Cu(3)-N(7)	1.947(10)
Ba(1)-O(8)	2.974(8)	Cu(3)-N(8)	1.938(10)
Ba(1)-Cu(2)	3.4518(17)	Cu(3)-O(5)	2.729(8)
Ba(1)-Cu(3)	3.4727(16)	Cu(4)-O(10)	1.927(8)
Ba(1)-Cu(4)	3.4816(16)	Cu(4)-N(6)	1.950(9)
Ba(1)-Cu(1)	3.4885(16)	Cu(4)-O(8)	1.967(7)
Cu(1)-O(1)	1.912(8)	Cu(4)-N(5)	1.981(11)
Cu(1)-N(3)	1.948(10)	Cu(4)-O(2)	2.597(8)
Cu(1)-O(5)	1.967(8)	O(1)-O(2)	4.046(11)
Cu(1)-N(4)	1.994(10)	O(4)-O(5)	4.042(11)
Cu(1)-O(11)	2.765(8)	O(7)-O(8)	4.030(11)
Cu(2)-O(4)	1.925(8)	O(10)-O(11)	4.086(11)
O(7)-Ba(1)-O(1)	130.9(3)	O(1)-Cu(1)-N(4)	91.5(4)
O(7)-Ba(1)-O(10)	117.0(2)	N(3)-Cu(1)-N(4)	95.3(4)
O(1)-Ba(1)-O(10)	87.1(2)	O(5)-Cu(1)-N(4)	168.8(4)
O(7)-Ba(1)-O(4)	84.0(2)	O(1)-Cu(1)-Ba(1)	47.6(2)
O(1)-Ba(1)-O(4)	115.9(2)	O(5)-Cu(1)-Ba(1)	55.6(2)
O(10)-Ba(1)-O(4)	127.4(2)	N(4)-Cu(1)-Ba(1)	113.6(3)
O(7)-Ba(1)-O(11)	55.7(2)	O(4)-Cu(2)-O(2)	85.4(3)
O(1)-Ba(1)-O(11)	81.2(2)	O(4)-Cu(2)-N(1)	158.0(4)
O(10)-Ba(1)-O(11)	96.1(2)	O(2)-Cu(2)-N(1)	91.0(4)
O(4)-Ba(1)-O(11)	132.1(2)	O(4)-Cu(2)-N(2)	89.6(4)
O(7)-Ba(1)-O(5)	80.1(2)	O(2)-Cu(2)-N(2)	172.0(4)
O(1)-Ba(1)-O(5)	55.4(2)	N(1)-Cu(2)-N(2)	95.9(4)
O(10)-Ba(1)-O(5)	134.8(2)	O(4)-Cu(2)-Ba(1)	49.3(2)
O(4)-Ba(1)-O(5)	94.1(2)	O(2)-Cu(2)-Ba(1)	58.4(2)
O(11)-Ba(1)-O(5)	57.6(2)	N(2)-Cu(2)-Ba(1)	113.6(3)
O(7)-Ba(1)-O(2)	131.8(2)	O(7)-Cu(3)-O(11)	84.0(3)
O(1)-Ba(1)-O(2)	93.2(2)	O(7)-Cu(3)-N(7)	161.5(4)
O(10)-Ba(1)-O(2)	77.5(2)	O(11)-Cu(3)-N(7)	92.3(4)
O(4)-Ba(1)-O(2)	55.9(2)	O(7)-Cu(3)-N(8)	90.4(4)
O(11)-Ba(1)-O(2)	171.7(2)	O(11)-Cu(3)-N(8)	168.1(4)
O(5)-Ba(1)-O(2)	123.8(2)	N(7)-Cu(3)-N(8)	96.3(4)
O(7)-Ba(1)-O(8)	92.3(2)	O(7)-Cu(3)-Ba(1)	47.7(2)
O(1)-Ba(1)-O(8)	134.4(2)	O(11)-Cu(3)-Ba(1)	55.6(2)
O(10)-Ba(1)-O(8)	55.8(2)	O(10)-Cu(4)-N(6)	91.7(4)
O(4)-Ba(1)-O(8)	77.2(2)	O(10)-Cu(4)-O(8)	85.3(3)
O(11)-Ba(1)-O(8)	124.0(2)	N(6)-Cu(4)-O(8)	173.1(4)
O(5)-Ba(1)-O(8)	169.1(2)	O(10)-Cu(4)-N(5)	159.6(4)
O(2)-Ba(1)-O(8)	56.5(2)	N(6)-Cu(4)-N(5)	95.1(4)
O(1)-Cu(1)-N(3)	164.0(4)	O(8)-Cu(4)-N(5)	89.8(4)
O(1)-Cu(1)-O(5)	82.7(3)	O(10)-Cu(4)-Ba(1)	48.2(2)
N(3)-Cu(1)-O(5)	92.8(4)	O(8)-Cu(4)-Ba(1)	58.6(2)



Complex  $[\text{Cu}_4\text{Ba}(\text{H}_2\text{L1})_2](\text{ClO}_4)_2 \cdot \text{EtOH} \cdot 4\text{H}_2\text{O}$  (**4.6a**) was further characterised by mass spectrometry. The relative intensity of the peaks in the LSIMS spectrum is very weak with respect to the peak at  $m/z$  306 corresponding to the NOBA matrix, which suggests that the complex is not very soluble within the matrix. The fragmentation pattern (Table 4.12) of the complex shows two peaks at  $m/z$  2073 and 2171 which correspond to the heteronuclear fragments  $[\text{Cu}_4\text{Ba}(\text{H}_2\text{L1})_2]^+$  and  $[\text{Cu}_4\text{Ba}(\text{H}_2\text{L1})_2(\text{ClO}_4)-2\text{H}]^+$  respectively.

**Table 4.12:** Peak attributions for  $[\text{Cu}_4\text{Ba}(\text{H}_2\text{L1})_2](\text{ClO}_4)_2 \cdot \text{EtOH} \cdot 4\text{H}_2\text{O}$

M/z	Rel. Intensity (%)	Fragments	Calc. Mass
306	100	NOBA matrix	306
969	5	$[\text{Cu}_2(\text{H}_2\text{L1}) + \text{H}]^+$	969
1037	8	$[\text{Cu}_2(\text{H}_2\text{L1})(\text{MeOH})_2 + 2\text{H}]^{2+}$	1036
2073	7	$[\text{Cu}_4\text{Ba}(\text{H}_2\text{L1})_2]^+$	2073
2171	1	$[\text{Cu}_4\text{Ba}(\text{H}_2\text{L1})_2(\text{ClO}_4)-2\text{H}]^+$	2171

An analogous zinc and barium sandwich complex was also synthesised. The barium salts were added first and left to react with the DHTMB and the diamine for long reflux (18 h) before adding the zinc(II) salts to the reaction mixture. In this case only this heteronuclear product was isolated from the reaction mixture. The yellow solid isolated analysing as  $[\text{Zn}_4\text{Ba}(\text{H}_2\text{L1})_2(\text{OH})](\text{ClO}_4) \cdot 3\text{H}_2\text{O}$  (**4.7**) was recrystallised and further characterised by X-ray crystallography.

Pale yellow crystals of  $[\text{Zn}_4\text{Ba}(\text{H}_2\text{L1})_2](\text{ClO}_4)_2 \cdot 2\text{Et}_2\text{O}$  (**4.7x**) were grown by slow diffusion of diethylether into a methanol solution of the heteronuclear complex **4.7**. All the X-ray data collection parameters are summarised in Table 16 of appendix 1 along with the details concerning the refinement and disorder. Perspective views of the cation  $[\text{Zn}_4\text{Ba}(\text{H}_2\text{L1})_2]^{2+}$  are shown in Figs. 4.15 and 4.16 (in order to appreciate clearly both macrocyclic ligands in the complex structure, one of them has been represented with white bonds and the other with black bonds) and selected bond lengths and angles relevant to the metal ion coordination are given in Table 4.13. The crystal structure is very similar to the previous copper and barium sandwich complex  $[\text{Cu}_4\text{Ba}(\text{H}_2\text{L1})_2](\text{ClO}_4)_2 \cdot \text{EtOH}$  (**4.6ax**). Two

of the macrocyclic ligands ( $H_2L1$ ) sandwich the barium ion. The two transition metal ions of each macrocyclic unit occupy the salen-type sites of the macrocycle while the barium ion coordinates the tetraphenolate central site of both macrocyclic units.

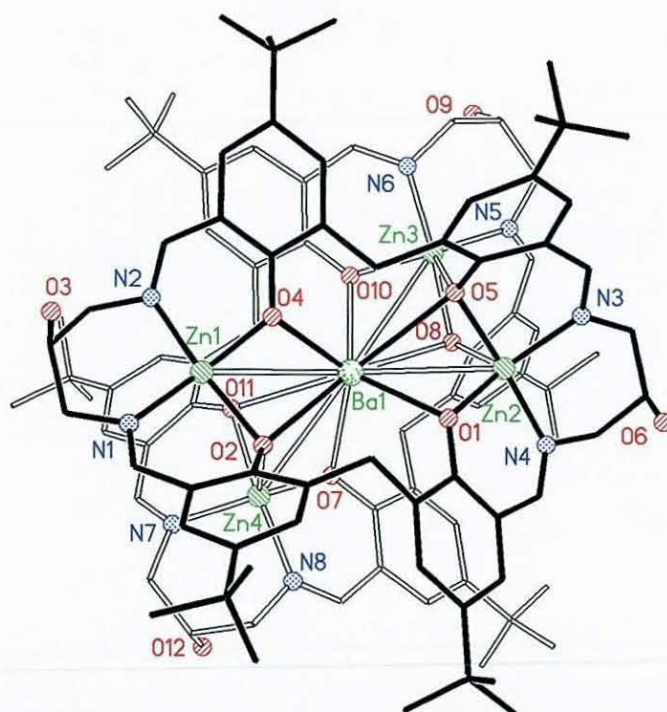


Fig. 4.15: Structure of the cation  $[Zn_4Ba(H_2L1)_2]^{2+}$

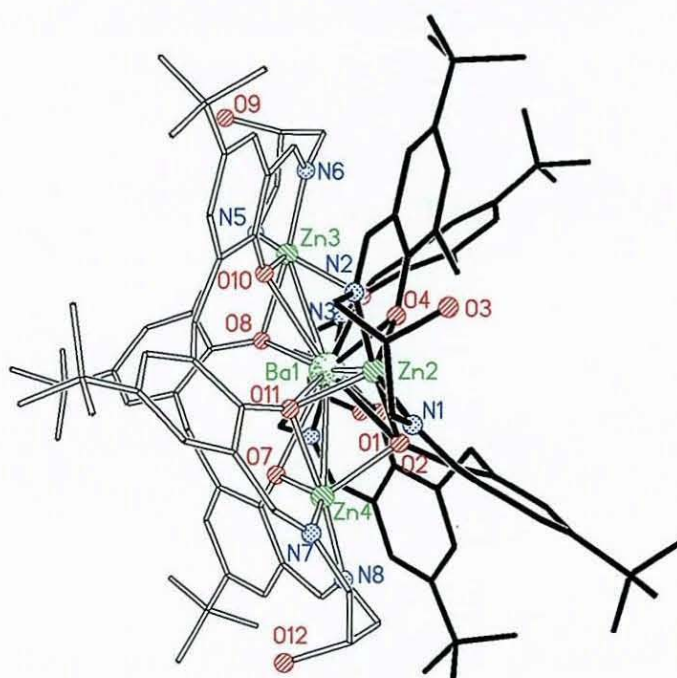
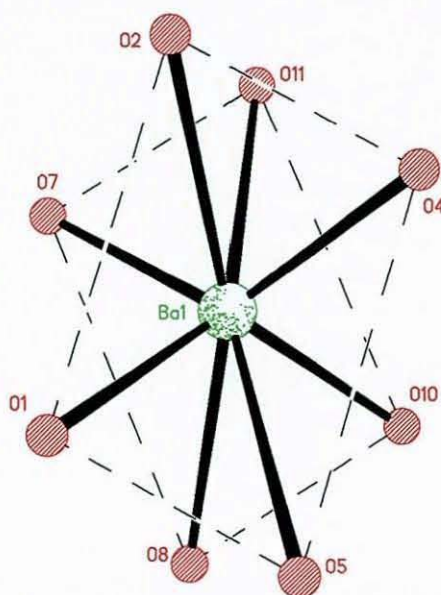


Fig. 4.16: Side-on view of the cation  $[Zn_4Ba(H_2L1)_2]^{2+}$



The geometry of the zinc(II) ions is square pyramidal, with two imine nitrogen and two phenolate oxygen donors of one of the macrocyclic units at the basal plane and a phenolate oxygen donor of the other macrocyclic unit as the apical ligand. Again, the 2,2'-methylenediphenol groups are completely deprotonated (there is no intramolecular hydrogen bonding), the phenol oxygen atoms are well separated (eg. O1...O2 4.099(16) Å, Table 4.13) and the saddle-shape of the macrocycle has been stretched.

As for the analogous copper and barium sandwich complex, the barium cation is eight-coordinate and has rectangular antiprism geometry, coordinating the four phenolic oxygen donors of the each macrocycle (oxygen atoms O1A, O2A, O4A and O5A belong to one macrocycle while O1B, O2B, O4B and O5B belong to the other macrocycle), lying on the intersection between the two  $O_4$  planes (Fig. 4.17). Again, the bond lengths of barium coordination are not equivalent, having four bond distances approximately 0.3 Å longer than the other four due to the fact that the phenolate oxygen atoms participating on that bond are also coordinating opposite copper ions of the other macrocyclic unit as the axial ligand, and therefore weakening the bond to the barium ion (Table 4.13).



**Fig. 4.17:** Coordination sphere of the barium cation in  $[Zn_4Ba(H_2L1)_2]^{2+}$



**Table 4.13:** Selected intramolecular distances [Å] and angles [°] for  $[\text{Zn}_4\text{Ba}(\text{H}_2\text{L}1)_2](\text{ClO}_4)_2 \cdot 2\text{Et}_2\text{O}$

Ba(1)-O(4)	2.608(12)	Zn(2)-O(1)	2.009(11)	Zn(3)-N(7)	2.056(14)
Ba(1)-O(7)	2.626(11)	Zn(2)-N(4)	2.051(13)	Zn(3)-N(8)	2.057(13)
Ba(1)-O(10)	2.627(10)	Zn(2)-O(8)	2.066(10)	Zn(3)-O(8)	2.168(11)
Ba(1)-O(1)	2.630(10)	Zn(2)-N(3)	2.080(14)	Zn(4)-O(7)	1.982(12)
Ba(1)-O(11)	2.901(10)	Zn(2)-O(5)	2.128(11)	Zn(4)-O(2)	2.064(11)
Ba(1)-O(8)	2.925(11)	Zn(1)-O(4)	2.013(12)	Zn(4)-N(9)	2.065(15)
Ba(1)-O(2)	2.957(11)	Zn(1)-N(2)	2.048(13)	Zn(4)-N(10)	2.067(14)
Ba(1)-O(5)	2.994(11)	Zn(1)-N(1)	2.055(14)	Zn(4)-O(11)	2.137(10)
Ba(1)-Zn(2)	3.405(2)	Zn(1)-O(11)	2.087(11)	O(1A)-O(2)	4.099(16)
Ba(1)-Zn(4)	3.413(2)	Zn(1)-O(2)	2.141(11)	O(4A)-O(5)	4.105(16)
Ba(1)-Zn(1)	3.418(2)	Zn(3)-O(10)	1.982(11)	O(1B)-O(8)	4.130(15)
Ba(1)-Zn(3)	3.437(2)	Zn(3)-O(5)	2.051(11)	O(4B)-O(11)	4.102(15)
O(4)-Ba(1)-O(7)	124.4(4)	O(1)-Zn(2)-O(5)	84.4(4)		
O(4)-Ba(1)-O(10)	86.5(3)	N(4)-Zn(2)-O(5)	174.3(5)		
O(7)-Ba(1)-O(10)	120.7(3)	O(8)-Zn(2)-O(5)	77.2(4)		
O(4)-Ba(1)-O(1)	115.8(3)	N(3)-Zn(2)-O(5)	87.7(5)		
O(7)-Ba(1)-O(1)	89.3(3)	O(4)-Zn(1)-N(2)	90.3(5)		
O(10)-Ba(1)-O(1)	123.9(3)	O(4)-Zn(1)-N(1)	143.3(5)		
O(4)-Ba(1)-O(11)	71.6(3)	N(2)-Zn(1)-N(1)	94.9(5)		
O(7)-Ba(1)-O(11)	59.3(3)	O(4)-Zn(1)-O(11)	104.0(4)		
O(10)-Ba(1)-O(11)	95.7(3)	N(2)-Zn(1)-O(11)	106.9(5)		
O(1)-Ba(1)-O(11)	139.3(3)	N(1)-Zn(1)-O(11)	109.1(5)		
O(4)-Ba(1)-O(8)	137.8(3)	O(4)-Zn(1)-O(2)	84.0(4)		
O(7)-Ba(1)-O(8)	96.0(3)	N(2)-Zn(1)-O(2)	174.0(5)		
O(10)-Ba(1)-O(8)	59.9(3)	N(1)-Zn(1)-O(2)	88.5(5)		
O(1)-Ba(1)-O(8)	71.7(3)	O(11)-Zn(1)-O(2)	76.6(4)		
O(11)-Ba(1)-O(8)	131.7(3)	O(10)-Zn(3)-O(5)	105.8(4)		
O(4)-Ba(1)-O(2)	59.6(3)	O(10)-Zn(3)-N(6)	142.7(5)		
O(7)-Ba(1)-O(2)	70.4(3)	O(5)-Zn(3)-N(6)	107.5(5)		
O(10)-Ba(1)-O(2)	138.4(3)	O(10)-Zn(3)-N(6)	91.3(5)		
O(1)-Ba(1)-O(2)	94.2(3)	O(5)-Zn(3)-N(6)	107.7(5)		
O(11)-Ba(1)-O(2)	53.1(3)	N(5)-Zn(3)-N(6)	94.3(5)		
O(8)-Ba(1)-O(2)	160.9(3)	O(10)-Zn(3)-O(8)	84.2(4)		
O(4)-Ba(1)-O(5)	94.0(3)	O(5)-Zn(3)-O(8)	76.6(4)		
O(7)-Ba(1)-O(5)	139.3(3)	N(5)-Zn(3)-O(8)	87.4(5)		
O(10)-Ba(1)-O(5)	69.5(3)	N(6)-Zn(3)-O(8)	174.5(5)		
O(1)-Ba(1)-O(5)	58.9(3)	O(7)-Zn(4)-O(2)	105.9(5)		
O(11)-Ba(1)-O(5)	160.3(3)	O(7)-Zn(4)-N(7)	141.5(5)		
O(8)-Ba(1)-O(5)	52.5(3)	O(2)-Zn(4)-N(7)	108.8(5)		
O(2)-Ba(1)-O(5)	131.1(3)	O(7)-Zn(4)-N(8)	90.1(5)		
O(1)-Zn(2)-N(4)	90.2(5)	O(2)-Zn(4)-N(7)	107.9(5)		
O(1)-Zn(2)-O(8)	106.4(4)	N(7)-Zn(4)-N(8)	94.7(6)		
N(4)-Zn(2)-O(8)	106.4(5)	O(7)-Zn(4)-O(11)	83.4(4)		
O(1)-Zn(2)-N(3)	140.7(5)	O(2)-Zn(4)-O(11)	77.1(4)		
N(4)-Zn(2)-N(3)	95.1(5)	N(7)-Zn(4)-O(11)	88.5(5)		
O(8)-Zn(2)-N(3)	109.3(5)	N(8)-Zn(4)-O(11)	172.7(5)		

Complex  $[\text{Zn}_4\text{Ba}(\text{H}_2\text{L1})_2(\text{OH})](\text{ClO}_4)\cdot 3\text{H}_2\text{O}$  (4.7) was further characterised by mass spectrometry. The LSIMS spectrum of the complex shows two peaks at  $m/z$  2077 and 2178 which correspond to the fragments  $[\text{Zn}_4\text{Ba}(\text{H}_2\text{L1})_2-2\text{H}]^+$  and  $[\text{Zn}_4\text{Ba}(\text{H}_2\text{L1})_2(\text{ClO}_4)-2\text{H}]^+$  respectively. The peaks at  $m/z$  1007, 1138 and 1139 also suggest the formation of heteronuclear species. The relative intensity of the peaks is very weak with respect to the peak at  $m/z$  306 corresponding to the NOBA matrix, which suggests again a lack of solubility in the LSIMS medium (Fig. 4.18, Table 4.14).

**Table 4.14:** Peak attributions for  $[\text{Zn}_4\text{Ba}(\text{H}_2\text{L1})_2(\text{OH})](\text{ClO}_4)\cdot 3\text{H}_2\text{O}$

M/z	Rel. Intensity (%)	Fragments	Calc. Mass
306	100	NOBA matrix	306
971	35	$[\text{Zn}_2(\text{H}_3\text{L1})-2\text{H}]^+$	973
1007	25	$[\text{Zn}_2\text{Ba}(\text{HL1})-\text{H}]^+$	1007
1138	20	$[\text{Zn}_2\text{Ba}(\text{HL1})(\text{MeOH})-2\text{H}]^+$	1138
1339	15	$[\text{Zn}_2\text{Ba}(\text{H}_2\text{L1})(\text{ClO}_4)(\text{EtOH})_2(\text{H}_2\text{O})_2+\text{H}]^+$	1337
2077	7	$[\text{Zn}_4\text{Ba}(\text{H}_2\text{L1})_2-2\text{H}]^+$	2077
2178	7	$[\text{Zn}_4\text{Ba}(\text{H}_2\text{L1})_2(\text{ClO}_4)-2\text{H}]^+$	2178

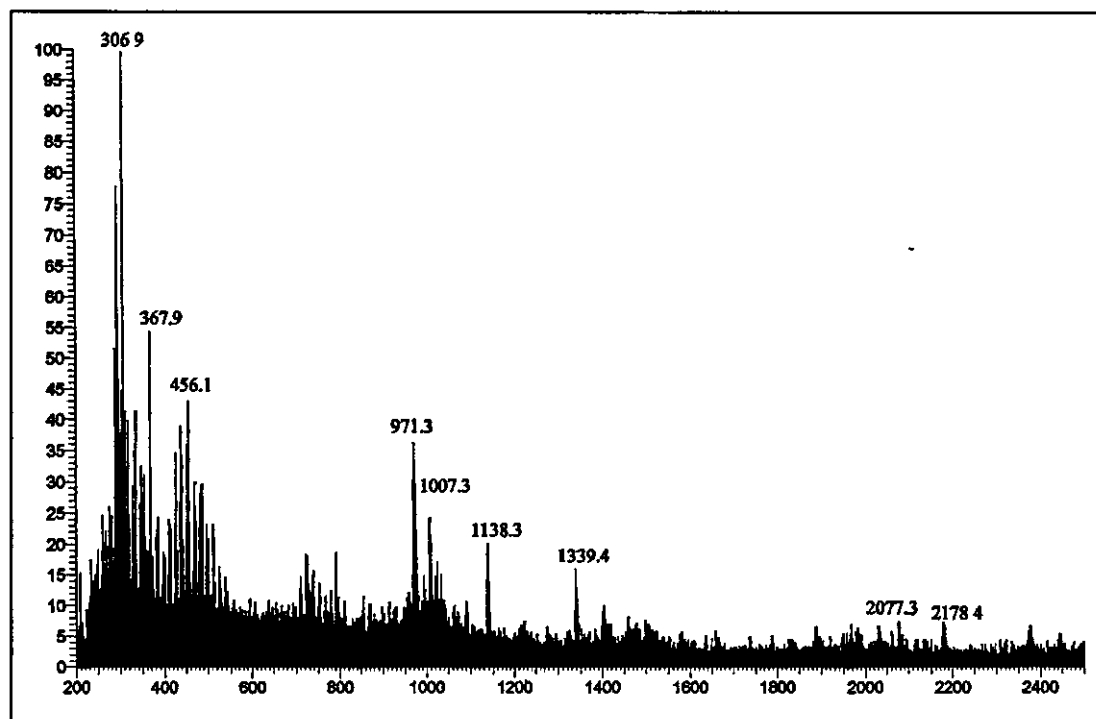


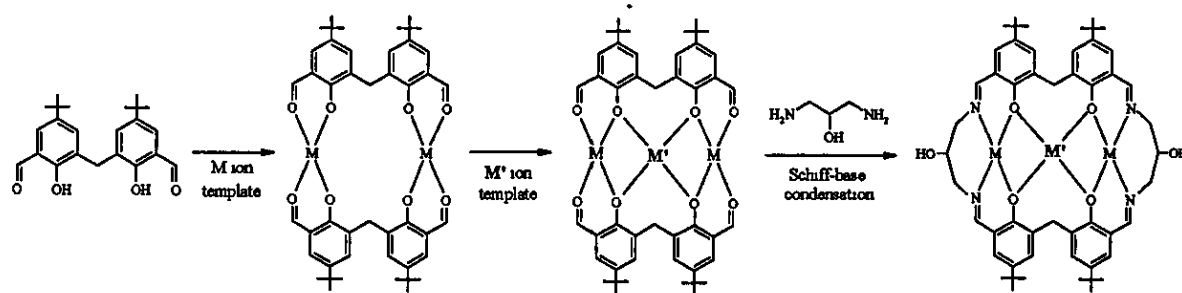
**Fig. 4.18:** LSIMS spectrum of  $[\text{Zn}_4\text{Ba}(\text{H}_2\text{L1})_2(\text{OH})](\text{ClO}_4)\cdot 3\text{H}_2\text{O}$

#### 4.2.4. Possible routes for the synthesis of the heteronuclear complexes of $H_6L1$

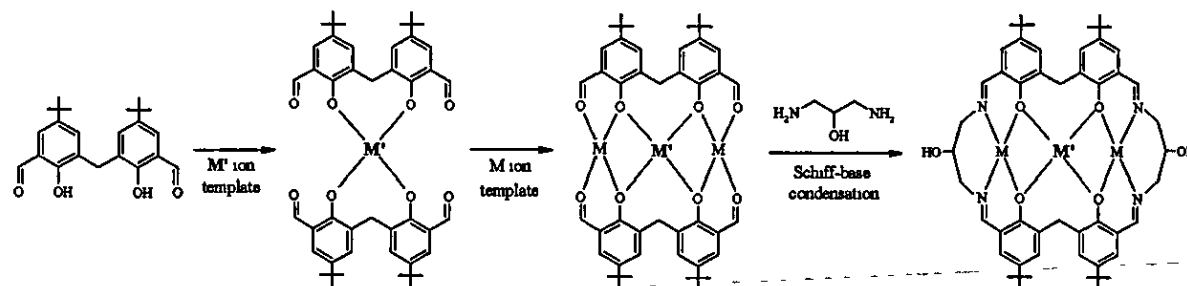
The mechanism for the synthesis of this series of heteronuclear complexes clearly involves a Schiff-base condensation (formation of an imine from an amine and a carbonyl compound) *via* the template route. In the template synthesis the metal assists the Schiff-base reaction that leads to the formation of the macrocycle.<sup>2,4</sup> The metal ions direct the course of the reaction and therefore, since either metal could act as template, the structure of the final product may be dependent on the order in which the components are added.

DHTMB molecules are expected to react with the metal ions to form polynuclear complexes. Such species are then expected to readily form symmetrical [2+2] Schiff-base macrocycles upon condensation with the diamine, once the components have assembled around the template metal ions in the appropriate arrangement. It is likely that the formation of heteronuclear complexes of  $H_6L1$  follow one of the routes outlined in Schemes 4.1, 4.2 and 4.3. Depending on the order in which the different reactants were added to the reaction mixture and the metal ion radii, three different pathways that would yield the same product are possible.

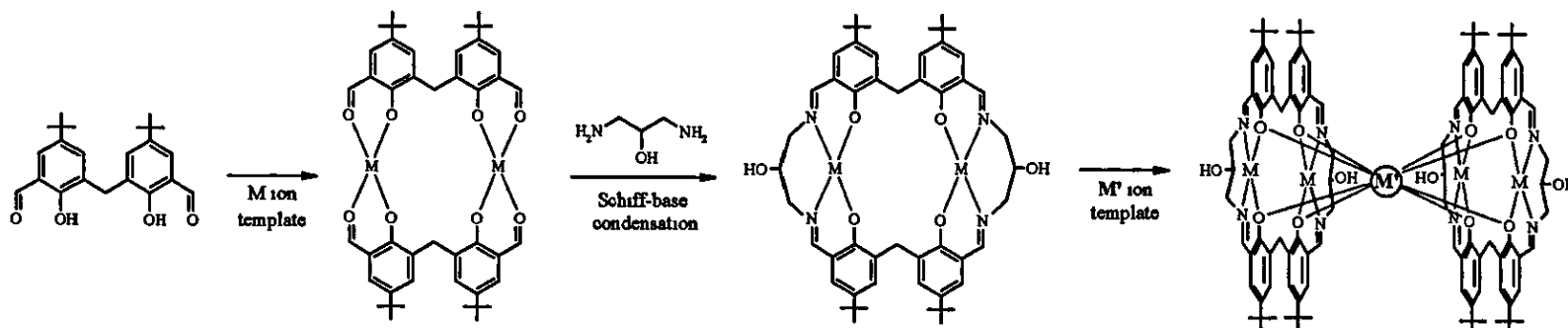
It is likely that the cyclisation step in the first pathway (Scheme 4.1) involves two molecules of the DHTMB which bind the two transition metal ions ( $M = Ni^{2+}$ ,  $Cu^{2+}$  or  $Zn^{2+}$ ). This dinuclear complex is essentially pre-organised for binding a third metal ion in the central site, which is occupied by the alkaline or alkaline earth metal ( $M' = Na^+$  or  $Ca^{2+}$ ). If the incoming metal ion is of suitable size, the overall conformation of the complex need not undergo major change. Then two diamine molecules condense with the aldehydes, forming the [2+2] macrocycle. Thus, in the first pathway the template species is the transition metal ion.



**Scheme 4.1:** heteronuclear complexes of  $\text{H}_6\text{L1}$  synthesised *via* M template condensation.



**Scheme 4.2:** heteronuclear complexes of  $\text{H}_6\text{L1}$  synthesised *via* M' template condensation



**Scheme 4.3:** heteronuclear "sandwich" complexes of  $\text{H}_6\text{L1}$  synthesised *via* M template condensation

In the second pathway (Scheme 4 2) two molecules of the DHTMB bind the alkaline or alkaline earth metal ion ( $M'$ ) in the preferred tetraphenolate site, then two transition metal ions ( $M$ ) bind the two equivalent  $N_2O_2$  sites and two diamine molecules condense with the aldehydes, again forming the macrocycle. In this case, the alkaline or alkaline earth metal ion is probably not assisting the Schiff-base formation as it is not coordinated to the carbonyl or amine groups although it is contributing to bringing the two DHTMB units together, so is a different kind of template reaction from that involving transition metal ions alone. Both cyclisation pathways are equivalent and would lead to the same products if the alkaline or alkaline earth metal ion radii are suitable for the central cavity of the macrocycle  $H_6L1$ .

If the central cavity of the [2+2] macrocycle is not large enough to accommodate  $M'$  (where  $M'=Ba^{2+}$ ), the alkali earth metal ion ( $M'$ ) can coordinate two preformed macrocyclic units forming sandwich complexes (Scheme 4 3). Alternatively, the large metal ion can influence the product of the initial cyclisation reaction by binding more than two DHTMB molecules generating larger [3+3] or [4+4] macrocyclic rings (as will be described in the subsequent sections 4.3 and 4.4).

### 4.3. Heteronuclear complexes of the pseudocalixarene macrocycle $H_9L8$

While the use of metal ions to template [2+2] Schiff-base macrocyclic condensation reactions from constituent amines and aldehydes or ketones is well known,<sup>2</sup> the formation of [3+3] products is rare.<sup>3-6</sup>

The reaction of the dialdehyde DHTMB with the diamine 1,3-diaminopropan-2-ol in the presence of an alkaline earth metal ion ( $Ca^{2+}$  or  $Ba^{2+}$  salts) as template and first row transition metal ions ( $Ni^{2+}$ ,  $Cu^{2+}$  and  $Zn^{2+}$  salts) yields a variety of heteronuclear complexes of the new [3+3] pseudo-calixarene macrocycle  $H_9L8$



The first heteronuclear complex of  $H_9L8$  ( $[Cu_3Ba(H_2L8)](ClO_4) \cdot 2H_2O$ ) was synthesised by reacting the barium salts and the ligand reagents on long reflux in the presence of a base, after which the copper(II) salts were added to the reaction mixture and further refluxed. The reaction yielded again a mixture of two different heteronuclear complexes isolated by crystallisation. The green crystals analysed as  $[Cu_3Ba(H_2L8)](ClO_4) \cdot 2H_2O$  (4.8a) and was the major product of the reaction (60%) while the brown crystals of the minor product analysed as the sandwich complex  $[Cu_4Ba(H_2L1)_2](ClO_4)_2 \cdot 2H_2O$  (4.8b), analogous to the one discussed previously (complex 4.6a). The new [3+3] macrocycle  $H_9L8$  was initially characterised by X-ray crystallographic studies

Green crystals of  $[Cu_3Ba(H_3L8)(MeOH)(ClO_4)](ClO_4)$  (4.8ax) were grown by slow diffusion of diethylether into a methanol solution of the heteronuclear complex  $[Cu_3Ba(H_2L8)](ClO_4) \cdot 2H_2O$  (4.8a). All the X-ray data collection parameters are summarised in Table 17 of appendix 1 along with the details concerning the refinement and disorder. A perspective view of the cation  $[Cu_3Ba(H_3L8)(MeOH)(ClO_4)]$  is shown in Fig. 4.20 and selected bond lengths and angles relevant to the metal ion coordination are given in Table 4.15.

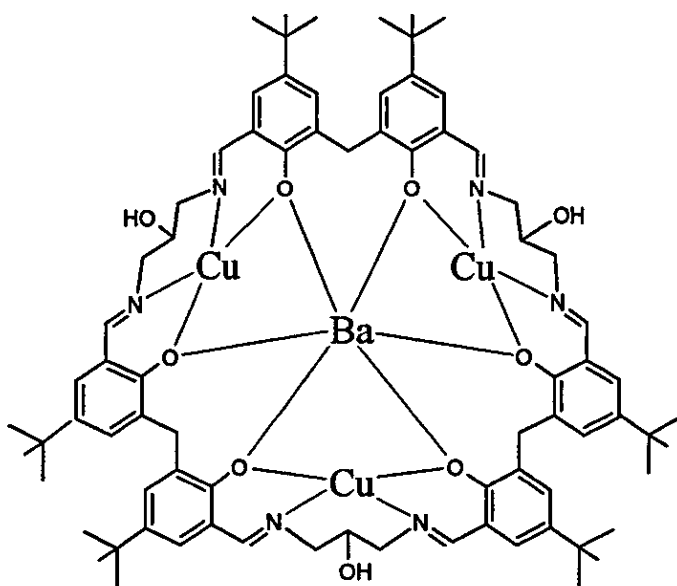
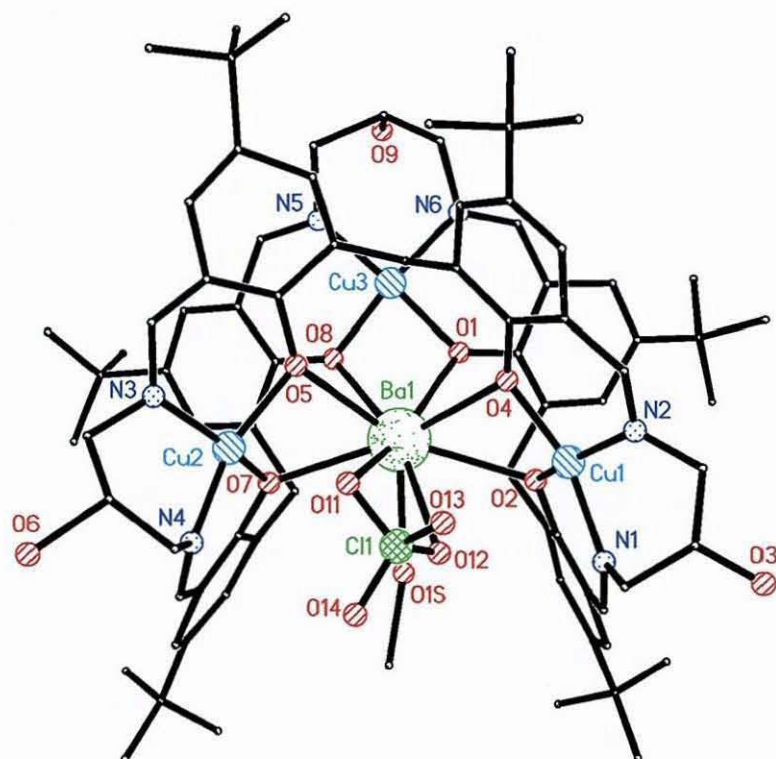


Fig. 4.19: Connectivity diagram for the cation  $[Cu_3Ba(H_3L8)]^{2+}$

The three copper(II) ions of each macrocyclic unit occupy the salen-type sites of the macrocycle while the barium ion coordinates the hexaphenolate central site of the macrocycle (Fig. 4.19). Two copper ions (Cu1 and Cu2) of the complex are four-coordinate and have identical macrocyclic donors, two phenolate oxygen and two imine nitrogen atoms. The geometry at each copper ion is distorted square planar. The other copper ion (Cu3) is five-coordinated and has square pyramidal geometry, with two phenol oxygen and two imine nitrogen macrocyclic donors in the basal plane and one alkoxo oxygen donor of the other macrocyclic unit as the apical ligand.



**Fig. 4.20:** Structure of the cation  $[\text{Cu}_3\text{Ba}(\text{H}_3\text{L8})(\text{MeOH})(\text{ClO}_4)]^+$

The general conformation of the cation  $[\text{Cu}_3\text{Ba}(\text{H}_3\text{L8})(\text{MeOH})(\text{ClO}_4)]^+$  is very different from the complexes discussed previously. The ligand wraps around the barium ion in a manner that resembles the seam of a tennis ball. This could be to optimise the match between the sizes of the cation and the macrocyclic hole. The macrocycle adopts a folded conformation which optimises the metal-donor atom distances, generating six approximately equal Ba-O bonds (Table 4.15).

**Table 4.15:** Selected interatomic distances [Å] and angles [°] for [Cu<sub>3</sub>Ba(H<sub>3</sub>L8)(MeOH)(ClO<sub>4</sub>)](ClO<sub>4</sub>)

Ba(1)-O(7)	2.665(18)	Cu(1)-O(2)	1.873(18)
Ba(1)-O(2)	2.745(18)	Cu(1)-N(2)	1.83(2)
Ba(1)-O(5)	2.74(2)	Cu(1)-N(1)	1.88(3)
Ba(1)-O(1)	2.698(18)	Cu(2)-N(4)	1.88(3)
Ba(1)-O(1S)	2.77(2)	Cu(2)-O(7)	1.925(19)
Ba(1)-O(8)	2.778(18)	Cu(2)-O(5)	1.96(2)
Ba(1)-O(4)	2.797(18)	Cu(2)-N(3)	1.94(3)
Ba(1)-O(12)	2.91(2)	Cu(3)-O(8)	1.839(19)
Ba(1)-O(11)	3.13(2)	Cu(3)-N(5)	1.91(2)
Ba(1)-Cu(2)	3.504(5)	Cu(3)-O(1)	1.896(18)
Ba(1)-Cu(1)	3.552(4)	Cu(3)-N(6)	1.92(2)
Cu(1)-O(4)	1.884(19)	Cu(3)-O(6)*	2.35(2)
<hr/>			
O(7)-Ba(1)-O(2)	145.2(6)	Cu(2)-Ba(1)-Cu(3)	103.29(11)
O(7)-Ba(1)-O(5)	61.4(6)	Cu(1)-Ba(1)-Cu(3)	112.71(11)
O(2)-Ba(1)-O(5)	146.4(5)	O(4)-Cu(1)-O(2)	90.0(8)
O(7)-Ba(1)-O(1)	124.2(5)	O(4)-Cu(1)-N(2)	97.1(10)
O(2)-Ba(1)-O(1)	75.2(5)	O(2)-Cu(1)-N(2)	157.9(9)
O(5)-Ba(1)-O(1)	107.7(6)	O(4)-Cu(1)-N(1)	158.6(10)
O(7)-Ba(1)-O(1S)	73.5(6)	O(2)-Cu(1)-N(1)	94.0(10)
O(2)-Ba(1)-O(1S)	72.6(6)	N(2)-Cu(1)-N(1)	87.1(11)
O(5)-Ba(1)-O(1S)	132.4(6)	O(4)-Cu(1)-Ba(1)	51.4(6)
O(1)-Ba(1)-O(1S)	109.8(6)	O(2)-Cu(1)-Ba(1)	49.8(6)
O(7)-Ba(1)-O(8)	73.4(5)	N(2)-Cu(1)-Ba(1)	146.3(8)
O(2)-Ba(1)-O(8)	124.6(5)	N(1)-Cu(1)-Ba(1)	117.9(8)
O(5)-Ba(1)-O(8)	74.7(5)	N(4)-Cu(2)-O(7)	91.7(10)
O(1)-Ba(1)-O(8)	52.0(5)	N(4)-Cu(2)-O(5)	159.0(10)
O(1S)-Ba(1)-O(8)	107.4(6)	O(7)-Cu(2)-O(5)	90.5(8)
O(7)-Ba(1)-O(4)	144.8(5)	N(4)-Cu(2)-N(3)	92.1(12)
O(2)-Ba(1)-O(4)	57.3(5)	O(7)-Cu(2)-N(3)	154.5(9)
O(5)-Ba(1)-O(4)	89.5(5)	O(5)-Cu(2)-N(3)	94.9(10)
O(1)-Ba(1)-O(4)	81.5(5)	N(4)-Cu(2)-Ba(1)	117.6(8)
O(1S)-Ba(1)-O(4)	124.0(6)	O(7)-Cu(2)-Ba(1)	48.8(6)
O(8)-Ba(1)-O(4)	120.2(5)	O(5)-Cu(2)-Ba(1)	51.3(6)
O(7)-Ba(1)-O(12)	94.3(6)	N(3)-Cu(2)-Ba(1)	145.6(8)
O(2)-Ba(1)-O(12)	65.4(6)	O(8)-Cu(3)-N(5)	94.7(10)
O(5)-Ba(1)-O(12)	100.6(6)	O(8)-Cu(3)-O(1)	80.0(8)
O(1)-Ba(1)-O(12)	139.7(6)	N(5)-Cu(3)-O(1)	173.5(9)
O(1S)-Ba(1)-O(12)	67.0(7)	O(8)-Cu(3)-N(6)	170.0(9)
O(8)-Ba(1)-O(12)	167.7(6)	N(5)-Cu(3)-N(6)	92.8(11)
O(4)-Ba(1)-O(12)	70.5(6)	O(1)-Cu(3)-N(6)	92.0(9)
O(7)-Ba(1)-O(11)	72.4(6)	O(8)-Cu(3)-O(6)*	95.0(8)
O(2)-Ba(1)-O(11)	103.9(6)	N(5)-Cu(3)-O(6)*	88.6(9)
O(5)-Ba(1)-O(11)	57.6(6)	O(1)-Cu(3)-O(6)*	95.6(8)
O(1)-Ba(1)-O(11)	152.0(6)	N(6)-Cu(3)-O(6)*	91.8(9)
O(1S)-Ba(1)-O(11)	96.1(7)	O(8)-Cu(3)-Ba(1)	48.3(6)
O(8)-Ba(1)-O(11)	130.3(6)	N(5)-Cu(3)-Ba(1)	127.3(7)
O(4)-Ba(1)-O(11)	75.2(6)	O(1)-Cu(3)-Ba(1)	46.2(6)
O(12)-Ba(1)-O(11)	43.1(7)	N(6)-Cu(3)-Ba(1)	121.7(7)
Cu(2)-Ba(1)-Cu(1)	124.95(10)	O(6)*-Cu(3)-Ba(1)	124.5(6)

Symmetry transformations used to generate equivalent atoms: (\*) x, -y+1/2, z+1/2



The barium cation is nine-coordinate and has a distorted tricapped trigonal antiprismatic geometry, coordinating the six phenolate oxygen atoms of the macrocycle, a methanol oxygen donor (O1S) and two oxygen atoms of a perchlorate molecule (O11 and O12). The six prismatic oxygen ligands (O5, O7, O8, O2, O4 and O12) define the vertices of the distorted trigonal prism. The three capping oxygen ligands (O1, O11 and O1S) are positioned outside the faces of the prism (Fig. 4.21).

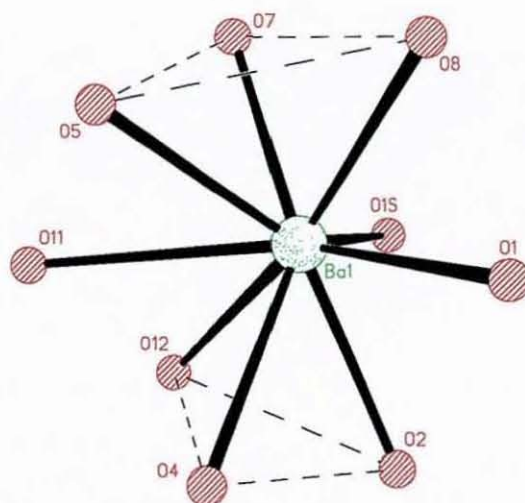


**Fig. 4.21:** Coordination sphere of the barium ion in the cation  $[\text{Cu}_3\text{Ba}(\text{H}_3\text{L8})(\text{MeOH})(\text{ClO}_4)]^+$

The LSIMS spectrum of the crystals of  $[\text{Cu}_3\text{Ba}(\text{H}_3\text{L8})(\text{MeOH})(\text{ClO}_4)](\text{ClO}_4)$  (**4.8ax**) shows two peaks corresponding to heteronuclear complexes of the macrocycle  $\text{H}_9\text{L8}$  (Fig. 4.22, Table 4.16). The main peak at  $m/z$  1688 is attributable to the heteronuclear fragment  $[\text{Cu}_3\text{Ba}(\text{H}_2\text{L8})(\text{ClO}_4)\text{-H}]^+$ . While the peak at  $m/z$  1587 is assigned to the heteronuclear fragment  $[\text{Cu}_3\text{Ba}(\text{H}_2\text{L8})\text{-H}]^+$ .

**Table 4.16:** Peak attributions for  $[\text{Cu}_3\text{Ba}(\text{H}_3\text{L8})(\text{MeOH})(\text{ClO}_4)](\text{ClO}_4)$

$m/z$	Rel. Intensity (%)	Fragments	Calc. Mass
1587	25	$[\text{Cu}_3\text{Ba}(\text{H}_2\text{L8})\text{-H}]^+$	1587
1688	100	$[\text{Cu}_3\text{Ba}(\text{H}_3\text{L8})(\text{ClO}_4)\text{-H}]^+$	1688

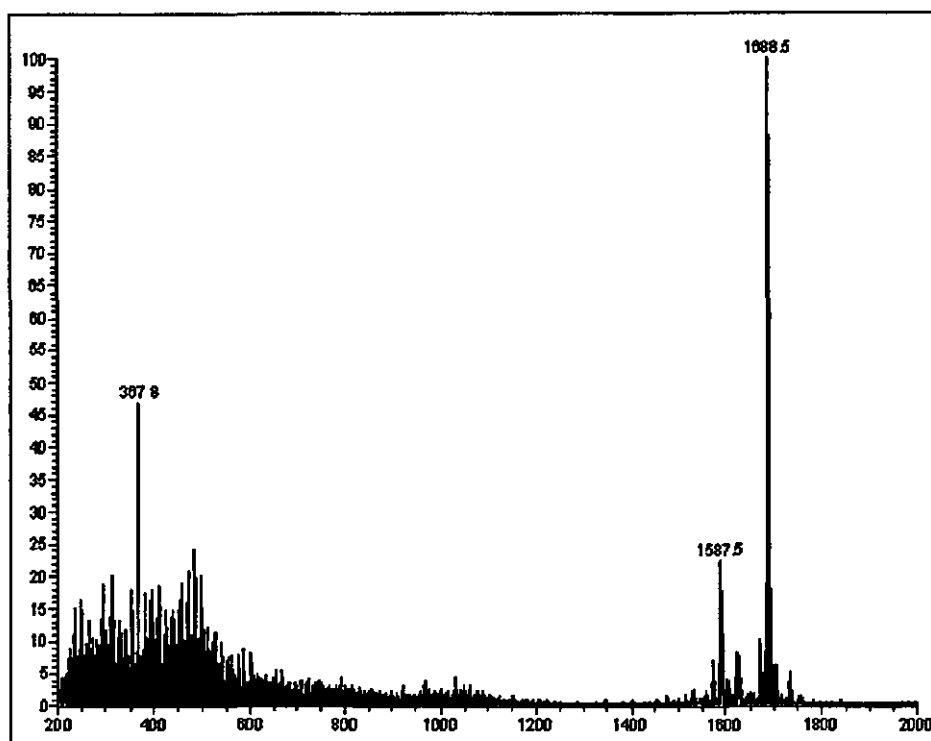


Fig. 4.22: LSIMS spectrum of  $[\text{Cu}_3\text{Ba}(\text{H}_3\text{L8})(\text{MeOH})(\text{ClO}_4)](\text{ClO}_4)$

The heteronuclear complexes of  $\text{H}_9\text{L8}$  listed in Table 4.17 were prepared by template techniques as described in the experimental chapter. As for the heteronuclear complexes of  $\text{H}_6\text{L1}$ , the heteronuclear complexes of  $\text{H}_9\text{L8}$  here described were synthesised adding triethylamine to the reaction mixture.

Table 4.17: Selected data for the heteronuclear complexes of  $\text{H}_9\text{L8}$  investigated

	Formula	Colour	IR bands ( $\text{cm}^{-1}$ )
4.9a	$[\text{Ni}_3\text{Ba}(\text{HL8})](\text{EtOH})\cdot\text{H}_2\text{O}$	Brown yellowish	3385 (b, m, $\nu_{\text{O-H}}$ ); 1621 (m, $\nu_{\text{C=N}}$ ); 1116 and 1081 (m, $\nu_{3(\text{ClO}_4^-)}$ )
4.10	$[\text{Cu}_3\text{Ca}(\text{H}_3\text{L8})](\text{NO}_3)_2\cdot 3\text{EtOH}\cdot 2\text{H}_2\text{O}$	Green	3409 (b, m, $\nu_{\text{O-H}}$ ); 1625 (s, $\nu_{\text{C=N}}$ ); 1443 and 1363 (m, $\nu_{\text{coordNO}_3^-}$ ); 1385 (m, $\nu_{\text{freeNO}_3^-}$ )
4.11	$[\text{Zn}_3\text{Ca}(\text{H}_3\text{L8})](\text{NO}_3)_2\cdot 2\text{EtOH}\cdot 2\text{H}_2\text{O}$	Yellow	3422 (b, m, $\nu_{\text{O-H}}$ ), 1638 (s, $\nu_{\text{C=N}}$ ); 1459 and 1362 (m, $\nu_{\text{coordNO}_3^-}$ ), 1390 (m, $\nu_{\text{freeNO}_3^-}$ )



Similarly to copper(II) and barium complexes, the synthesis of the nickel(II) and barium complex gave mixtures of different heteronuclear macrocyclic complexes, which could be separated by different solubility in DCM. The product soluble in DCM analysed as  $[\text{Ni}_3\text{Ba}(\text{HL8})](\text{EtOH})\cdot\text{H}_2\text{O}$  (4.9a), suggesting the formation of the heteronuclear complex of the [3+3] macrocycle  $\text{H}_9\text{L8}$ . The brown minor product insoluble in DCM (4.9b) will be described in section 4.5. The fragmentation pattern for the complex  $[\text{Ni}_3\text{Ba}(\text{HL8})](\text{EtOH})\cdot\text{H}_2\text{O}$  (Table 4.18) shows a peak at  $m/z$  1583 corresponding to the fragment  $[\text{Ni}_2\text{Ba}(\text{H}_4\text{L8})(\text{EtOH})(\text{H}_2\text{O})+2\text{H}]^+$ .

**Table 4.18:** Peak attributions for  $[\text{Ni}_3\text{Ba}(\text{HL8})](\text{EtOH})\cdot\text{H}_2\text{O}$

M/z	Rel. Intensity (%)	Fragments	Calc. Mass
957	37	$[\text{Ni}_2(\text{H}_3\text{L1})-2\text{H}]^+$	957
1439	50	$[\text{Ni}_3(\text{H}_4\text{L8})+\text{H}]^+$	1439
1459	49	$[\text{Ni}_3(\text{H}_4\text{L8})(\text{H}_2\text{O})+2\text{H}]^+$	1459
1494	40	$[\text{Ni}_3(\text{H}_4\text{L8})(\text{H}_2\text{O})_3+2\text{H}]^+$	1494
1583	33	$[\text{Ni}_2\text{Ba}(\text{H}_4\text{L8})(\text{EtOH})(\text{H}_2\text{O})+2\text{H}]^+$	1583

As previously mentioned in section 4.2.2, the products obtained in the synthesis of the heteronuclear calcium complexes is directly related to the order in which the reagents are added to reaction mixture. The heteronuclear calcium complexes 4.4 and 4.5 of the macrocycle  $\text{H}_6\text{L1}$  were synthesised by adding the transition metal and the calcium salts simultaneously to the reaction mixture. Alternatively, the heteronuclear calcium complexes  $[\text{Cu}_3\text{Ca}(\text{H}_3\text{L8})](\text{NO}_3)_2\cdot 3\text{EtOH}\cdot 2\text{H}_2\text{O}$  (4.10) and  $[\text{Zn}_3\text{Ca}(\text{H}_3\text{L8})](\text{NO}_3)_2\cdot 2\text{EtOH}\cdot 2\text{H}_2\text{O}$  (4.11) of the new [3+3] macrocyclic ligand  $\text{H}_9\text{L8}$  were isolated with good yields (80-85%) when the calcium salts were added and left to react with the ligands on long reflux before adding the transition metal salts to the reaction mixture.

The LSIMS spectrum of  $[\text{Cu}_3\text{Ca}(\text{H}_3\text{L8})](\text{NO}_3)_2\cdot 3\text{EtOH}\cdot 2\text{H}_2\text{O}$  (4.10) shows a peak at  $m/z$  1514 corresponding to the fragment  $[\text{Cu}_3\text{Ca}(\text{H}_2\text{L8})+\text{Na}]^+$ . There are also peaks at  $m/z$  1413 and 1444 assigned to doubly charged ions of the clusters  $[\text{Cu}_3\text{Ca}(\text{H}_6\text{L8})_2(\text{EtOH})(\text{H}_2\text{O})+2\text{H}]^{2+}$  and  $[\text{Cu}_3\text{Ca}(\text{H}_7\text{L8})_2(\text{NO}_3)(\text{OH})(\text{EtOH})+\text{H}]^{2+}$  respectively. The peaks at  $m/z$  1006 and 1068, corresponding to the fragments

$[\text{Cu}_2\text{Ca}(\text{HL1})-\text{H}]^+$  and  $[\text{Cu}_2\text{Ca}(\text{H}_2\text{L1})(\text{NO}_3)-2\text{H}]^+$ , also suggest the formation of a heteronuclear complex of the [2+2] macrocycle  $\text{H}_6\text{L1}$  (Table 4.19).

**Table 4.19:** Peak attributions for  $[\text{Cu}_3\text{Ca}(\text{H}_3\text{L8})](\text{NO}_3)_2 \cdot 3\text{EtOH} \cdot 2\text{H}_2\text{O}$

M/z	Rel. Intensity (%)	Fragments	Calc. Mass
1006	35	$[\text{Cu}_2\text{Ca}(\text{HL1})-\text{H}]^+$	1006
1068	50	$[\text{Cu}_2\text{Ca}(\text{H}_2\text{L1})(\text{NO}_3)-2\text{H}]^+$	1068
1413	40	$[\text{Cu}_3\text{Ca}(\text{H}_6\text{L8})_2(\text{EtOH})(\text{H}_2\text{O})+2\text{H}]^{2+}$	2826
1444	45	$[\text{Cu}_3\text{Ca}(\text{H}_7\text{L8})_2(\text{NO}_3)(\text{OH})(\text{EtOH})+\text{H}]^{2+}$	2888
1476	65	$[\text{Cu}_3(\text{H}_4\text{L8})+\text{Na}]^+$	1475
1514	30	$[\text{Cu}_3\text{Ca}(\text{H}_2\text{L8})+\text{Na}]^+$	1513

The spectrum of the complex  $[\text{Zn}_3\text{Ca}(\text{H}_3\text{L8})](\text{NO}_3)_2 \cdot 2\text{EtOH} \cdot 2\text{H}_2\text{O}$  (4.11) shows two peaks which again suggest formation of the heteronuclear complex. The peaks at  $m/z$  1405 and 1413 are assigned to doubly charged ions of the clusters  $[\text{Zn}_3\text{Ca}(\text{H}_6\text{L8})_2(\text{EtOH})]^{2+}$  and  $[\text{Zn}_3\text{Ca}(\text{H}_6\text{L8})_2(\text{NO}_3)+\text{H}]^{2+}$  respectively (Fig. 4.23, Table 4.20)

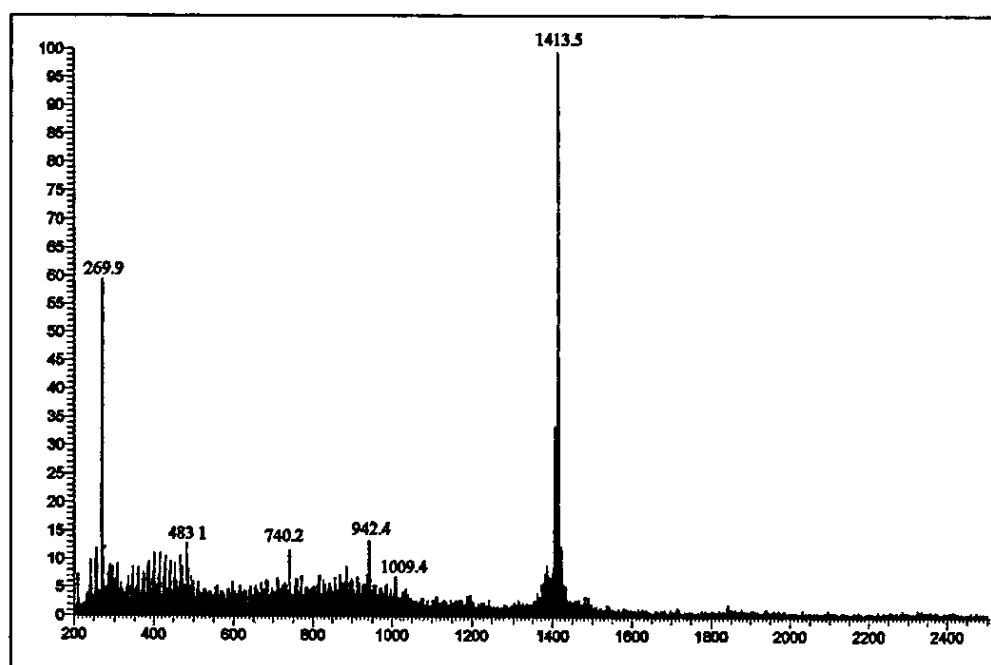


**Fig. 4.23:** LSIMS spectrum of  $[\text{Zn}_3\text{Ca}(\text{H}_3\text{L8})](\text{NO}_3)_2 \cdot 2\text{EtOH} \cdot 2\text{H}_2\text{O}$

**Table 4.20:** Peak attributions for  $[\text{Zn}_3\text{Ca}(\text{H}_3\text{L8})](\text{NO}_3)_2 \cdot 2\text{EtOH} \cdot 2\text{H}_2\text{O}$ 

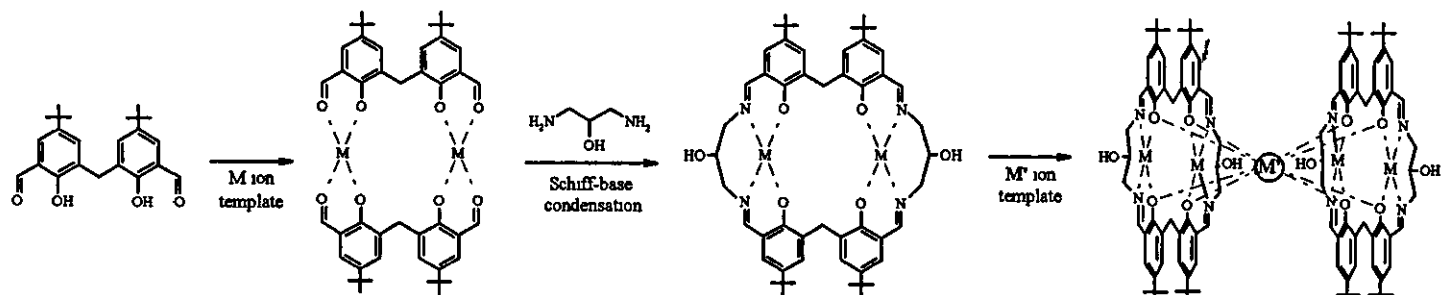
M/z	Rel. Intensity (%)	Fragments	Calc. Mass
1405	30	$[\text{Zn}_3\text{Ca}(\text{H}_6\text{L8})_2(\text{EtOH})]^{2+}$	2811
1413	100	$[\text{Zn}_3\text{Ca}(\text{H}_6\text{L8})_2(\text{NO}_3)+\text{H}]^{2+}$	2828

The LSIMS results for the complexes  $[\text{Cu}_3\text{Ca}(\text{H}_3\text{L8})](\text{NO}_3)_2 \cdot 3\text{EtOH} \cdot 2\text{H}_2\text{O}$  (4.10) and  $[\text{Zn}_3\text{Ca}(\text{H}_3\text{L8})](\text{NO}_3)_2 \cdot 2\text{EtOH} \cdot 2\text{H}_2\text{O}$  (4.11) suggest the presence of heteronuclear complexes possibly containing two  $\text{H}_6\text{L8}$  macrocyclic units. No structural data are available at the moment. The collective evidence of the analytical and spectroscopic results described previously is sufficient to suggest that the compounds under consideration are complexes of the macrocycle  $\text{H}_9\text{L8}$ . This conclusion is confirmed by the results of the X-ray diffraction study of the complex  $[\text{Cu}_3\text{Ba}(\text{H}_2\text{L8})](\text{ClO}_4) \cdot 3\text{EtOH} \cdot 4\text{H}_2\text{O}$ .

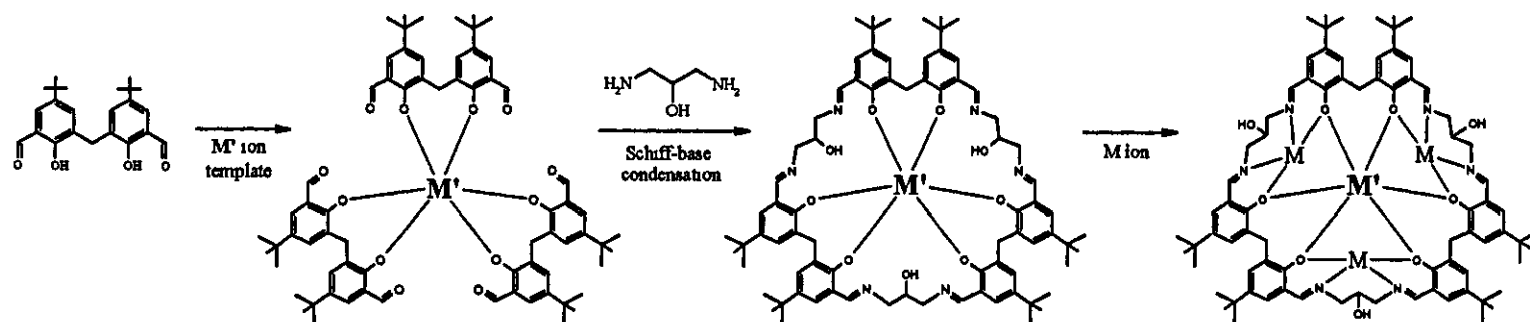
#### 4.3.1. Possible route for the synthesis of the heteronuclear complexes of $\text{H}_9\text{L8}$

As described previously, the cyclisation pathway is related to the variation of the template metal radii. The central cavity of the [2+2] macrocycle  $\text{H}_6\text{L1}$  can stretch in order to accommodate large metal ions such as  $\text{Na}^+$  or  $\text{Ca}^{2+}$  in the central tetraphenolate binding site, but it is not big enough to bind larger metal ions like  $\text{Ba}^{2+}$  (see section 4.2.3). If the transition metal ion acts as the template for the reaction, the dinuclear complexes of  $\text{H}_6\text{L1}$  are essentially pre-organised and the alkaline-earth metal ion either sits above the macrocycle coordinating four phenolate oxygen donors, in the case of  $\text{Ca}^{2+}$  ions, or bind the phenol oxygen donors of two macrocyclic units forming sandwich complexes, in the case of  $\text{Ba}^{2+}$  ions (Scheme 4.3)

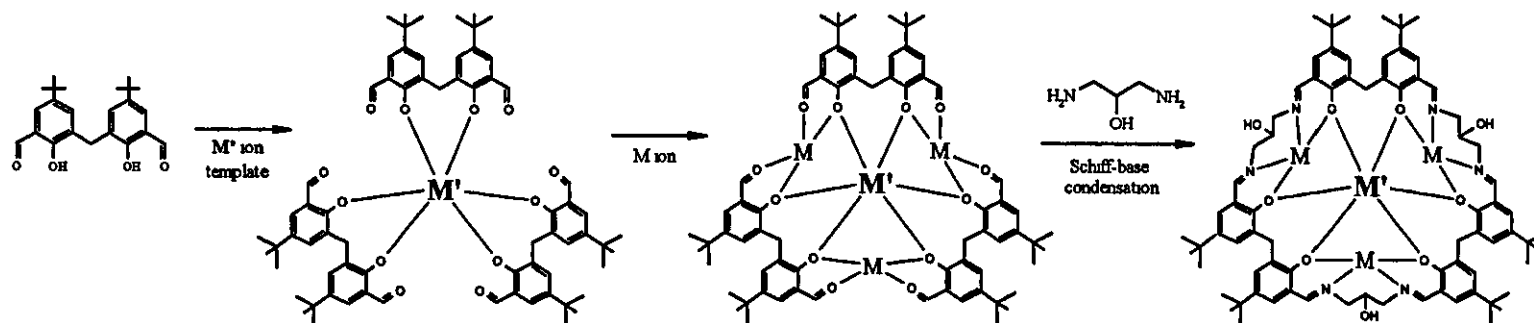
Alternatively, if the alkaline-earth metal ion acts as the template of the reaction, coordinates the ligand molecules around to form the expanded [3+3] macrocycle, which provides a suitable macrocyclic cavity for the  $\text{Ca}^{2+}$  and  $\text{Ba}^{2+}$  ions. It is possible that the formation of the heteronuclear complexes of  $\text{H}_9\text{L8}$  follow the route outlined in Scheme 4.4.



**Scheme 4.3:** heteronuclear “sandwich” complexes of  $H_6L1$  synthesised *via* template condensation.



**Scheme 4.4:** heteronuclear complexes of  $H_9L8$  synthesised *via* template condensation.



**Scheme 4.5:** heteronuclear complexes of  $H_5L8$  synthesised *via* template condensation

The cyclisation step involves three molecules of the DHTMB which bind the alkaline-earth metal ion ( $\text{Ca}^{2+}$  or  $\text{Ba}^{2+}$ ). Then three diamine molecules condense with the aldehydes, forming the [3+3] macrocycle. Thus, the template of the reaction is the alkali-earth metal ion. This mononuclear complex is essentially pre-organised for binding three transition metal ions in the three equivalent  $\text{N}_2\text{O}_2$  sites. If the incoming metal ion is of suitable size, the overall conformation of the complex need not undergo major change. However, if this was the only pathway occurring, the reaction should yield the [3+3] macrocyclic complex as the only product. Instead, when  $\text{Ba}^{2+}$  is used mixtures of heteronuclear complexes of [2+2], [3+3] and [4+4] macrocycles are obtained, suggesting that more than one cyclisation pathway is occurring.

It could also be possible that the alkaline-earth metal ion acts as the first template, coordinating three molecules of DHTMB and then the transition metal ions act as the cyclisation template, coordinating to the DHTMB molecules and thus facilitating the condensation of the diamine molecules with the aldehydes (Scheme 4.5). As the heteronuclear intermediate complex is not cyclic, it can rearrange to different macrocycles before condensing with the diamine molecules, and this would lead to mixtures of complexes with different macrocycles.

#### 4.4. Heteronuclear complexes of the pseudocalixarene macrocycle $\text{H}_{12}\text{L9}$

As previously described in section 4.2.3, simultaneous addition of barium and copper(II) perchlorate salts to an ethanol solution of DHTMB and further reaction with 1,3-diaminopropan-2-ol in the presence of base yielded a green brownish solid. A mixture of brown and green crystals was obtained by slow evaporation of an ethanol solution of the solid isolated. These crystals could be separated by different solubility in chloroform. The brown solid was characterised by X-ray crystallography, elemental analysis and mass spectrometry as the heteronuclear sandwich complex  $([\text{Cu}_4\text{Ba}(\text{H}_2\text{L1})_2](\text{ClO}_4)_2 \cdot \text{EtOH} \cdot 4\text{H}_2\text{O})$  (4.6a), described in section 4.2.3. The other product  $([\text{Cu}_4\text{Ba}(\text{H}_4\text{L9})](\text{ClO}_4)_2 \cdot 4\text{H}_2\text{O})$  (4.6b) containing a [4+4] macrocycle was recrystallised and initially characterised by X-ray crystallography.



Green crystals of  $[\text{Cu}_4\text{Ba}(\text{H}_4\text{L9})(\text{MeOH})_2]\cdot 3\text{H}_2\text{O}$  (4.6bx) were grown by slow diffusion of diethylether into a methanol solution of the heteronuclear complex  $[\text{Cu}_4\text{Ba}(\text{H}_4\text{L9})](\text{ClO}_4)_2\cdot 4\text{H}_2\text{O}$  (4.6b). All the X-ray data collection parameters are summarised in Table 18 of appendix 1 along with the details concerning the refinement and disorder. A perspective view of the complex is shown in Fig 4.25 and selected bond lengths and angles relevant to the metal ion coordination are given in Table 4.21.

The structure of  $[\text{Cu}_4\text{Ba}(\text{H}_4\text{L9})(\text{MeOH})_2]^{2+}$  contains the [4+4] ligand coordinated to four copper and one barium centres, using all 16 imine and phenol potential donor atoms to bind the metal ions. The four copper(II) ions of each macrocyclic unit occupy the salen-type sites of the macrocycle while the barium ion coordinates the octaphenolate central site.

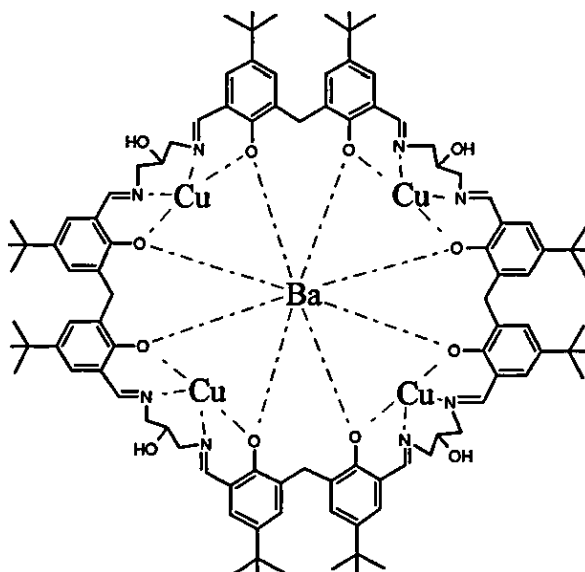
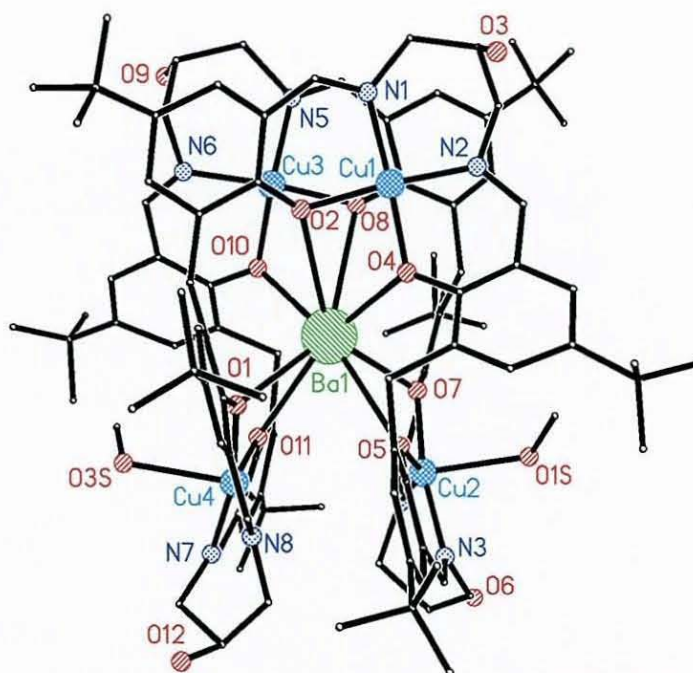


Fig. 4.24: Diagram showing the connectivity in the cation  $[\text{Cu}_4\text{Ba}(\text{H}_2\text{L9})]^{2+}$

The general conformation of this complex is different from the complexes discussed previously. Like the heteronuclear complex of the [3+3] macrocycle (see section 4.3.1), the ligand wraps around the barium ion. The macrocycle adopts a folded conformation which optimises the metal-donor atom distances generating eight Ba-O bonds, which distances range from 2.67(1) to 3.17(2) Å

(Table 4.21). The longer Ba-O bond distances (e.g. Ba1····O2 3.06(1)Å or Ba1····O8 3.17(2)Å) are due to the fact that these phenolate oxygen donors act as basal donors for the copper centres, as well as axial donors for the opposite copper centres and therefore weakening the bond to barium.



**Fig. 4.25:** Structure of the cation  $[\text{Cu}_4\text{Ba}(\text{H}_4\text{L9})(\text{MeOH})_2]^{2+}$

All four copper ions are five-coordinate and have square pyramidal geometry, with identical macrocyclic donors (two phenolate oxygen and two imine nitrogen atoms) as the basal ligands. The apical ligand for two of the copper ions (Cu1 and Cu3) is the phenolate oxygen donor that acts as the basal ligand of the opposite copper centre (Cu1····O8 2.58(2) Å and Cu3····O2 2.54(3) Å). The other two copper ions (Cu2 and Cu4) have the corresponding axial phenolate oxygen donors at a distance too long to be significant which would give a really weak interaction (Cu2····O11 3.82(4) Å and Cu4····O5 3.77(5) Å) due to the conformation of the macrocycle. Instead, Cu2 and Cu4 copper ions have a methanol oxygen atom (O1S and O3S respectively) as the axial donor.

**Table 4.21:** Selected interatomic distances [ $\text{\AA}$ ] and angles [ $^\circ$ ] for  
 $[\text{Cu}_4\text{Ba}(\text{H}_4\text{L9})(\text{MeOH})_2]\cdot 3\text{H}_2\text{O}$

Ba(1)-O(10)	2.665(13)	Ba(1)-Cu(1)	3.712(3)	Cu(2)-O(1S)	2.38(2)
Ba(1)-O(7)	2.670(14)	Ba(1)-Cu(4)	3.766(3)	Cu(3)-O(10)	1.921(13)
Ba(1)-O(4)	2.681(12)	Cu(1)-N(2)	1.92(2)	Cu(3)-O(8)	1.946(19)
Ba(1)-O(1)	2.697(15)	Cu(1)-O(4)	1.921(12)	Cu(3)-N(6)	1.98(3)
Ba(1)-O(5)	2.964(12)	Cu(1)-O(2)	1.971(17)	Cu(3)-N(5)	1.99(2)
Ba(1)-O(2)	3.062(13)	Cu(1)-N(1)	1.989(17)	Cu(4)-O(1)	1.917(12)
Ba(1)-O(11)	3.097(13)	Cu(2)-O(7)	1.900(13)	Cu(4)-N(8)	1.946(17)
Ba(1)-O(8)	3.169(15)	Cu(2)-N(3)	1.942(16)	Cu(4)-N(7)	1.911(17)
Ba(1)-Cu(3)	3.691(3)	Cu(2)-O(5)	1.957(12)	Cu(4)-O(11)	1.949(14)
Ba(1)-Cu(2)	3.688(3)	Cu(2)-N(4)	1.987(16)	Cu(4)-O(3S)	2.44(4)
O(10)-Ba(1)-O(7)	114.4(4)	O(4)-Cu(1)-Ba(1)	43.9(4)		
O(10)-Ba(1)-O(4)	115.5(4)	O(2)-Cu(1)-Ba(1)	55.5(4)		
O(7)-Ba(1)-O(4)	94.7(4)	O(7)-Cu(2)-N(3)	169.5(8)		
O(10)-Ba(1)-O(1)	95.6(5)	O(7)-Cu(2)-O(5)	89.1(5)		
O(7)-Ba(1)-O(1)	120.6(4)	N(3)-Cu(2)-O(5)	94.0(6)		
O(4)-Ba(1)-O(1)	117.6(4)	O(7)-Cu(2)-N(4)	92.6(6)		
O(10)-Ba(1)-O(5)	162.2(4)	N(3)-Cu(2)-N(4)	89.8(6)		
O(7)-Ba(1)-O(5)	57.1(4)	O(5)-Cu(2)-N(4)	150.2(8)		
O(4)-Ba(1)-O(5)	81.9(3)	O(7)-Cu(2)-O(1S)	84.8(6)		
O(1)-Ba(1)-O(5)	78.6(4)	N(3)-Cu(2)-O(1S)	84.8(8)		
O(10)-Ba(1)-O(2)	69.4(4)	O(5)-Cu(2)-O(1S)	104.7(7)		
O(7)-Ba(1)-O(2)	139.7(4)	N(4)-Cu(2)-O(1S)	105.2(8)		
O(4)-Ba(1)-O(2)	53.6(4)	O(7)-Cu(2)-Ba(1)	44.0(4)		
O(1)-Ba(1)-O(2)	97.8(4)	O(5)-Cu(2)-Ba(1)	53.2(4)		
O(5)-Ba(1)-O(2)	127.9(3)	N(4)-Cu(2)-Ba(1)	110.9(5)		
O(10)-Ba(1)-O(11)	80.5(4)	O(10)-Cu(3)-O(8)	86.2(6)		
O(7)-Ba(1)-O(11)	79.8(4)	O(10)-Cu(3)-N(6)	90.5(8)		
O(4)-Ba(1)-O(11)	163.8(3)	O(8)-Cu(3)-N(6)	172.5(8)		
O(1)-Ba(1)-O(11)	55.1(4)	O(10)-Cu(3)-N(5)	157.1(9)		
O(5)-Ba(1)-O(11)	82.4(3)	O(8)-Cu(3)-N(5)	89.1(10)		
O(2)-Ba(1)-O(11)	137.4(4)	N(6)-Cu(3)-N(5)	96.5(11)		
O(10)-Ba(1)-O(8)	53.0(5)	O(10)-Cu(3)-Ba(1)	43.9(4)		
O(7)-Ba(1)-O(8)	95.0(4)	O(8)-Cu(3)-Ba(1)	59.1(4)		
O(4)-Ba(1)-O(8)	69.0(3)	N(6)-Cu(3)-Ba(1)	114.1(6)		
O(1)-Ba(1)-O(8)	141.4(4)	O(1)-Cu(4)-N(8)	93.6(6)		
O(5)-Ba(1)-O(8)	138.1(4)	O(1)-Cu(4)-N(7)	166.6(9)		
O(2)-Ba(1)-O(8)	53.5(4)	N(8)-Cu(4)-N(7)	90.1(7)		
O(11)-Ba(1)-O(8)	126.4(3)	O(1)-Cu(4)-O(11)	88.7(6)		
Cu(3)-Ba(1)-Cu(4)	125.13(9)	N(8)-Cu(4)-O(11)	152.8(8)		
Cu(2)-Ba(1)-Cu(4)	69.32(7)	N(7)-Cu(4)-O(11)	93.8(7)		
Cu(1)-Ba(1)-Cu(4)	152.99(7)	O(1)-Cu(4)-O(3S)	84.5(10)		
N(2)-Cu(1)-O(4)	91.6(7)	N(8)-Cu(4)-O(3S)	108.7(12)		
N(2)-Cu(1)-O(2)	173.2(6)	N(7)-Cu(4)-O(3S)	82.1(12)		
O(4)-Cu(1)-O(2)	84.3(6)	O(11)-Cu(4)-O(3S)	98.5(11)		
N(2)-Cu(1)-N(1)	94.4(8)	O(1)-Cu(4)-Ba(1)	42.9(5)		
O(4)-Cu(1)-N(1)	159.4(6)	N(8)-Cu(4)-Ba(1)	111.1(5)		
O(2)-Cu(1)-N(1)	91.3(8)	N(7)-Cu(4)-Ba(1)	145.9(7)		
N(2)-Cu(1)-Ba(1)	117.9(5)	O(11)-Cu(4)-Ba(1)	55.1(4)		



The barium cation is eight-coordinate and has rectangular antiprism geometry, coordinating all eight phenolate oxygen atoms of the macrocycle (Fig. 4.26). As happened with the barium sandwich complexes  $[\text{Cu}_4\text{Ba}(\text{H}_2\text{L1})_2](\text{ClO}_4)_2 \cdot \text{EtOH}$  (**4.6ax**) and  $[\text{Zn}_4\text{Ba}(\text{H}_2\text{L1})_2](\text{ClO}_4)_2 \cdot 2\text{Et}_2\text{O}$  (**4.7x**), the bond lengths of barium coordination are not equivalent, having four bond distances approximately 0.3 Å longer than the other four (Table 4.21). The reason for four Ba-O bonds being longer is because the phenolate oxygen atoms participating in those bonds are also weakly coordinating as the axial ligand for the opposite copper ions, and thence weakening the bond to the barium ion.

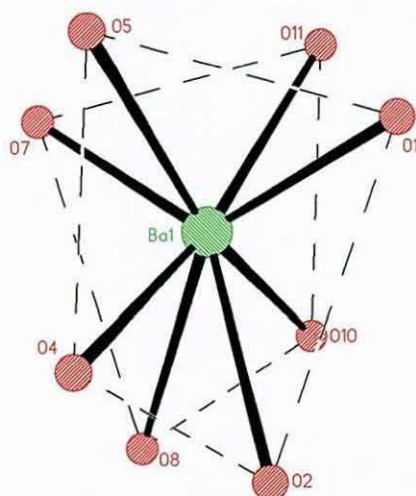


**Fig. 4.26:** Coordination sphere of the barium ion in the cation  $[\text{Cu}_4\text{Ba}(\text{H}_4\text{L9})]^{2+}$

Further characterisation of the green crude product (**4.6b**) was obtained by mass spectrometry. The LSIMS mass spectrum indicated the formation of heteronuclear entities in the complex. The spectrum showed peaks corresponding to complexes of different macrocyclic ligands, suggesting that more than one synthetic pathway are operating in the reaction mixture. The fragmentation pattern for the heteronuclear complex (Table 4.22, Fig. 4.27) shows two peaks at  $m/z$  1589 and 1688 suggesting the formation of heteronuclear complexes of the [3+3] macrocycle  $\text{H}_9\text{L8}$  as a minor product. The peaks at  $m/z$  2072 and 2171, corresponding to the fragments  $[\text{Cu}_4\text{Ba}(\text{H}_4\text{L9})-\text{H}]^+$  and  $[\text{Cu}_4\text{Ba}(\text{H}_4\text{L9})(\text{ClO}_4)-2\text{H}]^+$  respectively, suggest the formation of the heteronuclear complex of the [4+4] macrocycle  $\text{H}_{12}\text{L9}$ . However, these peaks could also be attributed to the fragments  $[\text{Cu}_4\text{Ba}(\text{H}_2\text{L1})_2-\text{H}]^+$

and  $[\text{Cu}_4\text{Ba}(\text{H}_2\text{L1})_2(\text{ClO}_4)_2-2\text{H}]^+$ , which correspond to the formation of the heteronuclear sandwich complex of the [2+2] macrocycle  $\text{H}_6\text{L1}$ . The peak at  $m/z$  1036 could be assigned to the doubly charged fragment  $[\text{Cu}_4\text{Ba}(\text{H}_4\text{L9})]^{2+}$  or also to  $[\text{Cu}_4\text{Ba}(\text{H}_2\text{L1})_2]^{2+}$ .

The presence of a mixture of complexes of  $(\text{H}_6\text{L1})_2$  and  $\text{H}_{12}\text{L9}$  in the product was not detected by the normal methods of characterisation as the differences between the equivalent heteronuclear complexes  $[\text{Cu}_4\text{Ba}(\text{H}_2\text{L1})_2]^{2+}$  and  $[\text{Cu}_4\text{Ba}(\text{H}_4\text{L9})]^{2+}$  are not obvious. In this case mass spectrometry was not a good way to distinguish between the complexes since they have the same molecular weight. Alternatively, it might be possible to distinguish between the equivalent heteronuclear complexes if the mass spectrometry was performed on the pure crystallised samples. Since the macrocycle is different, the fragmentation pattern should be different in each case (e.g. it might be possible to see peaks corresponding to one macrocyclic unit of the [2+2] macrocycle  $\text{H}_6\text{L1}$  in the case of the heteronuclear sandwich complex  $[\text{Cu}_4\text{Ba}(\text{H}_2\text{L1})_2]^{2+}$ , whereas this could not be possible in the case of the equivalent [4+4] macrocyclic complex  $[\text{Cu}_4\text{Ba}(\text{H}_4\text{L9})]^{2+}$ ). The other way to distinguish between them was studying the crystal structures.

**Table 4.22:** Peak attributions for  $[\text{Cu}_4\text{Ba}(\text{H}_4\text{L9})](\text{ClO}_4)_2 \cdot 4\text{H}_2\text{O}$

M/z	Rel. Intensity (%)	Fragments	Calc. Mass
1036	65	$[\text{Cu}_4\text{Ba}(\text{H}_4\text{L9})]^{2+}$ $[\text{Cu}_4\text{Ba}(\text{H}_2\text{L1})_2]^{2+}$	2073
1589	7	$[\text{Cu}_3\text{Ba}(\text{H}_2\text{L8}) + \text{H}]^+$	1589
1688	18	$[\text{Cu}_3\text{Ba}(\text{H}_3\text{L8})(\text{ClO}_4) - \text{H}]^+$	1688
2072	95	$[\text{Cu}_4\text{Ba}(\text{H}_4\text{L9}) - \text{H}]^+$ $[\text{Cu}_4\text{Ba}(\text{H}_2\text{L1})_2 - \text{H}]^+$	2072
2171	100	$[\text{Cu}_4\text{Ba}(\text{H}_4\text{L9})(\text{ClO}_4)_2 - 2\text{H}]^+$ $[\text{Cu}_4\text{Ba}(\text{H}_2\text{L1})_2(\text{ClO}_4)_2 - 2\text{H}]^+$	2171



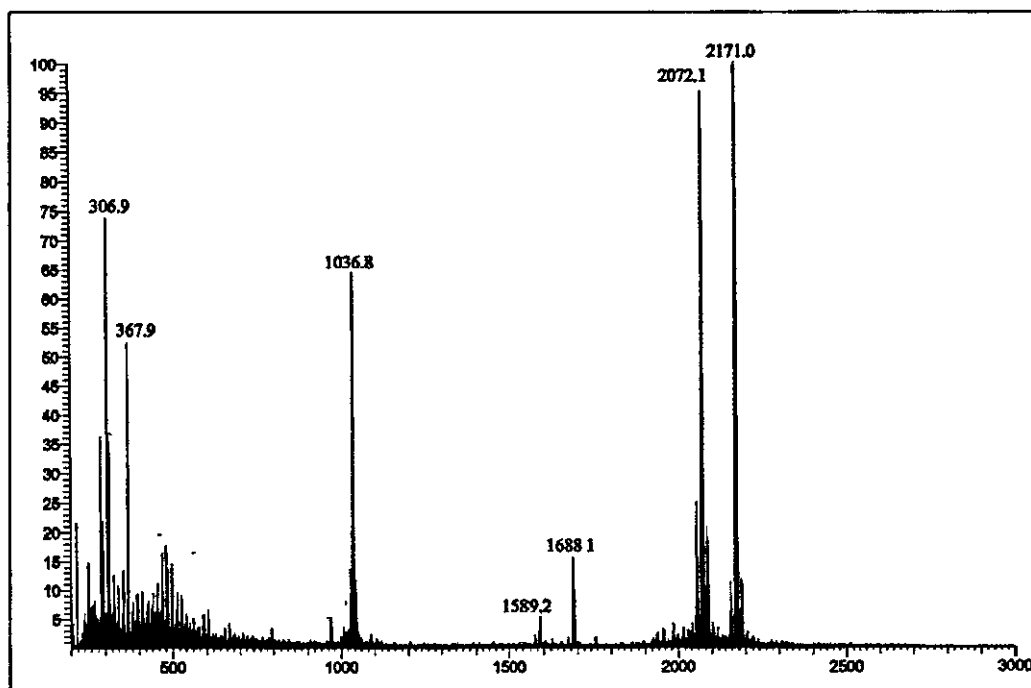


Fig. 4.27: LSIMS spectrum of  $[\text{Cu}_4\text{Ba}(\text{H}_4\text{L9})](\text{ClO}_4)_2 \cdot 4\text{H}_2\text{O}$

The crude product (4.6b) showed a band at  $1628\text{ cm}^{-1}$  in its IR spectrum attributed to the imine stretching bonds. The disappearance of the carbonyl and amine signals was taken as an indication of the formation of a closed macrocyclic ring rather than an open chain system. A broad band at  $3446\text{ cm}^{-1}$  indicates O-H stretching vibrations of water.

These IR and LSIMS characterisation results do not indicate whether the complex  $[\text{Cu}_4\text{Ba}(\text{H}_4\text{L9})](\text{ClO}_4)_2 \cdot 4\text{H}_2\text{O}$  (4.6b) is formed in the synthesis reaction or within the crystallisation solvents. The study and comparison of the crystal structures of the heteronuclear complexes  $[\text{Cu}_4\text{Ba}(\text{H}_2\text{L1})_2](\text{ClO}_4)_2 \cdot \text{EtOH}$  (4.6ax, described in section 4.2.3) and  $[\text{Cu}_4\text{Ba}(\text{H}_4\text{L9})(\text{MeOH})_2](\text{ClO}_4)_2$  (4.6bx) suggests a possible route for the formation of the [4+4] macrocyclic product *via* intramolecular rearrangement of the heteronuclear sandwich complex of  $\text{H}_6\text{L1}$ . The next section will discuss which process is more likely to occur.

#### 4.4.1. Possible routes for the synthesis of the heteronuclear complexes of $H_{12}L9$

The new [4+4] macrocycle has the same connectivity as the [2+2] macrocycle  $H_6L1$  but the ring has expanded to twice the size. The macrocycle  $H_{12}L9$  can be regarded as being constructed of four 2,2'-methylenediphenol units and four saturated side chains, inserting softer imine donors along with potentially bridging alcohol donors between them. The presence of more flexible links in the macrocycle extends the range of conformational possibilities and thus permits some response to the coordination preferences of the metal ions. Therefore, the new macrocycle would be expected to be considerably more flexible than the related [2+2] and [3+3] macrocycles

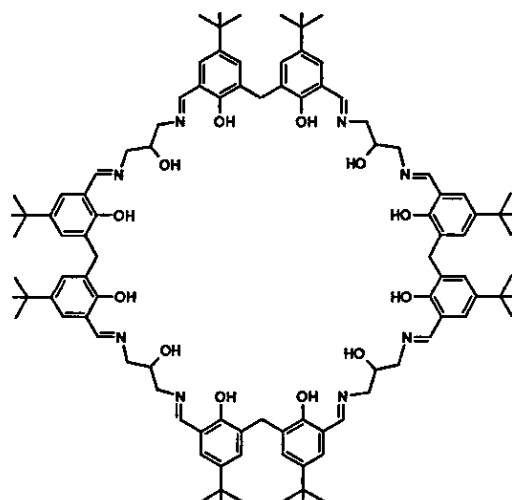


Fig. 4.28: Schiff-base pseudo-calixarene macrocycle  $H_{12}L9$ .

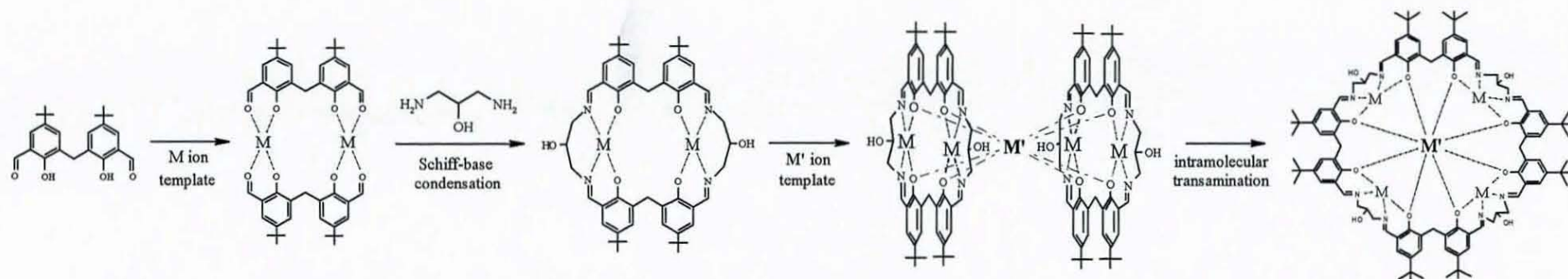
The exact mechanism by which the [4+4] macrocycle is formed is not clear, but two pathways are proposed depending on which of the metal ions, alkaline-earth or transition metal, is the template of the reaction. The first possibility is that  $H_{12}L9$  is formed as a result of the Schiff-base condensation of four DHTMB and four diamine molecules. In this case, the barium ion acts as the template of the reaction coordinating the ligand molecules around to form the expanded [4+4] macrocycle. The formation of the heteronuclear complexes of  $H_{12}L9$  would then follow the route outlined in Scheme 4.6. The cyclisation step involves four molecules of the DHTMB which bind the alkaline-earth metal ion. Then four

diamine molecules condense with the aldehydes, forming the [4+4] macrocycle. The mononuclear complex is essentially pre-organised for binding the transition metal ions in the four equivalent  $N_2O_2$  sites yielding the heteronuclear complex. However, if this was the only pathway occurring, the reaction should yield the [4+4] macrocyclic complex as the only product. Instead, when  $Ba^{2+}$  is used mixtures of heteronuclear complexes of [2+2], [3+3] and [4+4] macrocycles are obtained, suggesting that more than one cyclisation pathway is occurring.

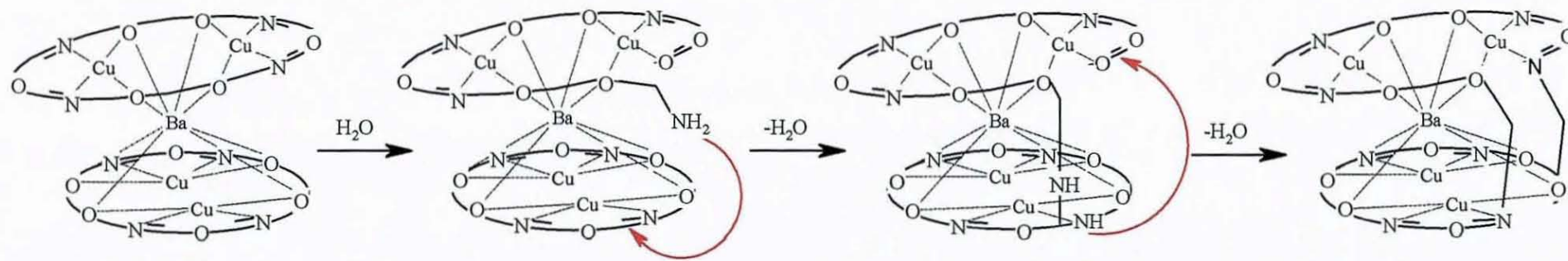
As explained in the case of the [3+3] macrocycle  $H_9L8$ , it could also be possible that the alkaline-earth metal ion acts as the first template, coordinating four molecules of DHTMB and then the transition metal ions act as the cyclisation template, coordinating to the DHTMB molecules and thus facilitating the condensation of the diamine molecules with the aldehydes (Scheme 4.7). The acyclic heteronuclear intermediate complex can rearrange to different macrocycles before condensing with the diamine molecules, yielding mixtures of complexes with different macrocycles.

The third pathway proposed suggests that the transition metal ion acts as the template of the reaction (Scheme 4.8). As described previously, the transition metal arranges the ligand molecules around it, forming dinuclear complexes of the [2+2] macrocycle  $H_6L1$ , which are essentially pre-organised. The barium ion is too large for the cavity in the [2+2] macrocycle, and the product of the barium template reaction is the sandwich complex of two [2+2] macrocyclic units  $[Cu_4Ba(H_2L1)_2](ClO_4)_2 \cdot EtOH$  (**4.6ax**) in which the alkaline-earth metal ion ( $Ba^{2+}$ ) binds the eight phenolate oxygen donors of two macrocyclic units. The small [2+2] rings can be transformed by ring opening and intramolecular rearrangement into the new conformationally flexible [4+4] ring, yielding the complex  $[Cu_4Ba(H_4L9)(MeOH)_2](ClO_4)_2$  (**4.6bx**). However, this rearrangement would only take part under reflux and not by crystallisation. When the mixtures of crystals of **4.6ax** and **4.6bx** are separated by different solubility and both products are recrystallised, clean samples are obtained and not mixtures again, suggesting that no rearrangement is taking part under crystallisation.





**Scheme 4.8:** heteronuclear complexes of  $\text{H}_{12}\text{L}_9$  synthesised *via* intramolecular rearrangement of the sandwich complex of  $\text{H}_6\text{L}_1$



**Scheme 4.9:** possible mechanism for the intramolecular rearrangement of the heteronuclear sandwich complex of  $\text{H}_6\text{L}_1$



In this case the barium ion is actually a little too small ( $r(\text{Ba}^{2+}) = 1.56 \text{ \AA}$ )<sup>176</sup> for the cavity of the new macrocycle  $\text{H}_{12}\text{L9}$ . It is not completely clear why the [4+4] macrocycle is formed but it seems that the driving force is the formation of a more flexible macrocyclic cavity which can accommodate the barium cation in order to optimise metal-ligand bonding distances and distribute the macrocyclic donor atoms in a favourable geometrical arrangement about the barium ion. A possible mechanism is shown in Scheme 4 9, based on that proposed for a related reaction in which a [2+2] sandwich-like complex undergoes rearrangement to a [4+4] analogue.<sup>182</sup>

In the cation  $[\text{Cu}_4\text{Ba}(\text{H}_2\text{L1})_2(\text{EtOH})]^{2+}$  the two dicopper [2+2] macrocyclic units are held together by the barium coordination but also by axial coordination of a phenolate oxygen from one macrocycle to a copper centre in the second unit. This structure suffers hydrolysis of an imine bond of one macrocycle, resulting in a terminal carbonyl and amine groups. The amine group can react with an imine group of the other macrocycle by nucleophilic attack at the carbon atom. One of the C-N single bonds then breaks. As a result a new intermolecular imine link has been formed and there is another terminal amine group, which undergoes Schiff-base condensation with the free carbonyl to form the product of the new expanded macrocycle. The resulting complex has the structure and conformation observed for the complex  $[\text{Cu}_4\text{Ba}(\text{H}_4\text{L9})(\text{MeOH})_2]$ . Similar attack by nucleophilic amine groups on coordinated imino ligands has been implicated in the mechanism of transamination reactions in related systems.<sup>183</sup>

Analogous metal-directed ring-expansion reactions in Schiff-base macrocycles have been previously observed. Templated expansion of a preformed [2+2] Schiff-base macrocycle to a [4+4] analogue was reported by McKee *et al.*<sup>182</sup> The macrocyclic enlargement was obtained from the barium [2+2] complex by transmetallation with manganese ions. Similarly, metal-directed expansion of a preformed [2+2] Schiff-base macrocycle to a [3+3] analogue has been reported by Love *et al.*<sup>184</sup> The reaction between a [2+2] Schiff-base polypyrrolic macrocycle and zinc acetate yielded the enlarged [3+3] macrocyclic complex.

#### 4.5. Other heteronuclear barium complexes

As explained previously, the presence of mixtures of the macrocyclic ligands in the heteronuclear complexes would not necessarily be detected by the normal methods of characterisation, as the differences between equivalent complexes with different macrocycles might not be obvious. Microanalytical, infrared spectroscopy and nuclear magnetic resonance results would be very similar, and recrystallisation would tend to eliminate the minor component. In some cases, the major difference between the complexes with different macrocycles would be their masses, so the obvious way of detecting the complexes was mass spectroscopy. However, the presence of a mixture of  $(H_6L1)_2$  and  $H_{12}L9$  ligands in the product was not detected by mass spectrometry as the equivalent heteronuclear complexes  $[M_4Ba(H_2L1)_2]^{2+}$  and  $[M_4Ba(H_4L9)]^{2+}$  have the same molecular weight. The only way to distinguish between them was studying the crystal structures, as in the case of the copper(II) complexes **4.6ax** and **4.6bx**. However, in the case of the complex **4.9b**,  $[Ni_4Ba(H_2L1)_2(EtOH)_2](ClO_4)_2 \cdot 3H_2O$  (or  $[Ni_4Ba(H_4L9)(EtOH)_2](ClO_4)_2 \cdot 3H_2O$ ), where no crystal structure was obtained it could not be concluded whether the heteronuclear complex contained the macrocyclic ligand  $(H_6L1)_2$  or  $H_{12}L9$ .

As previously outlined, simultaneous addition of barium and nickel(II) perchlorate salts to an ethanol solution of DHTMB and further reaction with 1,3-diaminopropan-2-ol in the presence of base yielded a mixture of two different heteronuclear complexes. One of the products analysed as  $[Ni_3Ba(H_2L8)](EtO) \cdot H_2O$  (**4.9a**), previously described in section 4.3. The other product of the reaction, analysed as  $[Ni_4Ba(H_2L1)_2(EtOH)_2](ClO_4)_2 \cdot 3H_2O$  (or  $[Ni_4Ba(H_4L9)(EtOH)_2](ClO_4)_2 \cdot 3H_2O$ , **4.9b**). The fragmentation pattern for the complex **4.9b** shows the main peak at  $m/z$  957 corresponding to a singly charged ion containing the dimetallic fragment  $[Ni_2(H_3L1) - 2H]^+$ . The peak at  $m/z$  1195 assigned to the trimetallic fragment  $[Ni_2Ba(H_2L1)(ClO_4)]^+$  suggests the formation of the heteronuclear complex (Fig 4.29, Table 4.23).

Table 4.23: Peak attributions for 4.9b

M/z	Rel. Intensity (%)	Fragments	Calc. Mass
957	100	$[\text{Ni}_2(\text{H}_3\text{L1})-2\text{H}]^+$	957
1026	10	$[\text{Ni}_2(\text{H}_3\text{L1})(\text{EtOH})(\text{H}_2\text{O})+3\text{H}]^+$	1026
1195	18	$[\text{Ni}_2\text{Ba}(\text{H}_2\text{L1})(\text{ClO}_4)]^+$	1195

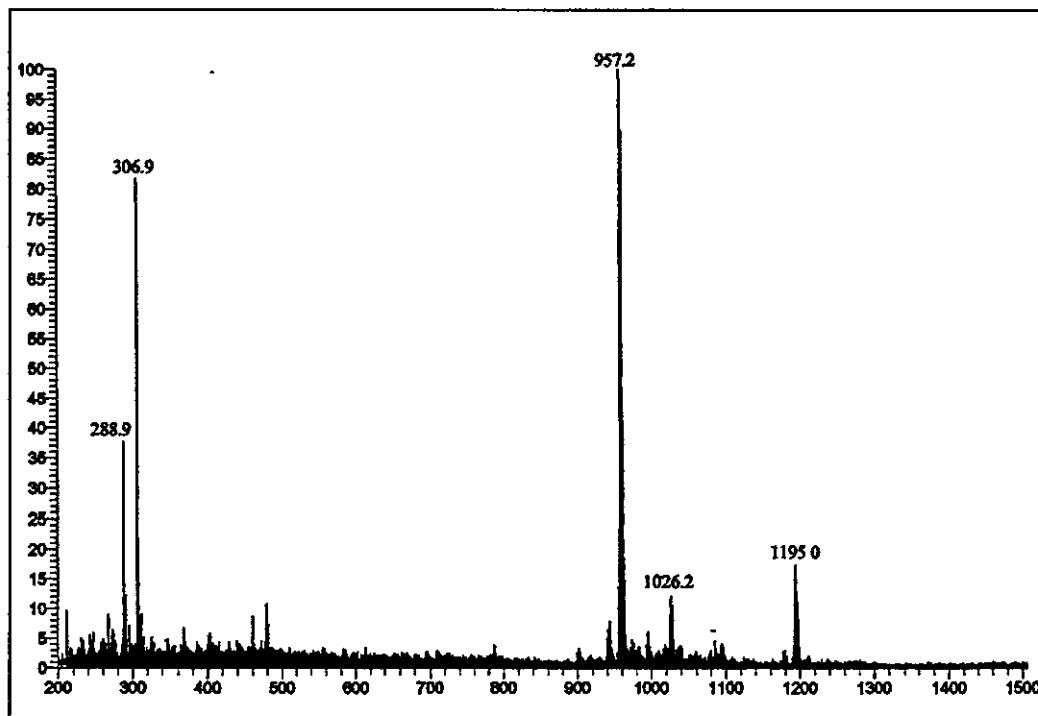


Fig. 4.29: LSIMS spectrum of 4.9b

The results obtained have shown that the heteronuclear complex of Ni(II) and barium with weakly coordinated anions to the barium centre can also be synthesised and detected by LSIMS or IR spectroscopy. However, these characterisation techniques do not reveal whether the macrocyclic ligand present in the complex is  $(\text{H}_6\text{L1})_2$  or  $\text{H}_{12}\text{L9}$ . However, the presence of a peak corresponding to the [2+2] macrocycle suggests that the complex obtained is probably the sandwich complex  $[\text{Ni}_4\text{Ba}(\text{H}_2\text{L1})_2(\text{EtOH})_2](\text{ClO}_4)_2 \cdot 3\text{H}_2\text{O}$  and not the [4+4] macrocyclic complex  $[\text{Ni}_4\text{Ba}(\text{H}_4\text{L9})(\text{EtOH})_2](\text{ClO}_4)_2 \cdot 3\text{H}_2\text{O}$

#### 4.6. Conclusions

The ability to bind hard metal ions in the tetraphenolate site reflects the pseudocalixarene nature of the host and demonstrates that the Schiff-base/calixarene hybrids synthesised retain some properties of each "parent" class as well as some new functionality focussed on the methylenediphenol groups.

One of the most important features highlighted in this chapter is the effect of the alkali or alkali-earth metal ion in the direction of the macrocyclic synthesis, and on the template process. The metal ion controls the stereochemistry in the intermediates of the reaction promoting cyclisation of the ligands and formation of a suitable macrocycle. The macrocycle would not form from the same reactants in the absence of the template. The formation of heteronuclear complexes of the large macrocycles  $H_9L8$  and  $H_{12}L9$  is an example of the template effect that the alkaline earth metal ion has in the reaction (except in the case of macrocyclic rearrangement).

The charge of guest cations is a significant factor which affects the cation-binding ability of the macrocycle due to the strong electrostatic interaction between the macrocyclic moieties and the guest cation. Moreover, the size-fit principle is important for this ion recognition, because only certain metal ions have the appropriate ionic diameter for the recognition site. As seen in the results, the matching of the template metal ion size to the macrocyclic cavity is one of the driving forces for the complex formation, the macrocyclic cavity being sufficiently large to bind the template metal ion. Thus, depending on the template metal radii and geometrical requirements, three macrocycles have been formed.

If the template of the reaction is the first row transition metal ion ( $Ni^{2+}$ ,  $Cu^{2+}$  or  $Zn^{2+}$ ) or the alkaline metal  $Na^+$ , the [2+2] macrocycle  $H_6L1$  is formed. The macrocyclic cavity of  $H_6L1$  seems suitable for the sodium ion radius (1.16 Å). The complexes obtained suggest that if both metal ions are added simultaneously

to the reaction mixture, the transition metal acts as the template of the reaction and the alkaline (or even the slightly smaller alkaline earth metal ( $r(\text{Ca}^{2+}) = 1.14 \text{ \AA}$ ) simply occupy the pre-formed central site of the macrocyclic cavity. In the case of the barium ion ( $r(\text{Ba}^{2+}) = 1.56 \text{ \AA}$ ), the metal ion is too large for the [2+2] macrocyclic cavity, and it sits above the plane of the macrocyclic donors set, leading to a new structure in which two of the [2+2] macrocyclic units sandwich the metal ion. A barium complex of the new [4+4] macrocycle  $\text{H}_{12}\text{L9}$  was also obtained as a second product of the reaction, together with the barium [2+2] sandwich complex. The new [4+4] macrocycle is possibly formed by barium template reaction, coordinating four molecules of DHTMB around it. It could also be possible that it forms as a result of the intramolecular rearrangement of the barium [2+2] sandwich complex under reflux, in order to optimise the bonding distances and distribute the macrocyclic donor atoms in a more favourably geometrical arrangement about the barium ion.

Alternatively, when the alkaline earth metal ion ( $\text{Ca}^{2+}$  or  $\text{Ba}^{2+}$ ) is added first to the reaction mixture, it seems to act as the template of the reaction. In this case the [2+2] macrocyclic cavity seems to be too small and the new [3+3] macrocycle  $\text{H}_9\text{L8}$  is formed. The [3+3] macrocyclic cavity is likely to be a good match for the metal ion size, since the macrocycle is flexible enough to wrap around to optimise the metal-donor atom distances. However, the [3+3] macrocycle has just six phenolate donors to coordinate the barium ion, and more external ligands are needed to complete the barium coordination. Instead, the [4+4] macrocycle seems to be the perfect fit for the barium heteronuclear complexes, since it has the eight phenolate donors required by the barium and is also flexible enough to wrap around the barium ion and optimise the metal ion coordination preferences.

In conclusion, the new pseudocalixarene macrocycles synthesized could be used as ion recognition systems that coordinate selectively alkaline or alkaline-earth metal ions in the phenolic central site. This could only be possible if, once the heteronuclear complexes were obtained, the alkali or alkali earth metal ions could be eliminated without breaking the macrocyclic ligand system (e.g. by



protonating the phenolate oxygen donors of the macrocycle) Similar selective calcium and barium receptors based on site-selective transmetallation of polynuclear zinc complexes have been reported by Nabeshima *et al.*<sup>185</sup> Based on the results, it can be concluded that the site-selectivity for the [2+2] macrocycle H<sub>6</sub>L1 is Na<sup>+</sup>>Ca<sup>2+</sup>>Ba<sup>2+</sup> and for the [3+3] macrocycle H<sub>9</sub>L8 is Ca<sup>2+</sup>>Ba<sup>2+</sup>>>Na<sup>+</sup>. This can be explained in terms of the heteronuclear complexes obtained depending on the experimental conditions and the yields of the synthesis. Heteronuclear sodium complexes of H<sub>6</sub>L1 were obtained with good yields (*ca.* 80%) either by sodium or transition metal template reaction. Heteronuclear calcium complexes of H<sub>6</sub>L1 were obtained with lower yields (*ca.* 60%) when the template of the reaction was the transition metal. Instead, heteronuclear calcium complexes of the H<sub>9</sub>L8 were synthesised with high yields (*ca.* 85%) if the calcium ion was the template of the reaction. From these results it can be concluded that the [2+2] macrocycle H<sub>6</sub>L1 would preferentially coordinate sodium ions over calcium ions and the [3+3] macrocycle H<sub>9</sub>L8 would preferentially coordinate calcium ions, since no sodium complexes of H<sub>9</sub>L8 were isolated. In the case of the barium ion, it can not be concluded which macrocycle is preferably formed in the synthesis of heteronuclear barium complexes since mixtures of complexes of H<sub>6</sub>L1, H<sub>9</sub>L8 and H<sub>12</sub>L9 were obtained for different experimental conditions. The processes occurring in the barium complexes syntheses are still unclear and need further investigation.

Future work should elucidate the role of both metals in the formation of heteronuclear macrocyclic complexes. The study should include further experiments to obtain the heteronuclear sandwich complex of H<sub>6</sub>L1 in other experimental conditions, i.e. reaction of the isolated dicopper complex with barium and base. Experiments to isolate alkaline or alkaline-earth homonuclear complexes should also be performed in order to study if the kinetic coordination template effect of metal dominates in the formation of the macrocycle and also which is the preferred macrocyclic cavity for the group 1 and 2 metal ions. The alkaline and alkaline-earth complexes isolated could then be treated with transition metal ions in order to obtain the heteronuclear complexes. In addition,

further studies should investigate the coordination of barium ions to the diphenolic dialdehyde DHTMB. Similar studies of coordination of the uranyl to di- and triphenol ligands have been reported.<sup>186</sup>

Further studies should also examine in detail the possible rearrangement route of the macrocycle H<sub>6</sub>L1. Heteronuclear sandwich complexes should be recrystallised in different set of solvents in order to study if the rearrangement process takes place and the influence of the solvent on it. The rearrangement of the macrocycle H<sub>6</sub>L1 to generate larger macrocycles provides a route to new pseudocalixarene hosts for large cations such as lanthanides, where the central site can be fine-tuned by the properties of the smaller transition metal ions in the system. The mechanism and general applicability of this reaction should be considered for further work.

# **CHAPTER V**

## **EXPERIMENTAL**

## **E.1. General experimental conditions**

### **E.1.1. Solvents and reagents**

Solvents used for preparative chemistry were chemically pure grade or HPLC grade and were used without further purification unless stated otherwise. Chemicals that were not synthesised in this work were Analar or reagent grade and were used without further purification. When the conditions required, solutions were degassed with nitrogen for at least 20 minutes prior to undertaking experiments.

### **E.1.2. Physical measurements**

Infrared spectra were recorded as KBr pellets or DCM solution in the range 4000-450  $\text{cm}^{-1}$  on a Perkin-Elmer System 2000 Fourier Transform spectrometer within the chemistry department at Loughborough University.

Elemental analyses were performed on a Perkin-Elmer 2400 elemental analyser by the chemistry department technicians (Mrs Pauline King, Mr Alastair Daley and Ms Sandra Dias) at Loughborough University.

Low resolution Fast Atom Bombardment (FAB, actually LSIMS) and low resolution Electrospray Ionization (ESI) mass spectra were performed by the EPSRC National Mass Spectrometry Service Centre at Swansea.

$^1\text{H}$  NMR spectra (500 MHz) were recorded on a Bruker AC250FT spectrometer with  $\delta$  referenced to external  $\text{SiMe}_4$  by the experimental officer Mr Mark Edgar within the chemistry department at Loughborough University.

Most of the crystallographic data were collected at 150K on a Bruker SMART 1000 CCD diffractometer using graphite monochromated  $\text{Mo-K}\alpha$  radiation ( $\lambda=0.71073 \text{ \AA}$ ) at Loughborough University. Some sets were collected at 150K on

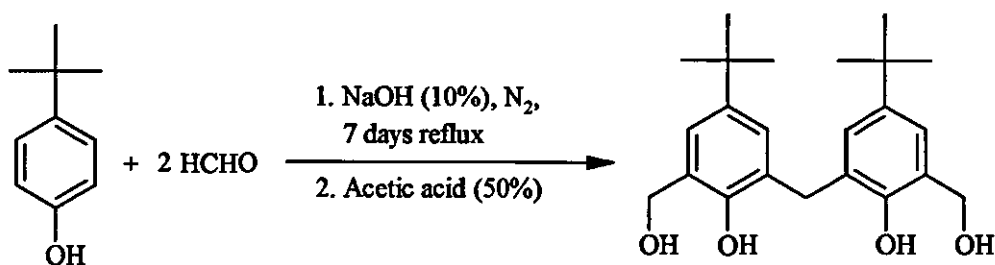
stations 9.8 and 16.2 of the Synchrotron Radiation Source at Daresbury<sup>186</sup> on a Bruker Apex II CCD diffractometer using synchrotron radiation.

Variable-temperature magnetic measurements were carried out by Dr C.J. Harding at The Open University, Milton Keynes, on polycrystalline samples using a Faraday type magnetometer (Oxford Instruments), equipped with a helium continuous-flow cryostat working in the temperature range 80–280 K, and an electromagnet operating at a magnetic field of 0.8 T. Diamagnetic corrections were estimated from standard Pascal values. Room temperature magnetic susceptibilities were measured using a Sherwood Scientific magnetic susceptibility balance within the chemistry department at Loughborough University.

## E.2. Chapter 2: Dinuclear complexes of $H_6L1$

### E.2.1. Organic preparations

#### E.2.1.1. Synthesis of 2,2'-dihydroxy-5,5'-di-*tert*-butyl-3,3'-methanediyl-dibenzylalcohol (DHTMBA)



This precursor was synthesised following a literature procedure<sup>110</sup> with some modifications. A mixture of 45 g of 4-*tert*-butylphenol, 60 mL of a 37% HCHO solution, and 140 mL of a 10% NaOH solution was placed in a 500 mL round bottomed flask fitted with a reflux condenser. This mixture was heated at  $50 \pm 5^\circ\text{C}$  for 8 or 9 days under an atmosphere of  $\text{N}_2$ . It was then cooled and the resinous bright yellow precipitate was collected by filtration, re-dissolved in a minimum of acetone (50 to 100 mL). A white insoluble product was filtered off if necessary.



The resulting yellow filtrate was then acidified with 200 mL of cold 50% aqueous acetic acid. The aqueous layer was extracted several times with diethylether (100 mL) (3-4 times). The combined ether layers were washed (3-4 times) with water to remove the excess acetic acid and dried over  $MgSO_4$ . The solvent was removed to give a coloured oil (the colour varying between pale yellow and red-purple). The oil was dissolved in 60-80 mL of toluene to which petroleum ether (bp 40-60°C) was added to turbidity. Within a day a white crystalline solid separated which was removed by filtration and washed with cold petroleum ether (Yield: 23-27 g, 43-48%).

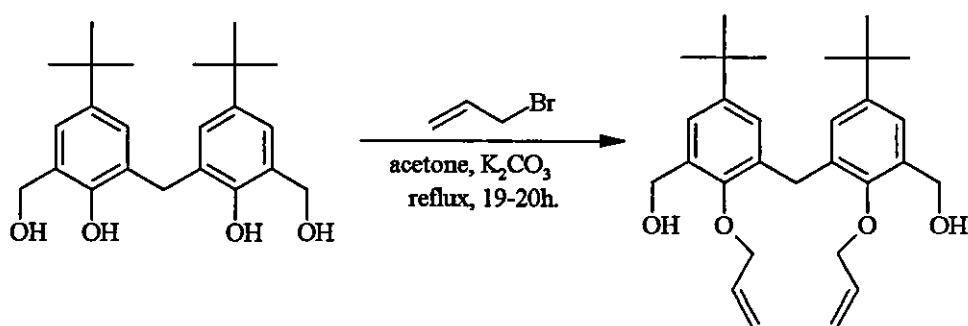
CHN Calc.: C 74.16%, H 8.66% for  $[C_{23}H_{32}O_4]$

Found: C 73.80%, H 9.13%

NMR ( $CDCl_3$ , ppm,  $^1H$ ): 7.26(d, 2, ArH), 6.94(d, 2, ArH), 4.77(s, 4,  $CH_2OH$ ), 3.88(s, 2,  $ArCH_2Ar$ ), 1.26(s, 18,  $C(CH_3)_3$ ).

IR (DCM,  $cm^{-1}$ ): 3420 (s,  $\nu_{OH}$ ); 1208 (s,  $\nu_{ArOH}$ ); 875 (m, 1,2,3,5 tetrasubstitution of Ar).

#### E.2.1.2. Synthesis of 2,2'-diallyloxy-5,5'-di-*tert*-butyl-3,3'-methanediyl-dibenzylalcohol (AOTMBA)



This compound was prepared using a method frequently applied to phenols.<sup>111</sup>

10 g (27 mmol) of DHTMBA, 7 g (58 mmol) of allylbromide, 7.42 g of anhydrous potassium carbonate and 100 mL of acetone were placed in a 250 mL three-necked round bottom flask fitted with a reflux condenser and sealed stirrer unit and refluxed for 20h with stirring. The reaction mixture was then poured into

200 mL of water and the aqueous layer was extracted three times with diethyl ether. Then, the organic layer was washed with a 2M sodium hydroxide solution and dried over anhydrous potassium carbonate. The solvent was removed under vacuum leaving a white solid, which could be recrystallised from dichloromethane/n-hexane. The yield is 9 g (74 %). Colourless crystals suitable for X-ray studies were obtained by slow evaporation of a solution of petroleum ether/diethylether (50:50).

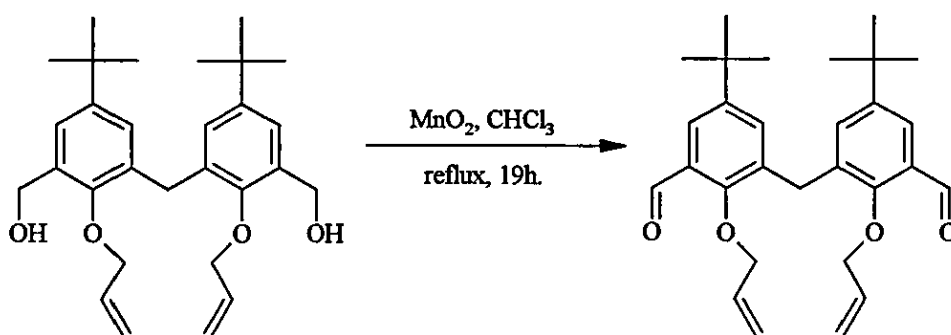
CHN Calc.: C 75.45%, H 8.95% for  $[C_{23}H_{40}O_4] \cdot 1/2H_2O$

Found: C 75.64%, H 9.06%

NMR ( $CDCl_3$ , ppm,  $^1H$ ): 7.24(d, 2, ArH), 7.01(d, 2 ArH), 6.07(m, 2, allyl =CH), 5.34(dd, 2, allyl =CH<sub>2</sub>), 5.30(dd, 2, allyl =CH<sub>2</sub>), 4.73(d, 4, CH<sub>2</sub>OH), 4.34(d, 4, allyl CH<sub>2</sub>), 4.70(s, 4, CH<sub>2</sub>OH), 4.07(s, 2, ArCH<sub>2</sub>Ar), 1.26(s, 18, C(CH<sub>3</sub>)<sub>3</sub>).

IR (DCM,  $cm^{-1}$ ): 3272 (s,  $\nu_{OH}$ ), 3081 (w,  $\nu_{allyl=CH_2}$ ), 883 (m, 1,2,3,5 tetrasubstitution of Ar).

### E.2.1.3. Synthesis of 2,2'-diallyloxy-5,5'-di-*tert*-butyl-3,3'-methanediyl-dibenzaldehyde (AOTMB)



The method used is similar to the one reported by Taniguchi *et al.*<sup>112</sup>

50 g of activated  $MnO_2$  were added to 9 g (20 mmol) of AOTMBA in 200 mL of chloroform. The reaction mixture was refluxed for 19-20 h. after which time  $MnO_2$  was filtered off and the organic layer dried over anhydrous magnesium sulphate. The solvent was removed under vacuum leaving a pale yellow oil that

crystallised under vacuum over a week. The solid was then washed with cold methanol to remove the yellow impurities. Colourless crystals suitable for X-ray studies were obtained by slow evaporation of a diethylether solution of the product. The yield is 7 g (78%). The oil did not always crystallise but could be used without further purification, since the NMR and elemental analysis data showed no partially oxidised product present

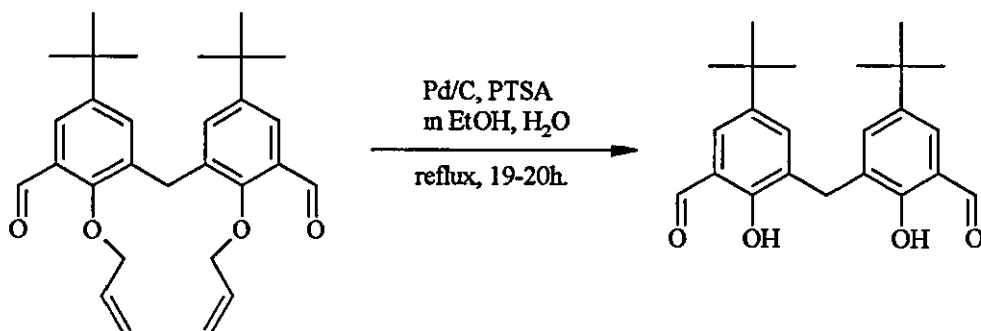
CHN Calc : C 76.11%, H 8.15% for  $[\text{C}_{29}\text{H}_{36}\text{O}_4] \cdot \frac{1}{2}\text{H}_2\text{O}$

Found: C 76.08%, H 8.15%

NMR ( $\text{CDCl}_3$ , ppm.  $^1\text{H}$ ): 10.4 (s, 2, CHO), 7.75 (d, 2, ArH), 7.30 (d, 2, ArH), 6.06 (m, 2, allyl=CH), 4.40 (dd, 2, allyl=CH<sub>2</sub>), 4.44 (dd, 2, allyl=CH<sub>2</sub>), 4.13 (s, 2, ArCH<sub>2</sub>Ar), 1.26 (s, 18, C(CH<sub>3</sub>)<sub>3</sub>).

IR (DCM,  $\text{cm}^{-1}$ ): 1660 ( $\nu_{\text{C}=\text{O}}$ ), 3081 (w,  $\nu_{\text{allyl}=\text{CH}_2}$ ), 885 (m, 1,2,3,5 tetrasubstitution of Ar).

#### E.2.1.4. Synthesis of 2,2'-dihydroxy-5,5'-di-*tert*-butyl-3,3'-methanediyl-dibenzaldehyde (DHTMB)



The method used is similar to the one reported by Boss *et al.*<sup>113</sup>

To a solution of AOTMB (7 g, 15.6 mmol) in 150 mL of ethanol, 1.5 g of Pd on activated charcoal and 0.7 g of *p*-toluenesulfonic acid in 5 mL of water were added. The stirred suspension was refluxed for 2 days after which time the reaction mixture was filtered hot. On cooling, the product precipitated out as a pale yellow powder, which was filtered off (1 g). An additional 3 g of DHTMB could be obtained on concentration of the resulting filtrate. Pale yellow crystals

suitable for X-Ray studies were obtained by slow evaporation of a diethylether solution of the product. The yield is 4 g (70%).

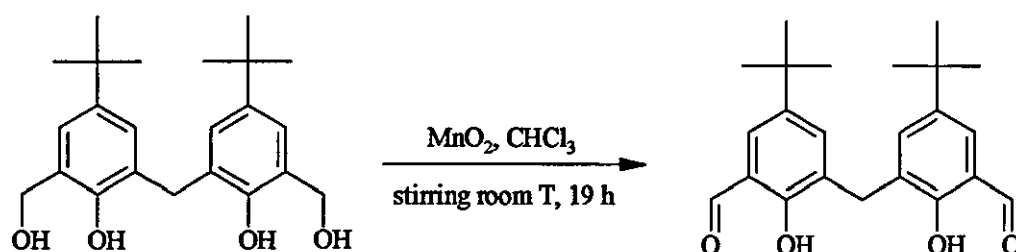
CHN Calc : C 74.97%, H 7.66% for  $[C_{23}H_{28}O_4]$

Found. C 74.51%, H 7.86%

$^1H$  NMR ( $CDCl_3$ , ppm,  $^1H$ ): 9.86(s, 2, CHO), 7.64(d, 2, ArH), 7.37(d, 2, ArH), 4.03(s, 2,  $ArCH_2Ar$ ), 1.26(s, 18,  $C(CH_3)_3$ )

IR (KBr,  $cm^{-1}$ ): 1658 (s,  $\nu_{C=O}$ ), 1270 (s,  $\nu_{ArOH}$ ), 1216 (s)

#### E.2.1.5. Synthesis of 2,2'-dihydroxy-5,5'-di-*tert*-butyl-3,3'-methanediyl-dibenzaldehyde (DHTMB) by direct oxidation



Formation of DHTMB was initially carried out according to the last procedure, involving four steps. This method has recently been replaced by simple manganese dioxide oxidation of the dialcohol into the dialdehyde reducing the number of steps to two, and in a higher overall yield (16% vs. 5%).

Powdered manganese dioxide, suitable for organic oxidations, was obtained commercially and activated by heating at  $120^\circ C$  for 48 h immediately prior to use. 13.6 g (0.156 mol) of cooled freshly activated manganese dioxide were added to a solution of 2 g (5.4 mmol) of 2,2'-dihydroxy-5,5'-di-*tert*-butyl-3,3'-methanediyl-dibenzylalcohol (DHTMBA) in chloroform (*ca.* 750 mL), and stirred for 19 h at room temperature. The manganese dioxide was removed by filtration. Removal of solvent by rotatory evaporation yielded a brown sticky product, which was dissolved in the minimum volume of ethanol by warming slightly. On cooling, the product precipitated out as a pale yellow powder, which was filtered

off. Additional crops of pale yellow solid were separated by continuous concentration of the resulting filtrate and dissolving again in the minimum volume of ethanol (Yield: 0.7 g; 35%).

CHN Calc. C 74.97%, H 7.66% for  $[C_{23}H_{28}O_4]$

Found: C 74.56%, H 7.88%

IR (KBr,  $cm^{-1}$ ): 1659 (s,  $\nu_{C=O}$ ), 1271 (s,  $\nu_{ArOH}$ ), 1216 (s).

## E.2.2. Complex syntheses

### E.2.2.1. $[Cu_2(H_4L1)Cl]Cl \cdot 2MeOH$ (2.1)

0.073 g (0.543 mmol) of anhydrous  $CuCl_2$  was dissolved in *ca.* 40 mL of EtOH (apple green colour) 0.2 g (0.543 mmol) of DHTMB were also dissolved in *ca.* 35 mL of hot methanol and added to the metal salt solution. This mix was heated up to reflux during 10 minutes, after which time a solution of 1,3-diaminopropan-2-ol (0.052 g, 0.543 mmol) in *ca.* 20 mL of methanol was added dropwise to the refluxing solution. The colour turned emerald green and after few minutes started to get darker, becoming dark green. The reaction mixture refluxed for 2 hours. After that time, the solution was filtered and concentrated under vacuum. A pale green product precipitated, so it was filtered off. (Yield: 0.11 g; 36%). Emerald green crystals suitable for X-ray study were obtained by slow diffusion of diethylether into an ethanol solution over a few days.

CHN Calc.: C 58.68%; H 6.75%; N 5.07% for  $[Cu_2(H_4L1)Cl]Cl \cdot 2MeOH$

Found: C 58.43%; H 6.56%; N 5.08%

LSI-MS  $m/z$  (%) (calc.). 889 (40) ( $[Na_2(H_4L1)-e]^+$ , 889); 970 (100)

$([Cu_2(H_4L1)+e]^+$ , 970), 1006 (15) ( $[Cu_2(H_4L1)Cl+H]^+$ ,  
1006); 1032 (7) ( $[Cu_2(H_4L1)(MeOH)_2-2H]^+$ , 1032)

IR (KBr,  $cm^{-1}$ ). 3327 (b, s,  $\nu_{O-H}$ ), 2952 (s,  $\nu_{C-CH_3}$ ); 1627 (s,  $\nu_{C=N}$ ); 1560 (w,  $\nu_{C-O}$ );  
1475 (m); 1436 (m); 1365 (m); 1221 (m).



**E.2.2.2.  $[\text{Zn}_2(\text{H}_4\text{L1})\text{Cl}]\text{Cl}\cdot\text{H}_2\text{O}$  (2.2)**

Anhydrous  $\text{ZnCl}_2$  (0.15 g, 1.086 mmol) and DHTMB (0.2 g, 0.543 mmol) were dissolved in ethanol (*ca.* 80 mL). The solution was refluxed for 10-15 minutes after which time a solution of 1,3-diaminopropan-2-ol (0.052 g, 0.543 mmol) in *ca.* 10 mL of ethanol was added dropwise to the refluxing solution. The solution colour changed from bright yellow to dark yellow. The reaction mixture refluxed for 2 hours. The solution was then cooled down, concentrated under vacuum to half the volume and left to evaporate slowly. A yellow solid precipitated, so it was filtered off (Yield: 0.26 g; 90%). This solid was dissolved in ethanol and diethylether was left diffusing into the solution. Yellow crystals suitable for X-ray studies were isolated in a few days.

CHN Calc.: C 58.76%, H 6.45%; N 5.27% for  $[\text{Zn}_2(\text{H}_4\text{L1})\text{Cl}]\cdot\text{Cl}\cdot\text{H}_2\text{O}$

Found. C 58.59%; H 6.52%; N 5.26%

LSI-MS  $m/z$  (calc): 973 (30) ( $[\text{Zn}_2(\text{H}_4\text{L1})+\text{e}]^+$ , 973); 1009 (60)  
 $([\text{Zn}_2(\text{H}_4\text{L1})\text{Cl}]^+$ , 1009).

IR (KBr,  $\text{cm}^{-1}$ ): 3422 (b, s,  $\nu_{\text{O-H}}$ ); 2963 (s,  $\nu_{\text{C-CH}_3}$ ); 1638 (s,  $\nu_{\text{C=N}}$ ); 1553 (w); 1262 (s), 1220 (m), 1097 (s); 1025 (m), 797 (m).

**E.2.2.3.  $[\text{Ni}_2(\text{H}_4\text{L1})\text{Cl}]\text{Cl}\cdot 4\text{H}_2\text{O}$  (2.3)**

$\text{NiCl}_2\cdot 6\text{H}_2\text{O}$  (0.13 g, 0.543 mmol) and DHTMB (0.2 g, 0.543 mmol) were dissolved in hot ethanol (*ca.* 100 mL). The pale green solution was refluxed for 10-15 minutes after which time a solution of 1,3-diaminopropan-2-ol (0.052 g, 0.543 mmol) in *ca.* 10 mL of methanol was added dropwise to the refluxing solution. The solution colour changed from pale green-yellowish to lime green and cloudy. The reaction mixture was allowed to reflux for 2 hours. The solution was then cooled down, concentrated under vacuum and left to evaporate slowly. A pale green solid precipitated, so it was collected (Yield: 0.17 g; 57%).

**CHN Calc.:** C 56.60%; H 6.76%; N 5.08% for  $[\text{Ni}_2(\text{H}_4\text{L1})\text{Cl}]\cdot\text{Cl}\cdot 4\text{H}_2\text{O}$

**Found:** C 56.57%; H 6.50%; N 4.70%

**ESI-MS m/z (%) (calc):** 479 (40) ( $[\text{Ni}_2(\text{H}_4\text{L1})\text{-}2\text{H}]^{2+}$ , 958); 957 (100)

( $[\text{Ni}_2(\text{H}_4\text{L1})\text{-H}]^+$ , 959); 995 (10) ( $[\text{Ni}_2(\text{H}_4\text{L1})\text{Cl}]^+$ , 995).

(relative abundance given for cone voltage = 90V)

**IR (KBr,  $\text{cm}^{-1}$ ):** 3383 (b,m, $\nu_{\text{O-H}}$ ); 2956 (m, $\nu_{\text{C-CH}_3}$ ); 1634 (s,  $\nu_{\text{C=N}}$ ); 1551 (w,  $\nu_{\text{C=O}}$ ),

1476 (m); 1364 (m); 1223 (m).

#### E.2.2.4. $[\text{Mn}_2(\text{H}_4\text{L1})\text{Cl}]\text{Cl}\cdot\text{H}_2\text{O}\cdot\text{EtOH}$ (2.4)

$\text{MnCl}_2\cdot 4\text{H}_2\text{O}$  (0.107 g, 0.543 mmol) and DHTMB (0.2 g, 0.543 mmol) were dissolved in hot ethanol (*ca.* 100 mL).  $\text{N}_2$  was bubbled through the mixture to avoid oxidation of the Mn(II) ions. This mixture was refluxed for 15 minutes after which time a solution of 1,3-diaminopropan-2-ol (0.054 g, 0.543 mmol) in *ca.* 10 mL of degassed ethanol was added dropwise to the bright yellow refluxing solution. The solution colour changed to bright orange yellowish and became slightly cloudy. The reaction mixture was allowed to reflux for 4 hours and left under nitrogen atmosphere overnight. The bright orange solid precipitated so it was filtered off and washed with ethanol (Yield: 0.22 g; 75%).

**CHN Calc.:** C 59.61%; H 6.85%; N 5.15% for  $[\text{Mn}_2(\text{H}_4\text{L1})\text{Cl}]\text{Cl}\cdot\text{H}_2\text{O}\cdot\text{EtOH}$

**Found:** C 59.33%; H 6.50%; N 4.86%

**LSI-MS m/z (%) (calc):** 898 (7) ( $[\text{Mn}(\text{H}_4\text{L1})\text{-e}]^+$ , 898), 951 (11) ( $[\text{Mn}_2(\text{H}_4\text{L1})\text{-}$

$2\text{H}]^+$ , 951); 987 (100) ( $[\text{Mn}_2(\text{H}_4\text{L1})\text{Cl-H}]^+$ , 987), 1040

(35) ( $[\text{Mn}_2(\text{H}_4\text{L1})(\text{Cl})_2(\text{H}_2\text{O})\text{-H}]^+$ , 1040)

**IR (KBr,  $\text{cm}^{-1}$ ):** 3384 (b, s,  $\nu_{\text{O-H}}$ ); 2958 (m,  $\nu_{\text{C-CH}_3}$ ); 1648 (s,  $\nu_{\text{C=N}}$ ); 1545 (w); 1480

(w); 1384 (w); 1364 (w); 1267 (m); 1219(w).

**E.2.2.5.  $[\text{Ni}_2(\text{H}_4\text{L1})(\text{H}_2\text{O})_3](\text{ClO}_4)_2 \cdot \text{H}_2\text{O}$  (2.5)**

0.2 g (0.543 mmol) of  $\text{Ni}(\text{ClO}_4)_2 \cdot 6\text{H}_2\text{O}$  and 0.2 g (0.543 mmol) of DHTMB were dissolved in EtOH (*ca.* 80 mL). The solution (light green colour) was refluxed for 15 minutes after which time a solution of 1,3-diaminopropan-2-ol (0.054 g, 0.543 mmol) in *ca.* 10 mL of EtOH was added dropwise to the refluxing solution. The solution was refluxing for 5 hours, after which it was filtered and concentrated under vacuum. Afterwards, it was left to evaporate slowly in EtOH. Pale green crystals suitable for X-ray analysis were obtained after few hours. They were filtered off and washed several times with  $\text{Et}_2\text{O}$  (0.152 g). The colour then changed from green to pale orange reddish. It was filtered off a second crop (0.08 g) of pale orange reddish powder after adding  $\text{Et}_2\text{O}$  to the green solution (Overall yield: 68%)

CHN Calc.: C 50.71%; H 6.06%; N 4.55% for  $[\text{Ni}_2(\text{H}_4\text{L1})(\text{H}_2\text{O})_3](\text{ClO}_4)_2 \cdot \text{H}_2\text{O}$

Found: C 51.09%; H 6.39%; N 4.26%

ESI-MS  $m/z$  (%) (calc.): 451 (30) ( $[\text{Ni}(\text{H}_6\text{L1})-\text{H}]^{2+}$ , 902); 479 (100) ( $[\text{Ni}_2(\text{H}_4\text{L1})-2\text{H}]^{2+}$ , 958), 901 (5) ( $[\text{Ni}(\text{H}_4\text{L1})-\text{H}]^{2+}$ , 901); 959 (40) ( $[\text{Ni}_2(\text{H}_4\text{L1})-\text{H}]^+$ , 959), 1059 (15) ( $[\text{Ni}_2(\text{H}_4\text{L1})(\text{ClO}_4)]^+$ , 1059)  
(Note: the relative abundance is given for cone voltage = 90V)

IR (KBr,  $\text{cm}^{-1}$ ) 3422 (b,m, $\nu_{\text{O-H}}$ ), 2960 (m, $\nu_{\text{C-CH}_3}$ ); 1635 (s,  $\nu_{\text{C=N}}$ ); 1561 (w,  $\nu_{\text{C-O}}$ ); 1477 (m); 1439 (m); 1394 (m), 1226 (m); 1107 (b, s,  $\nu_3(\text{ClO}_4^-)$ ), 624 (m,  $\nu_4(\text{ClO}_4^-)$ ).

**E.2.2.6.  $[\text{Co}_2(\text{H}_4\text{L1})(\text{H}_2\text{O})_3](\text{ClO}_4)_2 \cdot 3\text{EtOH}$  (2.6)**

$\text{Co}(\text{ClO}_4)_2 \cdot 6\text{H}_2\text{O}$  (0.198 g, 0.543 mmol) and DHTMB (0.2 g, 0.543 mmol) were dissolved in ethanol (*ca.* 80 mL). The orange solution was refluxed for 15 minutes under  $\text{N}_2$ , after which time a solution of 1,3-diaminopropan-2-ol (0.054 g, 0.543 mmol) in *ca.* 10 mL of degassed ethanol was added dropwise to the refluxing

solution The solution colour changed from orange to dark orange-brownish The reaction mixture was allowed to reflux for 3 hours. The solvent was removed under vacuum. The dark yellow brownish residue was dissolved in dichloromethane, a small amount of impurities was filtered off and the solution was evaporated to dryness (Yield: 0.25 g; 68%)

CHN Calc: C 51.52%; H 6.71%; N 4.14% for  $[\text{Co}_2(\text{H}_4\text{L1})(\text{H}_2\text{O})_3](\text{ClO}_4)_2 \cdot 3\text{EtOH}$   
 Found: C 51.78%; H 6.07%; N 4.00%

LSI-MS  $m/z$  (%) (calc): 902 (15) ( $[\text{Co}(\text{H}_4\text{L1})-\text{e}]^+$ , 902); 943 (14) ( $[\text{Co}_2(\text{H}_4\text{L1})(\text{H}_2\text{O})+\text{Na}]^+$ , 943); 959 (95) ( $[\text{Co}_2(\text{H}_4\text{L1})-\text{H}]^+$ , 959); 1059 (100) ( $[\text{Co}_2(\text{H}_4\text{L1})(\text{ClO}_4)-\text{H}]^+$ , 1059); 1131 (55) ( $[\text{Co}_2(\text{H}_4\text{L1})(\text{ClO}_4)(\text{H}_2\text{O})_4-\text{H}]^+$ , 1131).

IR (KBr,  $\text{cm}^{-1}$ ): 3440 (b,s, $\nu_{\text{O-H}}$ ); 2957 (m, $\nu_{\text{C-CH}_3}$ ), 1636 (s, $\nu_{\text{C=N}}$ ); 1560 (w), 1458 (m); 1364 (m); 1270 (m), 1222 (m); 1106 (b, s,  $\nu_3(\text{ClO}_4^-)$ ); 623 (m,  $\nu_4(\text{ClO}_4^-)$ )

#### E.2.2.7. $[\text{Co}_2(\text{H}_4\text{L1})(\text{H}_2\text{O})_3](\text{BF}_4)_2 \cdot 2\text{H}_2\text{O}$ (2.7)

$\text{Co}(\text{BF}_4)_2 \cdot 2\text{H}_2\text{O}$  (0.185 g, 0.543 mmol) and DHTMB (0.2 g, 0.543 mmol) were dissolved in ethanol (ca. 80 mL) The solution was refluxed under nitrogen atmosphere for 15 minutes, after which time a solution of 1,3-diaminopropan-2-ol (0.054 g, 0.543 mmol) in ca. 10 mL of ethanol was added dropwise to the refluxing solution. The reaction mixture was allowed to reflux for 2 hours. On standing, the yellow brownish solution turned dark brown A small amount of impurities was filtered off and the solvent was removed under vacuum. The dark brown residue was washed with dichloromethane (Yield: 0.26 g; 78%)

CHN Calc: C 50.99%, H 6.25%; N 4.57% for  $[\text{Co}_2(\text{H}_4\text{L1})(\text{H}_2\text{O})_3](\text{BF}_4)_2 \cdot 2\text{H}_2\text{O}$   
 Found: C 51.04%; H 6.53%; N 4.57%

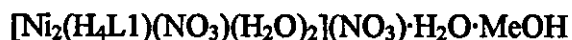
LSI-MS  $m/z$  (%) (calc): 903 (18) ( $[\text{Co}(\text{H}_4\text{L1})+\text{H}]^+$ , 903); 959 (100) ( $[\text{Co}_2(\text{H}_4\text{L1})-\text{H}]^+$ , 959); 1016 (10) ( $[\text{Co}_2(\text{H}_4\text{L1})(\text{H}_2\text{O})_3+\text{H}]^+$ , 1016), 1134 (40) ( $[\text{Co}_2(\text{H}_4\text{L1})(\text{EtOH})_3(\text{H}_2\text{O})_2-\text{H}]^+$ , 1134).

IR (KBr,  $\text{cm}^{-1}$ ). 3448 (b, s,  $\nu_{\text{O-H}}$ ); 2960 (s,  $\nu_{\text{C-CH}_3}$ ), 1647 (s,  $\nu_{\text{C=N}}$ ); 1560 (w,  $\nu_{\text{C-O}}$ );  
1458 (m); 1270 (m), 1223 (m); 1084 and 1055 (b,  $\nu_{3(\text{BF}_4^-)}$ ).

**E.2.2.8.  $[\text{Ni}_2(\text{H}_4\text{L1})(\text{NO}_3)(\text{H}_2\text{O})_2](\text{NO}_3)\cdot\text{H}_2\text{O}\cdot\text{MeOH}$  (2.8)**

0.235 g. (0.81 mmol) of  $\text{Ni}(\text{NO}_3)_2$  and 0.2 g. (0.543 mmol) of DHTMB were heated to reflux in *ca.* 80 mL of ethanol (light green colour) on a steam bath during 10 minutes, after which time a solution of 1,3-diaminopropan-2-ol (0.052 g, 0.543 mmol) in *ca.* 20 mL of methanol was added dropwise to the refluxing solution. The solution was allowed to reflux for 2 hours, after which the solution was cooled down, filtered and concentrated under vacuum. The mixture was dissolved in dichloromethane, filtered to eliminate impurities and concentrated under vacuum again. Afterwards, it was dissolved in methanol and left to crystallise by slow diffusion of diethylether into the solution. Pale green and yellow crystals were isolated in few days (Yield: 0.192 g, 60%).

CHN Calc : C 54.38 %; H 6.54 %; N 7.18 %



Found: C 54.55%; H 6.25%; N 7.13%

LSI-MS  $m/z$  (%) (calc.): 902 (5) ( $[\text{Ni}(\text{H}_4\text{L1})+\text{H}]^+$ , 902); 942 (9) ( $[\text{Ni}(\text{H}_4\text{L1})(\text{H}_2\text{O})+\text{Na}]^+$ , 942); 958 (100) ( $[\text{Ni}_2(\text{H}_4\text{L1})-2\text{H}]^+$ , 958); 980 (7) ( $[\text{Ni}_2(\text{H}_4\text{L1})(\text{H}_2\text{O})+2\text{H}]^+$ , 980).

IR (KBr,  $\text{cm}^{-1}$ ). 3387 (b, s,  $\nu_{\text{O-H}}$ ); 2956 (m,  $\nu_{\text{C-CH}_3}$ ); 1636 (s,  $\nu_{\text{C=N}}$ ); 1560 (w,  $\nu_{\text{C-O}}$ ),  
1475 and 1366 (s,  $\nu_{\text{coordinatedNO}_3^-}$ ); 1384 (s,  $\nu_{\text{freeNO}_3^-}$ )

**E.2.2.9.  $[\text{Zn}_2(\text{H}_4\text{L1})(\text{NO}_3)(\text{H}_2\text{O})_2](\text{NO}_3)\cdot 3\text{H}_2\text{O}$  (2.9)**

The complex was obtained from reaction of  $\text{Zn}(\text{NO}_3)_2\cdot 6\text{H}_2\text{O}$  (0.1615 g, 0.543 mmol) with DHTMB (0.2 g, 0.543 mmol), both dissolved in ethanol (*ca.* 90 mL) warming slowly. This mix was refluxed for 10-15 minutes after which time a solution of 1,3-diaminopropan-2-ol (0.052 g, 0.543 mmol) in *ca.* 10 mL of



methanol was added dropwise to the refluxing solution. The solution colour changed from white to bright yellow. The reaction mixture was refluxed for 2.5 hours. The solution was then cooled down, concentrated under vacuum and left to evaporate slowly. Yellow crystals suitable for X-ray studies were isolated within a week (Yield: 0.18 g; 58%).

CHN Calc: C 54.21%; H 6.30%, N 7.29% [ $\text{Zn}_2(\text{H}_4\text{L1})(\text{NO}_3)(\text{H}_2\text{O})_2](\text{NO}_3)\cdot 3\text{H}_2\text{O}$ ]

Found: C 54.01%; H 6.19%; N 7.87%

LSI-MS  $m/z$  (%) (calc.): 958 (15) ( $[\text{Zn}(\text{H}_4\text{L1})(\text{EtOH})+\text{H}]^+$ , 955); 971 (100)

( $[\text{Zn}_2(\text{H}_4\text{L1})-2\text{H}]^+$ , 971)

IR (KBr,  $\text{cm}^{-1}$ ): 3405 (b, s,  $\nu_{\text{O-H}}$ ); 2958 (s,  $\nu_{\text{C-CH}_3}$ ); 1646 (s,  $\nu_{\text{C=N}}$ ), 1560 (w,  $\nu_{\text{C=O}}$ );

1479 (m); 1438 and 1364 (s,  $\nu_{\text{coordinatedNO}_3^-}$ ); 1384 (s,  $\nu_{\text{freeNO}_3^-}$ ).

#### E.2.2.10. $[\text{Co}_2(\text{H}_3\text{L1})(\text{NO}_3)]\cdot 5\text{H}_2\text{O}$ (2.10)

$\text{Co}(\text{NO}_3)_2\cdot 6\text{H}_2\text{O}$  (0.16 g, 0.543 mmol) and DHTMB (0.2 g, 0.543 mmol) were dissolved in ethanol (*ca.* 80 mL). The dark orange solution was refluxed for 15 minutes, after which time a solution of 1,3-diaminopropan-2-ol (0.054 g, 0.543 mmol) in *ca.* 10 mL of ethanol was added dropwise to the refluxing solution. The solution colour changed from dark orange to dark orange-reddish. The reaction mixture was allowed to reflux for 3 hours. After that the solution was evaporated till dryness. The solid was washed with DCM and water (Yield: 0.25 g; 83%).

CHN Calc.: C 56.16%; H 6.79%; N 6.29% for  $[\text{Co}_2(\text{H}_3\text{L1})(\text{NO}_3)]\cdot 5\text{H}_2\text{O}$

Found: C 56.03%; H 6.41%; N 6.04%

LSI-MS  $m/z$  (%) (calc.): 902 (11) ( $[\text{Co}(\text{H}_4\text{L1})-\text{e}]^+$ , 902); 959 (33) ( $[\text{Co}_2(\text{H}_4\text{L1})-$

$\text{H}]^+$ , 959); 1022 (20) ( $[\text{Co}_2(\text{H}_4\text{L1})(\text{NO}_3)]^+$ , 1022), 1079

(7) ( $[\text{Co}_2(\text{H}_4\text{L1})(\text{NO}_3)(\text{H}_2\text{O})_3+2\text{H}]^+$ , 1079).

IR (KBr,  $\text{cm}^{-1}$ ): 3396 (b, s,  $\nu_{\text{O-H}}$ ); 2957 (m,  $\nu_{\text{C-CH}_3}$ ); 1636 (s,  $\nu_{\text{C=N}}$ ), 1479 (w);

1460 and 1364 (s,  $\nu_{\text{coordinatedNO}_3^-}$ ); 1384 (s,  $\nu_{\text{freeNO}_3^-}$ ); 1274 (s);

1221 (s).

**E.2.2.11.  $[\text{Zn}_2(\text{H}_4\text{L1})(\text{AcO})](\text{AcO})\cdot 5\text{H}_2\text{O}$  (2.11)**

$\text{Zn}(\text{AcO})_2\cdot 2\text{H}_2\text{O}$  (0.24 g, 0.543 mmol),  $\text{Na}(\text{AcO})$  (0.022 g, 0.27 mmol) and DHTMB (0.2 g, 0.543 mmol) were dissolved in hot ethanol (*ca.* 80 mL). The solution was refluxed for 15 minutes after which time a solution of 1,3-diaminopropan-2-ol (0.052 g, 0.543 mmol) in *ca.* 10 mL of ethanol was added dropwise to the refluxing solution. The reaction mixture refluxed for 4 hours. The solution was then cooled down, concentrated under vacuum to half the volume and diethylether was allowed to diffuse into the solution. Pale yellow crystals suitable for X-ray analysis were obtained within a week (Yield: 0.21 g; 53%). This reaction was performed in order to obtain the heteronuclear Zn-Na complex, but analyses show that this was not achieved. See discussion in Chapter 4.

CHN Calc.: C 56.90%; H 6.99%; N 4.74% for  $[\text{Zn}_2(\text{H}_4\text{L1})(\text{AcO})](\text{AcO})\cdot 5\text{H}_2\text{O}$

Found: C 56.51%; H 6.52%; N 4.17%

LSI-MS  $m/z$  (calc.): 971 (100) ( $[\text{Zn}_2(\text{H}_4\text{L1})-2\text{H}]^+$ , 971); 1033 (40)

( $[\text{Zn}_2(\text{H}_4\text{L1})(\text{AcO})]^+$ , 1033); 1095 (20) ( $[\text{Zn}_2(\text{H}_4\text{L1})(\text{AcO})_2+\text{H}]^+$ , 1093).

IR (KBr,  $\text{cm}^{-1}$ ): 3417 (b, s,  $\nu_{\text{O-H}}$ ); 2959 (s,  $\nu_{\text{C-CH}_3}$ ), 1642 (s,  $\nu_{\text{C=N}}$ ); 1593 (s); 1430 (s,  $\nu_{\text{COO}^-}$ ); 1393 (m); 1364 (m); 1216 (m); 1023 (m); 662 (m)

**E.2.2.12.  $[\text{Ni}_2(\text{H}_4\text{L1})(\text{MeOH})_2](\text{ClO}_4)_2\cdot \text{MeOH}$  (2.12)**

0.2 g (0.543 mmol) of  $\text{Ni}(\text{ClO}_4)_2\cdot 6\text{H}_2\text{O}$  and 0.2 g (0.543 mmol) of DHTMB were dissolved in EtOH (*ca.* 80 mL). The solution (lime green colour) was refluxed for 15 minutes after which time a solution of 1,3-diaminopropan-2-ol (0.054 g, 0.543 mmol) in *ca.* 10 mL of EtOH was added dropwise to the refluxing solution. The solution was refluxed for 2 hours. The colour of the solution was brown yellowish, but on standing the colour became green yellowish again. The solution was concentrated under vacuum to dryness, dissolved in methanol and left to evaporate slowly. After few days green crystals were formed, so they were filtered off and dissolved again in methanol. This green solution was left to crystallise

under diethylether diffusion Red crystals suitable for X-ray analysis were obtained within few days (Yield: 0.295 g; 87%)

**CHN Calc:** C52.62%; H6.26%; N4.46% for  $[\text{Ni}_2(\text{H}_4\text{L1})(\text{MeOH})_2](\text{ClO}_4)_2 \cdot \text{MeOH}$

**Found:** C 52.66%; H 6.22%; N 4.09%

**LSI-MS m/z (%) (calc.):** 901 (15) ( $[\text{Ni}(\text{H}_4\text{L1})+\text{e}]^+$ , 901); 941 (13)

( $[\text{Ni}(\text{H}_4\text{L1})(\text{H}_2\text{O})+\text{Na}]^+$ , 942); 957 (100) ( $[\text{Ni}_2(\text{H}_4\text{L1})-$

$\text{H}]^+$ , 959); 1059 (5) ( $[\text{Ni}_2(\text{H}_4\text{L1})(\text{ClO}_4)]^+$ , 1059).

**IR (KBr,  $\text{cm}^{-1}$ ):** 3425 (b, m,  $\nu_{\text{O-H}}$ ); 2960 (m,  $\nu_{\text{C-CH}_3}$ ), 1633 (s,  $\nu_{\text{C=N}}$ ); 1565 (w,  $\nu_{\text{C-O}}$ );

1475 (m); 1439 (m); 1394 (m), 1365 (m); 1225 (m); 1108

(b, s,  $\nu_3(\text{ClO}_4^-)$ ); 624 (m,  $\nu_4(\text{ClO}_4^-)$ ).

#### **E.2.2.13. $[\text{Mn}_2(\text{H}_2\text{L1})(\text{Cl})_2(\text{EtOH})_2] \cdot 6\text{H}_2\text{O}$ (2.13)**

$\text{MnCl}_2 \cdot 4\text{H}_2\text{O}$  (0.107 g, 0.543 mmol) and DHTMB (0.2 g, 0.543 mmol) were dissolved in hot EtOH (*ca.* 100 mL) The solution was refluxed for 10-15 minutes after which time a solution of 1,3-diaminopropan-2-ol (0.052 g, 0.543 mmol) in *ca.* 10 mL of MeOH was added dropwise to the refluxing solution The solution colour changed from pale yellow to yellow-brownish. The reaction mixture was refluxing for 2 hours. The dark brown solution was then cooled down and concentrated under vacuum. A yellow solid precipitated so it was filtered off (Yield: 0.173 g; 53%) This solid was dissolved in a mixture of dmf and dmsO and  $\text{Et}_2\text{O}$  was allowed to diffuse into the solution. Brown crystals suitable for X-ray studies were isolated within a week.

**CHN Calc.:** C 55.03%; H 7.26%; N 4.59% for  $[\text{Mn}_2(\text{H}_2\text{L1})(\text{Cl})_2(\text{EtOH})_2] \cdot 6\text{H}_2\text{O}$

**Found:** C 54.99%; H 7.39%; N 4.94%

**LSI-MS m/z (%) (calc.):** 951 (100) ( $[\text{Mn}_2(\text{H}_2\text{L1})+\text{e}]^+$ , 951); 973 (24)

( $[\text{Mn}_2(\text{H}_2\text{L1})+\text{Na}]^+$ , 973), 987 (17) ( $[\text{Mn}_2(\text{H}_2\text{L1})\text{Cl}+\text{H}]^+$ , 987); 997 (27)

( $[\text{Mn}_2(\text{H}_2\text{L1})(\text{EtOH})+\text{e}]^+$ , 997); 1011 (33) ( $[\text{Mn}_2(\text{H}_2\text{L1})\text{Cl}+\text{Na}]^+$ ,

1009), 1119 (28)  $[\text{Mn}_2(\text{H}_2\text{L1})(\text{Cl})_2(\text{dmsO})(\text{H}_2\text{O})+\text{H}]^+$ , 1119).

IR (KBr,  $\text{cm}^{-1}$ ): 3422 (b, s,  $\nu_{\text{O-H}}$ ); 2958 (m,  $\nu_{\text{C-CH}_3}$ ), 1617 (s,  $\nu_{\text{C=N}}$ ); 1550 (m,  $\nu_{\text{C-O}}$ );  
1439 (m); 1364 (w); 1309 (w); 1267 (m).

#### E.2.2.14. $[\text{Co}_2(\text{H}_2\text{L1})(\text{Cl})_2(\text{H}_2\text{O})_2]$ (2.14)

$\text{CoCl}_2 \cdot 6\text{H}_2\text{O}$  (0.129 g, 0.543 mmol) and DHTMB (0.2 g, 0.543 mmol) were dissolved in ethanol (*ca.* 80 mL). The solution was refluxed for 15 minutes, after which time a solution of 1,3-diaminopropan-2-ol (0.054 g, 0.543 mmol) in *ca.* 10 mL of ethanol was added dropwise to the refluxing solution. The solution colour changed from bright blue to emerald green and became a bit cloudy. The reaction mixture was allowed to reflux for 3 hours. A small amount of impurities was filtered off and the solvent was removed. The dark green brownish residue was washed with dichloromethane (Yield: 0.21 g; 73%).

CHN Calc : C 58.59%; H 6.43%; N 5.25% for  $[\text{Co}_2(\text{H}_2\text{L1})(\text{Cl})_2(\text{H}_2\text{O})_2]$

Found: C 58.63%; H 6.41%; N 5.08%

LSI-MS  $m/z$  (%) (calc.): 959 (45) ( $[\text{Co}_2(\text{H}_2\text{L1})+\text{e}]^+$ , 959), 995 (100)  
( $[\text{Co}_2(\text{H}_2\text{L1})(\text{Cl})]^+$ , 994); 1039 (5)  
( $[\text{Co}_2(\text{H}_2\text{L1})(\text{Cl})(\text{H}_2\text{O})_2]^+$ , 1030).

IR (KBr,  $\text{cm}^{-1}$ ): 3366 (b, m,  $\nu_{\text{O-H}}$ ), 2955 (s,  $\nu_{\text{C-CH}_3}$ ); 1630 (s,  $\nu_{\text{C=N}}$ ); 1560 (w);  
1477(m); 1438 (m); 1392 (m); 1363 (m); 1278 (w); 1222 (m)

#### E.2.2.15. $[\text{Fe}_2(\text{H}_2\text{L1})(\text{Cl})_2(\text{H}_2\text{O})_2]$ (2.15)

$\text{FeCl}_2 \cdot 4\text{H}_2\text{O}$  (0.108 g, 0.543 mmol) and DHTMB (0.2 g, 0.543 mmol) were dissolved in hot ethanol (100 mL). The solution was refluxed for 10-15 minutes after which time a solution of 1,3-diaminopropan-2-ol (0.052 g, 0.543 mmol) in *ca.* 10 mL of ethanol was added dropwise to the refluxing solution. The solution colour changed from black to black-reddish. The reaction mixture was left under reflux for 3 hours. A very small amount of impurities was filtered off. The solution was washed with acetonitrile and water and concentrated under vacuum to dryness (Yield: 0.18 g; 63%).

**CHN Calc.:** C 58.94%; H 6.47%; N 5.29% for  $[\text{Fe}_2(\text{H}_2\text{L1})(\text{Cl})_2(\text{H}_2\text{O})_2]$

**Found:** C 58.97%; H 6.10%; N 5.23%

**ESI-MS m/z (%) (calc.):** 476 (20) ( $[\text{Fe}_2(\text{H}_2\text{L1})]^{2+}$ , 952), 492 (20) ( $[\text{Fe}_2(\text{H}_2\text{L1})(\text{MeOH})]^{2+}$ , 984); 951 (100) ( $[\text{Fe}_2(\text{H}_2\text{L1})\text{-H}]^+$ , 951); 987 (60) ( $[\text{Fe}_2(\text{H}_2\text{L1})(\text{Cl})\text{-H}]^+$ , 987).  
(relative abundance given for cone voltage = 90V)

**IR (KBr,  $\text{cm}^{-1}$ ):** 3423 (b, s,  $\nu_{\text{O-H}}$ ); 2956 (m,  $\nu_{\text{C-CH}_3}$ ); 1618 (s,  $\nu_{\text{C=N}}$ ), 1549 (m,  $\nu_{\text{C=O}}$ ); 1442 (m); 1391 (w); 1363 (w); 1316 (w); 1268 (m); 1218 (m).

#### **E.2.2.16. $[\text{Mn}_2(\text{H}_2\text{L1})(\text{AcO})_2(\text{EtOH})]$ (2.16)**

$\text{Mn}(\text{AcO})_3 \cdot 2\text{H}_2\text{O}$  (0.144 g, 0.543 mmol) and DHTMB (0.2 g, 0.543 mmol) were dissolved in ethanol (80 mL). The solution was refluxed for 30 minutes after which time a solution of 1,3-diaminopropan-2-ol (0.054 g, 0.543 mmol) in *ca.* 10 mL of ethanol was added dropwise to the refluxing solution. The solution had a dark brown colour. The reaction mixture was allowed to reflux for 1 hour and after it was left to cool down. On standing, the solution turned dark green brownish. A small amount of impurities was filtered off and the solvent was removed. The dark green brownish residue was washed with DCM (Yield: 0.213 g; 70%).

**CHN Calc.:** C 62.47%, H 6.87%, N 5.02% for  $[\text{Mn}_2(\text{H}_2\text{L1})(\text{AcO})_2(\text{EtOH})]$

**Found:** C 62.96%, H 6.89%, N 4.28%

**ESI-MS m/z (%) (calc.):** 475 (100) ( $[\text{Mn}_2(\text{H}_2\text{L1})]^{2+}$ , 950); 495 (80) ( $[\text{Mn}(\text{H}_2\text{L1})(\text{EtOH})_2 + 2\text{H}]^{2+}$ , 990); 516 (10) ( $[\text{Mn}_2(\text{H}_2\text{L1})(\text{AcO}) + \text{Na}]^{2+}$ , 1033).  
(Note: the relative abundance is given for cone voltage = 20V)

**IR (KBr,  $\text{cm}^{-1}$ ):** 3422 (b, w,  $\nu_{\text{O-H}}$ ); 2956 (m,  $\nu_{\text{C-CH}_3}$ ); 1618 (s,  $\nu_{\text{C=N}}$ ); 1550 (m,  $\nu_{\text{C=O}}$ ), 1439 (m,  $\nu_{\text{COO}^-}$ ); 1268 (m)



**E.2.2.17.  $[\text{Mn}_2(\text{H}_2\text{L1})(\text{AcO})_2(\text{H}_2\text{O})_3]$** 

Same manganese complex was found for the synthesis with Mn(II) acetate as with Mn(III) acetate:  $\text{Mn}(\text{AcO})_2 \cdot 4\text{H}_2\text{O}$  (0.132 g, 0.543 mmol) and DHTMB (0.2 g, 0.543 mmol) were dissolved in ethanol (*ca.* 80 mL).  $\text{N}_2$  was bubbled through the mixture and it was refluxed for 15 minutes after which time a solution of 1,3-diaminopropan-2-ol (0.054 g, 0.543 mmol) in *ca.* 10 mL of degassed ethanol was added dropwise to the bright yellow refluxing solution. The solution became a little bit darker. The reaction mixture was allowed to reflux for 1 hour under nitrogen. It seems that the compound oxidised because the solution turned dark green brownish when the reaction was stopped. The solution was concentrated under vacuum to dryness. The dark green brownish residue was washed with dichloromethane. A small amount of solid was filtered off (Yield: 0.165 g; 54%)

**CHN Calc.:** C 59.88%, H 6.82%, N 4.98% for  $[\text{Mn}_2(\text{H}_2\text{L1})(\text{AcO})_2(\text{H}_2\text{O})_3]$

**Found:** C 59.56%, H 6.75%, N 4.98%

**ESI-MS  $m/z$  (%) (calc):** 475 (100) ( $[\text{Mn}_2(\text{H}_2\text{L1})]^{2+}$ , 950); 495 (80)

( $\text{Mn}(\text{H}_2\text{L1})(\text{EtOH})_2 + 2\text{H}^+$ , 990); 516 (10) ( $[\text{Mn}_2(\text{H}_2\text{L1})(\text{AcO}) + \text{Na}]^{2+}$ , 1033).

(Note: the relative abundance is given for cone voltage = 20V)

**IR (KBr,  $\text{cm}^{-1}$ ):** 3384 (b, m,  $\nu_{\text{O-H}}$ ), 2955 (s,  $\nu_{\text{C-CH}_3}$ ); 1618 (s,  $\nu_{\text{C=N}}$ ); 1551 (s,  $\nu_{\text{C=O}}$ ); 1438 (m,  $\nu_{\text{COO}^-}$ ); 1268 (m)

**E.2.2.18.  $[\text{Mn}_2(\text{H}_2\text{L1})(\text{OH})(\text{EtOH})_2](\text{CF}_3\text{SO}_3)$  (2.17)**

$\text{Mn}(\text{SO}_3\text{CF}_3)_2$  (0.1 g, 0.325 mmol) and DHTMB (0.12 g, 0.325 mmol) were dissolved in ethanol (*ca.* 80 mL). The mixture was refluxed for 15 minutes after which time a solution of 1,3-diaminopropan-2-ol (0.003 g, 0.325 mmol) in *ca.* 10 mL of ethanol was added dropwise to the pale yellow refluxing solution. The solution became brown yellowish. The reaction mixture was allowed to reflux for 1 hour and after it was left to cool. On standing, the solution turned dark green brownish. A small amount of impurities was filtered off and the solvent was removed. The dark green residue was washed with DCM (Yield: 0.198 g; 60%).

CHN Calc.: C 56.62%, H 6.42%, N 4.63% for  $[\text{Mn}_2(\text{H}_2\text{L1})(\text{OH})(\text{EtOH})_2](\text{CF}_3\text{SO}_3)$

Found: C 56.84%, H 6.26%, N 4.17%

ESI-MS  $m/z$  (%) (calc.): 475 (100) ( $[\text{Mn}_2(\text{H}_2\text{L1})]^{2+}$ , 950); 495 (25)

( $[\text{Mn}(\text{H}_2\text{L1})(\text{EtOH})_2+2\text{H}]^{2+}$ , 990); 1099 (5)  $[\text{Mn}_2(\text{H}_2\text{L1})(\text{CF}_3\text{SO}_3)-\text{H}]^+$ , 1099).

(Note: the relative abundance is given for cone voltage = 20V)

IR (KBr,  $\text{cm}^{-1}$ ): 3432 (b, s,  $\nu_{\text{O-H}}$ ); 2960 (m,  $\nu_{\text{C-CH}_3}$ ), 1616 (s,  $\nu_{\text{C=N}}$ ); 1552 (m,  $\nu_{\text{C-O}}$ );

1441 (m); 1396 (w), 1365 (w); 1269 (s,  $\nu_{\text{SO}_3^-}$ ); 1172 (w); 1031

(m,  $\nu_{\text{C-F}}$ ); 640 (w,  $\nu_{\text{C-F}}$ ).

#### E.2.2.19. $[\text{Co}_2(\text{HL1})](\text{ClO}_4)$ (2.18)

0.1 g (0.074 mmol) of the previous dinuclear Co(II) complex  $[\text{Co}_2(\text{HL1})(\text{H}_2\text{O})](\text{ClO}_4)_2 \cdot 3\text{EtOH} \cdot 3\text{H}_2\text{O}$  were dissolved in *ca.* 10 mL of ethanol and oxidised with 4 drops of  $\text{H}_2\text{O}_2$  (50%). The solution colour changed from dark yellow (Co(II) ions) to dark brown (Co(III) ions). It was evaporated to dryness and washed with DCM to eliminate impurities (Yield. 0.074 g; 95%)

CHN Calc.: C 59.07%; H 6.01%; N 5.29% for  $[\text{Co}_2(\text{HL1})](\text{ClO}_4)$

Found: C 59.27%, H 6.38%; N 4.65%

LSI-MS  $m/z$  (calc.): 849 (40) ( $[(\text{H}_6\text{L1})+\text{H}]^+$ , 846), 959 (100) ( $[\text{Co}_2(\text{H}_2\text{L1})+\text{e}]^+$ ,

959); 981 (55)  $[\text{Co}_2(\text{HL1})+\text{Na}]^+$ , 981).

IR (KBr,  $\text{cm}^{-1}$ ): 3420 (b, s,  $\nu_{\text{O-H}}$ ); 2964 (m,  $\nu_{\text{C-CH}_3}$ ); 1637 (b, s,  $\nu_{\text{C=N}}$ ), 1448 (w);

1394 (w); 1366 (w); 1089 (b, s,  $\nu_{3(\text{ClO}_4^-)}$ ); 626 (m,  $\nu_{4(\text{ClO}_4^-)}$ )

#### E.2.2.20. $[\text{Cu}_2(\text{H}_2\text{L1})] \cdot \text{H}_2\text{O}$ (2.19)

$\text{CuCl}_2 \cdot 2\text{H}_2\text{O}$  (0.08 g, 0.543 mmol),  $\text{CaCl}_2$  (0.03 g, 0.27 mmol) and DHTMB (0.2 g, 0.543 mmol) were dissolved in hot EtOH (*ca.* 80 mL). The solution was refluxed for 15 minutes after which time a solution of 1,3-diaminopropan-2-ol (0.052 g, 0.543 mmol) in *ca.* 10 mL of EtOH was added dropwise to the refluxing solution. The colour changed from light bright green to green and the solution

became cloudy. After 10 minutes it was not cloudy anymore and became darker green. After 15 minutes few drops of  $\text{Et}_3\text{N}$  were added to the mixture, which turned brown. The reaction mixture was left under reflux for 24 hours. A dark brown solid precipitated, so it was filtered off (Yield: 0.094 g; 35%). Brown crystals of  $[\text{Cu}_2(\text{H}_2\text{L1})](\text{Et}_2\text{O})\cdot(\text{dmsO})$  suitable for X-ray analysis were grown by diffusing  $\text{Et}_2\text{O}$  in a mixture of DMSO, DMF and DCM. The remaining brown solution analysed as the heteronuclear complex  $[\text{Cu}_2\text{Ca}(\text{HL1})]\cdot\text{Cl}$  (4.4), described in the heteronuclear complexes section (synthesis E 4.3)

**CHN Calc.:** C 63.33%; H 6.74%; N 5.68% for  $[\text{Cu}_2(\text{H}_2\text{L1})]\cdot\text{H}_2\text{O}$

**Found:** C 63.37%; H 6.55%; N 5.40%

**LSI-MS  $m/z$  (%) (calc.):** 845 (25) ( $[(\text{H}_6\text{L1})-\text{e}]^+$ , 845); 906 (15) ( $[\text{Cu}(\text{H}_4\text{L1})-\text{e}]^+$ , 906); 969 (13) ( $[\text{Cu}_2(\text{H}_2\text{L1})+\text{H}]^+$ , 969); 989 (22) ( $[\text{Cu}_2(\text{H}_2\text{L1})(\text{H}_2\text{O})+\text{H}]^+$ , 989); 1005 (7) ( $[\text{Cu}_2(\text{H}_4\text{L1})\text{Cl}+2\text{H}]^+$ , 1005).

**IR (KBr,  $\text{cm}^{-1}$ ):** 3356 (b, m,  $\nu_{\text{O-H}}$ ); 2924 (s,  $\nu_{\text{C-CH}_3}$ ); 1618 (s,  $\nu_{\text{C=N}}$ ), 1541 (s); 1440 (s); 1398 (m); 1362 (m); 1263 (m); 1254 (m); 1216 (m)

#### E.2.2.21. $[\text{Ni}_2(\text{H}_2\text{L1})]\cdot 3\text{H}_2\text{O}$ (2.20)

$\text{Ni}(\text{NO}_3)_2\cdot 6\text{H}_2\text{O}$  (0.158 g, 0.543 mmol),  $\text{Ca}(\text{NO}_3)_2\cdot 4\text{H}_2\text{O}$  (0.064 g, 0.27 mmol) and DHTMB (0.2 g, 0.543 mmol) were dissolved in hot EtOH (*ca.* 80 mL). The solution was refluxed for 15 minutes after which time a solution of 1,3-diaminopropan-2-ol (0.052 g, 0.543 mmol) in *ca.* 10 mL of EtOH was added dropwise to the refluxing solution. The colour changed from lime green yellowish to dark lime green. After 15 minutes few drops of  $\text{Et}_3\text{N}$  were added to the mixture, which turned brown-orange. The reaction mixture was left under reflux for 24 hours. A dark brown solid precipitated, so it was filtered off (Yield: 0.08 g; 29%). The remaining brown solution was analysed as the heteronuclear complex  $[\text{Ni}_2\text{Ca}(\text{HL1})(\text{EtOH})]\cdot\text{NO}_3$  (4.5) described in the heteronuclear complexes section (synthesis E.4.4)

**CHN Calc.:** C 61.68%; H 6.97%, N 5.53% for  $[\text{Ni}_2(\text{H}_2\text{L1})]\cdot 3\text{H}_2\text{O}$

**Found:** C 61.78%; H 6.59%; N 5.62%

**LSI-MS m/z (%) (calc.):** 942 (5) ( $[\text{Ni}(\text{H}_4\text{L1})(\text{H}_2\text{O})+\text{Na}]^+$ , 942); 959 (30)

( $[\text{Ni}_2(\text{H}_2\text{L1})-\text{H}]^+$ , 959); 1001 (8) ( $[\text{Ni}_2(\text{H}_2\text{L1})(\text{H}_2\text{O})+\text{Na}]^+$ , 1001).

**IR (KBr,  $\text{cm}^{-1}$ ):** 3406 (b, m,  $\nu_{\text{O-H}}$ ), 2952 (m,  $\nu_{\text{C-CH}_3}$ ); 1618 (s,  $\nu_{\text{C=N}}$ ); 1544 (m),

1449 (m); 1391 (w), 1363 (w); 1328 (w), 1269 (w), 1220 (w).

### **E.3. Polynuclear complexes of $\text{H}_6\text{L1}$**

#### **E.3.1. $[\text{Cu}_4(\text{H}_2\text{L1})(\text{OH})_2(\text{H}_2\text{O})_4](\text{NO}_3)_2$ (3.1)**

0.16 g (0.543 mmol) of  $\text{Cu}(\text{NO}_3)_2\cdot 6\text{H}_2\text{O}$  and 0.2 g (0.543 mmol) of DHTMB were dissolved in *ca.* 80 mL of ethanol (olive green colour). This mixture was heated up to reflux during 10 minutes, after which time a solution of 1,3-diaminopropan-2-ol (0.052 g, 0.543 mmol) in *ca.* 20 mL of methanol was added dropwise to the refluxing solution. The colour turned emerald green and after 10 minutes started to get darker, becoming dark green brownish. The reaction mixture was refluxing for 1 h. The solution was cooled, filtered and evaporated to dryness. The residue was then dissolved in dichloromethane, filtered to eliminate impurities and evaporated again before being dissolved in ethanol and left to evaporate slowly. A green product precipitated, so it was filtered off (Yield 0.28 g; 79%). A mixture of emerald green and brown crystals, suitable for X-ray study, was obtained by slow diffusion of diethylether into a dimethylformamide solution in a few days. It was possible to separate these by their different solubility. The brown crystals were soluble in ethanol, but not the green ones. Emerald green crystals were also obtained by slow evaporation of a mixture of ethanol, benzene and petroleum ether.

CHN Calc: C 47.12%; H 5.63%; N 6.34% for  $[\text{Cu}_4(\text{H}_2\text{L1})(\text{OH})_2(\text{H}_2\text{O})_4](\text{NO}_3)_2$

Found: C 47.10%; H 5.49%; N 6.34% (green solid, **3.1**)

Calc: C 46.68%; H 5.95%; N 6.05%

for  $[\text{Cu}_4(\text{H}_2\text{L1})(\text{OH})_2(\text{H}_2\text{O})(\text{EtOH})](\text{NO}_3)_2 \cdot 2\text{EtOH} \cdot \text{H}_2\text{O}$

Found: C 46.70%; H 5.84%; N 6.08% (green crystals, **3.1b**)

Calc: C 52.90%; H 6.05%; N 7.85% for  $[\text{Cu}_3(\text{H}_2\text{L1})(\text{NO}_3)](\text{NO}_3)(\text{dmf}) \cdot \text{H}_2\text{O}$

Found: C 52.92%; H 6.37%; N 7.90% (brown crystals, **3.1a**)

LSI-MS  $m/z$  (%) (calc) 1032 (37) ( $[\text{Cu}_3(\text{H}_2\text{L1}) + e]^{+}$ , 1032); 1091 (100)

( $[\text{Cu}_4(\text{L1}) + e]^{+}$ , 1093); 1111 (82) ( $[\text{Cu}_4(\text{L1})(\text{OH}) + \text{H}]^{+}$ ,

1111); 1127 (83) ( $[\text{Cu}_4(\text{H}_2\text{L1})(\text{OH})_2 - \text{H}]^{+}$ , 1128); 1156 (60)

( $[\text{Cu}_4(\text{H}_2\text{L1})(\text{OH})(\text{EtO}) - \text{H}]^{+}$ , 1156)

IR (KBr,  $\text{cm}^{-1}$ ): 3385 (b, m,  $\nu_{\text{O-H}}$ ); 2952 (m,  $\nu_{\text{C-CH}_3}$ ); 1647 (m,  $\nu_{\text{C=N}}$ ), 1475 (m);

1384 (s,  $\nu_{\text{freeNO}_3^-}$ ); 1221 (w); 1064 (w); 992 (w); 825 (w).

### E.3.2. $[\text{Cu}_3(\text{H}_2\text{L1})(\text{NO}_3)](\text{NO}_3)(\text{dmf})_3 \cdot \text{H}_2\text{O}$ (**3.2c**)

0.286 g (0.968 mmol) of  $\text{Cu}(\text{NO}_3)_2 \cdot 6\text{H}_2\text{O}$  were dissolved in hot ethanol (*ca.* 35 mL). 0.238 g (0.646 mmol) of DHTMB was also dissolved by slightly heating in ethanol (*ca.* 35 mL). The solutions were mixed (olive green colour) and refluxed during 10 minutes, after which time a solution of 1,3-diaminopropan-2-ol (0.062 g, 0.646 mmol) in *ca.* 20 mL of methanol was added dropwise to the refluxing solution. The colour turned to emerald green. The reaction mixture was left under reflux for 18 hours. During that time, the colour became brown. The solution was filtered and concentrated under vacuum. Brown and emerald green crystals were obtained by slow evaporation of the ethanol solution in a few days. These crystals were washed with chloroform to separate them. The green crystals were soluble, but not the brown ones. The green solution was evaporated to dryness (Yield: 0.13 g; 34%). Brown crystals suitable for X-ray study were obtained by slow diffusion of diethylether into an ethanol solution of the brown product and also by slow diffusion of diethylether into an ethanol/dmf solution of the brown product (Yield: 0.21 g; 51%)



**CHN Calc.:** C 46.80%; H 5.21%; N 7.35% for  $[\text{Cu}_4(\text{HL1})(\text{NO}_3)_3(\text{H}_2\text{O})_3]$

**Found:** C 46.63%; H 4.96%; N 7.63% (green solid, **3.2a**)

**Calc.:** C 43.43%, H 4.79%; N 6.56% for  $[\text{Cu}_3(\text{H}_3\text{L1})](\text{NO}_3)_3(\text{CHCl}_3)_2 \cdot 2\text{H}_2\text{O}$

**Found:** C 43.26%; H 4.83%, N 6.62% (brown solid, **3.2b**)

**Calc:** C 52.59%; H 6.30%; N 9.05% for  $[\text{Cu}_3(\text{H}_2\text{L1})(\text{NO}_3)](\text{NO}_3)(\text{dmf})_3 \cdot \text{H}_2\text{O}$

**Found:** C 52.58%; H 6.22%; N 8.75% (crystals in (EtOH/dmf)/Et<sub>2</sub>O, **3.2c**)

**LSI-MS of 3.2c** *m/z* (%) (calc.): 969 (95) ( $[\text{Cu}_2(\text{H}_2\text{L1})+\text{H}]^+$ , 969); 1029 (97) ( $[\text{Cu}_3(\text{HL1})-\text{H}]^+$ , 1029); 1089 (100) ( $[\text{Cu}_3(\text{H}_2\text{L1})(\text{OH})_2+\text{Na}]^+$ , 1088); 1094 (75) ( $[\text{Cu}_3(\text{H}_2\text{L1})(\text{NO}_3)+\text{H}]^+$ , 1094); 1136 (25) ( $[\text{Cu}_3(\text{H}_2\text{L1})(\text{NO}_3)(\text{EtOH})-\text{H}]^+$ , 1138)

**IR (KBr, cm<sup>-1</sup>):** 3420 (b,m,ν<sub>O-H</sub>); 2953 (m,ν<sub>C-CH<sub>3</sub></sub>); 1625 (m,ν<sub>C=N</sub>); 1563 (w,ν<sub>C-O</sub>); 1454 (w), 1383 (s, ν<sub>NO<sub>3</sub></sub>); 1280 (w), 1218 (w); 750 (w).

### **E.3.3. $[\text{Cu}_4(\text{H}_3\text{L1})(\text{OH})_2(\text{H}_2\text{O})_4](\text{NO}_3)_3$ (3.3)**

0.321 g (1.086 mmol) of  $\text{Cu}(\text{NO}_3)_2 \cdot 6\text{H}_2\text{O}$  and 0.2 g (0.543 mmol) of DHTMB were heated to reflux in ca. 80 mL of ethanol (olive green colour) on a steam bath during 10 minutes, after which time a solution of 1,3-diaminopropan-2-ol (0.052 g, 0.543 mmol) in ca. 20 mL of methanol was added dropwise to the refluxing solution. The resulting emerald green solution was left under reflux for 2 hours. After which the emerald green solid that precipitated was filtered from the cold solution. When the compound was dissolved in DMF the colour changed to dark brown within a week. Recrystallisation by slow diffusion of diethylether into the DMF solution of this complex gave brown crystals of the trinuclear complex  $[\text{Cu}_3(\text{H}_2\text{L1})](\text{NO}_3)_2(\text{dmf})_3$  in a few days (Yield: 0.15 g; 40%)

**CHN Calc.:** C 44.98%; H 5.45%; N 7.06% for  $[\text{Cu}_4(\text{H}_3\text{L1})(\text{OH})_2(\text{H}_2\text{O})_4](\text{NO}_3)_3$

**Found:** C 44.90%; H 4.87%; N 7.25% (green solid, **3.3**)

**Calc.:** C 52.03%; H 6.40%; N 9.40% for  $[\text{Cu}_3(\text{H}_2\text{L1})](\text{NO}_3)_2(\text{dmf})_3$

**Found.** C 52.15%; H 6.27%; N 9.38% (brown crystals, **3.3a**)

LSI-MS  $m/z$  (calc): 907 (25) ( $[\text{Cu}(\text{H}_3\text{L1})]^+$ , 907), 968 (100) ( $[\text{Cu}_2(\text{H}_2\text{L1})-\text{e}]^+$ , 968); 1031 (62) ( $[\text{Cu}_3(\text{L1})-\text{e}]^+$ , 1031); 1092 (17) ( $[\text{Cu}_3(\text{HL1})(\text{NO}_3)-\text{e}]^+$ , 1092); 1109 (25) ( $[\text{Cu}_4(\text{L1})(\text{OH})]^+$ , 1110); 1127 (40) ( $[\text{Cu}_4(\text{L1})(\text{OH})_2-\text{e}]^+$ , 1127); 1154 (15) ( $[\text{Cu}_4(\text{L1})(\text{NO}_3)]^+$ , 1155).

IR (KBr,  $\text{cm}^{-1}$ ): 3423 (b,m, $\nu_{\text{O-H}}$ ); 2955 (m, $\nu_{\text{C-CH}_3}$ ); 1674 (m, $\nu_{\text{C=O}}$ ); 1630 (m, $\nu_{\text{C=N}}$ ); 1570 (w,  $\nu_{\text{C=O}}$ ); 1459 (w); 1438 (w); 1384 (s,  $\nu_{\text{freeNO}_3^-}$ ); 1284 (w)

#### E.3.4. $[\text{Ni}_3(\text{HL1})(\text{NO}_3)] \cdot 6\text{H}_2\text{O}$ (3.4)

0.235 g (0.81 mmol) of  $\text{Ni}(\text{NO}_3)_2 \cdot 6\text{H}_2\text{O}$  and 0.2 g (0.543 mmol) of DHTMB were heated to reflux in *ca.* 80 mL of ethanol. The apple green solution was refluxed for 10-15 minutes after which time a solution of 1,3-diaminopropan-2-ol (0.052 g, 0.543 mmol) in *ca.* 10 mL of ethanol was added dropwise to the refluxing solution. The reaction mixture was allowed to reflux for 4 hours. The solution was then concentrated under vacuum and dissolved in dichloromethane (green brownish colour) to eliminate impurities. After that it was washed with water and rinsed with diethylether, yielding a green brownish solid (Yield: 0.29 g; 89%).

CHN Calc: C 52.65%; H 6.37%; N 5.90% for  $[\text{Ni}_3(\text{HL1})(\text{NO}_3)] \cdot 6\text{H}_2\text{O}$

Found: C 52.98%; H 6.16%; N 6.15%

LSI-MS  $m/z$  (%) (calc.): 901 (5) ( $[\text{Ni}(\text{H}_3\text{L1})-\text{H}]^+$ , 901); 957 (35) ( $[\text{Ni}_2(\text{H}_3\text{L1})-2\text{H}]^+$ , 957); 1164 (12) ( $[\text{Ni}_3(\text{H}_2\text{L1})(\text{NO}_3)_2+\text{Na}]^+$ , 1164).

IR (KBr,  $\text{cm}^{-1}$ ): 3426 (b, s,  $\nu_{\text{O-H}}$ ); 2956 (m, $\nu_{\text{C-CH}_3}$ ), 1638 (m, $\nu_{\text{C=N}}$ ); 1549 (w, $\nu_{\text{C=O}}$ ); 1460 (w); 1384 (m,  $\nu_{\text{NO}_3^-}$ ); 1364 (w), 1222 (w).

#### E.3.5. $[\text{Ni}_3(\text{L1})((\text{NH}_2)_2\text{CO})] \cdot 2\text{EtOH} \cdot 2\text{H}_2\text{O}$ (3.5)

0.185 g (0.543 mmol) of  $\text{Ni}(\text{BF}_4)_2 \cdot 6\text{H}_2\text{O}$ , 0.033 g (0.543 mmol) of urea ( $(\text{NH}_2)_2\text{CO}$ ) and 0.2 g (0.543 mmol) of DHTMB were dissolved in EtOH (*ca.* 80

mL). The solution (light green yellowish colour) was refluxed for 30 minutes after which time a solution of 1,3-diaminopropan-2-ol (0.054 g, 0.543 mmol) in *ca.* 10 mL of EtOH was added dropwise to the refluxing solution. The colour turned dark yellow brownish, it was allowed to reflux for 2 hours, after which it was filtered and concentrated under vacuum. Afterwards, it was dissolved in EtOH and left to evaporate slowly. After a few days a pale green solid (JNi1B) was filtered off, the mass spectrum revealed that there was no complex but metal salts. The dark brown liquid (JNi1A) was concentrated and left to evaporate slowly. The solid obtained was washed with DCM and water (Yield: 0.24 g; 74%)

CHN Calc.: C 56.89%, H 6.87%; N 6.98%  $[\text{Ni}_3(\text{L1})(\text{NH}_2)_2\text{CO}]\cdot 2\text{EtOH}\cdot 2\text{H}_2\text{O}$

Found: C 56.79%; H 6.87%; N 6.78%

ESI-MS *m/z* (%) (calc.). 479 (35)  $([\text{Ni}_2(\text{H}_4\text{L1})\text{-}2\text{H}]^{2+}$ , 958), 847 (5)  $([\text{H}_6\text{L1}+\text{H}]^+$ , 846); 957 (40)  $([\text{Ni}_2(\text{H}_3\text{L1})\text{-}2\text{H}]^+$ , 957); 1131 (5)  $([\text{Ni}_3(\text{H}_2\text{L1})(\text{NH}_2)_2\text{CO}](\text{OH})(\text{H}_2\text{O})_2]^+$ , 1131); 1165 (3)  $([\text{Ni}_3(\text{H}_2\text{L1})(\text{NH}_2)_2\text{CO}](\text{BF}_4)+\text{H}]^+$ , 1165)  
(Note: relative abundance given for cone voltage = 90V)

IR (KBr,  $\text{cm}^{-1}$ ): 3405 (b, m,  $\nu_{\text{O-H}}$ ); 2967 (m,  $\nu_{\text{C-CH}_3}$ ); 1660 (s, urea  $\nu_{\text{C=O}}$ ); 1616 (w,  $\nu_{\text{C=N}}$ ), 1456 (w), 1272 (m); 1218 (m); 739 (m); 711 (m).

### E.3.6. $[\text{Fe}_4(\text{L1})(\text{OH})_2(\text{EtO})_2](\text{NO}_3)_2\cdot\text{H}_2\text{O}$ (3.6)

$\text{Fe}(\text{NO}_3)_3\cdot 9\text{H}_2\text{O}$  (0.219 g, 0.543 mmol) and DHTMB (0.2 g, 0.543 mmol) were dissolved in hot ethanol (100 mL). The solution was refluxed for 10-15 minutes after which time a solution of 1,3-diaminopropan-2-ol (0.052 g, 0.543 mmol) in *ca.* 10 mL of ethanol was added dropwise to the refluxing solution. The reaction mixture was left under reflux for 4 hours. After that time it was left to slowly evaporate to dryness. The dark black residue was washed with DCM (Yield: 0.29 g; 84%).

CHN Calc: C 50.62%; H 5.77%; N 6.33% for  $[\text{Fe}_4(\text{L1})(\text{OH})_2(\text{EtO})_2](\text{NO}_3)_2 \cdot \text{H}_2\text{O}$

Found: C 50.52%; H 5.73%; N 6.31%

LSI-MS  $m/z$  (%) (calc): 932 (6) ( $[\text{Fe}(\text{H}_3\text{L1})(\text{MeOH})]^+$ , 932); 992 (4)

( $[\text{Fe}_2(\text{HL1})(\text{OH})+\text{Na}]^+$ , 992); 1064 (3) ( $[\text{Fe}_2(\text{H}_4\text{L1})(\text{NO}_3)(\text{EtO})+\text{e}]^+$ ,

1062); 1092 (2) ( $[\text{Fe}_2(\text{H}_2\text{L1})(\text{NO}_3)(\text{EtOH})(\text{MeO})]^+$ , 1092), 1299 (4)

( $[\text{Fe}_4(\text{L1})(\text{NO}_3)_2(\text{EtO})_2\text{Na}+2\text{e}]^+$ , 1299).

IR (KBr,  $\text{cm}^{-1}$ ): 3424 (b, m,  $\nu_{\text{O-H}}$ ); 2958 (s,  $\nu_{\text{C-CH}_3}$ ); 1623 (s,  $\nu_{\text{C=N}}$ ), 1543 (s,  $\nu_{\text{C=O}}$ ),

1443 and 1364 (m,  $\nu_{\text{coord.NO}_3^-}$ ); 1385 (m,  $\nu_{\text{freeNO}_3^-}$ ); 1270 (s).

### E.3.7. $[\text{Zn}_4(\text{H}_2\text{L1})(\text{EtO})_2(\text{EtOH})](\text{NO}_3)_2$ (3.7)

The complex was obtained from reaction of  $\text{Zn}(\text{NO}_3)_2 \cdot 6\text{H}_2\text{O}$  (0.323 g, 1.086 mmol) with DHTMB (0.2 g, 0.543 mmol), both were dissolved in ethanol (*ca.* 90 mL) and warmed. This mixture was refluxed for 15 minutes after which time a solution of 1,3-diaminopropan-2-ol (0.052 g, 0.543 mmol) in *ca.* 10 mL of ethanol was added dropwise to the refluxing solution. The solution colour changed from pale yellow to bright yellow. The reaction mixture was refluxed for 2 hours. The solution was then concentrated to half the volume and left to evaporate slowly to dryness. The solid obtained was washed with DCM and water (Yield: 0.28 g; 76%)

CHN Calc.: C 51.15%; H 6.15%; N 5.96% for  $[\text{Zn}_4(\text{H}_2\text{L1})(\text{EtO})_2(\text{EtOH})](\text{NO}_3)_2$

Found: C 51.76%; H 6.04%; N 6.11%

LSI-MS  $m/z$  (%) (calc): 969 (25) ( $[\text{Zn}_2(\text{H}_3\text{L1})-3\text{H}]^+$ , 969), 1033 (17)

( $[\text{Zn}_2(\text{H}_4\text{L1})(\text{NO}_3)-2\text{H}]^+$ , 1033); 1099 (10) ( $[\text{Zn}_4(\text{L1})+\text{e}]^+$ ,

1100); 1195 (11) ( $[\text{Zn}_4(\text{H}_2\text{L1})(\text{NO}_3)(\text{MeO})+\text{e}]^+$ , 1195),

1273 (10) ( $[\text{Zn}_4(\text{H}_2\text{L1})(\text{NO}_3)_2(\text{EtO})+2\text{H}]^+$ , 1273).

IR (KBr,  $\text{cm}^{-1}$ ): 3421 (b, m,  $\nu_{\text{O-H}}$ ); 2956 (m,  $\nu_{\text{C-CH}_3}$ ); 1637 (s,  $\nu_{\text{C=N}}$ ); 1545 (w,  $\nu_{\text{C=O}}$ ),

1458 and 1363 (m,  $\nu_{\text{coord.NO}_3^-}$ ); 1393 (m); 1219 (m).

**E.3.8. [Cu<sub>4</sub>(H<sub>2</sub>L1)(OH)<sub>2</sub>(EtOH)](ClO<sub>4</sub>)<sub>2</sub> (3.8)**

0.2 g (1.086 mmol) of Cu(ClO<sub>4</sub>)<sub>2</sub>·6H<sub>2</sub>O and 0.2 g (0.543 mmol) of DHTMB were heated to reflux in *ca.* 80 mL of ethanol (brown yellowish colour) during 10 minutes, after which time a solution of 1,3-diaminopropan-2-ol (0.052 g, 0.543 mmol) in *ca.* 20 mL of ethanol was added dropwise to the refluxing solution. The resulting green brownish solution was refluxed for 3 hours. The solution was evaporated to dryness and dissolved in dichloromethane. The emerald green solution was evaporated till dryness (Yield: 0.24 g; 64%)

CHN Calc.: C 47.20%; H 5.28%; N 4.08% for [Cu<sub>4</sub>(H<sub>2</sub>L1)(OH)<sub>2</sub>(EtOH)](ClO<sub>4</sub>)<sub>2</sub>

Found: C 47.30%; H 5.59%; N 4.26%

LSI-MS m/z (%) (calc.): 977 (14) ([Cu(H<sub>2</sub>L1)(H<sub>2</sub>O)<sub>4</sub>-2H]<sup>+</sup>, 977); 1031 (10) ([Cu<sub>3</sub>(H<sub>2</sub>L1)+e]<sup>+</sup>, 1031); 1130 (5) ([Cu<sub>4</sub>(H<sub>2</sub>L1)(OH)<sub>2</sub>+e]<sup>+</sup>, 1129); 1193 (5) ([Cu<sub>4</sub>(HL1)(ClO<sub>4</sub>)+e]<sup>+</sup>, 1193); 1337 (10) ([Cu<sub>4</sub>(H<sub>2</sub>L1)(ClO<sub>4</sub>)<sub>2</sub>(EtO)-2H]<sup>+</sup>, 1337)

IR (KBr, cm<sup>-1</sup>): 3448 (b, s, ν<sub>O-H</sub>); 2958 (m, ν<sub>C-CH<sub>3</sub></sub>), 1646 (s, ν<sub>C=N</sub>), 1560 (w, ν<sub>C-O</sub>), 1458 (m); 1394 (w); 1364 (m); 1270 (m); 1222 (m); 1104 (b, s, ν<sub>3(ClO<sub>4</sub>-)</sub>); 623 (m, ν<sub>4(ClO<sub>4</sub>-)</sub>).

**E.3.9. [Fe<sub>4</sub>(L1)(OH)<sub>2</sub>(EtO)<sub>2</sub>](ClO<sub>4</sub>)<sub>2</sub>·4EtOH (3.9)**

Fe(ClO<sub>4</sub>)<sub>2</sub>·6H<sub>2</sub>O (0.197 g, 0.543 mmol) and DHTMB (0.2 g, 0.543 mmol) were dissolved in ethanol (100 mL). The solution was refluxed for 10-15 minutes after which time a solution of 1,3-diaminopropan-2-ol (0.052 g, 0.543 mmol) in *ca.* 10 mL of ethanol was added dropwise to the refluxing solution. The reaction mixture was left under reflux for 4 hours. After that time the solution was left to evaporate to dryness. The black residue was washed with dichloromethane (Yield: 0.34 g, 83%).



CHN Calc.: C 48.97%; H 6.29%; N 3.57% for  $[\text{Fe}_4(\text{L1})(\text{OH})_2(\text{EtO})_2](\text{ClO}_4)_2 \cdot 4\text{EtOH}$

Found: C 58.09%; H 6.27%; N 3.05%

LSI-MS  $m/z$  (%) (calc.): 897 (17) ( $[\text{Fe}(\text{H}_4\text{L1})-\text{H}]^+$ , 897), 940 (15)

( $[\text{Fe}(\text{HL1})(\text{H}_2\text{O})+\text{Na}]^+$ , 940); 951 (15) ( $[\text{Fe}_2(\text{H}_2\text{L1})-\text{H}]^+$ , 951), 994 (14)

( $[\text{Fe}_2(\text{L1})(\text{H}_2\text{O})\text{Na}+\text{H}]^+$ , 994), 1266 (6) ( $[\text{Fe}_4(\text{L1})(\text{ClO}_4)(\text{OH})_4(\text{H}_2\text{O})_2]^+$ ,

1266); 1373 (5) ( $[\text{Fe}_4(\text{L1})(\text{ClO}_4)_2(\text{OH})_3(\text{EtOH})(\text{H}_2\text{O})]^+$ , 1375).

IR (KBr,  $\text{cm}^{-1}$ ): 3427 (b,s, $\nu_{\text{O-H}}$ ); 2956 (m, $\nu_{\text{C-CH}_3}$ ); 1619 (s, $\nu_{\text{C=N}}$ ); 1549 (m, $\nu_{\text{C=O}}$ );

1444 (m); 1394 (w); 1364 (w); 1319 (w); 1269 (m); 1221 (m);

1107 (b, s,  $\nu_3(\text{ClO}_4^-)$ ); 624 (m,  $\nu_4(\text{ClO}_4^-)$ )

### E.3.10. $[\text{Ni}_4(\text{H}_2\text{L1})(\text{OH})_2(\text{H}_2\text{O})](\text{ClO}_4)_2$ (3.10)

0.397 g (1.086 mmol) of  $\text{Ni}(\text{ClO}_4)_2 \cdot 6\text{H}_2\text{O}$  and 0.2 g (0.543 mmol) of DHTMB were heated to reflux in *ca.* 80 mL of ethanol (light green yellowish colour) on a steam bath during 10 minutes, after which time a solution of 1,3-diaminopropan-2-ol (0.052 g, 0.543 mmol) in *ca.* 20 mL of methanol was added dropwise to the refluxing solution. The colour turned light brown yellowish. After this, 0.075 mL (0.543 mmol) of  $\text{Et}_3\text{N}$  was added dropwise to the mixture. The solution was refluxed for 2 hours, after which it was filtered and concentrated under vacuum to dryness. The solid was dissolved in dichloromethane, filtered to eliminate impurities and concentrated to dryness under vacuum again (Yield: 0.27 g, 75%)

CHN Calc.: C 47.07%; H 5.16%; N 4.22% for  $[\text{Ni}_4(\text{H}_2\text{L1})(\text{OH})_2(\text{H}_2\text{O})](\text{ClO}_4)_2$

Found: C 47.02%; H 5.98%; N 4.61%

LSI-MS  $m/z$  (%) (calc.): 1239 (23) ( $[\text{Ni}_4(\text{H}_2\text{L1})(\text{ClO}_4)(\text{EtO})(\text{OH})+2\text{H}]^+$ , 1239);

1256 (90) ( $[\text{Ni}_4(\text{H}_2\text{L1})(\text{EtO})_3(\text{EtOH})-\text{H}]^+$ , 1256); 1298

(12) ( $[\text{Ni}_4(\text{H}_2\text{L1})(\text{ClO}_4)(\text{EtOH})_2(\text{OH})_2-\text{H}]^+$ , 1300)

IR (KBr,  $\text{cm}^{-1}$ ): 3447 (b, s,  $\nu_{\text{O-H}}$ ); 2939 (m,  $\nu_{\text{C-CH}_3}$ ), 2678 (s); 1628 (s,  $\nu_{\text{C=N}}$ ); 1543

(w,  $\nu_{\text{C=O}}$ ); 1144, 1107 and 1090 (b, s,  $\nu_3(\text{ClO}_4^-)$ ); 626 (m,  $\nu_4(\text{ClO}_4^-)$ ).

**E.3.11.  $[\text{Cu}_4(\text{H}_2\text{L1})(\text{OH})_2(\text{EtOH})](\text{Cl})_2$  (3.11)**

0.146 g (1.086 mmol) of anhydrous  $\text{CuCl}_2$  and 0.2 g (0.543 mmol) of DHTMB were dissolved in *ca.* 80 mL of hot ethanol (apple green colour). This mixture was refluxed for 10 minutes, after which time a solution of 1,3-diaminopropan-2-ol (0.052 g, 0.543 mmol) in *ca.* 20 mL of ethanol was added dropwise to the refluxing solution. The solution became darker and cloudy. After 10-15 minutes it started to get brownish green colour but it was not cloudy anymore. The reaction mixture was refluxed for 1.5 hours. After that time, the solution was left to cool, filtered and concentrated under vacuum to dryness. The solid was dissolved in DCM (olive green colour), filtered to eliminate some impurities and concentrated to dryness under vacuum again. The green brownish product was dissolved in EtOH and stirred overnight after adding some  $\text{Et}_3\text{N}$ . After that time it was evaporated to dryness, dissolved in DCM and impurities were filtered off. The resultant solution was evaporated to dryness (Yield. 0.24 g; 71%).

**CHN Calc.:** C 52.04%; H 5.82%; N 4.50% for  $[\text{Cu}_4(\text{H}_2\text{L1})(\text{OH})_2(\text{EtOH})](\text{Cl})_2$

**Found:** C 52.25%; H 5.96%; N 4.80%

**LSI-MS  $m/z$  (calc.):** 967 (42) ( $[\text{Cu}_2(\text{H}_3\text{L1})\text{-2H}]^+$ , 967); 1031 (100)

( $[\text{Cu}_3(\text{H}_2\text{L1})\text{+e}]^+$ , 1031); 1202 (5)

( $[\text{Cu}_4(\text{H}_2\text{L1})(\text{Cl})_2(\text{H}_2\text{O})_2\text{+e}]^+$ , 1202).

**IR (KBr,  $\text{cm}^{-1}$ ):** 3422 (b, m,  $\nu_{\text{O-H}}$ ); 2957 (m,  $\nu_{\text{C-CH}_3}$ ), 1637 (s,  $\nu_{\text{C=N}}$ ); 1542 (w,  $\nu_{\text{C=O}}$ );

1477 (m); 1458 (m), 1439 (m); 1364 (m); 1223 (m)

**E.3.12.  $[\text{Ni}_4(\text{H}_2\text{L1})(\text{OH})_2(\text{EtOH})_4](\text{Cl})_2$  (3.12)**

$\text{NiCl}_2 \cdot 6\text{H}_2\text{O}$  (0.194 g, 0.81 mmol) and DHTMB (0.2 g, 0.543 mmol) were dissolved in hot ethanol (*ca.* 100 mL). The golden yellow solution was refluxed for 10-15 minutes after which time a solution of 1,3-diaminopropan-2-ol (0.052 g, 0.543 mmol) in *ca.* 10 mL of ethanol was added dropwise to the refluxing solution. The solution colour turned green and cloudy. The reaction mixture was

refluxed for 4 hours. The solution was then evaporated to dryness. It was redissolved in dichloromethane (lime green colour solution) and some impurities were filtered off and evaporated to dryness (Yield: 0.18 g; 51%)

**CHN** Calc: C 55.90%; H 6.63%; N 4.49% for  $[\text{Ni}_4(\text{H}_2\text{L1})(\text{OH})_2(\text{EtOH})_4](\text{Cl})_2$

Found: C 55.88%; H 6.77%; N 2.36%

**LSI-MS**  $m/z$  (%) (calc): 957 (100) ( $[\text{Ni}_2(\text{H}_3\text{L1})-2\text{H}]^+$ , 957); 979 (15)

( $[\text{Ni}_2(\text{H}_3\text{L1})(\text{H}_2\text{O})+2\text{H}]^+$ , 979); 1163 (10) ( $[\text{Ni}_4(\text{H}_2\text{L1})(\text{Cl})_2(\text{OH})]^+$ , 1163); 1327 (10) ( $[\text{Ni}_4(\text{H}_2\text{L1})(\text{Cl})_2(\text{EtO})(\text{EtOH})_3-\text{H}]^+$ , 1329), 1349 (10) ( $[\text{Ni}_4(\text{H}_2\text{L1})(\text{Cl})_2(\text{OH})(\text{EtOH})_4+\text{H}]^+$ , 1349).

**IR** (KBr,  $\text{cm}^{-1}$ ): 3417 (b, m,  $\nu_{\text{O-H}}$ ); 2960 (s,  $\nu_{\text{C-CH}_3}$ ), 1648 (s,  $\nu_{\text{C=N}}$ ); 1547 (w,  $\nu_{\text{C=O}}$ ); 1480 (m); 1460 (s); 1363 (m); 1270 (m); 1216 (s).

### E.3.13. $[\text{Cu}_4(\text{H}_2\text{L1})(\text{OH})_2(\text{H}_2\text{O})_2](\text{BF}_4)_2$ (3.13)

0.375 g (1.086 mmol) of  $\text{Cu}(\text{BF}_4)_2 \cdot 6\text{H}_2\text{O}$  and 0.2 g (0.543 mmol) of DHTMB were dissolved in hot ethanol (*ca.* 80 mL). This mixture (brown yellowish colour) was refluxed during 10 minutes, after which time a solution of 1,3-diaminopropan-2-ol (0.062 g, 0.646 mmol) in *ca.* 20 mL of ethanol was added dropwise to the refluxing solution. The reaction mixture was left under reflux for 3 hours. During that time the colour became dark green. The solution was filtered and concentrated under vacuum to dryness, dissolved in dichloromethane and impurities filtered off. The resultant solution was evaporated to dryness, washed with water and rinsed with diethylether (Yield: 0.22 g; 61%)

**CHN** Calc.: C 46.65%; H 5.27%; N 4.18% for  $[\text{Cu}_4(\text{H}_2\text{L1})(\text{OH})_2(\text{H}_2\text{O})_2](\text{BF}_4)_2$

Found: C 46.35%; H 5.48%; N 4.47%

**LSI-MS**  $m/z$  (%) (calc): 977 (20) ( $[\text{Cu}(\text{H}_3\text{L1})(\text{H}_2\text{O})_4-2\text{H}]^+$ , 977); 1067 (19)

( $[\text{Cu}_3(\text{H}_2\text{L1})(\text{H}_2\text{O})_2+\text{e}]^+$ , 1067); 1264 (8)

( $[\text{Cu}_4(\text{H}_2\text{L1})(\text{BF}_4)(\text{EtOH})(\text{OH})_2+2\text{H}]^+$ , 1264); 1460

(21) ( $[\text{Cu}_4(\text{H}_2\text{L1})(\text{BF}_4)_2(\text{OH})(\text{EtOH})_3(\text{H}_2\text{O})_2]^+$ , 1460).

IR (KBr,  $\text{cm}^{-1}$ ): 3422 (b,m, $\nu_{\text{O-H}}$ ); 2958 (m, $\nu_{\text{C-CH}_3}$ ), 1639 (m, $\nu_{\text{C=N}}$ ), 1543 (w, $\nu_{\text{C-O}}$ );  
1444 (m); 1394 (w); 1364 (w); 1221 (m); 1061 (b, s,  $\nu_{\text{BF}_4}$ ).

### E.3.14. $[\text{Co}_4(\text{L1})(\text{OH})_4](\text{BF}_4)_2 \cdot 3\text{H}_2\text{O} \cdot 4\text{EtOH}$ (3.14)

$\text{Co}(\text{BF}_4)_2 \cdot 2\text{H}_2\text{O}$  (0.37 g, 1.086 mmol) and DHTMB (0.2 g, 0.543 mmol) were dissolved in ethanol (*ca.* 80 mL). The orange solution was refluxed for 15 minutes, after which time a solution of 1,3-diaminopropan-2-ol (0.054 g, 0.543 mmol) in *ca.* 10 mL of ethanol was added dropwise to the refluxing solution. The solution colour changed from orange to dark orange-red. The reaction mixture was allowed to reflux for 2 hours and after it was left to cool. On standing, the solution turned dark brown. A small amount of impurities was filtered off and the solvent was removed under vacuum. The dark brown residue was dissolved in dichloromethane, filtered to eliminate impurities and precipitated with diethylether (Yield. 0.33 g; 80%).

CHN Calc: C 46.35%; H 6.22%; N 3.60% for  $[\text{Co}_4(\text{L1})(\text{OH})_4](\text{BF}_4)_2 \cdot 3\text{H}_2\text{O} \cdot 4\text{EtOH}$   
Found: C 46.01%; H 6.27%; N 3.55%

LSI-MS  $m/z$  (%) (calc) 847 (80)  $([(\text{H}_6\text{L1})+\text{H}]^+)$ , 846), 937 (100)  
 $([\text{Co}(\text{H}_4\text{L1})(\text{H}_2\text{O})_2-\text{H}]^+)$ , 937); 977 (53)  $([\text{Co}_2(\text{H}_2\text{L1})(\text{H}_2\text{O})+\text{e}]^+)$ ,  
977); 1052 (30)  $([\text{Co}_3(\text{L1})(\text{OH})_2+\text{H}]^+)$ , 1050); 1327 (25)  
 $([\text{Co}_4(\text{L1})(\text{OH})_4(\text{EtOH})_4+\text{e}]^+)$ , 1327), 1384 (40)  
 $([\text{Co}_4(\text{L1})(\text{EtOH})_4(\text{OH})_6+\text{Na}]^+)$ , 1384

IR (KBr,  $\text{cm}^{-1}$ ): 3481 (b, s,  $\nu_{\text{O-H}}$ ); 2961 (m, $\nu_{\text{C-CH}_3}$ ); 1646 (s, $\nu_{\text{C=N}}$ ); 1458 (w); 1394  
(m); 1364 (m); 1269 (m); 1220 (m); 1084 (b, $\nu_{\text{BF}_4}$ ).

### E.3.15. $[\text{Ni}_4(\text{H}_2\text{L1})(\text{OH})_2(\text{EtO})](\text{AcO}) \cdot \text{H}_2\text{O}$ (3.15)

0.2 g (0.81 mmol) of  $\text{Ni}(\text{AcO})_2 \cdot 4\text{H}_2\text{O}$  and 0.2 g (0.543 mmol) of DHTMB were heated to reflux in *ca.* 100 mL of ethanol (green yellowish colour) during 10

minutes, after which time a solution of 1,3-diaminopropan-2-ol (0.052 g, 0.543 mmol) in *ca.* 20 mL of ethanol was added dropwise to the refluxing solution. The colour turned light brown yellowish. The solution was refluxing for 4 hours, after which the solution was filtered and concentrated under vacuum. The mixture was dissolved in dichloromethane, filtered to eliminate impurities and concentrated to dryness under vacuum again (Yield: 0.29 g; 87%).

**CHN Calc.:** C 54.59%, H 6.22%; N 4.55% for  $[\text{Ni}_4(\text{H}_2\text{L1})(\text{OH})_2(\text{EtO})](\text{AcO})\cdot\text{H}_2\text{O}$

**Found:** C 54.64%, H 6.36%; N 4.82%

**LSI-MS  $m/z$  (%) (calc):** 957 (82) ( $[\text{Ni}_2(\text{H}_4\text{L1})-\text{H}]^+$ , 959); 979 (84)

( $[\text{Ni}_2(\text{H}_4\text{L1})(\text{OH})+\text{H}]^+$ , 981); 1016 (52) ( $[\text{Ni}_2(\text{H}_4\text{L1})(\text{AcO})-\text{H}]^+$ ,

1018); 1073 (42) ( $[\text{Ni}_2(\text{H}_4\text{L1})(\text{AcO})(\text{H}_2\text{O})_3]^+$ , 1073); 1089 (44)

( $[\text{Ni}_4(\text{L1})(\text{OH})-\text{H}]^+$ , 1089), 1161 (57) ( $[\text{Ni}_4(\text{L1})(\text{EtO})(\text{EtOH})-\text{H}]^+$ , 1163)

**IR (KBr,  $\text{cm}^{-1}$ ):** 3410 (b, m,  $\nu_{\text{O-H}}$ ); 2956 (s,  $\nu_{\text{C-CH}_3}$ ); 1619 (s,  $\nu_{\text{C=N}}$ ); 1547 (m,  $\nu_{\text{C=O}}$ );

1449 (s,  $\nu_{\text{COO}^-}$ ); 1392 (m); 1363 (m); 1270 (m), 1218 (m).

#### E.4. Heteronuclear complexes

##### E.4.1. $[\text{Ni}_2\text{Na}(\text{H}_2\text{L1})(\text{H}_2\text{O})_2](\text{AcO})$ (4.2)

$\text{Ni}(\text{AcO})_2\cdot 4\text{H}_2\text{O}$  (0.135 g, 0.543 mmol),  $\text{Na}(\text{AcO})$  (0.022 g, 0.27 mmol) and DHTMB (0.2 g, 0.543 mmol) were dissolved in hot EtOH (*ca.* 80 mL). The solution was refluxed for 15 minutes after which time a solution of 1,3-diaminopropan-2-ol (0.052 g, 0.543 mmol) in *ca.* 10 mL of EtOH was added dropwise to the refluxing solution. The colour changed from lime green yellowish to brown yellowish. After 15 minutes a few drops of  $\text{Et}_3\text{N}$  were added to the mixture. The reaction mixture was left under reflux for 24 hours. A brown solid precipitated was filtered off. The remaining brown solution was evaporated to dryness and washed with DCM (Yield: 0.225 g; 77%)

**CHN Calc.:** C 60.25%; H 6.65%; N 5.20% for  $[\text{Ni}_2\text{Na}(\text{H}_2\text{L1})(\text{H}_2\text{O})_2](\text{AcO})$

**Found:** C 60.23%; H 6.41%; N 5.03%

LSI-MS  $m/z$  (%) (calc.): 959 (97) ( $[\text{Ni}_2(\text{H}_3\text{L1})]^+$ , 959); 979 (100)  
 $([\text{Ni}_2\text{Na}(\text{H}_2\text{L1})\text{-}2\text{H}]^+$ , 979).

IR (KBr,  $\text{cm}^{-1}$ ): 3422 (b, m,  $\nu_{\text{O-H}}$ ); 2958 (m,  $\nu_{\text{C-CH}_3}$ ); 1618 (s,  $\nu_{\text{C=N}}$ ); 1545 (m,  $\nu_{\text{C-O}}$ );  
 1450 (m,  $\nu_{\text{COO}^-}$ ); 1391 (w); 1363 (w); 1330 (w); 1269 (w); 1220 (w).

#### E.4.2. $[\text{Zn}_2\text{Na}(\text{H}_2\text{L1})(\text{AcO})(\text{EtOH})](\text{AcOH})$ (4.3)

DHTMB (0.2 g, 0.543 mmol) and Na(AcO) (0.022 g, 0.27 mmol) were dissolved in hot EtOH (*ca.* 80 mL). The yellow solution was refluxed for 15 minutes after which time a solution of 1,3-diaminopropan-2-ol (0.048 g, 0.543 mmol) in *ca.* 10 mL of EtOH was added dropwise to the refluxing solution. The colour became dark yellow-orange. It was left refluxing for 15 minutes and few drops of  $\text{Et}_3\text{N}$  were added to the solution. The reaction mixture was refluxing for 22 hours. After that time 0.24 g (1.086 mmol) of  $\text{Zn}(\text{AcO})_2 \cdot 2\text{H}_2\text{O}$  dissolved in *ca.* 10 mL of EtOH were added to the mixture and allowed to reflux for 4 hours. The solution was then left to cool down, filtered and evaporated under vacuum. The product was dissolved in DCM, some impurities filtered off and concentrated to dryness under vacuum. Then it was washed with  $\text{H}_2\text{O}$  and rinsed with  $\text{Et}_2\text{O}$  (Yield: 0.26 g; 83%).

CHN Calc.: C 60.05%; H 6.69%; N 4.83% for  $[\text{Zn}_2\text{Na}(\text{H}_2\text{L1})(\text{AcO})(\text{EtOH})](\text{AcOH})$   
 Found. C 60.13%; H 6.57%; N 4.16%

LSI-MS  $m/z$  (%) (calc.): 973 (95) ( $[\text{Zn}_2(\text{H}_3\text{L1})\text{+H}]^+$ , 973), 995 (15)  
 $([\text{Zn}_2\text{Na}(\text{H}_2\text{L1})]^+$ , 995), 1031 (30) ( $[\text{Zn}_2\text{Na}(\text{H}_2\text{L1})(\text{H}_2\text{O})_2]^+$ , 1031).

IR (KBr,  $\text{cm}^{-1}$ ): 3388 (b, w,  $\nu_{\text{O-H}}$ ), 2958 (s,  $\nu_{\text{C-CH}_3}$ ); 1634 (s,  $\nu_{\text{C=N}}$ ); 1581 (m,  $\nu_{\text{C-O}}$ );  
 1442 (m,  $\nu_{\text{COO}^-}$ ); 1393 (m); 1363 (w); 1265 (w); 1220 (w)

#### E.4.3. $[\text{Cu}_2\text{Ca}(\text{HL1})] \cdot \text{Cl}$ (4.4)

$\text{CuCl}_2 \cdot 2\text{H}_2\text{O}$  (0.08 g, 0.543 mmol),  $\text{CaCl}_2$  (0.03 g, 0.27 mmol) and DHTMB (0.2 g, 0.543 mmol) were dissolved in hot EtOH (*ca.* 80 mL). The solution was



refluxed for 15 minutes after which time a solution of 1,3-diaminopropan-2-ol (0.052 g, 0.543 mmol) in *ca.* 10 mL of EtOH was added dropwise to the refluxing solution. The colour changed from light bright green to green and the solution became cloudy. After 10 minutes it was not cloudy anymore and became darker green. After 15 minutes few drops of Et<sub>3</sub>N were added to the mixture, which turned brown. The reaction mixture was left under reflux for 24 hours. A dark brown solid precipitated, so it was filtered off. This dark brown solid was analysed as the dicopper(II) complex [Cu<sub>2</sub>(H<sub>2</sub>L1)]·H<sub>2</sub>O (2.19) described in the dinuclear complexes section (synthesis E.2.2.20). The remaining brown solution was evaporated to dryness (Yield: 0.18 g; 66%) analysing as the heteronuclear complex 4.4

CHN Calc.: C 59.90%; H 6.09%; N 5.37% for [Cu<sub>2</sub>Ca(HL1)]·Cl

Found: C 62.55%, H 6.48%; N 5.41%

LSI-MS *m/z* (%) (calc): 906 (30) ([Cu(H<sub>3</sub>L1)-H]<sup>+</sup>, 906); 969 (53)

([Cu<sub>2</sub>(H<sub>3</sub>L1)]<sup>+</sup>, 969); 1006 (20) ([Cu<sub>2</sub>Ca(HL1)-H]<sup>+</sup>, 1006), 1043 (100)

([Cu<sub>2</sub>Ca(H<sub>2</sub>L1)Cl]<sup>+</sup>, 1043); 1147 (15) ([Cu<sub>2</sub>Ca(HL1)(Cl)<sub>2</sub>(EtOH)<sub>2</sub>+2H]<sup>+</sup>, 1147).

IR (KBr, cm<sup>-1</sup>): 3374 (b, m, ν<sub>O-H</sub>); 2957 (m, ν<sub>C-CH<sub>3</sub></sub>); 1627 (s, ν<sub>C=N</sub>); 1555 (w),

1454 (m); 1393 (w); 1363 (w); 1263 (m); 1222 (w), 1070 (w).

#### E.4.4. [Ni<sub>2</sub>Ca(HL1)(EtOH)](NO<sub>3</sub>) (4.5)

Ni(NO<sub>3</sub>)<sub>2</sub>·6H<sub>2</sub>O (0.158 g, 0.543 mmol), Ca(NO<sub>3</sub>)<sub>2</sub>·4H<sub>2</sub>O (0.064 g, 0.27 mmol) and DHTMB (0.2 g, 0.543 mmol) were dissolved in hot EtOH (*ca.* 80 mL). The solution was refluxed for 15 minutes after which time a solution of 1,3-diaminopropan-2-ol (0.052 g, 0.543 mmol) in *ca.* 10 mL of EtOH was added dropwise to the refluxing solution. The colour changed from lime green yellowish to dark lime green. After 15 minutes few drops of Et<sub>3</sub>N were added to the mixture, which turned brown-orange. The reaction mixture was left under reflux for 24 hours. A dark brown solid precipitated, so it was filtered off. This dark brown

solid was analysed as the dinickel(II) complex  $[\text{Ni}_2(\text{H}_2\text{L1})(\text{H}_2\text{O})_3]$  (2.20) described in the dinuclear complexes section (synthesis E.2.2.21). The remaining brown solution was evaporated to dryness (Yield: 0.19 g, 63%) analysing as the heteronuclear complex 4.5

**CHN Calc.:** C 58.61%; H 6.37%; N 6.33% for  $[\text{Ni}_2\text{Ca}(\text{HL1})(\text{EtOH})](\text{NO}_3)$

**Found:** C 58.56%; H 6.61%; N 6.32%

**LSI-MS m/z (calc):** 479 (83) ( $[\text{Ni}_2(\text{H}_2\text{L1})]^{2+}$ , 958); 957 (100) ( $[\text{Ni}_2(\text{H}_3\text{L1})]^+$ , 959); 1058 (55) ( $[\text{Ni}_2\text{Ca}(\text{H}_2\text{L1})(\text{NO}_3)\text{-}2\text{H}]^+$ , 1058).

**IR (KBr,  $\text{cm}^{-1}$ ):** 3384 (b, m,  $\nu_{\text{O-H}}$ ); 2952 (s,  $\nu_{\text{C-CH}_3}$ ); 1619 (s,  $\nu_{\text{C=N}}$ ); 1544 (m,  $\nu_{\text{C-O}}$ ); 1449 and 1363 (m,  $\nu_{\text{coord.NO}_3}$ ); 1392 (m,  $\nu_{\text{freeNO}_3}$ ).

**E.4.5.  $[\text{Cu}_4\text{Ba}(\text{H}_2\text{L1})_2](\text{ClO}_4)_2\cdot\text{EtOH}\cdot 4\text{H}_2\text{O}$  (4.6a)**

**$[\text{Cu}_4\text{Ba}(\text{H}_4\text{L9})](\text{ClO}_4)_2\cdot 4\text{H}_2\text{O}$  (4.6b)**

$\text{Cu}(\text{ClO}_4)_2\cdot 6\text{H}_2\text{O}$  (0.2 g, 0.543 mmol),  $\text{Ba}(\text{ClO}_4)_2\cdot 3\text{H}_2\text{O}$  (0.1 g, 0.27 mmol) and DHTMB (0.2 g, 0.543 mmol) were dissolved in hot EtOH (*ca.* 80 mL). The solution was refluxed for 15 minutes after which time a solution of 1,3-diaminopropan-2-ol (0.052 g, 0.543 mmol) in *ca.* 10 mL of EtOH was added dropwise to the refluxing solution. The colour changed from brown yellowish to dark green. After 15 more minutes refluxing few drops of  $\text{Et}_3\text{N}$  were added. The reaction mixture was refluxing for 24 hours. The green brownish solution was then left to cool down and concentrated under vacuum to dryness. The resultant solid was washed with DCM and some copper salts were eliminated by filtration. The product was dissolved in EtOH and left to crystallise by diffusing  $\text{Et}_2\text{O}$  into the solution. After few days there were some brown crystals. It was also crystallised by slow evaporation of EtOH. In this case, after few days there was a mixture of brown crystals and green square plates, which were separated by different solubility in  $\text{CHCl}_3$  (the green crystals were soluble but not the brown ones). The green product (4.6b) was dissolved in MeOH and left to crystallise in  $\text{Et}_2\text{O}$  diffusion. Suitable X-ray green square plate crystals (4.6bx) grew within few

days (Yield: 0.44g; 69%). The brown product (4.6a) was left to crystallise by Et<sub>2</sub>O diffusion into a mixture of EtOH and MeOH. Brown crystals (4.6ax) appeared within a week (Yield: 0.195g; 30%).

**Green product (4.6b):**

**CHN Calc.:** C 53.28%; H 5.85%; N 4.78% for [Cu<sub>4</sub>Ba(H<sub>4</sub>L9)](ClO<sub>4</sub>)<sub>2</sub>·4H<sub>2</sub>O

**Found.** C 53.40%; H 5.75%; N 5.04%

**LSI-MS m/z (calc.):** 1036 (65) ([Cu<sub>2</sub>Ba(H<sub>2</sub>L1)<sub>2</sub>]<sup>2+</sup> or [Cu<sub>4</sub>Ba(H<sub>4</sub>L9)]<sup>2+</sup>, 2073); 1589 (7) ([Cu<sub>3</sub>Ba(H<sub>2</sub>L8)+H]<sup>+</sup>, 1589), 1688 (18) ([Cu<sub>3</sub>Ba(H<sub>3</sub>L8)(ClO<sub>4</sub>)-H]<sup>+</sup>, 1688); 2072 (95) ([Cu<sub>4</sub>Ba(H<sub>3</sub>L9)]<sup>+</sup> or [Cu<sub>4</sub>Ba(H<sub>2</sub>L1)<sub>2</sub>-H]<sup>+</sup>, 2072); 2171 (100) ([Cu<sub>4</sub>Ba(H<sub>4</sub>L9)(ClO<sub>4</sub>)-2H]<sup>+</sup> or [Cu<sub>4</sub>Ba(H<sub>2</sub>L1)<sub>2</sub>(ClO<sub>4</sub>)-2H]<sup>+</sup>, 2171).

**IR (KBr, cm<sup>-1</sup>):** 3446 (b, s, ν<sub>O-H</sub>); 2957 (m, ν<sub>C-CH<sub>3</sub></sub>); 1628 (s, ν<sub>C=N</sub>); 1559 (m); 1540 (m); 1457 (m); 1263 (m); 1122, 1108 and 1088 (m, ν<sub>3(ClO<sub>4</sub>-)</sub>); 668 (m, ν<sub>4(ClO<sub>4</sub>-)</sub>).

**Brown product (4.6a):**

**CHN Calc.:** C 53.28%; H 5.85%; N 4.78% [Cu<sub>4</sub>Ba(H<sub>2</sub>L1)<sub>2</sub>](ClO<sub>4</sub>)<sub>2</sub>·EtOH·4H<sub>2</sub>O

**Found:** C 53.24%; H 5.81%; N 4.96%

**LSI-MS m/z (%) (calc.):** 969 (5) ([Cu<sub>2</sub>(H<sub>3</sub>L1)]<sup>+</sup>, 969), 1037 (8) ([Cu<sub>2</sub>(H<sub>2</sub>L1)(MeOH)<sub>2</sub>]<sup>2+</sup>, 1037); 2073 (7) ([Cu<sub>4</sub>Ba(H<sub>2</sub>L1)<sub>2</sub>]<sup>+</sup>, 2073), 2171 (1) ([Cu<sub>4</sub>Ba(H<sub>2</sub>L1)<sub>2</sub>(ClO<sub>4</sub>)-2H]<sup>+</sup>, 2171).

**IR (KBr, cm<sup>-1</sup>):** 3462 (b, m, ν<sub>O-H</sub>); 2956 (m, ν<sub>C-CH<sub>3</sub></sub>); 1624 (s, ν<sub>C=N</sub>); 1559 (m); 1456 (m); 1393 (m); 1265 (m); 1104, 1068 and 1040 (b, m, ν<sub>3(ClO<sub>4</sub>-)</sub>)

**E.4.6. [Zn<sub>4</sub>Ba(H<sub>2</sub>L1)<sub>2</sub>(OH)](ClO<sub>4</sub>)<sub>3</sub>·3H<sub>2</sub>O (4.7)**

DHTMB (0.2 g, 0.543 mmol) and Ba(ClO<sub>4</sub>)<sub>2</sub>·3H<sub>2</sub>O (0.1 g, 0.27 mmol) were dissolved in hot EtOH (ca. 80 mL). The pale yellow solution was refluxed for 15 minutes after which time a solution of 1,3-diaminopropan-2-ol (0.048 g, 0.543

mmol) in *ca.* 10 mL of EtOH was added dropwise to the refluxing solution. The colour became dark yellow-orange. It was left refluxing for 15 minutes and few drops of Et<sub>3</sub>N were added to the solution. The reaction mixture was refluxing for 18 hours. 0.074 g (0.543 mmol) of anhydrous ZnCl<sub>2</sub> dissolved in *ca.* 10 mL of EtOH were added to the mixture and allowed to reflux for 5 hours. The colour became pale orange and the solution was cloudy. It was then left to cool down. A pale yellow solid precipitated and was filtered off. The orange solution was evaporated to dryness, dissolved in DCM to eliminate impurities, dried and washed with H<sub>2</sub>O (Yield: 0.16 g; 53%). Pale yellow crystals suitable for X-ray were obtained within few days by diffusion of Et<sub>2</sub>O into a MeOH solution of the product.

**CHN** Calc : C 55.48%; H 6.04%; N 4.97% for [Zn<sub>4</sub>Ba(H<sub>2</sub>L1)<sub>2</sub>(OH)](ClO<sub>4</sub>)·3H<sub>2</sub>O

Found: C 55.25%; H 6.01%; N 4.92% or [Zn<sub>4</sub>Ba(H<sub>4</sub>L9)(OH)](ClO<sub>4</sub>)·3H<sub>2</sub>O

**LSI-MS** m/z (%) (calc.): 971 (35) ([Zn<sub>2</sub>(H<sub>3</sub>L1)-2H]<sup>+</sup>, 973); 1007 (25)

([Zn<sub>2</sub>Ba(HL1)-H]<sup>+</sup>, 1007); 1138 (20) ([Zn<sub>2</sub>Ba(HL1)(MeOH)-2H]<sup>+</sup>, 1138);

1339 (15) ([Zn<sub>2</sub>Ba(H<sub>2</sub>L1)(ClO<sub>4</sub>)(EtOH)<sub>2</sub>(H<sub>2</sub>O)<sub>2</sub>+H]<sup>+</sup>, 1337); 2077 (7)

([Zn<sub>4</sub>Ba(H<sub>2</sub>L1)<sub>2</sub>-2H]<sup>+</sup>, 2077); 2178 (7) ([Zn<sub>4</sub>Ba(H<sub>2</sub>L1)<sub>2</sub>(ClO<sub>4</sub>)-2H]<sup>+</sup>, 2178)

**IR** (KBr, cm<sup>-1</sup>): 3448 (b, w, ν<sub>O-H</sub>); 2957 (m, ν<sub>C-CH<sub>3</sub></sub>), 1630 (s, ν<sub>C=N</sub>), 1551 (m, ν<sub>C-O</sub>),

1450 (m); 1394 (m); 1268 (m); 1103 and 1068 (b, m, ν<sub>3(ClO<sub>4</sub>-)</sub>); 624 (w, ν<sub>4(ClO<sub>4</sub>-)</sub>)

#### E.4.7. [Cu<sub>3</sub>Ba(H<sub>2</sub>L8)](ClO<sub>4</sub>)·2H<sub>2</sub>O (4.8a)

Ba(ClO<sub>4</sub>)<sub>2</sub>·3H<sub>2</sub>O (0.1 g, 0.27 mmol) and DHTMB (0.2 g, 0.543 mmol) were dissolved in hot EtOH (*ca.* 80 mL). The solution was refluxed for 15 minutes after which time a solution of 1,3-diaminopropan-2-ol (0.052 g, 0.543 mmol) in *ca.* 10 mL of dry EtOH was added dropwise to the refluxing solution. The colour changed from yellowish to orange. The reaction mixture was under reflux for 15 minutes. Few drops of Et<sub>3</sub>N were added to the mixture. After 18 hours refluxing 0.2 g of Cu(ClO<sub>4</sub>)<sub>2</sub>·6H<sub>2</sub>O (0.543 mmol) were added to the mixture and reflux was continued for another 5 hours. The colour turned dark green brownish. The

solution was concentrated under vacuum to dryness giving a dark green solid. The product was left to crystallise in Et<sub>2</sub>O diffusion into a MeOH solution, brown crystals suitable for X-ray analysis were obtained in few days (Yield: 0.072 g, 23%). Green square plate crystals were also grown by slow evaporation of an EtOH solution of the product (Yield: 0.187 g, 60%).

**CHN Calc:** C 54.31%; H 5.84%; N 4.87% [Cu<sub>3</sub>Ba(H<sub>2</sub>L8)](ClO<sub>4</sub>)·2H<sub>2</sub>O

**Found:** C 54.01%; H 5.82%; N 4.69% (green crystals, 4.8a)

**Calc:** C 51.11%; H 5.76%; N 4.85% [Cu<sub>4</sub>Ba(H<sub>2</sub>L1)<sub>2</sub>](ClO<sub>4</sub>)<sub>2</sub>·2H<sub>2</sub>O

**Found:** C 51.03%; H 5.54%; N 4.87% (brown crystals, 4.8b)

**LSI-MS m/z (%) (calc.):** 1031 (40) ([Cu<sub>3</sub>(HL1)]<sup>+</sup>, 1031), 1203 (23)

([Cu<sub>2</sub>Ba(H<sub>2</sub>L1)(ClO<sub>4</sub>)]<sup>+</sup>, 1203); 1587 (25) ([Cu<sub>3</sub>Ba(H<sub>2</sub>L8)-H]<sup>+</sup>,

1587), 1688 (100) ([Cu<sub>3</sub>Ba(H<sub>3</sub>L8)(ClO<sub>4</sub>)-H]<sup>+</sup>, 1688); 2072 (10)

([Cu<sub>4</sub>Ba(H<sub>2</sub>L1)<sub>2</sub>-H]<sup>+</sup>, 2072); 2173 (9) ([Cu<sub>4</sub>Ba(H<sub>2</sub>L1)<sub>2</sub>(ClO<sub>4</sub>)]<sup>+</sup>, 2173)

**IR (KBr, cm<sup>-1</sup>):** 3423 (b, m, ν<sub>O-H</sub>); 2955 (s, ν<sub>C-H</sub>); 1625 (s, ν<sub>C-N</sub>); 1547 (m),

1450 (s); 1267 (s), 1102 (b, s, ν<sub>3(ClO<sub>4</sub>-)</sub>), 624 (m, ν<sub>4(ClO<sub>4</sub>-)</sub>).

**E.4.8. [Ni<sub>3</sub>Ba(HL8)](EtOH)·H<sub>2</sub>O (4.9a)**

**[Ni<sub>4</sub>Ba(H<sub>2</sub>L1)<sub>2</sub>(EtOH)<sub>2</sub>](ClO<sub>4</sub>)<sub>2</sub>·3H<sub>2</sub>O (4.9b)**

Ni(ClO<sub>4</sub>)<sub>2</sub>·6H<sub>2</sub>O (0.198 g, 0.543 mmol), Ba(ClO<sub>4</sub>)<sub>2</sub>·3H<sub>2</sub>O (0.105 g, 0.27 mmol) and DHTMB (0.2 g, 0.543 mmol) were dissolved in hot EtOH (ca. 80 mL). The solution was refluxed for 15 minutes after which time a solution of 1,3-diaminopropan-2-ol (0.052 g, 0.543 mmol) in ca. 10 mL of EtOH was added dropwise to the refluxing solution. The colour changed from lime green yellowish to dark lime green. After 15 minutes few drops of Et<sub>3</sub>N were added to the mixture, which turned brown yellowish. The reaction mixture was under reflux for 24 hours. The solution was then left to cool down, evaporated to dryness and washed with DCM. A pale brown solid insoluble in DCM was filtered off (Yield: 0.23 g; 70%). The remaining brown yellowish solution soluble in DCM was dried and washed with water and diethylether (Yield: 0.08 g; 27%).

**Brown yellowish product (4.9a):**

CHN Calc.: C 58.69%; H 6.28%; N 5.13% for  $[\text{Ni}_3\text{Ba}(\text{H}_2\text{L8})](\text{EtO})\cdot\text{H}_2\text{O}$

Found: C 58.47%; H 6.30%; N 5.33%

LSI-MS  $m/z$  (%) (calc.). 957 (37) ( $[\text{Ni}_2(\text{H}_3\text{L1})\text{-}2\text{H}]^+$ , 957); 1439 (50)

( $[\text{Ni}_3(\text{H}_4\text{L8})\text{+H}]^+$ , 1439); 1459 (49) ( $[\text{Ni}_3(\text{H}_4\text{L8})(\text{H}_2\text{O})\text{+}2\text{H}]^+$ , 1459); 1494 (40) ( $[\text{Ni}_3(\text{H}_4\text{L8})(\text{H}_2\text{O})_3\text{+}2\text{H}]^+$ , 1494); 1583 (33) ( $[\text{Ni}_2\text{Ba}(\text{H}_4\text{L8})(\text{EtOH})(\text{H}_2\text{O})\text{+}2\text{H}]^+$ , 1583).

IR (KBr,  $\text{cm}^{-1}$ ): 3385 (b, m,  $\nu_{\text{O-H}}$ ); 2954 (m,  $\nu_{\text{C-CH}_3}$ ); 1621 (m,  $\nu_{\text{C-N}}$ ); 1541 (w);

1445 (s), 1392 (s); 1363 (s); 1269 (w); 1116 and 1081 (m,  $\nu_3(\text{ClO}_4^-)$ ).

**Brown product (4.9b):**

CHN Calc: C 54.06%, H 6.13%; N 4.67% for  $[\text{Ni}_4\text{Ba}(\text{H}_2\text{L1})_2(\text{EtOH})_2](\text{ClO}_4)_2\cdot 3\text{H}_2\text{O}$

Found: C 54.03%; H 5.90%; N 4.36% or  $[\text{Ni}_4\text{Ba}(\text{H}_4\text{L9})(\text{EtOH})_2](\text{ClO}_4)_2\cdot 3\text{H}_2\text{O}$

LSI-MS  $m/z$  (%) (calc.): 957 (100) ( $[\text{Ni}_2(\text{H}_3\text{L1})\text{-}2\text{H}]^+$ , 957); 1026 (10)

( $[\text{Ni}_2(\text{H}_3\text{L1})(\text{EtOH})(\text{H}_2\text{O})\text{+}3\text{H}]^+$ , 1026); 1195 (18) ( $[\text{Ni}_2\text{Ba}(\text{H}_2\text{L1})(\text{ClO}_4)]^+$ , 1195).

IR (KBr,  $\text{cm}^{-1}$ ): 3448 (b, m,  $\nu_{\text{O-H}}$ ); 2957 (m,  $\nu_{\text{C-CH}_3}$ ); 1621 (s,  $\nu_{\text{C-N}}$ ); 1560 (m),

1457 (m); 1306 (m); 1270 (m), 1226 (w); 1100 (b, m,  $\nu_3(\text{ClO}_4^-)$ ); 623 (w,  $\nu_4(\text{ClO}_4^-)$ ).

**E.4.9.  $[\text{Cu}_3\text{Ca}(\text{H}_3\text{L8})](\text{NO}_3)_2\cdot 3\text{EtOH}\cdot 2\text{H}_2\text{O}$  (4.10)**

$\text{Ca}(\text{NO}_3)_2\cdot 4\text{H}_2\text{O}$  (0.064 g, 0.27 mmol) and DHTMB (0.2 g, 0.543 mmol) were dissolved in hot EtOH (*ca.* 80 mL). The solution was refluxed for 15 minutes after which time a solution of 1,3-diaminopropan-2-ol (0.052 g, 0.543 mmol) in *ca.* 10 mL of EtOH was added dropwise to the refluxing solution. The colour changed from pale to dark yellow. After 15 minutes few drops of  $\text{Et}_3\text{N}$  were added to the mixture. After 18 hours refluxing, 0.126 g of  $\text{Cu}(\text{NO}_3)_2\cdot 6\text{H}_2\text{O}$  (0.543 mmol) were added to the mixture. The solution became dark green and cloudy, but after 10 minutes it was not cloudy anymore. The reaction mixture was left under reflux for 4 hours. A brown solid was filtered off. The green solution was evaporated to



dryness (Yield: 0.26 g; 85%)

CHN Calc.: C 56.33%; H 6.39%; N 6.08%  $[\text{Cu}_3\text{Ca}(\text{H}_3\text{L8})](\text{NO}_3)_2 \cdot 3\text{EtOH} \cdot 2\text{H}_2\text{O}$

Found: C 56.38%; H 6.19%; N 6.09%

LSI-MS  $m/z$  (%) (calc.). 1006 (35)  $([\text{Cu}_2\text{Ca}(\text{HL1})\text{-H}]^+)$ , 1006);

1068 (50)  $([\text{Cu}_2\text{Ca}(\text{H}_2\text{L1})(\text{NO}_3)\text{-2H}]^+)$ , 1068); 1413 (40)

$([\text{Cu}_3\text{Ca}(\text{H}_6\text{L8})_2(\text{EtOH})(\text{H}_2\text{O})\text{+2H}]^{2+})$ , 2826); 1444 (45)

$([\text{Cu}_3\text{Ca}(\text{H}_7\text{L8})_2(\text{NO}_3)(\text{OH})(\text{EtOH})\text{+H}]^{2+})$ , 2888); 1476 (65)

$([\text{Cu}_3(\text{H}_4\text{L8})\text{+Na}]^+)$ , 1475); 1514 (30)  $([\text{Cu}_3\text{Ca}(\text{H}_2\text{L8})\text{+Na}]^+)$ , 1513).

IR (KBr,  $\text{cm}^{-1}$ ): 3409 (b, m,  $\nu_{\text{O-H}}$ ), 2953 (m,  $\nu_{\text{C-CH}_3}$ ); 1625 (s,  $\nu_{\text{C=N}}$ ); 1542 (m,  $\nu_{\text{C-O}}$ ),

1443 and 1363 (m,  $\nu_{\text{coord.NO}_3^-}$ ); 1385 (m,  $\nu_{\text{freeNO}_3^-}$ ); 1267 (m).

#### E.4.10. $[\text{Zn}_3\text{Ca}(\text{H}_3\text{L8})](\text{NO}_3)_2 \cdot 2\text{EtOH} \cdot 2\text{H}_2\text{O}$ (4.11)

DHTMB (0.2 g, 0.543 mmol) and  $\text{Ca}(\text{NO}_3)_2 \cdot 4\text{H}_2\text{O}$  (0.064 g, 0.27 mmol) were dissolved in hot EtOH (*ca.* 80 mL). The pale yellow solution was refluxed for 15 minutes after which time a solution of 1,3-diaminopropan-2-ol (0.048 g, 0.543 mmol) in *ca.* 10 mL of EtOH was added dropwise to the refluxing solution. The colour became dark yellow-orange. It was left refluxing for 15 minutes and few drops of  $\text{Et}_3\text{N}$  were added to the solution. The reaction mixture was refluxed for 22 hours. After that time 0.162 g (0.543 mmol) of  $\text{Zn}(\text{NO}_3)_2 \cdot 6\text{H}_2\text{O}$  dissolved in *ca.* 10 mL of EtOH were added to the mixture and allowed to reflux for 4 hours. The solution was then left to cool down, filtered and evaporated under vacuum. The product was washed with DCM and  $\text{H}_2\text{O}$  (Yield: 0.28 g; 86%).

CHN Calc.: C 56.86%; H 6.40%; N 6.47%  $[\text{Zn}_3\text{Ca}(\text{H}_3\text{L8})](\text{NO}_3)_2 \cdot 2\text{EtOH} \cdot 2\text{H}_2\text{O}$

Found: C 56.79%; H 6.41%; N 6.34%

LSI-MS  $m/z$  (%) (calc.): 1405 (30)  $([\text{Zn}_3\text{Ca}(\text{H}_6\text{L8})_2(\text{EtOH})]^{2+})$ , 2811); 1413

(100)  $([\text{Zn}_3\text{Ca}(\text{H}_6\text{L8})_2(\text{NO}_3)\text{+H}]^{2+})$ , 2828).

IR (KBr,  $\text{cm}^{-1}$ ): 3422 (b, m,  $\nu_{\text{O-H}}$ ); 2953 (s,  $\nu_{\text{C-CH}_3}$ ); 1638 (s,  $\nu_{\text{C=N}}$ ), 1544 (w,  $\nu_{\text{C-O}}$ );

1459 and 1362 (m,  $\nu_{\text{coord.NO}_3^-}$ ); 1390 (m,  $\nu_{\text{freeNO}_3^-}$ ); 1322 (m); 1267 (m).

## REFERENCES

1. L. F. Lindoy, *The Chemistry of Macrocyclic Ligand Complexes*, Cambridge University Press: Cambridge, UK, 1989.
2. E. C. Constable, *Coordination Chemistry of Macrocyclic Compounds*, Oxford University Press: New York, 1999.
3. P. A. Vigato, S. Tamburini and D. E. Fenton, *Coord. Chem. Rev.*, 1990, **106**, 25
4. P. Guerriero, S. Tamburini and P. A. Vigato, *Coord. Chem. Rev.*, 1995, **139**, 17.
5. H. Ōkawa, H. Furutachi, D. E. Fenton, *Coord. Chem. Rev.*, 1998, **174**, 51.
6. P. A. Vigato and S. Tamburini, *Coord. Chem. Rev.*, 2004, **248**, 1717.
7. V. McKee, *Adv. Inorg. Chem.*, 1993, **40**, 323.
8. D. E. Fenton, *Biocoordination Chemistry*, 1st ed., Oxford University Press: Oxford, UK, 1995
9. S. J. Lippard and J. M. Berg, *Principles of Bioinorganic Chemistry*, University Science Book: Mill Valley (California), 1994
10. I. Bertini, H. B. Gray, S. J. Lippard and J. S. Valentine, *Bioinorganic Chemistry*, University Science Books. Mill Valley (California), 1994.
11. D. E. Fenton, *Adv. Inorg. Bio. Mechanisms*, 1983, **12B**, 187.
12. L. F. Lindoy, *Synthesis of Macrocycles: The Design of Selective Complexing Agents*, R.M. Izatt and J.J. Christensen Eds., John Wiley, New York, 1987, 53.
13. S. R. Cooper, *Crown Compounds: Toward Future Applications*, VCH Publisher Inc., New York, 1992.
14. D. E. Fenton and H. Ōkawa, *Chem. Ber.*, 1997, **130**, 433
15. S. R. Collinson and D.E. Fenton, *Coord. Chem. Rev.*, 1996, **148**, 19.
16. D. E. Fenton, *Pure Appl. Chem.*, 1986, **58**, 1437.
17. L. F. Lindoy, *Pure Appl. Chem.*, 1989, **61**, 1575.
18. O. Kahn, *Adv. Inorg. Chem.*, 1995, **43**, 179.
19. S. Murray, *Adv. Inorganic Chem.*, 1995, **43**, 261.
20. A. Martell, J. Penitka and D. Kong, *Coord. Chem. Rev.*, 2001, **55**, 216.
21. C. J. Harding, Q. Lu, J. F. Malone, D. J. Marrs, N. Martin, V. McKee and J. Nelson, *Dalton Trans.*, 1995, 1739.

- 22 N A. Bailey, M. M. Eddy, D. E. Fenton, G. Jones, S. Moss and A. Mukhopadhyay, *Chem. Commun.*, 1981, 628.
23. N A. Bailey, M. M. Eddy, D. E. Fenton, S. Moss and A. Mukhopadhyay, *Dalton Trans.*, 1984, 2281.
24. D. E. Fenton and R. Moody, *Dalton Trans.*, 1987, 219.
25. S. S. Tandon and V. McKee, *Dalton Trans.*, 1989, 19.
- 26 S. K. Dutta, U. Flörke, S. Mohanta and K. Nag, *Inorg. Chem.*, 1998, 5029.
27. S. R. Korupoju and P. S. Zacharias, *Chem. Commun.*, 1998, 1267
28. J. Nelson, V. McKee and G. Morgan, *Prog. Inorg. Chem.*, 1998, 47, 167.
29. H. Houjou, S. K. Lee, Y. Hishikawa, Y. Nagawa and K. Hiratani, *Chem. Commun.*, 2000, 2197.
30. S. Schmidt, W. Bauer, F. W. Heinemann, H. Lanig and A. Grohmann, *Angew. Chem. Int. Ed.*, 2000, 39(5), 913.
31. R. D. Hancock, *Chelate Ring Size and Metal Ion Selection*, J. Chem. Ed., 1992, 69, 615.
32. S. Gou and D. E. Fenton, *Inorg. Chim. Acta*, 1994, 223, 169.
33. H. Adams, N. A. Bailey, P. Bertrand, C. O. Rodrigues de Barbarin, D. E. Fenton and S. Gou, *Dalton Trans.*, 1995, 275.
34. S. J. Weininger and F. R. Stermitz, *Organic Chemistry*, Ed. Reverté, Barcelona, 1988.
35. R. C. Long and D. N. Hendrickson, *J. Am. Chem. Soc.*, 1983, 105, 1513.
36. H. Ōkawa, J. Nishio, M. Ohba, M. Tadokoro, N. Matsumoto, M. Koikawa, S. Kida and D. E. Fenton, *Inorg. Chem.*, 1993, 32, 2949.
37. M. Yonemura, N. Usuki, Y. Nakamura, M. Ohba and H. Ōkawa, *Dalton Trans.*, 2000, 3624.
38. A. Atkins, D. Black, A. J. Blake, A. Marin-Becerra, S. Parsons, L. Ruiz-Ramirez and M. Schroder, *Chem. Commun.*, 1996, 457.
39. A. Hori, M. Yonemura, M. Ohba and H. Ōkawa, *Bull. Chem. Soc. Jpn.*, 2001, 74, 495.
40. M. J. Grannas, B. F. Hoskins and R. Robson, *Inorg. Chem.*, 1994, 33, 1071.
41. K. K. Nanda, S. Mohanta, U. Florke, S. K. Dutta and K. Nag, *Dalton Trans.*, 1995, 3831.

- 42 V. McKee and S. S. Tandon, *Dalton Trans.*, 1991, 221.
43. J. McCrea, V. McKee, T. Metcalfe, S. S. Tandon and J. Wikaira, *Inorg. Chim. Acta*, 2000, **297**, 220
44. R. Robson, *Inorg. Nucl. Chem. Letters*, 1970, **6**, 125.
45. N. H. Pilkington and R. Robson, *Aust. J. Chem.*, 1970, **23**, 2225.
46. R. Menif and A. E. Martell, *Chem. Commun.*, 1989, 1521.
47. R. Menif, A. E. Martell, P. J. Squattrito and A. Clearfield, *Inorg. Chem.*, 1990, **29**, 4723.
- 48 B F. Hoskins, N. J. McLeod and H. A. Schaap, *Aust. J. Chem.*, 1976, **29**, 515.
49. H. Wada, K. Motoda, M. Ohba, H. Sakiyama, N. Matsumoto and H. Ōkawa, *Bull. Chem. Soc. Jpn.*, 1995, **68**, 1105.
50. T Aono, H Wada, M. Yonemura, H. Furutachi, M. Ohba and H. Ōkawa, *Dalton Trans.*, 1997, 3029.
51. T. Aono, H. Wada, M. Yonemura, M. Ohba, H. Ōkawa and D. E. Fenton, *Dalton Trans.*, 1997, 1527.
52. L. K. Thompson, S. K. Mandal, S. S. Tandon, J. N. Bridson and M. K. Park, *Inorg. Chem.*, 1996, **35**, 3117
53. M. J. MacLachlan, M. K. Park and L. K. Thompson, *Inorg. Chem.*, 1996, **35**, 5492.
54. D. Black, A. J. Blake, R. L. Finn, L. F. Lindoy, A. Nezhadali, G. Rougnaghi, P. A. Tasker and M. Schröder, *Chem. Commun.*, 2002, 340
55. O. J. Gelling, A. Meetsma and B. L. Feringa, *Inorg. Chem.*, 1990, **29**, 2816
56. N. A. Bailey, D. E. Fenton, R. Moody, P. J. Scrimshire, E. Belorizky, P. H. Fries and J. M. Latour, *Dalton Trans.*, 1988, 2817.
57. P. Guerriero, P. A. Vigato, J. G. Bunzyl and E. Moret, *Dalton Trans.*, 1990, 647.
58. M. Qian, S. Gou, S. Chantrapromma, S. S. S. Raj, H. K. Fun, Q. Zeng, Z. Yu and X. You, *Inorg. Chim. Acta*, 2000, **305**, 83.
59. W. Huang, S. Gou, D. Hu, S. Chantrapromma, H. K. Fun and Q. Meng, *Inorg. Chem.*, 2001, **40**, 1712
60. J. D. Crane, D. E. Fenton, J. M. Latour and A. J. Smith, *Dalton Trans.*, 1991, 2979.

61. M. Yonemura, Y. Matsumura, M. Ohba, H. Ōkawa and D. E. Fenton, *Chem. Letters*, 1996, 601
62. P. Lacroix, O. Kahn, F. Theobald, J. Leroy and C. Wakselman, *Inorg. Chim. Acta*, 1988, **142**, 129.
63. L. K. Thompson, S. K. Mandal, S. S. Tandon, J. N. Bridson and M. K. Park, *Inorg. Chem.*, 1996, **35**, 3117.
64. The United Kingdom Chemical Database Service, C D.S.; D. A. Fletcher, R. F. McMeeking and D. J. Parkin, *J. Chem. Inf. Comput. Sci.* 1996, **36**, 746.
65. F. H. Allen, *Acta Crystallogr.*, 2002, **B58**, 380.
66. D. E. Fenton, *Adv. Inorg. Bioinorg. Mech.*, 1983, **2**, 187.
67. S. S. Tandon, L. K. Thompson, J. N. Bridson and C. Benelli, *Inorg. Chem.*, 1995, **34**, 5507.
68. S. S. Tandon, L. K. Thompson, J. N. Bridson, V. McKee and A. J. Downard, *Inorg. Chem.*, 1992, 4635.
69. E. Spodine, Y. Moreno, M. T. Garland, O. Pena and R. Baggio, *Inorg. Chim. Acta*, 2000, **309**, 57.
70. A. J. Downard, V. McKee and S. S. Tandon, *Inorg. Chim. Acta*, 1990, **173**, 181.
71. S. S. Tandon and V. McKee, *Chem. Commun.*, 1988, 385.
72. S. S. Tandon and V. McKee, *Inorg. Chem.*, 1989, **28**, 2901
73. P. E. Kruger and V. McKee, *Chem. Commun.*, 1997, 1341.
74. S. S. Tandon and V. McKee, *Chem. Commun.*, 1988, 1334
75. J. McCrea, V. McKee, T. Metcalfe, S. S. Tandon and J. Wikaira, *Inorg. Chim. Acta*, 2000, **297**, 220.
76. F. M. Launay, Ph D Thesis, The Queen's University Of Belfast, 2001.
77. M. Bell, A. J. Edwards, B. F. Hoskins, E. H. Kachab and R. Robson, *Chem. Commun.*, 1987, 1852.
78. A. J. Edwards, B. F. Hoskins, R. Robson, J. C. Wilson, B. Moubaraki and K. S. Murray, *Dalton Trans.*, 1994, 1837.
79. K. K. Nanda, K. Venkatsubramanian, D. Majumdar and K. Nag, *Inorg. Chem.*, 1994, **33**, 1581
80. S. Mohanta, K. K. Nanda, R. Werner, W. Haase, A. K. Mukherjee, S. K. Dutta and K. Nag, *Inorg. Chem.*, 1997, **36**, 4656.

81. M. Yonemura, H. Ōkawa, M. Ohba, D. E. Fenton and L. K. Thompson, *Chem. Commun.*, 2000, 817.
82. Y. Nakamura, M. Yonemura, K. Arimura, N. Usuki, M. Ohba and H. Ōkawa, *Inorg. Chem.*, 2001, **40**, 3739.
83. P. E. Kruger, F. Launay and V. McKee, *Chem. Commun.*, 1999, 639.
84. S. Cromie, F. Launay and V. McKee, *Chem. Commun.*, 2001, 1918.
85. B. F. Hoskins, R. Robson and P. Smith, *Chem. Commun.*, 1990, 488.
86. D. C. Gutsche, *Calixarenes Revisited*, J F. Stoddart Ed, The Royal Society of Chemistry, Cambridge, 1998.
87. D. C. Gutsche, *Calixarenes*, The Royal Society of Chemistry, Cambridge, 1989.
88. A. J. Edwards, B. F. Hoskins, E. H. Kechab, A. Markiewicz, K. S. Murray, and R. Robson, *Inorg. Chem.*, 1992, **31**, 3585.
89. M. Bell, A. J. Edwards, B. F. Hoskins, E. H. Kachab and R. Robson, *J. Am. Chem. Soc.*, 1989, **111**, 3603.
90. V. Böhmer, *Angew. Chem. Int. Ed. Engl.*, 1995, **34**, 713.
91. B. Masci, *J. Org. Chem.*, 2001, **66**, 1497.
92. P. Thuéry and B. Masci, *Dalton Trans.*, 2003, 2411.
93. B. Masci, S. L. Mortera, D. Persiana and P. Thuéry, *J. Org. Chem.*, 2006, **71**, 504.
94. P. Thuéry, M. Nierlich, J. Vicens and H. Takemura, *Polyhedron*, 2001, **20**, 3183.
95. B. Masci, M. Gabrieli, S. L. Mortera, M. Nierlich and P. Thuéry, *Polyhedron*, 2002, **21**, 1125.
96. P. Thuéry and B. Masci, *Polyhedron*, 2003, **22**, 3499.
97. P. Thuéry and B. Masci, *Polyhedron*, 2004, **23**, 649.
98. S. Goetz, PhD Thesis, Loughborough University, 2002.
99. J. Barreira Fontecha, S. Goetz and V. McKee, *Acta Cryst.*, 2004, **C60**, o776.
100. H. Shimakoshi, T. Takemoto, I. Aritome and Y. Hisaeda, *Tetrahedron Lett.*, 2002, **43**, 4809.
101. H. Shimakoshi, T. Takemoto, I. Aritome and Y. Hisaeda, *Inorg. Chem.*, 2005, **44**, 9134.
102. T. Steiner, *Angew. Chem. Int. Ed.*, 2002, **41**, 48.



103. G. A. Jeffrey, *An Introduction to Hydrogen Bonding*, Oxford University Press, Oxford, 1997.
104. G. Gilli and P. Gilli, *J. Mol. Struct.*, 2000, **552**, 1.
105. P. Gilli, V. Bertolasi, V. Ferretti and G. Gilli, *J. Am. Chem. Soc.*, 1994, **116**, 909.
106. D. C. Gutsche, B. Dhawan, K. H. No and R. Muthukrishnan, *J. Am. Chem. Soc.*, 1981, **103**, 3782.
107. J. Barreira Fontecha, S. Goetz and V. McKee, *Angew. Chem. Int. Ed. Engl.*, 2002, **41**, 4553.
108. R. G. Pearson, *Chemical Hardness*, Wiley-VCH, 1997.
109. J. Ribas Gispert, *Química de Coordinación*, ed. Universitat de Barcelona, 2000.
110. B. Dhawan and D. C. Gutsche, *J. Org. Chem.* 1983, **48**, 1539.
111. A. I. Vogel, *Vogel's Textbook of Practical Organic Chemistry*, 5th. ed., Prentice Hall, 1996.
112. S. Taniguchi, *Bull. Chem. Soc. Jpn.* 1984, **57**, 2683.
113. R. Boss and R. Scheffold, *Angew. Chem. Int. Ed. Engl.*, 1976, **15**, 558.
114. J. Coates, *Interpretation of Infrared Spectra, Encyclopedia of Analytical Chemistry*, ed. R. A. Meyers, pp. 10815-10837, John Wiley & Sons Ltd, Chichester, 2000
115. S. K. Mandal and K. J. Nag, *Dalton Trans.* 1984, 2141.
116. J. Barreira Fontecha, S. Goetz and V. McKee, *Dalton Trans.*, 2005, 923.
117. F. Mellon, R. Self and J. R. Startin, *Mass Spectrometry of Natural Substances in Food*, The Royal Society of Chemistry, Cambridge, 2000.
118. A. K. Brisdon, *Inorganic Spectroscopic Methods*, Oxford University Press, New York, 1998.
119. J. J. Manura and J. D. Manura, *Isotope Distribution Calculator, SIS*, 1996.  
[http //www sisweb com/cgi-bin/mass10 pl](http://www.sisweb.com/cgi-bin/mass10.pl)
120. D. Lee, P. L. Hung, B. Springler and S. J. Lippard, *Inorg. Chem.*, 2002, **41**, 521.
121. C. H. L. Kennard, E. J. O'Reilly and G. Smith, *Polyhedron*, 1984, **3**, 689.
122. A. M. Barrios and S. J. Lippard, *J. Am. Chem. Soc.*, 1999, **121**, 11751.

123. I. L. Eremenko, S. E. Nefedov, A. A. Sidirov, M. A. Golubnichaya, P. V. Danilov, V. N. Ikorskii, Y. G. Shvedenkov, V. M. Novotortsev and I. I. Moiseev, *Inorg. Chem.* 1999, **38**, 3764
124. D. Volkmer, B. Hommerich, K. Griesar, W. Haase and B. Krebs, *Inorg. Chem.*, 1996, **35**, 3792.
125. G. B. Deacon and R. J. Phillips, *Coord. Chem. Rev.* 1980, **33**, 227.
126. M. D. Glick, R. L. Lindvedt, T. J. Anderson and J. L. Mack, *Inorg. Chem.*, 1976, **15**, 2258
127. A. McAuley, K. Beveridge, S. Subramanian and T. W. Whitcombe, *Dalton Trans.*, 1991, 1821.
128. K. K. Nanda, R. Das, K. Venkatsubramanian, P. Paul and K. Nag, *Dalton Trans.*, 1993, 2515.
129. S. Brooker and P. D. Croucher, *Chem. Commun.*, 1995, 2075.
130. S. Brooker and P. D. Croucher, *Chem. Commun.*, 1995, 1493.
131. H. Duval, V. Bulach, J. Fischer and R. Weiss, *Inorg. Chem.*, 1999, **38**, 5495.
132. T. Thanyasiry and E. Sinn, *Dalton Trans.*, 1989, 1187.
133. A. Fabretti, A. Giusti, V. Albano, C. Castellari, D. Gatteschi and R. Sessoli, *Dalton Trans.*, 1991, 2133.
134. F. A. Cotton and G. Wilkinson, *Advanced Inorganic Chemistry*, 5<sup>th</sup> Ed., John Wiley & Sons, New York, 1988, 745.
135. R. L. Carlin, *Magnetochemistry*, Springer-Verlag, Heidelberg, 1986.
136. J. McCleverty, *Chemistry of the First-row Transition Metals*, Oxford University Press, New York, 1999.
137. N. A. Law, T. E. Machonkin, J. P. McGorman, E. J. Larson, J. W. Kampf, and V. L. Pecoraro, *Chem. Commun.*, 1995, 2015.
138. K. D. Karlin, *Science*, 1993, **261**, 701.
139. A. M. Barrios and S. J. Lippard, *J. Am. Chem. Soc.*, 2000, **122**, 9172.
140. H. Adams, S. Clunas, D. E. Fenton and S. E. Spey, *Dalton Trans.*, 2003, 625.
141. O. Kahn, *Molecular Magnetism*, VCH: New York, 1993.
142. K. K. Nanda, A. Addison, W. N. Paterson, E. Sinn, L. K. Thompson and U. Sakaguchi, *Inorg. Chem.*, 1998, **37**, 1028

143. D. Christodoulou, M. G. Kanatzidis, D. Coucouvanis, *Inorg. Chem.*, 1990, **29**, 191.
144. D. Gatteschi, A. Caneschi, R. Sessoli and A. Comia, *Chem. Soc. Rev.*, 1996, 101.
145. W. Radecka-Paryzek, V. Patroniak and J. Lisowski, *Coord. Chem. Rev.*, 2005, **249**, 2156.
146. C. H. Weng, S. C. Cheng, H. M. Wei, H. H. Wei and C. J. Lee, *Inorg. Chim. Acta*, 2006, **359**, 2029.
147. S. G. Naik, A. Mukherjee, R. Raghunathan, M. Nethaji, S. Ramasesha and A. R. Chakravarty, *Polyhedron*, 2006, **25**, 2135.
148. V. McKee, J. Nelson, D. J. Speed and R. M. Town, *Dalton Trans.*, 2001, 3641.
149. J. Gao, J. H. Reibenspies, R. A. Zingaro, F. R. Woolley, A. E. Martell and A. Clearfield, *Inorg. Chem.*, 2005, **44**, 232.
150. P. J. van Koningsbruggen, J. W. van Hal, R. A. G. de Graaff, J. G. Haasnoot and J. Reedijk, *Dalton Trans.*, 1993, 2163.
151. Y. Journaux, J. Sletten and O. Kahn, *Inorg. Chem.*, 1986, **25**, 439.
152. L. Merz and W. Hasse, *Dalton Trans.*, 1980, 875.
153. M. Lubben, R. Hage, A. Meetsma, K. Byma and B. L. Feringa, *Inorg. Chem.*, 1995, **34**, 2217.
154. K. Motoda, H. Sakiyama, N. Matsumoto, H. Ōkawa and D.E. Fenton, *Dalton Trans.*, 1995, 3419.
155. E. Ruiz, P. Alemany, S. Alvarez and J. Cano, *Inorg. Chem.*, 1997, **36**, 3683.
156. C. J. Harding, V. McKee, J. Nelson and Q. Lu, *Chem. Commun.*, 1993, 1768
157. Q. Lu, J. M. Latour, C. J. Harding, N. Martin, D. J. Marrs, V. McKee and J. Nelson, *Dalton Trans.*, 1994, 1471.
158. O. Kahn, *Struct. Bonding*, 1987, **68**, 89.
159. P. Zanello, S. Tamburini, P. A. Vigato and G. A. Mazzocchin, *Coord. Chem. Rev.* 1987, **77**, 165.
160. M. Yonemura, Y. Matsumura, H. Furutachi, M. Ohba, H. Ōkawa and D. E. Fenton, *Inorg. Chem.*, 1997, **36**, 2711.

- 161 M. Yonemura, M. Ohba, K. Takahashi, H. Ōkawa and D. E. Fenton, *Inorg. Chim. Acta*, 1998, **283**, 72.
162. M. Yonemura, K. Arimura, K. Inoue, N. Usuki, M. Ohba and H. Ōkawa, *Inorg. Chem.*, 2002, **41**, 582.
163. G. Fachinetti, C. Floriani, P. F. Zanazzi, *J. Am. Soc.*, 1978, **100**, 7405.
164. Y. Inada, K. Mochizuki, T. Tsuchiya, H. Tsuji, S. Funahashi, *Inorg. Chim. Acta*, 2005, **358**, 3009.
165. O. Atakol, H. Nazir, C. Arici, S. Durmus, I. Svoboda and H. Fuess, *Inorg. Chim. Acta*, 2003, **342**, 295.
166. K. Smith, C. H. Liu and G. A. El-Hiti, *Org. Biomol. Chem.*, 2006, **4(5)**, 917
167. L. P. C. Nielsen, C. P. Stevenson, D. G. Blackmond and E. N. Jacobsen, *J. Am. Chem. Soc.*, 2004, **126**, 1360.
168. K. Omura, T. Uchida, R. Irie and T. Katsuki, *Chem. Commun.*, 2004, 2060.
169. T. Fukuda and T. Katsuki, *Synlett*, 1995, 825.
170. G. Bartoli, M. Bosco, A. Carlone, M. Locatelli, M. Massaccesi, P. Melchiorre and L. Sambri, *Org. Lett.* 2004, **6**, 2173.
171. F. C. J. M. van Veggel, M. Bos, S. Harkema, H. van de Bovenkamp, W. Verboom, J. Reedijk and D. N. Reinhoudt, *J. Org. Chem.*, 1991, **56**, 225.
172. F. Gao, W.-J. Ruan, J.-M. Chen, Y.-H. Zhang and Z.-A. Zhu, *Spectrochimica Acta A*, 2005, **62**, 886.
- 173 C. Redshaw, *Coord. Chem. Rev.*, 2003, **244**, 45
174. P. Thuéry, Z. Asfari, J. Vicens, V. Lamare and J.-F. Dozol, *Polyhedron*, 2002, **21**, 2497.
175. N. P. Clague, J. D. Crane, D. J. Moreton, E. Sinn, S. J. Teat and N. A. Young, *Dalton Trans.*, 1999, 3535.
176. R. D. Shannon, *Acta Cryst.*, 1976, **A32**, 751.
177. G. Guillemot, E. Solari, C. Rizzoli and C. Floriani, *Chem. Eur. J.*, 2002, **8**, 2072.
178. S. M. Nelson, F. E. Esho and M. G. B. Drew, *Dalton Trans.*, 1983, 1857.
179. M. G. B. Drew, F. E. Esho and S. M. Nelson, *Dalton Trans.*, 1983, 1653.
180. S. M. Nelson and M. G. B. Drew, *Dalton Trans.*, 1982, 407.

181. H. M. El-Kaderi, M. J. Heeg and C. H. Winter, *Organometallics*, 2004, **23**, 4995.
182. S. Brooker, V. McKee and W. B. Shepard, *Dalton Trans.*, 1987, 2555.
183. S. M. Nelson, *Pure Appl. Chem.*, 1980, **52**, 2461.
184. G. Givaja, A. J. Blake, C. Wilson, M. Schröder and J. B. Love, *Chem. Commun.*, 2005, 4423.
185. S. Akine, T. Taniguchi, T. Saiki and T. Nabeshima, *J. Am. Chem. Soc.*, 2005, **127**, 541.
186. P. Thuéry, Z. Asfari, M. Nierlich, J. Vicens and B. Masci, *Polyhedron*, 2002, **21**, 1949.
187. R. J. Cernik, W. Clegg, C. R. A. Catlow, G. Bushnell-Wye, J. V. Flaherty, G. N. Graves, M. Hamichi, I. Burrows, D. J. Taylor and S. J. Teat, *J. Synchrotron Radiat.*, 1997, **4**, 279.
188. P. v. d. Sluis and A. L. Spek, *Acta Crystallogr., Sect. A*, 1990, **46**, 194
189. G. M. Sheldrick, SHELXTL version 6.10, Bruker-AXS, Madison WI 2000.

## SINGLE CRYSTAL X-RAY CRYSTALLOGRAPHY

The single crystals were mounted in oil on the tip of a quartz glass capillary and placed under a stream of nitrogen.

The data sets were corrected for Lorentz and polarisation effects. The data sets were solved by direct methods or by patterson methods and refined by full-matrix least squares on  $F^2$ . The structures were solved and refined using SHELXTL version 6.10 suites of program [Sheldrick, 2000]<sup>189</sup>. The crystal data and structure refinement table for all the structures is tabulated in appendix 1. Full details of the refinements in CIF format are available on CD-ROM which can be found in the back cover (appendix 3).



# **APPENDIX I**

## **CRYSTAL STRUCTURE DATA**

**Table 1. Crystal data and structure refinement for [Cu<sub>2</sub>(H<sub>4</sub>L1)(Cl)]Cl·1.6Et<sub>2</sub>O·EtOH (2.1x)**

The X-ray reflection data were collected at 150K on a Bruker SMART1000 CCD diffractometer using graphite monochromated Mo-K $\alpha$  radiation ( $\lambda = 0.71073 \text{ \AA}$ ) at Loughborough University.

Identification code	jbcu3	
Empirical formula	C62 H92 Cl2 Cu2 N4 O9	
Formula weight	1235.38	
Temperature	150(2) K	
Wavelength	0.71073 $\text{\AA}$	
Crystal system	Triclinic	
Space group	P-1	
Unit cell dimensions	a = 13.707(3) $\text{\AA}$ b = 14.568(3) $\text{\AA}$ c = 16.827(4) $\text{\AA}$	$\alpha = 103.472(3)^\circ$ $\beta = 95.935(3)^\circ$ $\gamma = 93.429(3)^\circ$
Volume	3237.9(12) $\text{\AA}^3$	
Z	2	
Density (calculated)	1.267 $\text{Mg/m}^3$	
Absorption coefficient	0.794 $\text{mm}^{-1}$	
F(000)	1312	
Crystal size	0.35 x 0.14 x 0.07 $\text{mm}^3$	
Theta range for data collection	1.50 to 25.00 $^\circ$	
Index ranges	-16 $\leq h \leq$ 16, -17 $\leq k \leq$ 17, -20 $\leq l \leq$ 20	
Reflections collected	22825	
Independent reflections	11280 [R(int) = 0.0455]	
Completeness to theta = 25.00 $^\circ$	99.0 %	
Absorption correction	Multiscan	
Max. and min. transmission	1.00 and 0.88	
Refinement method	Full-matrix least-squares on F <sup>2</sup>	
Data / restraints / parameters	11280 / 0 / 733	
Goodness-of-fit on F <sup>2</sup>	0.924	
Final R indices [I > 2 $\sigma$ (I)]	R1 = 0.0568, wR2 = 0.1308	
R indices (all data)	R1 = 0.1062, wR2 = 0.1478	
Largest diff. peak and hole	0.962 and -0.453 $\text{e.\AA}^{-3}$	

**Refinement and disorder details for [Cu<sub>2</sub>(H<sub>4</sub>L1)(Cl)]Cl·2Et<sub>2</sub>O·EtOH (2.1x)**

One of the pendant alcohols was modelled with 70:30 distribution over two sites, while the other pendant alcohol was refined with 95.5 occupancy of two overlapping sites. Hydrogen atoms bonded to carbon were inserted at calculated positions using a riding model; those bonded to oxygen were located from difference maps and not further refined except for those of the ethanol and pendant alcohol groups which were inserted at calculated positions using a riding model. The largest residual electron density peak (0.96) is 1.5 Angstrom from the coordinated chloride ion and mid-way along the Cu-Cu vector.

**Table 2. Crystal data and structure refinement for [Zn<sub>2</sub>(H<sub>4</sub>L1)(Cl)]Cl·Et<sub>2</sub>O·0.5EtOH·0.55H<sub>2</sub>O (2.2x)**

The X-ray reflection data were collected at 150K on a Bruker SMART1000 CCD diffractometer using graphite monochromated Mo-K $\alpha$  radiation ( $\lambda = 0.71073 \text{ \AA}$ ) at Loughborough University.

Identification code	jzn3	
Empirical formula	C57 H80 20 Cl2 N4 O8.10 Zn2	
Formula weight	1152.69	
Temperature	150(2) K	
Wavelength	0.71073 $\text{\AA}$	
Crystal system	Triclinic	
Space group	P-1	
Unit cell dimensions	a = 13.8372(7) $\text{\AA}$	$\alpha = 103.4880(10)^\circ$
	b = 14.7550(7) $\text{\AA}$	$\beta = 95.6630(10)^\circ$
	c = 16.8022(8) $\text{\AA}$	$\gamma = 93.0300(10)^\circ$
Volume	3309.4(3) $\text{\AA}^3$	
Z	2	
Density (calculated)	1.157 Mg/m <sup>3</sup>	
Absorption coefficient	0.854 mm <sup>-1</sup>	
F(000)	1218	
Crystal size	0.52 x 0.42 x 0.42 mm <sup>3</sup>	
Theta range for data collection	1.83 to 25.00 $^\circ$ .	
Index ranges	-16 $\leq h \leq$ 16, -17 $\leq k \leq$ 17, -19 $\leq l \leq$ 19	
Reflections collected	23643	
Independent reflections	11600 [R(int) = 0.0167]	
Completeness to theta = 25.00 $^\circ$	99.4 %	
Absorption correction	Multiscan	
Max. and min. transmission	1.00 and 0.70	
Refinement method	Full-matrix least-squares on F <sup>2</sup>	
Data / restraints / parameters	11600 / 108 / 805	
Goodness-of-fit on F <sup>2</sup>	1.083	
Final R indices [I > 2 $\sigma$ (I)]	R1 = 0.0723, wR2 = 0.2136	
R indices (all data)	R1 = 0.0827, wR2 = 0.2257	
Largest diff. peak and hole	1.414 and -0.528 e $\text{\AA}^{-3}$	

**Refinement and disorder details for [Zn<sub>2</sub>(H<sub>4</sub>L1)(Cl)]Cl·Et<sub>2</sub>O·0.5EtOH·0.55H<sub>2</sub>O (2.2x)**

This complex is isomorphous with the copper equivalent. The detailed structure differs in the occupancy of the solvate sites and in the 5-/6-coordinate disorder at the zinc sites. One disordered *t*-butylphenol group was refined with 60.40 occupancy of two positions; one of the pendant alcohols showed 80:20 disorder over two positions; the ethanol solvate was modelled with partial (25:25) occupancy of two overlapping positions and the diethylether solvate molecules were each refined with 50% occupancy. No hydrogen atoms bonded to oxygen were located or included in the model.

**Table 3. Crystal data and structure refinement for  $[\text{Ni}_2(\text{H}_4\text{L1})(\text{H}_2\text{O})(\text{EtOH})_2](\text{ClO}_4)_2 \cdot 4\text{EtOH}$  (2.5x)**

The X-ray reflection data were collected at 150K on a Bruker SMART1000 CCD diffractometer using graphite monochromated Mo-K $\alpha$  radiation ( $\lambda = 0.71073 \text{ \AA}$ ) at Loughborough University.

Identification code	jni2	
Empirical formula	C <sub>64</sub> H <sub>104</sub> Cl <sub>2</sub> N <sub>4</sub> Ni <sub>2</sub> O <sub>21</sub>	
Formula weight	1453.83	
Temperature	150(2) K	
Wavelength	0.71073 $\text{\AA}$	
Crystal system	Orthorhombic	
Space group	Pnma	
Unit cell dimensions	a = 27 9805(12) $\text{\AA}$	$\alpha = 90^\circ$
	b = 13.7050(6) $\text{\AA}$	$\beta = 90^\circ$
	c = 18 8743(8) $\text{\AA}$	$\gamma = 90^\circ$
Volume	7237.8(5) $\text{\AA}^3$	
Z	4	
Density (calculated)	1.334 $\text{Mg/m}^3$	
Absorption coefficient	0.666 $\text{mm}^{-1}$	
F(000)	3096	
Crystal size	0.53 x 0.30 x 0.27 $\text{mm}^3$	
Theta range for data collection	1.46 to 25.00 $^\circ$	
Index ranges	-33 $\leq h \leq$ 33, -16 $\leq k \leq$ 16, -22 $\leq l \leq$ 22	
Reflections collected	50518	
Independent reflections	6664 [R(int) = 0.0234]	
Completeness to theta = 25.00 $^\circ$	100.0 %	
Absorption correction	Multiscan	
Max. and min. transmission	1.00 and 0.87	
Refinement method	Full-matrix least-squares on F <sup>2</sup>	
Data / restraints / parameters	6664 / 3 / 477	
Goodness-of-fit on F <sup>2</sup>	1.196	
Final R indices [I > 2 $\sigma$ (I)]	R1 = 0.0764, wR2 = 0.1899	
R indices (all data)	R1 = 0.0840, wR2 = 0.1949	
Largest diff. peak and hole	0.768 and -0.601 $\text{e \AA}^{-3}$	

**Refinement and disorder details for  $[\text{Ni}_2(\text{H}_4\text{L1})(\text{H}_2\text{O})(\text{EtOH})_2](\text{ClO}_4)_2 \cdot 4\text{EtOH}$  (2.5x)**

The pendant alcohol group of the macrocycle is disordered 75:25 over two positions. The cations lie on mirror planes, as do the perchlorate anions, one of which is disordered (modelled as 45:5 % over two sites on the mirror plane), and the uncoordinated ethanol solvate molecules. Hydrogen atoms bonded to oxygen atoms were located from difference maps and not further refined. The quality of the refinements is not improved by reducing the symmetry.

**Table 4. Crystal data and structure refinement [Ni<sub>2</sub>(H<sub>4</sub>L1)(NO<sub>3</sub>)(EtOH)<sub>2</sub>]Et<sub>2</sub>O·1.5EtOH·NO<sub>3</sub>·H<sub>2</sub>O (2.8x)**

The X-ray reflection data were collected at 150K on a Bruker SMART1000 CCD diffractometer using graphite monochromated Mo-K $\alpha$  radiation ( $\lambda = 0.71073 \text{ \AA}$ ) at Loughborough University.

Identification code	jbn12a	
Empirical formula	C63 H87 N6 Ni2 O17 50	
Formula weight	1325 81	
Temperature	150(2) K	
Wavelength	0.71073 $\text{\AA}$	
Crystal system	Monoclinic	
Space group	P2 <sub>1</sub>	
Unit cell dimensions	a = 13 5710(14) $\text{\AA}$ b = 28.532(3) $\text{\AA}$ c = 17.7737(18) $\text{\AA}$	$\alpha = 90^\circ$ $\beta = 103.299(2)^\circ$ $\gamma = 90^\circ$
Volume	6697.6(12) $\text{\AA}^3$	
Z	4	
Density (calculated)	1.315 Mg/m <sup>3</sup>	
Absorption coefficient	0 633 mm <sup>-1</sup>	
F(000)	2812	
Crystal size	0.16 x 0 21 x 0 52 mm <sup>3</sup>	
Theta range for data collection	1 43 to 25 00 $^\circ$ .	
Index ranges	-16<= <i>h</i> <=16, -33<= <i>k</i> <=33, -21<= <i>l</i> <=21	
Reflections collected	45222	
Independent reflections	22631 [R(int) = 0 0564]	
Completeness to theta = 25 00 $^\circ$	99 6 %	
Absorption correction	Multiscan	
Max. and min. transmission	1.00 and 0 78	
Refinement method	Full-matrix least-squares on F <sup>2</sup>	
Data / restraints / parameters	22631 / 7 / 1613	
Goodness-of-fit on F2	1 045	
Final R indices [I>2sigma(I)]	R1 = 0 0824, wR2 = 0 2154	
R indices (all data)	R1 = 0 0984, wR2 = 0.2256	
Absolute structure parameter	0 627(18)	
Largest diff. peak and hole	1.391 and -1.255 e $\text{\AA}^{-3}$	

**Refinement and disorder details for [Ni<sub>2</sub>(H<sub>4</sub>L1)(NO<sub>3</sub>)(EtOH)<sub>2</sub>]Et<sub>2</sub>O·1.5EtOH·NO<sub>3</sub>·H<sub>2</sub>O (2.8x)**

The oxygen atoms O(6A) and O(3B) on the pendant alcohol groups of two different macrocyclic units are disordered over two position with 50% occupancy each. Hydrogen atoms bonded to carbon were inserted at calculated positions using a riding model. The hydrogen atoms on the pendant alcohol groups, the phenol groups, the oxygen atoms belonging to the coordinated ethanol molecules and those belonging to the solvate molecules were not located or included in the model.

**Table 5. Crystal data and structure refinement for [Zn<sub>2</sub>(H<sub>4</sub>L1)(NO<sub>3</sub>)(EtOH)](NO<sub>3</sub>)·H<sub>2</sub>O (2.9x)**

The X-ray reflection data were collected at 150K on a Bruker SMART1000 CCD diffractometer using graphite monochromated Mo-K $\alpha$  radiation ( $\lambda = 0.71073 \text{ \AA}$ ) at Loughborough University.

Identification code	jbzn2	
Empirical formula	C <sub>54</sub> H <sub>72.50</sub> N <sub>6</sub> O <sub>13</sub> 2.5 Zn <sub>2</sub>	
Formula weight	1148.42	
Temperature	150(2) K	
Wavelength	0.71073 $\text{\AA}$	
Crystal system	Tetragonal	
Space group	I4 <sub>1</sub> /a	
Unit cell dimensions	a = 41.2744(13) $\text{\AA}$	$\alpha = 90^\circ$
	b = 41.2744(13) $\text{\AA}$	$\beta = 90^\circ$
	c = 13.2831(6) $\text{\AA}$	$\gamma = 90^\circ$
Volume	22628.8(14) $\text{\AA}^3$	
Z	16	
Density (calculated)	1.348 Mg/m <sup>3</sup>	
Absorption coefficient	0.915 mm <sup>-1</sup>	
F(000)	9672	
Crystal size	0.45 x 0.12 x 0.10 mm <sup>3</sup>	
Theta range for data collection	0.70 to 25.00 $^\circ$ .	
Index ranges	-48 $\leq$ h $\leq$ 49, -48 $\leq$ k $\leq$ 48, -15 $\leq$ l $\leq$ 15	
Reflections collected	80813	
Independent reflections	9961 [R(int) = 0.0466]	
Completeness to theta = 25.00 $^\circ$	100.0 %	
Absorption correction	Multiscan	
Max. and min. transmission	1.00 and 0.89	
Refinement method	Full-matrix least-squares on F <sup>2</sup>	
Data / restraints / parameters	9961 / 0 / 729	
Goodness-of-fit on F <sup>2</sup>	1.050	
Final R indices [I > 2 $\sigma$ (I)]	R1 = 0.0453, wR2 = 0.1197	
R indices (all data)	R1 = 0.0628, wR2 = 0.1300	
Largest diff. peak and hole	0.740 and -0.425 e $\text{\AA}^{-3}$	

**Refinement and disorder details for [Zn<sub>2</sub>(H<sub>4</sub>L1)(NO<sub>3</sub>)(EtOH)](NO<sub>3</sub>)·H<sub>2</sub>O (2.9x)**

The coordinated nitrate and one pendant alcohol are both disordered and were modelled with 60:40 occupancy of two related positions. Hydrogen atoms bonded to carbon were inserted at calculated positions using a riding model. Hydrogen atoms bonded to oxygen were all located and not further refined except for that bound to the disordered alcohol, which was not included in the refinement.



**Table 6. Crystal data and structure refinement for [Zn<sub>2</sub>(H<sub>4</sub>L1)(AcO)](AcO)·5H<sub>2</sub>O·4Et<sub>2</sub>O (2.11x)**

The X-ray reflection data were collected at 150K on a Bruker SMART1000 CCD diffractometer using graphite monochromated Mo-K $\alpha$  radiation ( $\lambda = 0.71073 \text{ \AA}$ ) at Loughborough University.

Identification code	jzn4b	
Empirical formula	C72 H122 N4 O12 67 Zn2	
Formula weight	1377.14	
Temperature	150(2) K	
Wavelength	0.71073 $\text{\AA}$	
Crystal system	Hexagonal	
Space group	P6 <sub>3</sub> /m	
Unit cell dimensions	a = 27.654(3) $\text{\AA}$	$\alpha = 90^\circ$
	b = 27.654(3) $\text{\AA}$	$\beta = 90^\circ$
	c = 15.936(2) $\text{\AA}$	$\gamma = 120^\circ$
Volume	10554.4(19) $\text{\AA}^3$	
Z	6	
Density (calculated)	1.300 Mg/m <sup>3</sup>	
Absorption coefficient	0.746 mm <sup>-1</sup>	
F(000)	4460	
Crystal size	0.79 x 0.16 x 0.13 mm <sup>3</sup>	
Theta range for data collection	0.85 to 22.49 $^\circ$	
Index ranges	-29 $\leq h \leq$ 29, -29 $\leq k \leq$ 29, -17 $\leq l \leq$ 17	
Reflections collected	59721	
Independent reflections	4810 [R(int) = 0.1074]	
Completeness to theta = 22.49 $^\circ$	100.0 %	
Absorption correction	Multiscan	
Max. and min. transmission	1.00 and 0.50	
Refinement method	Full-matrix least-squares on F <sup>2</sup>	
Data / restraints / parameters	4810 / 361 / 323	
Goodness-of-fit on F <sup>2</sup>	1.050	
Final R indices [I > 2 $\sigma$ (I)]	R1 = 0.1232, wR2 = 0.3188	
R indices (all data)	R1 = 0.1614, wR2 = 0.3412	
Largest diff. peak and hole	1.213 and -1.563 e. $\text{\AA}^{-3}$	

**Refinement and disorder details for [Zn<sub>2</sub>(H<sub>4</sub>L1)(AcO)](AcO)·5H<sub>2</sub>O·4Et<sub>2</sub>O (2.11x)**

The saturated side chain of the macrocycle was disordered over two equivalent sets of positions and modelled with 70:30 site occupancy. Hydrogen atoms bonded to carbon were inserted at calculated positions using a riding model; those bonded to oxygen atoms were located from difference maps and not further refined. The hydrogen atoms of the phenol-phenolate H-bond were not located or included in the model. The cation was treated using the SQUEEZE<sup>188</sup> procedure of PLATON. The 'missing' electron count refined to 251 extra electrons per formula unit, which were assigned to one acetate anion, five water and four ether solvate molecules.

**Table 7. Crystal data and structure refinement for  $[\text{Ni}_2(\text{H}_4\text{L1})(\text{MeOH})_2]_2(\text{ClO}_4)_4 \cdot 2\text{Et}_2\text{O} \cdot 3\text{MeOH} \cdot \text{EtOH}$  (2.12x)**

The X-ray reflection data were collected at 150K on a Bruker SMART1000 CCD diffractometer using graphite monochromated Mo-K $\alpha$  radiation ( $\lambda = 0.71073 \text{ \AA}$ ) at Loughborough University.

Identification code	jniodd	
Empirical formula	C62 H90 Cl2 N4 Ni2 O19	50
Formula weight	1397.71	
Temperature	150(2) K	
Wavelength	0.71073 $\text{\AA}$	
Crystal system	Orthorhombic	
Space group	Pca2 <sub>1</sub>	
Unit cell dimensions	a = 26 6163(6) $\text{\AA}$	$\alpha = 90^\circ$
	b = 13.6515(3) $\text{\AA}$	$\beta = 90^\circ$
	c = 38.3297(9) $\text{\AA}$	$\gamma = 90^\circ$
Volume	13927 2(5) $\text{\AA}^3$	
Z	8	
Density (calculated)	1 333 Mg/m <sup>3</sup>	
Absorption coefficient	0 688 mm <sup>-1</sup>	
F(000)	5912	
Crystal size	0.58 x 0 24 x 0 22 mm <sup>3</sup>	
Theta range for data collection	1.06 to 25.00 $^\circ$ .	
Index ranges	-31 $\leq h \leq$ 31, -16 $\leq k \leq$ 16, -45 $\leq l \leq$ 45	
Reflections collected	97288	
Independent reflections	24533 [R(int) = 0 0349]	
Completeness to theta = 25 00 $^\circ$	100 0 %	
Absorption correction	Multiscan	
Max. and min. transmission	1 00 and 0.85	
Refinement method	Full-matrix least-squares on F <sup>2</sup>	
Data / restraints / parameters	24533 / 1 / 1665	
Goodness-of-fit on F2	1 045	
Final R indices [I > 2 $\sigma$ (I)]	R1 = 0 0532, wR2 = 0.1387	
R indices (all data)	R1 = 0 0613, wR2 = 0 1471	
Absolute structure parameter	0.510(10)	
Largest diff. peak and hole	0.790 and -0 489 e $\text{\AA}^{-3}$	

**Refinement and disorder details for  $[\text{Ni}_2(\text{H}_4\text{L1})(\text{MeOH})_2]_2(\text{ClO}_4)_4 \cdot 2\text{Et}_2\text{O} \cdot 3\text{MeOH} \cdot \text{EtOH}$  (2.12x)**

All the hydrogen atoms belonging to the macrocycle were inserted at calculated positions except those on the alkoxo oxygen atoms, the coordinated methanol molecules and the phenol oxygen atoms, which were not included in the model. The hydrogen at the oxygen atoms of the solvate molecules were not included in the model either. The oxygen atoms O(3), O(6) and O(12) of the pendant alcohol groups are disordered over two sites, one with 70% occupancy and the other with 30% occupancy whereas the oxygen atom O(9) of the remaining pendant alcohol group was refined with 80:20 occupancy of two overlapping sites. The model was refined as a racemic twin.

**Table 8. Crystal data and structure refinement for  $[\text{Mn}_2(\text{H}_2\text{L1})(\text{Cl})_2(\text{dmf})(\text{dmsO})]\cdot 1.5\text{dmf}\cdot 0.3\text{Et}_2\text{O}$  (2.13x)**

The X-ray reflection data were collected at 150K on a Bruker SMART1000 CCD diffractometer using graphite monochromated Mo-K $\alpha$  radiation ( $\lambda = 0.71073 \text{ \AA}$ ) at Loughborough University.

Identification code	jbmnl1sol	
Empirical formula	C62 H90.50 Cl2 Mn2 N6 O9 S	
Formula weight	1304.96	
Temperature	150(2) K	
Wavelength	0.71073 $\text{\AA}$	
Crystal system	Monoclinic	
Space group	P2 <sub>1</sub> /c	
Unit cell dimensions	a = 11 8935(8) $\text{\AA}$	$\alpha = 90^\circ$
	b = 19.5914(13) $\text{\AA}$	$\beta = 100.6830(10)^\circ$
	c = 32 009(2) $\text{\AA}$	$\gamma = 90^\circ$
Volume	7329.3(9) $\text{\AA}^3$	
Z	4	
Density (calculated)	1.183 Mg/m <sup>3</sup>	
Absorption coefficient	0.499 mm <sup>-1</sup>	
F(000)	2762	
Crystal size	0.28 x 0.15 x 0.10 mm <sup>3</sup>	
Theta range for data collection	1.66 to 25.00 $^\circ$ .	
Index ranges	-14 $\leq h \leq$ 14, -23 $\leq k \leq$ 23, -38 $\leq l \leq$ 37	
Reflections collected	51860	
Independent reflections	12907 [R(int) = 0.0486]	
Completeness to theta = 25.00 $^\circ$	100.0 %	
Absorption correction	Multiscan	
Max. and min. transmission	1.00 and 0.88	
Refinement method	Full-matrix least-squares on F <sup>2</sup>	
Data / restraints / parameters	12907 / 45 / 866	
Goodness-of-fit on F <sup>2</sup>	1.079	
Final R indices [I > 2 $\sigma$ (I)]	R1 = 0.0658, wR2 = 0.1874	
R indices (all data)	R1 = 0.0925, wR2 = 0.2055	
Largest diff. peak and hole	1.200 and -0.493 e. $\text{\AA}^{-3}$	

**Refinement and disorder details for  $[\text{Mn}_2(\text{H}_2\text{L1})(\text{Cl})_2(\text{dmf})(\text{dmsO})]\cdot 1.5\text{dmf}\cdot 0.3\text{Et}_2\text{O}$  (2.13x)**

In addition to the coordinated dmf and dmsO molecules, the lattice contained a partial-occupancy ether molecule, refined isotropically with 30% occupancy, one disordered dmf molecule, modelled as 50% occupancy of each of two overlapping sites and a further 50% occupancy dmf molecule. One of the pendant alcohol groups of the macrocycle was disordered and refined with 50% occupancy of two related positions (O3 and O3') and one of the *t*-butyl groups was modelled with 60:40 occupancy of two positions. The hydrogen atoms of the pendant alcohols were not located or included in the model.

**Table 9. Crystal data and structure refinement for [Cu<sub>2</sub>(H<sub>4</sub>L1)]·dmsO·Et<sub>2</sub>O (2.19x)**

The X-ray reflection data were collected at 150K on station 9.8 of the Synchrotron Radiation Source at Daresbury<sup>187</sup> on a Bruker Apex II CCD diffractometer using synchrotron radiation.

Identification code	jcua3a	
Empirical formula	C <sub>58</sub> H <sub>78</sub> Cu <sub>2</sub> N <sub>4</sub> O <sub>8</sub> S	
Formula weight	1118.38	
Temperature	120(2) K	
Wavelength	0.68970 Å	
Crystal system	Triclinic	
Space group	P-1	
Unit cell dimensions	a = 11.123(4) Å	α = 100.415(7)°
	b = 15.799(6) Å	β = 107.201(6)°
	c = 18.739(7) Å	γ = 105.817(7)°
Volume	2901.7(19) Å <sup>3</sup>	
Z	2	
Density (calculated)	1.280 Mg/m <sup>3</sup>	
Absorption coefficient	0.823 mm <sup>-1</sup>	
F(000)	1184	
Crystal size	0.11 x 0.02 x 0.01 mm <sup>3</sup>	
Theta range for data collection	1.36 to 20.57°	
Index ranges	-11 ≤ h ≤ 11, -16 ≤ k ≤ 15, -18 ≤ l ≤ 18	
Reflections collected	13731	
Independent reflections	6297 [R(int) = 0.0975]	
Completeness to theta = 20.57°	98.2 %	
Absorption correction	Multiscan	
Max. and min. transmission	1.00 and 0.098	
Refinement method	Full-matrix least-squares on F <sup>2</sup>	
Data / restraints / parameters	6297 / 241 / 702	
Goodness-of-fit on F <sup>2</sup>	1.216	
Final R indices [I > 2σ(I)]	R1 = 0.0898, wR2 = 0.2149	
R indices (all data)	R1 = 0.1480, wR2 = 0.2442	
Extinction coefficient	0.0082(17)	
Largest diff. peak and hole	0.925 and -0.841 e Å <sup>-3</sup>	

**Refinement and disorder details for [Cu<sub>2</sub>(H<sub>4</sub>L1)]·dmsO·Et<sub>2</sub>O (2.19x)**

The pendant alcohol groups of the macrocycle are both disordered and were modelled with 70:30 occupancy of two related positions. In addition, the lattice contained a disordered dmsO molecule, modelled as 40:60 of each of two overlapping sites. Hydrogen atoms bonded to carbon were inserted at calculated positions using a riding model and those bonded to oxygen were located from difference maps and not further refined.

**Table 10. Crystal data for [Cu<sub>3</sub>(H<sub>2</sub>L1)(OH)(H<sub>2</sub>O)](NO<sub>3</sub>)·4EtOH (3.2d)**

The X-ray reflection data were collected at 150K on a Bruker SMART1000 CCD diffractometer using graphite monochromated Mo-K $\alpha$  radiation ( $\lambda = 0.71073 \text{ \AA}$ ) at Loughborough University.

Identification code	jbcu4m	
Empirical formula	C <sub>58</sub> H <sub>82</sub> Cu <sub>3</sub> N <sub>6</sub> O <sub>17</sub>	
Formula weight	1325.92	
Temperature	150(2) K	
Wavelength	0.71073 $\text{\AA}$	
Crystal system	Orthorhombic	
Space group	Ibam	
Unit cell dimensions	a = 19.2306(17) $\text{\AA}$	$\alpha = 90^\circ$
	b = 20.6124(18) $\text{\AA}$	$\beta = 90^\circ$
	c = 34.221(3) $\text{\AA}$	$\gamma = 90^\circ$
Volume	13565(2) $\text{\AA}^3$	
Z	8	
Density (calculated)	1.298 Mg/m <sup>3</sup>	
Absorption coefficient	0.998 mm <sup>-1</sup>	
F(000)	5560	
Crystal size	0.06 x 0.22 x 0.61 mm <sup>3</sup>	
Theta range for data collection	1.45 to 25.00 $^\circ$ .	
Index ranges	-22 $\leq h \leq$ 22, -24 $\leq k \leq$ 24, -40 $\leq l \leq$ 40	
Reflections collected	46939	
Independent reflections	6103 [R(int) = 0.0855]	
Completeness to theta = 25.00 $^\circ$	100.0 %	
Absorption correction	Multiscan	
Max. and min. transmission	1.00 and 0.79	
Refinement method	Full-matrix least-squares on F <sup>2</sup>	
Data / restraints / parameters	6103 / 113 / 310	
Goodness-of-fit on F <sup>2</sup>	1.060	
Final R indices [I > 2 $\sigma$ (I)]	R1 = 0.1065, wR2 = 0.2849	
R indices (all data)	R1 = 0.1438, wR2 = 0.3094	
Largest diff. peak and hole	3.612 and -1.677 e $\text{\AA}^{-3}$	

**Refinement and disorder details for [Cu<sub>3</sub>(H<sub>2</sub>L1)(OH)(H<sub>2</sub>O)](NO<sub>3</sub>)·4EtOH (3.2d)**

Hydrogen atoms bonded to carbon were inserted at calculated positions using a riding model. No hydrogen atoms bonded to oxygen were located or included in the model. The cation was treated using the SQUEEZE<sup>188</sup> procedure of PLATON. The 'missing' electron count refined to 137 extra electrons per formula unit, which were assigned to one nitrate anion and four ethanol solvate molecules.

**Table 11. Crystal data for [Cu<sub>3</sub>(H<sub>2</sub>L1)(NO<sub>3</sub>)](NO<sub>3</sub>)(dmf)<sub>3</sub> (3.3a)**

The X-ray reflection data were collected at 150K on a Bruker SMART1000 CCD diffractometer using graphite monochromated Mo-K $\alpha$  radiation ( $\lambda = 0.71073 \text{ \AA}$ ) at Loughborough University.

Identification code	jbcu7sol	
Empirical formula	C61 H85 Cu3 N9 O15	
Formula weight	1375.00	
Temperature	150(2) K	
Wavelength	0.71073 $\text{\AA}$	
Crystal system	Monoclinic	
Space group	P2 <sub>1</sub> /c	
Unit cell dimensions	a = 17.2344(13) $\text{\AA}$	$\alpha = 90^\circ$
	b = 22.1300(16) $\text{\AA}$	$\beta = 103.4880(10)^\circ$
	c = 17.6582(13) $\text{\AA}$	$\gamma = 90^\circ$
Volume	6549.0(8) $\text{\AA}^3$	
Z	4	
Density (calculated)	1.395 Mg/m <sup>3</sup>	
Absorption coefficient	1.036 mm <sup>-1</sup>	
F(000)	2884	
Crystal size	0.45 x 0.24 x 0.04 mm <sup>3</sup>	
Theta range for data collection	1.52 to 25.00 $^\circ$	
Index ranges	-20 $\leq$ h $\leq$ 20, -26 $\leq$ k $\leq$ 26, -20 $\leq$ l $\leq$ 20	
Reflections collected	46309	
Independent reflections	11521 [R(int) = 0.0424]	
Completeness to theta = 25.00 $^\circ$	99.9 %	
Absorption correction	Multiscan	
Max. and min. transmission	1.00 and 0.88	
Refinement method	Full-matrix least-squares on F <sup>2</sup>	
Data / restraints / parameters	11521 / 0 / 859	
Goodness-of-fit on F <sup>2</sup>	1.066	
Final R indices [ $I > 2\sigma(I)$ ]	R1 = 0.0646, wR2 = 0.1637	
R indices (all data)	R1 = 0.0852, wR2 = 0.1761	
Largest diff. peak and hole	1.592 and -0.687 e $\text{\AA}^{-3}$	

**Refinement and disorder details for [Cu<sub>3</sub>(H<sub>2</sub>L1)(NO<sub>3</sub>)](NO<sub>3</sub>)(dmf)<sub>3</sub> (3.3a)**

The macrocycle shows rotational disorder in one of the tert-butyl groups and this has been modelled with 50:50 occupancy of two sites. Additionally, the carbons of one of the saturated section are disordered 60:40 over two related sites. The alcohol group on this chain is not disordered and its associated proton was located from difference maps. The pendant alcohol on the opposite side of the macrocycle has been modelled with 50:50 occupancy of two related sites; the proton on this group has not been included. There are several residual electron density peaks of 1.2 - 1.5 electrons/ Angstrom in the region of the copper ions.



**Table 12. Crystal data for  $[\text{Cu}_4(\text{H}_2\text{L1})(\text{OH})_2(\text{H}_2\text{O})(\text{EtOH})] \cdot (\text{NO}_3)_2 \cdot 2\text{EtOH} \cdot \text{H}_2\text{O}$  (3.1b)**

The X-ray reflection data were collected at 150K on a Bruker SMART1000 CCD diffractometer using graphite monochromated Mo-K $\alpha$  radiation ( $\lambda = 0.71073 \text{ \AA}$ ) at Loughborough University.

Identification code	jbcu2sol	
Empirical formula	C <sub>56</sub> H <sub>88</sub> Cu <sub>4</sub> N <sub>6</sub> O <sub>19</sub>	
Formula weight	1403.48	
Temperature	150(2) K	
Wavelength	0.71073 $\text{\AA}$	
Crystal system	Monoclinic	
Space group	$P2_1/c$	
Unit cell dimensions	$a = 11.867(2) \text{ \AA}$	$\alpha = 90^\circ$
	$b = 14.125(3) \text{ \AA}$	$\beta = 93.406(3)^\circ$
	$c = 41.220(7) \text{ \AA}$	$\gamma = 90^\circ$
Volume	$6897(2) \text{ \AA}^3$	
Z	4	
Density (calculated)	$1.352 \text{ Mg/m}^3$	
Absorption coefficient	$1.285 \text{ mm}^{-1}$	
F(000)	2936	
Crystal size	$0.31 \times 0.13 \times 0.04 \text{ mm}^3$	
Theta range for data collection	$0.99$ to $25.00^\circ$ .	
Index ranges	$-13 \leq h \leq 14$ , $-16 \leq k \leq 16$ , $-48 \leq l \leq 48$	
Reflections collected	47670	
Independent reflections	12095 [R(int) = 0.0902]	
Completeness to $\theta = 25.00^\circ$	99.7 %	
Absorption correction	Multiscan	
Refinement method	Full-matrix least-squares on $F^2$	
Data / restraints / parameters	12095 / 66 / 696	
Goodness-of-fit on $F^2$	0.940	
Final R indices [ $I > 2\sigma(I)$ ]	$R1 = 0.0763$ , $wR2 = 0.2119$	
R indices (all data)	$R1 = 0.1516$ , $wR2 = 0.2415$	
Largest diff. peak and hole	$1.267$ and $-0.926 \text{ e \AA}^{-3}$	

**Refinement and disorder details for  $[\text{Cu}_4(\text{H}_2\text{L1})(\text{OH})_2(\text{H}_2\text{O})(\text{EtOH})] \cdot (\text{NO}_3)_2 \cdot 2\text{EtOH} \cdot \text{H}_2\text{O}$  (3.1b)**

The saturated chains on either side of the macrocycle were disordered over two equivalent sets of positions and modelled with 60/40 and 50/50 site occupancy. The solvate molecules bridging each pair of copper ions is also disordered and has been modelled as 50:50 H<sub>2</sub>O-EtOH in each case. The terminal carbon atom at one of the ethanol molecules is further split equally between two related sites. The highest residual peaks are in this region. The hydrogen atoms of the phenol-phenol H-bond, and the bound solvates were not located. The uncoordinated solvate molecules and nitrate ions were too highly disordered for individual atoms to be resolved; this was treated using the SQUEEZE<sup>188</sup> procedure of PLATON. This indicated two voids of 1016  $\text{\AA}^3$  and 468 electrons per cell, or 117 per asymmetric unit. This was assigned to two nitrate counter ions (seen in the IR spectrum), 2 EtOH and one water molecule per asymmetric unit - these were included in the formula, F(000) etc.

**Table 13. Crystal data and structure refinement for [Cu<sub>2</sub>Na(H<sub>2</sub>L1)(H<sub>2</sub>O)]·AcO·10EtOH·4H<sub>2</sub>O (4.1x)**

The X-ray reflection data were collected at 150K on a Bruker SMART1000 CCD diffractometer using graphite monochromated Mo-K $\alpha$  radiation ( $\lambda = 0.71073 \text{ \AA}$ ) at Loughborough University.

Identification code	jcuna	
Empirical formula	C74 H137 Cu2 N4 Na O23	
Formula weight	1600.95	
Temperature	150(2) K	
Wavelength	0.71073 $\text{\AA}$	
Crystal system	Monoclinic	
Space group	C2/c	
Unit cell dimensions	a = 30.118(3) $\text{\AA}$	$\alpha = 90^\circ$
	b = 12.0762(13) $\text{\AA}$	$\beta = 90.299(2)^\circ$
	c = 18.2775(19) $\text{\AA}$	$\gamma = 90^\circ$
Volume	6647.7(12) $\text{\AA}^3$	
Z	4	
Density (calculated)	1.600 Mg/m <sup>3</sup>	
Absorption coefficient	0.736 mm <sup>-1</sup>	
F(000)	3448	
Crystal size	0.55 x 0.10 x 0.09 mm <sup>3</sup>	
Theta range for data collection	1.35 to 25.00 $^\circ$	
Index ranges	-35 $\leq h \leq$ 35, -14 $\leq k \leq$ 14, -21 $\leq l \leq$ 21	
Reflections collected	21862	
Independent reflections	5776 [R(int) = 0.1080]	
Completeness to theta = 25.00 $^\circ$	98.7%	
Absorption correction	Multiscan	
Max. and min. transmission	1.00 and 0.53	
Refinement method	Full-matrix least-squares on F <sup>2</sup>	
Data / restraints / parameters	5776 / 42 / 325	
Goodness-of-fit on F <sup>2</sup>	1.489	
Final R indices [I > 2 $\sigma$ (I)]	R1 = 0.1412, wR2 = 0.3925	
R indices (all data)	R1 = 0.1868, wR2 = 0.4172	
Largest diff. peak and hole	2.186 and -1.229 e. $\text{\AA}^{-3}$	

#### Refinement and disorder details for [Cu<sub>2</sub>Na(H<sub>2</sub>L1)(H<sub>2</sub>O)]·AcO·10EtOH·4H<sub>2</sub>O (4.1x)

The pendant alcohol was disordered over two equivalent sets of positions and modelled with 50:50 site occupancy, while one disordered *t*-butylphenol group was refined with 60:40 occupancy over two positions. Hydrogen atoms bonded to carbon were inserted at calculated positions using a riding model. No hydrogen atoms bonded to oxygen were located or included in the model. The uncoordinated solvate molecules and acetate ions were too highly disordered for individual atoms to be resolved, this was treated using the SQUEEZE<sup>188</sup> procedure of PLATON. This indicated two voids of 2131 Angstrom and 713 electrons per cell, or 365 per asymmetric unit. This was assigned to one acetate counter ion (seen in the IR spectrum), ten ethanol and four water molecules per asymmetric unit - these were included in the formula, F(000) etc.

**Table 14. Crystal data and structure refinement for  $[\text{Zn}_2\text{Na}(\text{H}_2\text{L1})(\text{AcO})(\text{EtOH})_2 \cdot 2\text{EtOH}$  (4.3x)**

The X-ray reflection data were collected at 150K on a Bruker SMART1000 CCD diffractometer using graphite monochromated Mo-K $\alpha$  radiation ( $\lambda = 0.71073 \text{ \AA}$ ) at Loughborough University.

Identification code	jzn2	
Empirical formula	C <sub>59</sub> H <sub>82</sub> N <sub>4</sub> Na O <sub>10</sub> 50 Zn <sub>2</sub>	
Formula weight	1169.02	
Temperature	150(2) K	
Wavelength	0.71073 $\text{\AA}$	
Crystal system	Triclinic	
Space group	P-1	
Unit cell dimensions	a = 12.6218(19) $\text{\AA}$ b = 13.276(2) $\text{\AA}$ c = 18.469(3) $\text{\AA}$	$\alpha = 96.194(2)^\circ$ $\beta = 92.955(2)^\circ$ $\gamma = 97.699(2)^\circ$
Volume	3042.0(8) $\text{\AA}^3$	
Z	2	
Density (calculated)	1.276 $\text{Mg/m}^3$	
Absorption coefficient	0.854 $\text{mm}^{-1}$	
F(000)	1238	
Crystal size	0.45 x 0.20 x 0.10 $\text{mm}^3$	
Theta range for data collection	1.11 to 25.00 $^\circ$ .	
Index ranges	-14 $\leq h \leq$ 15, -15 $\leq k \leq$ 15, -21 $\leq l \leq$ 21	
Reflections collected	21410	
Independent reflections	10577 [R(int) = 0.0596]	
Completeness to theta = 25.00 $^\circ$	98.9 %	
Absorption correction	Multiscan	
Max and min. transmission	1.00 and 0.75	
Refinement method	Full-matrix least-squares on F <sup>2</sup>	
Data / restraints / parameters	10577 / 144 / 767	
Goodness-of-fit on F <sup>2</sup>	0.973	
Final R indices [ $I > 2\sigma(I)$ ]	R1 = 0.0671, wR2 = 0.1561	
R indices (all data)	R1 = 0.1168, wR2 = 0.1730	
Largest diff. peak and hole	1.255 and -0.489 $\text{e \AA}^{-3}$	

**Refinement and disorder details for  $[\text{Zn}_2\text{Na}(\text{H}_2\text{L1})(\text{AcO})(\text{EtOH})_2 \cdot 2\text{EtOH}$  (4.3x)**

Two disordered *t*-butylphenol groups were refined with 50.50 occupancy of two positions. The coordinated ethanol molecule was modelled with 50% occupancy. Hydrogen atoms bonded to carbon were inserted at calculated positions using a riding model; those bonded to the ethanol and pendant alcohol oxygen atoms were inserted at calculated positions using a riding model.

**Table 15. Crystal data and structure refinement for [Cu<sub>4</sub>Ba(H<sub>2</sub>L1)<sub>2</sub>](ClO<sub>4</sub>)<sub>2</sub>·EtOH (4.6ax)**

The X-ray reflection data were collected at 150K on a Bruker SMART1000 CCD diffractometer using graphite monochromated Mo-K $\alpha$  radiation ( $\lambda = 0.71073 \text{ \AA}$ ) at Loughborough University.

Identification code	jcubab (jcu4ba)	
Empirical formula	C103.75 H112 50 Ba Cl2 Cu4 N8 O21	
Formula weight	2269.92	
Temperature	150(2) K	
Wavelength	0.71073 $\text{\AA}$	
Crystal system	Tetragonal	
Space group	P4 <sub>2</sub> 2 <sub>1</sub> 2	
Unit cell dimensions	a = 29 378(4) $\text{\AA}$	$\alpha = 90^\circ$
	b = 29 378(4) $\text{\AA}$	$\beta = 90^\circ$
	c = 31 324(6) $\text{\AA}$	$\gamma = 90^\circ$
Volume	27034(7) $\text{\AA}^3$	
Z	8	
Density (calculated)	1.115 Mg/m <sup>3</sup>	
Absorption coefficient	1.001 mm <sup>-1</sup>	
F(000)	9320	
Crystal size	0.48 x 0.38 x 0.09 mm <sup>3</sup>	
Theta range for data collection	0.95 to 25.00 $^\circ$ .	
Index ranges	-31 $\leq h \leq$ 33, -26 $\leq k \leq$ 34, -37 $\leq l \leq$ 22	
Reflections collected	66202	
Independent reflections	23108 [R(int) = 0.0801]	
Completeness to theta = 25.00 $^\circ$	97.8 %	
Absorption correction	Multiscan	
Refinement method	Full-matrix least-squares on F <sup>2</sup>	
Data / restraints / parameters	23108 / 1496 / 1261	
Goodness-of-fit on F <sup>2</sup>	1.486	
Final R indices [I > 2 $\sigma$ (I)]	R1 = 0.0862, wR2 = 0.2359	
R indices (all data)	R1 = 0.1538, wR2 = 0.2674	
Absolute structure parameter	-0.01(2)	
Largest diff. peak and hole	2.146 and -1.441 e $\text{\AA}^{-3}$	

**Refinement and disorder details for [Cu<sub>4</sub>Ba(H<sub>2</sub>L1)<sub>2</sub>](ClO<sub>4</sub>)<sub>2</sub>·EtOH (4.6ax)**

One of the pendant alcohols was modelled with 60.40 distribution over two sites. Hydrogen atoms bonded to carbon were inserted at calculated positions using a riding model; those bonded to oxygen were not located or included in the model.

**Table 16. Crystal data and structure refinement for  $[\text{Zn}_4\text{Ba}(\text{H}_2\text{L1})_2](\text{ClO}_4)_2 \cdot 2\text{Et}_2\text{O}$  (4.7x)**

The X-ray reflection data were collected at 150K on a Bruker SMART1000 CCD diffractometer using graphite monochromated Mo-K $\alpha$  radiation ( $\lambda = 0.71073 \text{ \AA}$ ) at Loughborough University.

Identification code	jznba2b	
Empirical formula	C <sub>56</sub> H <sub>70</sub> O <sub>50</sub> Ba <sub>0.50</sub> Cl <sub>4</sub> N <sub>4</sub> O <sub>11</sub> Zn <sub>2</sub>	
Formula weight	1210.52	
Temperature	150(2) K	
Wavelength	0.71073 $\text{\AA}$	
Crystal system	Triclinic	
Space group	P-1	
Unit cell dimensions	a = 11.864(2) $\text{\AA}$ b = 18.465(4) $\text{\AA}$ c = 27.189(5) $\text{\AA}$	$\alpha = 87.173(3)^\circ$ $\beta = 86.663(3)^\circ$ $\gamma = 79.886(3)^\circ$
Volume	5849.1(19) $\text{\AA}^3$	
Z	4	
Density (calculated)	1.375 $\text{Mg/m}^3$	
Absorption coefficient	1.255 $\text{mm}^{-1}$	
F(000)	2510	
Crystal size	0.22 x 0.18 x 0.18 $\text{mm}^3$	
Theta range for data collection	0.75 to 22.50 $^\circ$	
Index ranges	-12 $\leq h \leq$ 12, -19 $\leq k \leq$ 19, -29 $\leq l \leq$ 29	
Reflections collected	33440	
Independent reflections	15263 [R(int) = 0.1286]	
Completeness to theta = 22.50 $^\circ$	99.8%	
Absorption correction	Multiscan	
Max. and min. transmission	1.00 and 0.26	
Refinement method	Full-matrix least-squares on F <sup>2</sup>	
Data / restraints / parameters	15263 / 188 / 632	
Goodness-of-fit on F <sup>2</sup>	1.086	
Final R indices [ $I > 2\sigma(I)$ ]	R1 = 0.1411, wR2 = 0.3327	
R indices (all data)	R1 = 0.2037, wR2 = 0.3750	
Largest diff. peak and hole	6.249 and -1.925 $\text{e.\AA}^{-3}$	

**Refinement and disorder details for  $[\text{Zn}_4\text{Ba}(\text{H}_2\text{L1})_2](\text{ClO}_4)_2 \cdot 2\text{Et}_2\text{O}$  (4.7x)**

Hydrogen atoms bonded to carbon were inserted at calculated positions using a riding model and their temperature factor fixed. The hydrogen atoms on the pendant alcohol groups were not located or included in the model. All the light atoms (C, N and O) were left as isotropic since attempts to refine anisotropically (using DELU and ISOR restraints) resulted in large numbers of non-positive definite atoms. This is probably a result of the poor data quality (ca. 50% of the reflections had  $I > 2\sigma(I)$ ). Better quality crystals should be obtained.

**Table 17. Crystal data and structure refinement for [Cu<sub>3</sub>Ba(H<sub>3</sub>L8)(MeOH)(ClO<sub>4</sub>)](ClO<sub>4</sub>) (4.8ax)**

The X-ray reflection data were collected at 150K on a Bruker SMART1000 CCD diffractometer using graphite monochromated Mo-K $\alpha$  radiation ( $\lambda = 0.71073 \text{ \AA}$ ) at Loughborough University.

Identification code	jcubasq	
Empirical formula	C <sub>79</sub> H <sub>96</sub> Ba Cl <sub>2</sub> Cu <sub>3</sub> N <sub>6</sub> O <sub>18</sub>	
Formula weight	1816.48	
Temperature	150(2) K	
Wavelength	0.71073 $\text{\AA}$	
Crystal system	Monoclinic	
Space group	P2 <sub>1</sub> /c	
Unit cell dimensions	a = 19.769(9) $\text{\AA}$ b = 23.760(10) $\text{\AA}$ c = 21.473(9) $\text{\AA}$	$\alpha = 90^\circ$ $\beta = 108.120(6)^\circ$ $\gamma = 90^\circ$
Volume	9586(7) $\text{\AA}^3$	
Z	4	
Density (calculated)	1.259 Mg/m <sup>3</sup>	
Absorption coefficient	1.177 mm <sup>-1</sup>	
F(000)	3732	
Crystal size	0.25 x 0.20 x 0.02 mm <sup>3</sup>	
Theta range for data collection	1.08 to 22.50 $^\circ$ .	
Index ranges	-21 $\leq h \leq$ 21, -25 $\leq k \leq$ 25, -23 $\leq l \leq$ 23	
Reflections collected	54711	
Independent reflections	12539 [R(int) = 0.4964]	
Completeness to theta = 22.50 $^\circ$	100.0 %	
Absorption correction	Multiscan	
Max. and min. transmission	1.00 and 0.44	
Refinement method	Full-matrix least-squares on F <sup>2</sup>	
Data / restraints / parameters	12539 / 268 / 625	
Goodness-of-fit on F <sup>2</sup>	1.243	
Final R indices [I > 2 $\sigma$ (I)]	R1 = 0.1310, wR2 = 0.3155	
R indices (all data)	R1 = 0.3525, wR2 = 0.3851	
Extinction coefficient	0.046(2)	
Largest diff. peak and hole	2.092 and -1.055 e $\text{\AA}^{-3}$	

**Refinement and disorder details for [Cu<sub>3</sub>Ba(H<sub>3</sub>L8)(MeOH)(ClO<sub>4</sub>)](ClO<sub>4</sub>)·Et<sub>2</sub>O (4.8ax)**

Two of the pendant alcohols were modelled with 50% distribution over two sites. Hydrogen atoms bonded to carbon were inserted at calculated positions using a riding model and their temperature factor fixed. The hydrogen atoms on the pendant alcohol groups were not located or included in the model. Some of the atoms were left as isotropic since attempts to refine anisotropically (using DELU and ISOR restraints) resulted in large numbers of non-positive definite atoms. This is probably a result of the poor data quality. Better quality crystals should be obtained.



**Table 18. Crystal data and structure refinement for [Cu<sub>4</sub>Ba(H<sub>4</sub>L9)(MeOH)<sub>2</sub>]-3H<sub>2</sub>O (4.6bx)**

The X-ray reflection data were collected at 150K on station 16.2 of the Synchrotron Radiation Source at Daresbury<sup>187</sup> on a Bruker Apex II CCD diffractometer using synchrotron radiation.

Identification code	jcuba81	
Empirical formula	C104 H120 Ba Cu4 N8 O15	
Formula weight	2113.58	
Temperature	150(2) K	
Wavelength	0.84640 Å	
Crystal system	Monoclinic	
Space group	C2/c	
Unit cell dimensions	a = 41 415(9) Å	α = 90°
	b = 42.163(9) Å	β = 101 949(3)°
	c = 28.256(6) Å	γ = 90°
Volume	48271(18) Å <sup>3</sup>	
Z	16	
Density (calculated)	1 163 Mg/m <sup>3</sup>	
Absorption coefficient	1.070 mm <sup>-1</sup>	
F(000)	17472	
Crystal size	0 23 x 0.16 x 0 03 mm <sup>3</sup>	
Theta range for data collection	3 69 to 25 00°.	
Index ranges	-41 ≤ h ≤ 41, -42 ≤ k ≤ 42, -28 ≤ l ≤ 28	
Reflections collected	104427	
Independent reflections	25091 [R(int) = 0 1576]	
Completeness to theta = 25 00°	99 6 %	
Absorption correction	Multiscan	
Refinement method	Full-matrix least-squares on F <sup>2</sup>	
Data / restraints / parameters	25091 / 1181 / 2442	
Goodness-of-fit on F <sup>2</sup>	1.788	
Final R indices [I > 2σ(I)]	R1 = 0.1279, wR2 = 0 3223	
R indices (all data)	R1 = 0.2377, wR2 = 0 3672	
Largest diff. peak and hole	1 841 and -1 069 e Å <sup>-3</sup>	

**Refinement and disorder details for [Cu<sub>4</sub>Ba(H<sub>4</sub>L9)(MeOH)<sub>2</sub>]-3H<sub>2</sub>O (4.6bx)**

One the pendant alcohol was modelled with 70 30 distribution over two sites Hydrogen atoms bonded to carbon were inserted at calculated positions using a riding model and their temperature factor fixed. The hydrogen atoms on the pendant alcohol groups were not located or included in the model.

## **APPENDIX II**

### **CONFERENCES AND PUBLICATIONS**

## CONFERENCES AND PUBLICATIONS

### Conferences:

- December 2002 RSC UK Macrocyclic and Supramolecular Chemistry Group Meeting, University of York. *Poster Presented.*
- April 2003 9<sup>th</sup> BCA/CCG Intensive course "X-ray structure analysis", University of Durham
- July 2003 Coordination Chemistry Discussion Group Meeting, University of Manchester *Poster Presented.*
- January 2004 UK Macrocycles and Supramolecular Chemistry Meeting, University of Sheffield. *Poster Presented.*
- July 2004 XXIX International Symposium on Macrocyclic Chemistry, Cairns, Australia. *Poster Presented.*

### Publications:

- J Barreira Fontecha, S. Goetz and V. McKee, *Angew. Chem. Ed. Engl.*, 2002, **41**, 4553.
- J. Barreira Fontecha, S. Goetz and V. McKee, *Acta Cryst.*, 2004, **C60**, o776.
- A. Abuskhuma, J M Briody, M. McCann, M. Devereux, K. A. Kavanagh, J Barreira Fontecha and V. McKee, *Polyhedron*, 2004, **23**, 1249.
- J. Barreira Fontecha, S. Goetz and V. McKee, *Dalton Trans.*, 2005, 923.
- N. Sanchez Ballester, J. Barreira Fontecha, J. Wikaira and V. McKee, *Acta Cryst.*, 2005, **E61**, o567.

